Steady State and Laser Flash Photolysis Studies of Ferrocenyl Group VI Fischer-Carbenes and Metalloporphyrins

This Thesis is Presented for the Degree of

Doctor of Philosophy

By

Jonathan Rochford B.Sc.

Under the Supervision of Dr. Mary Pryce

at

Dublin City University

School of Chemical Sciences

December 2004

Declaration

I hereby certify that this thesis, which I know submit for assessment on the programme of study leading to the award of Doctor of Philosophy is entirely my own work and has not been taken from the work of others save and to the extent that such work has been cited and acknowledged within the text of my work.

Signed: Jana Mari Rockford

Student ID No: 96039671

December 2004

Table of Contents

Dedication

I would like to dedicate this work to my family for their patience and support over the last four years (particularly in the last year), without which I almost certainly could not have reached my goals and I am forever grateful

Acknowledgements

I'd like to thank my supervisor, Dr Mary Pryce, for giving me the opportunity to carry out my studies I consider myself lucky to have studied under the guidance of someone with unlimited patience and optimism when it comes to chemistry I am also very grateful to Dr Pryce for allowing me the freedom, and encouraging me, to try my own ideas in the laboratory I would also like to say a special thanks to Prof Conor Long for his invaluable advise over the past four years

Many thanks to Dr Denise Rooney of the National Universtiy of Ireland Maynooth and her students Margaret, Ciara and Kevin, for the advise and productive meetings over the last few years Thanks also to Prof John McGarvey of Queens University Belfast and to Dr Stanley Botchway of Rutherford Appleton Laboratories for their assistance with the time resolved fluorescence studies Thanks to Dr Sylvia Draper of Trinity College Dublin for the x-ray crystallography studies and to Dr Elena Cariati of Universita di Milano for carrying out nonlinear optical studies

I'm sure a few names are left out below but it's been a long time and it's hard to keep track of the many faces I've had the pleasure of working alongside with over the last few years Firstly a massive thank you to my fellow researchers in X246 Jennifer, Davnat, Peter (cheers for the tunes), Karl, Kieran, Kevin, Claire, Tony, Mohammed and Gemma – thanks for some great times! Thanks also to the Hans Vos research group (especially for putting up with my taste in music!) – Adrian, Helen, Luke, Scott, Marco you crazy Italian, Bill, Fiona Frehill, Noel, Stefania, Dec, Eric, Fiona Lynch, Wes, Linda, Rob and the German contingent, Andy, Sabine and Thomas

A big thank you to Moss (for always being Moss), Lorraine, Ray 'razor' Tully, Shane (sorry for addicting you to music!), Daithi, Tommy, Robbie, Daz (keep on keepin' on), Noel 'nobby' Brennan, Steve, Dave Savage, John, Paddy Kane, Johann, Fayner, Ian and Deborah, Cathal, Maire, Aoife, Daragh, Leon, Dave Cummins, Kathleen, Clodagh, Richard, Ger, Neil, Fadi, Frankie

I'm sure I've left more than a few names out but all of those Friday nights in the Slipper must have killed a few brain cells Finally, none of this work could have happened without the invaluable work of the technical staff Vinnie, Ambrose, John, Damien (keep on banging those drums), Mick, Maurice, Veronica, Mary and Ann, I'm very grateful for your help during my time in D C U

Abstract

Chapter one begins with a theoretical description of the electronic structure of the various compounds studied in this thesis, which includes group VI Fischer carbenes, ferrocene and *meso*-substituted porphyrins This is followed by an introduction to the principles of photophysics and non-linear optics Chapter one finishes with an outline of the experimental techniques of laser flash photolysis and electric field induced second harmonic generation (EFISHG)

Chapter two opens with a literature survey of the photochemistry of Fischer carbene complexes covering the areas of photoinduced CO loss, *syn-anti* isomerisation and ketene formation The synthesis of some ferrocenyl chromium and tungsten methoxy Fischer carbene complexes, $(CO)_5M{=}C(OMe)Fc$ and 1,1'-$[(CO)_5M{=}C(OMe)]_2Fc$ (M = Cr, W), is then presented and their photochemistry is investigated in cyclohexane using the techniques of steady state and laser flash photolysis Electrochemical, X-ray crystallographic and EFISHG data are also presented

An investigation into the photochemistry of some additional ferrocenyl Fischer carbene complexes containing a vinyl spacer is presented in chapter three Photoinduced CO loss of the complexes $(CO)_5M{=}C(OMe)C_2H_2Fc$ and $(CO)_5M{=}C(Pyrrolidine)C_2H_2Fc$ (M = Cr, W) is investigated in cyclohexane using the techniques of steady state and laser flash photolysis The results of photoinduced *cis-trans* isomerisation of the complexes $(CO)_5M{=}C(OMe)C_2H_2Fc$ and $(CO)_5M{=}C(OMe)C_2H_2Ph$ (M = Cr, W) are also discussed Electrochemical, X-ray crystallographic and EFISHG data are also included

Chapter four contains a literature survey of the synthetic techniques for the synthesis of *meso*-substituted porphyrin compounds covering the development of the area from the early methods of Rothemund and Adler to the modern stepwise techniques of Lindsey et al The experimental details for the synthesis of some novel thienyl and ferrocenyl porphyrins are reported and their methods discussed

A photophysical investigation of some novel *meso*-substituted thienyl porphyrins is presented in chapter 5 using the techniques of electronic absorption spectroscopy, fluorescence spectroscopy, laser flash photolysis, time correlated single photon counting and cyclic voltammetry These novel *meso*-substituted thienyl porphyrins show some characteristic photophysical properties in contrast to conventional *meso*-substituted tetra-aryl porphyrins and may find interesting applications in non-linear optical materials and other photonic devices

Chapter six opens with a literature survey of ferrocenyl porphyrins followed by an investigation into the photophysical properties of some novel *meso*-substituted ferrocenyl/ferrocenium porphyrins using the techniques of fluorescence spectroscopy, spectro-electrochemistry, laser flash photolysis, time correlated single photon counting and cyclic voltammetry Efficient quenching of the porphyrin luminescence was observed due to the appended ferrocenyl moiety, which acts as an electron-donor and quenches the S_1, S_2 and T_1 excited states of the porphyrins by an electron-transfer mechanism On decreasing the electron-transfer efficiency of the iron centre by oxidising the ferrocene moiety to the ferrocemum ion the luminescent properties of the porphyrin ring are switched on again

Finally chapter seven discusses future work for chapters 2,3,5 and 6 Also the synthesis and properties of some novel thiophene ligands and their ruthenium complexes are presented and their potential applications as non-linear optical materials for second and third harmonic generation are discussed

The overall aim of this thesis was to study the photochemistry/photophysics of organometallic donor-acceptor compounds, which incorporated the Fischer carbene unit as an acceptor moiety Ferrocene and porphyrin units were chosen as the donor moieties The synthesis of porphyrin systems containing the Fischer carbene acceptor group was unsuccessful

Chapter 1

Theoretical Background and Experimental Techniques

1 Introduction

Ferrocene was first discovered by Kealy and Pauson in 1951,[1] however, it was Wilkinson, Woodward and Fischer who first suggested its '*sandwich*' type structure almost a year later [2] The discovery of ferrocene attracted a large amount of interest at the time due to its novel bonding interaction between the metal centre and the two cyclopentadienyl rings, but nobody could have predicted the impact it would have on the field of organometallic chemistry Even today, ferrocene is still studied in a wide variety of research areas ranging from polymerisation catalysis[3] and anionic liquids[4] to drug development[5] and materials science [6] Since their discovery in 1964, Fischer-carbenes have also proven to be extremely versatile, finding applications such as stoichiometric- and catalytic-reagents in organic synthesis [7] They have also attracted recent interest in the ever-developing field of molecular photonics [8]

Generally photochemical investigations of Fischer-carbenes have focused on monometallic type complexes that have been widely used in organic synthesis [9] To date there have been no publications on the photochemical investigations of bimetallic Fischer-carbene systems By introducing ferrocene as a donor group in such systems applications may be found in molecular photonics as non-linear optical materials, as well as in organic synthesis [8(d e) 10] The Fischer-carbene moiety acts as an efficient electron acceptor in such π-conjugated donor-acceptor type systems due to the electron deficiency at the central carbene-carbon The photochemistry of simple di- and tri-metallic heteroatom stabilised Fischer-carbene complexes containing ferrocene as a donor group were investigated and will be discussed in chapters 2 and 3

In order to discuss the photochemical and electrochemical properties of these compounds it is first necessary to develop an understanding of the bonding and electronic structure involved in both Fischer-carbenes and ferrocene, therefore their electronic structures are reviewed A theoretical description of the electronic structure of the porphyrin macrocycle is also given to aid in the understanding of the photophysical and electrochemical properties of the thienyl and ferrocenyl porphyrins, which will be discussed in chapters 5 and 6

1 1 Basic principles of photophysics

The absorption of radiation by a molecule with energy (hν) in the visible and ultraviolet regions of the spectrum generally results in the formation of an electronically and vibrationally excited state of the absorbing species Knowledge of the various energy relaxation pathways available following electronic excitation is essential to the understanding of the photophysics and photochemistry of any molecule (whether it is classed as organic, inorganic or organometallic), as well as to the rational design of functional systems

Characterisation of an electronically excited molecule also involves a detailed knowledge of its electronic distribution and molecular geometry According to the Franck-Condon principle, electronic transitions take place on a much faster time scale than the rate at which nuclei can respond, as the nuclei have a much greater mass than the electrons The direct absorption of light therefore generates an excited electronic configuration that has the ground state nuclear coordinates, but is not a well defined metastable state of the system This initial state is known as the Franck-Condon (FC) excited state

Vibrational relaxation of the FC state is fast compared to relaxation processes that regenerate the ground state As a result, the nuclear and electronic relaxation processes can be treated separately in terms of a potential energy surface (PES) that is based on the configurational wave function for the excited state A distinct PES is assigned to each relevant electronic excited state and the system within each PES is treated as a distinct chemical entity with properties, which can be discussed in terms of its electronic wavefunction

The behaviour of an electronically excited molecule typically involves a sequence of distinct steps illustrated in figure 1 – 1 Following the generation of a FC excited state, rapid vibrational relaxation occurs to the lowest vibrational level of the newly populated electronic excited state This thermally equilibrated excited state is also known as a '*thexi*' state *Thexi* states have a definite structure, chemical reactivity and absorption spectrum and can therefore be considered as higher energy isomers of the ground state

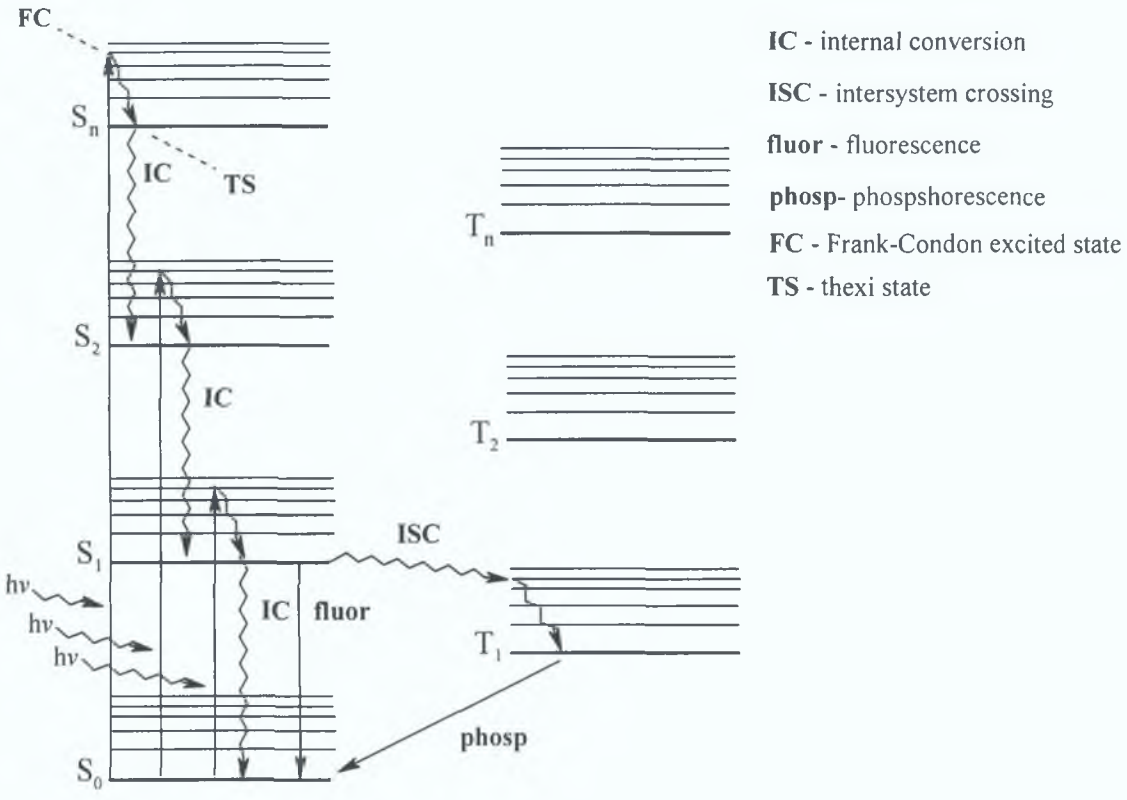

Fig. 1 - 1

A number of processes can take place from the *thexi* state. Internal conversion and/or intersystem crossing may occur to a lower energy electronic state. Non-radiative relaxation between two states (e.g. $S_1 \rightarrow S_0$, $S_n \rightarrow S_1$, $T_n \rightarrow T_1$ where $n > 1$) is called internal conversion (ic) while a relaxation between two states of different multiplicity (e.g. $S_1 \rightarrow T_1$) is called intersystem crossing (isc). If a high-energy singlet state S_n is initially populated rapid internal conversion usually occurs to the first excited singlet state S_1. As with the initially populated FC state, rapid vibrational relaxation of all the lower energy excited states to their potential energy minima occurs. Emission can then occur in which a molecule discards its excitation energy as a photon in the form of fluorescence and/or phosphorescence from the S_1 and T_1 excited states respectively. Whether fluorescence or phosphorescence occurs depends on the efficiency of internal conversion and intersystem crossing from the S_1 excited state. Fluorescence and phosphorescence are easily distinguished as they both occur on different timescales. As fluorescence involves the spontaneous emission of radiation usually from $S_1 \rightarrow S_0$, i.e. both states are of the same multiplicity, it is an allowed

process and typically occurs within a few nanoseconds Phosphorescence can persist for much longer periods of time as it involves relaxation from a triplet excited state to a lower energy singlet state, which is spin-forbidden The processes of intersystem crossing and phosphorescence are both spin-forbidden but exist in systems with appreciable spin-orbit coupling (spin-orbit coupling is more efficient for heavier atoms, a phenomenon known as '*the heavy atom effect*')

As the excited states of the absorbing species have a definite structure, chemical reactivity and greater energy than the ground state species, reaction may also occur from this state The rate of reaction must be very fast however to compete with the relaxation processes

In a metal complex the molecular orbitals involved in the metal-ligand bonds are generally not equally delocalised between the metal and the ligands but predominantly located at the metal or the ligands Electronic transitions involving these orbitals can therefore be classified according to the localisation of their electron density before and after excitation In simple homoleptic mononuclear complexes three types of electronic excitations can be distinguished

1 Those primarily centred on the metal orbital (metal-centred MC or ligand-field LF d-d transitions)
2 Those primarily centred on the ligand orbitals (ligand-centred LC $\pi-\pi^*$, $n-\pi^*$ transitions)
3 Charge transfer (CT) transitions involving the electrons on the central metal and the ligands The charge transfer process can be further subdivided into charge transfer from the metal-to-ligand (MLCT, $d-\pi^*$), ligand-to-metal (LMCT, σ- or π-d) or metal-to-solvent charge transfer (MSCT)

For heteroleptic systems, intraligand charge transfer (ILCT) transitions become possible, however ILCT transitions are usually at higher energy than metal based transitions Also, on introduction of a second metal to a complex intravalence charge transfer (IVCT) transitions become possible Due to the spatial distribution of electron density involved upon charge transfer excitation these transitions are very sensitive to

solvent polarity and can usually be identified by their solvatochromic behaviour Generally, the products that result from CT excitation are strongly reducing and/or oxidising and their reactivity is directly connected to their redox properties

In many cases LC states occur at very high energies, and are frequently followed by facile deactivation to lower excited states within the same molecule If intraligand photoactivity is observed it is often similar to that of the free ligand but modified by coordination

Specific bond weakening in an excited state may cause greatly enhanced chemical activity In many cases LF excitation leads to a weakening of metal-ligand bonds As a result a ligand may be released without any change in the oxidation state of the metal This process is very important for the generation of catalysts because the active species is a coordinatively unsaturated complex, which provides an access for a suitable substrate An understanding of why particular intermediates are generated, and of the wavelength dependence of photochemical pathways, is thus gained through knowledge of the possible excited states of the ground state species

1 2 The electronic structure of Fischer carbene complexes

The concept of a double bond between transition metals and carbon constitutes one of the most important elements in the field of organometallic chemistry The first example of a metal-carbon double bond was by Fischer and Maasbol in 1964 with the synthesis of $(CO)_5W=C(Ph)(OMe)$ [11] Soon after the discovery of Fischer-type complexes their chemistry was systematically explored and Fischer-carbenes have since been established as valuable species in organic synthesis as well as in catalytic processes [7] Schrock later prepared a number of tantalum complexes including $(Me_3CCH_2)_3Ta=CH(CMe_3)$ and $(\eta^5\text{-}C_5H_5)_2MeTa=CH_2$ [12]

Two different patterns of reactivity emerged during the development of these systems resulting in their classification as Fischer- and Schrock-type carbenes Fischer-type carbenes are 18-electron species having a metal in a low oxidation state (0 or 1+) They are stabilised by phenyl or heteroatom substituents at the carbene carbon where the heteroatom is usually oxygen, nitrogen or sulphur Schrock–type carbenes are usually electron deficient (10-16e^-) with a metal in a high oxidation state (3+) and having only hydrogen or simple alkyl substituents at the carbene carbon Fischer-type carbenes are electron deficient at the carbene carbon and are thus susceptible to nucleophilic attack at this site In contrast, the carbene carbon shows nucleophillic character in Schrock-type complexes even though they have a more electron deficient metal centre than their Fischer-type counterparts

Hall and Taylor used *ab-initio* calculations in a study to differentiate between the electronic structures of Fischer- and Schrock-type carbene complexes [13] They explained their results by examining the metal centre and the carbene ligand as individual fragments Calculations on a variety of free carbenes indicated that heteroatom and phenyl substituents preferentially stabilise a singlet ground state, whereas alkyl and hydride substituents stabilised a triplet ground state at the carbene carbon

In terms of valence bond formalism, the atomic orbitals of the central carbene carbon atom can be considered as sp^2 hybridised Two of these sp^2-hybrid orbitals form σ-bonds to each of the substituents Assuming a singlet ground state for the free ligand, the remaining sp^2-hybrid orbital is filled and can donate electron density to the metal centre to form a metal-carbon σ-bond The remaining p-orbital on the carbene carbon is unfilled and orientated perpendicular to the sp^2 plane This empty p-orbital can thus accept electron density from a metal non-bonding d-orbital forming a metal-carbon π-bond analogous to metal-carbonyl back donation (scheme 1 - 1) This type of bonding is characteristic of Fischer-type complexes due to the stabilisation of the singlet carbene fragment by the phenyl or heteroatom substituent Conversely, Schrock-type carbenes may be viewed as a triplet-state carbene spin-coupled to two electrons on the metal centre

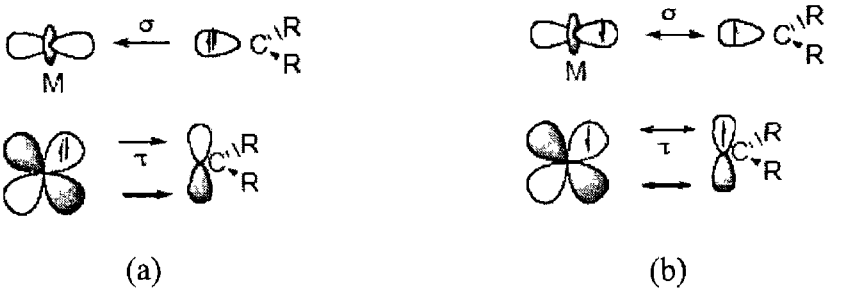

Scheme 1- 1 Bonding scheme for (a) Fischer-type and (b) Schrock-type carbenes

In the Fischer-type complex the π-electrons are polarised towards the metal while in the Schrock-type complex the π-electrons are evenly distributed In a theoretical study carried out by Vyboishchikov and Frenking, Fischer-type complexes were interpreted as metal-carbene donor-acceptor complexes with metal-carbon bond orders close to that of typical metal-carbon single bonds [14] In the same study, Schrock–type complexes were shown to have higher double bond character due to the covalent nature of the metal-carbene bond in these systems

The first application of molecular electronic structure calculations of a transition metal carbene was reported by Block et al [15] It was shown that nucleophillic attack at the carbene carbon of the Fischer type complex $(CO)_5Cr{=}C(OCH_3)CH_3$ is frontier orbital controlled rather than charge controlled This was explained as a result of the

energetic localisation of the LUMO of the complex, which is mainly carbene carbon $2p_x$ in character Block and Fenske later went on to perform molecular orbital calculations on a series of free carbene ligands and their respective Fischer-type complexes [16] They concluded from their results that no single characteristic of the free ligand's electronic structure is the sole determinant of the ligands σ-donor/π-acceptor strength Although the energetic placement of the ligands HOMO and LUMO are extremely important with respect to the extent of metal-carbene interaction, the spatial localisation, degeneracy and symmetry must also be taken into account

Nakatsuji et al have reported the barrier to rotation around the Cr=C bond of $(CO)_5Cr=C(OH)H$ as 0 41 kcal mol^{-1} in contrast to 65 kcalmol^{-1} for the C=C double bond in ethylene and 3 kcal mol^{-1} for an aliphatic C-C bond [17] This small barrier to rotation was explained by the degeneracy of the metal d-orbitals in the complex with respect to rotation about the $M\text{-}C_{carbene}$ axis Van der Waal forces and any steric factors involving bulky substituents on the carbene carbon therefore determine any barrier to rotation about this axis Jacobsen and Ziegler later reported that the preference of a staggered or eclipsed arrangement is determined by the substituents at the carbene ligand aswell as the metal-carbene bond distance [18] The eclipsed configuration of $(CO)_5Cr=C(OCH_3)CH_3$ is 0 5 – 0 7 kcal mol^{-1} more stable than the staggered configuration

On rotation of the carbene ligand into the staggered configuration the steric repulsion between the equatorial carbonyl ligands and the methoxy moiety of the carbene ligand is reduced This however results in a reduced π-bonding interaction and an elongation of the M=C bond The balance of steric repulsion and the electronic interaction between the metal and carbene fragments thus determines whether the eclipsed or staggered configuration is favoured Increasing the steric bulk of the carbene substituents thus increases the stabilisation energy gained in adapting the staggered configuration The electronic interaction between the metal d-orbitals and the carbene p-orbital decreases however and the M=C bond becomes less sensitive to the electronic nature of the carbene substituents

Wang et al. recently carried out a study on four Fischer-type chromium complexes $(CO)_5Cr=C(OCH_3)C\equiv CPh$, $(CO)_5Cr=C(NH_2)Me$, $(CO)_5Cr=C(NH_2)Ph$ and $(CO)_5Cr=C(NMe_2)Ph$.[19] It was shown that the π-bond character of these Fischer-type carbene complexes is best represented by a Cr-C-X (where X = N, O) three-centred four–electron bond with the π-electron density mainly located at either the d*yz* orbital of chromium or the p_z orbital of the heteroatom 'X' in the carbene ligand (scheme 1 – 2).

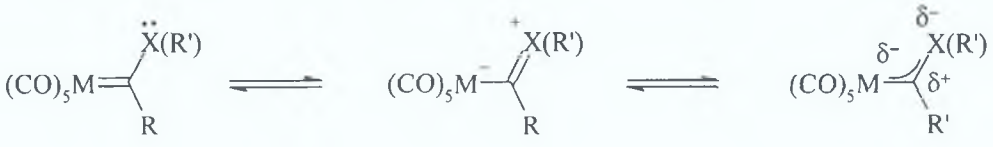

Scheme 1 - 2: A schematic representation of the hybrid resonance forms for a heteroatom stabilised Fischer carbene depicting possible π-bond delocalisation between M-$C_{carbene}$ and X-$C_{carbene}$ (X = N or O).

These studies also indicated that amino carbenes are poorer π-acceptors than alkoxy carbenes, and that each of these ligands are poorer π-acceptors than carbonyl ligands. The Cr-$C_{carbene}$ bond length is ~ 0.1 Å longer in amino carbenes than in alkoxy carbenes. A stronger π-bond therefore exists between the metal centre and the axial carbonyl ligand in amino carbenes.

The electronic structure and electronic spectral characterisation of a Fischer-type carbene complex is essential to understanding its photophysics and excited state chemistry. There have been a number of theoretical studies on Fischer type carbene complexes where the molecular orbital energies have been calculated. In all cases the molecular orbitals of the $(CO)_5M$ (M=Cr, W) fragment are correlated to the molecular orbitals of the carbene fragment. Fong and Cooper reported a simplified molecular orbital diagram for Fischer carbenes where they assumed C_{2v} local symmetry for the carbene moiety.[20] The pentacarbonyl fragment has C_{4v} symmetry, which results in a splitting of the d orbitals into b_2, e, a_1 and b_1 states. The important feature of the ordering of the occupied levels is that the b_2(d*yz*) level is the HOMO as it cannot form a π-bond with the carbene ligand, although it is still involved in π-bond interactions with the three CO ligands in the *yz*-plane. The b_1(d*xz*) orbital is stabilised by π-

accceptor interactions with the three CO ligands in the *xz*-plane and the carbene p_x orbital The $a_2(dxy)$ orbital does not overlap with the carbene ligand as it lies in an orthogonal plane with respect to the p_x orbital, however it lies lower in energy than both the $b_2(dyz)$ and $b_1(dxz)$ orbitals due to its π-accceptor interactions with the four CO ligands in the *xy*-plane (fig 1 – 2)

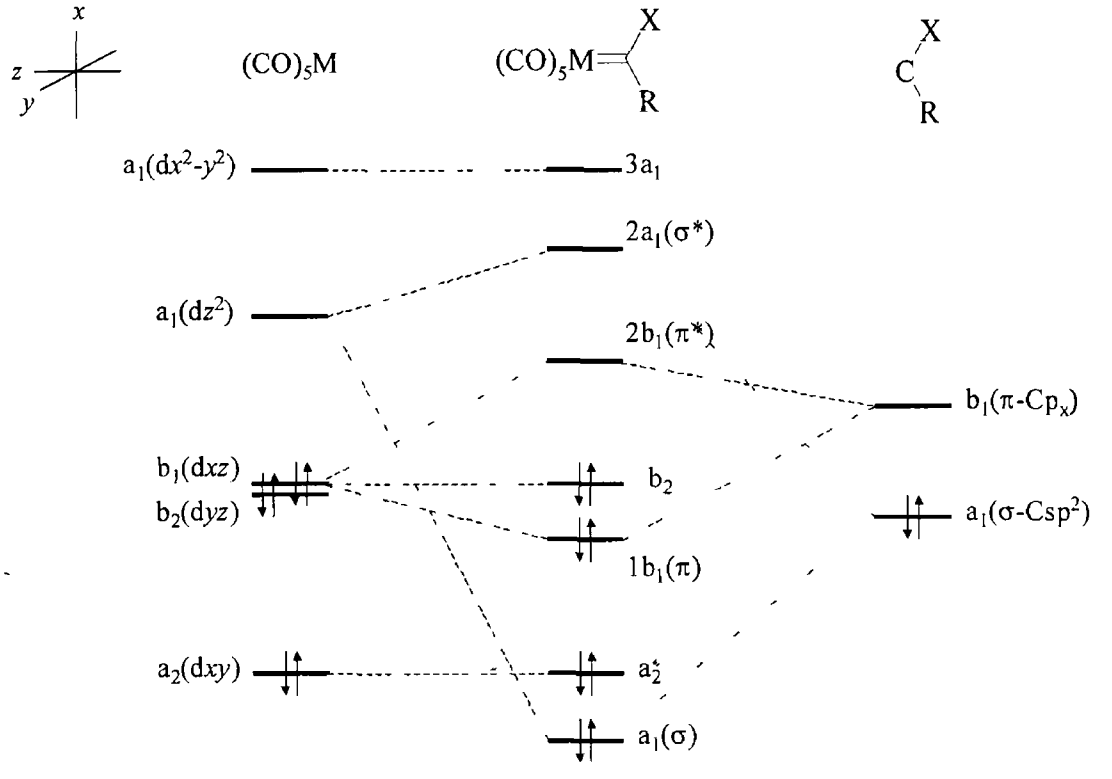

Fig 1 - 2 A schematic molecular orbital diagram for Fischer carbenes (M = Cr, Mo, W, X = OR, NR_2)

The LUMO is assigned to the $2b_1(\pi^*)$ orbital, which is primarily ligand $C(p_x)$ in character, as the lowest allowed absorption in these complexes shows strong MLCT characteristics According to the molecular orbital diagram the lowest energy MLCT band is assigned to the electronic transition $^1A_1(b_2^2) \rightarrow {}^1A_2(b_2{}^1 2b_1{}^1)$ The next two bands are assigned to the LF transitions $^1A_1(b_2^2) \rightarrow {}^1B_2(b_2{}^1 2a_1{}^1)$ and $^1A_1(b_2^2) \rightarrow {}^1B_2(b_2{}^1 3a_1{}^1)$, of increasing energy respectively

1.3 The electronic structure of ferrocene

The cyclopentadienyl (Cp) rings of ferrocene may be orientated in an eclipsed (D_{5h}) or staggered (D_{5d}) conformation. The energy of rotation about the Fe-Cp axis is very small (~ 4 $kJmol^{-1}$) and ground state structures of ferrocene may show either of these conformations. There is also very little difference in electronic states between the D_{5h} and D_{5d} symmetries. The bonding in ferrocene is best treated by the linear combination of atomic orbitals (LCAO) approximation. The primary orbital interactions that form the metal-ligand bonds in ferrocene occur between the Fe orbitals and the π-orbitals of the Cp ligand. If D_{5d} symmetry is assumed, so that there is a centre of symmetry in the ferrocene molecule through the Fe atom, there will be centro-symmetric (*g*) and anti-symmetric (*u*) combinations. The five p-orbitals on the planar Cp ligand, of D_{5h} symmetry, can be combined to produce five molecular orbitals (fig. 1 - 3).

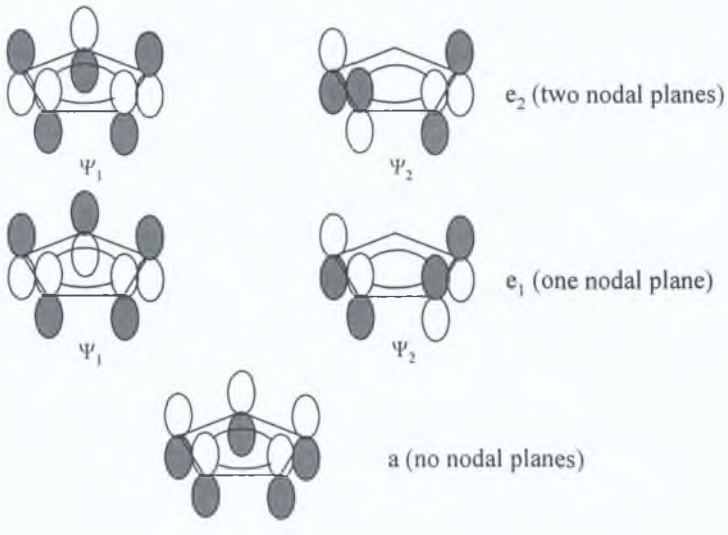

Fig. 1 - 3: The π-molecular orbitals of the cyclopentadienyl ligand (D_{5h})

One combination is fully symmetrical about the Cp ring (*a*) and there are two doubly degenerate combinations (e_1 and e_2) having one and two planar nodes at right angles to the plane of the ring. The relative energies of these orbitals increase as the number of nodes increases. The a_1 and e_1 orbitals are both fully occupied in the electronic configuration of the Cp ligand whereas the e_2 orbitals are anti-bonding and unfilled.

By combining the π-molecular orbitals of the two Cp ligands, the symmetry-adapted linear combination of molecular orbitals are formed, i e the sum and difference of the corresponding molecular orbitals on the Cp ligand are taken, i e (a - a), (a + a), ($e_1\psi_1$ - $e_1\psi_1$), ($e_1\psi_1$ + $e_1\psi_1$), ($e_1\psi_2$ - $e_1\psi_2$), ($e_1\psi_2$ + $e_1\psi_2$) etc This results in three sets of ligand molecular orbitals of gerade (*g*) and ungerade (*u*) symmetry with respect to the centre of inversion, a low lying filled pair of a_{1g} and a_{2u} symmetry, a filled pair of e_{1g} and e_{1u} symmetry and an unfilled anti-bonding pair of e_{2g} and e_{2u} symmetry By taking into account the symmetry and energy of these ligand molecular orbitals, the molecular orbital bonding picture of ferrocene can be constructed For example, ' a + a ' gives rise to a molecular orbital of a_{1g} symmetry This ligand orbital can in theory overlap with the Fe 4s and $3dz^2$ orbitals as they are also of a_{1g} symmetry (fig 1 – 4) This interaction gives rise to bonding and anti-bonding molecular orbitals of the complex a_{1g} and a_{1g}^* respectively Each combination of ligand molecular orbitals and metal molecular orbitals leads to a bonding molecular orbital [($\psi_{\text{ligand molecular orbital}}$)+($\psi_{\text{metal atomic orbital}}$)] and a corresponding anti-bonding molecular orbital [($\psi_{\text{ligand molecular orbital}}$)-($\psi_{\text{metal atomic orbital}}$)] providing that the energies of the two component sets are sufficiently close for overlap

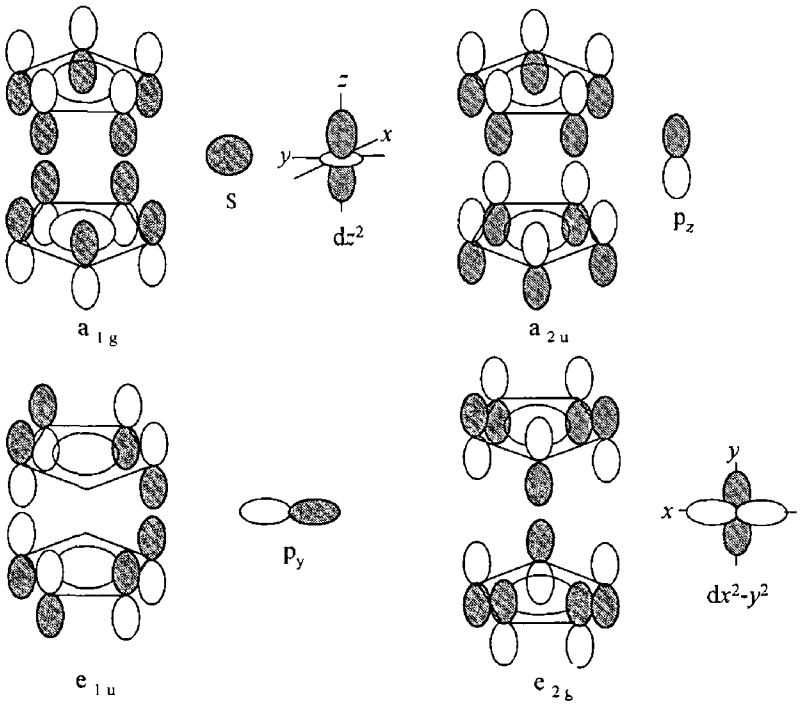

Fig 1 - 4 Examples of symmetry matching for the a_{1g} , a_{2u} , e_{1u} and e_{2g} ligand molecular orbitals with the Fe atomic orbitals

A molecular orbital diagram for ferrocene (D_{5d}) is shown in fig 1 – 5 Due to a difference in energies the a_{1g} molecular orbital is mainly ligand based with some Fe 4s and $3dz^2$ character Similarly, the a_{2u} level has very little Fe $4p_z$ character due to energy difference with the ligand a_{2u} molecular orbital with which it is formally able to combine The e_{1g} molecular orbital arises from the bonding combination of the ligand e_1 orbitals with the Fe 3d*xz* and 3d*yz* orbitals This is the only symmetry combination of orbitals in the two Cp rings that has appreciable overlap with the metal 3d orbitals to act as an efficient donor It is thus this interaction that is mainly responsible for the stability of the complex The corresponding anti-bonding orbitals, e_{1g}*, are unfilled in the ground state of ferrocene but they are involved in excited state transitions Again, the e_{1u} bonding molecular orbitals are mainly ligand based with some Fe $3p_x$ and $3p_y$ character The a_{1g}' molecular orbital is mainly Fe $3dz^2$ in character as the ligand a_{1g} molecular orbital points between the nodes of the metal dz^2 orbital resulting in little overlap The e_{2g} (dx^2-y^2, d*xy*) metal orbitals are considered non-bonding due to poor overlap with the ligand e_{2g} molecular orbitals

As each of the occupied molecular orbitals are symmetric about the axis of rotation no inherent barrier to internal rotation is predicted The very low values observed for this rotation (~ 4 $kJmol^{-1}$) may be attributed to van der Waals forces between the two Cp rings The attachment of additional groups or ligands destroys the D_{5d}/D_{5h} symmetry of ferrocene thus altering the molecular orbital diagram [21]

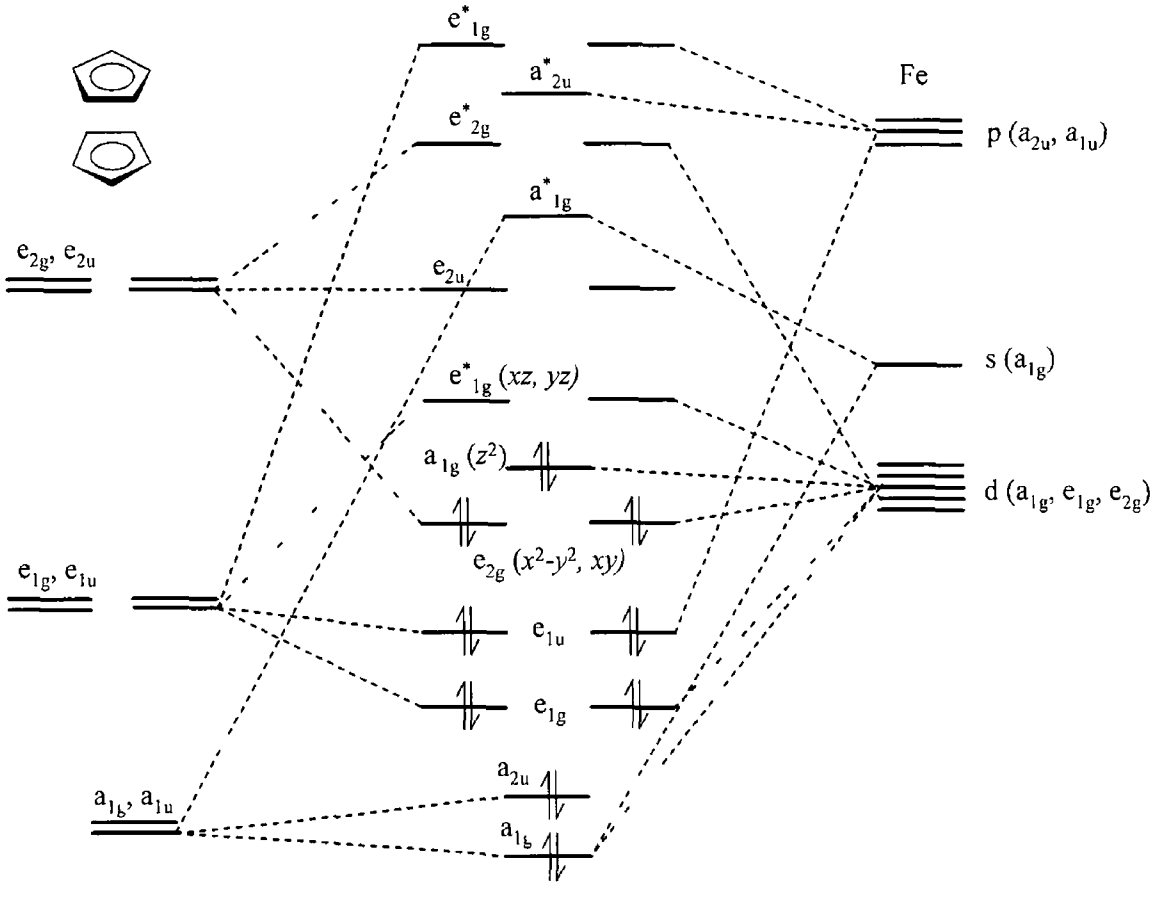

Fig 1 - 5 Molecular orbital diagram for ferrocene (D_{5d})

1 4 Photophysical properties of the porphyrin macrocycle

Porphyrins are intensely coloured materials with distinct absorption features The word '*porphyrin*' is actually derived from the Greek word '*porphura*' meaning purple Metalloporphyrins can be classed as either regular or irregular and, in terms of their absorption, into three categories normal, hypso and hyper Hypso absorption spectra are blue shifted with respect to normal porphyrins and hyper absorption spectra show prominent extra absorption bands in the region $\lambda > 320$ nm A regular porphyrin is one whose optical absorption and emission spectra are determined essentially by the π electrons of the porphyrin ring, with only minor perturbation from the electrons of the central metal ion substituent In irregular porphyrins there is extensive interaction between the π-electrons of the porphine ring and the electrons of the central metal ion and its ligands

The electronic absorption spectrum of a typical regular porphyrin such as zinc-tetraphenylpophyrin (ZnTPP) consists of several bands (closed shell metal ions cause weak perturbations to the porphine ring π-orbitals and their absorption spectra in general are of the regular type) Two weak transitions to the first excited state ($S_0 \rightarrow S_1$) occur in the region 500-600 nm and are commonly known as the 'Q' bands (Q – quasi allowed) The lowest-energy transition, sometimes called α, is attributed to the lowest singlet excited state and is denoted by Q(0,0) The higher-energy band, sometimes called β, at relatively constant energy separation from Q(0,0) is a higher vibrational mode and is denoted by Q(1,0) In the parent free base porphyrin the presence of an extra two hydrogens leads to a reduction of the overall porphyrin symmetry, from a D_{4h} to a D_{2h} point group As a consequence of this reduction in symmetry the Q(0,0) splits into $Q_x(0,0)$ and $Q_y(0,0)$ Each band has a vibronic overtone $Q_x(1,0)$ and $Q_y(1,0)$ thus resulting in four Q-bands overall A strong transition to the second excited state ($S_0 \rightarrow S_2$) known as the 'B' (strongly allowed) or 'Soret' band occurs in the region of 400 - 430 nm and is denoted by B(0,0) High resolution spectra in the vapour phase or at low temperature show another band at slightly higher energy, attributed to addition of one mode of vibrational excitation and is denoted by B(1,0) Internal conversion from S_2 to S_1 is rapid so fluorescence is only detected from S_1

Several other less intense bands labelled N, L and M occur at shorter wavelengths (N about 325 nm, M about 215 nm and L anywhere in between these bands) However, this discussion will be restricted to the Soret and Q-band absorption for porphyrins [22]

Theoretical analysis of the Soret and Q bands has shown that they arise from $\pi-\pi^*$ transitions and can be explained by considering the four frontier orbitals using Gouterman's four orbital model (fig 1 – 6) [23] This model describes the low-lying $\pi-\pi^*$ excited states of porphyrins in terms of the transitions between the two highest occupied molecular orbitals a_{2u} and a_{1u} (HOMO and HOMO-1) to the two degenerate lowest energy unoccupied molecular orbitals e_g (LUMOs) For a molecule with D_{4h} symmetry, the orbitals e_g are strictly degenerate whereas the a_{2u} and a_{1u} orbitals are non-degenerate The electronic configuration of a ground state porphyrin is $^1A_{1g}$ $(a_{1u}^2 a_{2u}^2)$ Accordingly, the lowest singlet excited configurations are $^1(a_{2u}^1 e_g^1)$ and $^1(a_{1u}^1 e_g^1)$ The degenerate nature of these singlet states causes strong configurational interaction between them The resulting resonance yields the relatively weak visible Q(0,0) band, in which the transition dipoles of the two configurations are deconstructive, and the intense Soret B(0,0) band, in which the transition dipoles of the two configurations are constructive The closer the energy of the configurations $^1(a_{2u}^1 e_g^1)$ and $^1(a_{1u}^1 e_g^1)$, the weaker the Q(0,0) band In free base porphyrins, the central protons lift the degeneracy of the e_g orbitals, causing the Q(0,0) bands of the metal complexes to split into $Q_x(0,0)$ and $Q_y(0,0)$ with each band having a vibronic overtone, $Q_x(1,0)$ and $Q_y(1,0)$

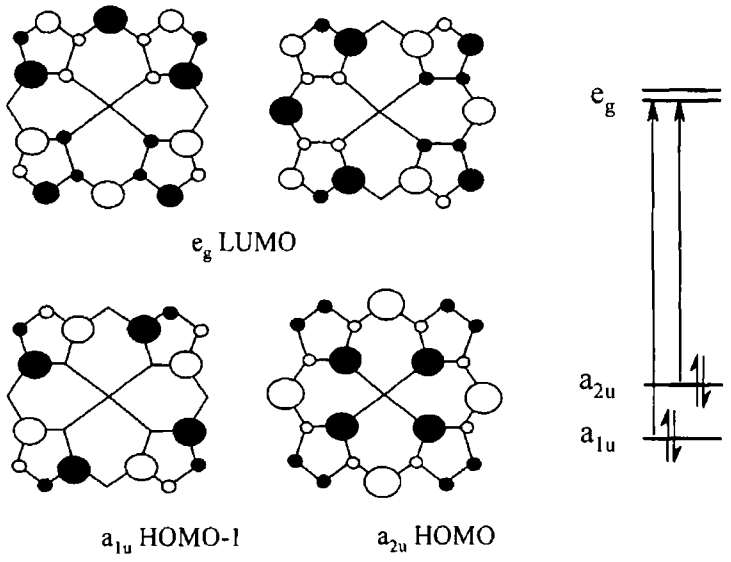

Fig 1 – 6 The four frontier orbitals of a regular metalloporphyrin The a_{1u} orbital has nodes at all four *meso* positions whereas the a_{2u} orbital has considerable charge at these sites

The a_{1u} orbital is not expected to be influenced by *meso*-substituents as it has nodes at the *meso*-carbons whereas the a_{2u} orbital has considerable electron density on the *meso*-carbons and is expected to be strongly influenced by *meso*-substituents In contrast, the a_{1u} orbital has a larger charge density at the β–carbons than the a_{2u} orbital and is thus more sensitive to pyrrole substitution on the porphine ring Also, the a_{1u} orbital has nodes through the nitrogens and cannot interact directly with the metal Less electronegative metals shift the a_{2u} orbitals to higher energy, whereas more electronegative metals stabilise a_{2u}

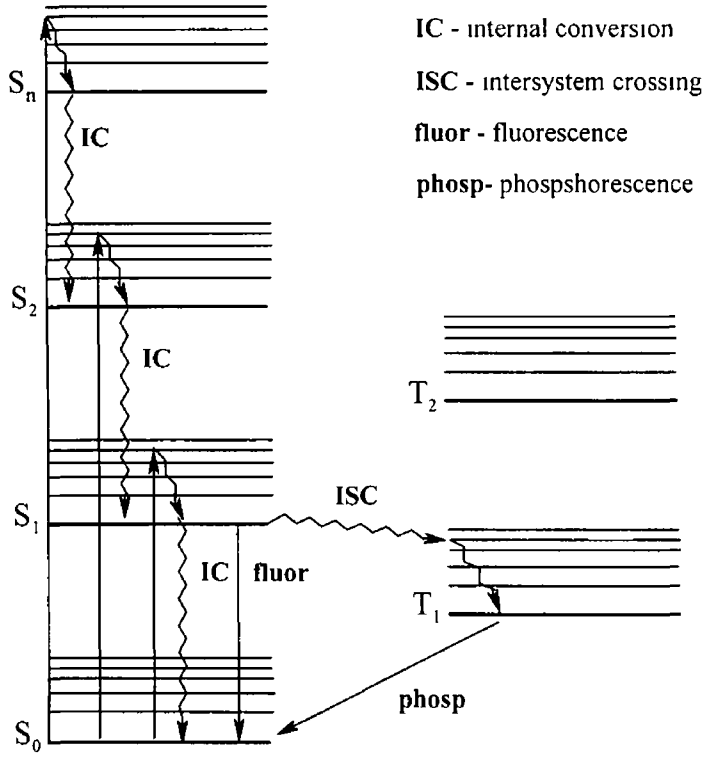

Fig 1 – 7 Jablonski diagram for a regular porphyrin

Excitation from the ground state S_0 to any of the upper singlet excited states S_n leads to rapid radiationless decay to the lowest excited singlet state S_1 within a few picoseconds or less From the S_1 excited state, the porphyrin molecule can emit radiation through fluorescence, non-radiatively decay to S_0 or undergo intersystem crossing to the lowest triplet state T_1 Fluorescence decay lifetimes are typically in the nanosecond range for regular porphyrins From the T_1 state, the porphyrin molecule can emit radiation through phosphorescence The triplet state of regular porphyrins are easily monitored in solution at room temperature through use of a flash photolysis set up, with lifetimes in the microsecond range

In free base and closed shell metalloporphyrins, possible transitions are confined to the delocalised π-system of the porphine ring The presence of open shell transition metal ions in the porphyrin core can lead to additional transitions MLCT (d-π*) transitions can occur between the highest occupied metal d orbital and the empty e_g on the porphyrin, LMCT (π-d) transitions can occur from the a_{1u} and a_{2u} orbitals of the porphyrin to the empty d orbitals on the metal Also, ligand field (d-d) transitions can occur via promotion of electrons within the metal d-orbital manifold

1 5 The technique of laser flash photolysis

The conventional technique of flash photolysis was developed by Porter and Norrish m the 1950's in order to observe short-lived intermediates present in photochemical processes [24] They subsequently received the Nobel Prize in 1967 for their pioneering work

The technique of flash photolysis involves the irradiation of a sample with an intense pulse of light within a very short time thereby producing a high concentration of excited state species or photoproducts within that time interval Pulsed monochromatic laser radiation is therefore ideal for this purpose The evolution of the system in time can be monitored by UV-vis absorption spectroscopy By observing the change in absorbance of the excited state species over time as it undergoes thermal relaxation to the parent compound, or another stable photoproduct, the rate of reaction can be calculated using first or second order kinetics This is assuming that thermal relaxation of the excited state does not occur within the lifetime of the laser pulse and that the absorption spectrum of the excited state species is sufficiently different from that of the parent compound for a change to be observed Identification of intermediates can be facilitated if their absorption spectra are characteristic and well resolved from the absorption spectra of the parent compound However, if a reactive intermediate possesses a low molar extinction coefficient it may not be detected

The structural information obtained upon laser flash photolysis of a particular system with UV-vis detection is minimal, however, it becomes a much more powerful technique when used m conjunction with time-resolved infra-red (TRIR) and time-resolved resonance Raman (TRrR) spectroscopy The absorption patterns observed in the carbonyl-stretching region of metal-carbonyl systems (1700 – 2200 cm^{-1}) are a direct indication of the symmetry/geometry of the molecule Kelly et al pioneered laser flash photolysis of group VI metal carbonyl systems with UV-vis detection [25] Fischer-carbenes, because of their high solubility in non-polar solvents and high molar extinction coefficients, are amenable to the technique of laser flash photolysis The first laser flash photolysis study of Fischer-carbene systems was carried out by McGarvey et al in 1988 on the catalytically important $(CO)_5W{=}C(OMe)Ph$ complex,[26] however, relatively few time resolved studies have been carried out since

1 6 Laser flash photolysis set up with UV-vis detection

A schematic diagram of the flash photolysis instrumentation used in this study is presented in Fig 1 - 8 The excitation source is a neodymium yttrium aluminium garnet (Nd YAG) laser which operates at a fundamental frequency of 1064 nm Nd atoms are implanted in the host YAG crystals of approximately one part per hundred The YAG host material has the advantage of having a relatively high thermal conductivity to remove wasted heat, thus allowing these crystals to be operated at high repetition rates of many pulses per second By use of non-linear optics, the fundamental frequency of 1064 nm can be frequency doubled, tripled or quadrupled to generate a second, third or fourth harmonic at 532, 355 and 266 nm respectively This allows certain photochemical processes within a system to be selected The power of the laser can also be amplified by varying the applied voltage across the amplifier flash tube At 355 nm the energy is typically 45 mJ per pulse The lifetime of the laser pulse is approximately 10 ns The laser pulse is directed via a Pellin-Broca prism through an optical trigger onto the sample cuvette The optical trigger prepares the transient digitiser (a Hewlett Packard HP 54510A oscilloscope) for detection of a transient species

Any changes induced in the sample are monitored by a 275 W Xenon arc lamp positioned at a right angle to the direction of the laser pulse The monitoring beam passes through the sample and is directed to the entrance slit of an applied photophysics f/3 4 monochromator via a circular lens UV-vis filters are employed between the Xenon arc lamp and the sample during the course of the experiment to avoid excessive photodegradation of the sample A Hamatsu five stage photomultiplier operating at 850 V is placed at the exit slit of the monochromator The absorbance changes are measured by an oscilloscope via a variable load transistor As mentioned above, the oscilloscope is activated by an optical trigger placed between the laser source and the sample cuvette The oscilloscope is interfaced to an Olivetti PCS 286 microcomputer via an IEEE bus cable All signals are stored on floppy disc

A general procedure describing sample preparation for laser flash photolysis experiments is given in appendix A1 A typical transient signal is obtained as follows The amount of monitoring light being transmitted through the sample solution before the laser flash, 'I_0', is initially recorded I_0 (mV) corresponds to the amount of light detected by the photomultiplier tube when the Xenon arc lamp shutter is open less the voltage generated by stray light, i e when the lamp shutter is closed When the Xenon arc lamp shutter is opened while simultaneously firing the laser, the laser pulse passes through the sample cuvette and the amount of monitoring light transmitted through is 'I_t' Since $A = \log (I_0/I_t)$, according to the Beer-Lambert law, the change in intensity of the monitoring beam transmitted through the sample is measured as a function of time and wavelength A typical trace therefore shows the change in absorbance/voltage with time, which corresponds to the time-resolved absorbance and may be analysed by first or second order kinetics

Transient absorption difference spectra are accumulated in a 'point by point' manner (typically every 10 nm) with consistent time-base and voltage settings Transient absorption difference spectra are very useful in showing the absorption maxima and minima of the transient species

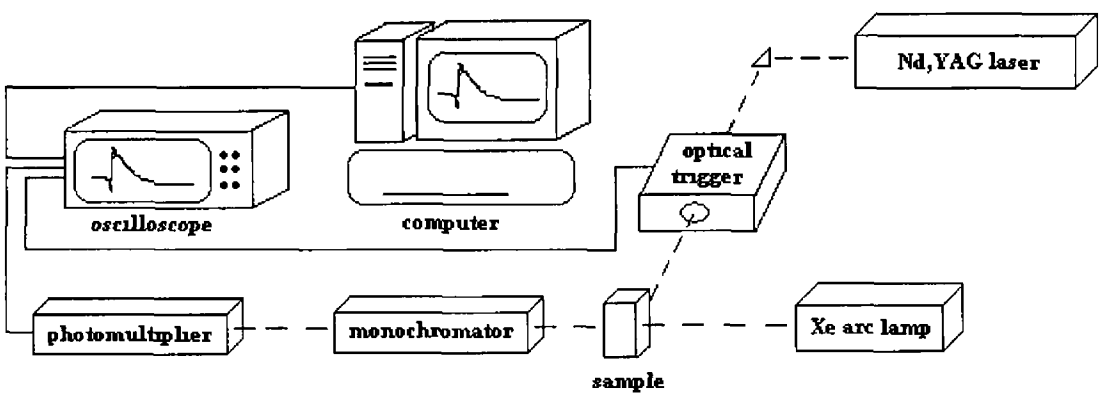

Fig 1 – 8 Laser flash photolysis set-up

1 7 Principles of nonlinear optics

When electromagnetic radiation of high intensity, e g laser, interacts with a non-linear optical material new electromagnetic fields may be generated Molecular dipoles in the material interact with the electromagnetic field of the incident light causing its phase, frequency, amplitude or polarisation to be altered The study of these interactions is known as non-linear optics (NLO) Materials able to manipulate photonic signals efficiently are of importance in technologies such as optical communication, optical computing, and dynamic image processing In general, progress in these areas would benefit from the availability of readily processed materials with sufficiently large NLO responses, thus extensive research efforts have been directed at synthesising more efficient photon manipulating materials

In linear optics, when the fluctuating electric field E of monochromatic radiation of frequency ω strikes a molecule it sets the electron cloud into oscillatory motion thus causing an instantaneous displacement of the electron density of the molecule In this distorted form the molecule is polarised, i e it undergoes a momentary charge displacement forming an induced electric dipole moment known as polarisation P, which oscillates at the fundamental frequency of the incident monochromatic radiation The magnitude of P depends on the strength of the perturbing electric field E and the ease with which E can distort the electron cloud of the molecule (eqn 1)

$$P = \alpha E\cos 2\pi\omega t \qquad \text{(eqn 1)}$$

The parameter 'α' is known as the polarisability of the molecule, a volumetric measure of the molecules' electron cloud displacement in the path of incident light, relative to the nuclear framework The polarisabihty α is closely related to the structure and bonding properties of the molecule and is always non-zero

If the incident light frequency ω is in a transparent region of the molecular spectrum, much of the light passes through the sample, but a small fraction ($\sim 10^{-3}$) is scattered in all directions Most of the scattered light emerges at the same frequency as the incident light and is known as Rayleigh scattering, as photons neither gain nor lose

energy in their collisions with the molecules A very small portion of these collisions ($\sim 10^{-6}$) are inelastic, and a net transfer of energy occurs giving rise to scattered light with modified frequencies These frequency changes are associated with transitions between vibrational levels (ω_k) of the system, i e $\omega \pm \omega_k$, and can give rise to Raman spectra of the system involved

In the case of bulk or macroscopic materials equation 1 takes a different form where χ is the linear susceptibility of a collection of molecules (eqn 2) The macroscopic susceptibilities are related to the corresponding molecular susceptibilities, or polarisabilities, by local field effects that take into account intermolecular interactions and molecular packing density

$$P = \chi E cos 2\pi\omega t \qquad \text{(eqn 2)}$$

The non-linear optical phenomenon arises from the breakdown of equation 1 at sufficiently intense electric fields, such as lasers As the applied field strengths increase, the polarisation response of the system is no longer linear Only after the advent of the laser could optical fields of sufficient intensity be produced to observe this effect The non-linear polarisation of the molecule, which is a function of the applied electric field, is now represented by a schematic power series expansion in the electric field

$$P_i = \mu_g + \alpha_{ij} E_j cos 2\pi\omega t + \beta_{ijk} E_j E_k cos^2 2\pi\omega t + \gamma_{ijkl} E_j E_k E_l cos^3 2\pi\omega t + \qquad \text{(eqn 3)}$$

where P_i is the i^{th} component of the polarisation, μ_g is the permanent ground-state dipole moment and the frequency dependent α_{ij}, β_{ijk} and γ_{ijkl} represent the linear, quadratic and cubic polarisabilities respectively (the subscripts i, j, k refer to the components expressed in a molecular frame) Accordingly, the macroscopic polarisation of a material is represented by a similar series expansion where P_0 is the static dipole of the material and $\chi^{(1)}$,$\chi^{(2)}$ and $\chi^{(3)}$ represent the linear, quadratic and cubic macroscopic susceptibilities respectively

$$P_I = P_0 + \chi^{(1)}_{IJ} E_J cos 2\pi\omega t + \chi^{(2)}_{IJK} E_J E_K cos^2 2\pi\omega t + \chi^{(3)}_{IJKL} E_J E_K E_L cos^3 2\pi\omega t + \qquad \text{(eqn 4)}$$

It should be noted that as the order of the molecular or macroscopic susceptibilities increases the non-linear effect becomes increasingly difficult to observe A variety of non-linear optical effects can occur through β and γ (or $\chi^{(2)}$ and $\chi^{(3)}$), however, in the following discussion we will refer to second-order effects only β can give rise to four different non-linear optical effects, they are second-harmonic generation (SHG, $\beta(-2\omega,\omega,\omega)$) also known as "three-wave mixing", the linear-electrooptic effect (LEOE, $\beta(-\omega,\omega,0)$), sum-frequency generation (SFG, $\beta(-\omega_1,-\omega_2,\omega_1,\omega_2)$) and optical rectification (OREC, $\beta(0,-\omega,-\omega)$) Experimentally SHG is of greatest interest and is most frequently measured therefore this discussion will be restricted to second-order effects

1.8 The molecular quadratic polarisability (β)

For centrosymmetric systems the effect of symmetrically related polarisations cancel each other out, therefore the expression for P cannot contain any even terms such as β or $\chi^{(2)}$. Most second-order NLO materials have therefore been composed of non-centrosymmetric one-dimensional charge-transfer molecules. Incorporation of achiral molecules, hydrogen bonding, ionic chromophores or steric hindrance into crystal matrices can enhance the chances of a non-centrosymmetric configuration. Typically molecules designed for SHG contain a conjugated π-electron system, asymmetrically substituted by electron donor and acceptor groups. Such systems, sometimes known as 'push-pull' or 'donor-π-acceptor' compounds, are characterised in solution by an intense absorption band in the UV-visible region that is associated with an intramolecular charge transfer (ICT) transition. It should also be noted that SHG requires phase matching where the waves of the fundamental frequency, ω, and of the doubled frequency, 2ω, should be in phase. With birefringent crystals, phase matching can be achieved for certain directions of the incident and generated waves as the refractive index is frequency dependent. The transfer of energy involved in SHG results from the perturbation of the electronic wavefunction of the molecule by the electric field of the photon which, for a very short time interval ($< 10^{-14}$s), becomes indistinguishable from the potential and kinetic energy of the perturbed electrons. It can be viewed in terms of the electric field of the incident radiation modifying the electronic ground state of the molecule. The original electronic ground state is no longer a quantum state for the molecule when it is perturbed by the electric field. The new quantum state can be described as a linear combination of the ground and excited states of the molecule in its unperturbed state. As the ground and excited states of the molecule have different electronic distributions within the molecule, mixing of these states results in a net charge redistribution or polarisation. Although the mixing introduces excited state character into the ground state, it does not result in a population of any excited state. The instantaneous formation of these polarised states has been sometimes referred to as virtual transitions where the molecule is regarded as having attained a higher energy non-stationary energy level, i.e. a virtual state, which returns to a lower energy stationary state by emitting a photon. These processes are simultaneous and cannot be separated in time.

These concepts are the basis of the quantum-mechanical 'sum-over-states' (SOS) perturbation theory for the description of the molecular polarisation Thus, the electronic states created by the perturbing field are treated as an infinite expansion over a complete set of unperturbed excited states and the components of the molecular first hyperpolarisability can be related exactly to all the excited states of the molecule [27] [28] [29] Oudar and Chemla simplified this approach by assuming that the NLO response is dominated by the quadratic hyperpolarisability tensor β_{ijk} that is one dimensional along the ICT axis thus restricting the superposition to one excited state The second-order response was taken to be the sum of two contributions, i e β_{add} and β_{ct}, where β_{add} is the additive portion, accounting for the interaction between the individual substituents and the conjugated π-network, and β_{ct} the contribution arising from the interaction of donor and acceptor moieties [30] [31] It was shown experimentally, however, that β_{ct} is responsible for a large proportion of the first hyperpolarisability, which was later confirmed theoretically by Zyss [32]

$$\beta \cong \beta_{CT} = \frac{3}{2\varepsilon_0\hbar^2}\frac{\omega_{gc}^2\left(\mu_{cc}-\mu_{gg}\right)\mu_{gc}^2}{\left[\left(\hbar\omega_{ge}\right)^2-\left(\hbar\omega\right)^2\right]\left[\left(\hbar\omega_{gc}\right)^2-\left(2\hbar\omega\right)^2\right]} \qquad \text{(eqn 5)}$$

$$= \beta_0\frac{\omega_{gc}^4}{\left[\left(\hbar\omega_{ge}\right)^2-\left(\hbar\omega\right)^2\right]\left[\left(\hbar\omega_{gc}\right)^2-\left(2\hbar\omega\right)^2\right]} \qquad \text{(eqn 6)}$$

$$\beta_0 = \frac{3\varepsilon_0^2\left(\mu_{ee}-\mu_{gg}\right)\mu_{ge}^2}{\left(\hbar\omega_{ge}\right)^2} \qquad \text{(eqn 7)}$$

According to Oudar and Chemla β can be expressed according to equation 5, where $\hbar\omega_{ge}$ is the energy difference between the ground and charge-transfer excited states, $\hbar\omega$ is the energy of the incident photon, $(\mu_{ee} - \mu_{gg})$ is the difference between the ground and excited sate dipole moments and μ_{ge} is the transition dipole moment between the ground and excited states Extrapolation to zero of equation 5 ($\hbar\omega$= 0 0 eV) allows estimation of the static first hyperpolarisability, β_0, which is used to compare the nonlinearity of different molecules

The two-level model therefore makes it possible to establish trends in the nonlinearity-molecular structure relationship in terms of relatively simple physical properties It is clear from equation 7 that the hyperpolarisability will be enhanced with decreasing ICT transition energy, increasing oscillator strengths for the ICT transition, increasing transition dipole moment and increasing change of dipole moment

It was shown by Marder using the two-state analysis of a four π-orbital system, i e single donor and acceptor orbitals linked via two bridge orbitals, that the optimum value for β is dependent on the coulombic energy difference between the donor and acceptor orbitals [33] It was found that the strongest donor-acceptor pair does not necessarily lead to the largest non-linearity and that the degree of bond-length-alternation, i e bridge length, and the importance of the donor and acceptor orbital interaction with those of the bridge must be considered

This two-level model holds quite well for many organic donor-π-acceptor type systems as it describes β in terms of an electronic charge transfer excitation between the ground and excited state, however, it fails for octopolar compounds, some organometallics and some recently developed unconventional chromophores

1 9 Electric Field Induced Second Harmonic Generation (EFISH)[34]

In a typical EFISH experiment, the molecule of interest is dissolved in an appropriate solvent and put into an optical cell The molecular dipoles are then aligned in solution using a high voltage dc pulse, which is provided by electrodes on opposite sides of the cell This serves to break the macroscopic centrosymmetry of the solution thus allowing measurement of its nonlinearity Molecules with a permanent dipole μ align with the dc field The EFISH experiment therefore gives a projection of the first hyperpolarisability vector along the dipole direction, i e the net second-order effect observed is the product $\mu\beta_{vec}$ where μ is the dipole moment of the molecule and β_{vec} is the vectorial component of the first hyperpolarisability For dipolar molecules, which obey the two-level model, β_{vec} is usually dominated by the first hyperpolarisability along the charge transfer axis (β_{CT})

1 10 Bibliography

[1] T J Kealy, P L Pauson, *Nature* **1951**, 168, 1039

[2] (a) G Wilkinson, M Rosenblum, M C Whiting, R B Woodward, *J Amer Chem Soc* **1952**, 74, 2125 (b) E O Fischer, W Pfab, *Naturforsch Teil* B **1952**, 7, 372

[3] H B Tatistcheff, L F Hancock, M S Wrightonm, *J Phys Chem* **1995**, 99, 7689

[4] M L Mutch, J S Wilkes, *Proc Electrochemical Soc* **1998**, 98, 254

[5] M Zora, B Yucel, N B Peynircioglu, *J Organomet Chem* **2002**, 656, 11

[6] M Malaun, R Kowallick, A M McDonagh, M Marcaccio, R L Paul, I Asselberghs, K Clays, A Persoons, B Bildstein, C Fiorini, J-M Nunzi, M D Ward, J A McCleverty, *J Chem Soc , Dalton Tran* **1991**, 3025

[7] (a) K H Dotz, *Angew Chem Int Ed Engl* **1984**, 23, 587 (b) W D Wulff, '*Metal-Carbene Cycloadditions*' in '*Comprehensive Organic Synthesis*', Wiley-Interscience New York, **1988** (c) L S Hegedus, '*Transition Metals in the Synthesis of Complex Organic Molecules*', **1994**, University Science Books (d) M Doyle in '*Comprehensive Organometallic Chemistry II*', E W Abel, F G Stone, G Wilkinson, Eds , Pergamon Press Oxford, **1995**, Vol 12, 387 (e) W D Wulff in '*Comprehensive Organometallic Chemistry II*', E W Abel, F G Stone, G Wilkinson, Eds , Pergamon Press Oxford, **1995**, Vol 12, 469 (f) L S Hegedus in '*Comprehensive Organometallic Chemistry II*', E W Abel, F G Stone, G Wilkinson, Eds , Pergamon Press Oxford, **1995**, Vol 12, 549 (g) D F Harvey, D M Sigano, *Chem Rev* **1996**, 96, 271 (h) L S Hegedus, *Tetrahedron* **1997**, 53 (12), 4105 (i) F Zaragoza-Dorwald, '*Metal Carbenes in Organic Synthesis*', **1999**, Wiley-VCH

[8] (a) H Fischer, F Leroux, G Roth, R Stumpf, *Organometallics* **1996**, 15, 3723 (b) G Roth, H Fischer, T Meyer-Friedrichsen, J Heck, S Houbrechts, A Persoons, *Organometallics* **1998**, 17, 1511 (c) E Licandro, S Maiorana, A Papagni, P Hellier, L Capella, A Persoons, S Houbrechts, *J Organomet Chem* **1999**, 583, 111 (d) K N Jayaprakash, C R Paresh, I Matsuoka, M M Bhadbhade, V G Puranik, P K Das, H Nishira, A Sarkar, *Organometallics* **1999**, 18, 3851-3858 (e) O Briel, A Fehn, W Beck, *J Organomet Chem* **1999**, 578, 247

[9] K O Doyle, M L Gallagher, M T Pryce, A D Rooney, *J Organomet Chem* **2001**, 617-618, 269

[10] (a) J A Connor, J P Lloyd, *J Chem Soc Dalton Trans* **1972**, 1470 (b) J A Connor, J P Lloyd, *J Chem Soc Perkin Trans* I **1973**, 17 (c) K H Dotz, R Dietz, D Neugebauer, *Chem Ber* **1979**, 112, 1486 (d) J Barluenga, A Fernandez-Acebes, A A Trabanco, J Florez, *J Amer Chem Soc* **1997**, 119, 7591 (e) M Zora, E U Gungor, *Tetrahedron Lett* **2001**, 42, 4733

[11] E O Fischer, A Maasbol, *Angew Chem* **1964**, 76, 645

[12] (a) R R Schrock, *J Amer Chem Soc* **1975**, 97, 6578 (b) R R Schrock, *Acc Chem Res* **1979**, 12, 98

[13] T E Taylor, M B Hall, *J Amer Chem Soc* **1984**, 106, 1576

[14] S F Vyboishchikov, G Frenking, *Chem Eur J* **1998**, 4 (8), 1428

[15] T F Block, R F Fenske, *J Organomet Chem* **1977**, 139, 235

[16] T F Block, R F Fenske,C P Casey, *J Amer Chem Soc* **1976**, 98, 441

[17] H Nakatsuji, J Ushio, S Han, T Yonezawa, *J Amer Chem Soc* **1983**, 105, 426

[18] H Jacobsen, T Ziegler, *Organometallics* **1995**, 14, 224

[19] C C Wang, Y Wang, H J Liu, K J Liu, L K Chou, K S Chan, *J Phys Chem* A **1997**, 101, 8887

[20] L K Fong, N J Cooper, *J Amer Chem Soc* **1984**, 106, 2595

[21] (a) S Barlow, H E Bunting, C Ringham, J C Green, G U Bublitz, S G Boxer, J W Perry, S R Marder, *J Amer Chem Soc* **1999**, 121, 3715 (b) J C Calabrese, L T Cheng, J C Green, S R Marder, W Tam, *J Amer Chem Soc* **1991**, 113, 7227 (c) D R Kanis, M A Ratner, T J Marks, *Chem Rev* **1994**, 94, 195

[22] For a more detailed discussion of porphyrin electronic structure see (a) E J Baerends, G Ricciardi, A Rosa, S J A van Gisbergen, *Coord Chem Rev* **2002**, 230, 5 (b) A Ghosh in *The Porphyrin Handbook*, eds K M Kadish, K M Smith, R Guilard, Academic Press Boston, 2000, Vol 7, ch 47 (c) C Lecomte, M -M Rohmer, M Benard in *The Porphyrin Handbook*, eds K M Kadish, K M Smith, R Guilard, Academic Press Boston, 2000, Vol 7, ch 48

[23] P J Spellane, M Gouterman, A Antipas, S Kim, Y C Liu, *Inorg Chem* **1980**, 19, 386

[24] R G W Norrish, G Porter, *Nature* (London) **1949**, 164, 658.

[25] (a) J M Kelly, D V Bent, E Koerner von Gustorf, *J Chem Soc , Chem Commun* **1973**,105 (b) J M Kelly, D V Bent, H Hermann, D Schultefrohlinde,

E Koerner von Gustorf, *J Organomet Chem* **1974**, 69, 259 (c) R Bonneau, J M Kelly, *J Am Chem Soc* **1980**, 102, 1220

[26] S E J Bell, K C Gordon, J J McGarvey, *J Amer Chem Soc* **1988**, 110, 3107

[27] J L Oudar, D S Chemla, *Opt Comm* **1975**, 13, 164

[28] J L Oudar, H LePerson, *Opt Comm* **1975**, 15, 258

[29] J L Oudar, D S Chemla, J Jerphagnon, *J Phys Rev B* **1975**, 12, 4534

[30] J L Oudar, D S Chemla, *J Chem Phys* **1977**, 66, 2664

[31] J L Oudar, *J Chem Phys* **1977**, 67, 446

[32] J Zyss, *J Chem Phys* **1979**, 71, 909

[33] S R Marder, D N Beratan, L -T Cheng, *Science* **1991**, 252, 103

[34] For a recent overview of experimental techniques used to measure optical nonlinearites see C E Powell, M G Humphrey, *Coord Chem Rev* **2004**, 248, 725

Chapter 2

A Steady State and Laser Flash Photolysis Study of Ferrocenyl Fischer Carbene Complexes

2 1 Aims and objectives

Synthesis of the new organometallic bis-carbene ferrocenyl complexes, 1,1'-$[(CO)_5M{=}C(OMe)]_2$-Fc (M = Cr, W) is reported The aim of this chapter is to investigate the photochemistry of these new complexes as well as their mono-carbene analogues, $(CO)_5M{=}C(OMe)Fc$ (M = Cr, W), by the techniques of steady state and laser flash photolysis The electronic interaction between the ferrocenyl and Fischer-carbene moieties is also investigated by crystallographic, solvatochromic and electrochemical methods The nonlinear optical response of the complexes $(CO)_5Cr{=}C(OMe)Fc$ and 1,1'-$[(CO)_5Cr{=}C(OMe)]_2$-Fc is investigated by the electric field induced second harmonic generation (EFISHG) technique

2 2 Literature Survey

2 2 1 Photoinduced CO loss from Fischer carbene complexes and their applications in organic synthesis

Photoinduced CO loss by a group VI carbene complex was first reported by Ofele and Herberhold in 1970 when the bis-amino complex $(CO)_5Cr$=C(1,3-dimethyl-4-imidazolin-2-ylidene) was irradiated in boiling THF The only photoproduct observed was the bis-carbene complex *cis*-di(1,3-dimethyl-4-imidazolin-2-ylidene)$Cr(CO)_4$, albeit in low yields [1] Due to the fact that this reaction was carried out in boiling THF, CO loss cannot be unambiguously attributed to a photochemical process, as CO loss is a well known thermal process for group VI metal carbonyls Fischer et al later reported the synthesis of *cis*- and *trans*-tetracarbonyl carbene complexes upon irradiation of a variety of group VI methoxy-carbene complexes in the presence of various phosphines as trapping ligands at room temperature [2] Low temperature photolysis studies showed the formation of the *cis* isomer to be the most favoured Photoinduced CO loss was also observed by Casey et al who reported photoinduced exchange of ^{12}CO by ^{13}CO in the complexes, $(CO)_5W$=CPh_2 and $(CO)_5W$=C(OMe)Ph [3] The same group later reported the preparation of a tetracarbonyl tungsten-carbene-alkene chelated complex by photoinduced CO loss (rxn 2 – 1) [4]

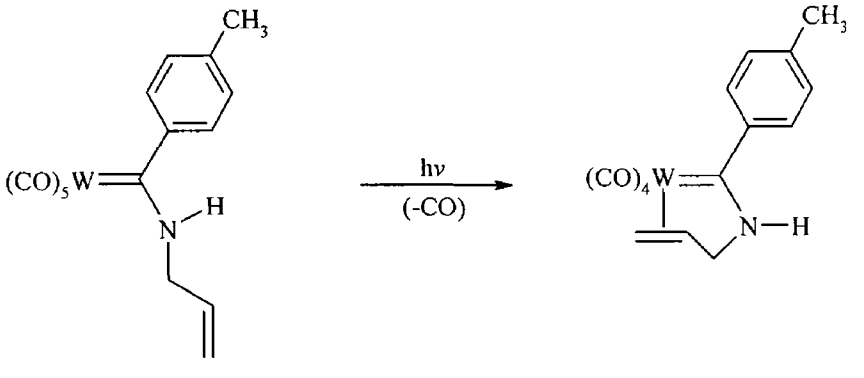

Rxn 2 - 1

This was the first reported case of a stable metal-carbene-alkene complex and was early evidence that these complexes as well as metallacyclobutanes could be key intermediates in metal catalysed reactions such as olefin metathesis,[5] cyclopropanation[6] and benzannulation [7]

In contrast to these results, independent studies by Dahlgren and Zink, and Rausch indicated photoinduced carbene replacement to be the primary photochemical process of the complexes $(CO)_5W{=}C(OMe)R$ (R=Me,Ph) and $(CO)_5W{=}CPh_2$.[5, 8] Foley et al. have shown that ultraviolet irradiation of $(CO)_5W{=}C(OMe)Ph$ yielded solely CO loss, thereby contradicting the observations made by Dahlgren for the same complex.[9]

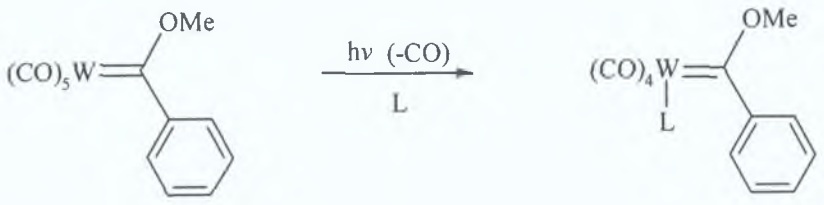

hν = 313, 366 or 436 nm

L = CH_3CN, THF, Et_2O, Ph—≡—Ph, Ph—≡—Me, Me—≡—Me, Ph—≡—H, H—≡—H

Rxn. 2 - 2

Quantum yields following irradiation at either 366 or 315 nm were unusually low (~ 0.01) for photoinduced CO dissociation. These values dropped to virtually zero when irradiation was directed into the W=C metal-to-ligand charge transfer (MLCT) band at 436 nm. These results indicate efficient intersystem crossing from the initially populated LF state to the low lying MLCT state.

The 352 nm absorption band of $(CO)_5W{=}C(OMe)Ph$ is assigned to the high-energy LF transition corresponding to the one-electron transition $^1A(b_2^2) \rightarrow {}^1B_2(b_2{}^1 3a_1{}^1)$, assuming local C_{2v} symmetry for the carbene moiety.[10] This transition populates the tungsten $dx^2\text{-}y^2$ valence orbital resulting in labilisation of an equatorial M-CO bond, which leads directly to loss of a *cis*-CO ligand. Population of the low-energy LF excited state of $(CO)_5W{=}C(OMe)Ph$ by the transition $^1A(b_2^2) \rightarrow {}^1B_2(b_2{}^1 2a_1{}^1)$ also results in *cis*-CO loss. This transition corresponds to population of the tungsten dz^2 orbital, which theoretically should result in labilisation of an axial W-CO bond, and therefore *trans*-CO loss (the same transition can sometimes lead to loss of the carbene ligand in chromium carbene complexes due to a weaker $Cr\text{-}C_{carbene}$ bond[11]). Since population of the low-energy LF excited state also leads to the formation of *cis*-$(CO)_4W{=}C(OMe)Ph$ within the laser pulse lifetime, Casey et. al proposed that an

axial CO ligand initially dissociates in the primary photochemical process but fast *trans-cis* interconversion of the vacant site occurs within a few nanoseconds of photoinduced CO loss Fluxional exchange of CO ligands has since been observed in ^{13}C-NMR studies of an unsaturated Fischer carbene complex [12]

The alkyne-carbene complexes synthesised by Foley et al [9] have considerable metallacyclobutene character, however, due to their instability in solution at ambient temperatures their exact structure could not be confirmed (scheme 2 – 1) These complexes decompose at room temperature via the proposed metallacyclobutene intermediate to give products that depend markedly upon the steric nature of the alkyne

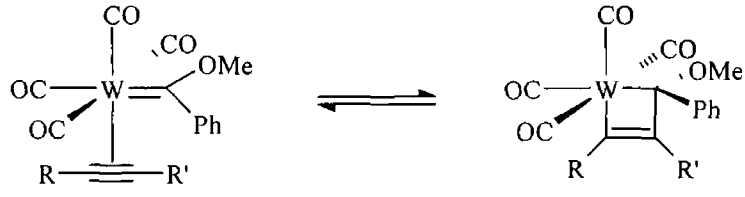

Scheme 2 - 1

The metal-carbene-alkyne adducts of diphenylacetylene and methylphenylacetylene decompose by a mechanism first proposed by Dotz et al to form indenyl ethers and naphthol derivatives (scheme 2 – 2) [7] The process is initiated, thermally or photochemically, by the dissociation of CO from complex I to produce the coordinatively unsaturated carbene complex II [13] Intermediate II is trapped by the alkyne present in solution, which binds the metal in such a way that the bulkier substituent R_L is placed parallel to the axial CO ligand to avoid unfavourable steric interactions with the carbene ligand in complex III [14] This steric effect is ultimately responsible for the regiochemistry observed in the final products The alkyne then undergoes insertion into the metal-carbon double bond to afford the η^3-metallatrienes *E*-IV and *Z*-IV Only the *E*-isomer undergoes cyclisation with the double bond giving rise to the indene (VII) and naphtol (X) products The *Z*-isomer undergoes CO insertion and reductive elimination to form the furan derivative V [15] Dotz and co-workers have shown that $(CO)_5Cr{=}C(OMe)Ph$ gives solely naphthol derivatives as opposed to the indene derivative which is predominantly formed by the tungsten analogue [7(a)] One explanation for this is that the tungsten complex is less likely to

undergo CO insertion due to the greater W-CO bond strength (178 kJmol^{-1}) compared to that of the Cr-CO bond (108 kJmol ^{1})

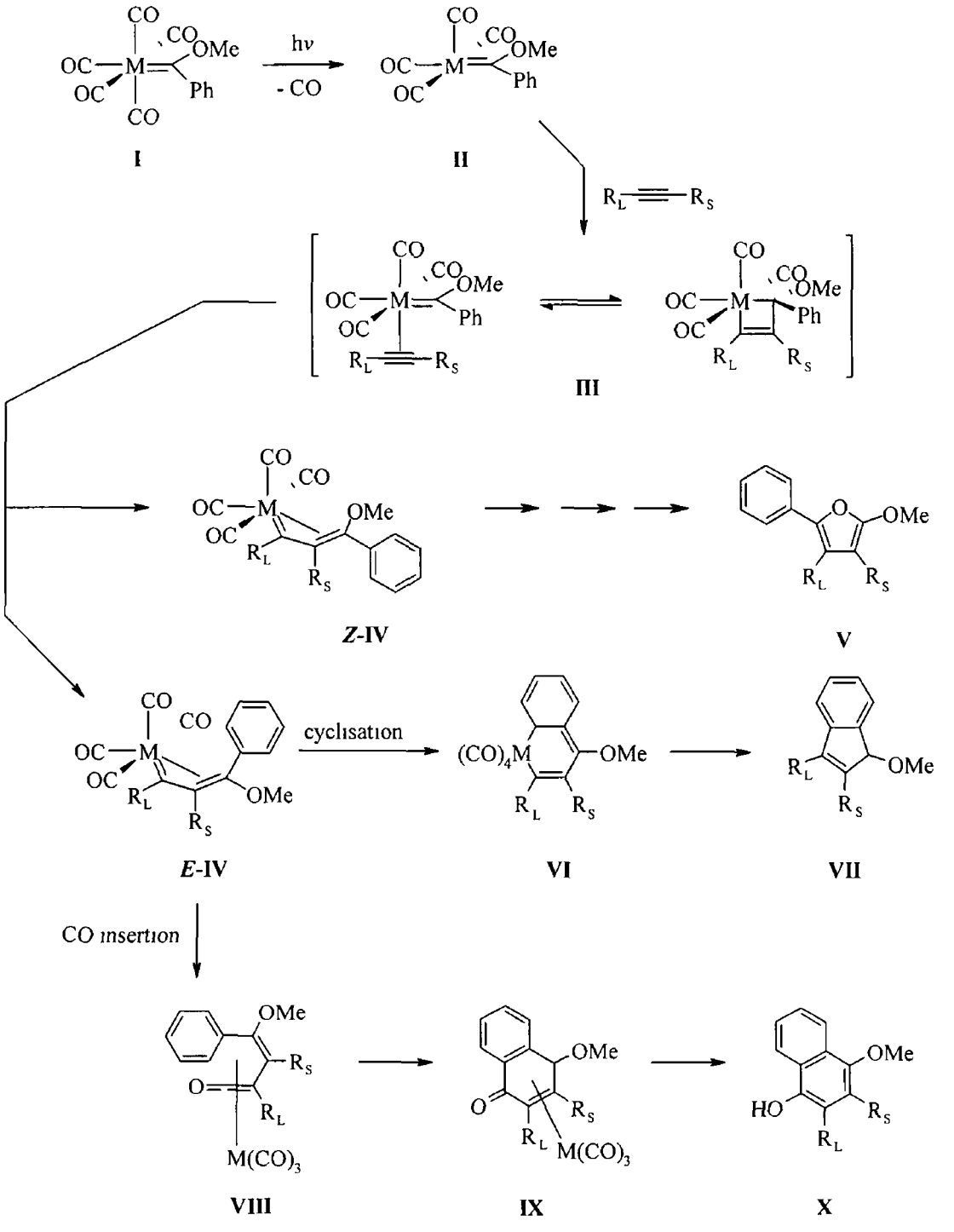

Scheme 2 - 2 The Dotz benzannulation reaction

Terminal alkynes, phenylacetylene and *n*-butylacetylene, both result in the production of polyacetylenes [9] Katz proposed that these metal-carbene-alkyne complexes undergo reaction as shown m scheme 2 – 3 [16]

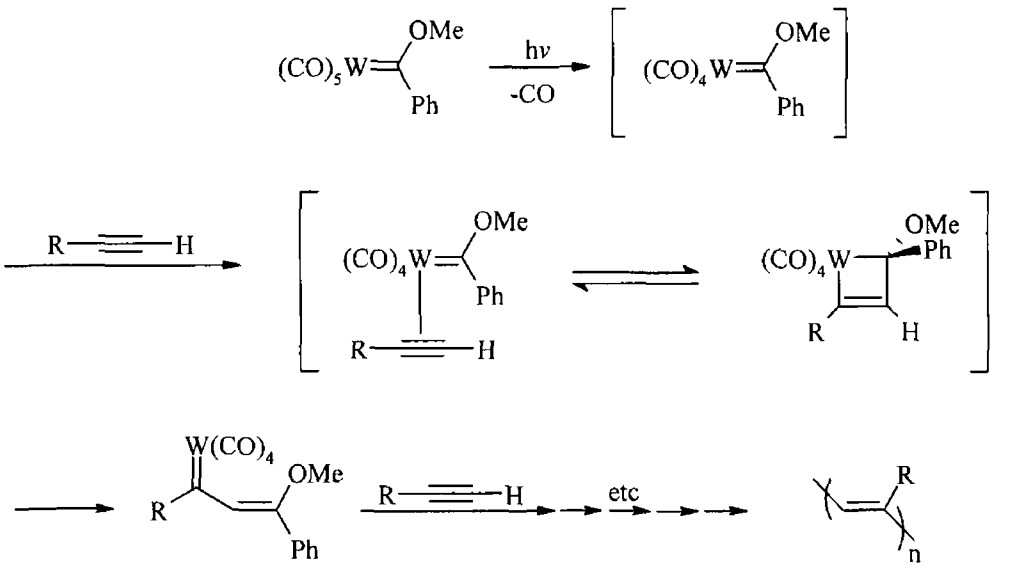

Scheme 2 – 3

Polyacetylene formation from terminal alkynes and indene/naphtol formation from internal alkynes suggests that there is some steric control involved in the reaction mechanism with increased steric hinderance favouring production of indenes and naphtols Dimethylacetylene was shown to have mixed reactivity supporting the latter proposal (rxn 2 – 3) [9]

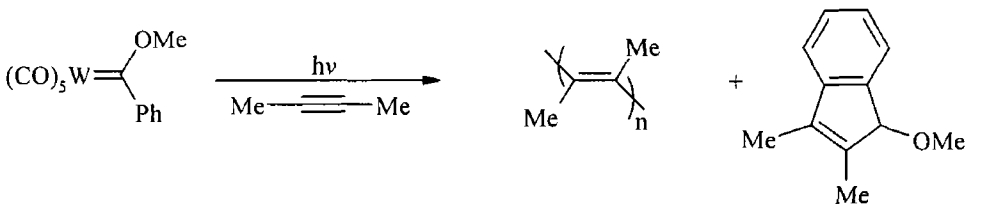

Rxn 2 – 3

Rausch and co-workers reported that photoinduced decomposition of $(CO)_5W{=}CPh_2$ was not inhibited in a CO atmosphere [8] This suggests that a process not involving CO loss is occurring upon photolysis Casey however discovered that exchange of ^{12}CO for ^{13}CO in $(CO)_5W{=}CPh_2$ could be initiated photochemically [3] Foley et al concluded

that the thermal instability of $(CO)_5W{=}CPh_2$ in solution at room temperature prohibited definitive conclusions to be made regarding the photochemistry of these types of Fischer-carbene complexes [9] Fong and Cooper's results confirm that CO loss is the primary photochemical process of the same complex [10] They also observed photoinduced metathesis upon population of the high-energy LF state of $(CO)_5W{=}CPh_2$ (scheme 2 – 4) This electronic transition $[^1A_1(b_2^2)\rightarrow{}^1B_2(b_2{}^1 3a_1{}^1)]$ populates the dx^2-y^2 metal orbital, which is anti-bonding with respect to an equatorial CO ligand thus allowing direct access to the *cis*-alkene/alkyne complex required for metallacyclobutane formation Irradiation of the MLCT band of $(CO)_5W{=}CPh_2$ at 485 nm did not result in metathesis, however, this is consistent with the authors' theory that carbonyl dissociation is a function of ligand field excitation, and that CO dissociation is the primary photochemical process involved in photochemically induced metathesis

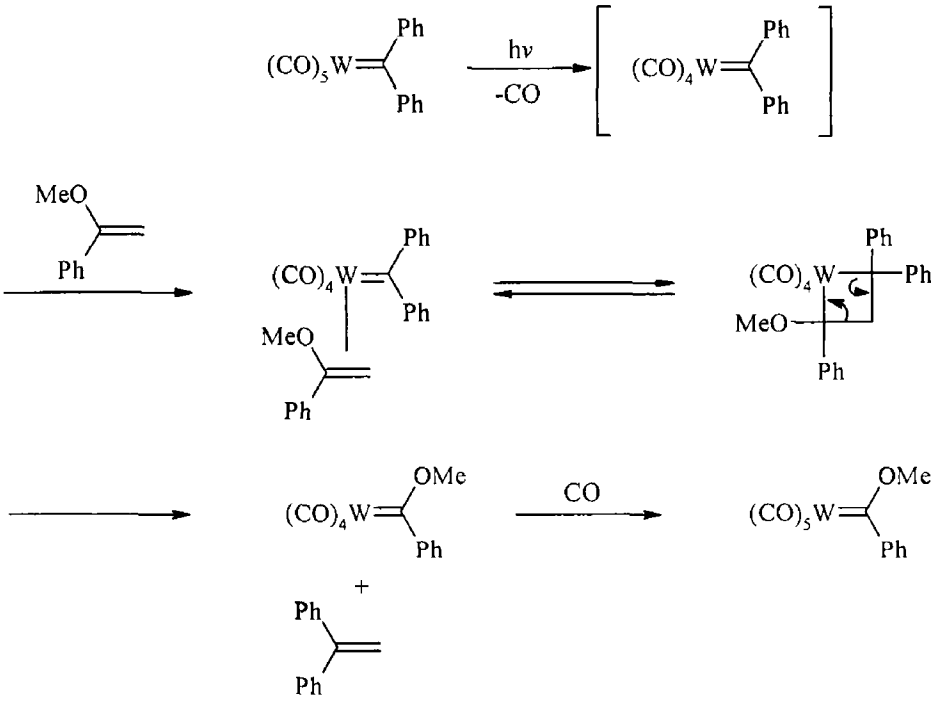

Scheme 2 - 4

The cyclopropanation of alkenes with Fischer-carbenes under thermal conditions is also a well known reaction Olefin metathesis and cyclopropanation only occurs when the carbene and alkene moieties are coplanar when forming the metallacyclobutane intermediate (whether metathesis or cyclopropanation occurs is dependent on the

electronic nature of the alkene and of the metal-carbene involved) Casey confirmed the intermediacy of a metallacyclobutane in cyclopropane formation, and CO loss as the primary photochemical process in its formation [6] A chelated tungsten-carbene-alkene complex was isolated after photoinduced CO loss and a cyclopropane product was formed on continued photolysis of the isolated species (scheme 2 – 5)

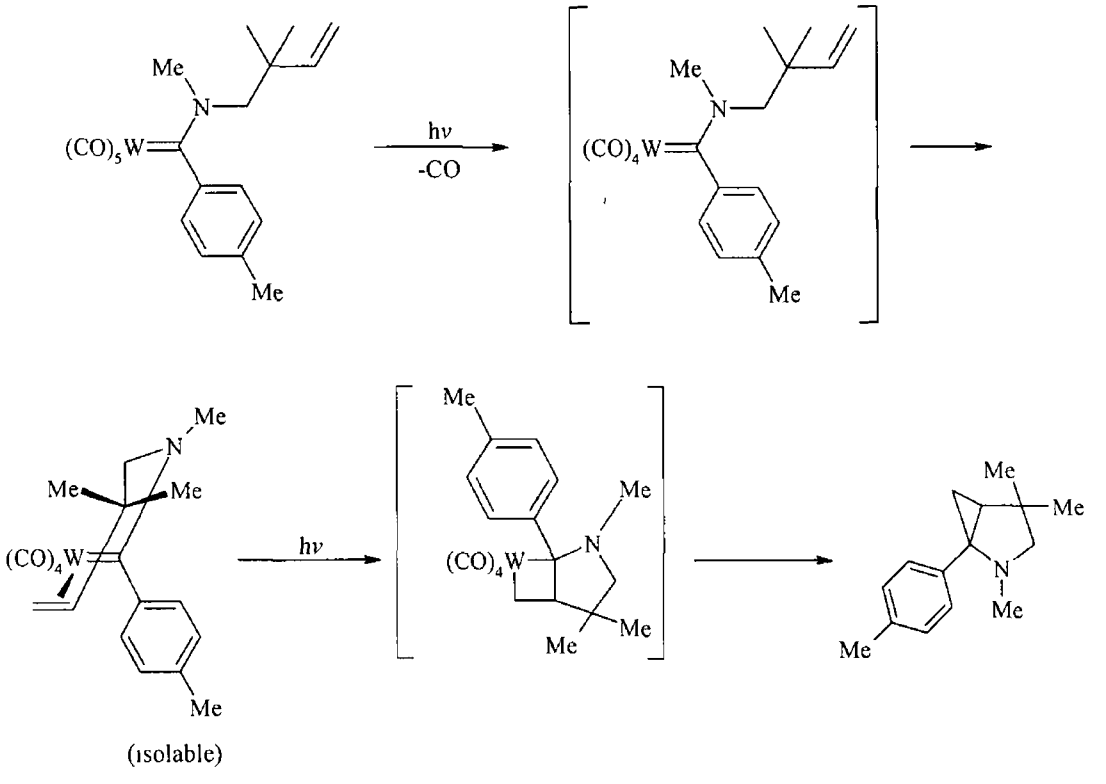

Scheme 2 - 5

Irradiation of the isolated species (shown in scheme 2 – 5) into its MLCT band is thought to decrease the bond order of the W-$C_{carbene}$ and the $C_{carbene}$-N bonds thus increasing the conformational mobility required for metallacyclobutane formation No olefin metathesis products were observed as they would have required the concurrent formation of the unstable $(CO)_5W{=}CH_2$ complex, which is unfavoured By placing a methoxy group on the alkene moiety of a similar catalyst, it has been shown that metathesis can also occur, under certain conditions, with concurrent formation of the relatively stable $(CO)_5W{=}C(OMe)H$ complex [17]

The *cis*- and *trans*-tetracarbonyl-tungsten-carbene-alkene complexes shown in scheme 2 – 6 were generated by LF photolysis of their pentacarbonyl precursors at – 78^{0}C

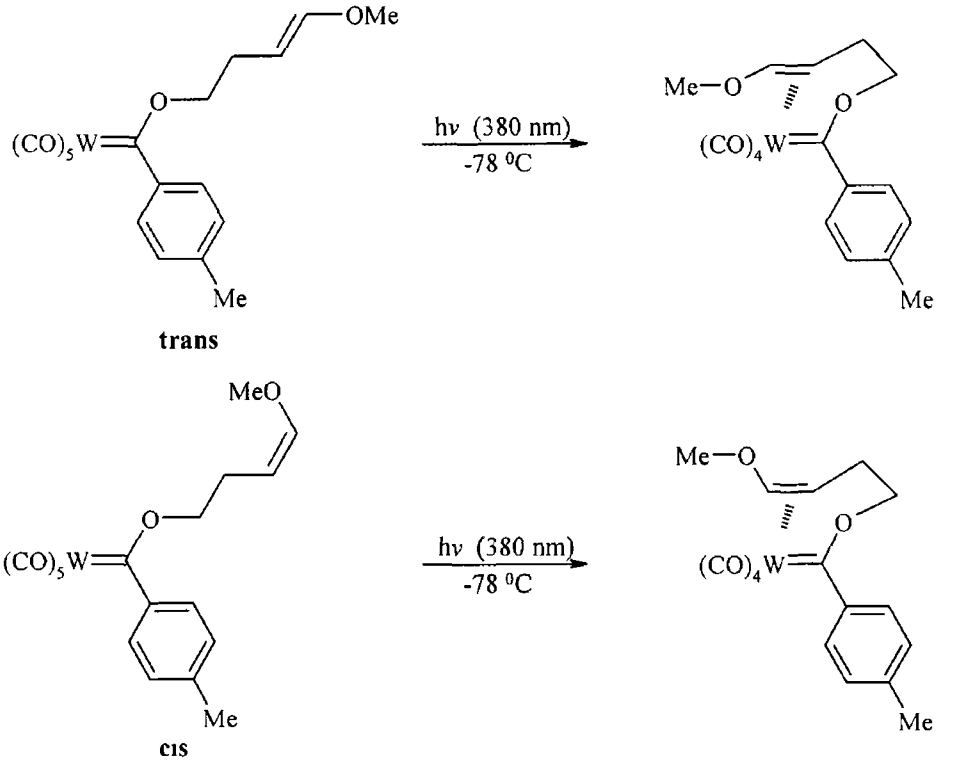

Scheme 2 - 6

The thermal decomposition of either the *cis*- or *trans*-carbene in benzene leads to the non-stereospecific formation of *exo*- and *endo*-cyclopropanes aswell as the olefin metathesis product 5-(methylphenyl)-2,3-dihydrofuran It is proposed that cyclisation of the tungsten-carbene-alkene complex to a metallacyclobutane occurs followed by fragmentation to either cyclopropane or to a new tungsten-carbene-alkene complex in which the dihydrofuran is complexed to the heteroatom stabilised carbene (scheme 2 – 7)

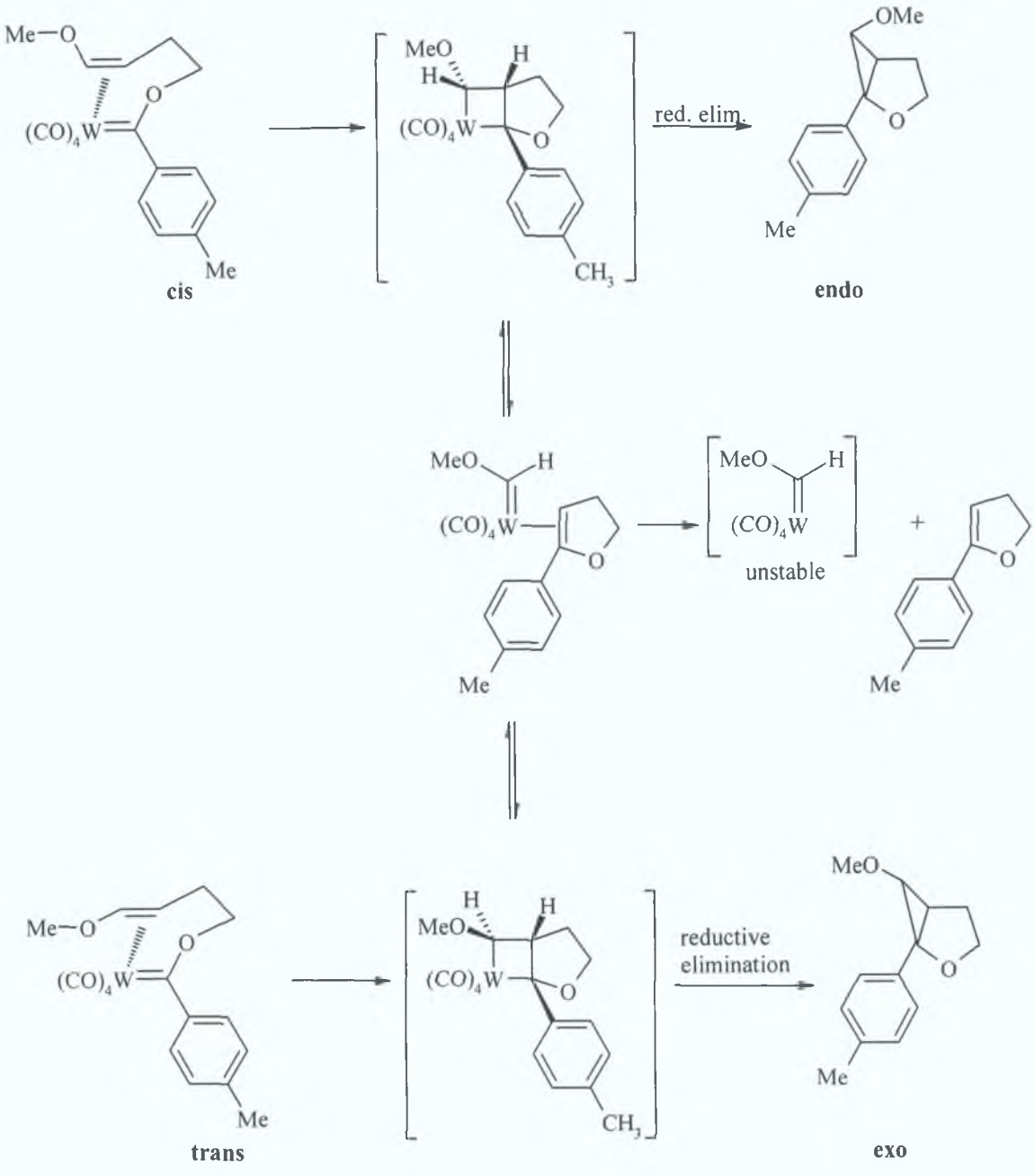

Scheme 2 - 7

Campos et al. have recently carried out a number of experimental and theoretical studies on the photoreactivity of chromium-imine-carbene complexes with alkynes and alkenes, a reaction first investigated by Hegedus et al. using the latter.[18] Irradiation of the chromium-imine-carbene complexes in the presence of alkenes lead to the formation of 1-pyrrolines via a two step process.[19] Initially, a *N*-cyclopropyl ketimine is formed following cyclopropanation, which in turn undergoes a photoinduced [1,3]-sigmatropic rearrangement (scheme 2 – 8).

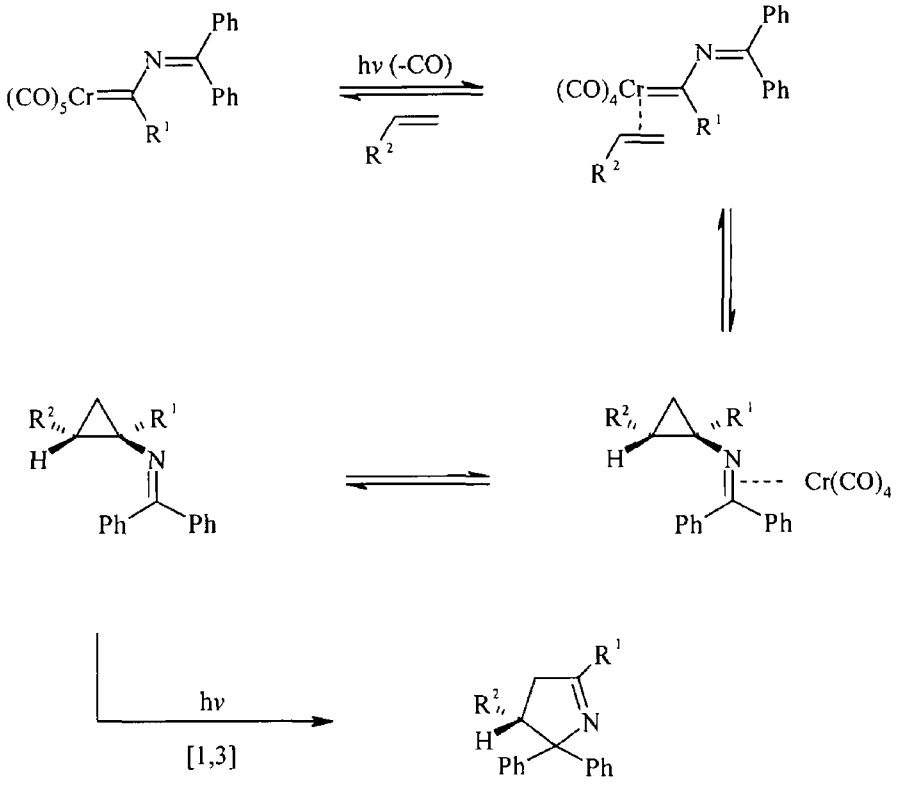

Scheme 2 – 8

Irradiation of the chromium-imme-carbene complexes in the presence of alkynes however leads to the formation of 2*H*-pyrrole derivatives via metallacycle formation, followed directly by reductive elimination of the metal moiety (scheme 2 – 9) [20]

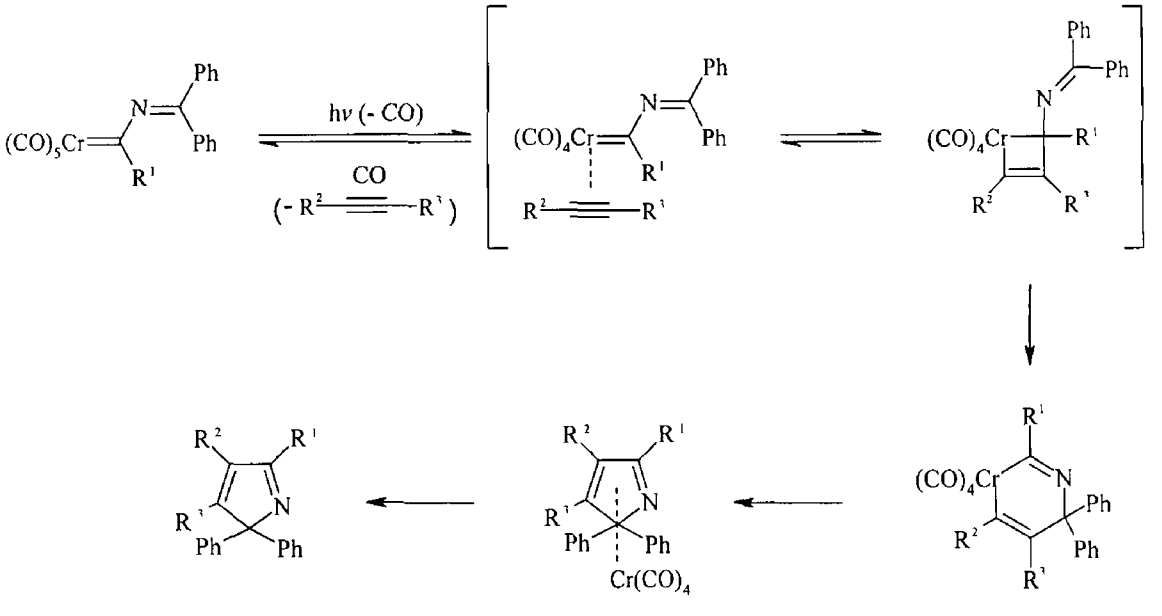

Scheme 2 – 9

2 2 2 *Anti – syn* isomerisation of Fischer carbene complexes

Owing to the π-bond character of the $C_{carbene}$-O bond in methoxy stabilised Fischer carbenes, an equilibrium between *anti*- and *syn*-configurations exists

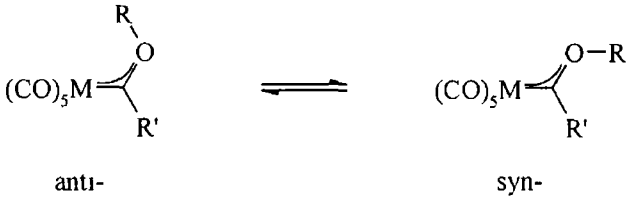

anti- syn-

Fig 5 -1

This isomerisation takes place via rotation of the methoxy group around the $C_{carbene}$-O bond [21] The *anti–syn* ratio in solution is dependent on the metal, the R-group, the solvent and also the temperature The *anti*-configuration is favoured energetically because of the electrostatic repulsion between the formally negative $M(CO)_5$ group and the oxygen lone pair in the *syn*-isomer This only applies, however, in the case of complexes with a rather long M-$C_{carbene}$ bond, since otherwise the steric interaction between the methoxy group and one of the equatorial carbonyl ligands forces the equilibrium towards the *syn*-isomer $(CO)_5W$=C(OMe)Ph occurs almost exclusively in the *anti*-configuration at room temperature, whereas nearly equal amounts of both isomers are found for the chromium analogue under identical conditions [21]

The resonant Raman spectrum of $(CO)_5W$=C(OMe)Ph generated following laser flash photolysis into its LF absorption bands has been reported by McGarvey et al [22] Photoinduced CO loss occurs for this complex, on population of either of its two LF excited states A transient species was observed in $CDCl_3$ with a lifetime of 7 5 μs following photolysis at 355 nm The deuterated complex $(CO)_5W$=C(OCD_3)Ph, displayed a similar transient species with an increased lifetime of 9 1 μs On photolysis in acetonitrile solution the tetracarbonyl species *cis*-$(CH_3CN)(CO)_4W$=C(OMe)Ph was formed However, the microsecond transient species was still observable at the isosbestic point of the reaction indicating that this transient species was in competition with the formation of the isolable acetonitrile adduct [23] The transient species therefore cannot be attributed to the solvation of an unsaturated CO loss intermediate

McGarvey and co-workers suggested that rapid rearrangement of the initial coordinatively unsaturated species takes place, thus leading to a partial bonding interaction between the metal centre and the methyl group of the carbene moiety This type of intramolecular coordination in which a hydrogen atom is bonded to both a carbon atom and a metal atom, saturated or unsaturated, is known as an 'agostic-interaction' [24] The agostic interaction occurs in competition with solvation of the coordinatively unsaturated photofragment and is the dominant species in non-coordinating solvents, however, it occurs at a comparable rate to the solvated species formed in coordinating solvents such as acetonitrile (scheme 2 – 11)

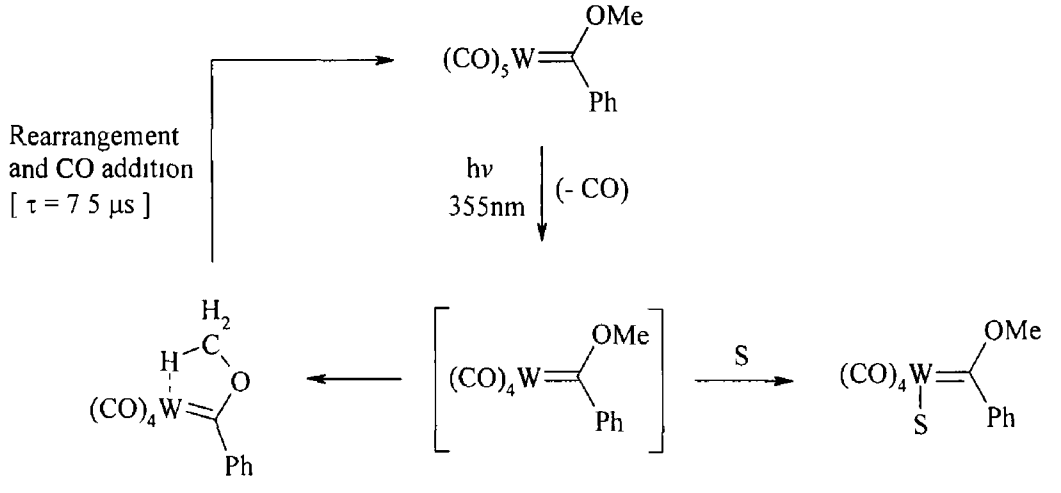

Scheme 2 – 11

The 352 nm absorption band of $(CO)_5W=C(OMe)Ph$ has been assigned to the high-energy LF transition corresponding to the one-electron transition $^1A(b_2^2)\rightarrow{}^1B_2(b_2{}^1 3a_1{}^1)$, assuming C_{2v} symmetry for the complex [10] This transition populates the tungsten $dx^2\text{-}y^2$ valence orbital resulting in labilisation of an equatorial M-CO bond and thus leads directly to loss of a *cis*-CO ligand facilitating the formation of an agostic interaction The transient species attributed to an agostic interaction aswell as *cis*-CO loss are also observed after excitation of $(CO)_5W=C(OMe)Ph$ at 405 nm This wavelength is thought to populate the low-energy LF excited state of $(CO)_5W=C(OMe)Ph$ by the transition $^1A(b_2^2)\rightarrow{}^1B_2(b_2{}^1 2a_1{}^1)$

This transition corresponds to population of the tungsten dz^2 orbital resulting in labilisation of an axial W-CO bond and therefore *trans*-CO loss (the same transition can sometimes lead to loss of the carbene ligand in some chromium carbene complexes due to a weaker Cr-$C_{carbene}$ bond) [11] Since 405 nm photolysis leads to the formation of *cis*-$(CO)_4W$=C(OMe)Ph within the laser pulse lifetime fast *trans-cis* interconversion of the vacant site occurs within a few nanoseconds of photoinduced CO loss Fluxional exchange of CO ligands has since been observed in ^{13}C-NMR studies of an unsaturated Fischer carbene complex [12]

A similar study was carried out by Servaas et al on $(CO)_5M$=C(OMe)Ph (M = Cr, W) using transient resonant Raman spectroscopy and matrix isolation [21] The lowest energy absorption bands of these complexes contain both MLCT and low-energy LF transitions therefore it is difficult to solely populate either of these excited states Following irradiation of the low-energy LF/MLCT band, almost complete *anti-syn* photoisomerisation was observed for both complexes in Ar, CO and CH_4 matrices at 10K [note $(CO)_5Cr$=C(OMe)Ph is initially present in the matrix as a mixture of *anti* and *syn* isomers in contrast to just the *anti* isomer for the tungsten complex] A new band was observed at 1,271 cm^{-1} for both the tungsten and chromium complexes in the resonant Raman studies following MLCT excitation and is attributed to the $\nu(C_{carbene}$-O) of the *syn*-isomers (the *anti*-isomers show this band at 1235 and 1234 cm^{-1} respectively) Irradiation of both complexes into their low-energy LF bands also gives rise to efficient *anti-syn* isomerisation, which suggests that *trans*-CO loss is not an efficient photoprocess for these complexes due to fast non-radiative decay to the lower energy MLCT state After prolonged photolysis of the low-energy LF bands, loss of a *cis*-CO ligand from the *syn*-isomers of both complexes was observed Photolysis of the syn-isomer resulted solely in photoisomerisation to the *anti*-isomer

This difference in behaviour between the *anti*- and *syn*-isomers was attributed to an increase in energy of the MLCT states of the *syn*-isomer, which reduces the probability of intersystem crossing This subsequently allows the low-energy LF excited state to dominate the photochemistry of these complexes Further photolysis of *syn*-[*cis*-$(CO)_4W$=C(OMe)Ph] results in the formation of an agostic interaction between a hydrogen of the methoxy group and tungsten as previously observed by McGarvey et al [22, 23] (scheme 2 – 12) No agostic interaction was observed for the chromium analogue

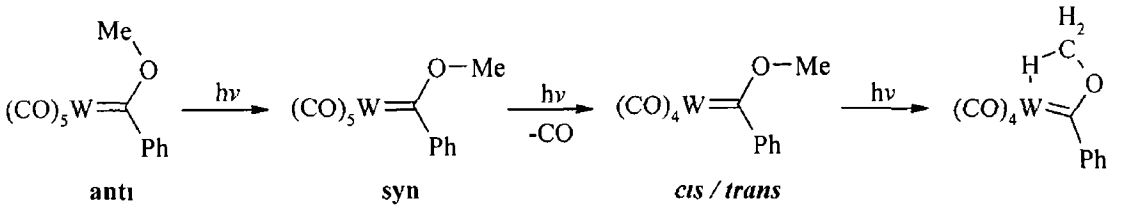

anti **syn** ***cis / trans***

Scheme 2 - 12

The work of McGarvey et al differs from that of Servaas et al in that Servaas et al observed *cis*-CO loss and formation of an agostic interaction for the tungsten-carbene complex on irradiation of the MLCT band, aswell as the low-energy LF band albeit in solution at room temperature [22] McGarvey et al suggested that irradiation of the MLCT band of $(CO)_5W$=C(OMe)Ph in solution at room temperature gives rise to thermal occupation of one of the higher LF states resulting in *cis*-CO loss thus allowing an agostic interaction to occur Occupation of this state is prevented in the matrix at 10K Gut et al in a later study on $(CO)_5W$=C(OMe)Ph suggested that *anti-syn* photoisomerisation and photoinduced CO loss occur as independent single-photon processes after LF excitation in solution at room temperature [25] Quantum yields for photoisomerisation and photoinduced CO loss were reported, $\Phi_{anti\ syn}$(308 nm) = 0 3, $\Phi_{CO\ loss}$(308 nm) = 0 017 These values are consistent with earlier studies [9 26] The quantum yield for *anti-syn* isomerisation is an order of magnitude greater than that for CO loss due to efficient non-radiative decay of the LF excited state to the lower energy MLCT state Gut and co-workers proposed that laser excitation of the high-energy LF state of $(CO)_5W$=C(OMe)Ph is followed by four possible relaxation pathways

i) radiationless decay to the ground state via the lower energy MLCT state

ii) *anti-syn* isomerisation via the lower energy MLCT state

iii) CO loss and formation of *cis*-$(CO)_4W$=C(OMe)Ph which recombines with CO to regenerate the starting pentacarbonyl species

iv) solvation to generate a tetracarbonyl species

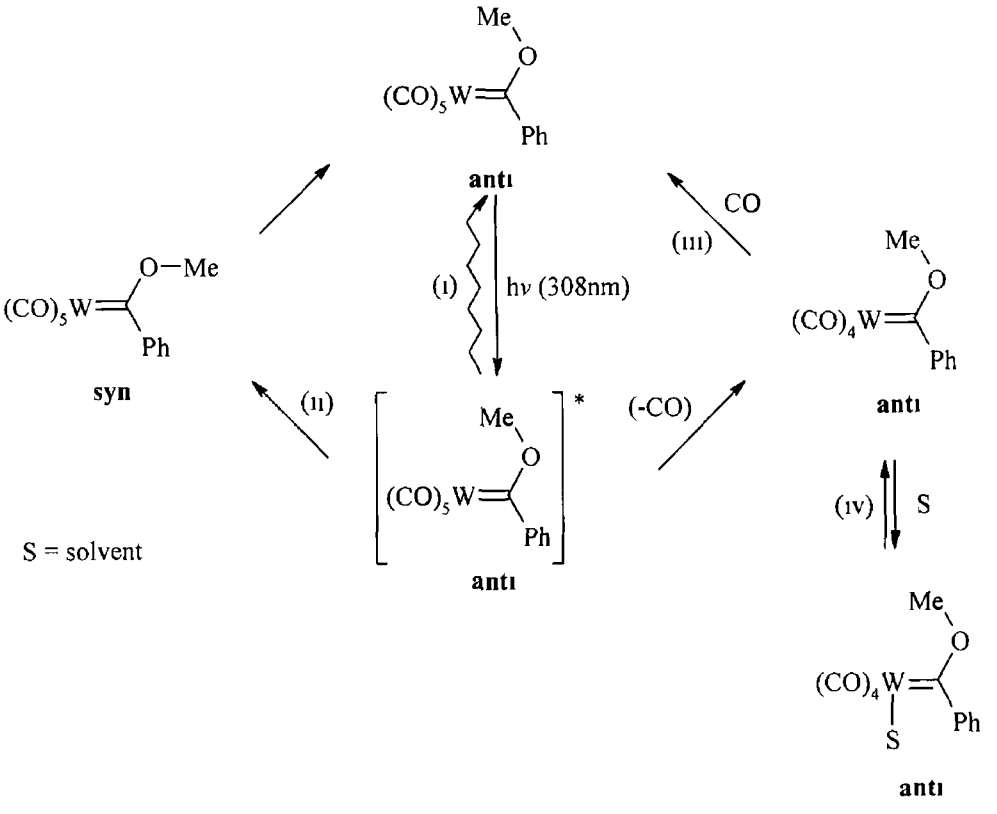

Scheme 2 – 13

Rooney et al investigated the photochemistry of the tungsten-carbene complexes $(CO)_5W=C(OMe)Me$, $(CO)_5W=C(OEt)Ph$ and $(CO)_5W=C(OMe)$*p*-Tolyl using laser flash photolysis, time-resolved resonance Raman spectroscopy and matrix isolation [27] The transients observed for all three complexes upon pulsed irradiation of both LF and MLCT bands result from *anti-syn* isomerisation, which was confirmed by the matrix isolation and Raman studies $(CO)_5W=C(OMe)Me$ exhibits transient species 1-2 orders of magnitude longer than the aryl-substituted carbenes This is consistent with the higher activation enthalpy for *anti-syn* isomerisation of $(CO)_5W=C(OMe)Me$ compared to $(CO)_5W=C(OMe)Ph$, i e 51 kJmol^{-1} and 37 kJmol^{-1} respectively Rooney et al suggest that the aryl moiety exerts electronic stabilisation, possibly by π-delocalisation, during the isomerisation process The *syn*-isomers of the aryl substituted carbenes exhibit a blue shift of the λ_{max} of the MLCT band whereas *syn*-$(CO)_5W=C(OMe)Me$ exhibits a red shift of its MLCT band from the *anti*-isomer (similar to previously reported silyl substituted carbenes) [28]

According to the authors, this shift to higher energy of the MLCT band of aryl substituted *syn*-carbenes suggests that, aswell as rotation of the alkoxy fragment, the aryl group rotates away from the plane of the carbene ligand thus minimising steric interaction with the alkoxy group, and at the same time reducing the degree of π-interaction with the carbene-carbon $2p_x$ orbital. Stabilisation of the *syn*-isomer of aryl substituted carbenes therefore arises mostly from donation of the lone pair at oxygen of the alkoxy group. This increased $C_{carbene}$-O π-interaction increases the bond order of the *syn*-isomer compared to the *anti*-isomer. The only shifts observed in the resonant Raman studies were for the aryl substituted carbenes and consisted of a shift to higher energy of the $\nu(C_{carbene}\text{-}O)$ bonds from 1235 cm^{-1} to 1266-1270cm^{-1} which is consistent with previous work by Servaas et. al.[21]

The *anti-syn* isomerisation of the aryl-substituted carbenes, $(CO)_5W{=}C(OEt)Ph$ and $(CO)_5W{=}C(OMe)$*p*-Tolyl, was photochemically irreversible as observed previously. In contrast, photochemically reversible *anti-syn* isomerisation was observed for $(CO)_5W{=}C(OMe)Me$ in matrix isolation studies. Rooney et. al proposed that upon MLCT excitation of the *syn*-isomer in aryl substituted carbenes the aryl ring rotates to a more conjugated position thus increasing resonance stabilisation in the excited state. This excited state is a local minimum with respect to the potential energy surface of the *syn*-isomer. As *anti-syn* isomerisation is not observed for these complexes, it was suggested that this excited state undergoes radiationless decay back to the *syn*-isomer from which it was initially formed (scheme 2 – 14).

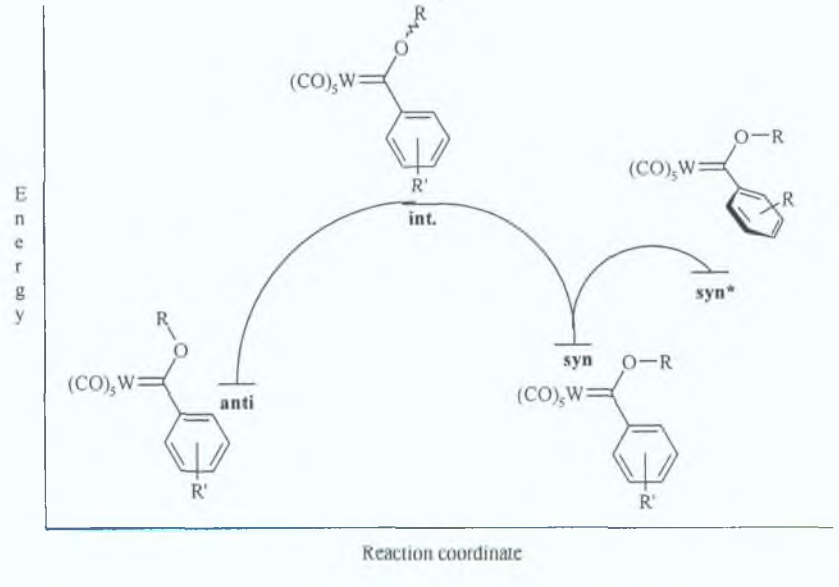

Scheme 2 - 14

2 2 3 Metal-ketene formation from Fischer-carbene complexes

Fischer-carbenes have been converted photochemically to a range of compounds, which includes amino-acids and peptides, β-lactams from imines, β-lactones from aldehydes, cyclobutanones from alkenes in addition to the products of intramolecular benzannulation reactions [7] These reactions are all photochemically driven by MLCT excitation of the carbene complex It is proposed that excitation into this state results in the formation of a metal-ketene transient formed by insertion of one of the equatorial carbonyl ligands into the metal-carbene bond (scheme 2 – 15)

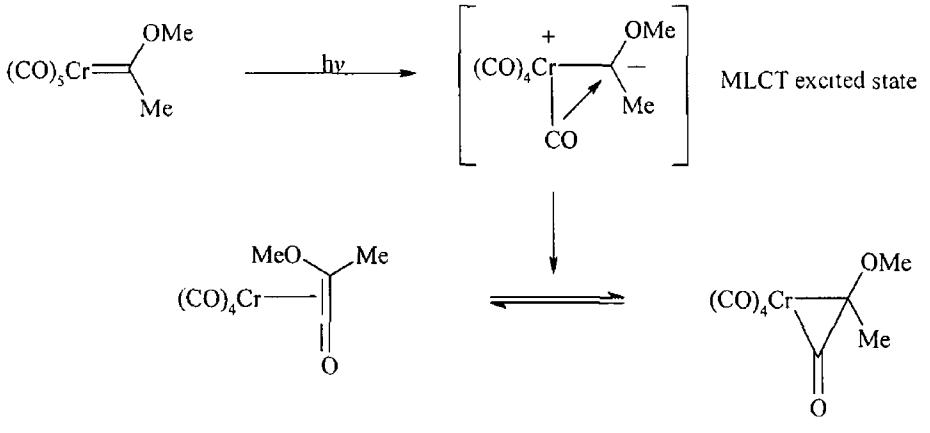

Scheme 2 – 15

Studies on η^5-CpW≡CTolyl have shown that migration of CO from the metal onto the carbyne-carbon upon MLCT excitation results in formation of a η^1- ketenyl complex in the presence of triphenylphosphine (rxn 2 – 4) [29]

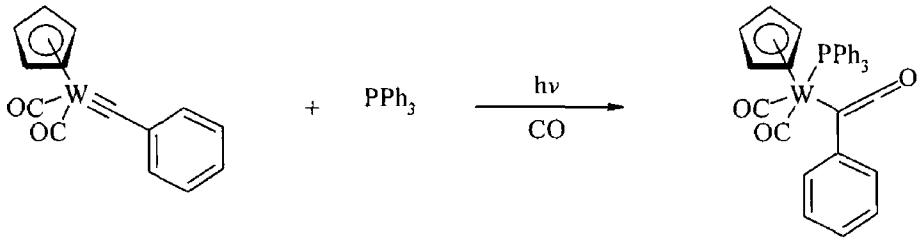

Rxn 2 – 4

The formation of ketene intermediates upon irradiation of chromium carbene complexes was first postulated by Hegedus and McGuire when they reported the synthesis of β-lactams by the photolysis of ether solutions containing various imines and the chromium carbene complex $(CO)_5Cr=C(OMe)Me$ (rxn 2 – 5) [30]

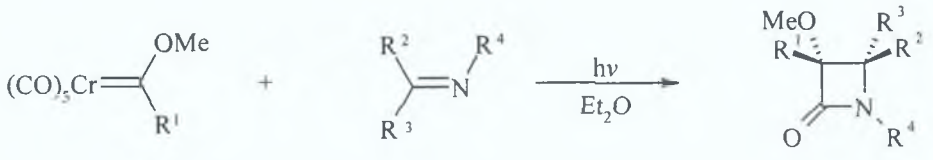

Rxn. 2 - 5

This reaction was stereospecific, producing only one diastereomer of the product. In contrast, under thermal conditions the chemistry of the α-carbon dominates, producing new carbene complexes (scheme 2 – 16).[31]

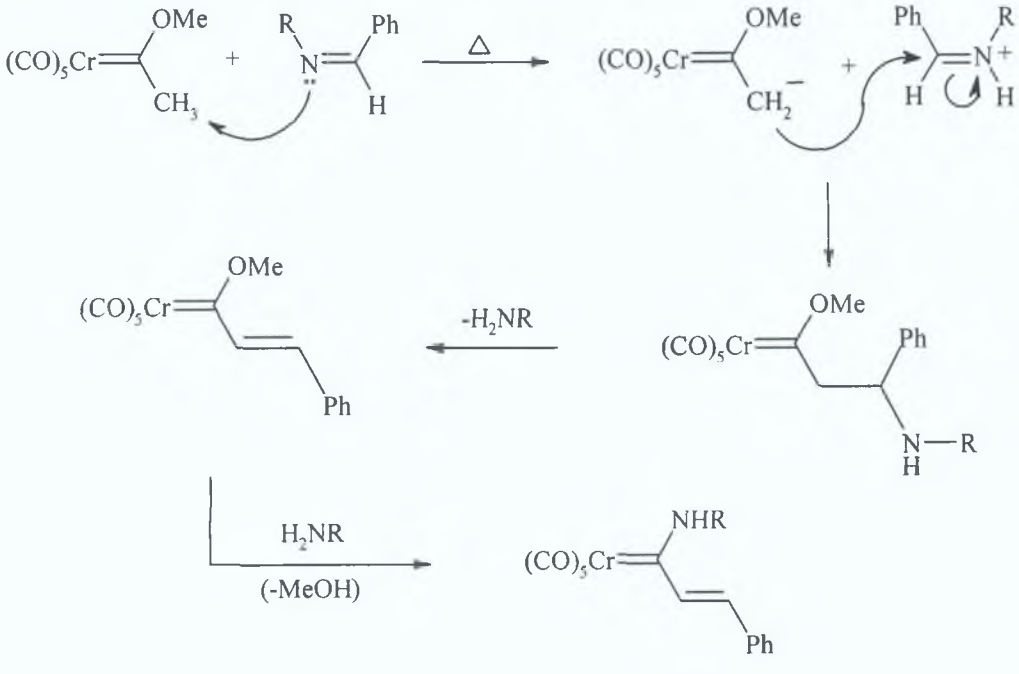

Scheme 2 - 16

Initially photoinduced elimination of a carbonyl ligand from the chromium carbene complex was believed to be the primary photoprocess in β-lactam formation, as CO dissociation from chromium complexes is well known under thermal conditions. However, β-lactam formation is not observed upon reaction of chromium carbene complexes with imines under thermal conditions. Also, high yields of β-lactam products are observed when the photochemical reaction is carried out under high pressures of CO.[31] These results suggest that the mechanism does not involve CO loss.

Strong evidence for the intermediacy of chromium-ketene complexes in the synthesis of β-lactams by the photolytic reaction of chromium carbene complexes and imines was observed by Hegedus when in an attempt to carry out a 1,3-cycloaddition of *p*-methoxyphenyl azide to the amino carbene $(CO)_5Cr{=}C(NMe_2)H$ the unexpected glycinamide was produced (rxn 2 – 6) [30]

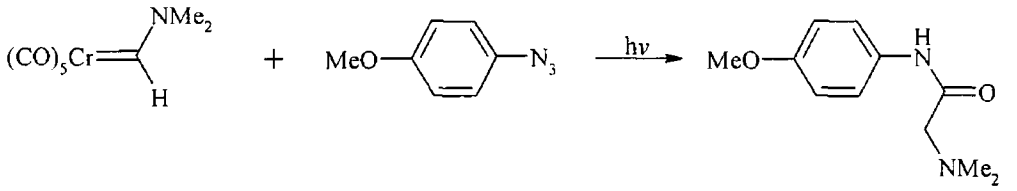

Rxn 2 - 6

In the presence of alcohols or amines, MLCT irradiation of the chromium carbenes led to analogous photochemistry, with β-lactam formation (rxn 2 – 7) [30]

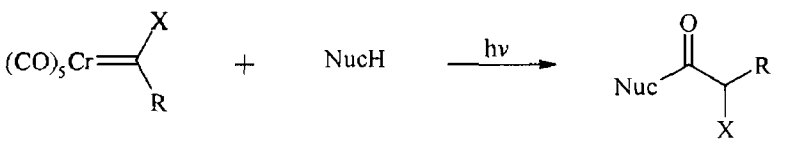

X = -OMe, $-NR_2$
NucH = MeOH, NR'_2

Rxn 2 - 7

The reactions involved in glycinamide and β-lactam formation are similar in that the products formed all consist of the carbene carbon, one CO ligand and the nucleophile Although there is no direct evidence of ketene formation both classes of compounds are potentially derived from nucleophillic attack on a ketene (scheme 2 – 17) The formation of ketene intermediates is inferred from subsequent reactions and has never been spectroscopically observed, due to its reactivity and unstability

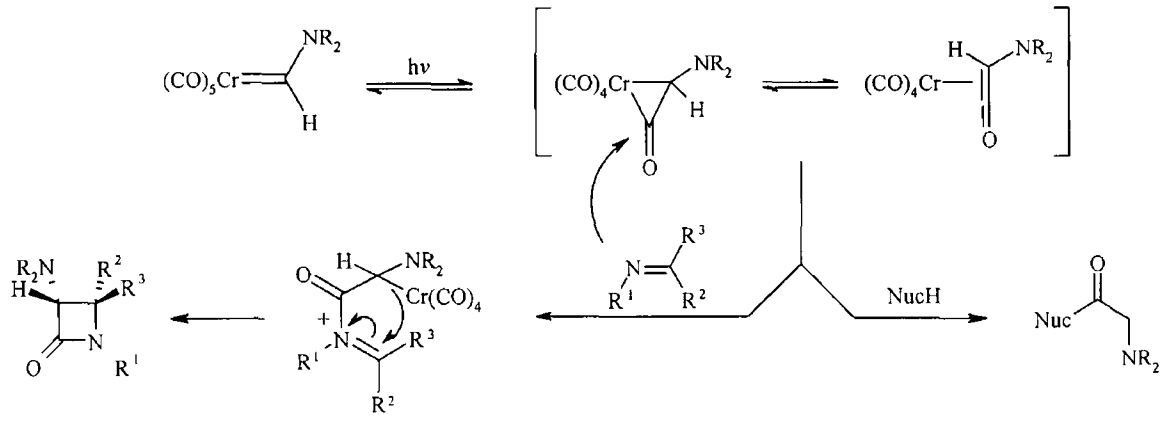

Scheme 2 - 17

The chromium ketene complex does not undergo typical free-ketene cycloaddition reactions with olefins, as it is only reactive towards nucleophillic reagents The reaction of free ketenes with imines to form β-lactams proceeds via a dipolar, non-concerted pathway This reaction occurs via nucleophillic attack of the imine at the ketene carbonyl to producing a zwitterionic intermediate, which undergoes a conrotatory ring closure to form the β-lactam (scheme 2 – 18) Free ketenes are generated in situ from acid halides and trimethylamine

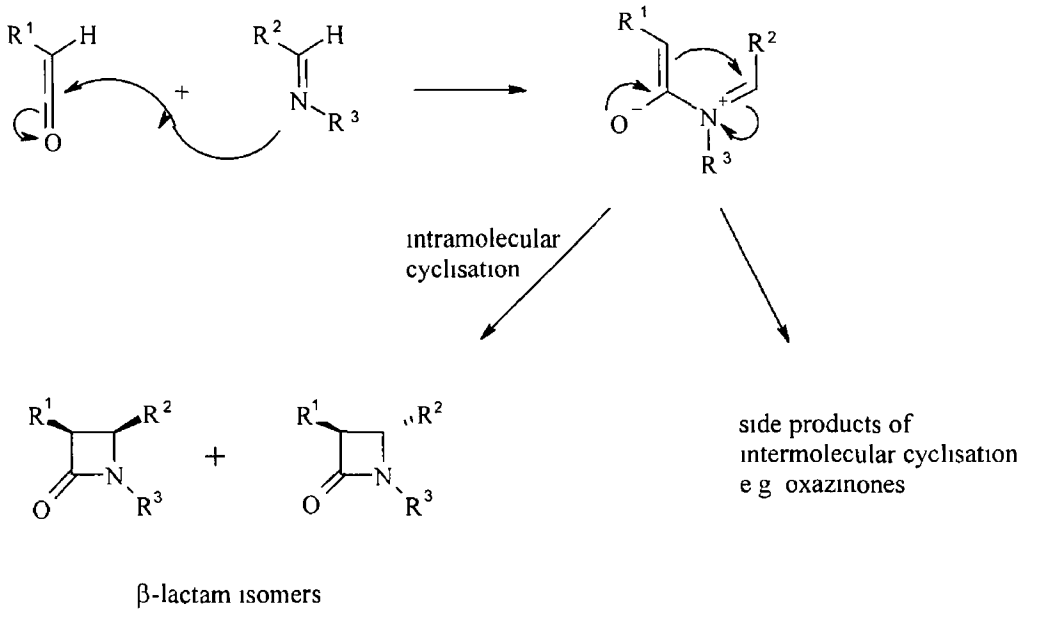

Scheme 2 - 18

Lower yields are often observed in the reaction of free ketenes with imines due to intermolecular reaction of the zwitterionic intermediate with further ketene rather than intramolecular cyclisation to form a β-lactam ring Intermolecular reactions are prevented in chromium ketene intermediates by the presence of the metal moiety, which results in higer yields for β-lactam formation [32]

Rooney et al have investigated the complexes $(CO)_5M=C(OMe)Me$ (M=Cr,W) by steady state photolysis, in the presence of imine, and matrix isolation [11] The chromium complex is known to react with N-benzylidenemethylamine in hexane to form a β-lactam (rxn 2 – 8)

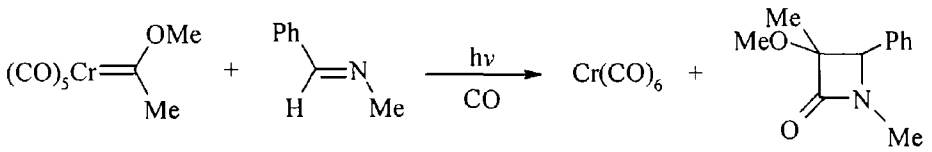

Rxn 2 - 8

Following irradiation of the MLCT band and upon further irradiation of both the low- and high-energy LF bands of the tungsten analogue no β-lactam products were observed Matrix isolation experiments gave no evidence for a metal-ketene complex upon MLCT excitation of both complexes The only photochemistry observed was *anti-syn* isomerisation Rooney et al proposed that the metal-ketene intermediate requires thermal activation and occurs in solution at room temperature Only thermal processes requiring less than 5 kJmol^{-1} of activation energy can occur in a matrix at 10 K

The chromium complex was more susceptible to loss of the carbene ligand than its tungsten analogue upon excitation of their respective low-energy LF states in solution at room temperature and in solid CO matrices at 10 K Rooney et al proposed that a chromium-ketene complex forms upon population of the chromium carbenes low-energy LF excited state in contrast to previous reports [30 31 32] On population of the LF excited state electron density is passed into the chromium dz^2 orbital from the HOMO denoted by the electronic transition $^1A_1(b_2^2) \rightarrow {}^1B_2(b_2{}^1 2a_1{}^1)$ This LF transition is anti-bonding with respect to the $Cr\text{-}C_{carbene}$ σ-bond and leads its dissociation Rooney et al

suggested that the Cr-$C_{carbene}$ π-bond remains intact This allows the carbene to undergo intramolecular nucleophillic attack on an adjacent equatorial carbonyl ligand to form the chromium-ketene transient complex

Fischer has previously reported such intramolecular carbene nucleophillic attack When the uncoordinated ketene $Ph_2C=C=O$ was formed under thermal conditions from the bis-phenyl carbene complexes $(CO)_5M=CPh_2$ (M = Cr and W) the chromium analogue gave higher yields of the final product than the tungsten carbene [33] $(CO)_5Cr=C(OMe)Me$ was also reported to lose a carbonyl ligand more readily than its tungsten analogue on irradiation of their respective high-energy LF bands in both N_2 and Ar matrices at 12 K Rooney et al suggested that due to the greater bond strength for W-CO (178 $kJmol^{-1}$) than Cr-CO (108 $kJmol^{-1}$) 'in-cage' recombination of the CO trapped in the matrix occurs for the tungsten complex [11] The carbonyl ligand will contain more vibrational energy on photoejection from the chromium complex and therefore will have a higher probability of escaping the matrix cage

Rooney and co-workers also studied the photochemistry of two classes of chromium amino-carbene complexes in low temperature matrices at 12 K using IR and UV spectroscopy aswell as UV monitored time-resolved laser flash photolysis in solution at room temperature at 355 nm excitation [34] The class-I compounds that are known to have little or no photoreactivity with imines to form β-lactams consist of $(CO)_5Cr=C(NMe_2)Me$, $(CO)_5Cr=C(NBz_2)Me$ and $(CO)_5Cr=C(NMe_2)Ph$ Class-II compounds which are known to undergo efficient photochemical reactions with imines to form β-lactams consist of $(CO)_5Cr=C(NMe_2)H$, $(CO)_5Cr=C(NBz_2)H$ and $(CO)_5Cr=C(NH_2)Me$

No transient species that could be assigned to a chromium-ketene complex for both class I and II compounds in matrix and flash photolysis experiments were detected All transient species observed were assigned to CO loss products as the symmetry of amino-carbene complexes preclude *anti-syn* photoisomerisation as observed in methoxy-carbenes Photoinduced CO loss is therefore suggested as the primary photochemical process in these complexes with chromium-ketene complex formation occurring subsequently by a thermal process

Class-II compounds were shown to react with N_2, ethene and CO in matrix isolation experiments Also, the transient species formed upon CO loss from class-II complexes showed significant solvent dependency on the rate of recombination with CO in solution, to regenerate the parent complex (scheme 2 – 19)

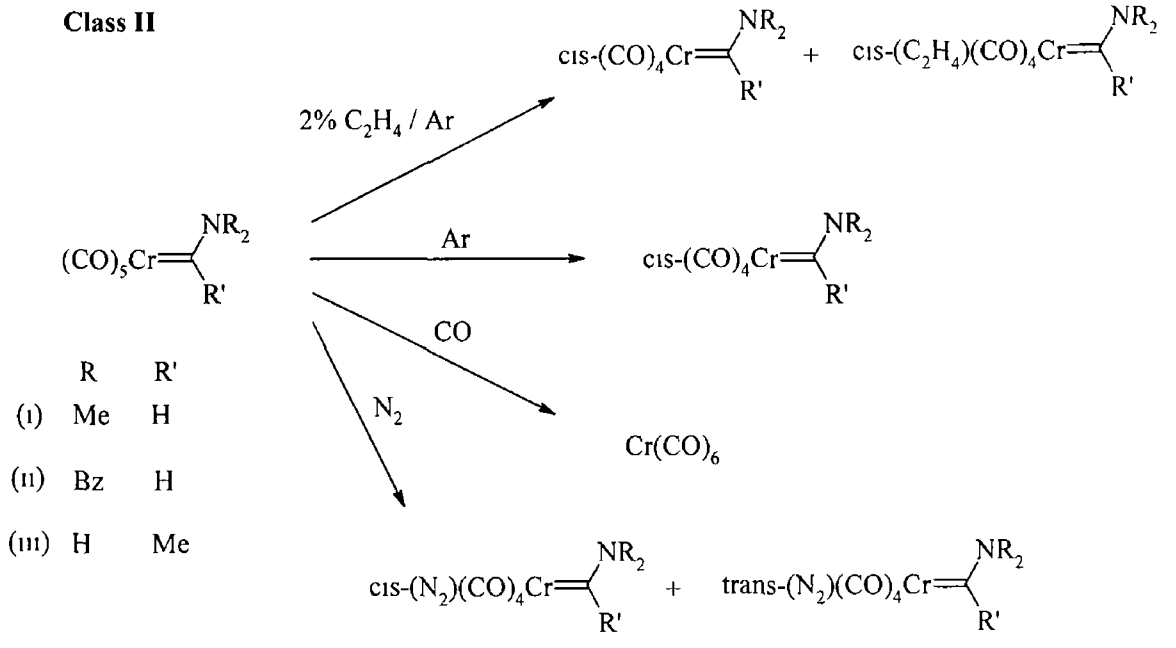

Scheme 2 - 19

In contrast, class-I compounds did not react with N_2, ethene or CO in low temperature matrices and showed little or no solvent dependency for recombination with CO after laser flash photolysis in solution (scheme 2 – 20) These results indicate that the vacant site formed upon photoinduced CO loss from class-I compounds is blocked The blocked site prevents any reaction occurring with N_2, ethene or CO in the 'matrix cage' and also prevents any solvent acting as a token ligand in solution, which is a well established process for many unsaturated metal carbonyl transient species The blocking of the vacant site in these unsaturated chromium-carbene species is a result of the bulky carbene ligand rearranging itself to reduce steric strain

Although these results indicate that there is a relationship between the vacant site being blocked and low synthetic activity, Rooney et al suggest that this is not universal for all carbene complexes as β-lactam formation is thought to be dependent on metal-ketene formation which is independent of CO loss [32]

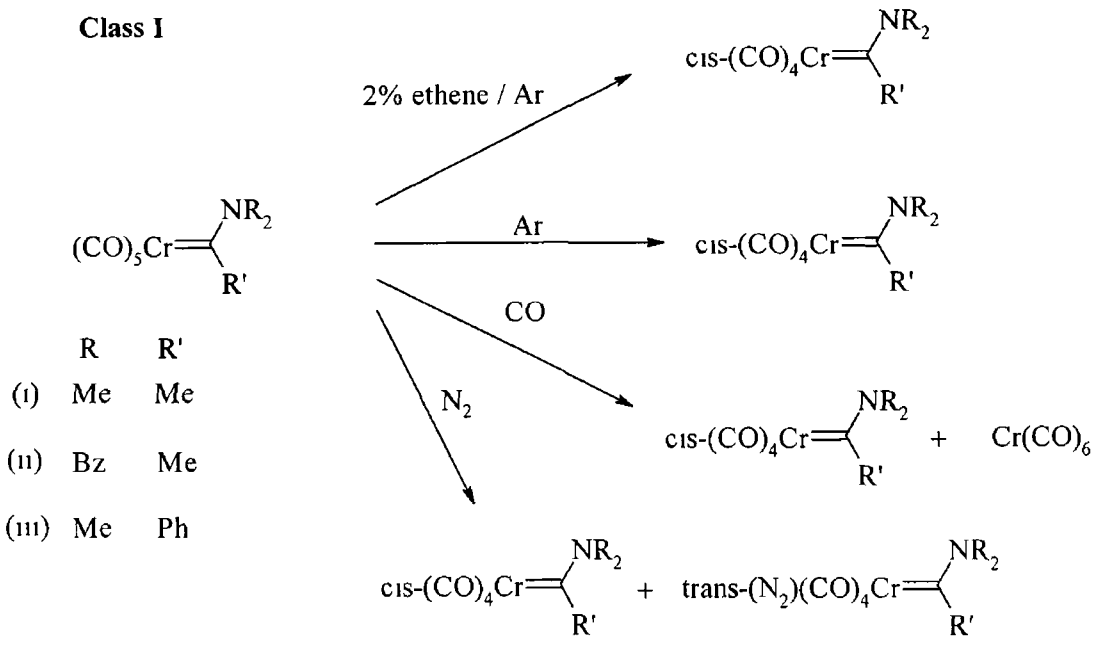

Scheme 2 - 20

In a separate laser flash photolysis study on the diamino carbene complex $(CO)_5Cr$](N,N'-Dimethylimidazole)] (fig 2 – 2), which has a low reactivity towards β-lactam formation, evidence for an unsolvated transient species was observed after photoinduced CO loss [35] This unsaturated transient species is relatively stable due to its electron rich chromium centre It was therefore concluded that although steric effects may influence the synthetic activity of some carbene complexes the electronic nature of the substituents on the carbene ligand must also have a reasonable influence on their synthetic reactivity

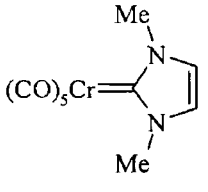

Fig 2 - 2

McGarvey et al have investigated the photochemistry of $(CO)_5W=C(X)SiPh_3$ (X = OEt, C_4H_8N) by laser flash photolysis coupled with time-resolved resonance Raman spectroscopy [28] Thermolysis of the amino-carbene results in CO loss and formation of the 16-electron species $(CO)_4W=C(C_4H_8N)SiPh_3$ The vacant site in this coordinatively unsaturated intermediate is blocked by one of the silyl phenyl groups

In contrast, thermolysis of the ethoxy carbene results in cleavage of the tungsten-carbene bond and formation of several products including $HSiPh_3$, $EtSiPh_3$, $Ph_3SiC(O)Et$ and ethane [36] Excited state absorption measurements of $(CO)_5W=C(C_4H_8N)SiPh_3$ following 355 nm excitation in pentane showed the formation of a 16-electron species attributed to *cis*-CO loss as shown in rxn 2 – 9 (bubbling CO gas through the solution regenerated the parent compound) No photoproduct is observed on photolysis at 416 nm as this wavelength lies within the MLCT transition while CO loss is associated with population of the higher energy *LF* state On photolysis of $(CO)_5W=C(C_4H_8N)SiPh_3$ at 355 nm in acetomtrile, as opposed to pentane, similar changes occur in the UV spectrum with the growth of an extra band at 420 nm attributed to the tetracarbonyl product *cis*-$(CH_3CN)(CO)_4W=C(C_4H_8N)SiPh_3$

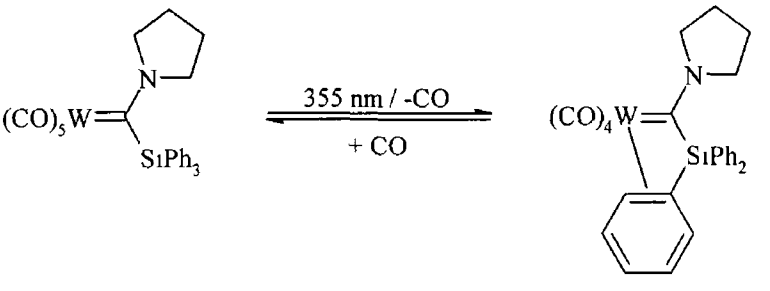

Rxn 2 - 9

Dissimilar behaviour was observed for the ethoxy carbene, $(CO)_5W=C(OEt)SiPh_3$, when compared to the ammo analogue Excitation at 355 or 416 nm in pentane or acetomtrile resulted in the observation of a transient species in the region 340-500 nm whose absorption decayed exponentially on a microsecond timescale The lifetime of this transient was independent of CO concentration yet dependent on solvent and temperature Also, *cis*-$(CH_3CN)(CO)_4W=C(OEt)SiPh_3$ was not observed following photolysis in acetonitrile McGarvey et al suggested that the quantum yield for CO loss is very low due to efficient intersystem crossing to a low-lying MLCT state and that *anti-syn* isomerisation of the ethoxy moiety on the carbene carbon occurs from this excited state, which gives rise to the observed transient species

In the following section, the synthesis and characterisation of some ferrocenyl Fischer-carbenes is reported The photochemistry and electrochemistry of these complexes is discussed

2 3 Experimental

2 3 1 Reagents

All reactions were performed under an inert atmosphere of argon Anhydrous diethyl ether was used as received (Fluka Chemicals) Aldrich Chemical Company supplied all other solvents Pentane was of HPLC grade and used without any further purification Dichloromethane was dried over $MgSO_4$ prior to use All solvents used for steady state photolysis and laser flash photolysis experiments were of spectroscopic grade and used without further purification Argon and carbon monoxide gases were supplied by Air Products and IIG respectively Chromium and tungsten hexacarbonyl, ferrocene, ferrocenecarboxaldehyde, *n*-butyl lithium (2 5 M solution in hexanes), N,N,N',N'-tetramethylethylenediamine, trimethylamine, chlorotrimethylsilane and pyrrolidine (Aldrich Chemical Company) were all used without further purification Methyl lithium (1 4M solution in diethyl ether) and trimethyloxomum tetrafluoroborate (Fluka Chemicals) were also used without further purification Silica gel (Merck) was used as received All mobile phases were dried over $MgSO_4$ prior to use

2 3 2 Equipment

All infrared spectra were obtained on a Perkin-Elmer 2000 FTIR spectrometer in 0 1 mm sodium chloride liquid solution cells using spectroscopic grade pentane as the solvent ^{1}H and ^{13}C NMR spectra were recorded on a Bruker model AC 400 MHz spectrometer in the appropriate deuterated solvent at room temperature with external TMS as a standard All UV spectra were measured in spectroscopic grade solvents on a Hewlett Packard 8452A-photodiode array spectrometer using a 1cm quartz cell All samples were prepared for steady state and laser flash photolysis by the freeze-pump-thaw procedure as described in the appendix

2.3.3 Synthesis

2.3.3.1 $(CO)_5Cr=C(OMe)Fc$

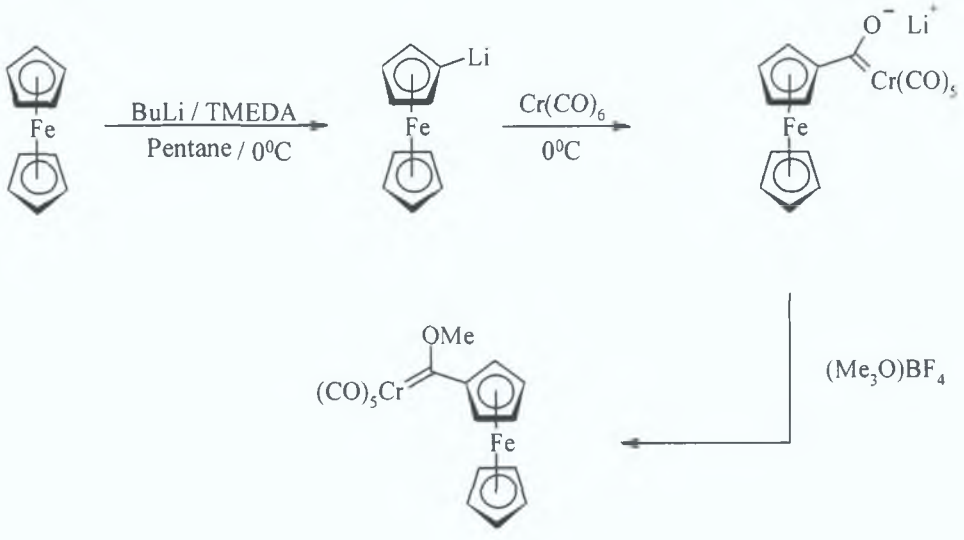

Scheme 2 - 21

$(CO)_5Cr=C(OMe)Fc$ was prepared by a procedure previously reported by Connor and Lloyd.[37] A suspension of ferrocenyl-lithium was first prepared and used in-situ. 5.40 mmol (1 g) of ferrocene was dissolved in 200 ml of pentane. On cooling this solution to 0 ^{0}C 5.40 mmol of *n*-BuLi (2.16 ml of 2.5 M *n*-BuLi in hexane solution) was slowly added via syringe followed by 5.40 mmol (0.44 ml) of N,N,N',N'-tetramethylethylenediamine (TMEDA). The reaction mixture was allowed to reach room temperature and left to stir for 24 hours. The solution was then cooled again to 0 ^{0}C and 5.4 mmol (1.2 g) of $Cr(CO)_6$ was added. The reaction mixture was again allowed to reach room temperature and stirred for 2 hours at which point the solvent was removed under reduced pressure. The resulting residue was dissolved in 25 ml of water and added to a separating funnel containing 25 ml of dichloromethane. Trimethyloxonium tetraflouroborate salt (~ 8.11 mmol/1.2 g) was added to this mixture until the water phase reached a pH of 3-4. The aqueous phase was then rinsed four times with 25 ml aliquots of dichloromethane. The organic extracts were combined, dried over magnesium sulphate and the solvent removed under reduced pressure resulting in a crude solid material. The product was purified on a silica gel column by flash chromatography using pentane:dichloromethane (9:1) as the mobile phase. Unreacted chromium hexacarbonyl was eluted off the column first followed by

unreacted ferrocene $(CO)_5Cr=C(OMe)Fc$ eluted off the column as the third band with a deep red colour The solvent was removed under reduced pressure resulting in a deep red powder with a yield of 1 68 g (3 94 mmol, 73 % yield)

IR (νCO) 1940 , 1952 , 2057 cm^{-1} (pentane)

^1H NMR ($CDCl_3$) δ 4 18 (5H, s), 4 62 (3H, s), 4 72 (2H, m), 4 93 (2H, m) ppm

^{13}C NMR ($CDCl_3$) δ 66 00, 70 51, 721 21, 74 62, 93 56, 217 30, 222 91, 333 24 ppm

2 3.3 2 1,1'-[(CO)$_5$Cr=C(OMe)]$_2$-Fc

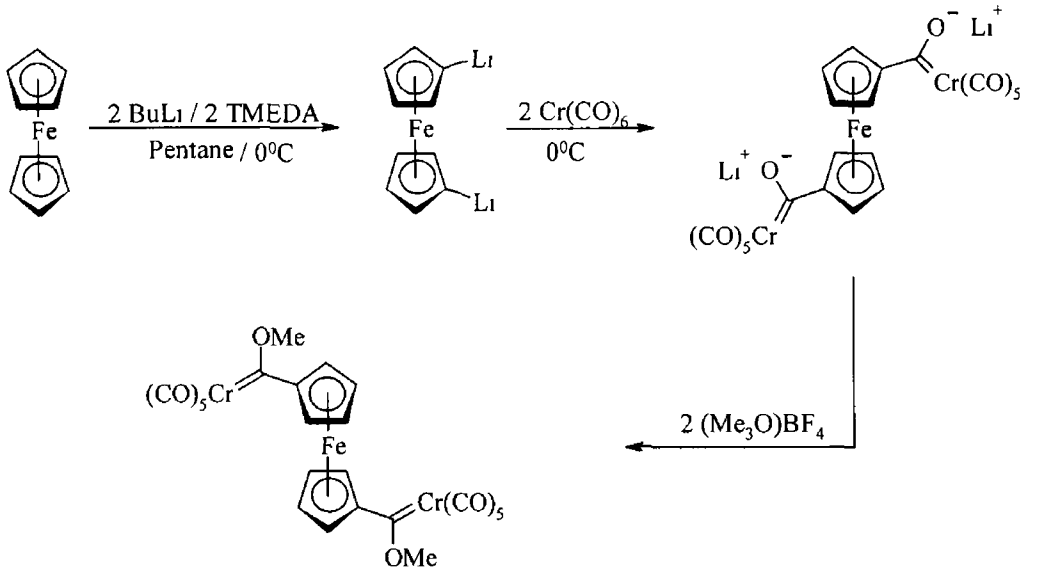

Scheme 2 – 22

1,1'-[(CO)$_5$Cr=C(OMe)]$_2$-Fc was prepared by a procedure similar to that for (CO)$_5$Cr=C(OMe)Fc with the following modifications 2 70 mmol (500 mg) of ferrocene was dissolved in 100 ml of pentane under an atmosphere of argon for formation of the 1,1'-dilithioferrocene salt A two fold excess of *n*-BuLi, i e 5 40 mmol (2 16 ml of 2 5 M *n*-BuLi in hexane solution), and TMEDA (0 44 ml, 5 4 mmol) are used resulting in the 1,1'-dilithioferrocene salt A twofold excess of Cr(CO)$_6$ (1 20 g, 5 4 mmol) and the trimethyloxonium tetraflouroborate salt (~ 8 11mmol/1 20 g) was therefore required for formation of the bis-carbene complex The crude product was again purified on a silica gel column by flash chromatography using pentane dichloromethane (9 1) as the mobile phase Unreacted chromium hexacarbonyl was eluted off the column first followed by unreacted ferrocene and (CO)$_5$Cr=C(OMe)Fc as a deep red band 1,1'-[(CO)$_5$Cr=C(OMe)]$_2$-Fc was eluted off the column as the fourth band using a slightly more polar mobile phase, i e pentane dichloromethane (8 2) The solvent was removed under reduced pressure resulting in a dark brown powder with a yield of 1 10 g (1 65 mmol, 61 % yield)

IR (νCO) 1944 , 1958 , 2056 cm^{-1} (pentane)

^{1}H NMR ($CDCl_3$) δ 4 67 (6H, s), 4 72 (4H, m), 4 96 (4H, m) ppm

^{13}C NMR ($CDCl_3$) δ 66 92, 74 11, 77 71, 94 62, 217 38, 223 04, 337 10 ppm

Anal Calcd for $C_{24}H_{14}O_{12}FeCr_2$ C 44 06, H 2 16 Found C 44 04, H 2 05

2 3 3 3 $(CO)_5W=C(OMe)Fc$

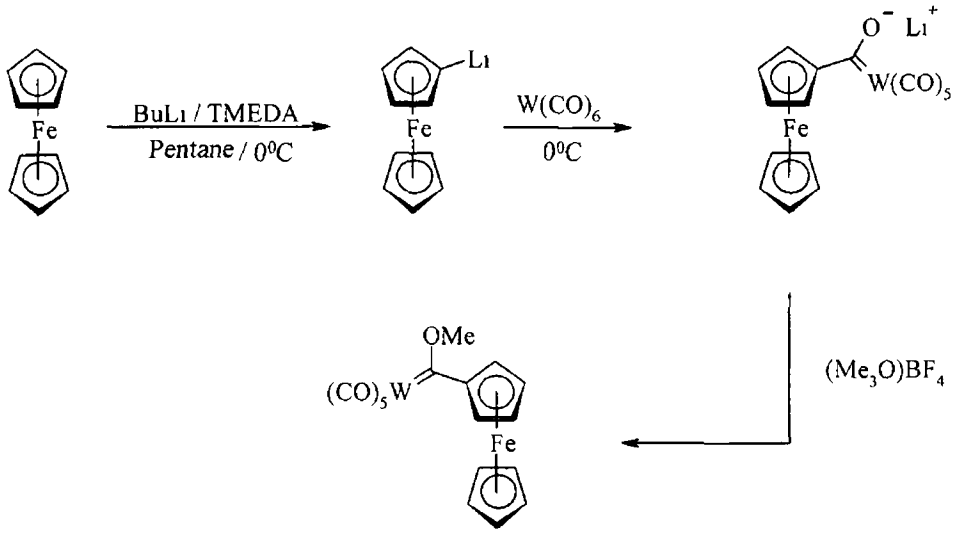

Scheme 2 - 23

$(CO)_5W=C(OMe)Fc$ was prepared in a similar manner to $(CO)_5Cr=C(OMe)Fc$ adapted from the method of Connor [38] A suspension of ferrocenyl-lithium was first prepared and used in-situ 2 70 mmol (0 50 g) of ferrocene was dissolved in 100 ml of pentane On cooling this solution to 0 ^{0}C 2 70 mmol of *n*-BuLi (1 08 ml of 2 5 M *n*-BuLi in hexane solution) were slowly added via syringe followed by 2 70 mmol (0 22 ml) of N,N,N',N'-tetramethylethylenediamine (TMEDA) The reaction mixture was allowed to reach room temperature and left stirring for 24 hours The solution was then cooled again to 0 ^{0}C and 2 70 mmol (0 95 g) of $W(CO)_6$ was added The reaction mixture was again allowed to reach room temperature and stirred for an additional 2 hours at which point the solvent was removed under reduced pressure The resulting residue was dissolved in 15 ml of water and added to a separating funnel containing 15 ml of dichloromethane Trimethyloxonium tetraflouroborate salt (~ 2 50 mmol/0 37 g) was added to this mixture until the water phase reached a pH of 3-4 The aqueous phase was then rinsed four times with 15 ml aliquots of dichloromethane The organic extracts were then combined, dried over magnesium sulphate and the solvent removed under reduced pressure resulting in a deep red crude product The product was purified on a silica gel column by flash chromatography using pentane dichloromethane (9 1) as the mobile phase Unreacted tungsten hexacarbonyl was eluted off the column first followed by unreacted ferrocene $(CO)_5W=C(OMe)Fc$ eluted off the column as the third band with a deep red colour

The solvent was removed under reduced pressure resulting in a deep red powder with a yield of 0 87g (1 57 mmol, 58 % yield)

IR (νCO) 1937 , 1949 , 2065 cm ^{1} (pentane)

^{1}H NMR ($CDCl_3$) δ 4 20 (5H, s), 4 46 (3H, s), 4 78 (2H, m), 4 92 (2H, m) ppm

^{13}C NMR ($CDCl_3$) 68 60, 70 80, 73 23, 75 10, 95 17, 191 14, 197 99, 202 35, 307 53 ppm

2.3.3.4 1,1'-[$(CO)_5W$=C(OMe)]$_2$-Fc

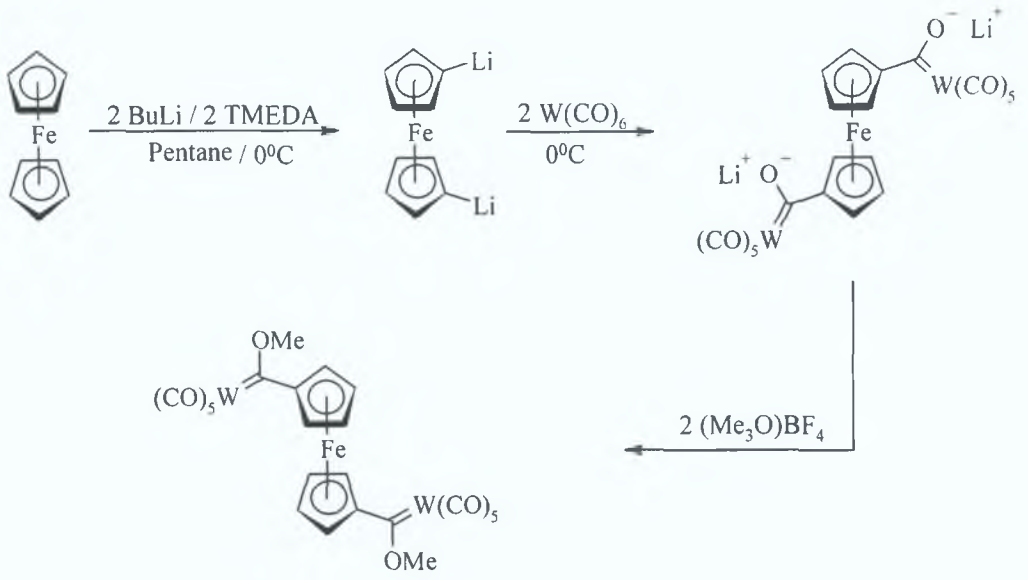

Scheme 2 – 24

1,1'-[$(CO)_5W$=C(OMe)]$_2$-Fc was prepared in a similar manner to 1,1'-[$(CO)_5Cr$=C(OMe)]$_2$-Fc. 1.35 mmol (250 mg) of ferrocene was dissolved in 100 ml of pentane under an atmosphere of argon for formation of the 1,1'-dilithioferrocene salt. A two fold excess of *n*-BuLi, i.e. 2.70 mmol (1.08 ml of 2.5 M *n*-BuLi in hexanes), and TMEDA (0.22 ml, 2.70 mmol) were used resulting in formation of the 1,1'-dilithioferrocene salt. A two-fold excess of $W(CO)_6$ (2.70 mmol, 0.95 g) and the trimethyloxonium tetraflouroborate salt (~ 2.50 mmol/0.37 g) were required for formation of the bis-carbene complex. The crude product was again purified on a silica gel column by flash chromatography using pentane:dichloromethane (9:1) as the mobile phase. Unreacted chromium hexacarbonyl was eluted off the column first followed by unreacted ferrocene and $(CO)_5W$=C(OMe)Fc as a deep red band. 1,1'-[$(CO)_5W$=C(OMe)]$_2$-Fc was eluted off the column as the fourth band using a slightly more polar mobile phase, i.e. pentane:dichloromethane (8:2). The solvent was removed under reduced pressure resulting in a dark red/brown powder with a yield of 1.065 g (1.16 mmol, 43 % yield).

IR (νCO): 1935, 1942 , 1955, 2064 cm^{-1} (pentane).

^{1}H NMR ($CDCl_3$): δ 4.50 (6H, s), 4.77 (4H, m), 4.96 (4H, m) ppm.

^{13}C NMR ($CDCl_3$): 69.07, 74.91, 76.59, 96.22, 197.64, 202.04, 311.00.

Anal. Calcd. for $C_{24}H_{14}O_{12}FeW_2$: C 31.40, H 1.54. Found: C 31.40, H 1.54.

2.4 Results

2.4.1 Photochemistry of $(CO)_5Cr=C(OMe)Fc$

2.4.1.1 Laser flash photolysis of $(CO)_5Cr=C(OMe)Fc$ in cyclohexane

$(CO)_5Cr=C(OMe)Fc$ is a deep red solid with a UV-vis spectrum exhibiting two low-energy bands in the visible region of the spectrum at 514 nm ($\varepsilon = 3.29 \times 10^3\ M^{-1}cm^{-1}$) and 422 nm ($\varepsilon = 7.55 \times 10^3\ M^{-1}cm^{-1}$) and also a slightly obscured band at 340 nm ($\varepsilon = 2.62 \times 10^3\ M^{-1}cm^{-1}$) in cyclohexane solution.

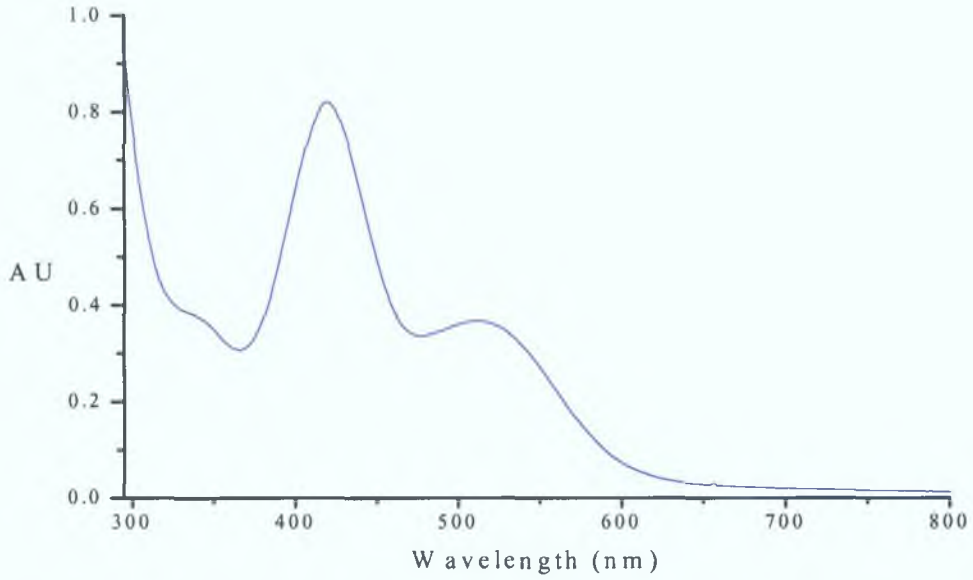

Fig. 2 – 3: UV-vis spectrum of $(CO)_5Cr=C(OMe)Fc$ in cyclohexane.

The photochemistry of $(CO)_5Cr=C(OMe)Fc$ was investigated by UV-vis monitored laser flash photolysis with λ_{exc} = 355 and 532 nm in cyclohexane under one atmosphere of carbon monoxide and also under one atmosphere of argon at room temperature. Following flash photolysis of $(CO)_5Cr=C(OMe)Fc$ at λ_{exc} = 355 nm in cyclohexane under one atmosphere of carbon monoxide at room temperature depletion of the parent compound is evident at 340 nm as is shown in fig. 2 - 4. This signal recovers to the pre-flash absorbance level, which is indicative of a photoreversible process. An average of ten shots were collected in order to reduce the signal-to-noise ratio of the signal as it was of very low intensity. For this reason, a difference absorbance spectrum could not be plotted.

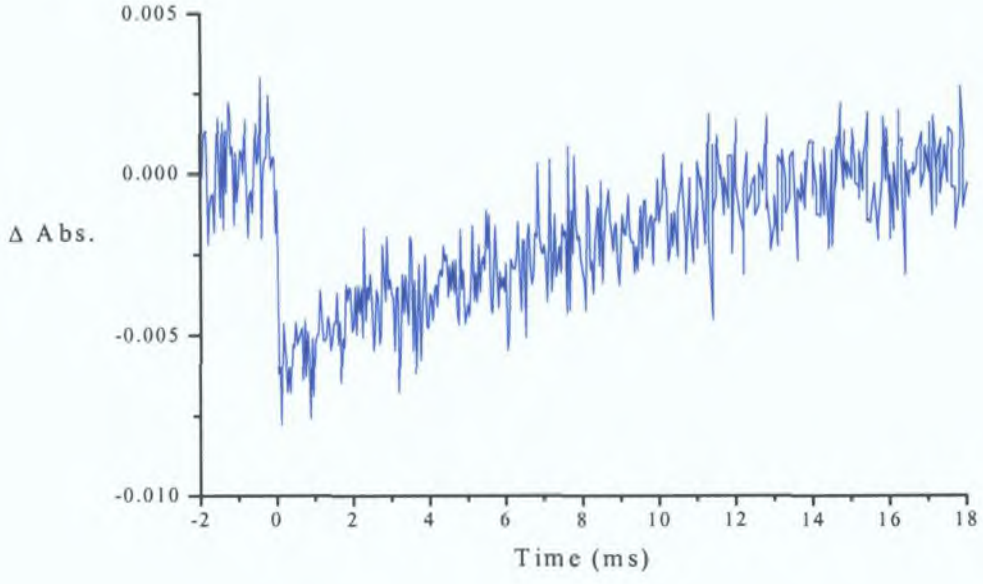

Fig. 2 - 4: Depletion of the parent compound with recovery at 340 nm following laser flash photolysis (λ_{exc} = 355 nm) of $(CO)_5Cr{=}C(OMe)Fc$ in cyclohexane under one atmosphere of carbon monoxide, ($k_{obs} = 134.05 \pm 13\ s^{-1}$, $\tau = 7.46 \pm 0.75$ ms).

The observed rate constant for the regeneration of the parent compound at 340 nm was calculated to be $134.05 \pm 13\ s^{-1}$ ($\tau = 7.46 \pm 0.75$ ms), however, there may be a substantial error associated with this value due to the low intensity of the signal. When the sample was placed under an atmosphere of argon a similar transient signal was observed at 340 nm. The absorbance of this transient signal did not recover to the pre-flash absorbance level however. The UV-vis spectra recorded throughout this experiment show a gradual decomposition of the parent compound (fig. 2 - 5) indicating that recovery of the parent compound does not occur in the absence of CO. The photoproduct therefore has a dependence on CO concentration. Accurate measurement of the lifetime of this transient species under various concentrations of CO was prevented due to the weak intensity of the signals observed. No photochemistry was observed for $(CO)_5Cr{=}C(OMe)Fc$ following irradiation at λ_{exc} = 532 nm in cyclohexane.

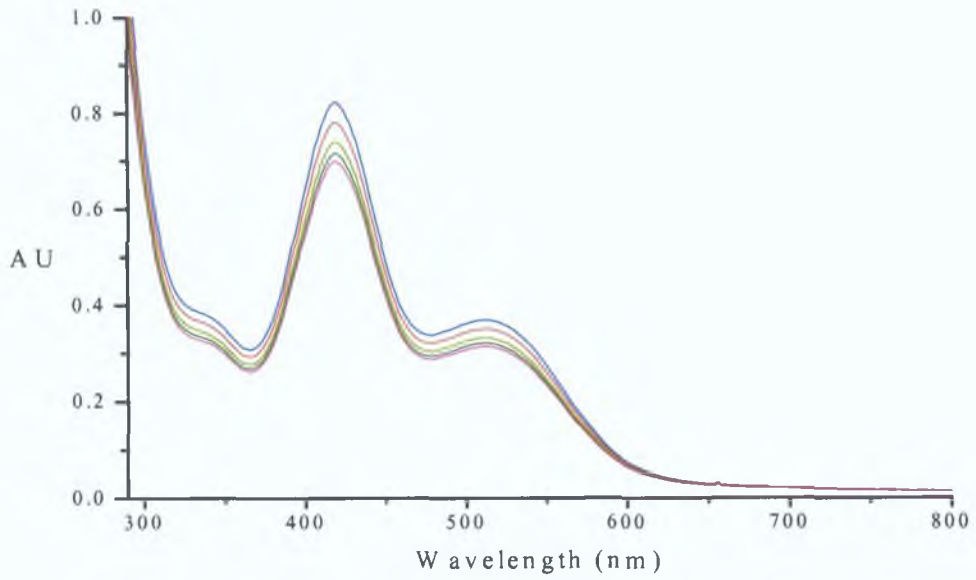

Fig. 2 - 5: UV-vis spectra recorded during laser flash photolysis of $(CO)_5Cr{=}C(OMe)Fc$ at 355 nm excitation wavelength in cyclohexane under one atmosphere of argon.

2.4.1.2 Steady state photolysis of $(CO)_5Cr=C(OMe)Fc$ in cyclohexane under one atmosphere of argon in the presence of triphenylphosphine

The photochemistry of $(CO)_5Cr=C(OMe)Fc$ was investigated in the presence of excess triphenylphosphine in an attempt to trap any CO loss species that may form following irradiation at 355 nm. No changes were observed during steady-state photolysis of $(CO)_5Cr=C(OMe)Fc$ at $\lambda_{exc} > 500$ nm. A small amount of *cis*-$(PPh_3)(CO)_4Cr=C(OMe)Fc$ was formed following steady-state photolysis at $\lambda_{exc} > 390$ nm. Formation of the photoproduct was more efficient at $\lambda_{exc} > 320$ nm. An increase in intensity of the low-energy absorption band of the parent compound at 514 nm was observed during the photolysis with a concomitant decrease and red shift of the higher lying band at 422 nm. A slight increase in absorbance was also observed for the high-energy band at 340 nm. Figure 2 - 6 shows the changes observed in the UV-vis spectrum during the photolysis. Isosbestic points were observed at 372 and 440 nm.

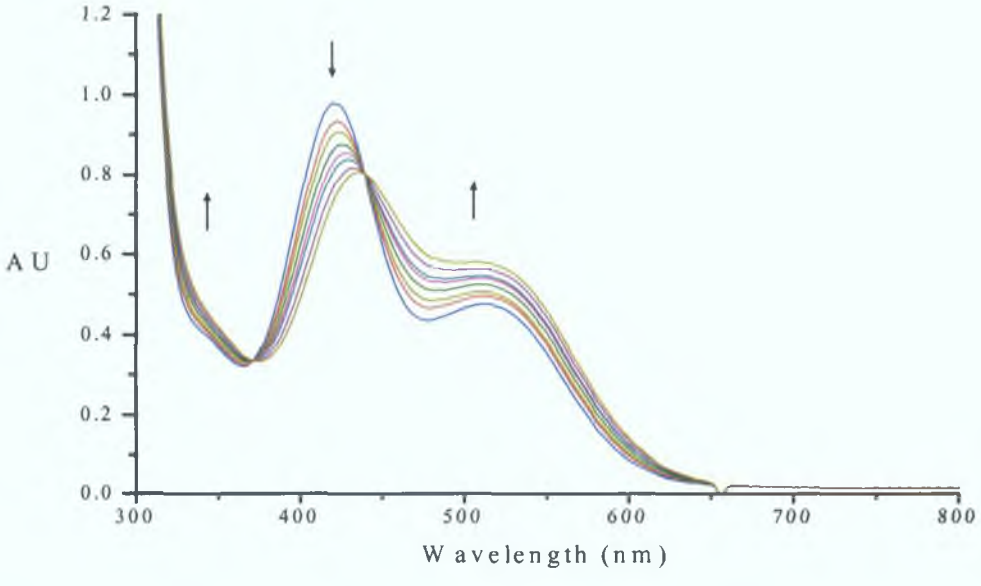

Fig. 2 - 6: UV-vis spectra recorded during steady state photolysis of $(CO)_5Cr=C(OMe)Fc$ at $\lambda_{exc} > 320$ nm in cyclohexane under one atmosphere of argon in the presence of excess triphenylphosphine.

The solution, a light reddish-brown colour, appeared to become slightly darker during the photolysis. After 60 min. of photolysis, when no more changes were apparent in the UV-vis spectrum, the solvent was removed from the sample under reduced pressure and an infrared spectrum (fig. 2 - 7) was recorded of the residual solid in the

carbonyl region of the spectrum. The parent compound was still present at 1940, 1951 and 2057 cm^{-1}, in addition to new peaks at 1895, 1902, 1923, 2000 and 2008 cm^{-1}. The latter ν(CO) absorption bands are indicative of the tetracarbonyl species *cis*-$(PPh_3)(CO)_4Cr{=}C(OMe)Fc$. The presence of two peaks in close proximity at 2000 and 2008 cm^{-1} suggest that there are possibly two isomers of the tetracarbonyl species present. As before, these results suggest that CO loss occurs during photolysis in this region of the spectrum.

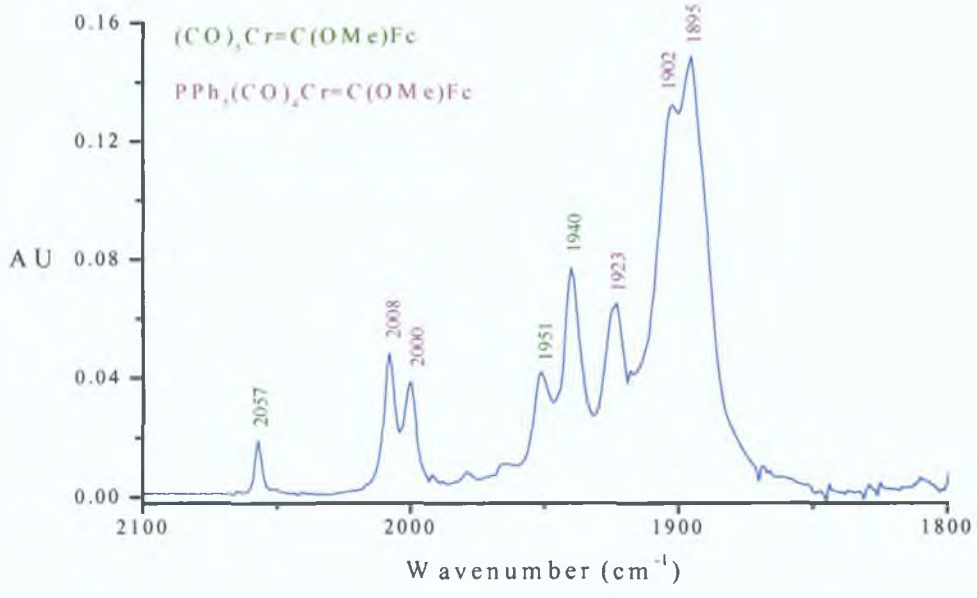

Fig. 2 - 7: Infrared spectrum recorded after steady state photolysis of $(CO)_5Cr{=}C(OMe)Fc$ at $\lambda_{exc} > 320$ nm in cyclohexane under one atmosphere of argon in the presence of excess triphenylphosphine.

2.4.1.3 Laser flash photolysis of $(CO)_5Cr=C(OMe)Fc$ in cyclohexane under one atmosphere of argon in the presence of triphenylphosphine

Absorption measurements were recorded, following pulsed laser excitation at 355 nm of $(CO)_5Cr=C(OMe)Fc$ in cyclohexane under one atmosphere of argon at room temperature in the presence of excess triphenylphosphine. Again, a difference absorption spectrum could not be plotted, again due to low intensity of the signals observed. Following flash photolysis at 355 nm, a rapid increase in the absorbance was observed in the range 320 – 380 nm and 610 – 690 nm. These signals did not recover to the pre-flash absorbance level. Figure 2 - 8 shows the signal observed at 380 nm. The observed changes in the UV-vis and infrared spectra during the experiment are similar to those described in the previous section.

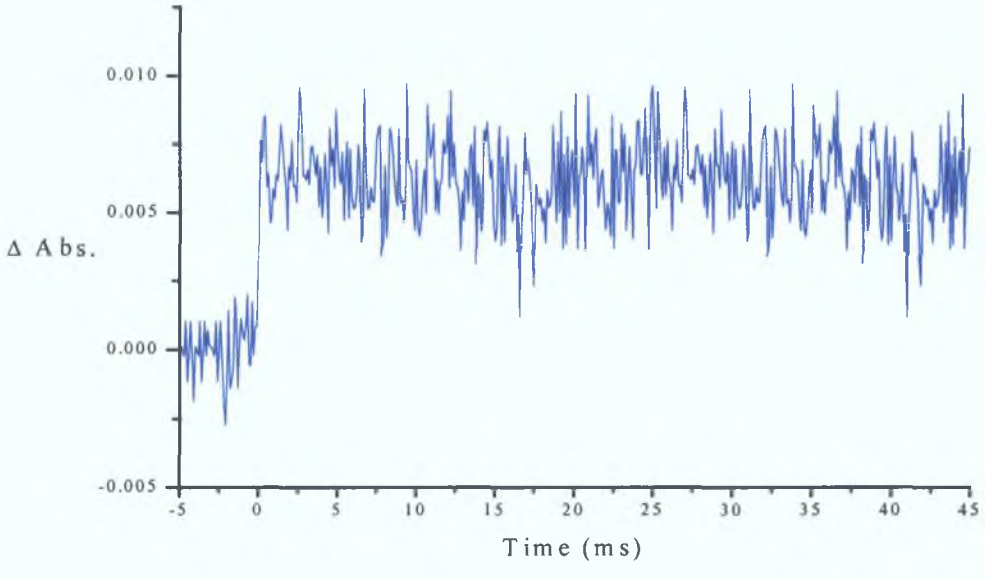

Fig. 2 - 8: Signal observed at 380 nm following laser flash photolysis of $(CO)_5Cr=C(OMe)Fc$ at 355 nm in the presence of excess triphenylphosphine.

2.4.2 Photochemistry of 1,1'-$[(CO)_5Cr{=}C(OMe)]_2Fc$

2.4.2.1 Laser flash photolysis of 1,1'-$[(CO)_5Cr{=}C(OMe)]_2Fc$ in cyclohexane

1,1'-$[(CO)_5Cr{=}C(OMe)]_2Fc$ is a dark brown solid with a UV-vis spectrum exhibiting a low-energy band in the visible region at 464 nm (ε = 7.84 x 10^3 $M^{-1}cm^{-1}$) with a shoulder at 514 nm (ε = 3.14 x 10^3 $M^{-1}cm^{-1}$) and also a higher energy band at 330 nm (ε = 3.04 x 10^3 $M^{-1}cm^{-1}$) in cyclohexane solution (fig. 2 – 9). No transient species were observed following flash photolysis of 1,1'-$[(CO)_5Cr{=}C(OMe)]_2Fc$ at 355 nm in cyclohexane under one atmosphere of carbon monoxide at room temperature. The UV-vis spectrum remained unchanged throughout the photolysis experiment. When this experiment was repeated in the absence of CO, under an atmosphere of argon, weak transients were observed in the region 600 – 510 nm and also between 400 – 360 nm. A transient signal indicating depletion of the parent compound was observed in the region 490 – 430 nm. The absorbance of the UV-vis spectrum decreased slightly as the experiment proceeded indicating some decomposition of the parent compound (fig. 2 – 9). As with the analogous mono-carbene complex $(CO)_5Cr{=}C(OMe)Fc$, a transient absorbance difference spectrum could not be plotted due to the low intensity of the signals observed.

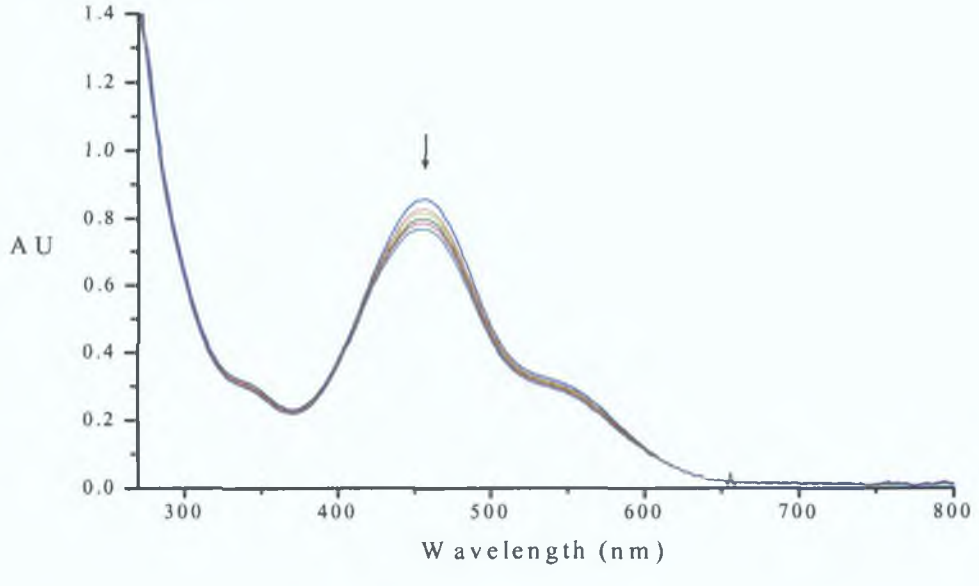

Fig. 2 - 9: UV-vis spectra recorded during laser flash photolysis of 1,1'-$[(CO)_5Cr{=}C(OMe)]_2Fc$ following 355 nm excitation, in cyclohexane under one atmosphere of argon.

A typical transient signal monitored at 540 nm is shown in fig. 2 - 10 (k_{obs} = 454 ± 45 s^{-1}, τ = 2 ± 0.22 ms). Also, the recovery observed at 460 nm is shown in fig. 2 - 11 (k_{obs} = 383 ± 38 s^{-1}, τ = 2 ± 0.26 ms). Both signals fail to recover to the pre-flash absorbance level consistent with the slight depletion observed in the UV-vis spectrum throughout the experiment. On gradually increasing the CO concentration in the sample cell a decrease in lifetime was apparent, thus indicating formation of a CO loss species. Accurate lifetime measurements were again prevented due to the weak intensity of the transient signals. Photolysis was therefore carried out in the presence of a trapping ligand as before, i.e. PPh_3, to confirm formation of a CO loss species. No photochemistry was observed following flash photolysis at 532 nm.

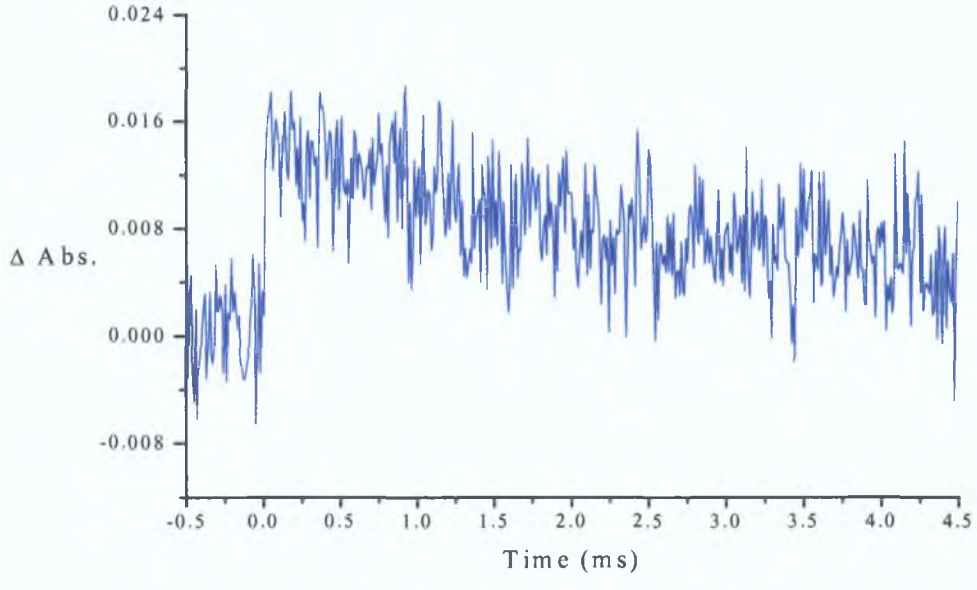

Fig. 2 - 10: Transient signal obtained following laser flash photolysis of 1,1'-$[(CO)_5Cr{=}C(OMe)]_2Fc$ at 355 nm excitation, in cyclohexane under one atmosphere of argon at 540 nm (k_{obs} = 454 ± 45 s^{-1}, τ = 2 ± 0.22 ms).

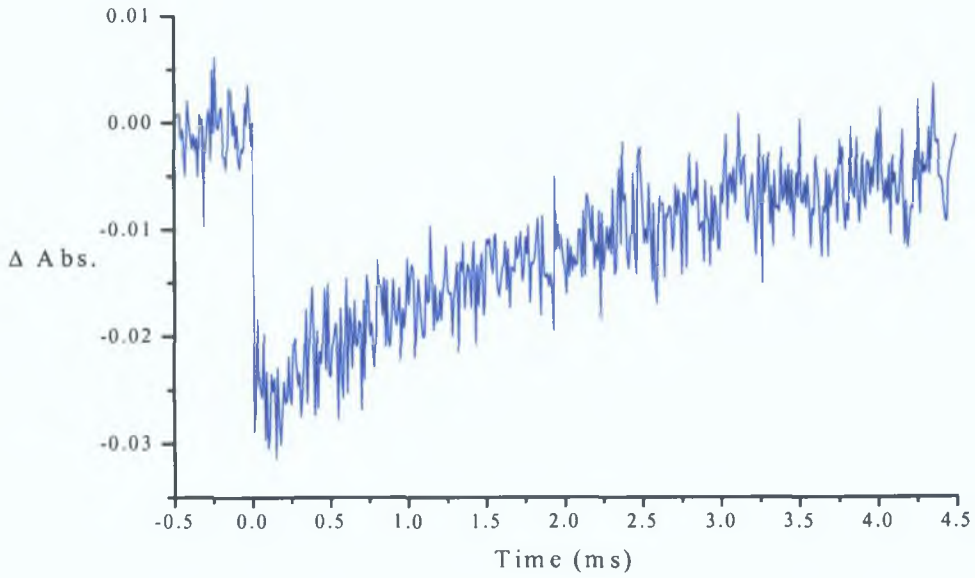

Fig. 2 - 11: Recovery observed following laser flash photolysis of 1,1'-$[(CO)_5Cr{=}C(OMe)]_2Fc$ at 355 nm excitation, in cyclohexane under one atmosphere of argon at 460 nm ($k_{obs} = 383 \pm 38\ s^{-1}$, $\tau = 2 \pm 0.26$ ms).

2.4.2.2 Steady state photolysis of 1,1'-$[(CO)_5Cr=C(OMe)]_2Fc$ in cyclohexane under one atmosphere of argon in the presence of triphenylphosphine

As with the analogous monocarbene complex $(CO)_5Cr=C(OMe)Fc$, the photochemistry of 1,1'-$[(CO)_5Cr=C(OMe)]_2Fc$ was investigated in cyclohexane under 1 atmosphere of argon at room temperature in the presence of an excess of triphenylphosphine in an attempt trap the proposed CO loss transient species formed following flash photolysis at 355 nm. No photochemistry was observed at $\lambda_{exc} > 500$ or $\lambda_{exc} > 400$ nm photolysis indicating that the two lower energy bands of 1,1'-$[(CO)_5Cr=C(OMe)]_2Fc$ at 514 and 464 nm are inactive with respect to CO loss from this complex. The sample was subjected to irradiation at $\lambda_{exc} > 320$ nm for a period of 75 min. A colour change from a reddish brown to a reddish purple was observed during the photolysis. The changes observed in the UV-vis spectrum were similar to those for $(CO)_5Cr=C(OMe)Fc$. Fig. 2 - 12 shows the changes observed in the UV-vis spectrum, which was monitored continuously during the photolysis.

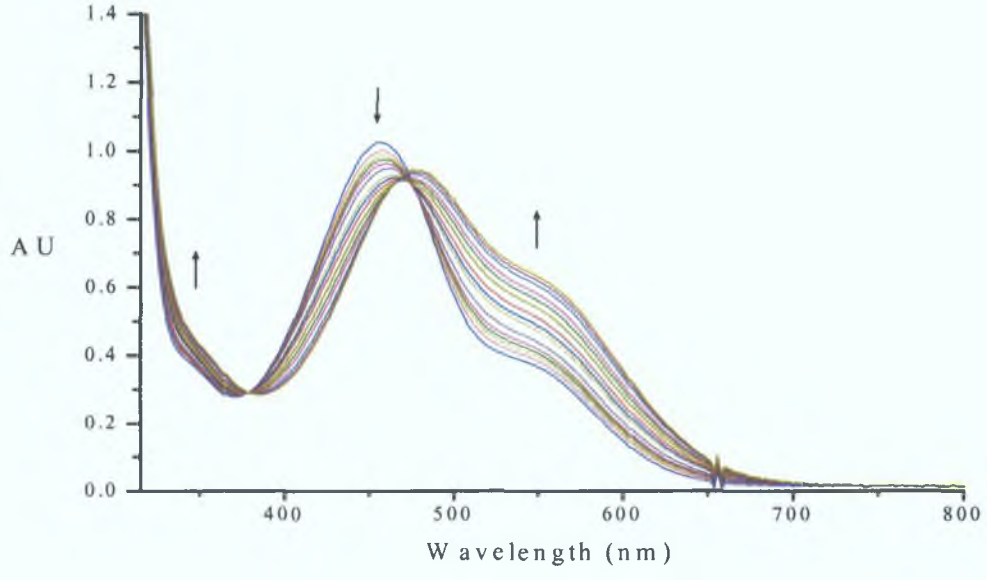

Fig. 2 - 12: UV-vis spectra recorded during steady state photolysis of 1,1'-$[(CO)_5Cr=C(OMe)]_2Fc$ at $\lambda_{exc} > 320$ nm in cyclohexane under one atmosphere of argon in the presence of a triphenylphosphine.

The lower energy absorption band of the parent compound at 514 nm increased in intensity as the photolysis proceeded with a concomitant decrease in the higher lying band at 464 nm, which also underwent a slight red shift to 476 nm. The higher energy band at 330 nm increased in intensity during the photolysis. An isosbestic point was observed at 378 nm.

When no more changes were apparent in the UV-vis spectrum, the solvent was removed from the sample under reduced pressure and an infrared spectrum (1700 – 2200 cm^{-1}) was recorded of the residual purple solid (fig. 2 - 13). A number of new peaks were observed which are possibly due to the formation of more than one tetracarbonyl species. The exact assignments of these peaks have not yet been resolved as there are a number of possible products present, however some pentacarbonyl starting material was still present (evident by the ν(CO) at 2056 cm^{-1}).

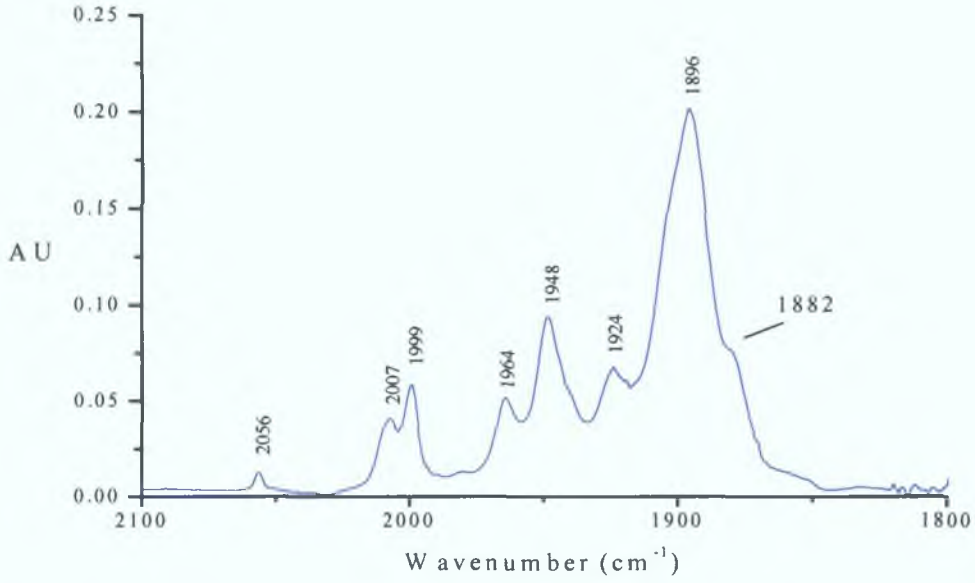

Fig. 2 - 13: Infrared spectrum recorded after steady state photolysis of 1,1'-$[(CO)_5Cr{=}C(OMe)]_2Fc$ at λ_{exc} > 320 nm in cyclohexane under one atmosphere of argon in the presence of excess triphenylphosphine.

The above experiment was repeated in the absence of trapping ligand resulting in the decomposition of the parent compound (fig. 2 - 14). The only new peak observed in the infrared spectrum was a small grow-in of chromium hexacarbonyl at 1981 cm^{-1} confirming the decomposition of the parent compound.

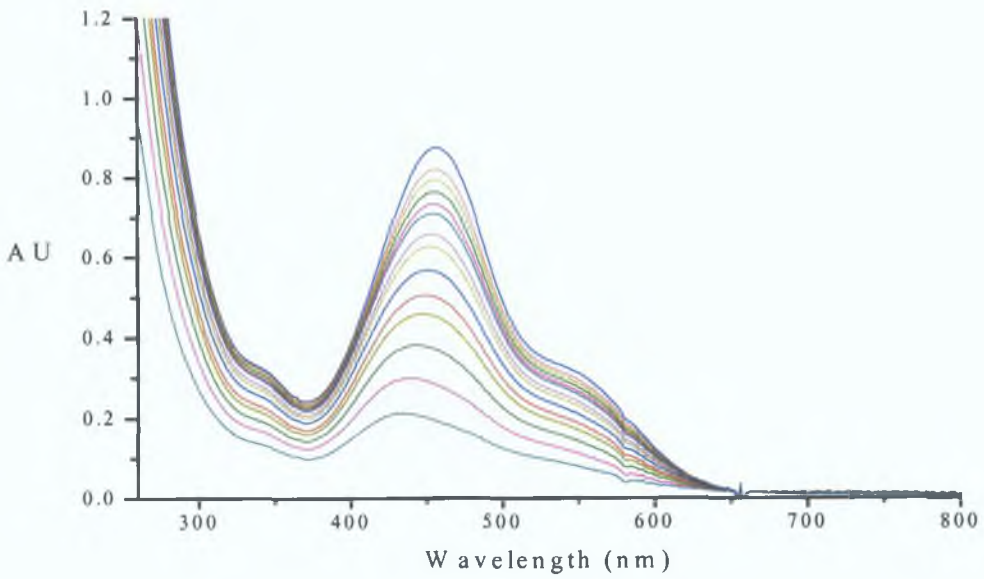

Fig. 2 - 14: UV-vis spectra recorded during steady state photolysis of 1,1'-$[(CO)_5Cr{=}C(OMe)]_2Fc$ at $\lambda_{exc} > 320$ nm in cyclohexane under one atmosphere of argon.

2.4.2.3 Laser flash photolysis of 1,1'-$[(CO)_5Cr{=}C(OMe)]_2Fc$ in cyclohexane under one atmosphere of argon in the presence of triphenylphosphine

Absorption measurements, following pulsed laser excitation at 355 nm of 1,1'-$[(CO)_5Cr{=}C(OMe)]_2Fc$ in cyclohexane under one atmosphere of argon at room temperature in the presence of excess triphenylphosphine showed a rapid increase in the absorbance which was permanent in the range 600 – 490 nm and 390 – 330 nm (very low intensity). A very weak depletion was also observed in the region 460 – 420 nm. Again, it was not possible to obtain a transient absorption difference spectrum due to the low intensity of the signals observed. The changes observed in the UV-vis spectrum throughout the experiment correspond to those observed following steady state photolysis under identical conditions. Fig. 2 - 15 shows the rise in absorbance observed at 530 nm. An infrared spectrum recorded at the end of the flash photolysis experiment was similar to that recorded following steady state photolysis as discussed in the previous section.

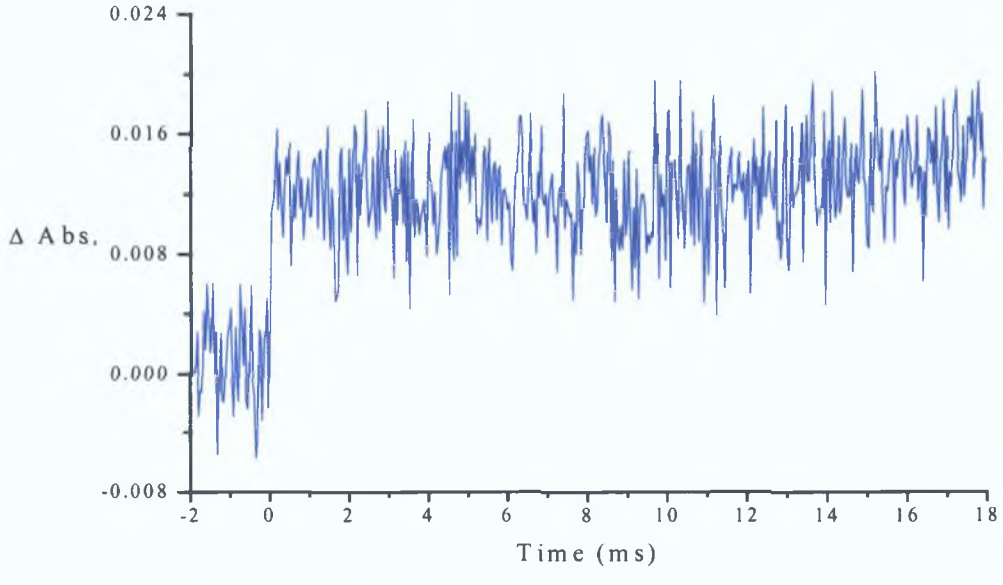

Fig. 2 - 15: Signal observed at 530 nm following laser flash photolysis of 1,1'-$[(CO)_5Cr{=}C(OMe)]_2Fc$ at 355 nm excitation in cyclohexane under one atmosphere of argon in the presence of excess triphenylphosphine.

2.4.3 Photochemistry of $(CO)_5W=C(OMe)Fc$

2.4.3.1 Laser flash photolysis of $(CO)_5W=C(OMe)Fc$ in cyclohexane

$(CO)_5W=C(OMe)Fc$ is a deep red solid with a UV-vis spectrum exhibiting low-energy bands in the visible region of the spectrum at 526 nm ($\varepsilon = 1.19 \times 10^3\ M^{-1}cm^{-1}$) and 408 nm ($\varepsilon = 3.36 \times 10^3\ M^{-1}cm^{-1}$) and a higher energy band at 352 nm ($\varepsilon = 2.03 \times 10^3\ M^{-1}cm^{-1}$) in cyclohexane solution (fig. 2 – 16). The photochemistry of $(CO)_5W=C(OMe)Fc$ was investigated by UV-vis monitored laser flash photolysis with λ_{exc} = 355 and 532 nm in cyclohexane under one atmosphere of carbon monoxide and also under one atmosphere of argon at room temperature.

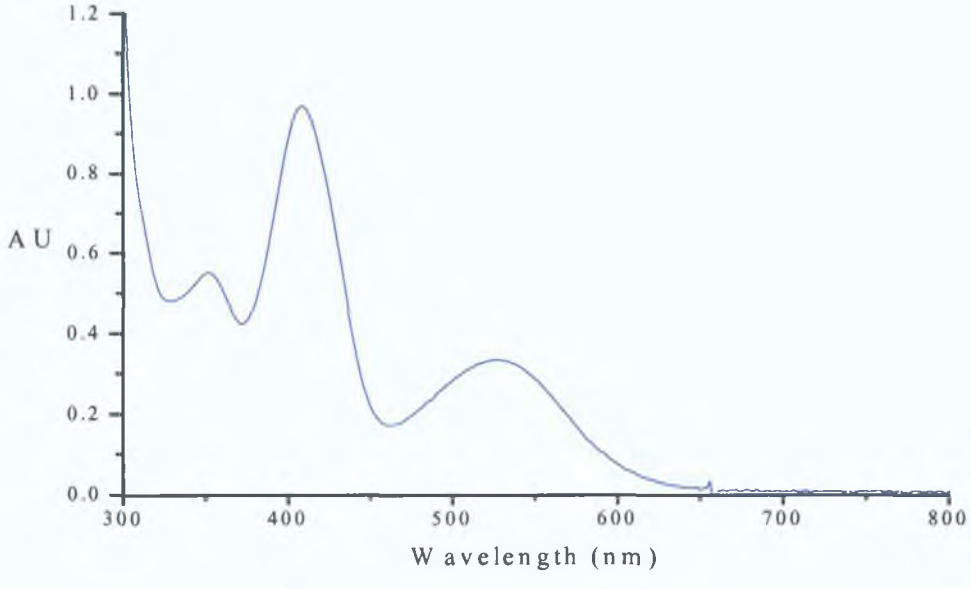

Fig. 2 – 16: The UV-vis spectrum of $(CO)_5W=C(OMe)Fc$ in cyclohexane.

Following flash photolysis at 355 nm under one atmosphere of carbon monoxide depletion of the parent compound is evident in the region of 300 - 340 nm, a typical depletion is shown in fig. 2 – 17. This species recovers to the pre-flash absorbance level, which is indicative of a photoreversible process. Two transient species were also observed between 370 – 480 nm (fig. 2 – 18). Due to the low intensity of the signals observed a transient absorbance difference spectrum could not be plotted. The UV-vis spectrum remained unchanged throughout the experiment.

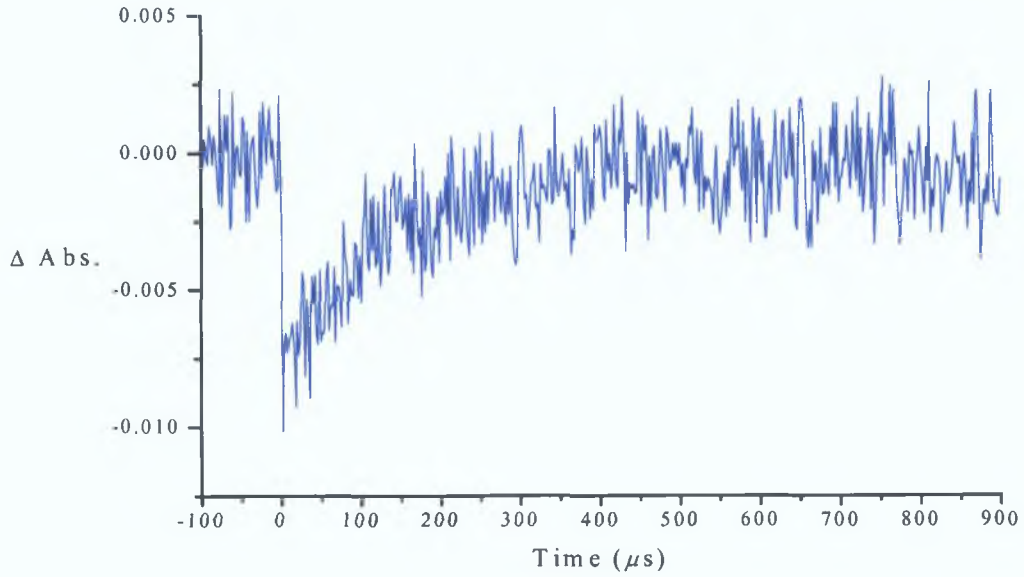

Fig. 2 - 17: Transient signal observed at 310 nm following laser flash photolysis of $(CO)_5W$=C(OMe)Fc at 355 nm excitation, in cyclohexane under one atmosphere of carbon monoxide (k_{obs} = 5387 ± 539 s^{-1}, τ = 185 ± 18.56 μs).

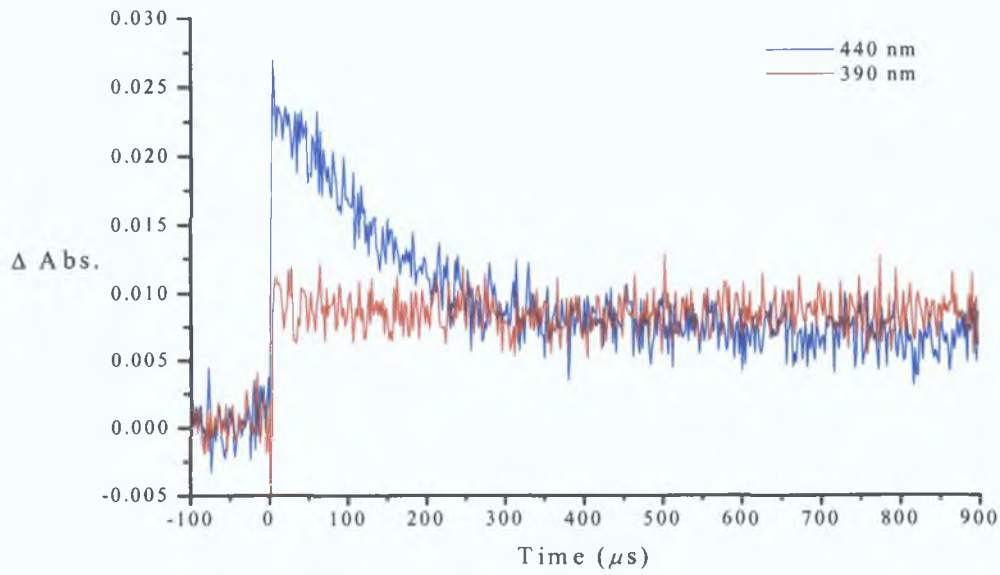

Fig. 2 - 18: Rise in absorption and transient decay observed following photolysis of $(CO)_5W$=C(OMe)Fc at 355 nm excitation in cyclohexane under one atmosphere of carbon monoxide at 390 and 440 nm (k_{obs} = 5334 ± 533 s^{-1}, τ = 187 ± 18.75 μs) respectively.

The observed rate constants for regeneration of the parent compound at 310 nm and the decay of the transient species observed at 440 nm were calculated as k_{obs} = 5387 ± 539 s^{-1} (τ = 185 ± 18 56 μs) and k_{obs} = 5334 ± 533 s^{-1} (τ = 187 ± 18 75 μs) respectively The transient signal observed at 440 nm does not return to the pre-irradiated baseline due to the presence of a second transient species, which can be monitored at 390 nm This second transient species did not return to the pre-irradiated baseline when monitored over 45 ms however the UV-vis spectrum remained unchanged throughout the experiment thus indicating that the parent compound is regenerated, i e the transient species formed is too long-lived to be monitored by the instrumentation available No photochemistry was observed following excitation at 532 nm

The sample was placed under an atmosphere of argon to investigate whether the lifetime of the transient species at 440 nm was dependent on CO concentration A transient signal was observed from 340 – 500 nm Similar transient species were observed as under one atmosphere of carbon monoxide at 390 and 440 nm (fig 2 – 19) The UV-vis spectra recorded throughout the experiment show a slight decomposition of the parent compound (fig 2 - 20) This confirms that the recovery of the parent compound is not photoreversible and has a dependence on carbon monoxide concentration suggesting that CO loss may be occurring No photochemistry was observed for $(CO)_5W$=C(OMe)Fc following irradiation at 532 nm in cyclohexane under similar conditions

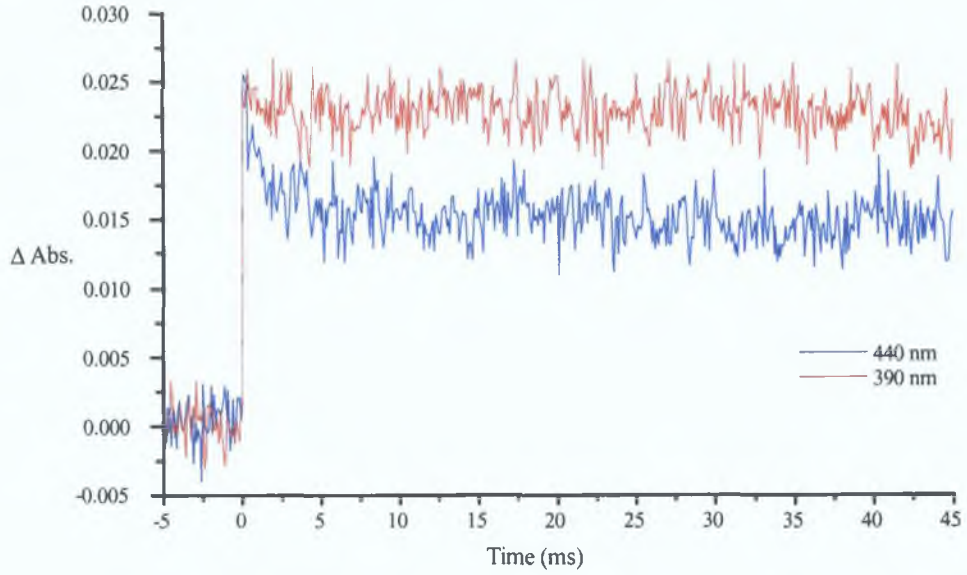

Fig. 2 - 19: Transient signals observed at 390 and 440 nm following photolysis of $(CO)_5W{=}C(OMe)Fc$ at 355 nm, in cyclohexane under one atmosphere of argon.

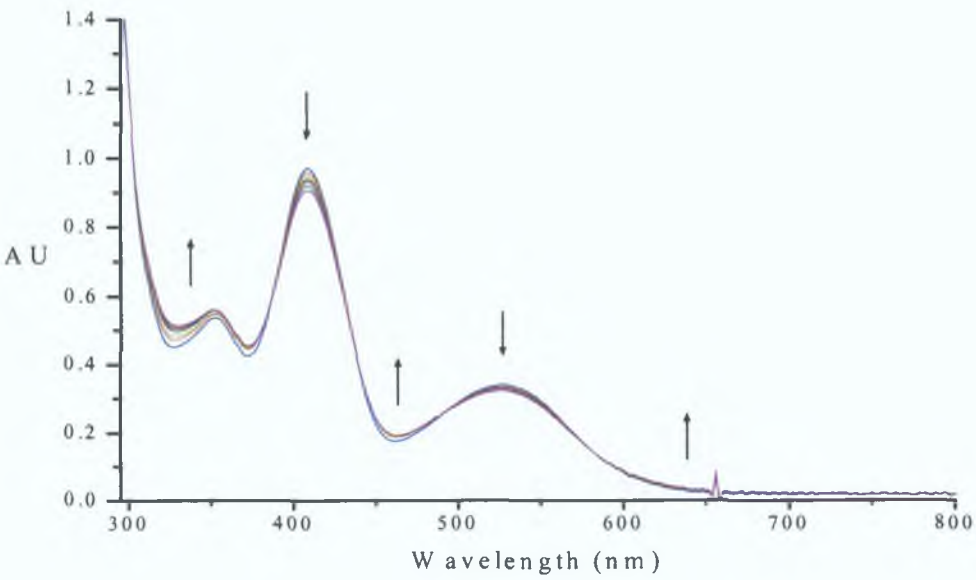

Fig. 2 - 20: UV-vis spectra recorded during laser flash photolysis of $(CO)_5W{=}C(OMe)Fc$ at 355 nm in cyclohexane under one atmosphere of argon.

2.4.3.2 Steady state photolysis of $(CO)_5W$=C(OMe)Fc in cyclohexane under one atmosphere of argon

A sample of $(CO)_5W$=C(OMe)Fc was irradiated at room temperature in cyclohexane under one atmosphere of argon. No changes were observed in the UV-vis spectrum during photolysis at $\lambda_{exc} > 390$ or 500 nm. Changes were observed however following photolysis at $\lambda_{exc} > 320$ nm (for up to 160 min). The UV-vis spectra recorded throughout the experiment show an increase in absorption of the band at 352 nm and also in the valleys between the absorption maxima of the parent compound. A slight decrease in absorption also occurred at high energy resulting in an isosbestic point at 312 nm (fig. 2 - 21). An infrared spectrum recorded at the end of the experiment following the photolysis only showed the presence of the parent compound $(CO)_5W$=C(OMe)Fc.

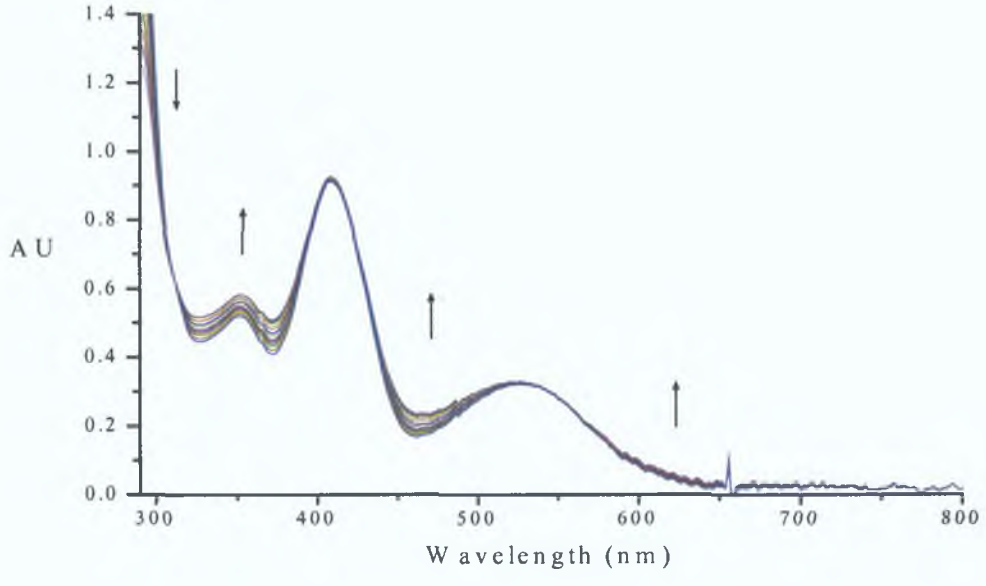

Fig. 2 - 21: UV-vis spectra recorded during steady state photolysis of $(CO)_5W$=C(OMe)Fc at $\lambda_{exc} > 320$ nm in cyclohexane under one atmosphere of argon.

2.4.3.3 Steady state photolysis of $(CO)_5W$=C(OMe)Fc in cyclohexane under one atmosphere of argon in the presence of triphenylphosphine

The photochemistry of $(CO)_5W$=C(OMe)Fc was investigated in the presence of excess triphenylphosphine in an attempt to trap the CO loss species that was thought to form following excitation at 355 nm. $(CO)_5W$=C(OMe)Fc was irradiated in cyclohexane under one atmosphere of argon at room temperature in the presence of excess triphenylphosphine. A small amount of *cis*-$(PPh_3)(CO)_4W$=C(OMe)Fc was formed following steady-state photolysis at $\lambda_{exc} > 320$ nm. No changes were observed during photolysis at $\lambda_{exc} > 390$ or 500 nm.

An increase in intensity of the low-energy absorption band of the parent compound at 526 nm was observed during photolysis with a concomitant decrease and red shift of the higher lying band at 408 nm. An increase in absorption was also observed for the high-energy band at 352 nm. Figure 2 - 22 shows the changes observed in the UV-vis spectrum, monitored during the photolysis. Isosbestic points were observed at 395 and 416 nm.

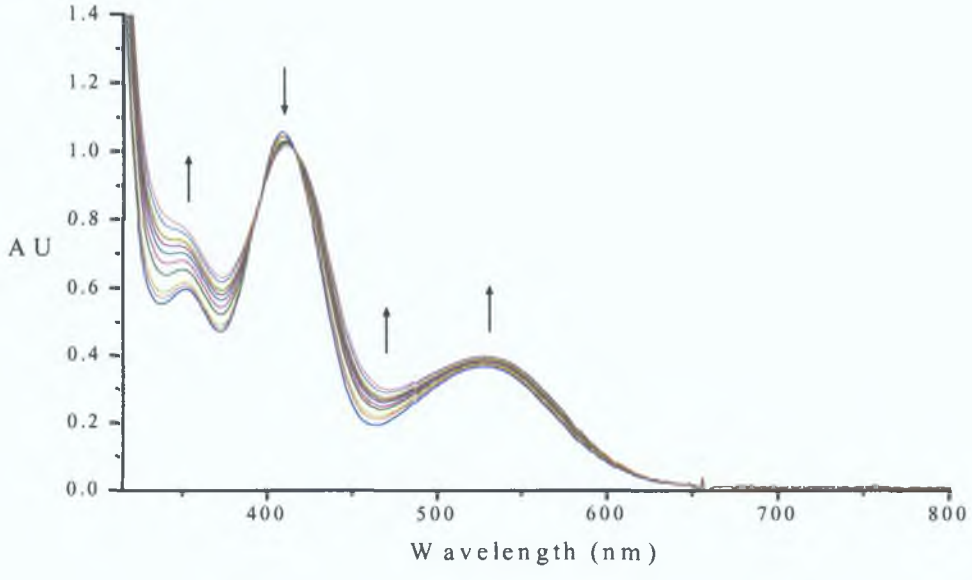

Fig. 2 - 22: UV-vis spectra recorded during steady state photolysis of $(CO)_5W$=C(OMe)Fc at $\lambda_{exc} > 320$ nm in cyclohexane under one atmosphere of argon in the presence of excess triphenylphosphine.

After 50 min. of photolysis, when no more changes were apparent in the UV-vis spectrum, the solvent was removed under reduced pressure and an infrared spectrum (fig. 2 - 23) was recorded of the residual solid. The parent compound was present at 1940, 1951 and 2057 cm^{-1}, however peaks indicative of the tetracarbonyl species *cis*-$(PPh_3)(CO)_4W{=}C(OMe)Fc$ were also present. As before, these results suggest that CO loss occurs following photolysis in this region of the spectrum.

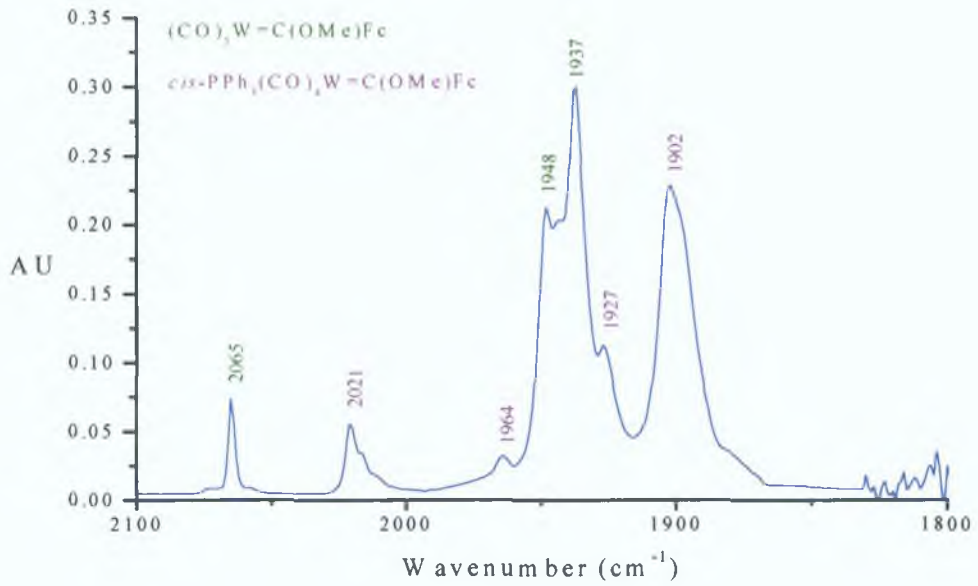

Fig. 2 - 23: Infrared spectrum recorded after steady state photolysis of $(CO)_5W{=}C(OMe)Fc$ at $\lambda_{exc} > 320$ nm in cyclohexane under one atmosphere of argon in the presence of excess triphenylphosphine.

2.4.3.4 Laser flash photolysis of $(CO)_5W$=C(OMe)Fc in cyclohexane under one atmosphere of argon in the presence of triphenylphosphine

Laser flash photolysis at λ_{exc} = 355 nm was carried out on $(CO)_5W$=C(OMe)Fc in cyclohexane, under one atmosphere of argon in the presence of excess triphenylphosphine at room temperature. Again, a transient absorption difference spectrum was not obtained due to the low intensity of the signals. Following flash photolysis at 355 nm, a transient signal such as that shown in fig. 2 – 24 was observed between 490 – 310 nm. These signals did not return to the pre-flash absorbance level. Also, the signals are observed in the same region that absorption occurs in the UV-vis spectrum. An infrared spectrum recorded after the flash photolysis experiment showed similar changes to those observed at the end of the steady state photolysis experiment under comparable conditions.

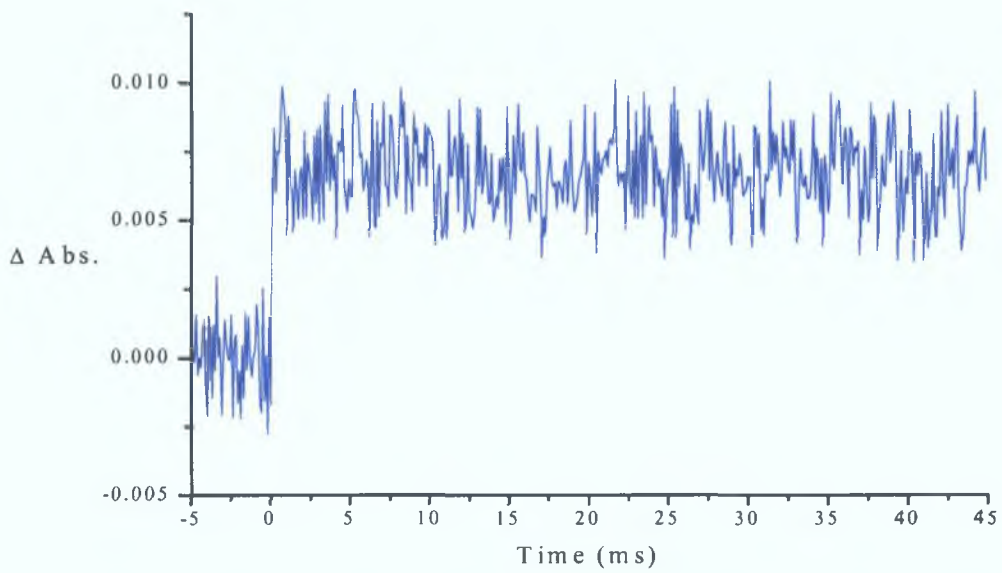

Fig. 2 - 24: Signal observed at 330 nm following laser flash photolysis of $(CO)_5W$=C(OMe)Fc at 355 nm under one atmosphere of argon in the presence of excess triphenylphosphine.

2.4.4 Photochemistry of 1,1'-[$(CO)_5W$=C(OMe)]$_2$Fc

2.4.4.1 Laser flash photolysis of 1,1'-[$(CO)_5W$=C(OMe)]$_2$Fc in cyclohexane

1,1'-[$(CO)_5W$=C(OMe)]$_2$Fc is a dark red/brown solid with a UV-vis spectrum exhibiting low-energy bands in the visible region of the spectrum at 548 nm (ε = 5.68 x 10^3 $M^{-1}cm^{-1}$) and 430 nm (ε = 1.55 x 10^4 $M^{-1}cm^{-1}$) and a higher energy band at 352 nm (ε = 7.96 x 10^3 $M^{-1}cm^{-1}$) in cyclohexane solution (fig. 2 – 25). The photochemistry of 1,1'-[$(CO)_5W$=C(OMe)]$_2$Fc was investigated by UV-vis monitored laser flash photolysis with λ_{exc} = 355 and 532 nm in cyclohexane under one atmosphere of carbon monoxide and also under one atmosphere of argon at room temperature. However, no transient signals were observed in this study.

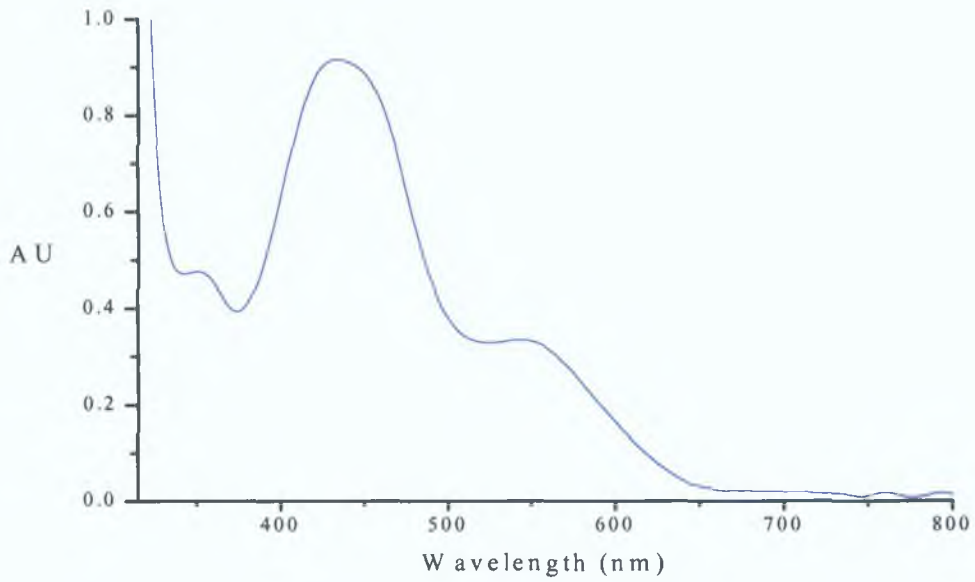

Fig. 2 – 25: UV-vis absorption spectrum of 1,1'-[$(CO)_5W$=C(OMe)]$_2$Fc in cyclohexane.

2.4.4.2 Steady state photolysis of 1,1'-[(CO)$_5$W=C(OMe)]$_2$Fc in cyclohexane under one atmosphere of argon in the presence of triphenylphosphine

The photochemistry of 1,1'-[(CO)$_5$W=C(OMe)]$_2$Fc was subsequently investigated in the presence of excess triphenylphosphine in an attempt to trap any possible CO loss species that may occur following irradiation at λ_{exc} > 320 nm. One sample was irradiated (λ_{exc} > 320 nm) in cyclohexane under one atmosphere of argon at room temperature in the presence of excess triphenylphosphine for a total of two hours. An increase in intensity of the low-energy absorption band of the parent compound at 548 nm was observed during the photolysis with a concomitant decrease and red shift of the higher lying band at 430 nm. A slight increase was also observed of the high-energy band at 352 nm. Figure 2 - 26 shows the changes observed in the UV-vis spectrum, monitored throughout the photolysis. Isosbestic points were observed at 392 and 468 nm.

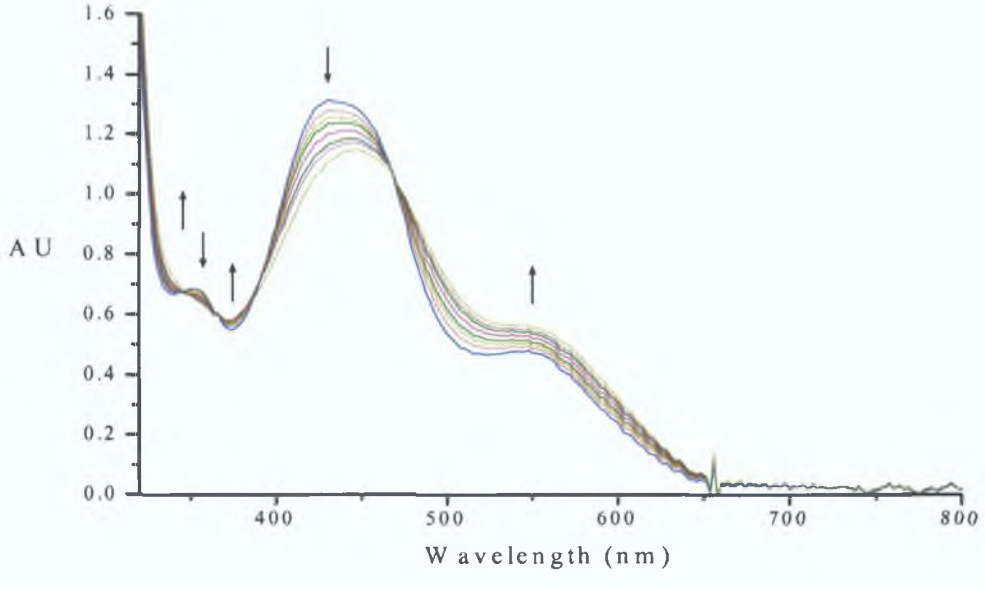

Fig. 2 - 26: UV-vis spectra recorded during steady state photolysis of 1,1'-[(CO)$_5$W=C(OMe)]$_2$Fc at λ_{exc} > 320 nm in cyclohexane under one atmosphere of argon in the presence of excess triphenylphosphine.

The solution, a light reddish-brown colour, appeared to become slightly darker during the photolysis. After 120 min. of photolysis, when no more changes were apparent in the UV-vis spectrum, the solvent was removed under reduced pressure and an infrared spectrum (fig. 2 - 27) was recorded of the residual solid.

From the IR spectrum, in addition to the bis-pentacarbonyl starting material at 1938, 1948 and 2064 cm^{-1}, at least two photoproducts were evident at 1881, 1897, 1964, 2010 and 2016 cm^{-1}, i.e. 1,1'-[*cis*-$(PPh_3)(CO)_4W{=}C(OMe)]_2Fc$ and 1-[*cis*-$(PPh_3)(CO)_4W{=}C(OMe)]$-1'-$[(CO)_5W{=}C(OMe)]Fc$. No changes were observed when the same sample was irradiated at $\lambda_{exc} > 390$ or 500 nm.

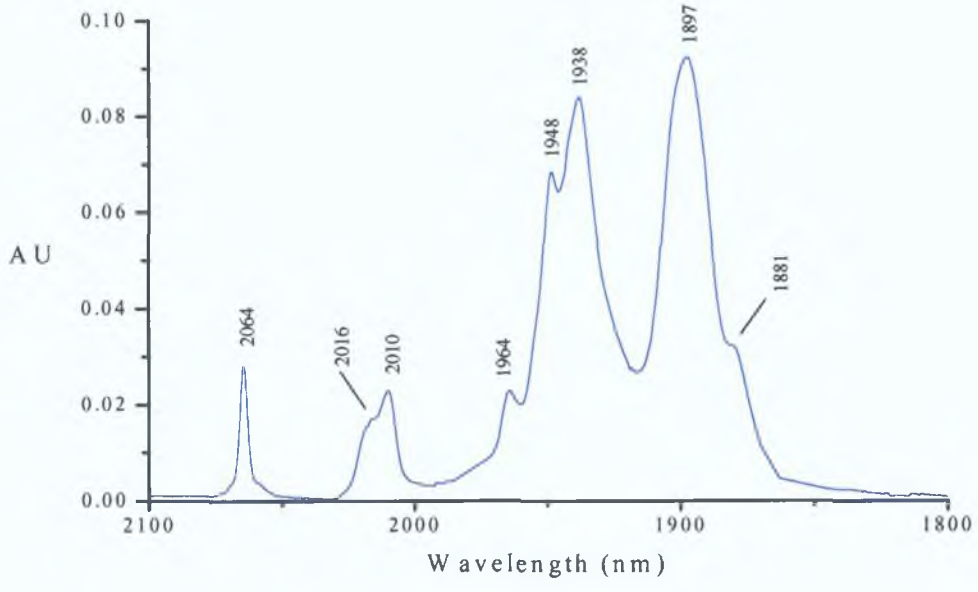

Fig. 2 - 27: Infrared spectrum recorded following steady state photolysis ($\lambda_{exc} > 320$ nm) of 1,1'-$[(CO)_5W{=}C(OMe)]_2Fc$ in cyclohexane under one atmosphere of argon in the presence of excess of triphenylphosphine.

2.4.5 Solvatochroism

The solvatochromic data for the two low-energy bands of compounds $(CO)_5M{=}C(OMe)Fc$ and 1,1'-$[(CO)_5M{=}C(OMe)]_2Fc$ (M = Cr, W) is shown in table 2 – 1. Some examples of solvatochromic behaviour are shown in figure 2 – 28 and figure 2 – 29 (all spectra have been normalised at the high-energy LF band).

	Cyclohexane	Toluene	Dichloromethane	Methanol	Acetonitrile
$(CO)_5Cr{=}C(OMe)Fc$	422	416	416	408	406
	522	518	518	518	518
$(CO)_5W{=}C(OMe)Fc$	408	406	404	400	400
	526	532	530	530	530
1,1'-$[(CO)_5Cr{=}C(OMe)]_2$-Fc	458	452	448	444	442
	520 (sh)	520 (sh)	520 (sh)	520 (sh)	520 (sh)
1,1'-$[(CO)_5W{=}C(OMe)]_2$-Fc	430	426	428	410	412
	548	538	524 (sh)	524 (sh)	524 (sh)

Table 2 – 1

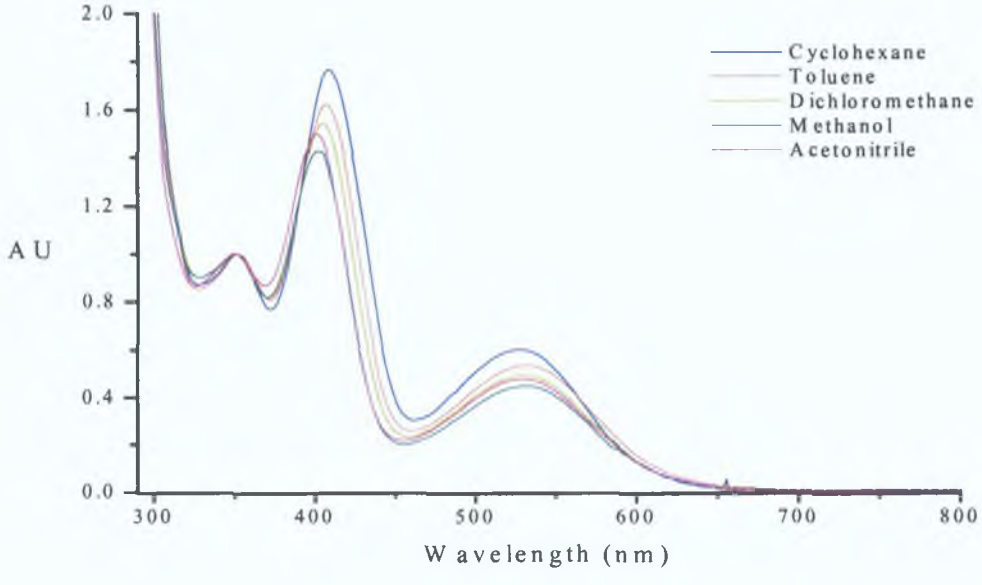

Fig. 2 – 28: UV-vis spectra displaying the solvatochromic behaviour of $(CO)_5W{=}C(OMe)Fc$ in various solvents.

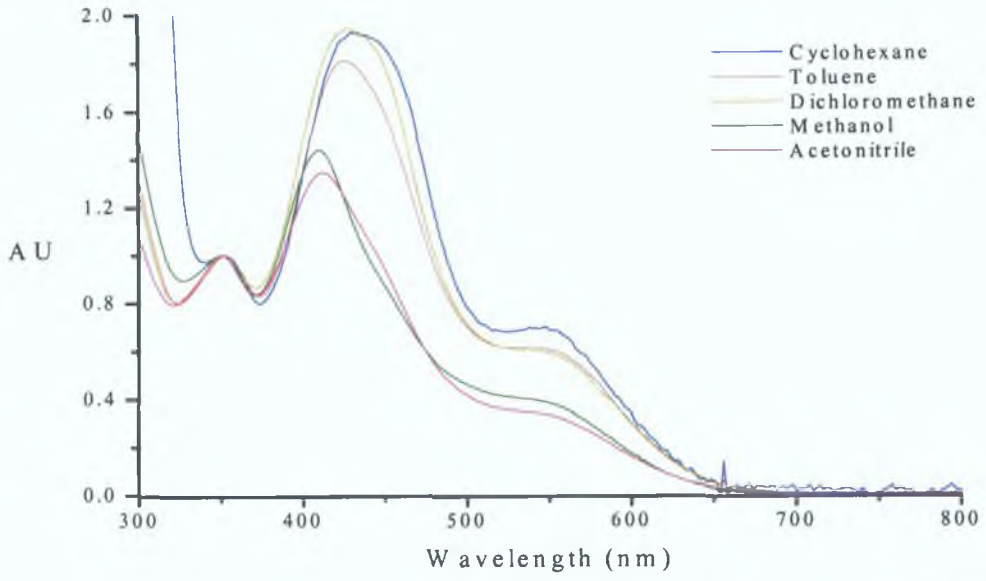

Fig. 2 – 29: UV-vis spectra displaying the solvatochromic behaviour of 1,1'-$[(CO)_5W{=}C(OMe)]_2Fc$ in various solvents.

2.4.6 Electrochemistry

Electrochemistry was performed in dry acetonitrile under argon with 0.1 M [*n*-BuN_4][BF_4] as supporting electrolyte. A three-electrode set up was used for all measurements with a glassy carbon working electrode (2 mm diameter), a platinum wire auxiliary electrode and a saturated calomel reference electrode. $E_{1/2}$ values were determined as $(E_{pa} + E_{pc})/2$, where E_{pa} and E_{pc} are the anodic and cathodic peak potentials, respectively (it is assumed that $E_{1/2} \approx E^{0'}$ for all measurements). All potentials are quoted in reference to the ferrocene/ferrocenium couple. Table 2 - 2 contains a list of the redox potentials recorded. An example of a typical cyclic voltammogram for $(CO)_5Cr{=}C(OMe)Fc$ is shown in figure 2 – 30.

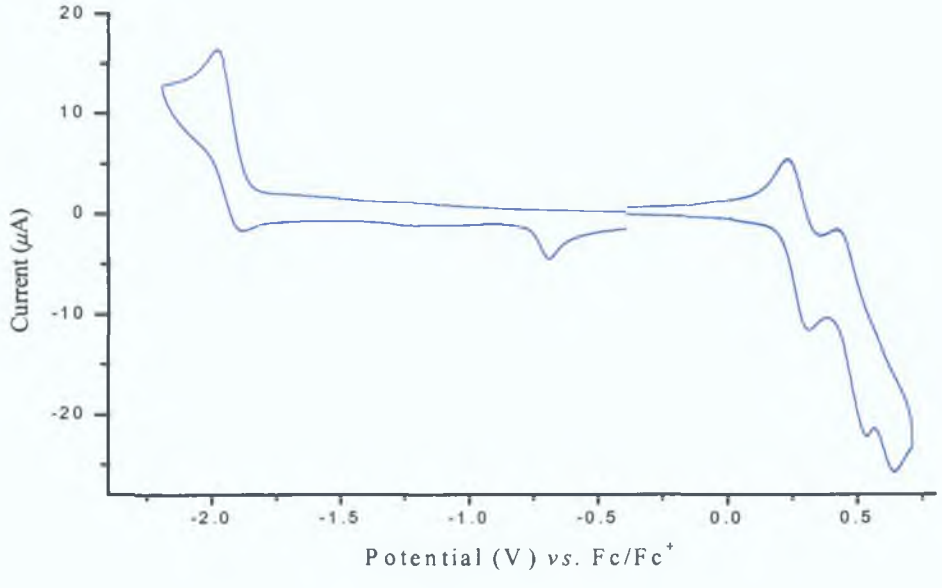

Fig. 2 – 30: Cyclic voltammogram of $(CO)_5Cr{=}C(OMe)Fc$ dissolved in dry acetonitrile containing 0.1 M [*n*-Bu_4N][BF_4]. The working electrode was a 1 mm radius glassy carbon disk and the scan rate was 0.1 Vs^{-1}.

	oxidation				
	1st			2nd	
	E_{pa}	E_{pc}	$E_{1/2}$	E_{pa}	E_{pc}
$(CO)_5Cr=C(OMe)Fc$	0 270	0 276	0 273	0 493	0 468
$1,1'-[(CO)_5Cr=C(OMe)]_2-Fc$	0 462	0 471	0 467	0 635	~
$(CO)_5W=C(OMe)Fc$	0 286	0 274	0 280	0 697	~
$1,1'-[(CO)_5W=C(OMe)]_2-Fc$	0 414	~	~	~	~

Table 2 - 2

	3^{rd}	reduction		
$E_{1/2}$	E_{pa}	E_{pc}	E_{pa}	$E_{1/2}$
0 481	0 599	-1 939	-1 921	-1 930
~	~	-1 635	~	~
~	~	-1 896	-1 899	-1 898
~	~	-1 899	~	~

Compounds $(CO)_5Cr=C(OMe)Fc$, $(CO)_5W=C(OMe)Fc$ and 1,1'-$[(CO)_5Cr=C(OMe)]_2$-Fc each display a reversible first oxidation step at half-wave potentials of $E_{1/2}$ = 0 273, 0 280 and 0 467 V respectively, which is ascribed to the ferrocene/ferrocenium couple [38] This ferrocene based HOMO orbital is therefore stabilised by successive substitution with the Fischer carbene unit Oxidation of this orbital in the bis-carbene complex 1,1'-$[(CO)_5W=C(OMe)]_2$-Fc is irreversible, however it does show an anodic peak at E_{ap} = 0 414 V indicating stabilisation of this orbital with respect to the mono-carbene analogue $(CO)_5W=C(OMe)Fc$ The bis-chromium carbene complex 1,1'-$[(CO)_5Cr=C(OMe)]_2$-Fc shows the greatest stabilisation of the HOMO orbital A second reversible oxidation is observed for $(CO)_5Cr=C(OMe)Fc$ at $E_{1/2}$ = 0 481 V and is assigned to oxidation of the metal carbene moiety [38] This oxidation occurs at a higher potential for the tungsten analogue $(CO)_5W=C(OMe)Fc$ however it is no longer reversible, E_{ap} = 0 697 V This process is also irreversible and at a higher potential for the bis-chromium carbene complex 1,1'-$[(CO)_5Cr=C(OMe)]_2$-Fc , E_{ap} = 0 635 V No further oxidation processes are observed for the bis-tungsten carbene complex 1,1'-$[(CO)_5W=C(OMe)]_2$-Fc $(CO)_5Cr=C(OMe)Fc$ also shows a third irreversible oxidation at E_{ap} = 0 599 V

Reduction of the complexes $(CO)_5M=C(OMe)Fc$ and 1,1'-$[(CO)_5M=C(OMe)]_2$-Fc (M = Cr, W) involves population of the carbene p_x LUMO orbital and is reversible for each of the mono-carbene complexes $(CO)_5Cr=C(OMe)Fc$ and $(CO)_5W=C(OMe)Fc$ undergo reduction at half-wave potentials of $E_{1/2}$ = -1 930 and –1 898 V respectively The bis-carbene complexes both display an irreversible reduction at E_{cp} = -1 635 and –1 899 V for the chromium and tungsten complexes respectively Although 1,1'-$[(CO)_5Cr=C(OMe)]_2$-Fc has the most stabilised HOMO orbital of the four complexes studied it also shows the most stabilised LUMO orbital (based on E_{cp} values as it displays an irreversible reduction) Thus, of the four complexes studied, 1,1'-$[(CO)_5Cr=C(OMe)]_2$-Fc displays the lowest HOMO-LUMO energy gap

2.4.7 X-ray crystal structure analysis

Crystals of $(CO)_5Cr=C(OMe)Fc$,[i] 1,1'-$[(CO)_5Cr=C(OMe)]_2Fc$ and 1,1'-$[(CO)_5W=C(OMe)]_2Fc$ were grown from saturated chloroform/cyclohexane (1 :1) solutions in an inert atmosphere.

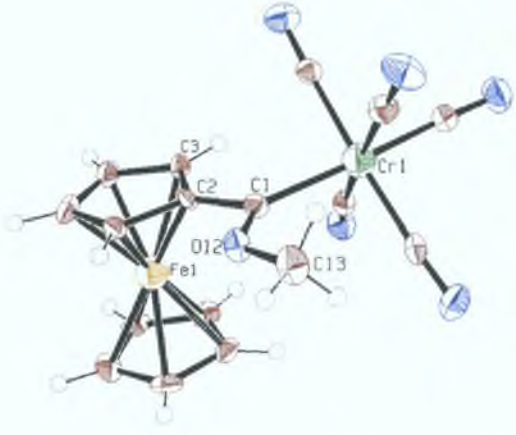

Fig. 2 – 31: ORTEP-III[39] diagram showing the x-ray crystal structure of $(CO)_5Cr=C(OMe)Fc$. Crystal data and experimental parameters are summarised in appendix A2.

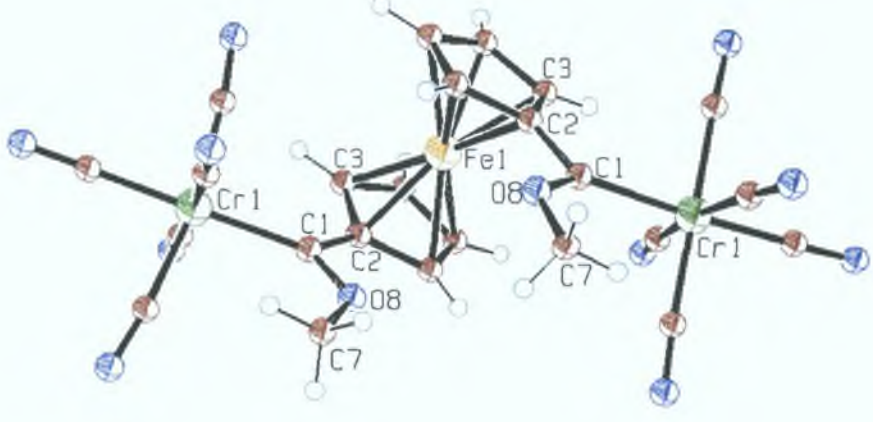

Fig. 2 – 32: ORTEP-III[39] diagram showing the x-ray crystal structure of 1,1'-$[(CO)_5Cr=C(OMe)]_2Fc$. Crystal data and experimental parameters are summarised in appendix A3.

[i] Collection of crystallographic data was carried out by Dr. Sylvia Draper, Department of Chemistry, Trinity College Dublin.

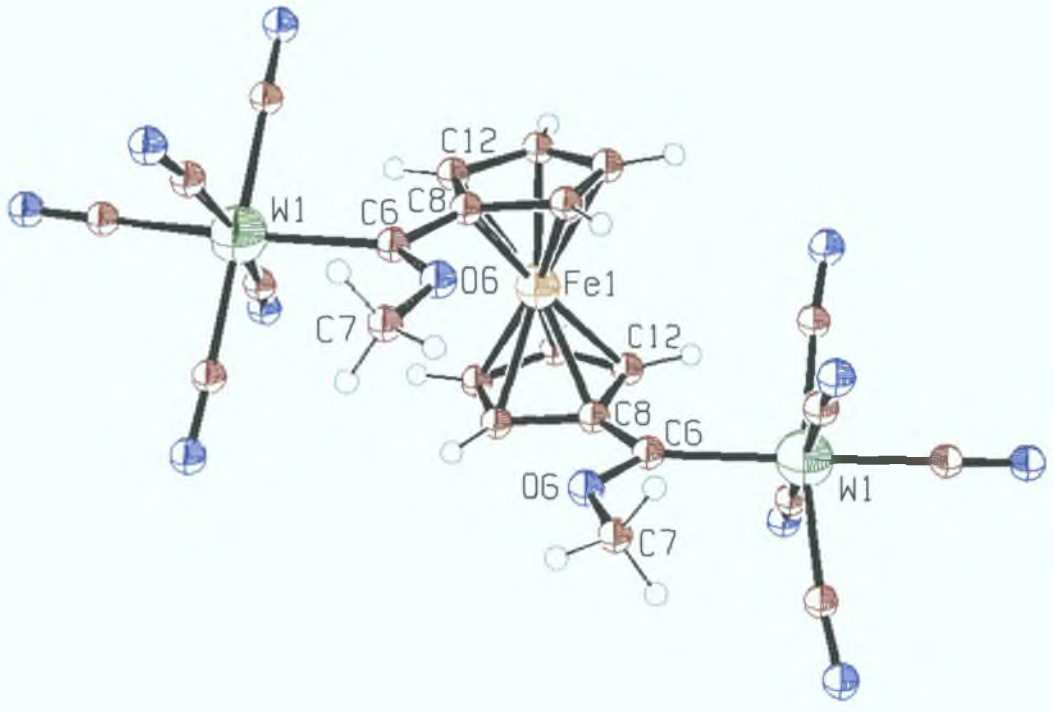

Fig. 2 – 33: ORTEP-III[39] diagram showing the x-ray crystal structure of 1,1'-$[(CO)_5W{=}C(OMe)]_2Fc$. Crystal data and experimental parameters are summarised in appendix A4.

$(CO)_5Cr{=}C(OMe)Fc$ displays a nearly perfect coplanar conformation between the ferrocenyl donor and the carbene substituent with a dihedral angle of 2.26^0 between C_3 and the O_{12}-C_1-C_2 plane. 1,1'-$[(CO)_5Cr{=}C(OMe)]_2Fc$ is slightly more distorted with a dihedral angle of 5.33^0 between C_3 and the O_8-C_1-C_2 plane. 1,1'-$[(CO)_5W{=}C(OMe)]_2Fc$ displays a dihedral angle of 4.94^0 between C_{12} and the O_6-C_8-C_{12} plane. The π-π overlap of the two bis-carbene systems however is not suppressed to a significant extent as evident in their UV-vis and electrochemistry data.

Cr-$C_{carbene}$ bond lengths of 2.088 and 2.072 Å are observed for both the mono- and bis-chromium substituted complexes respectively in comparison to 2.051 Å reported for the mono-carbene complex (*E,E'*)-$(CO)_5Cr{=}C(OMe)C_4H_4Fc$, which features a butadiene spacer between the ferrocene and Fischer-carbene units.[38] There is thus greater double bond character found in the Cr-$C_{carbene}$ bond of (*E,E'*)-$(CO)_5Cr{=}C(OMe)C_4H_4Fc$ than for the directly bonded systems. A W-$C_{carbene}$ bond length of 2.212 Å is observed for 1,1'-$[(CO)_5W{=}C(OMe)]_2Fc$.

$(CO)_5Cr=C(OMe)Fc$, 1,1'-$[(CO)_5Cr=C(OMe)]_2Fc$ and 1,1'-$[(CO)_5W=C(OMe)]_2Fc$ show $C_{carbene}$-$O_{methoxy}$ bond lengths of 1 420, 1 327 and 1 326 Å respectively indicating substantial double bond character, which is more pronounced in the bis-carbene systems These complexes therefore have a predominantly polar ground state, as observed in the UV-vis studies (resonance structure II, fig 2 – 33 and fig 2 – 34), which is typical of Fischer-carbene systems The butadiene bridged complex *E,E'*-$(CO)_5Cr=C(OMe)C_4H_4Fc$ shows an analogous $C_{carbene}$-$O_{methoxy}$ bond length of 1 332 Å [38]

The $C_{carbene}$-C_{Cp} bonds in $(CO)_5Cr=C(OMe)Fc$, 1,1'-$[(CO)_5Cr=C(OMe)]_2Fc$ and 1,1'-$[(CO)_5W=C(OMe)]_2Fc$ have slight double bond character with bond lengths of 1 462, 1 466 and 1 455 Å respectively indicating a small contribution from the fulvene type resonance structure also in these systems (resonance structure III, fig 2 – 33 and fig 2 – 34)

The π-systems of each of these complexes display a staggered configuration with respect to the Fischer-carbene moiety, however this does not appear to affect the communication between the carbene and pentacarbonyl units, presumably due to the low barrier for rotation of the Cr=C bond in such systems [40] It should be also noted that each of the methoxy substituents crystallise in the *anti*-configuration, which favours the formation of an agostic interaction following photodissociation of a CO ligand

Figure 2 – 33 shows a crystal packing diagram for $(CO)_5Cr=C(OMe)Fc$, which crystallises in the orthorhombic Pca2(1) space group Eight molecules of (*E*)-$(CO)_5Cr=C(C_4H_8N)C_2H_2Fc$ are contained in the unit cell Figures 2 – 34 and 2 – 35 show the crystal packing diagrams for 1,1'-$[(CO)_5Cr=C(OMe)]_2Fc$ and 1,1'-$[(CO)_5W=C(OMe)]_2Fc$ respectively, which both crystallise in the orthorhombic Pbcn space group with a total of six molecules contained in their unit cells

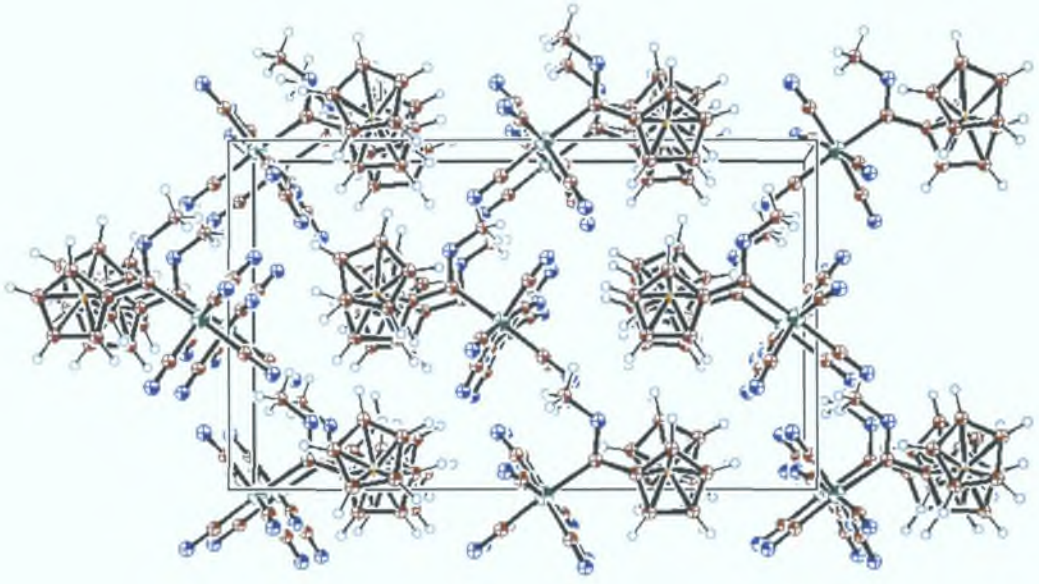

(a)

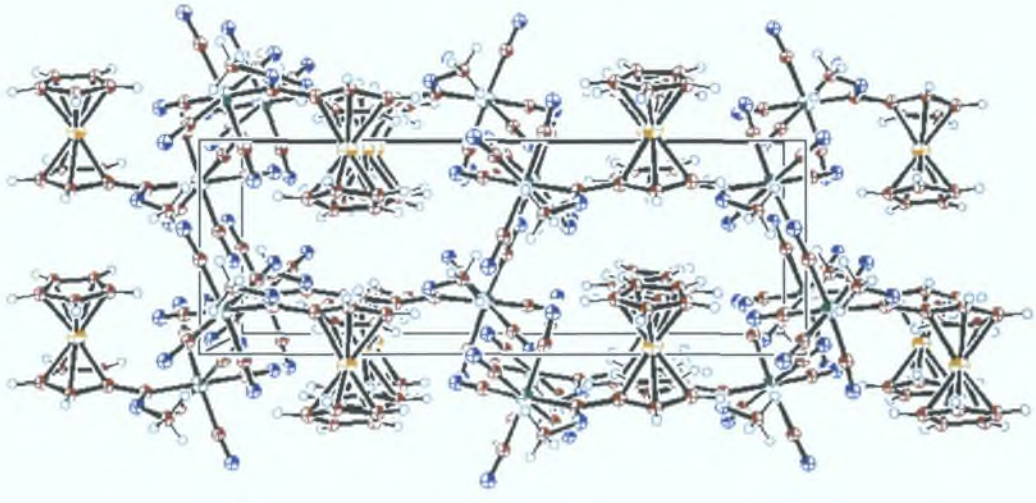

(b)

Fig. 2 – 33: Crystal packing diagrams for the $(CO)_5Cr{=}C(OMe)Fc$ unit cell viewed (a) normal to the (010) plane and (b) normal to the (001) plane.

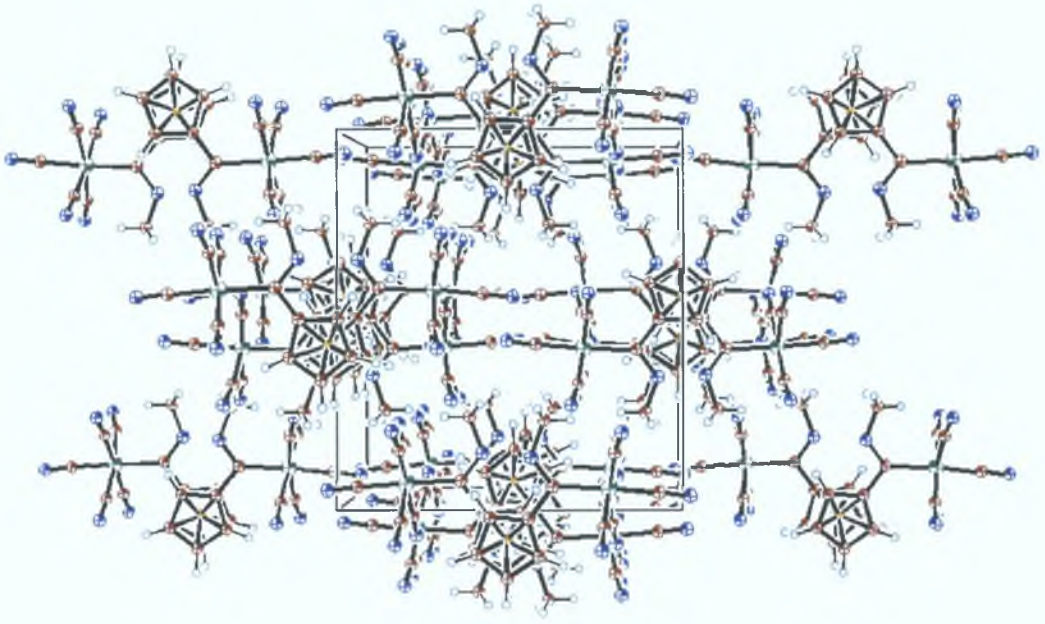

(a)

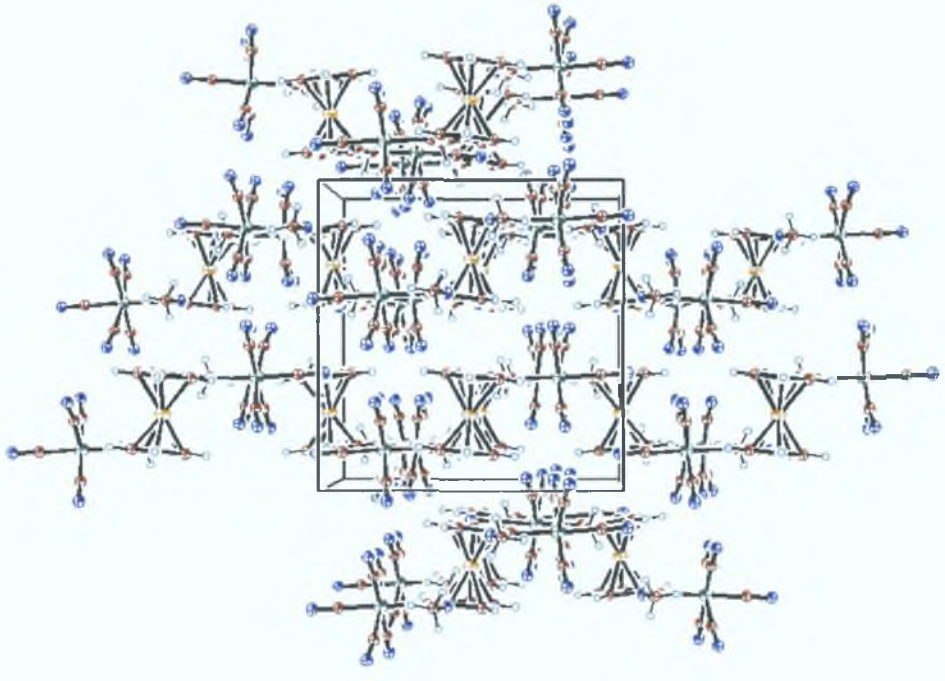

(b)

Fig. 2 – 34: Crystal packing diagrams for the 1,1'-$[(CO)_5Cr{=}C(OMe)]_2Fc$ unit cell viewed (a) normal to the (001) plane and (b) normal to the (010) plane.

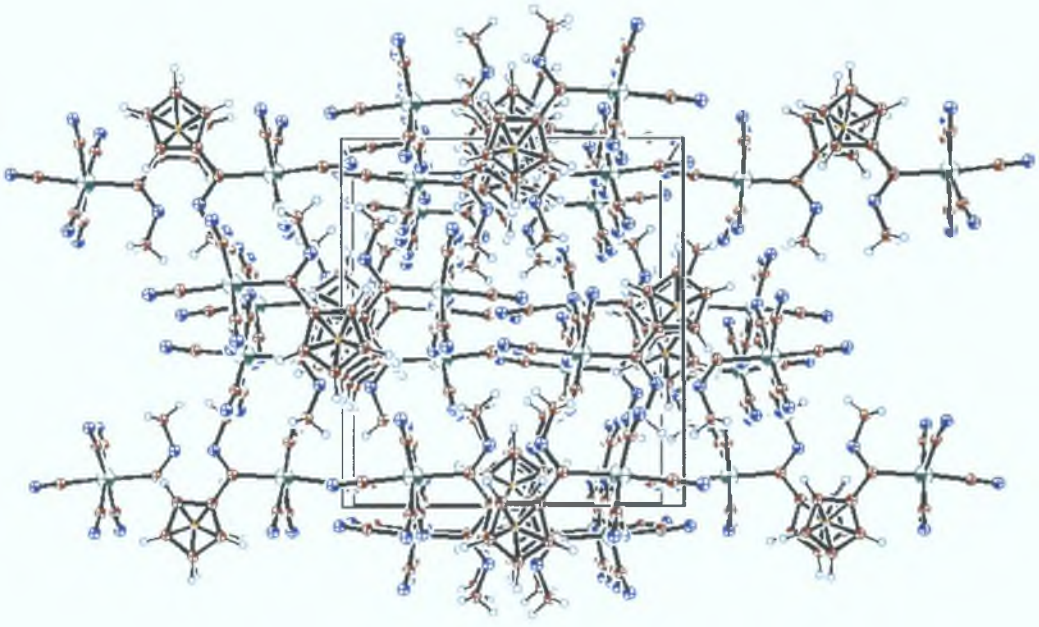

(a)

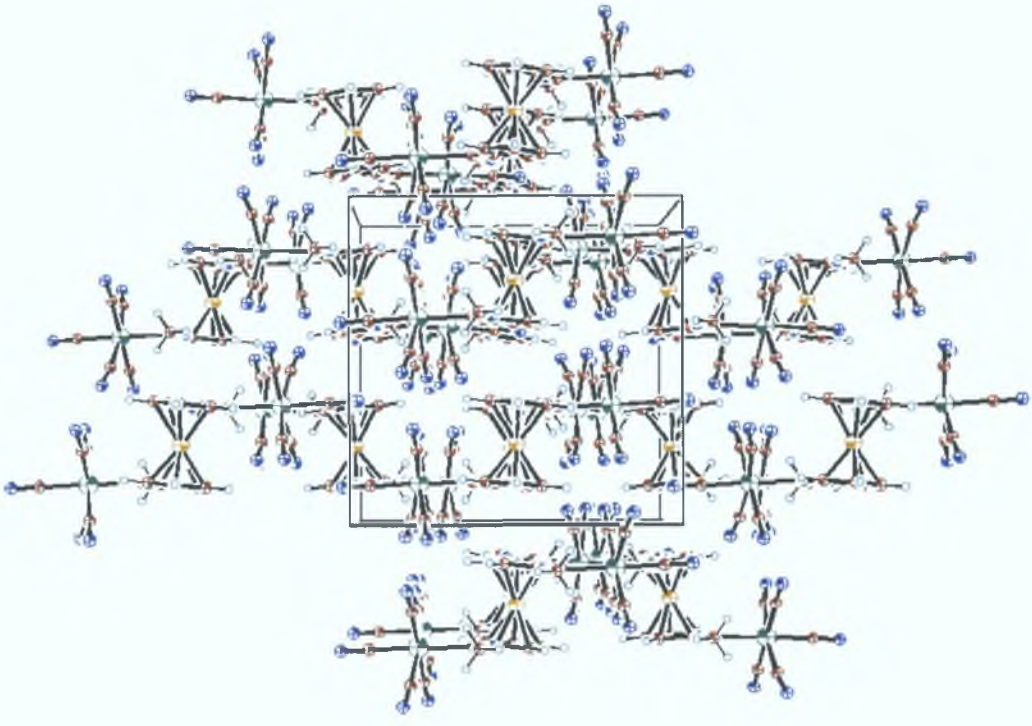

(b)

Fig. 2 – 35: Crystal packing diagrams for the 1,1'-$[(CO)_5W{=}C(OMe)]_2Fc$ unit cell viewed (a) normal to the (001) plane and (b) normal to the (010) plane.

2 4 8 Nonlinear optical properties

The nonlinear optical properties of the complexes $(CO)_5Cr=C(OMe)Fc$ and 1,1'-$[(CO)_5Cr=C(OMe)]_2Fc$ were investigated by the technique of Electric Field Induced Second Harmonic Generation (EFISH), the results of which are displayed in table 2 – 3 [11] All measurements were performed in chloroform solution with a fundamental frequency of 1 907 μm The term $\mu\beta$ represents the product of the molecular dipole and the second-order hyperpolarisability vector along the dipole direction

	$\mu\beta_{1\,907}$ (10^{-48})
$(CO)_5Cr=C(OMe)Fc$	403
1,1'-$[(CO)_5Cr=C(OMe)]_2$-Fc	338

Table 2 - 3

The $\mu\beta$ values of $(CO)_5Cr=C(OMe)Fc$ and 1,1'-$[(CO)_5Cr=C(OMe)]_2Fc$ obtained are quite modest, however this is expected due to the absence of a conjugated bridge between the donor and acceptor moieties These values do compare well with the archetypical organic donor-(π-bridge)-acceptor chromophore often used as a reference for the EFISH technique (*E*)-4-(dimethylamino)-4'-nitrostilbene (DANS), which has a $\mu\beta$ value of 482 x 10^{48} esu [41]

[11] EFISH measurements were carried out by Dr Elena Cariati, Dipartimento di Chimica Inorganica, Metallorgamca e Analitica, Universita di Milano

2 5 Discussion

2 5 1 UV-vis spectra and electrochemistry

Owing to the complex electronic structure of $(CO)_5M{=}C(OMe)Fc$ and 1,1'-$[(CO)_5M{=}C(OMe)]_2Fc$ (M = Cr, W) it was not possible to correctly assign the bands in the UV-vis spectra of these complexes Due to the lack of theoretical studies on these complexes, any assignments made here are done so tentatively based on Fischer carbenes substituted with an organic-donor group [10 37 42 43 44 45] while also taking into account the theoretical studies carried out on ferrocene-(π-bridge)-acceptor type complexes [46 47]

$(CO)_5M{=}C(OMe)Fc$ and 1,1'-$[(CO)_5M{=}C(OMe)]_2Fc$ (M = Cr, W) show similar UV-vis spectra Each complex exhibits a low-energy transition, which occurs at 522 and 520 nm for the mono- and bis-chromium complexes and at 526 and 548 nm for the mono- and bis-tungsten complexes respectively in cyclohexane solution This transition is not present in the UV-vis spectrum of $(CO)_5M{=}C(OMe)Ph$ (M = Cr, W) and is therefore most likely a ferrocene based transition [21] Ferrocene-(π-bridge)-acceptor type complexes typically exhibit a MLCT based electronic transition in this region of the spectrum, which involves the redistribution of electron density from the Fe (dz^2/dx^2-y^2/dxy) based HOMO to the acceptor based LUMO (π^*) [46] This band is therefore expected to be sensitive to the solvent polarity aswell as the strength of the acceptor and thus the HOMO-LUMO energy gap The first oxidation of these complexes are ferrocene based, thus the HOMO is assigned to the dz^2/dx^2-y^2/dxy orbitals of the iron centre The first oxidation of the mono-carbene complexes $(CO)_5M{=}C(OMe)Fc$ (M = Cr, W) occurs at 273 and 280 mV positive of the Fc/Fc^+ couple for the chromium and tungsten complexes respectively The HOMO is thus stabilised on substituting one of the Cp rings with an acceptor moiety On substitution of both Cp rings this effect is more pronounced with the bis-carbene complex 1,1'-$[(CO)_5Cr{=}C(OMe)]_2Fc$ exhibiting its first oxidation at 467 mV positive of the Fc/Fc^+ couple 1,1'-$[CO)_5W{=}C(OMe)]_2Fc$ does not show any reversible redox couples, however its first oxidation occurs with an anodic peak (E_{pa}) at 414 mV positive of the Fc/Fc^+ couple

On exchanging chromium for tungsten in the mono-carbene complex $(CO)_5M{=}C(OMe)Fc$ (M = Cr, W) the low-energy MLCT band shows a red shift of 4 nm when recorded in cyclohexane This red shift increases to 14 nm when monitored in toluene $(CO)_5W{=}C(OMe)Fc$ is also slightly easier to reduce than its chromium analogue ($\Delta E_{1/2}$ = 32 mV) This MLCT transition shows very little solvatochromic behaviour thus indicating that there is weak electronic coupling between the ferrocene and carbene moieties in these complexes The sensitivity of the low-energy MLCT transition to the group VI metal does confirm that it has some carbene character, however it is probably predominantly $(dz^2/dx^2\text{-}y^2/dxy)\rightarrow\pi^*$ (HOMO→bridge) in nature with some $(dz^2/dx^2\text{-}y^2/dxy)\rightarrow C_{carbene}(p_x)$ (HOMO→LUMO) character re Calabrese et al [47] [48] Shown in scheme 2 – 1 are the possible resonance structures for the ferrocenyl Fischer-carbene complexes $(CO)_5M{=}C(OMe)Fc$ (M = Cr, W)

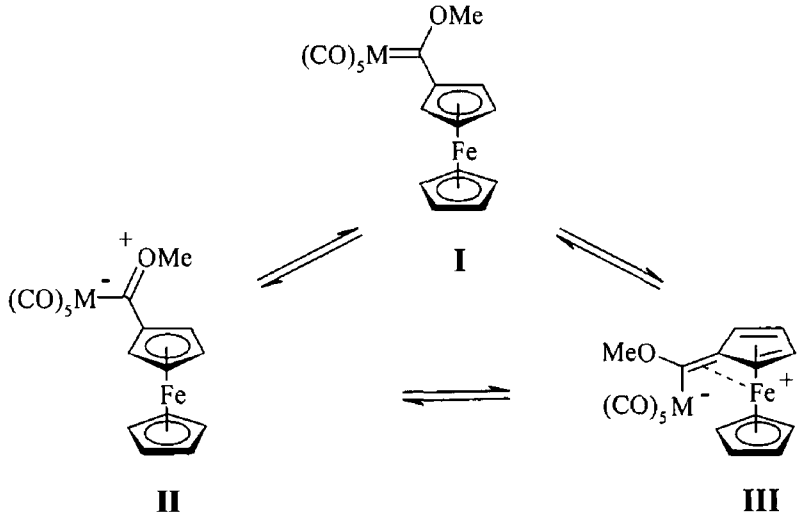

Scheme 2 – 1 Possible resonance structures for $(CO)_5M{=}C(OMe)Fc$ (M = Cr, W)

The low-energy MLCT transition of 1,1'-$[(CO)_5Cr{=}C(OMe)]_2Fc$ (λ_{max} = 520 nm) is similar to that of the mono-chromium complex, $(CO)_5Cr{=}C(OMe)Fc$ (λ_{max} = 522 nm) The bis-tungsten complex, 1,1'-$[(CO)_5W{=}C(OMe)]_2Fc$, shows more pronounced solvatochroism however, in comparison to the mono-tungsten complex, with a blue shift of the low-energy band (λ_{max} = 548 and 524 nm in cyclohexane and acetomtrile respectively) This negative solvatochromic behaviour suggests a contribution from resonance form III (scheme 2 – 2) in the ground state (see crystal structures for $C_{carbene}\text{-}C_{Cp}$ bond lengths) [49] Such strong solvatochroism is not observed for

$(CO)_5W=C(OMe)Fc$ thus dismissing the possibility of a fulvene type structure (resonance form III scheme 2 – 1) in its ground state

This increased solvatochromic behaviour for 1,1'-$[(CO)_5W=C(OMe)]_2Fc$ suggests an increased electronic coupling in comparison to the mono-tungsten complex and thus increased HOMO→LUMO character in the low-energy MLCT band (λ_{max} = 548 nm) The oscillator strength of this band is also increased slightly on going from the mono- to the bis-tungsten complex (ε = 1 19 x 10^3 *vs* 5 68 x 10^3 $M^{-1}cm^{-1}$) The low-energy MLCT band of 1,1'-$[(CO)_5Cr=C(OMe)]_2Fc$ (λ_{max} = 520 nm) is unfortunately obscured by its higher energy band and therefore appears as a shoulder, however it does not show any appreciable solvatochromic behaviour 1,1'-$[(CO)_5W=C(OMe)]_2Fc$ is the only complex of the four studied which undergoes irreversible oxidation of the ferrocene based HOMO orbital The irreversibility of this redox process may be due to the electron deficient Fe centre as shown in resonance form III (scheme 2 – 2) As 1,1'-$[(CO)_5Cr=C(OMe)]_2Fc$ undergoes a reversible oxidation of its ferrocene based HOMO orbital such a resonance form must not be as significant in its ground state structure

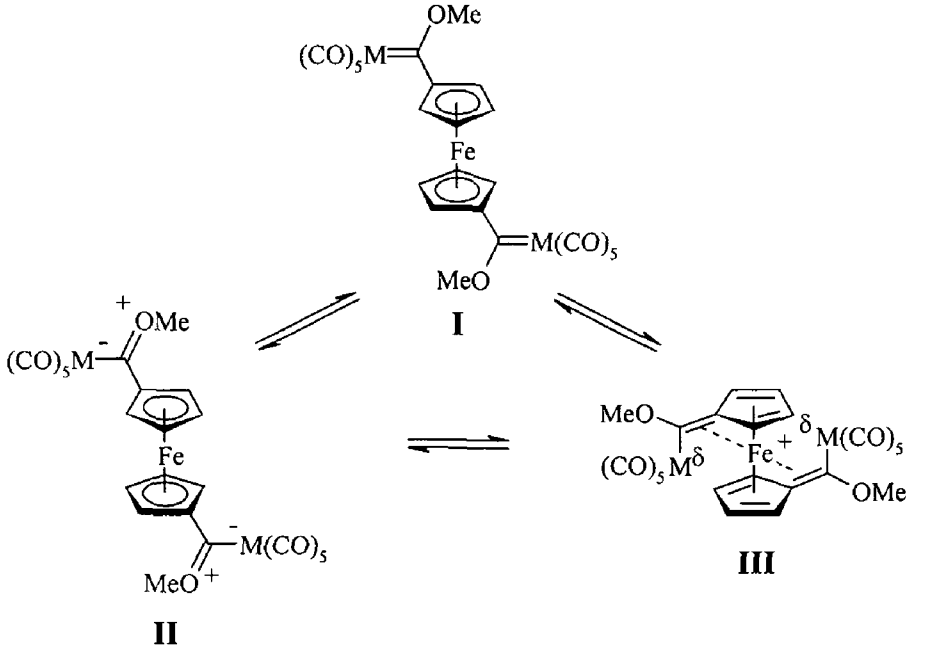

Scheme 2 – 2 Possible resonance structures for 1,1'-$[(CO)_5M=C(OMe)]_2Fc$ (M = Cr, W)

The higher energy band for these complexes occurs at 422 and 458 nm for the mono- and bis-chromium complexes and at 408 and 430 nm for the mono- and bis-tungsten complexes respectively in cyclohexane solution There is most likely a bridge→acceptor transition, i e $\pi \rightarrow C_{carbene}(p_x)$, in this region of the spectrum [46] This transition should be sensitive to the LUMO energy aswell as the solvent polarity Fischer-carbenes also exhibit MLCT transitions in this region of the spectrum, i e $d_{yz} \rightarrow C_{carbene}(p_x)$, where the d*yz* orbital is based on the chromium or tungsten metal [50] Such transitions typically display negative solvatochroism due to the zwitterionic ground state of these complexes [51] Ferrocenyl LF transitions and low-energy Fischer-carbene LF transitions (chromium/tungsten based $d_{yz} \rightarrow d_{z^2}$) may also occur in this region

The negative solvatochromic behaviour of this transition for each complex indicates that the Fischer–carbene based MLCT transition is dominant in this region of the spectrum There is therefore an appreciable contribution of resonance form II in the ground state of each of these complexes (scheme 2 – 1, scheme 2 – 2), which is evident in the crystal structures obtained However, this absorption becomes much broader for the bis-carbene complexes in comparison to the mono-carbene analogues, which is possibly due to increased mixing with the $\pi \rightarrow C_{carbene}(p_x)$ transition This may also be responsible for the red shift of 36 nm observed on going from $(CO)_5Cr{=}C(OMe)Fc$ to 1,1'-$[(CO)_5Cr{=}C(OMe)]_2Fc$, in cyclohexane A similar shift of 22 nm is observed for the mono- and bis-tungsten analogues This band appears relatively broad and intense (ε = 1 55 x 10^4 $M^{-1}cm^{-1}$) for 1,1'-$[(CO)_5W{=}C(OMe)]_2Fc$ with respect to the mono-tungsten analogue and both of the chromium complexes

The higher energy bands, which appear at 340 and 330 nm for the mono- and bis-chromium carbene complexes respectively and at 352 nm for both tungsten carbene complexes, are assigned to the high-energy carbene-based LF transition (chromium/tungsten based $d_{yz} \rightarrow d_{x^2-y^2}$) This assignment is based on steady state and laser flash photolysis studies as discussed in the following section

2 5 2 Steady state and laser flash photolysis

Similar photochemistry was observed for all Fischer-carbenes, $(CO)_5M=C(OMe)Fc$ and 1,1'-$[(CO)_5M=C(OMe)]_2Fc$ (M = Cr, W) investigated in this study Irradiation of the high-energy Fischer-carbene LF band, by steady state photolysis at $\lambda_{exc} > 320$ nm in cyclohexane in the presence of excess triphenylphosphine, resulted in formation of a tetracarbonyl species In accordance with previous literature reports, loss of a CO ligand '*cis*' to the carbene ligand is expected following irradiation of this band due to population of the dx^2-y^2 chromium/tungsten orbital [2 3 4 5 6 8 10] All complexes showed similar changes in their UV-vis absorption spectra An increase in intensity of the low-energy CT absorption bands of the parent compound was observed during the photolysis with a concomitant decrease and red shift of the higher lying CT transitions A slight increase was also observed of the high-energy Fischer-carbene LF based transition

A small amount of *cis*-$(PPh_3)(CO)_4Cr=C(OMe)Fc$ was also formed following steady-state photolysis of $(CO)_5Cr=C(OMe)Fc$ at $\lambda_{exc} > 390$ nm in the presence of excess triphenylphosphine in cyclohexane solution This suggests that the low-energy Fischer-carbene LF state also absorbs in this region of the spectrum, as proposed in the previous section The inefficiency of CO loss following population of this excited state is most probably due to efficient intersystem crossing to the CT states, which are inactive with respect to CO loss [21] No CO loss was observed following irradiation of $(CO)_5W=C(OMe)Fc$ or 1,1'-$[(CO)_5M=C(OMe)]_2Fc$ (M = Cr, W) at $\lambda > 390$ nm due to increased intersystem crossing between the low-energy Fischer-carbene LF state and the CT states of these systems

At the end of the photolysis experiments infrared spectra were obtained and, for all four compounds, ' evidence for tetracarbonyl photoproducts was observed Tetracarbonyl formation did not go to completion as indicated by the presence each of the parent compounds following photolysis In the case of the mono-carbene complexes two tetracarbonyl species may have formed This is evident by the two sets of ν(CO) at 1895, 1902 cm^{-1} and at 2000, 2008 cm^{-1} for *cis*-$(PPh_3)(CO)_4Cr=C(OMe)Fc$ The tungsten analogue only displays a single ν(CO) at

1902 and 2021 cm ^{1}, however the broadness of these peaks may mask further carbonyl stretches

Although these two species have not yet been isolated it is thought that there may be two structural isomers of the same tetracarbonyl complex, *cis*-$(PPh_3)(CO)_4M{=}C(OMe)Fc$ (M = Cr, W), present It is suggested here that free-rotation of the *cis*-$(PPh_3)(CO)_4M$ (M = Cr, W) moiety about the metal-carbene bond is restricted by the presence of the bulky ferrocene group and the methoxy group thereby giving rise to two isomers (fig 2 - 36) This proposal is based on the assumption however that the methoxy moiety remains in the *anti*-configuration as for the pentacarbonyl precursors (see crystal structures, section 2 3 7)

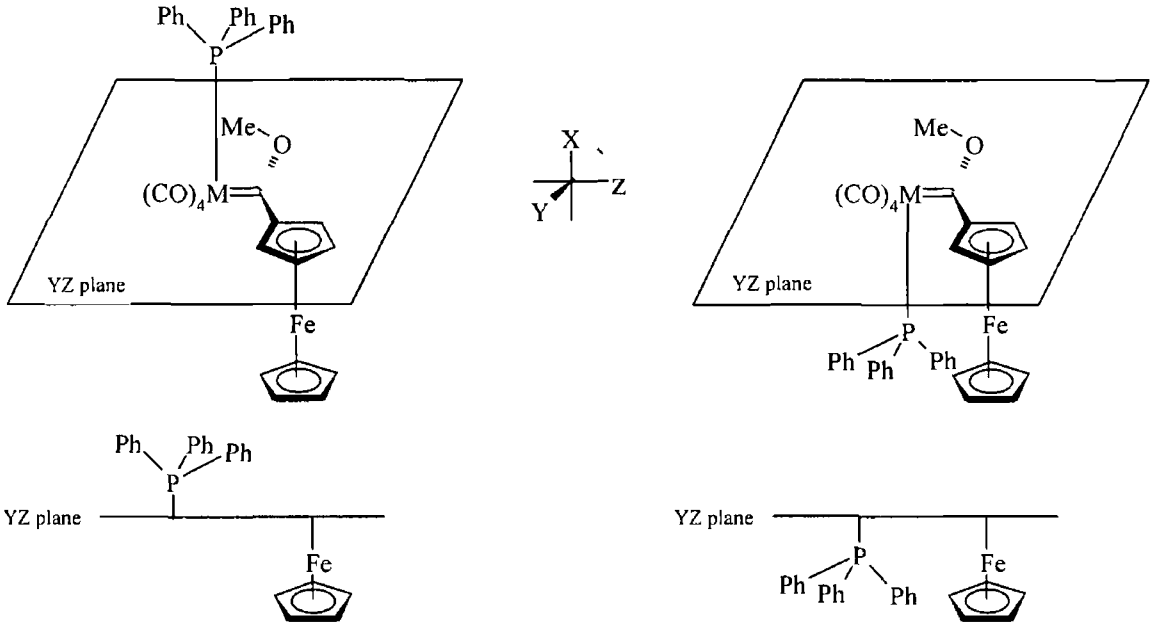

Fig 2 – 36 Proposed isomers for *cis*-$(PPh_3)(CO)_4M{=}C(OMe)Fc$ (M = Cr, W)

The infrared spectra recorded following photolysis of 1,1'-$[(CO)_5M{=}C(OMe)]_2Fc$ (M = Cr, W) in the presence of excess triphenylphosphine showed a very similar pattern for the ν(CO) to those of the mono-carbene complexes This suggests formation of analogous isomers at the metal centres There are also shoulders present at 1881 and 1882 cm ^{1}, which may be due to CO substitution at both of the chromium and tungsten centres respectively In theory, this would give rise to four isomers for the bis-carbene complexes following tetracarbonyl formation at both of the carbene moieties

Following laser flash photolysis of $(CO)_5Cr=C(OMe)Fc$ at 355 nm in cyclohexane under one atmosphere of carbon monoxide weak transient signals were observed. These transient signals indicated depletion of the parent compound with a λ_{min} at 340 nm. These signals recovered to the pre-irradiated baseline after *ca.* 7 ms. When the experiment was carried out under one atmosphere of argon the signals observed did not return to the pre-irradiated baseline. It is therefore most likely that photoinduced CO loss occurs following irradiation of $(CO)_5Cr=C(OMe)Fc$ at 355 nm. Six possible transient species that may form following laser flash photolysis of $(CO)_5Cr=C(OMe)Fc$ at 355 nm are given in scheme 2 – 3.

It has been postulated that population of the Fischer-carbene MLCT transition gives rise to the metal-ketene transient species (T-I, scheme 2 – 3) *via* CO insertion into the metal-carbene bond, however it has remained elusive to spectroscopic characterisation and its presence has only been imparted by subsequent chemical reaction.[11, 34] No evidence for *anti-syn* isomerisation of $(CO)_5Cr=C(OMe)Fc$ was observed for this complex (T-II, scheme 2 – 3).[25, 27] Considering the *anti*-configuration of the methoxy group as observed in the crystal structure (fig. 2 – 31), an intramolecular agostic interaction involving one of the methoxy-hydrogens is quite possible (T-III scheme 2 – 3). However, to date such intramolecular agostic interactions have only been reported for tungsten Fischer-carbene complexes.[21, 22, 23] The lifetime of the transient species observed here is also 3 orders of magnitude longer lived than that observed by McGarvey et. al following photoinduced CO loss from the $(CO)_5W=C(OMe)Ph$.[22] It is unlikely that the transient species is T-IV, as previous studies of solvated intermediates have reported much shorter lifetimes. For example, $Cr(CO)_5$(cyclohexane) decays with a second order rate constant of 2.3×10^{-6} $M^{-1}s^{-1}$ on reaction with CO.[52] The η^3-vinylcarbene species T-V is unprecedented as the vinyl moiety is contained in the Cp ring of the ferrocene unit. However a number of η^3-vinylcarbene complexes have previously been isolated, fully characterised and identified as intermediates in the Dotz benzannulation reaction.[7(g - h), 12] Further investigations are in progress to verify the nature of this transient species. Transient species T-VI is also unprecedented for Fischer-carbene complexes however it cannot be ruled out without further experimental evidence. This species contains a 5-membered ring involving an agostic interaction between the chromium centre and the hydrogen of the Cp carbon β to the carbene carbon atom.

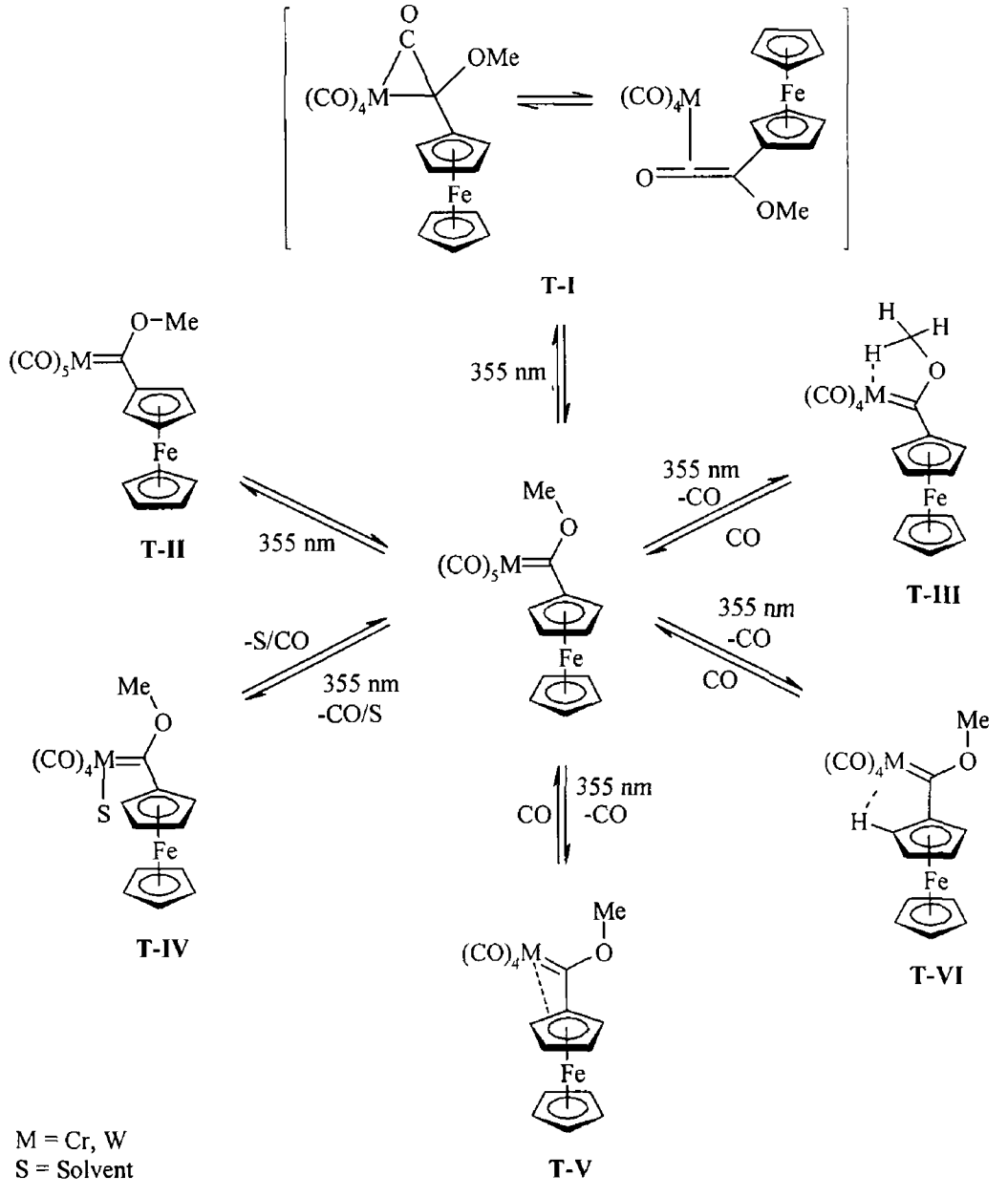

Scheme 2 – 3 Possible transient species (that may form) following laser flash photolysis of $(CO)_5M{=}C(OMe)Fc$ (M = Cr, W) in cyclohexane at 355 nm

As expected CO loss was not as efficient for the tungsten complex However, following laser flash photolysis of $(CO)_5W{=}C(OMe)Fc$ two transient species were observed One of these species is independently observable at 390 nm and was not observed to recover to the pre-flash absorbance level The UV-vis spectrum remained unchanged throughout the experiment indicating that the parent compound is regenerated, i e the transient species formed was too long lived to be monitored by the experimental set-up available This transient species is most likely similar to that

observed for the chromium analogue and likewise cannot be assigned without further investigation

The second transient species observed following flash photolysis of $(CO)_5W=C(OMe)Fc$ at 440 nm has a lifetime of 187 μs and does not return to the pre-irradiated baseline due to the presence of the long-lived species In comparison to the literature, this shorter-lived transient species is possibly due to *anti-syn* isomerisation of the methoxy group (T-II, scheme 2 – 3) [27] The partial double bond character of the $C_{carbene}$-O bond (resonance form II, scheme 2 – 1) restricts rotation of the methyl group about this bond *Anti-syn* isomerisation of alkoxy Fischer-carbenes has been attributed to population of the MLCT excited state, which reduces the bond order of the $C_{carbene}$-O bond thus allowing free rotation of the methoxy group

No transient signals were observed following laser flash photolysis of 1,1'-$[(CO)_5Cr=C(OMe)]_2Fc$ at 355 nm under one atmosphere of carbon monoxide However, weak transient signals were observed in the region of 380 and 540 nm when the experiment was repeated under one atmosphere of argon A depletion was also observed in the region of 460 nm These signals are most likely due to a similar transient species as observed for the mono-chromium complex Again, they cannot be assigned without further experimental evidence Neither of these signals recovered fully to the pre-flash absorption level due to decomposition of the parent compound, as is evident in the UV-vis spectra recorded throughout the experiment (fig 2 – 9) The lifetimes of these signals are *ca* 2 ms, which is slightly shorter than for the mono-carbene complex

No transient signals were observed following laser flash photolysis of 1,1'-$[(CO)_5W=C(OMe)]_2Fc$ at 355 nm This is not surprising as the bis-chromium carbene complex showed very weak signals, and tungsten Fischer-carbenes are known to have much lower quantum yields than their chromium counterparts for CO loss [25] However, when 1,1'-$[(CO)_5W=C(OMe)]_2Fc$ was irradiated in the presence of triphenylphosphine, evidence for a tetracarbonyl photoproduct was observed

On repeating the flash photolysis experiments under an atmosphere of argon in the presence of excess triphenylphosphine $(CO)_5Cr=C(OMe)Fc$, $(CO)_5W=C(OMe)Fc$ and 1,1'-$[(CO)_5Cr=C(OMe)]_2Fc$ all showed the formation of tetracarbonyl photoproduct as was observed in the steady-state experiments thereby confirming photoinduced CO loss following excitation of the higher energy Fischer-carbene LF transition (as mentioned above 1,1'-$[(CO)_5W=C(OMe)]_2Fc$ showed no observable photochemistry following laser flash photolysis experiments) No changes were observed in the UV-vis spectra during steady-state photolysis of $(CO)_5M=C(OMe)Fc$ or 1,1'-$(CO)_5M=C(OMe)]_2Fc$ (M = Cr, W) at $\lambda_{exc} > 500$ nm or following flash photolysis at 532 nm excitation Irradiation of the low-energy CT transitions are thus inactive with respect to CO loss and *anti-syn* isomerisation of the four complexes studied

2 6 Conclusion

The photochemistry of four organometalhc complexes was investigated using a combination of laser flash photolysis, and steady state photolysis in the presence of triphenylphosphine For all complexes, tetracarbonyl photoproducts were observed when a solution containing the organometallic compound and excess triphenylphosphine was photolysed Following laser flash photolysis transients assigned to a CO loss species were observed, however these transient species could not be accurately assigned without further experimental evidence UV-vis, electrochemical and crystal data all support the presence of electronic communication between the Fischer-carbene and ferrocenyl units in the systems studied

2 7 Bibliography

[1] K Ofele, M Herberhold, *Angew Chem Int Ed* **1970**, 9, 739

[2] E O Fischer, H Fischer, *Chem Ber* **1974**, 107, 657

[3] C P Casey, A J Shusterman, *J Mol Catal* **1970**, 8, 1

[4] C P Casey, A J Shusterman, N W Vollendorf, K J Haller, *J Amer Chem* **1982**, 104, 2417

[5] R M Dahlgren, J I Zink, *Inorg Chem* **1977**, 16, 3154

[6] C P Casey, N W Vollendorf, K J Haller, *J Am Chem Soc* **1984**, 106, 3754

[7] (a) K H Dotz, *Angew Chem Int Ed Engl* **1975**, 14, 644 (b) K E Garrett, J B Sheridan, D B Pourreau, W C Feng, G L Geoffroy, D L Staley, A L Rheingold, *J Amer Chem Soc* **1989**, 111, 8383 (c) B A Anderson, W D Wulff, *J Am Chem Soc* **1990**, 112, 8615 (d) M A Huffman, L S Liebeskind, *J Am Chem Soc* **1990**, 112, 8617 (e) K H Dotz, T Schafer, F Kroll, K Harms, *Angew Chem Int Ed Engl* **1992**, 31 (9), 1236 (f) M Torrent, M Duran, M Sola, *Organometallics* **1998**, 17, 1492 (g) M L Waters, T A Brandvold, L Isaacs, W D Wulff, A L Rheingold, *Organometallics* **1998**, 17, 4298 (h) J Barluenga, F Aznar, I Guitierrez, A Martin, S Garcia-Granda, M A Llorca-Baragano, *J Am Chem Soc* **2000**, 122, 1314

[8] B H Edwards, M D Rausch, *J Organomet Chem* **1981**, 210, 91

[9] H C Foley, L M Strubinger, T S Targos, G L Geoffroy, *J Am Chem Soc* **1983**, 105, 3064

[10] L K Fong, N J Cooper, *J Am Chem Soc* **1984**, 106, 2595

[11] M L Gallagher, J B Greene, A D Rooney, *Organometallics* **1997**, 16, 5260

[12] J Barluenga, F Aznar, A Martin, S Garcia-Granda, E Perez-Carreno, *J Am Chem Soc* **1994**, 116, 11191

[13] H Fischer, J Muhlemeier, R Markl, K H Dotz, *Chem Ber* **1982**, 115, 1355

[14] (a) K H Dotz, R Dietz, *Chem Ber* **1978**, 111, 2517 (b) K H Dotz, I Pruskil, *Chem Ber* **1980**, 113, 2876 (c) W D Wulff, P C Tang, J S McCallum, *J Am Chem Soc* **1981**, 103, 7677 (d) K H Dotz, J Muhlemeier, U Schubert, O Orama, *J Organomet Chem* **1983**, 247, 187

[15] J S McCallum, F A Kunng, S R Gilbertson, W D Wulff, *Organometallics* **1988**, 7, 2346

[16] T J Katz, S J Lee, *J Am Chem Soc* **1980**, 102, 422

[17] C P Casey, N L Hornung, W P Kosar, *J Am Chem Soc* **1987**, 109, 4908

[18] L S Hegedus, L M Schultze, J Montgomery, *Organometallics* **1989**, 8, 2189

[19] P J Campos, D Sampedro, M A Rodriguez, *Organometallics* **2002**, 21, 4076

[20] P J Campos, D Sampedro, M A Rodriguez, *J Org Chem* **2003**, 68, 4674

[21] P C Servaas, D J Stufkens, A Oskam, *J Organomet Chem* **1990**, 390, 61

[22] J N Bechara, S E J Bell, J J McGarvey, J J Rooney, *J Chem Soc, Chem Comm* **1986**, 1785

[23] S E J Bell, K C Gordon, J J McGarvey, *J Am Chem Soc* **1988**, 110, 3107

[24] For examples of agostic interactions see the following references (a) R J Kazlauskas, M S Wrighton, *J Am Chem Soc* **1982**, 104, 6005 (b) G K Yang, K S Peters, V Vaida, *J Am Chem Soc* **1986**, 108, 2511 (c) M P Coles, V C Gibson, W Clegg, M R J Elsegood, *Polyhedron* **1988**, 17, 2483 (d) A Toupadakis, G J Kudas W A King, B L Scott, J Huhmann-Vincent, *Organometallics* **1988**, 17, 5315 (e) X-L Luo, R H Crabtree, *J Am Chem Soc* **1989**, 111, 2527

[25] H P Gut, N Welte, U Link, H Fischer, U E Steiner, *Organometallics* **2000**, 19, 2354

[26] D B Pourreau, G L Geoffroy, *Adv Organomet Chem* **1985**, 24, 249

[27] A D Rooney, J J McGarvey, K C Gordon, *Organometallics* **1995**, 14, 107

[28] A D Rooney, J J McGarvey, K C Gordon, R A McNicholl, U Schubert, W Hepp, *Organometallics* **1993**, 12, 1277

[29] J B Sheridan, D B Pourreau, G L Geoffroy, *Organometallics* **1988**, 7, 289

[30] M A McGuire, L S Hegedus, *J Am Chem Soc* **1982**, 104, 5538

[31] L S Hegedus, M A McGuire, L M Schultze, C Yijun, O P Anderson, *J Am Chem Soc* **1984**, 106, 2680

[32] C Borel, L S Hegedus, J Krebs, Y Satoh, *J Am Chem Soc* **1987**, 109, 1101

[33] H Fischer, *Angew Chem Int Ed Engl* **1983**, 22 (11), 874

[34] K O Doyle, M L Gallagher, M T Pryce, A D Rooney, *J Organomet Chem* **2001**, 617-618, 269

[35] S Oishi, K Tokumaru, *J Phy Org Chem* **1989**, 2, 323

[36] (a) U Schubert, W Hepp, J Muller, *Organometallics* **1986**, 5, 173 (b) W Hepp, U Schubert, *J Organometallic Chem* **1987**, 321, 317 (c) U Schubert, H Hornig, *J Organomet Chem* **1987**, 335, 307 (d) U Schubert, *J Organomet Chem* **1988**, 358, 215 (e) W Hepp, U Schubert, *J Organomet Chem* **1990**, 385, 221

[37] J A Connor, J P Lloyd, *J Chem Soc Dalton Trans* **1972**, 1470

[38] K N Jayaprakash, P C Ray, I Matsuoka, M M Bhadbhade, V G Puranik, P K Das, H Nishihara, A Sarkar, *Organometallics*, **1998**, 18, 3851

[39] The ORTEP-III program was used to draw all x-ray crystal structures, L J Farrugia, *J Appl Cryst* **1997**, 30, 565

[40] H Nakatsuji, J Ushio, S Han, T Yonezawa, *J Am Chem Soc* **1983**, 105, 426-434

[41] S R Marder, L -T Cheng, B G Tiemann, A C Friedli, M Blanchard-Desce, J W Perry, J Skindhøj, *Science* **1994**, 263, 511

[42] S Robin-Le Guen, P Le Toul, B Caro, R Pichon, N Kervarec, *J Organomet Chem* **2001**, 626, 37

[43] L L Lancellotti, R Tubino, S Luzzati, E Licandro, S Maiorana, A Papagni, *Synthetic Metals*, **1998**, 93, 27

[44] M Y Darensbourg, D J Darensbourg, *Inorg Chem* , **1970**, 9, 32

[45] J A Connor, E M Jones, *J Chem Soc (A)*, **1971**, 1974

[46] S Barlow, H E Bunting, C Ringham, J C Green, G U Bublitz, S G Boxer, J W Perry, S R Marder, *J Am Chem Soc* , **1999**, 121, 3715

[47] J C Calabrese, L T Cheng, J C Green, S R Marder, W Tam, *J Am Chem Soc* , **1991**, 113, 7227

[48] As ferrocene is directly linked to the Fischer carbene moiety in these systems, the bridge π^*-orbitals referred to here are comprised of the cyclopentadienyl π^*-orbitals

[49] Such fulvene type structures are well documented and have been isolated as salts, S Barlow, L M Henling, M W Day, W P Schaefer, J C Green, T Hascall, S R Marder, *J Am Chem Soc* **2002**, 124, 6285

[50] See chapter 1 page 10

[51] (a) E Licandro, S Maiorana, A Papagni, P Hellier, L Capella, A Persoons, S Houbrechts, *J Organomet Chem* , **1999**, 583, 111 (b) C C Wang, Y Wang, H J Liu, K J Liu, L K Chou, K S Chan, *J Phys Chem* A **1997**, 101, 8887

[52] C J Breheny, J M Kelly, C J Long, S O'Keeffe, M T Pryce, G Russell, M W Walsh, *Organometallics* **1998**, 17, 3690

Chapter 3

Steady State and Laser Flash Photolysis Studies of Vinylferrocene substituted Fischer Carbene Complexes (*E*)-$(CO)_5M{=}C(X)C_2H_2Fc$ (M = Cr, W; X = OMe, C_4H_8N). A Comparative Study of Methoxy- and Pyrrolidino- Stabilised Fischer Carbene Complexes

3 1 Aims and objectives

The aim of this chapter was to synthesis two new organometallic complexes, (*E*)-$(CO)_5Cr{=}C(NC_4H_8)C_2H_2Fc$ and (*E*)-$(CO)_5W{=}C(NC_4H_8)C_2H_2Fc$ (Fc = ferrocene), and compare their photochemistry with the methoxy analogues The synthesis of (*E*)-$(CO)_5Cr{=}C(OCH_3)C_2H_2Fc$ and (*E*)-$(CO)_5W{=}C(OCH_3)C_2H_2Fc$ have previously been reported in the literature The photochemistry of the methoxy and pyrrolidino stabilised Fischer carbene complexes (*E*)-$(CO)_5M{=}C(X)C_2H_2Fc$ (M = Cr, W, X = -OMe, $-NC_4H_8$) was investigated by steady state and laser flash photolysis in cyclohexane solution A comparison is made between the electronic interaction of the vinylferrocene moiety with the methoxy- and pyrrohdino-carbene moieties using the results of UV-vis, electrochemical and X-ray crystallographic analysis The nonlinear optical response of the complexes (*E*)-$(CO)_5Cr{=}C(OMe)C_2H_2Fc$ and (*E*)-$(CO)_5Cr{=}C(NC_4H_8)C_2H_2Fc$ is reported by the electric field induced second harmonic generation (EFISHG) technique

3 2 Introduction

Organometallic based non-linear optical (NLO) materials consisting of conjugated donor-(π-bridge)-acceptor systems have been intensely investigated in recent years because of their potential applications in emerging photonic technologies [1] Transition metals introduce a number of parameters not found in organic systems, which may influence their NLO properties Organometallic complexes often display low energy metal-to-ligand charge-transfer transitions in the UV-vis region of the spectrum that can give rise to large optical non-linearities If the charge transfer excited state dipole moment (μ_{ee}) is significantly different than the ground state dipole moment (μ_{gg}), this excited state will have a large oscillator strength and can contribute greatly to the first hyperpolarisability (β) Ever since Green reported efficient second harmonic generation for (*cis*)-[1-ferrocenyl-2-(4-nitrophenyl)ethylene] (fig 3 – 1), ferrocene-(π-bridge)-acceptor systems have become one of the most extensively studied classes of organometallic compounds for non-linear optics [2]

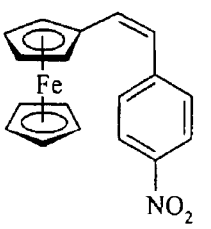

Fig 3 - 1

A theorectical two level model developed by Oudar and Chemla for organic donor-(π-bridge)-acceptor type systems relates the static molecular hyperpolarisability [3] (β_0) to characteristics of the molecule's optical transitions This model makes it possible to establish trends in the non-linearity/molecular structure relationship in terms of relatively simple physical properties, eqn (1) [4 5]

$$\beta_0 = \frac{3\varepsilon_0^2(\mu_{ee} - \mu_{gg})\mu_{ge}^2}{(\hbar\omega_{ge})^2} \qquad \text{eqn (1)}$$

It is clear from eqn. (1) that the hyperpolarisability will be enhanced with increasing transition dipole moment (μ_{ge}), increasing change of dipole moment (μ_{ee} - μ_{gg}), decreasing energy ($\hbar\omega_{ge}$) and increasing oscillator strength (ε_0) of the charge transfer transition. It was shown by Marder using the two-state analysis of a four π-orbital system, i.e. single donor and acceptor orbitals linked *via* two bridge orbitals, that the optimum value for β is dependent on the coulombic energy difference between the donor and acceptor orbitals.[6] The author also showed that strong donor-acceptor pairs, i.e. with a small coulombic energy difference, do not necessarily lead to the largest non-linearity and that the degree of bond-length-alternation, i.e. bridge length, and the importance of the donor and acceptor orbital overlap with those of the bridge must be considered. This two-level model holds quite well for many organic donor-(π-bridge)-acceptor type systems as their hyperpolarisability is dominated by a single low-energy charge transfer transition, however it fails for some organometallics, octopolar compounds and some unconventional chromophores.[7]

There have been a number of studies concentrating on structure property relationships with respect to NLO activity.[6, 8] Calabrese et al. initially showed that by increasing the acceptor strength on a series of vinyl ferrocene complexes a red shift of the low-energy transitions was observed with a corresponding increase in the non-linearity of the complex.[8(a)] Calabrese also showed that extending the donor-acceptor distance by increasing the number of vinyl units in the spacer group leads to an increase in the π-bridge orbital energy and a decrease in the π^*-bridge orbital energy thus resulting in a decrease in both of the low energy transitions and a corresponding increase in β. Alain et al. have synthesised a number of ferrocene derivatives displaying large optical non-linearities.[8(f), (g)] These compounds exhibit positive solvatochromic behaviour with the low-energy band increasing in oscillator strength as the acceptor strength is increased indicating greater metal-ligand communication.

Metallocene donors typically show two low-energy transitions in the UV-vis region of the spectrum. In an effort to gain an understanding of metallocene based chromophores and how they contribute to the first hyperpolarisability of non-linear optical materials Barlow et al. carried out a study that combined experimental and theoretical techniques on metallocene-(π-bridge)-acceptor type systems.[8(h)] For the

compounds studied (some examples are shown in fig. 3 – 2) both of the low energy transitions were shown to have appreciable charge-transfer character, as each band is red shifted to the same extent on increasing the acceptor strength. The higher energy band was assigned to a π→acceptor transition in agreement with previous studies,[6] where the π-orbital (HOMO-3) consists of a combination of the highest occupied cyclopentadienyl orbital and the highest occupied π-bridge orbital. The acceptor orbital (LUMO) is mainly localised on the acceptor moiety. The lower energy transition was assigned as a metal→acceptor (HOMO→LUMO) transition, which was dismissed in previous studies due to negligible overlap of the respective orbitals.[8(j)-(l)] Both transitions were also shown to have large dipole changes when populated, thus confirming that both of these excited states may contribute significantly to the non-linearity of the complexes.

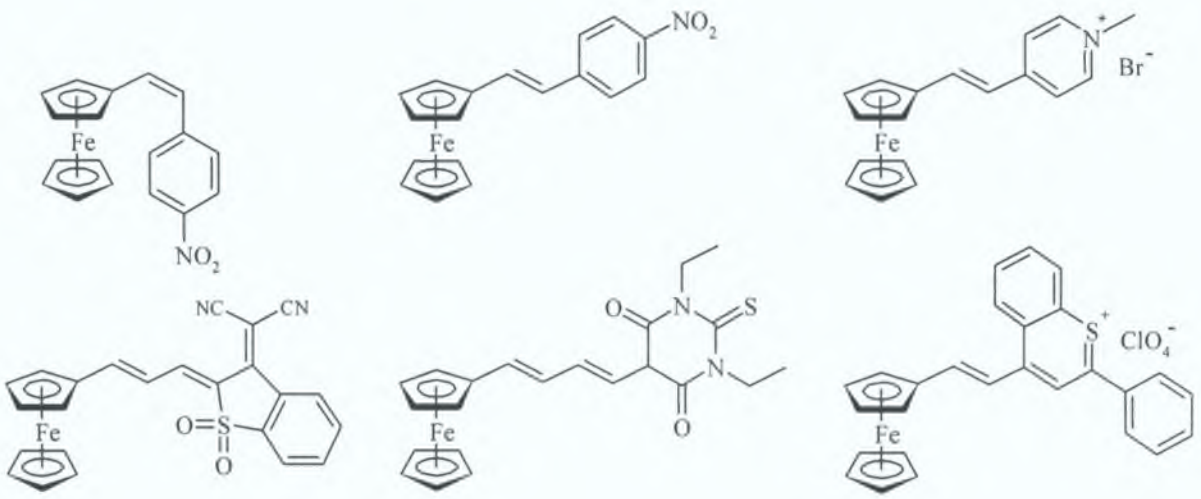

Fig. 3 - 2

By employing two metal centres in an NLO chromophore, thus creating heterobimetallic organometallic complexes, the electronic properties of the system can be manipulated to a higher degree by modifying both the electron-donor and electron-acceptor fragments. Doisneau et al. first implemented this hypothesis when they utilised Pd^{II} to act as an electron acceptor in the bis-metallic ferrocenyl oxazoline complex shown in figure 3 – 3.[9] The electron withdrawing effect of the Pd^{II} moiety increases the strength of the acceptor and EFISH measurements show that β is doubled upon coordination to the Pd^{II} moiety.

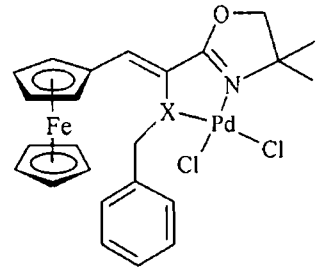

X = S, SO

Fig 3 – 3

Unfortunately, from a structure-property point of view, due to the complexity of UV-vis spectra for heterobimetallic organometallic systems, the origin of NLO activity for this class of compound is even more difficult to ascertain, and to date has received very limited interest This is not surprising due to the number of possible transitions involved in their UV-vis spectra, ligand based ($n \rightarrow \pi^*$, $\pi \rightarrow \pi^*$), ligand field ($d \rightarrow d$), metal-ligand charge-transfer (MLCT, i e $d \rightarrow \pi^*$–bridge, $d \rightarrow \pi^*$-acceptor), ligand-metal charge-transfer (LMCT, $\pi \rightarrow d$), intravalence/metal-metal charge-transfer (IVCT/MMCT, $d \rightarrow d'$) and intraligand charge-transfer (ILCT, $\pi \rightarrow \pi^*$)

One of the most common acceptor units used in ferrocenyl based heterobimetallic NLO systems has been metal-carbonyls,[1] most notably group-VI metals [10] Kotz et al reported the first example of such complexes when they investigated the electrochemistry of mono-, and bis-ferrocenyl phosphines and their Mo and W pentacarbonyl and tetracarbonyl complexes [11] For NLO studies the metal-carbonyl moiety has typically been linked *via* an arene ligand or *via* the lone pair on a nitrogen atom utilising pyridyl- or cyano-type ligands (some examples are shown in fig 3 – 4)

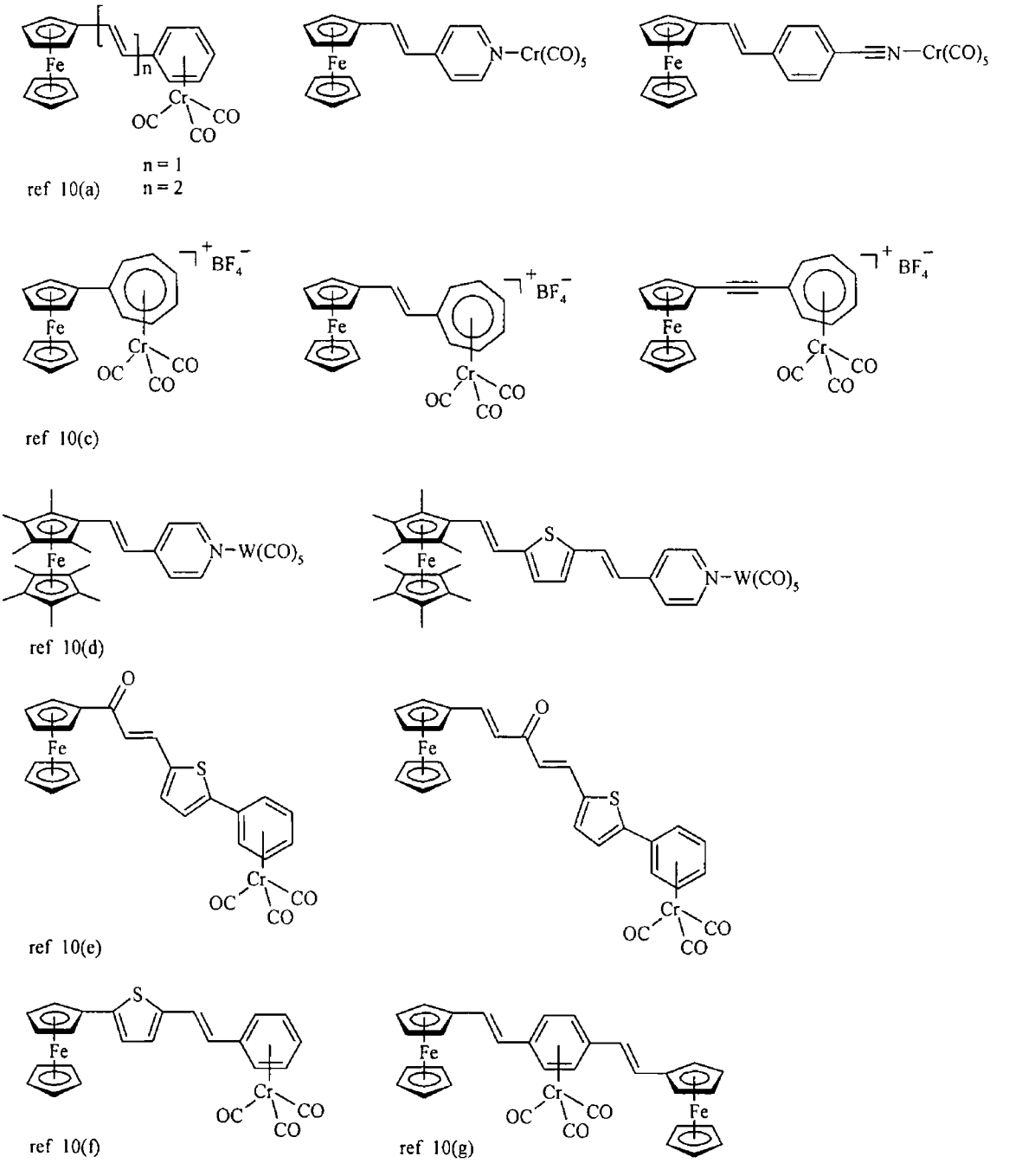

Fig 3 – 4

Maiorana et al first acknowledged the potential of group-VI Fischer-carbene pentacarbonyl units as the acceptor moiety in NLO systems [12] In recent years the use of Fischer-carbenes as the acceptor moiety in NLO systems has been receiving increased attention [13] Due to the unique electronic structure of the Fischer-carbene unit these systems are expected to show large changes in their dipole moment on MLCT excitation (scheme 3 – 1)

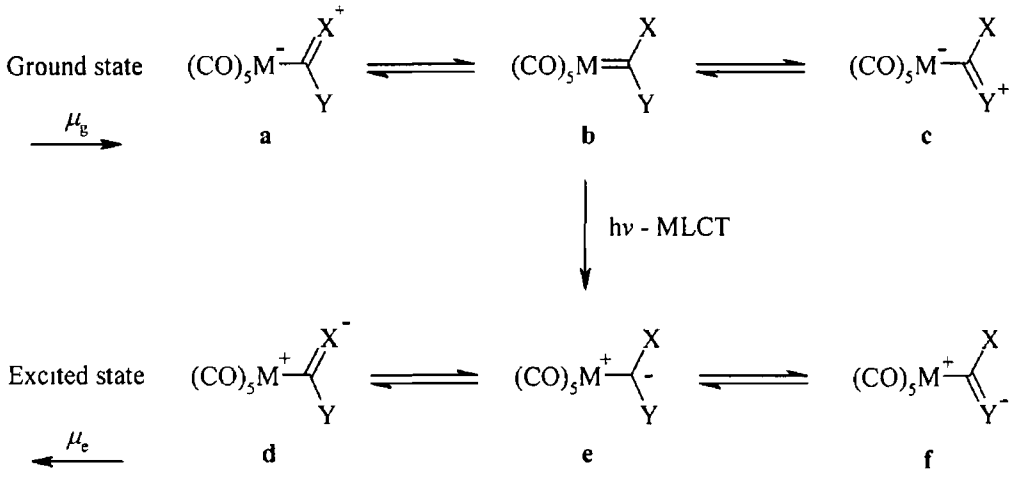

Scheme 3 – 1 Resonance structures for the ground and MLCT excited states of group-VI Fischer-carbene complexes depicting ground (μ_g) and excited (μ_e) state dipole moments

Connor and Lloyd[14] reported the first example of a ferrocenyl Fischer-carbene complex as far back as 1972 however the next reported example was not for another 25 years[15] (fig 3 – 5 **a** and **b** respectively) In both of these cases the carbene complex was used as an organic synthon [16] Fischer-carbenes are well known intermediates in numerous organic transformations as discussed previously in chapter 2

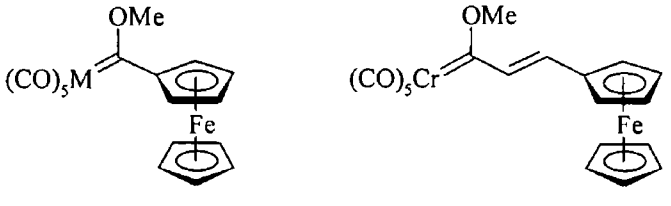

Fig 3 – 5

Beck et al later reported the synthesis of some highly conjugated ferrocenyl Fischer-carbenes however their NLO and photophysical properties were never reported (fig 3 – 6) [13(e)]

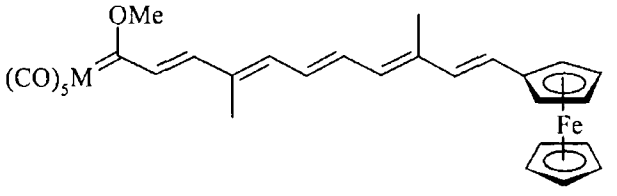

M = Cr, W

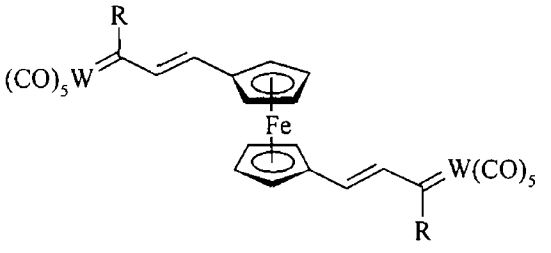

R = OMe, NMe_2

Fig 3 - 6

Jayaprakash et al reported the first NLO investigation of ferrocenyl Fischer-carbenes (fig 3 – 7) [13(d)] Very high values were reported for the first hyperpolarisabilities, with one of the compounds exhibiting one of the largest β values for any organometallic complex (M = W, n = 4)

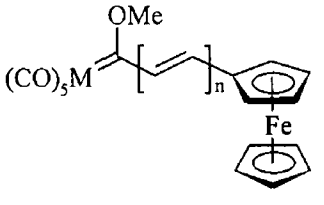

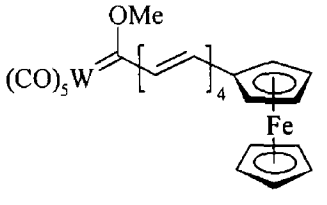

M = Cr, W
n = 1,2,3

Fig 3 – 7

In the following chapter the photochemistry of the methoxy Fischer-carbene complexes $(CO)_5M{=}C(OMe)C_2H_2Fc$ (M = Cr, W) is investigated aswell as their ammo analogues $(CO)_5M{=}C(C_4H_8N)C_2H_2Fc$ (M = Cr, W)

3 3 Experimental

3 3 1 Reagents

All reactions were performed under an inert atmosphere of argon Anhydrous diethyl ether was used as received (Fluka Chemicals) Aldrich Chemical Company supplied all other solvents Pentane was of HPLC grade and used without any further purification Dichloromethane was dried over $MgSO_4$ prior to use All solvents used for steady state photolysis and laser flash photolysis experiments were of spectroscopic grade and used without further purification Air Products and IIG supplied argon and carbon monoxide gases respectively Chromium and tungsten hexacarbonyl, ferrocenecarboxaldehyde, trimethylamine, chlorotrimethylsilane and pyrrolidine (Aldrich Chemical Company) were all used without further purification Methyl lithium (1 4 M solution in diethyl ether) and trimethyloxomum tetrafluoroborate (Fluka Chemicals) were also used without further purification Silica gel (Merck) was used as received All mobile phases were dried over $MgSO_4$ prior to use

3 3 2 Equipment

All infrared spectra were obtained on a Perkin-Elmer 2000 FTIR spectrometer with 0 1mm sodium chloride liquid solution cells using spectroscopic grade pentane as solvent ^{1}H and ^{13}C NMR spectra were recorded on a Bruker model AC 400 MHz spectrometer in the appropriate deuterated solvent at room temperature with TMS as a standard All UV-vis spectra were measured in spectroscopic grade solvents on a Hewlett Packard 8452A-photodiode array spectrometer using a 1cm quartz cell All samples were prepared for steady state and laser flash photolysis by the freeze-pump-thaw procedure as described in the appendix

3 3 3 Synthesis

3 3 3 1 $(CO)_5Cr=C(OMe)Me$

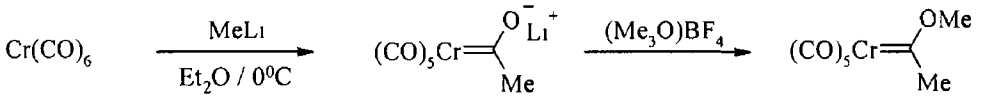

Scheme 3 - 2

$(CO)_5Cr=C(OMe)Me$ was prepared according to Fischer's procedure[17] with some modifications 9 09 mmol (2 0g) of $Cr(CO)_6$ was weighed out and dissolved in 25 ml of dry diethyl ether This solution was then cooled to 0 ^{0}C and a 10 % excess of MeLi (3 70 ml of a 2 5 M solution in diethyl ether) was slowly added dropwise by syringe The reaction mixture was allowed to reach room temperature and left stirring for 1 hour resulting in a dark brown solution at which point the solvent was removed under reduced pressure The resulting residue was dissolved in 25 ml of water and added to a separating funnel containing 25 ml of dichloromethane Trimethyloxonium tetrafluoroborate salt was added to this mixture until the aqueous phase reached a pH of 3 - 4 (~ 8 mmol/1 2 g) The product was extracted from the aqueous phase with four 25 ml aliquots of dichloromethane The organic extracts were combined, dried over magnesium sulphate and the solvent removed under reduced pressure resulting in a light brown oil Washing with cold pentane resulted in a yellow solid (1 86 g, 7 45 mmol, 82 % yield) which was subsequently characterised Analytical data were in agreement with the reported data [17]

IR (νCO) 2065, 1947 (broad) cm ^{1} (pentane)

^{1}H NMR ($CDCl_3$) δ 2 88 (3H, s), 4 64 (3H, s) ppm

3 3 3 2 (*E*)-$(CO)_5Cr{=}C(OMe)C_2H_2Fc$

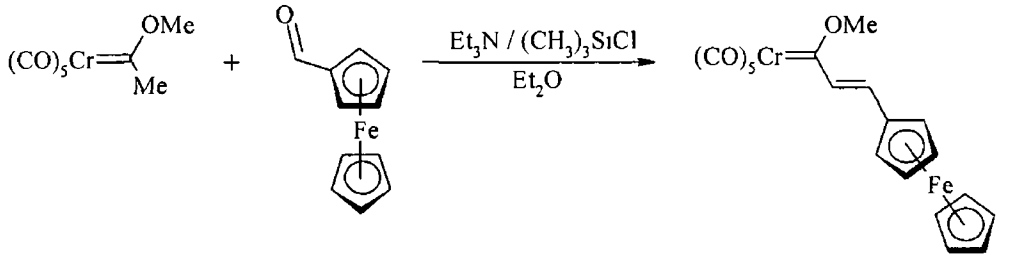

Rxn 3 - 1

(*E*)-$(CO)_5Cr{=}C(OMe)C_2H_2Fc$ was prepared according to a previously reported method with some modifications [15] To 25 ml of diethyl ether, 20 mmol (2 8 ml) trimethylamine, 15 mmol (2 3 ml) chlorotrimethylsilane and 5 mmol (1 07 g) ferrocenecarboxaldehyde was added 5 mmol (1 32 g) of $(CO)_5Cr{=}C(OMe)Me$ in 5 ml of diethyl ether The reaction mixture was allowed to stir at room temperature for 24 hours, during which time the solution changed colour from a reddish-brown to a dark purple The solvent was removed under reduced pressure and the resulting residue was passed through a silica gel column by flash chromatography using pentane dichloromethane (9 1) as the mobile phase (*E*)-$(CO)_5Cr{=}C(OMe)C_2H_2Fc$ eluted off the column as a dark purple band in 63 % yield (1 33 g, 3 15 mmol) behind the light yellow starting material $(CO)_5Cr{=}C(OMe)Me$ and traces of chromium hexacarbonyl at the solvent front Analytical data were in agreement with the reported data [15]

IR (νCO) 2056, 1955, 1945 cm ^{1} (pentane)

^{1}H NMR ($CDCl_3$) δ 4 20 (5H,s), 4 60 – 4 62 (4H, m), 4 68 (3H, s), 7 15 (1H, d, ^{3}J = 15 2 Hz), 7 47 (1H, d, ^{3}J = 15 2 Hz) ppm

^{13}C NMR ($CDCl_3$) 66 02, 70 32, 70 72, 73 07, 78 70, 137 88, 138 51, 217 67, 224 73, 323 07 ppm

3 3 3 3 (*E*)-$(CO)_5Cr{=}C(OMe)C_2H_2Ph$

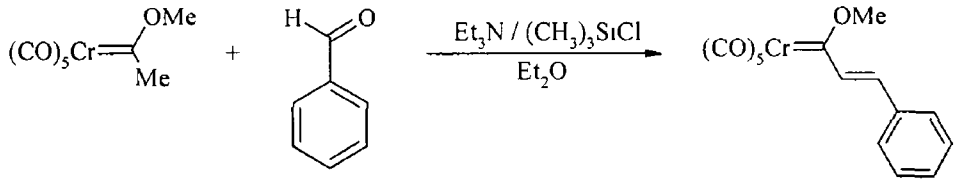

Rxn 3 - 2

To 25 ml of diethyl ether, 20 mmol (2 80 ml) trimethylamine, 15 mmol (2 3 ml) chlorotrimethylsilane and 5 mmol (1 07 g) benzaldehyde was added 5 mmol (1 32 g) of $(CO)_5Cr{=}C(OMe)Me$ in 5 ml of diethyl ether The reaction mixture was allowed to stir at room temperature for 24 hours, during which time the colour changed from reddish-brown to dark purple The solvent was removed under reduced pressure and the resulting residue was passed through a silica gel column by flash chromatography using pentane as the mobile phase (*E*)-$(CO)_5Cr{=}C(OMe)C_2H_2Ph$ eluted off the column as a red band in 44 % yield (744 mg, 2 20 mmol) behind the light yellow starting material $(CO)_5Cr{=}C(OMe)Me$ and traces of chromium hexacarbonyl at the solvent front Analytical data were in agreement with the reported data [18]

IR (νCO) 2060, 1962, 1950 cm ^{1} (pentane)

^{1}H NMR ($CDCl_3$) δ 7 95 (1H, d, ^{3}J = 15 6 Hz), 7 59 (2H, m), 7 42 (3H, m), 6 99 (1H, d, ^{3}J = 15 6 Hz), 4 83 (3H,s) ppm

3 3 3 4 $(CO)_5W=C(OMe)Me$

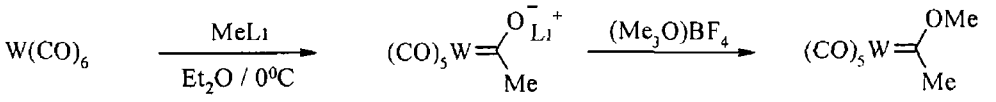

Scheme 3 - 3

$(CO)_5W=C(OMe)Me$ was prepared in a similar manner to $(CO)_5Cr=C(OMe)Me$ 2 84 mmol (1g) of $W(CO)_6$ were weighed out and added to 15 ml of dry diethyl ether This solution was then cooled to 0 ^{0}C and a 10 % excess of MeLi (1 25 ml of a 2 5 M solution in diethyl ether) was slowly added dropwise by syringe The reaction mixture was allowed to reach room temperature and left stirring for 1 hour resulting in a dark brown solution at which point the solvent was removed under reduced pressure The resulting residue was dissolved in 25 ml of water and added to a separating funnel containing 25 ml of dichloromethane Trimethyloxomum tetrafluoroborate salt (~ 3 mmol/0 44 g) was added to this mixture until the aqueous phase reached a pH of 3 - 4 The product was extracted from the aqueous phase with four 25 ml aliquots of dichloromethane The organic extracts were then combined, dried over magnesium sulphate and the solvent removed under reduced pressure resulting in a light brown oil Washing this oil with cold pentane resulted in a yellow solid (0 76 g, 1 82 mmol, 64 % yield) which was subsequently characterised Analytical data were in agreement with the reported data

IR (νCO) 1946, 1961, 2074 cm ^{1} (pentane)

^{1}H NMR ($CDCl_3$) δ 2 87 (3H, m), 4 59 (3H, s) ppm

3 3 3 5 (*E*)-$(CO)_5W{=}C(OMe)C_2H_2Fc$

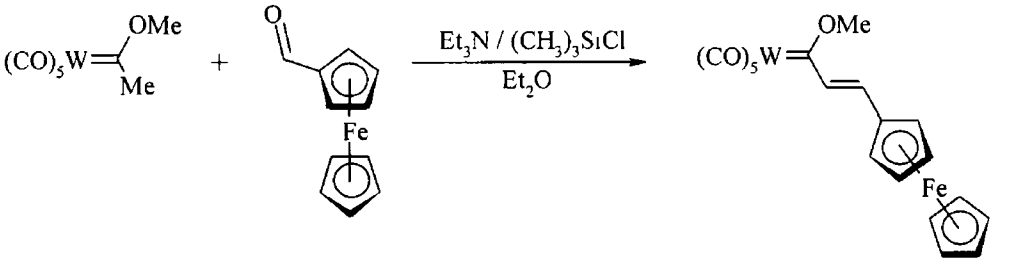

Rxn 3 - 3

(*E*)-$(CO)_5W{=}C(OMe)C_2H_2Fc$ was prepared according to a previously reported method with some modifications [15] To 15 ml of diethyl ether, 10 mmol (1 40 ml) trimethylamine, 7 50 mmol (1 15 ml) chlorotrimethylsilane and 2 50 mmol (0 54 g) ferrocenecarboxaldehyde was added 2 50 mmol (0 76 g) of $(CO)_5W{=}C(OMe)Me$ in 5ml of diethyl ether The reaction mixture was allowed to stir at room temperature for 24 hours The solution changed in colour from reddish-brown to dark purple over the course of the reaction The solvent was removed under reduced pressure and the resulting residue was passed through a silica gel column by flash chromatography using pentane dichloromethane (9 1) as the mobile phase Compound (*E*)-$(CO)_5W{=}C(OMe)C_2H_2Fc$ eluted off the column as a dark purple band in 52 % yield (593 mg, 1 30 mmol) behind the light yellow starting material $(CO)_5W{=}C(OMe)Me$ and traces of tungsten hexacarbonyl at the solvent front Analytical data were in agreement with the reported data

IR (νCO) 2065, 1952, 1941 cm ^{1} (pentane)

^{1}H NMR ($CDCl_3$) δ 4 14 (5H,s), 4 47 (3H, s), 4 55 (4H, m), 7 19 (2H, s) ppm

^{13}C NMR ($CDCl_3$) 67 33, 68 89, 69 37, 71 80, 76 20, 77 43, 140 10, 141 83, 196 94, 202 77, 299 66 ppm

3 3 3 6 (*E*)-$(CO)_5Cr{=}C(C_4H_8N)C_2H_2Fc$

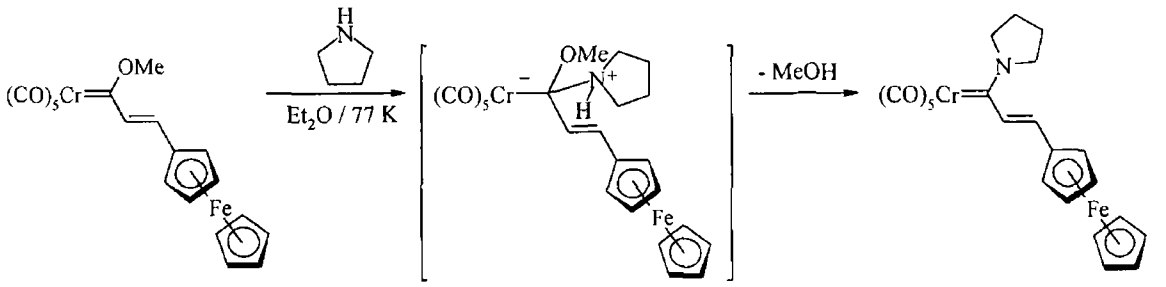

Scheme 3 – 4

1 20 mmol (0 10 ml) of pyrrolidine was added *via* syringe to a diethyl ether solution (25 ml) of (*E*)-$(CO)_5Cr{=}C(C_4H_8N)C_2H_2Fc$ (1 mmol/0 42 g) at 77 K The reaction was allowed to reach room temperature during which time the solution changed from a deep purple colour to an orange-red colour After leaving to stir for an additional 5 minutes, the solvent and excess pyrrolidine were removed under reduced pressure and the crude complex were purified by flash chromatography on a silica gel column using pentane dichloromethane (9 1) in 92 % yield (446 mg, 0 92 mmol)

Orange-red solid

IR (νCO) 1928, 1935, 2053 cm^{-1} (pentane)

^1H NMR ($CDCl_3$) δ 2 03 (4H, m), 3 60 (2H, dd), 4 09 (2H, dd), 4 13 (5H, s), 4 24 (2H, m), 4 32 (2H, m), 6 17 (1H, d, ^3J = 16 Hz), 6 68 (1H, d, ^3J = 16 Hz) ppm

^{13}C NMR ($CDCl_3$) 25 51, 25 84, 55 50, 59 94, 67 45, 68 35, 69 66, 69 91, 82 82, 127 55, 136 92, 218 63, 224 02, 262 50 ppm

Anal Calcd for $C_{22}H_{19}NO_5CrFe$ C 54 46, H 3 95, N 2 89 Found C 54 16, H 3 67, N 2 63

3 3 3 7 (*E*)-$(CO)_5W{=}C(C_4H_8N)C_2H_2Fc$

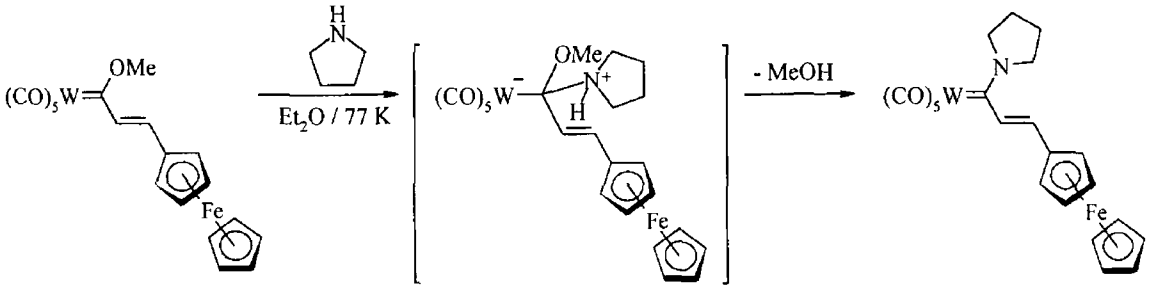

Scheme 3 – 5

(*E*)-$(CO)_5W{=}C(C_4H_8N)C_2H_2Fc$ was synthesised in an identical manner to the chromium analogue in 90 % yield (555 mg, 0 90 mmol)

Red solid

IR (νCO) 1924, 2060 cm ^{1} (pentane)

^{1}H NMR ($CDCl_3$) δ 2 04 (4H, m), 3 57 (2H, m), 3 99 (2H, m), 4 13 (5H, s), 4 29 (2H, m), 4 36 (2H, m), 6 63 (2H, s) ppm

^{13}C NMR ($CDCl_3$) δ 25 27, 25 99, 53 79, 62 75, 67 88, 69 83, 70 35, 77 62, 82 13, 136 53, 136 81, 199 74, 203 62, 242 96 ppm

Anal Calcd for $C_{22}H_{19}NO_5CrFe$ C 42 82, H 3 10, N 2 27 Found C 42 73, H 2 93, N 2 08

3.4 Results

3.4.1 Photochemistry of (*E*)-$(CO)_5Cr=C(OMe)C_2H_2Fc$

3.4.1.1 Laser flash photolysis of (*E*)-$(CO)_5Cr=C(OMe)C_2H_2Fc$ in cyclohexane at λ_{exc} = 355 nm

(*E*)-$(CO)_5Cr=C(OMe)C_2H_2Fc$ is a dark purple solid with a UV-vis spectrum exhibiting two low energy bands in the visible region of the spectrum at 548 nm (ε = 6.45 x 10^4 $M^{-1}cm^{-1}$) and 466 nm (ε = 6.81 x 10^4 $M^{-1}cm^{-1}$) and a higher lying band at 334 nm (ε = 1.15 x 10^5 $M^{-1}cm^{-1}$) in cyclohexane (fig. 3 – 10).

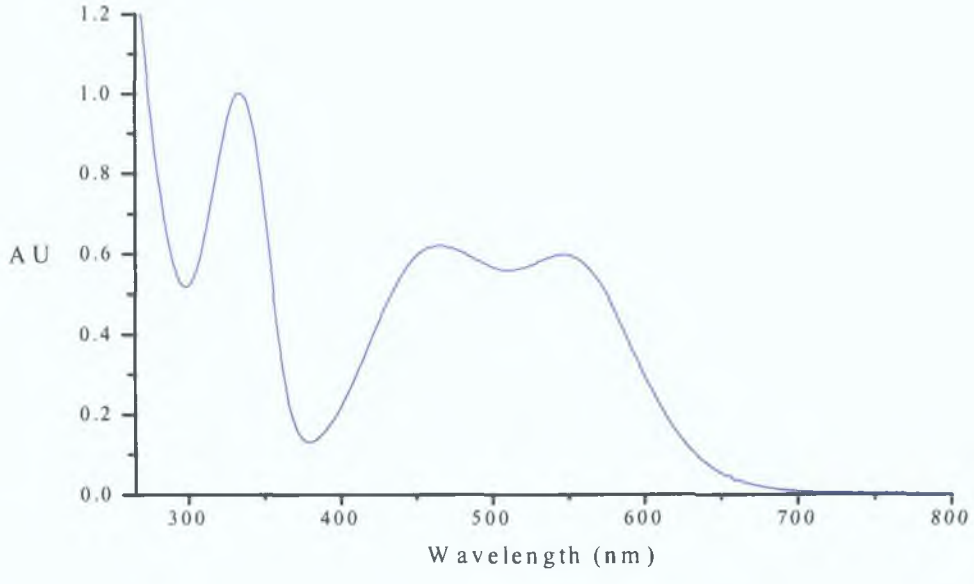

Fig. 3 – 10: UV-vis spectrum of (*E*)-$(CO)_5Cr=C(OMe)C_2H_2Fc$ in cyclohexane.

Following laser flash photolysis at 355 nm in cyclohexane under one atmosphere of carbon monoxide at room temperature, a single transient species was observed with λ_{max} at 380 and 290 nm. Depletion of the parent compound was observed from 390 – 630 nm and 290 – 340 nm. This depletion occurs within the lifetime of the laser pulse (10 ns), followed by an exponential recovery to the pre-flash absorbance level. The UV-vis spectrum remained unchanged throughout the experiment.

Figure 3 – 11 shows a typical transient signal observed at 550 nm, $\tau = 6 \pm 0.64$ ms ($k_{obs} = 156 \pm 16$ s^{-1}), which corresponds to the low energy absorption band of the parent compound. Figure 3 – 12 shows the transient signal observed at 290 nm, $\tau = 7 \pm 0.66$ ms ($k_{obs} = 153 \pm 15$ s^{-1}). The transient absorption difference spectra are given in figure 3 – 13.

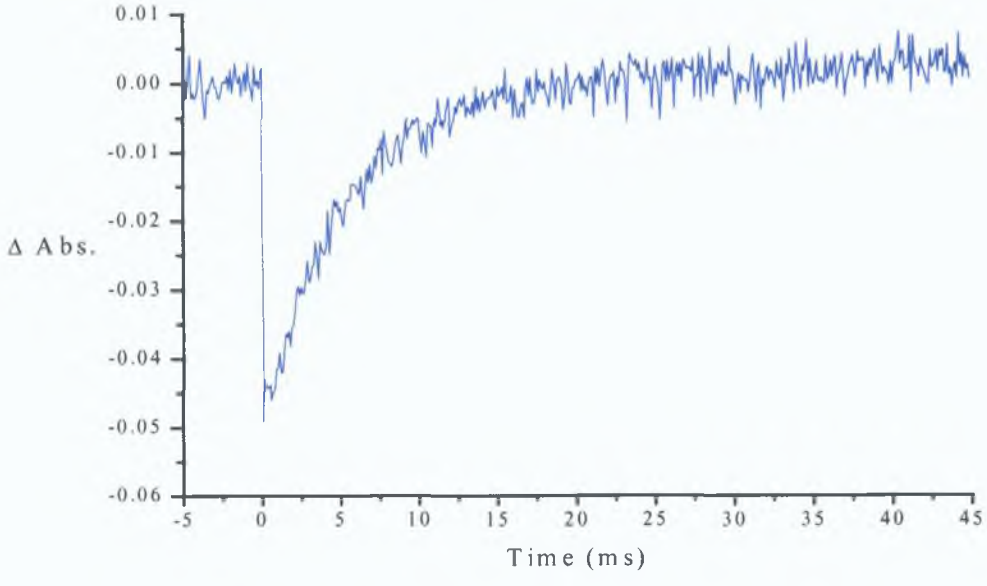

Fig. 3 – 11: Transient signal observed at 550 nm following laser flash photolysis ($\lambda_{exc} = 355$ nm) of (*E*)-$(CO)_5Cr{=}C(OMe)C_2H_2Fc$ in cyclohexane under one atmosphere of carbon monoxide, $\tau = 6 \pm 0.64$ ms ($k_{obs} = 156 \pm 16$ s^{-1}).

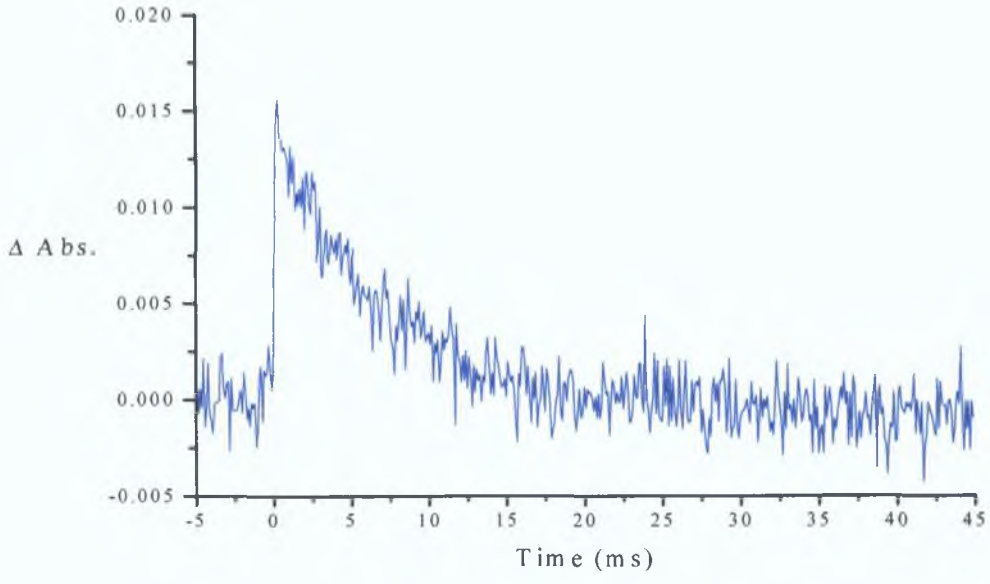

Fig. 3 – 12: Transient signal observed at 290 nm following laser flash photolysis (λ_{exc} = 355 nm) of (*E*)-$(CO)_5Cr{=}C(OMe)C_2H_2Fc$ in cyclohexane under one atmosphere of carbon monoxide, $\tau = 7 \pm 0.66$ ms ($k_{obs} = 153 \pm 15$ s^{-1}).

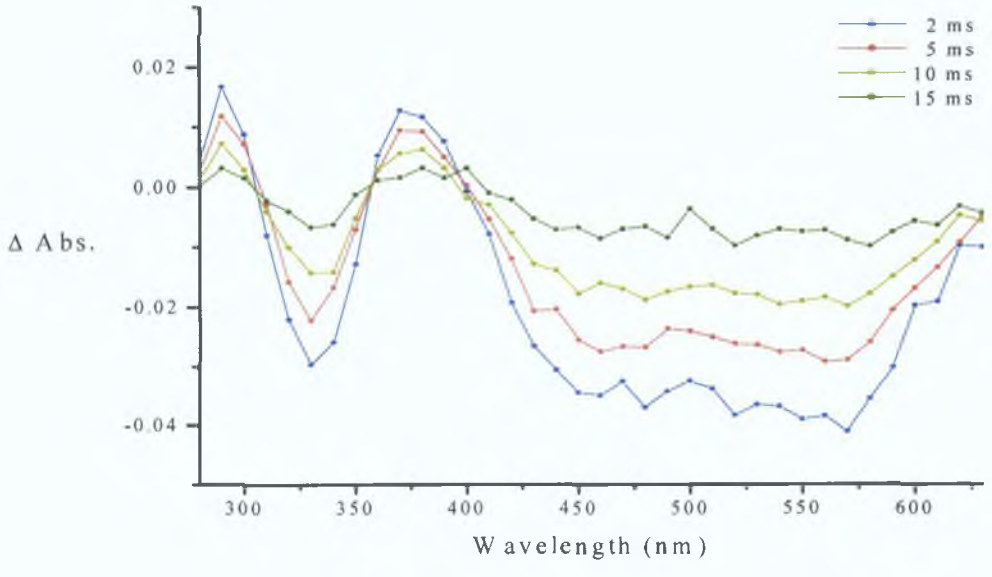

Fig. 3 - 13: Transient absorption difference spectra recorded at different time delays following flash photolysis (λ_{exc} = 355 nm) of (*E*)-$(CO)_5Cr{=}C(OMe)C_2H_2Fc$ in cyclohexane under one atmosphere of carbon monoxide. The transient absorbance difference spectra are plotted point-by-point every 10 nm.

There was no evidence for recovery of the parent compound following flash photolysis under an atmosphere of argon. Shown in figure 3 – 14 are the transient absorption difference spectra. Figure 3 - 15 shows an overlay of two transients recorded at 550 nm under one atmosphere of carbon monoxide and also under one atmosphere of argon. The UV-vis spectra recorded throughout the experiment show a gradual decomposition of the parent compound (fig. 3 - 16).

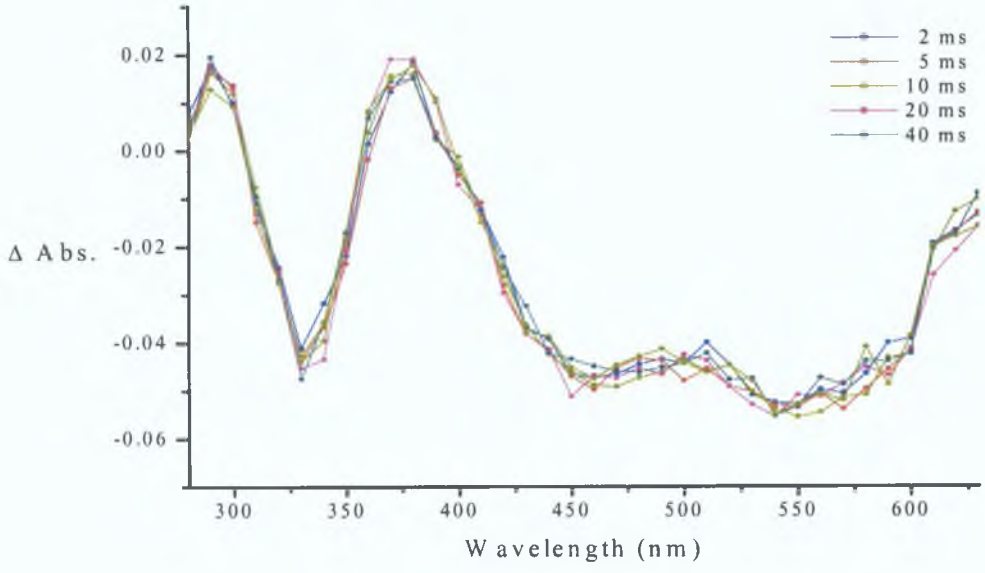

Fig. 3 - 14: Transient absorption difference spectra recorded at different time delays following flash photolysis (λ_{exc} = 355 nm) of (*E*)-$(CO)_5Cr{=}C(OMe)C_2H_2Fc$ in cyclohexane under one atmosphere of argon. The transient absorbance difference spectra are plotted point-by-point every 10 nm.

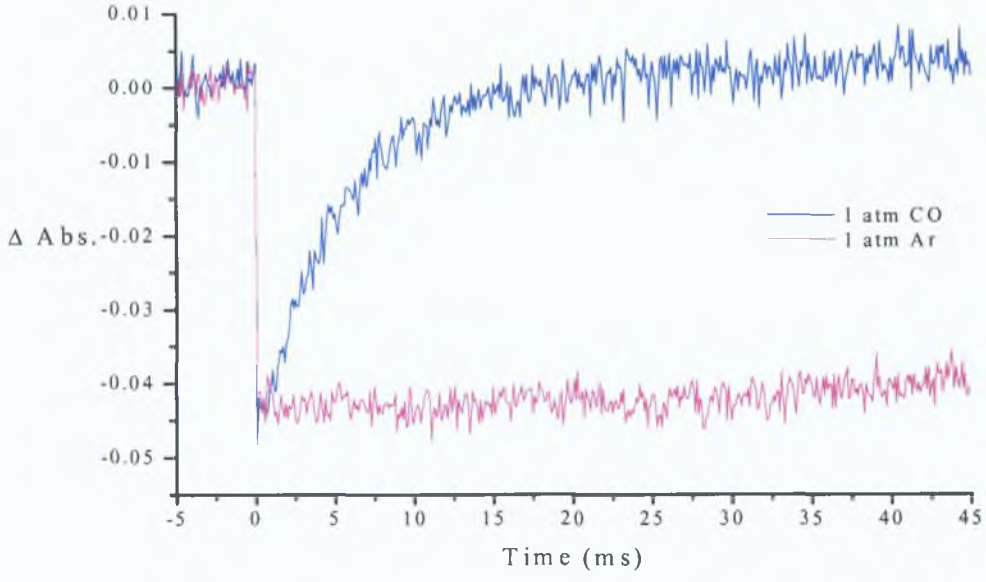

Fig. 3 - 15: Signals recorded at 550 nm following laser flash photolysis (λ_{exc} = 355 nm) of (*E*)-$(CO)_5Cr{=}C(OMe)C_2H_2Fc$ in cyclohexane under one atmosphere of carbon monoxide and one atmosphere of argon at 550 nm.

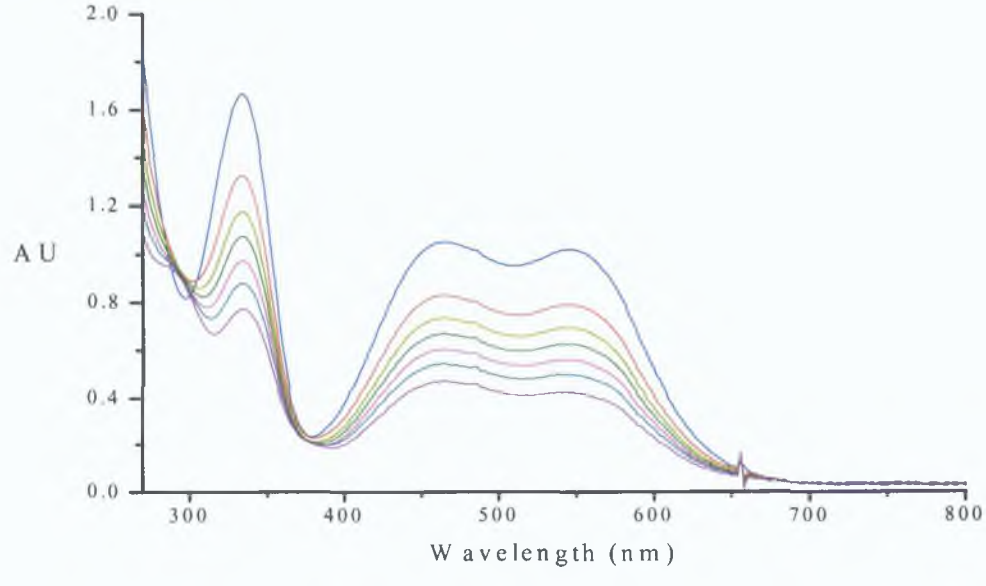

Fig. 3 - 16: UV-vis spectra recorded during laser flash photolysis (λ_{exc} = 355 nm) of (*E*)-$(CO)_5Cr{=}C(OMe)C_2H_2Fc$ in cyclohexane under one atmosphere of argon.

3.4.1.2 Laser flash photolysis of (*E*)-$(CO)_5Cr=C(OMe)C_2H_2Fc$ in cyclohexane at λ_{exc} = 532 nm

A single transient species was observed following laser flash photolysis of (*E*)-$(CO)_5Cr=C(OMe)C_2H_2Fc$ at 532 nm in cyclohexane under one atmosphere of argon at room temperature with a λ_{max} at 610 nm (fig. 3 – 17). The lifetime of this species was very short lived in comparison to the CO loss product observed following 355 nm excitation and is tentatively assigned to a species resulting from photoinduced *trans-cis* isomerisation, τ = 190 ± 19 ns (k_{obs} = 5 ± 0.5 x 10^6 s^{-1}). The UV-vis absorption spectrum remained unchanged throughout the experiment. The lifetime of this species was unchanged under atmospheric conditions, i.e. in the presence of oxygen as a triplet quencher, suggesting that the photoinduced *trans-cis* isomerisation of the vinyl spacer in (*E*)-$(CO)_5Cr=C(OMe)C_2H_2Fc$ occurs *via* a singlet excited state.

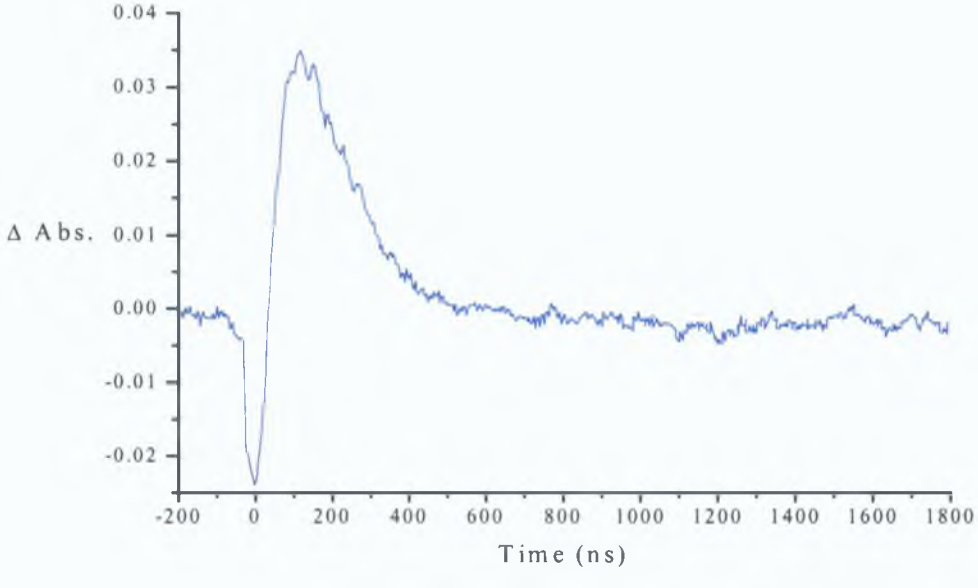

Fig. 3 - 17: Transient signal observed at 610 nm following laser flash photolysis (λ_{exc} = 532 nm) of (*E*)-$(CO)_5Cr=C(OMe)C_2H_2Fc$ in cyclohexane under one atmosphere of argon (τ = 190 ± 19 ns , k_{obs} = 5 ± 0.5 x 10^6 s^{-1}).

3 4 1 3 Determination of the second order rate constant for the reaction of the species formed following laser flash photolysis of $(CO)_5Cr=C(OMe)C_2H_2Fc$ with CO in cyclohexane

The second order rate constant for the reaction of a transient species with CO can be determined from the slope of the line obtained by plotting the observed rate constant versus CO concentration A variable CO experiment was carried out on the complex (*E*)-$(CO)_5Cr=C(OMe)C_2H_2Fc$ to confirm that CO loss occurs following flash photolysis at 355 nm The lifetime of the transient species was measured as it recombined with the CO present in solution to regenerate the parent compound, (*E*)-$(CO)_5Cr=C(OMe)C_2H_2Fc$ Only transient signals observed at 550 nm were monitored (as this is where the strongest signal was observed, fig 3 – 18) as the CO concentration varied systematically over the range 2 25 x 10^{-3} M to 9 0 x 10^{-3} M (i e 0 25 – 1 0 atm CO) As the concentration of CO is increased the lifetime of the transient species decreases accordingly, thus confirming formation of a CO loss species Figure 3 – 19 shows a plot of k_{obs} *vs* CO concentration The slope of the line represents the second order rate constant for the reaction of the transient species with CO at room temperature, $k_2 = 16 \pm 1\ 63\ M^{-1}s^{-1}$

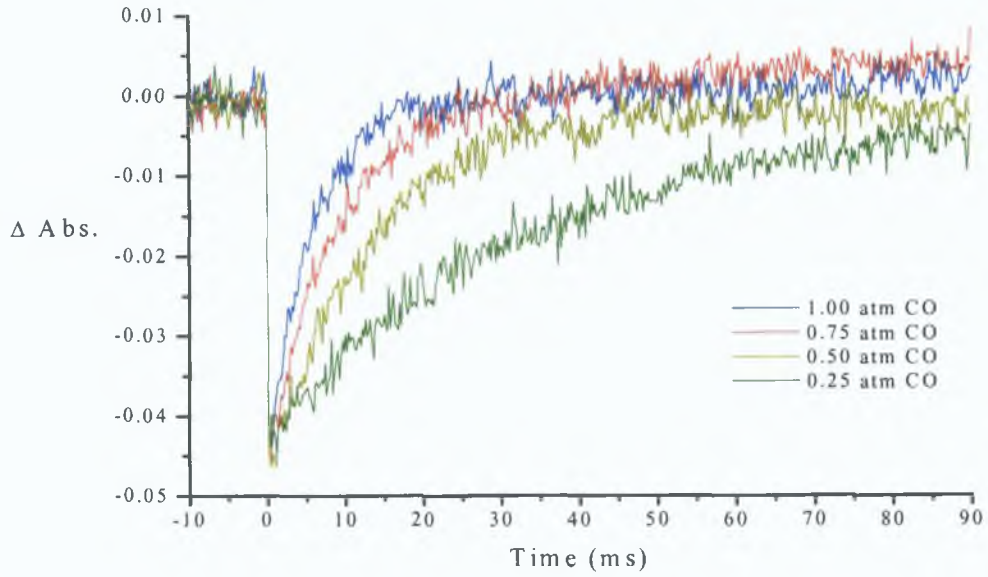

Fig. 3 – 18: An overlay of the signals recorded at 550 nm for (*E*)-$(CO)_5Cr{=}C(OMe)C_2H_2Fc$ following laser flash photolysis (λ_{exc} = 355 nm) with various concentrations of CO.

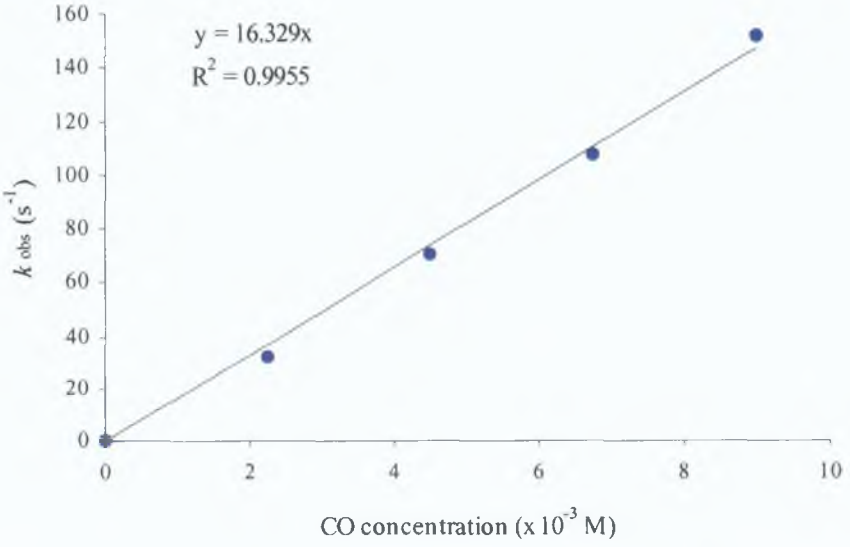

Fig. 3 – 19: Plot of k_{obs} *vs.* CO concentration for the decay of the transient species in cyclohexane at room temperature to the regenerate the parent compound (*E*)-$(CO)_5Cr{=}C(OMe)C_2H_2Fc$.

3 4 1 4 Activation parameters for the reaction of the species formed following laser flash photolysis of $(CO)_5Cr=C(OMe)C_2H_2Fc$ with CO in cyclohexane

Activation parameters were obtained by measuring k_2 over the temperature range 283 - 308 K From Eyring and Arrhenius plots, which were then constructed, it was possible to obtain the activation parameters for the reaction of the transient species with CO Given in figure 3 - 20 and figure 3 – 21 are the Arrhenius plot and the Eyring plot respectively (note the CO concentration was kept constant at 9 0 x 10^{-3}M)

1 / Temperature (x 10^{3} K^{-1})	ln (k_{obs} / [CO])
3 53	9 07
3 47	9 25
3 41	9 46
3 36	9 62
3 30	9 77
3 25	9 94

(a)

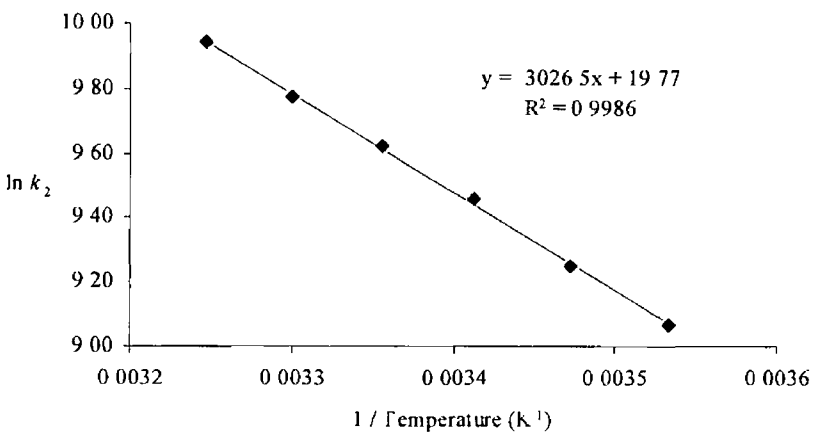

(b)

Fig 3 – 20 Arrhenius data (a) and plot (b) for the reaction of the transient species with CO in cyclohexane

1 / Temperature (x 10^{3} K^{1})	ln [(k_{obs}/ [CO]) / T]
3 53	3 42
3 47	3 59
3 41	3 78
3 36	3 92
3 30	4 06
3 25	4 21

(a)

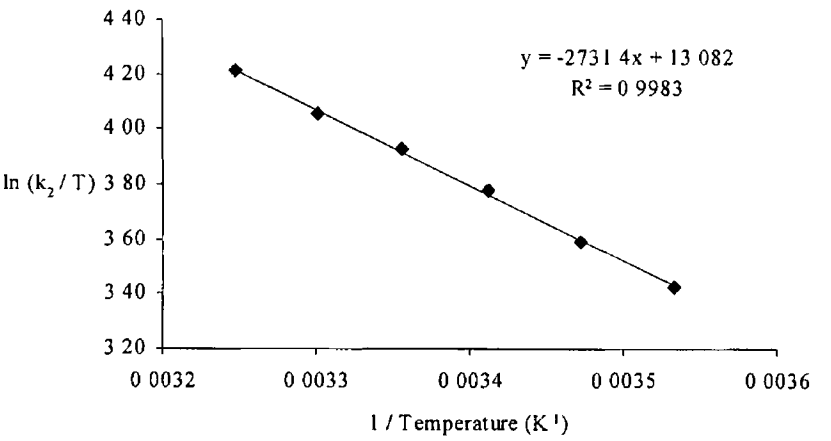

(b)

Fig 3 – 21 Eyring data (a) and plot (b) for the reaction of (cyclohexane)$(CO)_4Cr{=}C(OMe)C_2H_2Fc$ with CO in cyclohexane

The Arrhenius equation is given by '$\ln [k_{obs}/CO_{conc}] = -E^{\neq}_{act}/RT + \ln A$' Therefore a plot of $\ln k_2$ *vs* 1/T results in a straight line, with slope '$-E^{\neq}_{act}/R$' and intercept '$\ln A$' The activation energy of reaction of the transient species with CO (9 0 x 10^{3} M) in cyclohexane was therefore calculated as $E^{\neq}_{act} = 25 \pm 3$ kJ mol^{1}

The Eyring equation is given by '$\ln [(k_{obs}/CO_{conc})/T] = - (\Delta H^{\neq}/RT) + (\Delta S^{\neq}/R) + \ln (k/h)$' A plot of $\ln [k_2/T]$ *vs* 1/T gives a straight line, with slope '$-\Delta H^{\neq}/R$' and intercept '$(\Delta S^{\neq}/R) + \ln (k/h)$' Thus, the standard enthalpy and entropy for the reaction of the transient species with CO (9 0 x 10^{3} M) in cyclohexane are $\Delta H^{\neq} = 23 \pm 2$ kJ mol^{1} and $\Delta S^{\neq} = -89 \pm 9$ J K^{1} mol^{1}

3.4.1.5 Laser flash photolysis of (*E*)-$(CO)_5Cr=C(OMe)C_2H_2Fc$ in cyclohexane in the presence of excess triphenylphosphine at λ_{exc} = 355 nm

Following laser flash photolysis of (*E*)-$(CO)_5Cr=C(OMe)C_2H_2Fc$ in the presence of excess triphenylphosphine (λ_{exc} = 355 nm), a depletion in the absorbance of the parent compound was observed in the range 430 – 630 nm and between 320 – 340 nm (fig. 3 – 22). A transient species was also observed from 420 – 350 nm (λ_{max} = 370 nm). The purple solution became gradually darker during the photolysis. The lower energy absorption band of the parent compound at 548 nm increased in absorbance as the photolysis proceeded with a concomitant decrease in the higher lying band at 466 nm. An increase in absorption also occurred on the high-energy side of the 334 nm band (see fig. 3 – 23 in the following section). An isosbestic point was observed at 362 nm. An infrared spectrum recorded after the experiment showed new ν(CO) peaks at 1900, 1913, 1931 and 2006 cm^{-1} confirming formation of the tetracarbonyl species (*E*)-*cis*-$(PPh_3)(CO)_4Cr=C(OMe)C_2H_2Fc$ (see fig. 3 – 24 in the following section).[19]

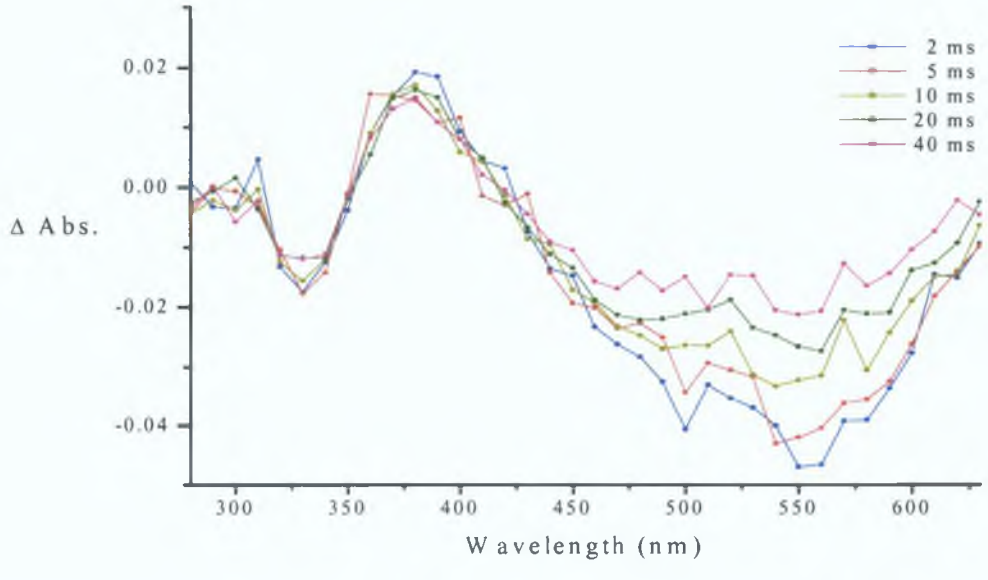

Fig. 3 - 22: Absorbance difference spectra recorded at different time delays following laser flash photolysis (λ_{exc} = 355 nm) of (*E*)-$(CO)_5Cr=C(OMe)C_2H_2Fc$ in cyclohexane under one atmosphere of argon in the presence of excess triphenylphosphine. The transient absorbance difference spectra are plotted point-by-point every 10 nm.

3 4 1 6 Steady state photolysis of (*E*)-$(CO)_5Cr=C(OMe)C_2H_2Fc$ in cyclohexane in the presence of excess triphenylphosphine

The photochemistry of (*E*)-$(CO)_5Cr=C(OMe)C_2H_2Fc$ was investigated in cyclohexane under one atmosphere of argon at room temperature in the presence of a large excess of triphenylphosphine in an attempt to trap the tetracarbonyl transient species The sample was irradiated at λ_{exc} > 550, > 400 and > 320 nm No photochemistry was observed at λ_{exc} > 550 nm, however, a small amount of tetracarbonyl was formed following irradiation at λ_{exc} > 400 nm Formation of the photoproduct was most efficient at λ_{exc} > 320 nm The observed changes in the UV-vis spectrum (fig 3 – 23) correspond to those observed following laser flash photolysis (λ_{exc} = 355 nm) An isosbestic point was observed at 362 nm, which is indicative of a clean reaction After 60 mm of photolysis, when no more changes were apparent in the UV-vis spectrum, the solvent was removed under reduced pressure and an infrared spectrum was recorded of the residual solid Peaks indicative of the formation of the tetracarbonyl species (*E*)-*cis*-$(PPh_3)(CO)_4Cr=C(OMe)C_2H_2Fc$ were present confirming occurrence of CO loss (fig 3 – 24) No peaks from the parent compound were present indicating complete conversion to the tetracarbonyl species

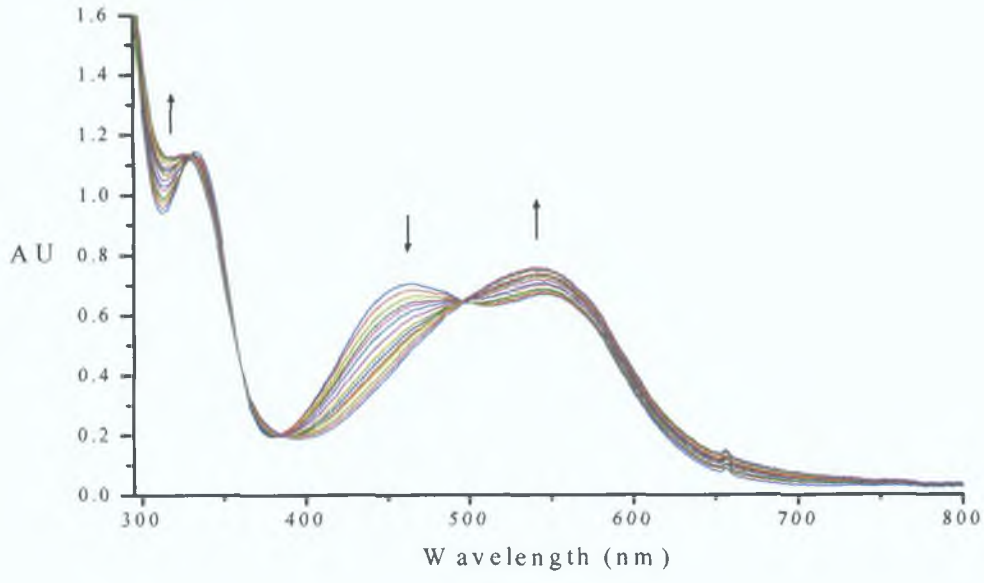

Fig. 3 - 23: UV-vis spectra recorded during steady state photolysis (λ_{exc} > 320 nm) of (*E*)-$(CO)_5Cr{=}C(OMe)C_2H_2Fc$ in cyclohexane under one atmosphere of argon in the presence of excess triphenylphosphine.

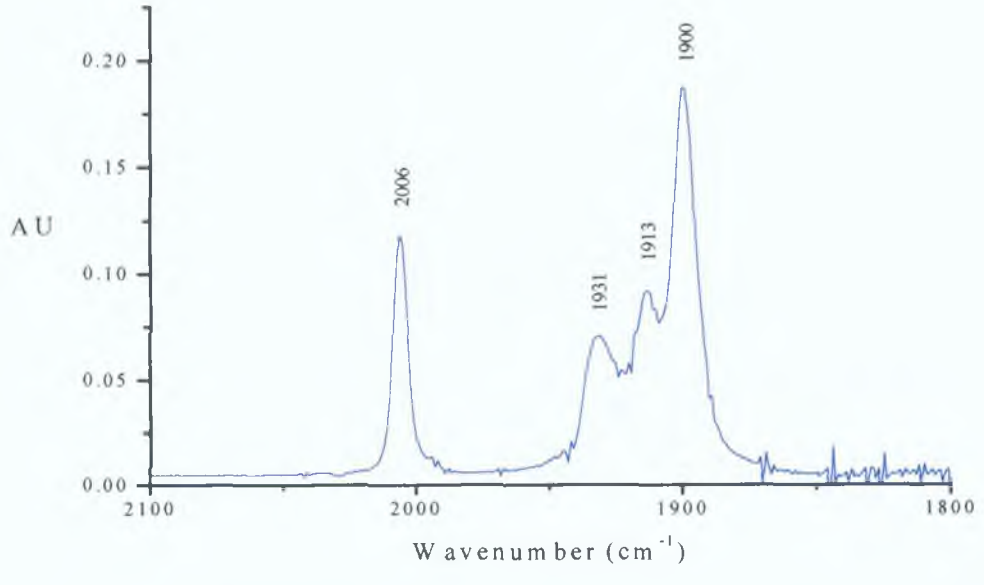

Fig. 3 - 24: Infrared spectrum of (*E*)-*cis*-$(PPh_3)(CO)_4Cr{=}C(OMe)C_2H_2Fc$ recorded following steady state photolysis (λ_{exc} > 320 nm) of $(CO)_5Cr{=}C(OMe)C_2H_2Fc$ in cyclohexane under one atmosphere of argon in the presence of excess triphenylphosphine.

3.4.2 Photochemistry of (*E*)-$(CO)_5Cr=C(OMe)C_2H_2Ph$

3.4.2.1 Laser flash photolysis of (*E*)-$(CO)_5Cr=C(OMe)C_2H_2Ph$ in cyclohexane at λ_{exc} = 355 nm

(*E*)-$(CO)_5Cr=C(OMe)C_2H_2Ph$ is a red solid with a UV-vis spectrum exhibiting two low-energy bands in the visible region of the spectrum at 472 nm and also a higher lying band at 324 nm in cyclohexane solution (fig. 3 – 25).

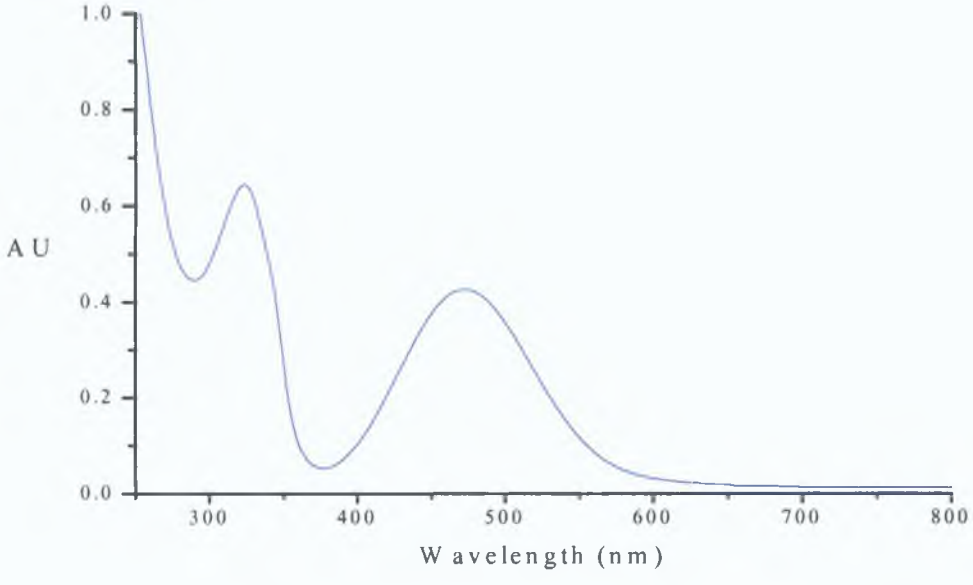

Fig. 3 – 25: UV-vis spectrum of (*E*)-$(CO)_5Cr=C(OMe)C_2H_2Ph$ in cyclohexane solution.

Following laser excitation at 355 nm in cyclohexane under one atmosphere of carbon monoxide at room temperature, a single transient species was observed with a λ_{max} at 370 nm. A depletion in absorbance of the parent compound was also observed in the range 420 - 600 nm as evident in the transient absorbance difference spectrum (fig. 3 – 26). This depletion occurs within the lifetime of the laser pulse (10 ns) and decays with a lifetime of τ = 40 ± 4 ms, k_{obs} = 25 ± 3 s^{-1} (fig. - 27). The UV-vis absorption spectrum remained unchanged throughout the experiment.

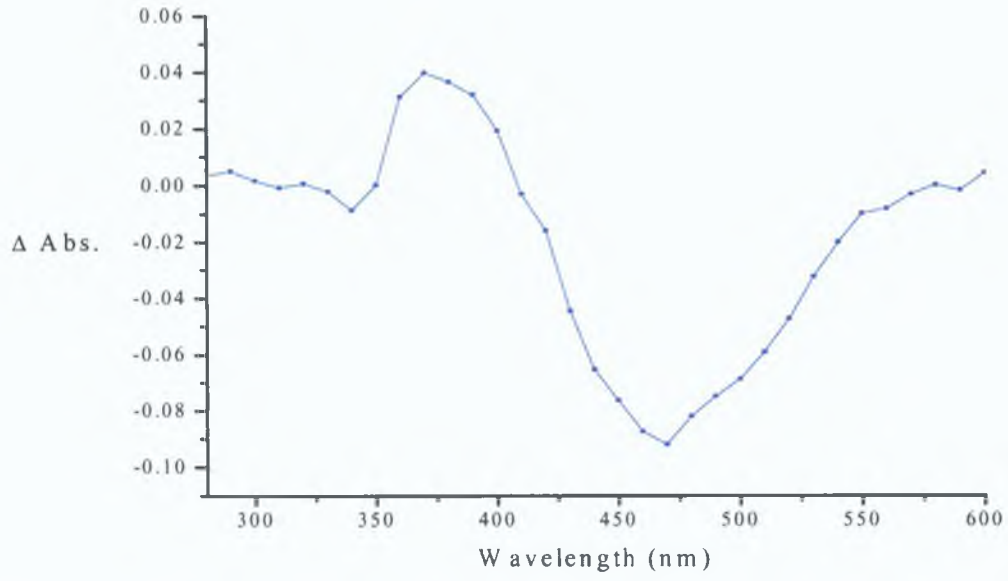

Fig. 3 - 26: Transient absorption difference spectrum recorded 2 ms following flash photolysis (λ_{exc} = 355 nm) of (*E*)-$(CO)_5Cr{=}C(OMe)C_2H_2Ph$ in cyclohexane under one atmosphere of carbon monoxide. The transient absorbance difference spectrum is plotted point-by-point every 10 nm.

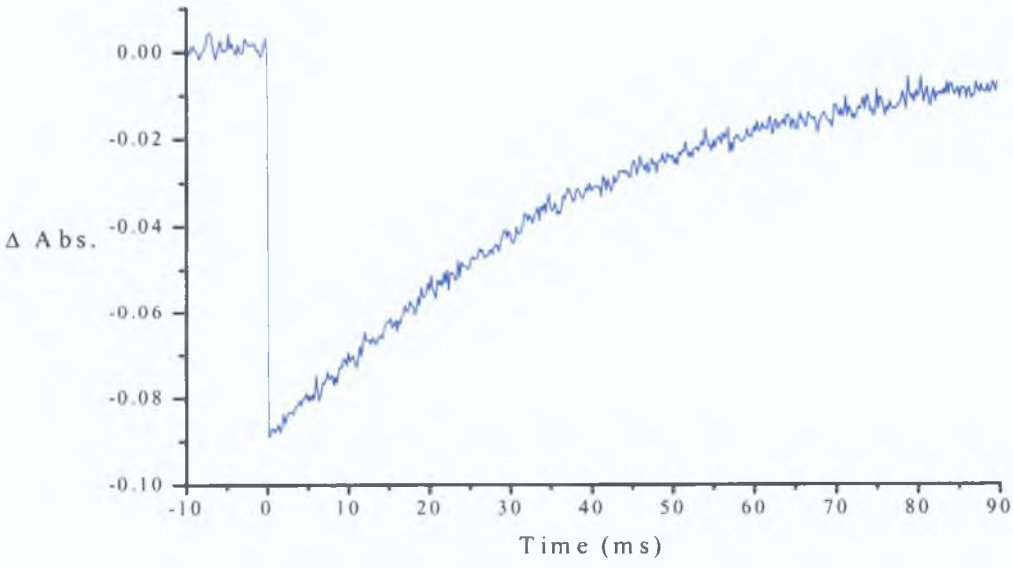

Fig. 3 - 27: Recovery of parent compound observed at 470 nm observed following laser flash photolysis (λ_{exc} = 355 nm) of (*E*)-$(CO)_5Cr{=}C(OMe)C_2H_2Ph$ in cyclohexane under one atmosphere of carbon monoxide (τ = 40 ± 4 ms, k_{obs} = 25 ± 3 s^{-1}).

3 4 2 2 Laser flash photolysis of (*E*)-$(CO)_5Cr=C(OMe)C_2H_2Ph$ in cyclohexane at λ_{exc} = 532 nm

A single transient species was observed following laser flash photolysis of (*E*)-$(CO)_5Cr=C(OMe)C_2H_2Ph$ at 532 nm in cyclohexane under one atmosphere of argon at room temperature with λ_{max} at 610 nm (fig – 28) The lifetime of this species was very short lived when compared to the transient signal observed following laser flash photolysis at 355 nm excitation This transient signal is tentatively assigned to the *cis*-isomer of the parent compound, which regenerates the parent *trans*-isomer (τ = 262 ± 26 ns, k_{obs} = 3 82 ± 0 40 x 10^6 s^{-1}) A depletion and recovery of the parent compound was also observed at 420 nm (τ = 278 ± 28 ns, k_{obs} = 3 60 ± 0 36 x 10^6 s^{-1}) and is shown in figure 3 – 29 The rate of recovery of the parent compound at 420 nm corresponds to the rate of decay of the transient species at 610 nm The UV-vis spectrum remained unchanged throughout the experiment The transient signals showed similar lifetimes when recorded under an atmosphere of argon, carbon monoxide and air, i e in the presence of oxygen as a triplet quencher The consistency of these measurements in the presence of argon, carbon monoxide or oxygen suggests that the photoinduced *trans-cis* isomerisation of the vinyl spacer occurs *via* a singlet excited state and also rules out the possibility of a CO loss transient species

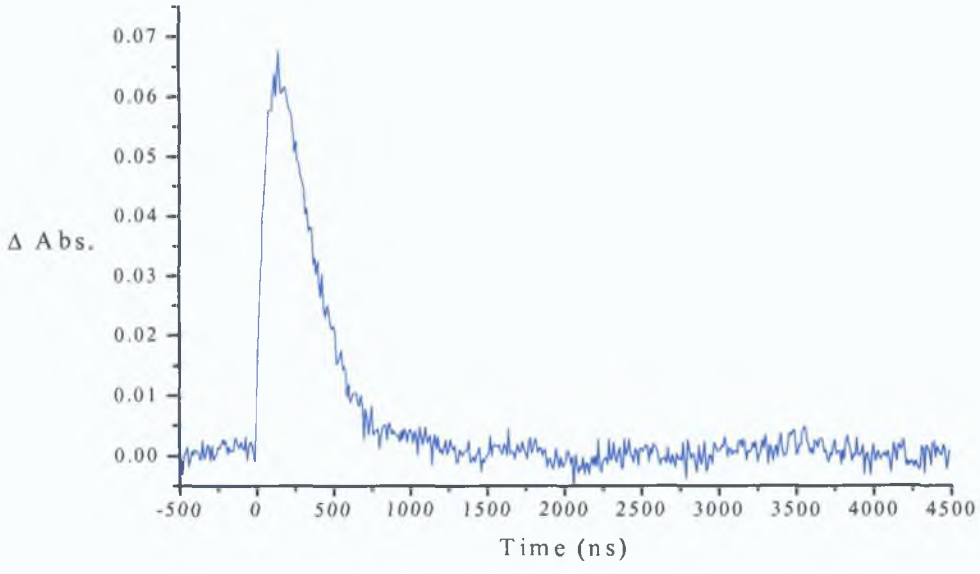

Fig. 3 - 28: Transient signal observed at 610 nm following laser flash photolysis (λ_{exc} = 532 nm) of (*E*)-$(CO)_5Cr{=}C(OMe)C_2H_2Ph$ in cyclohexane under one atmosphere of carbon monoxide isomer ($\tau = 262 \pm 26$ ns, $k_{obs} = 3.82 \pm 0.40 \times 10^6$ s^{-1}).

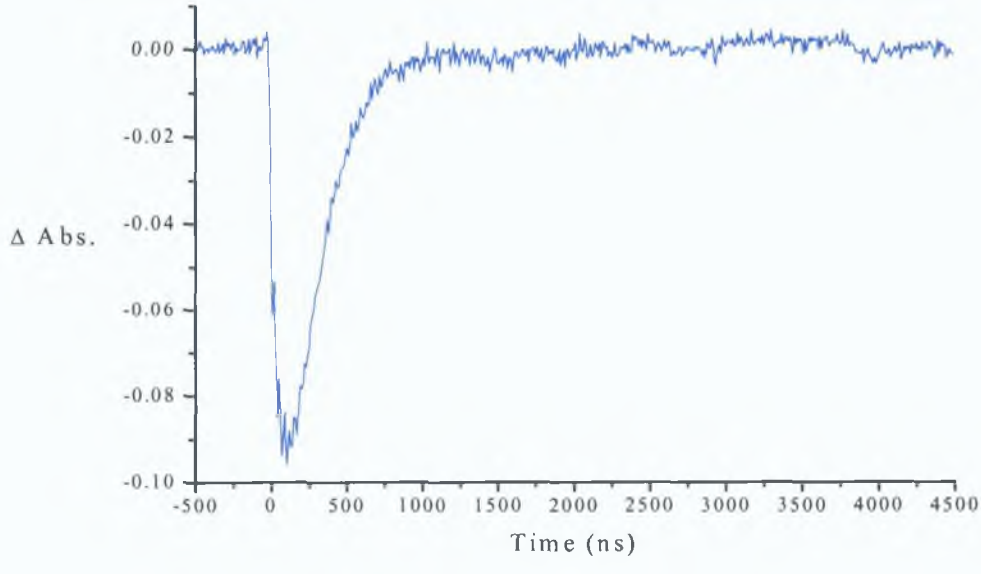

Fig. 3 - 29: Depletion and recovery observed at 420 nm following laser flash photolysis (λ_{exc} = 532 nm) of (*E*)-$(CO)_5Cr{=}C(OMe)C_2H_2Ph$ in cyclohexane under one atmosphere of carbon monoxide ($\tau = 278 \pm 28$ ns, $k_{obs} = 3.60 \pm 0.36 \times 10^6$ s^{-1}).

3.4.3 Photochemistry of (*E*)-$(CO)_5W{=}C(OMe)C_2H_2Fc$

3.4.3.1 Laser flash photolysis of (*E*)-$(CO)_5W{=}C(OMe)C_2H_2Fc$ in cyclohexane at λ_{exc} = 355 nm

(*E*)-$(CO)_5W{=}C(OMe)C_2H_2Fc$ is a dark purple solid with a UV-vis spectrum exhibiting two low energy bands in the visible region of the spectrum at 560 nm (ε = 2.65 x 10^3 $M^{-1}cm^{-1}$) and 444 nm (ε = 3.97 x 10^3 $M^{-1}cm^{-1}$), a higher lying band at 338 nm (ε = 4.72 x 10^3 $M^{-1}cm^{-1}$) and a shoulder at *ca.* 280 nm (ε = 3.76 x 10^3 $M^{-1}cm^{-1}$) in cyclohexane solution (fig. 3 – 30).

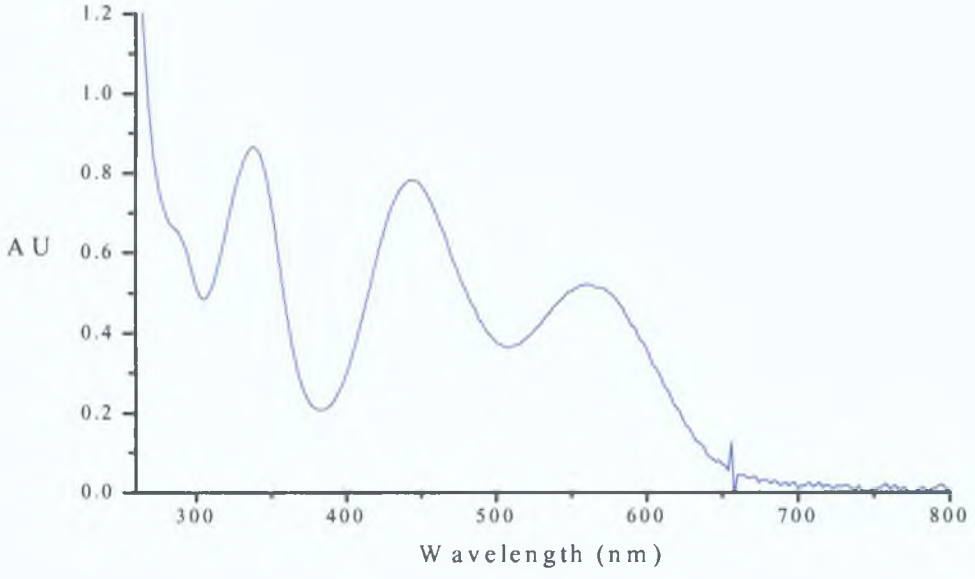

Fig. 3 – 30: UV-vis spectrum of (*E*)-$(CO)_5W{=}C(OMe)C_2H_2Fc$ in cyclohexane solution.

A weak transient signal with a λ_{max} at 380 nm was observed following laser excitation at 355 nm in cyclohexane under one atmosphere of carbon monoxide at room temperature (fig. 3 – 31). A weak depletion was also observed at 440 nm (fig. 3 – 32). These signals were not observed to return to the pre-flash absorption level however the UV-vis spectrum remained unchanged throughout the experiment, thus indicating regeneration of the parent compound. As the transient signals were extremely weak it was impossible to generate a transient absorbance difference spectrum.

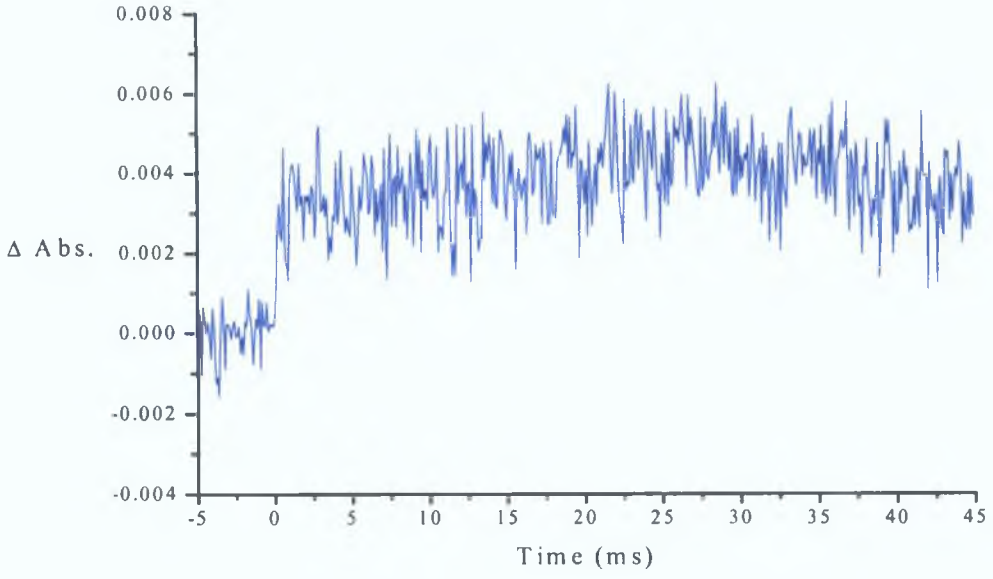

Fig. 3 - 31: Transient signal observed at 380 nm following laser flash photolysis (λ_{exc} = 355 nm) of (*E*)-$(CO)_5W{=}C(OMe)C_2H_2Fc$ in cyclohexane under one atmosphere of carbon monoxide.

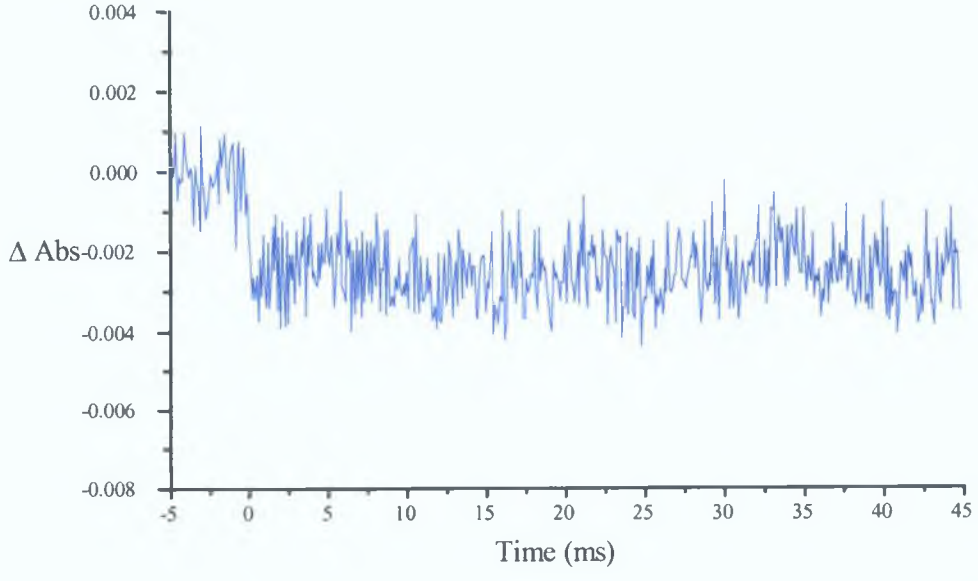

Fig. 3 - 32: Signal observed at 440 nm following laser flash photolysis (λ_{exc} = 355 nm) of (*E*)-$(CO)_5W{=}C(OMe)C_2H_2Fc$ in cyclohexane under one atmosphere of carbon monoxide.

When the experiment was repeated under one atmosphere of argon similar transient signals were observed, however, the UV-vis spectra recorded throughout the experiment showed a gradual decomposition of the parent compound (fig. 3 - 33). No photochemistry was observed for (*E*)-$(CO)_5W{=}C(OMe)C_2H_2Fc$ under similar conditions following 532 nm laser excitation.

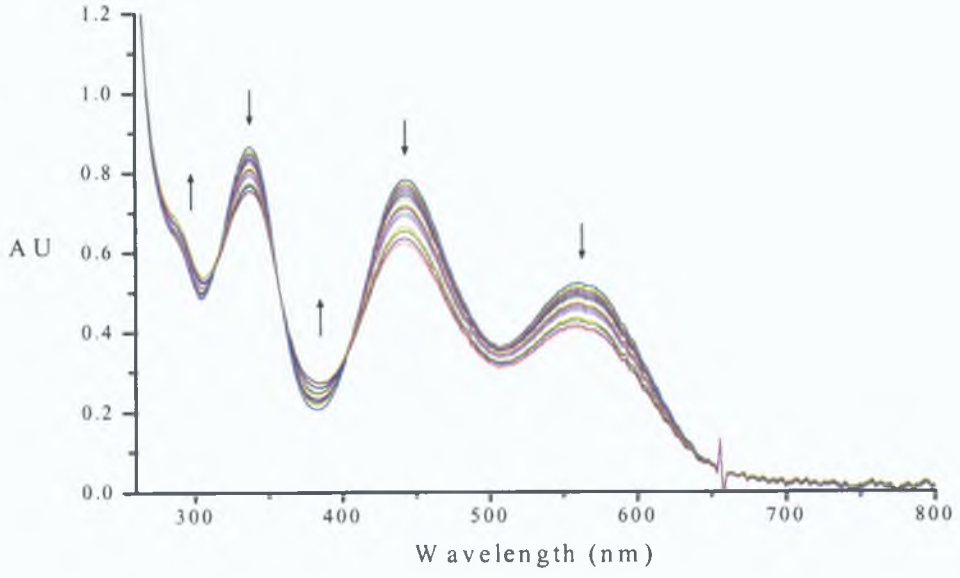

Fig. 3 - 33: UV-vis spectra recorded during laser flash photolysis (λ_{exc} = 355 nm) of (*E*)-$(CO)_5W{=}C(OMe)C_2H_2Fc$ in cyclohexane under one atmosphere of argon.

3.4.3.2 Steady state photolysis of (*E*)-$(CO)_5W$=C(OMe)C_2H_2Fc in cyclohexane in the presence of excess triphenylphosphine at λ_{exc} = 355 nm

The photochemistry of (*E*)-$(CO)_5W$=C(OMe)C_2H_2Fc was investigated in cyclohexane under 1 atm of argon at room temperature in the presence of excess triphenylphosphine in an attempt to trap any tetracarbonyl that may be formed following photolysis. The sample was initially irradiated at λ_{exc} > 550 nm however no changes were observed in the UV-vis absorption spectrum. Subsequent irradiation at λ_{exc} > 400 nm only resulted in a slight change in the UV-vis absorption spectrum. Similar changes were observed at λ_{exc} > 320 nm with a greater efficiency. The sample was irradiated at λ_{exc} > 320 nm for a total of 35 min. All three absorption bands of the parent compound at 548, 466 and 334 nm decreased in absorbance as the photolysis proceeded with a concomitant increase in absorbance in the valleys between each absorption band (fig. 3 – 34). Isosbestic points were observed at 372 and 394 nm.

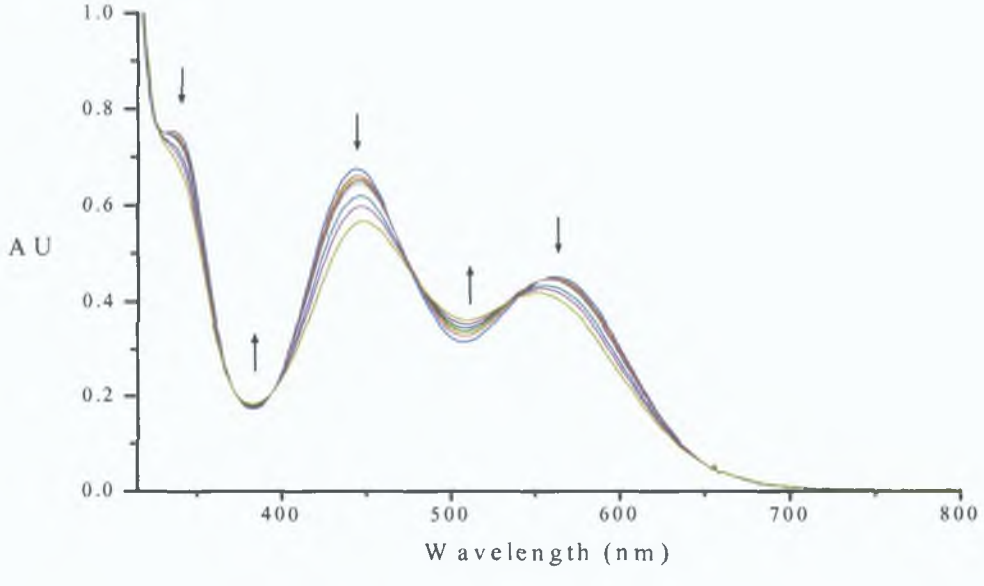

Fig. 3 - 34: UV-vis absorption spectra recorded during steady state photolysis of (*E*)-$(CO)_5W$=C(OMe)C_2H_2Fc at λ_{exc} > 320 nm in cyclohexane under one atmosphere of argon in the presence of excess triphenylphosphine.

After 35 min. of photolysis, when no more changes were apparent in the UV-vis spectrum, the solvent was removed under reduced pressure and an infrared spectrum of the solid was recorded. Peaks indicative of the formation of the tetracarbonyl species (*E*)-*cis*-$(PPh_3)(CO)_4W{=}C(OMe)C_2H_2Fc$ were present at 1900, 1927, 1964 and 2016 cm^{-1} thus confirming CO loss following irradiation at $\lambda_{exc} > 320$ nm (fig. 3 – 35).

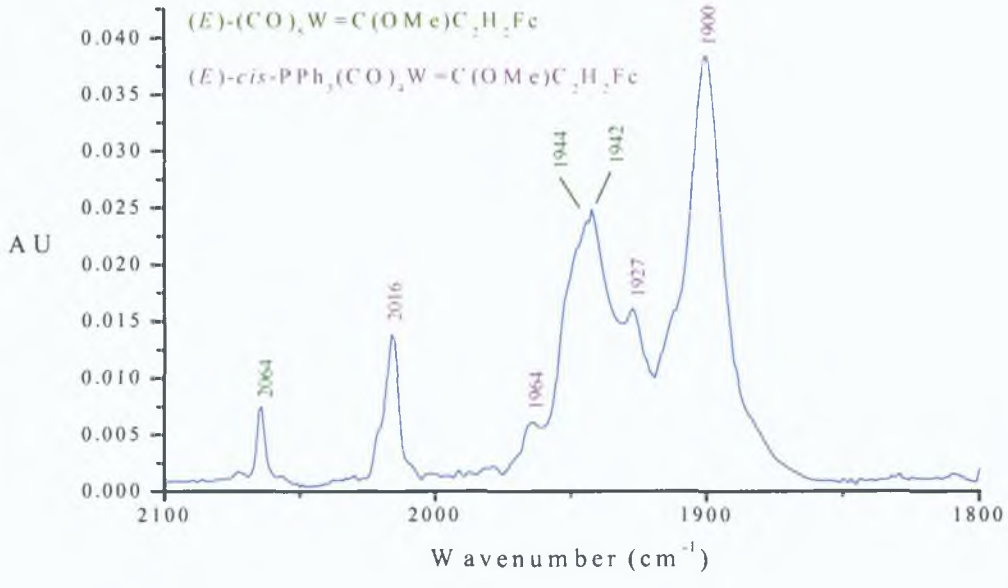

Fig. 3 - 35: The infrared spectrum recorded following steady state photolysis of (*E*)-$(CO)_5W{=}C(OMe)C_2H_2Fc$ at $\lambda_{exc} > 320$ nm in cyclohexane under one atmosphere of argon in the presence of excess triphenylphosphine.

3.4.3.3 Laser flash photolysis of (*E*)-$(CO)_5W{=}C(OMe)C_2H_2Fc$ in cyclohexane in the presence of excess triphenylphosphine

No transient signals were observed, following pulsed laser excitation at 355 nm of (*E*)-$(CO)_5W{=}C(OMe)C_2H_2Fc$ in cyclohexane under one atmosphere of argon at room temperature in the presence of excess triphenylphosphine. Similar changes were observed however in the UV-vis spectrum as during steady state photolysis (fig. 3 – 34 in the previous section).

3.4.4 Photochemistry of (*E*)-$(CO)_5Cr=C(C_4H_8N)C_2H_2Fc$

3.4.4.1 Laser flash photolysis of (*E*)-$(CO)_5Cr=C(C_4H_8N)C_2H_2Fc$ in cyclohexane at λ_{exc} = 355 nm

(*E*)-$(CO)_5Cr=C(C_4H_8N)C_2H_2Fc$ is a red solid with a UV-vis spectrum exhibiting two absorption bands with λ_{max} at 315 nm ($\varepsilon = 1.10 \times 10^4$ $M^{-1}cm^{-1}$) and 360 nm ($\varepsilon = 6.54 \times 10^3$ $M^{-1}cm^{-1}$) in cyclohexane solution (fig. 3 – 36). There is further broad band of low intensity with a λ_{max} at *ca.* 444 nm ($\varepsilon = 2.33 \times 10^3$ $M^{-1}cm^{-1}$), which absorbs to approximately 560 nm. The large difference observed in the UV-vis spectrum for (*E*)-$(CO)_5Cr=C(C_4H_8N)C_2H_2Fc$, when compared to the methoxy analogue, is due to rotation of the vinylferrocene π-system out of plane with the Fischer-carbene π-system (this is further elaborated in the X-ray crystal structure discussion section).

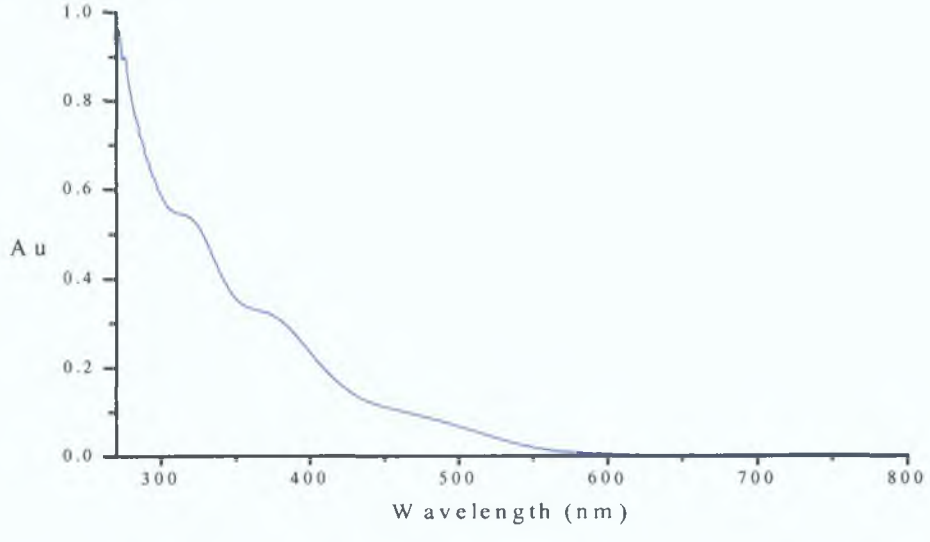

Fig. 3 - 36: UV-vis spectrum of (*E*)-$(CO)_5Cr=C(C_4H_8N)C_2H_2Fc$ in cyclohexane.

Transient absorption measurements were recorded following laser flash photolysis (λ_{exc} = 355 nm) in cyclohexane under one atmosphere of carbon monoxide at room temperature. The transient absorbance difference spectrum is shown in figure 3 – 37 with λ_{max} at 360 and 420 nm. Only a very small decay in absorbance of the transient species is observed, as regeneration of the parent compound occurs on a timescale too long lived to be monitored by the instrumentation.

The depletion observed at 330 nm corresponds to the strongest absorbing band of the parent compound The UV-vis absorption spectrum remained unchanged throughout the experiment

When the experiment was repeated under one atmosphere of argon the profile of the transient absorption difference spectrum recorded was very similar to that recorded under one atmosphere of CO Again, there were no changes in the UV-vis spectrum indicating that the parent compound was regenerated, on a longer timescale than was possible to measure with the experimental set-up Figure 3 - 38 shows an overlay of two transients recorded at 420 nm under one atmosphere of carbon monoxide and also under one atmosphere of argon The signal recorded under one atmosphere of carbon monoxide shows only a slight decay when compared to that recorded under one atmosphere of argon An infrared spectrum of the sample recorded after the experiment showed only absorption of the parent compound

No transient signals were observed following laser flash photolysis of (*E*)-$(CO)_5Cr{=}C(C_4H_8N)C_2H_2Fc$ at 532 nm However, when this experiment was carried out, it was only possible to monitor at *ca* $\lambda > 450$ nm due to the strong absorption of (*E*)-$(CO)_5Cr{=}C(C_4H_8N)C_2H_2Fc$ at higher energy

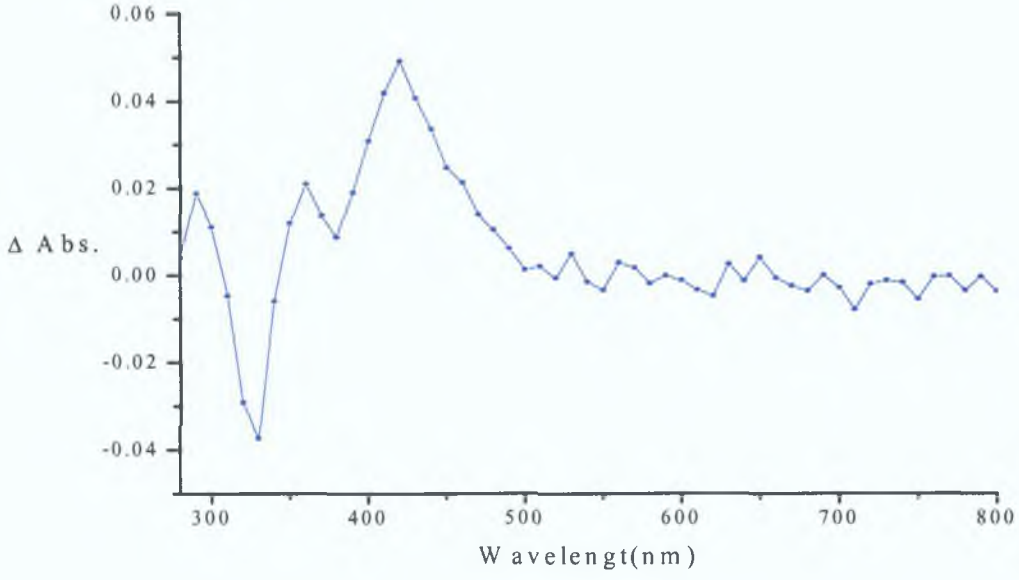

Fig. 3 - 37: Transient absorption difference spectra recorded at 2 ms following flash photolysis (λ_{exc} = 355 nm) of (*E*)-$(CO)_5Cr{=}C(C_4H_8N)C_2H_2Fc$ in cyclohexane under one atmosphere of carbon monoxide. The transient absorbance difference spectrum is plotted point-by-point every 10 nm.

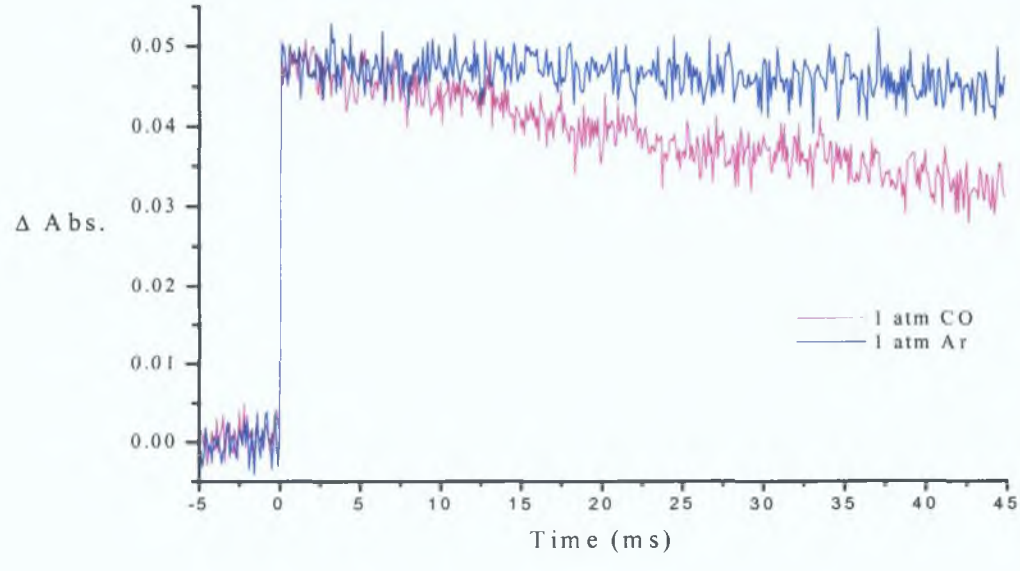

Fig. 3 - 38: Signals observed at 420 nm following laser flash photolysis (λ_{exc} = 355 nm) of (*E*)-$(CO)_5Cr{=}C(C_4H_8N)C_2H_2Fc$ in cyclohexane under one atmosphere of carbon monoxide and one atmosphere of argon.

3.4.4.2 Laser flash photolysis of (*E*)-$(CO)_5Cr=C(C_4H_8N)C_2H_2Fc$ in cyclohexane in the presence of excess triphenylphosphine at λ_{exc} = 355 nm

The transient absorption difference spectrum recorded, following flash photolysis of (*E*)-$(CO)_5Cr=C(C_4H_8N)C_2H_2Fc$ at 355 nm in cyclohexane under one atmosphere of argon at room temperature in the presence of excess triphenylphosphine is given in figure 3 – 39. Figure 3 - 40 shows a typical signal observed at 380 nm. The solution changed from a pale to a dark yellow colour during the photolysis. The absorption band of the parent compound at 360 nm increased in intensity as the photolysis proceeded with a concomitant decrease in the higher lying band at 315 nm (see fig. 3 – 41 in the following section). An isosbestic point was observed at 396 nm. An infrared spectrum recorded after the experiment confirmed formation of the tetracarbonyl species (*E*)-*cis*-$(PPh_3)(CO)_4Cr=C(C_4H_8N)C_2H_2Fc$ (see fig. 3 – 42 in the following section).

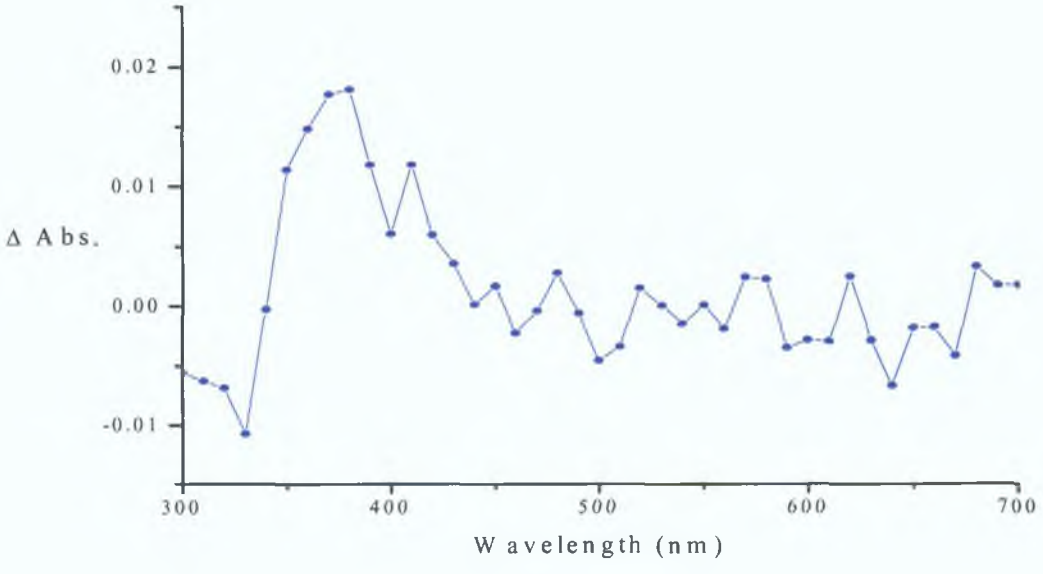

Fig. 3 - 40: Transient difference absorption spectrum recorded 2 ms following flash photolysis (λ_{exc} = 355 nm) of (*E*)-$(CO)_5Cr=C(C_4H_8N)C_2H_2Fc$ in cyclohexane under one atmosphere of argon in the presence of excess triphenylphosphine. The absorbance difference spectrum is plotted point-by-point every 10 nm.

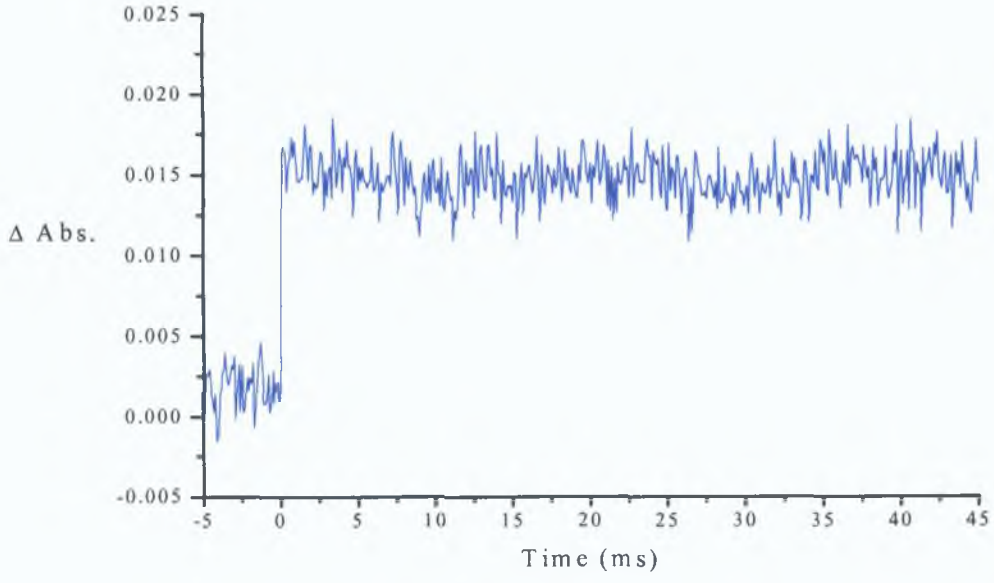

Fig. 3 - 40: Signal observed at 380 nm following laser flash photolysis (λ_{exc} = 355 nm) of (*E*)-$(CO)_5Cr{=}C(C_4H_8N)C_2H_2Fc$ in cyclohexane under one atmosphere of argon in the presence of triphenylphosphine.

3.4.4.3 Steady state photolysis of (*E*)-$(CO)_5Cr=C(C_4H_8N)C_2H_2Fc$ in cyclohexane in the presence of triphenylphosphine

The photochemistry of (*E*)-$(CO)_5Cr=C(C_4H_8N)C_2H_2Fc$ was investigated in cyclohexane under one atmosphere of argon at room temperature in the presence of an excess of triphenylphosphine as a trapping ligand to determine whether CO loss was occurring, as was the case with the methoxy analogue (*E*)-$(CO)_5Cr=C(OMe)C_2H_2Fc$. The sample was initially irradiated at λ_{exc} > 400 nm however no changes were observed in the UV-vis absorption spectrum. Efficient reaction was observed however following irradiation at λ_{exc} > 320 nm. The changes observed in the UV-vis spectra (fig. 3 - 41) correspond to those observed following laser flash photolysis (λ_{exc} = 355 nm).

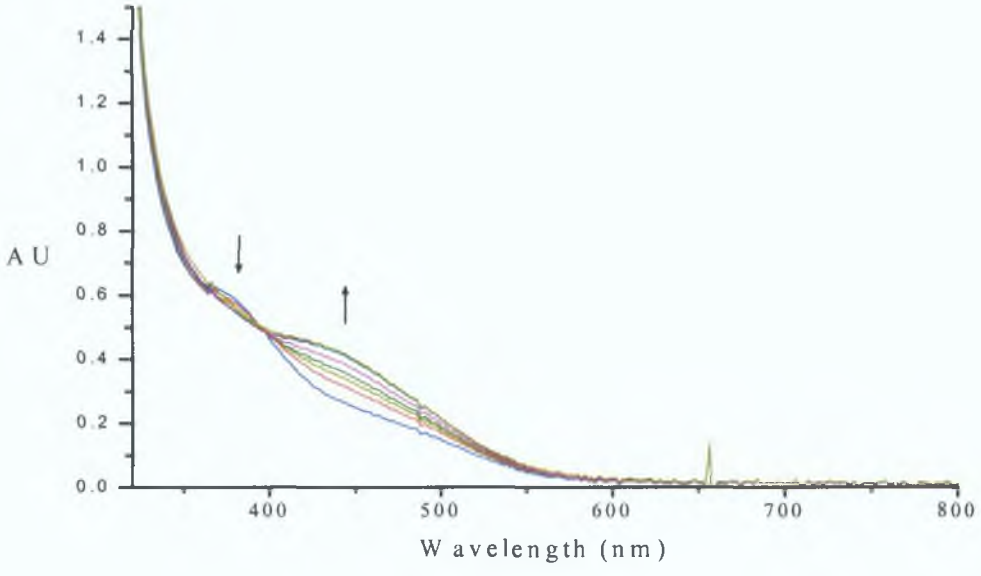

Fig. 3 - 41: UV-vis spectra recorded during steady state photolysis of (*E*)-$(CO)_5Cr=C(C_4H_8N)C_2H_2Fc$ at λ_{exc} > 320 nm in cyclohexane under one atmosphere of argon in the presence of excess triphenylphosphine.

After 120 min. of photolysis, when no more changes were apparent in the UV-vis spectrum, the solvent was removed under reduced pressure and an infrared spectrum was recorded of the residual solid (fig. 3 - 42). Peaks indicative of the formation of the tetracarbonyl species (*E*)-*cis*-$(PPh_3)(CO)_4Cr=C(C_4H_8N)C_2H_2Fc$ were present, therefore confirming CO loss as a photochemical process.

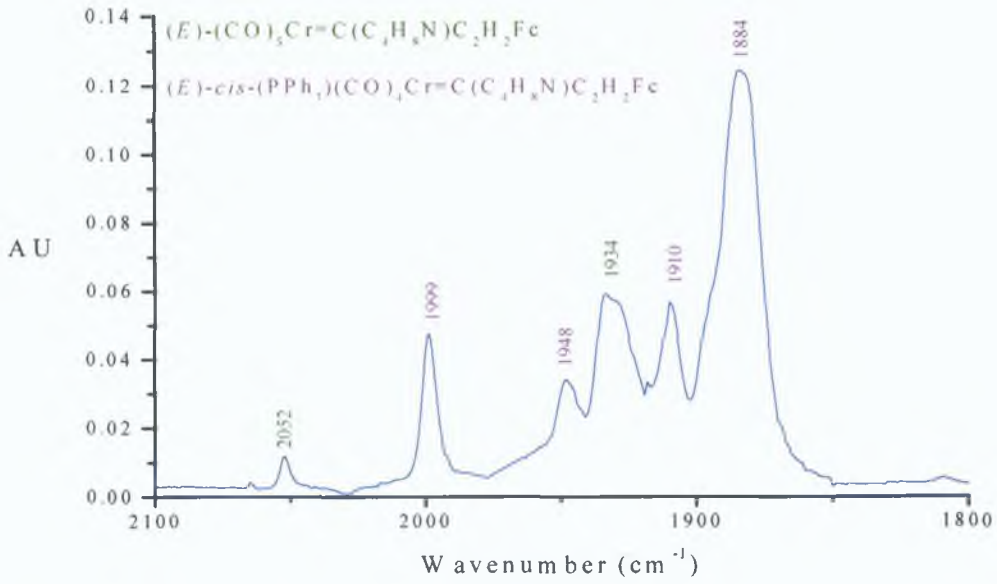

Fig. 3 - 42: Infrared spectrum of the residual solid following steady state photolysis of (*E*)-$(CO)_5Cr{=}C(C_4H_8N)C_2H_2Fc$ at λ_{exc} > 320 nm in cyclohexane under one atmosphere of argon in the presence of excess triphenylphosphine. The peaks at 1884, 1910, 1948 and 1999 cm^{-1} correspond to (*E*)-*cis*-$(PPh_3)(CO)_4Cr{=}C(C_4H_8N)C_2H_2Fc$ and the remaining peaks at 1934 and 2052 cm^{-1} correspond to the parent compound.

3.4.5 Photochemistry of (*E*)-$(CO)_5W=C(C_4H_8N)C_2H_2Fc$

3.4.5.1 Laser flash photolysis of (*E*)-$(CO)_5W=C(C_4H_8N)C_2H_2Fc$ in cyclohexane

(*E*)-$(CO)_5W=C(C_4H_8N)C_2H_2Fc$ is a red solid with a UV-vis spectrum exhibiting two unresolved bands at 298 nm ($\varepsilon = 6.68 \times 10^3\ M^{-1}cm^{-1}$) and 322 nm ($\varepsilon = 7.03 \times 10^3\ M^{-1}cm^{-1}$) in addition to two broad shoulders in the visible region of the spectrum at 380 nm ($\varepsilon = 4.52 \times 10^3\ M^{-1}cm^{-1}$) and 470 nm ($\varepsilon = 1.39 \times 10^3\ M^{-1}cm^{-1}$). The UV-vis absorption spectrum extends as far as 600 nm as is shown in figure 3 – 43. The change observed in the UV-vis absorption spectrum following aminolysis of the methoxy analogue are similar to those observed for the chromium carbene.

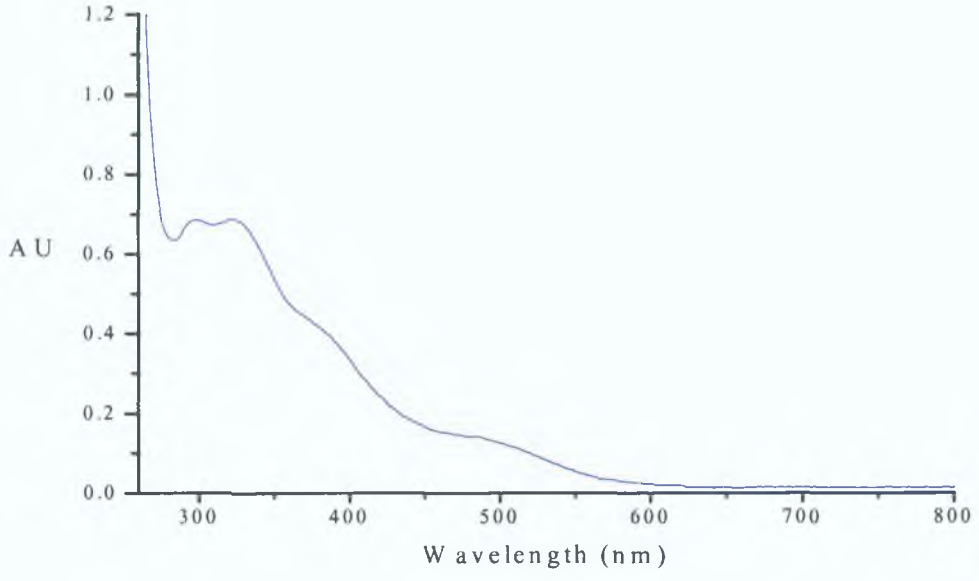

Fig. 3 – 43: UV-vis spectrum of (*E*)-$(CO)_5W=C(C_4H_8N)C_2H_2Fc$ in cyclohexane.

Following laser excitation at 532 nm in cyclohexane, under one atmosphere of carbon monoxide or one atmosphere of argon at room temperature, no transient signals were observed. When the sample was subsequently subjected to laser flash photolysis at 355 nm no photochemistry was again observed.

3.4.5.2 Steady state photolysis of (*E*)-$(CO)_5W=C(C_4H_8N)C_2H_2Fc$ in cyclohexane in the presence of excess triphenylphosphine

The photochemistry of (*E*)-$(CO)_5W=C(C_4H_8N)C_2H_2Fc$ was subsequently investigated in cyclohexane under 1 atm of argon at room temperature in the presence of excess triphenylphosphine to determine if CO loss occurs. The sample was initially irradiated at $\lambda_{exc} > 400$ nm however no changes were observed in the UV-vis absorption spectrum. The sample was then subjected to $\lambda_{exc} > 320$ nm for a total of 90 min. The lower energy shoulder of the parent compound at 470 nm increased in absorbance from 390 to 510 nm as the photolysis proceeded with a concomitant decrease in the higher lying shoulder from 330 to 390 nm. The high-energy bands at 298 and 322 nm were obscured by the absorbance of triphenylphosphine. An isosbestic point was observed at 390 nm (fig. 3 – 44).

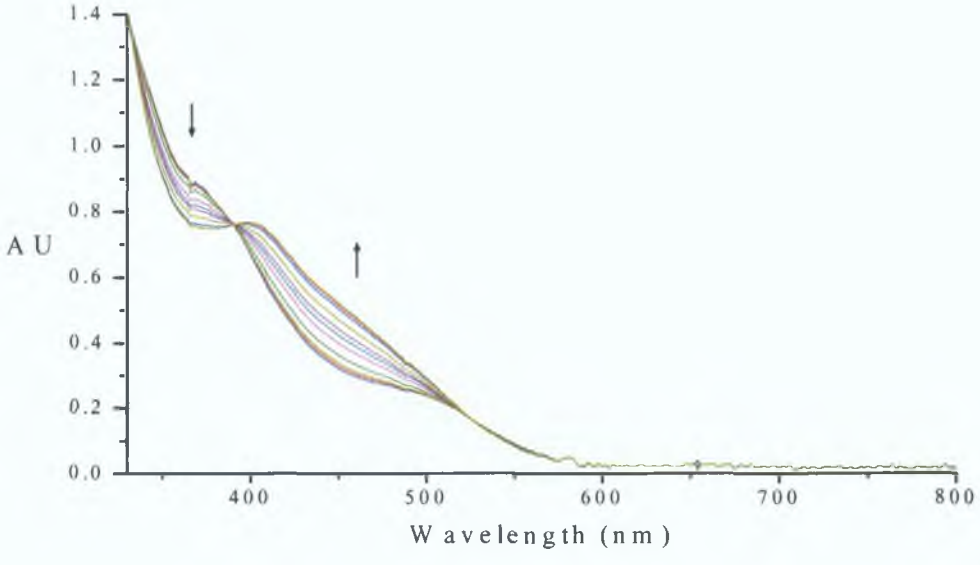

Fig. 3 - 44: UV-vis spectra recorded during steady state photolysis of (*E*)-$(CO)_5W=C(C_4H_8N)C_2H_2Fc$ at $\lambda_{exc} > 320$ nm in cyclohexane under one atmosphere of argon in the presence of excess triphenylphosphine.

When no more changes were apparent in the UV-vis spectrum, the solvent was removed under reduced pressure and an infrared spectrum was recorded of the residual solid. Peaks indicative of the formation of the tetracarbonyl species (*E*)-cis-$(PPh_3)(CO)_4W=C(C_4H_8N)C_2H_2Fc$ were present confirming CO loss as a photoprocess

(fig. 3 – 45). No peaks indicative of the parent compound were present in the infrared spectrum indicating that the reaction went to completion.

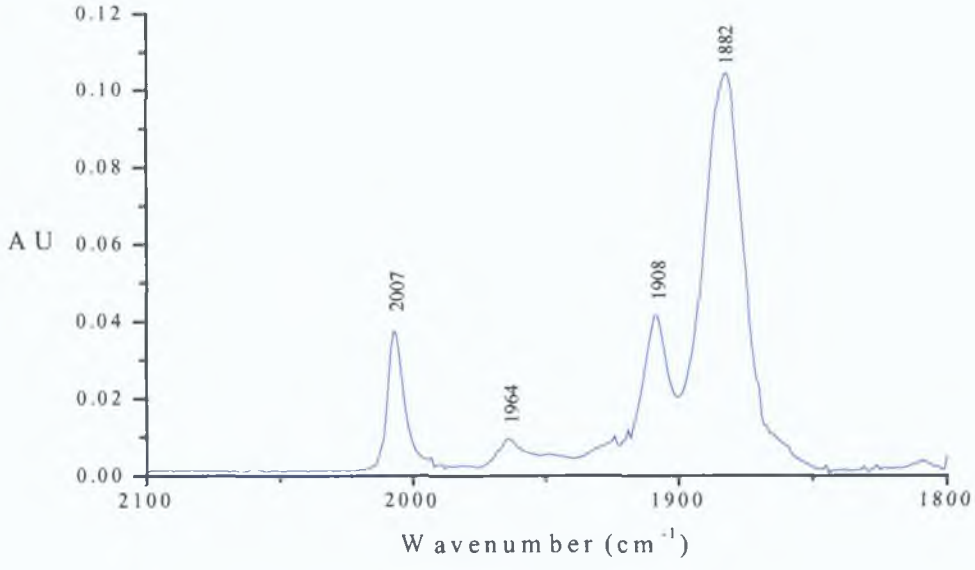

Fig. 3 - 45: Infrared spectrum of (*E*)-*cis*-$(PPh_3)(CO)_4W{=}C(C_4H_8N)C_2H_2Fc$ recorded after steady state photolysis of (*E*)-$(CO)_5W{=}C(C_4H_8N)C_2H_2Fc$ at $\lambda_{exc} > 320$ nm in cyclohexane under one atmosphere of argon in the presence of excess triphenylphosphine.

No transient signals were observed following laser excitation at 355 nm of (*E*)-$(CO)_5W{=}C(C_4H_8N)C_2H_2Fc$ in cyclohexane under one atmosphere of argon at room temperature in the presence of excess triphenylphosphine. Similar changes were observed however in the UV-vis spectrum as during steady state photolysis under comparable conditions.

3.4.6 Solvatochroism

The solvatochromic data for the two low energy bands of compounds (*E*)-$(CO)_5M{=}C(OMe)C_2H_2Fc$ where M = Cr, W is shown in table 3 – 1. UV-vis spectra were also recorded for the pyrrolidino derivatives in the various solvents however as none of the absorption bands are sufficiently resolved their λ_{max} could not be recorded accurately. Some examples of solvatochromic behaviour are shown in figure 3 – 46 and figure 3 – 47.

	Cyclohexane	Toluene	Dichloromethane	Methanol	Acetonitrile
(*E*)-$(CO)_5Cr{=}C(OMe)C_2H_2Fc$	464	460	456	450	448
	552	560	556	560	560
(*E*)-$(CO)_5W{=}C(OMe)C_2H_2Fc$	444	442	440	436	434
	560	570	570	570	568

Table 3 – 1

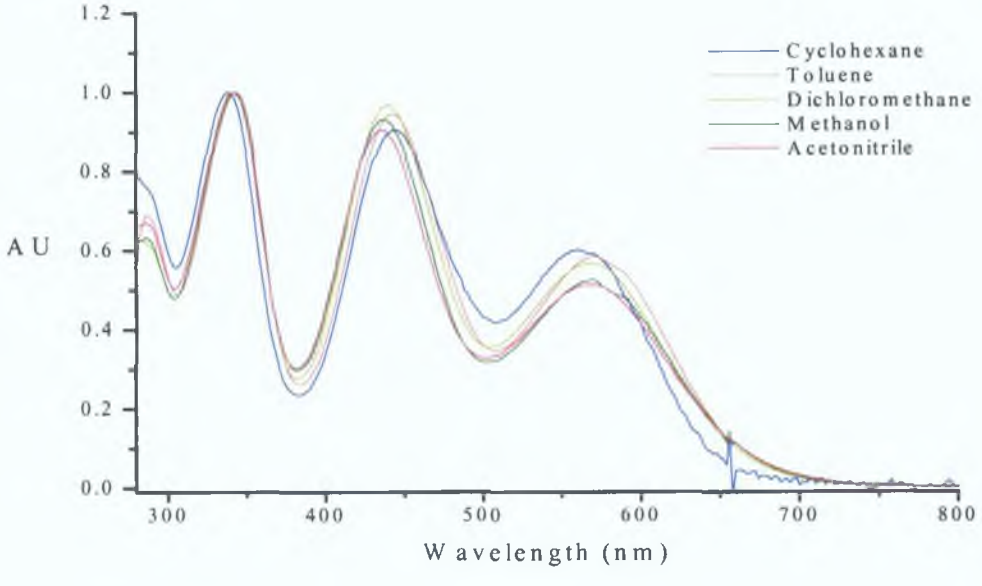

Fig. 3 – 46: UV-vis spectra displaying the solvatochromic behaviour of (*E*)-$(CO)_5W{=}C(OMe)C_2H_2Fc$ in various solvents (all spectra have been normalised at the high energy band).

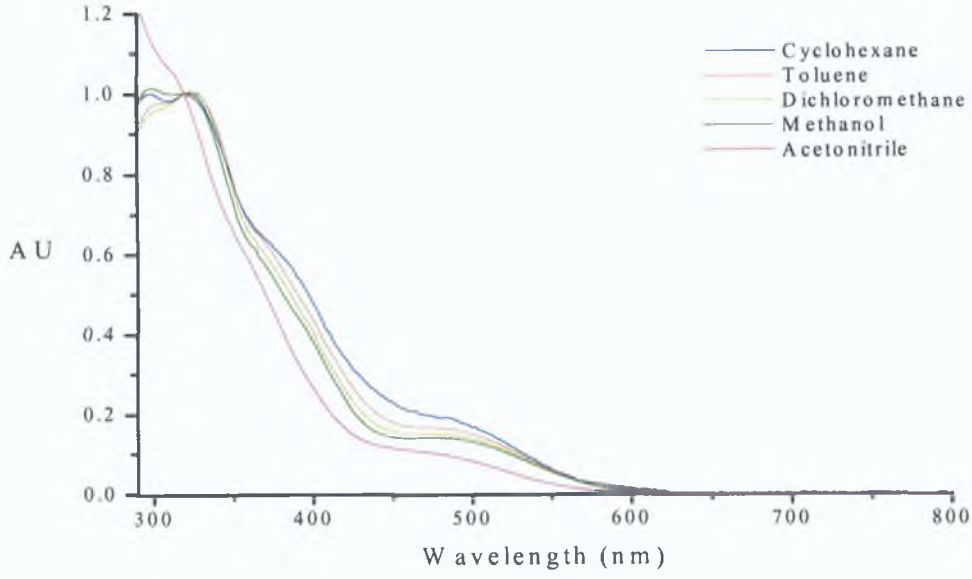

Fig. 3 – 47: UV-vis spectra displaying the solvatochromic behaviour of (*E*)-$(CO)_5W{=}C(C_4H_8N)C_2H_2Fc$ in various solvents.

3.4.7 Electrochemistry

Electrochemistry was performed in dry acetonitrile under argon with 0.1 M [*n*-BuN_4][BF_4] as supporting electrolyte. A three-electrode set up was used for all measurements with a glassy carbon working electrode (2 mm diameter), a platinum wire auxiliary electrode and a saturated calomel reference electrode. $E_{1/2}$ values were determined as $(E_{pa} + E_{pc})/2$, where E_{pa} and E_{pc} are the anodic and cathodic peak potentials, respectively (it is assumed that $E_{1/2} \approx E^{0'}$ for all measurements). All potentials are quoted in reference to the ferrocene/ferrocenium couple. Table 3 - 2 contains a list of the redox potentials recorded. Shown in figure 3 – 48 is a typical example of a cyclic voltammogram recorded for (*E*)-$(CO)_5Cr{=}C(C_4H_8N)C_2H_2Fc$.

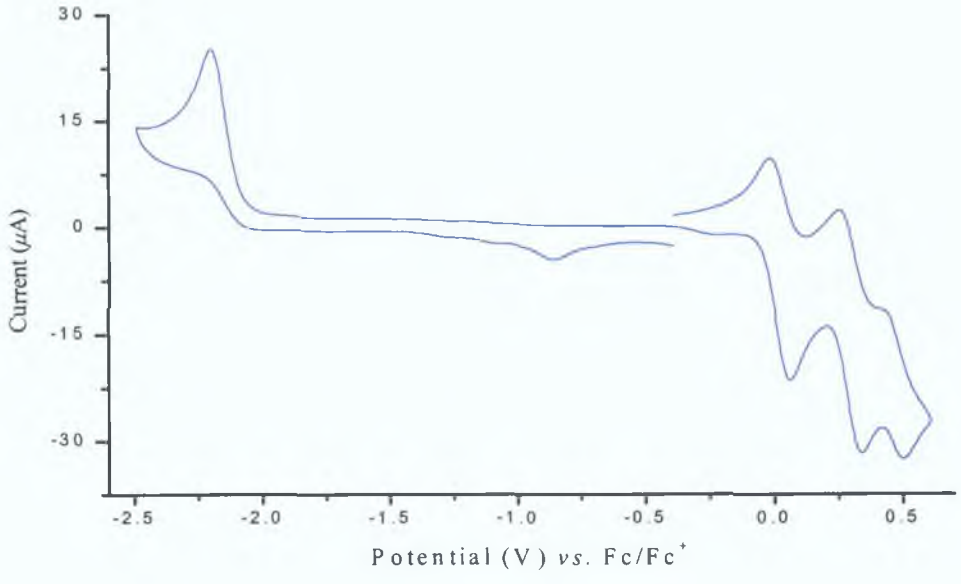

Fig. 3 – 48: Cyclic voltammogram of (*E*)-$(CO)_5Cr{=}C(C_4H_8N)C_2H_2Fc$ in acetonitrile.

	1st
	$E_{1/2}$
(*E*)-$(CO)_5Cr{=}C(OMe)C_2H_2Fc$	0 146
(*E*)-$(CO)_5Cr{=}C(C_4H_8N)C_2H_2Fc$	0 028
(*E*)-$(CO)_5W{=}C(OMe)C_2H_2Fc$	0 146
(*E*)-$(CO)_5W{=}C(C_4H_8N)C_2H_2Fc$	0 110

oxidation				reduction		
2nd			3rd			
E_{pa}	E_{pc}	$E_{1/2}$	$E_{1/2}$	E_{pc}	E_{pa}	$E_{1/2}$
0 465	0 451	0 458	~	-1 548	-1 530	-1 539
0 282	0 299	0 291	0 466	-2 149	~	~
0 552	~	~	~	-1 514	~	~
0 415	~	~	~	-2 119	-2 128	-2 124

Table 3 - 2

Each of the compounds studied show reversible first oxidation steps in the potential range of $E_{1/2}$ = 0 028 to 0 146 V, which is ascribed to the ferrocene/ferrocenium couple [13(d)] This redox couple is identical for both the Cr and W methoxy carbene complexes, $E_{1/2}$ = 0 146 V Its is reduced however to $E_{1/2}$ = 0 028 V, following aminolysis, for (*E*)-$(CO)_5Cr{=}C(C_4H_8N)C_2H_2Fc$ The ferrocene/ferrocemum couple of the tungsten analogue (*E*)-$(CO)_5W{=}C(C_4H_8N)C_2H_2Fc$ is reduced to a lesser extent with $E_{1/2}$ = 0 110 V The ferrocene HOMO orbital in these systems is therefore more strongly stabilised for the methoxy carbene systems However, it is most sensitive to a change in the group VI metal centre for the amino carbenes than for the methoxy carbenes A second reversible oxidation is observed at $E_{1/2}$ = 0 458 and 0 251 V for (*E*)-$(CO)_5Cr{=}C(OMe)C_2H_2Fc$ and (*E*)-$(CO)_5Cr{=}C(C_4H_8N)C_2H_2Fc$ respectively and is assigned to oxidation of the metal carbene moiety [13(d)] (*E*)-$(CO)_5Cr{=}C(C_4H_8N)C_2H_2Fc$ also shows a third irreversible oxidation at E_{ap} = 0 466 V Oxidation of the tungsten carbene moieties of the complexes (*E*)-$(CO)_5W{=}C(OMe)C_2H_2Fc$ and (*E*)-$(CO)_5W{=}C(C_4H_8N)C_2H_2Fc$ are irreversible in contrast to their chromium analogues, E_{pa} = 0 552 and 0 415 V respectively

Each of the compounds studied also show a reduction of the carbene moiety in a potential range of $E_{1/2}$ = –1 539 to –2 124 V This reduction involves population of the carbene-p_x LUMO orbital and is reversible for each of the complexes apart from (*E*)-$(CO)_5Cr{=}C(C_4H_8N)C_2H_2Fc$ (fig 3 – 48) [13(d)] By observing the trend in the E_{pc} results for all four complexes it is clear that the LUMO of these complexes is stabilized on going from the amino to the methoxy carbenes and also on going from the chromium to the tungsten analogues

3.4.8 The X-ray crystal structure of (*E*)-$(CO)_5Cr=C(C_4H_8N)C_2H_2Fc$

The molecular structure of (*E*)-$(CO)_5Cr=C(C_4H_8N)C_2H_2Fc$ was confirmed by single crystal x-ray diffraction. Crystals of (*E*)-$(CO)_5Cr=C(C_4H_8N)C_2H_2Fc$ were grown from a saturated chloroform/cyclohexane (*1 :1*) solution under an atmosphere of argon. Crystal data and experimental parameters are summarised in appendix A5.

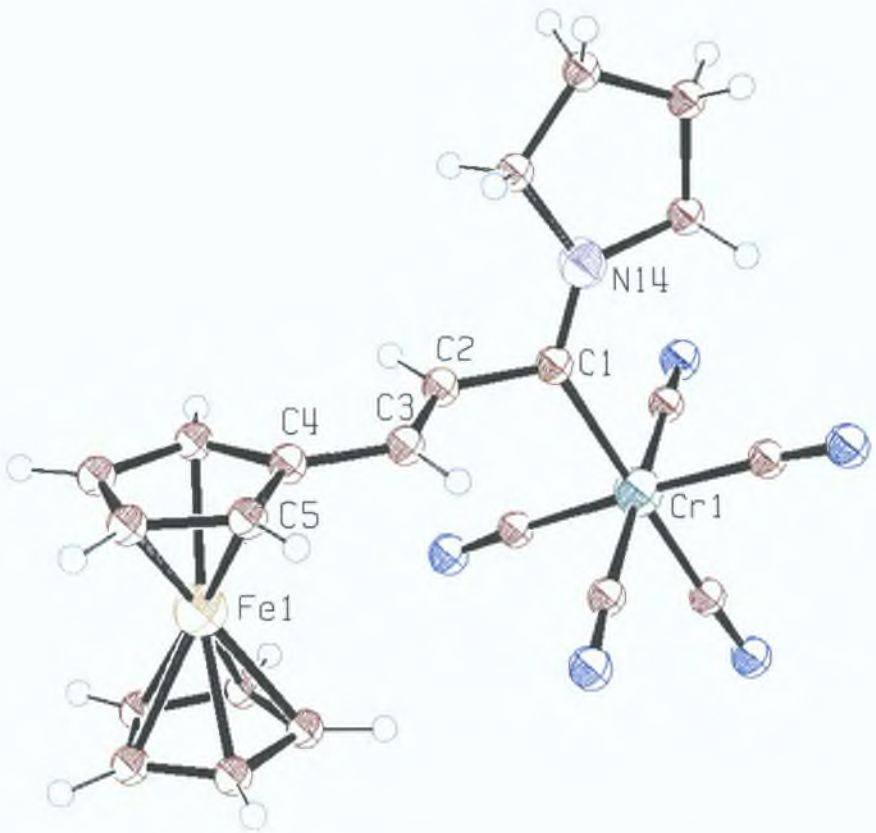

Fig. 3 – 49: ORTEP-III[20] diagram showing the x-ray crystal structure of (*E*)-$(CO)_5Cr=C(C_4H_8N)C_2H_2Fc$.

The most striking feature of the molecular structure of (*E*)-$(CO)_5Cr=C(C_4H_8N)C_2H_2Fc$ in contrast to $(CO)_5Cr=C(OMe)Fc$, reported in the previous chapter, and (*E,E'*)-$(CO)_5Cr=C(OMe)C_4H_4Fc$, previously reported by Jayaprakash et. al,[13(d)] is that the π-network of the Fischer-carbene moiety is out of plane with the π-network of the vinylferrocene moiety. A dihedral angle of 68.11^0 exists between C_3 and the N_{14}-C_1-C_2 plane. The vinyl spacer is almost coplanar with the Cp ring with a dihedral angle of 11.95^0 between C_5 and the C_2-C_3-C_4 plane. A similar structure was previously reported for the tungsten aminocarbene complex (*E*)-

$(CO)_5W=C(NMe_2)C_2H_2Fc$ [21] The π-π overlap of the Fischer-carbene and ferrocene systems is effectively suppressed as evident in the UV-vis and electrochemical data for (*E*)-$(CO)_5Cr=C(C_4H_8N)C_2H_2Fc$

A Cr-$C_{carbene}$ and $C_{carbene}$-N bond lengths of 2 119 Å and 1 303 Å respectively are observed for (*E*)-$(CO)_5Cr=C(C_4H_8N)C_2H_2Fc$ A Cr-$C_{carbene}$ bond length of 2 051 Å was reported for (*E,E'*)-$(CO)_5Cr=C(OMe)C_4H_4Fc$ [13(d)] This suggests a greater contribution from the polar resonance structure in the ground state of (*E*)-$(CO)_5Cr=C(C_4H_8N)C_2H_2Fc$ (resonance structure II, scheme 3 – 6) in comparison to (*E,E'*)-$(CO)_5Cr=C(OMe)C_4H_4Fc$ The latter compound shows a greater contribution from the fulvene-type resonance structure in comparison to (*E*)-$(CO)_5Cr=C(C_4H_8N)C_2H_2Fc$, however this is not surprising considering the large dihedral angle between the Fischer-carbene and vinylferrocene π-systems $C_{carbene}$-C_2 and C_3-C_4 bond lengths of 1 491 and 1 477 Å are observed for (*E*)-$(CO)_5Cr=C(C_4H_8N)C_2H_2Fc$ The shorter C_2-C_3 vinyl bond length of 1 264 Å emphasises the lack of conjugation in (*E*)-$(CO)_5Cr=C(C_4H_8N)C_2H_2Fc$ which is in contrast to vinyl bond lengths of 1 344 and 1 327 Å observed for (*E,E'*)-$(CO)_5Cr=C(OMe)C_4H_4Fc$ [13(d)] The π-systems of each of these complexes, amino and methoxy, display a staggered configuration with respect to the chromium pentacarbonyl moiety, however this does not appear to affect communication between the carbene and pentacarbonyl units, presumably due to the low barrier for rotation of the Cr=C bond in such systems [22]

Figure 3 – 50 shows a crystal packing diagram for (*E*)-$(CO)_5Cr=C(C_4H_8N)C_2H_2Fc$, which crystallises in the orthorhombic Pbca space group Eight molecules of (*E*)-$(CO)_5Cr=C(C_4H_8N)C_2H_2Fc$ are contained in the unit cell

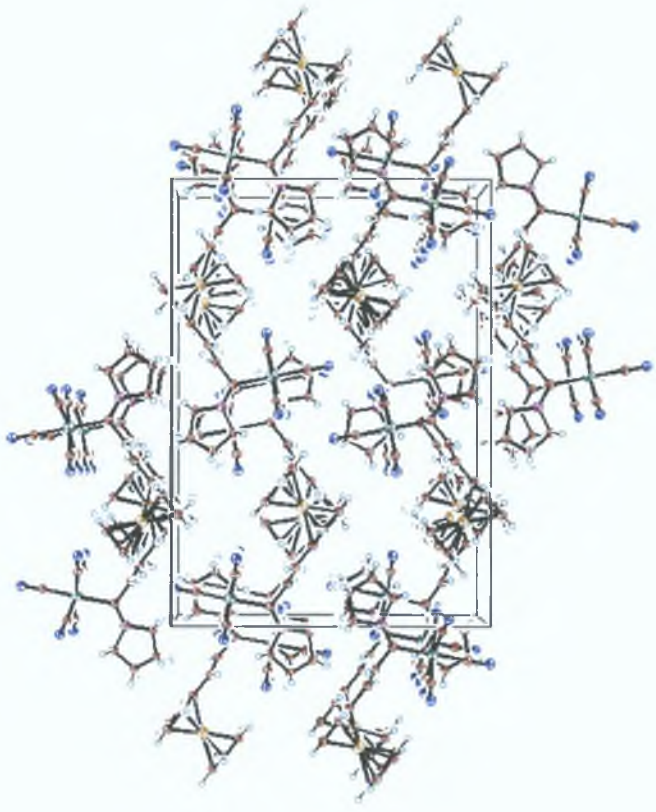

Fig. 3 – 50: Crystal packing diagram for the (*E*)-$(CO)_5Cr{=}C(C_4H_8N)C_2H_2Fc$ unit cell viewed normal to the (100) plane.

3.4 9 Nonlinear optical properties

The nonlinear optical properties of the complexes (*E*)-$(CO)_5Cr{=}C(OMe)C_2H_2Fc$ and (*E*)-$(CO)_5Cr{=}C(C_4H_8N)C_2H_2Fc$ were investigated by the technique of Electric Field Induced Second Harmonic Generation (EFISH), the results of which are displayed in table 2 – 3 All measurements were performed in chloroform solution with a fundamental frequency of 1 907 μm The term $\mu\beta$ represents the product of the molecular dipole and the second-order hyperpolarisability vector along the dipole direction

	$\mu\beta_{1.907}$ (10^{-48})
(*E*)-$(CO)_5Cr{=}C(OMe)C_2H_2Fc$	304
(*E*)-$(CO)_5Cr{=}C(C_4H_8N)C_2H_2Fc$	326

Table 3 - 3

The second-order hyperpolarisability of (*E*)-$(CO)_5Cr{=}C(OMe)C_2H_2Fc$ has been reported previously by Jayaprakash et al as 46 8 x 10^{30} esu by the Hyper Rayleigh Scattering (HRS) technique with a fundamental frequency of 1 064 μm [13(d)] The second-order hyperpolarisability of (*E*)-$(CO)_5Cr{=}C(C_4H_8N)C_2H_2Fc$ has not been previously reported Surprisingly both of these complexes display a decreased nonlinearity in comparison to $(CO)_5Cr{=}C(OMe)Fc$ with lacks a conjugated bridge between the donor and acceptor moieties ($\mu\beta$ = 403 x 10^{48} esu, chapter 2 section 2 3 8) It is noteworthy however that there is a slight increase in the nonlinearity following aminolysis of the Fischer carbene moiety

3 5 Discussion

3 5 1 UV-vis spectra and electrochemistry of (*E*)-$(CO)_5M{=}C(OMe)C_2H_2Fc$ and (*E*)-$(CO)_5M{=}C(NC_4H_8)C_2H_2Fc$ (M = Cr, W)

The ferrocenyl Fischer-carbene complexes (*E*)-$(CO)_5M{=}C(OMe)C_2H_2Fc$ and (*E*)-$(CO)_5M{=}C(NC_4H_8)C_2H_2Fc$ (M = Cr, W) display similar photochemistry following flash photolysis at 355 nm The chromium and tungsten methoxy complexes (*E*)-$(CO)_5M{=}C(OMe)C_2H_2Fc$ (M = Cr, W) each exhibit an intense low energy band in the visible region of the spectrum at 548 and 560 nm respectively adjacent to a higher energy band of similar intensity at 466 and 444 nm respectively in cyclohexane Higher lying bands are also observed at 334 and 338 nm for the chromium and tungsten complexes respectively (*E*)-$(CO)_5Cr{=}C(NC_4H_8)C_2H_2Fc$ exhibits two absorption bands with λ_{max} at 315 and 360 nm in cyclohexane solution and also a broad low intensity shoulder on the low-energy side of these two bands, which absorbs to approximately 560 nm The tungsten analogue (*E*)-$(CO)_5W{=}C(NC_4H_8)C_2H_2Fc$ has two high-energy bands very close in energy at 298 and 322 nm A lower lying band appears as a shoulder at *ca* 380 nm and is red shifted by ~ 20 nm in comparison to the chromium analogue The lower energy shoulder absorbs slightly further out to *ca* 600 nm

By substituting the methoxy group on the carbene ligand with the more efficient electron donating pyrrolidine group the carbene carbon becomes slightly less electron deficient Amino carbenes are therefore poorer π-acceptors than their alkoxy analogues This is evident in their infrared spectra with the $\nu(CO_{trans})$ stretching frequency at 2056 and 2065 cm^{-1} for (*E*)-$(CO)_5Cr{=}C(OMe)C_2H_2Fc$ and (*E*)-$(CO)_5W{=}C(OMe)C_2H_2Fc$ respectively whereas the same $\nu(CO_{trans})$ band occurs at 2053 and 2060 cm^{-1} for (*E*)-$(CO)_5Cr{=}C(NC_4H_8)C_2H_2Fc$ and (*E*)-$(CO)_5W{=}C(NC_4H_8)C_2H_2Fc$ respectively There is also an increase in reduction potential of the carbene moiety of *ca* 0 60 V following aminolysis (table 3 – 2) This may be responsible for the significant red shift of the low-energy UV-vis absorption bands observed on going from (*E*)-$(CO)_5M{=}C(OMe)C_2H_2Fc$ to (*E*)-$(CO)_5M{=}C(NC_4H_8)C_2H_2Fc$ (M = Cr, W) Also, the vinylferrocene π-system is out of

plane with the Fischer-carbene π-system in the pyrrolidino Fischer-carbene complexes, which may prevent efficient communication between the ferrocene and carbene moieties in the pyrrolidino complexes.

On comparing the crystal structures of ferrocenyl methoxy-carbene complexes it is clear that the π-system of the ferrocene/vinylferrocene moieties are in the same plane as the π-system of the methoxy-carbene fragment; $(CO)_5Cr{=}C(OMe)Fc$ (dihedral angle = 2.26^0),[23] 1,1'-$[(CO)_5Cr{=}C(OMe)]_2Fc$ (dihedral angle = 5.33^0)[23] and (*E,E'*)-$(CO)_5Cr{=}C(OMe)C_4H_4Fc$ (dihedral angle = 8.66^0).[13(d)] This is not the case for (*E*)-$(CO)_5Cr{=}C(NC_4H_8)C_2H_2Fc$ where the π-system of the vinylferrocene moiety is out of plane with the carbene π-system (dihedral angle = 68.11^0). It should be noted that the π-systems of each of these complexes, pyrrolidino and methoxy, display a staggered configuration with respect to the chromium pentacarbonyl moiety. This does not hinder communication between the carbene and pentacarbonyl units as there exists a low barrier for rotation about the Cr=C bond in such systems.[22]

The UV-vis absorption spectra of (*E*)-$(CO)_5M{=}C(OMe)C_2H_2Fc$ (M = Cr, W) are very similar to those described in chapter 2 for the complexes $(CO)_5M{=}C(OMe)Fc$ (M = Cr, W) and similar assignments are made on this basis. The lower energy band of (*E*)-$(CO)_5M{=}C(OMe)C_2H_2Fc$ (λ_{max} = 552 and 560 nm for M = Cr , W respectively) is therefore assigned to a ferrocene based MLCT transition incorporating both (dz^2/dx^2-y^2/dxy)$\rightarrow C_{carbene}(p_x)$ (HOMO→LUMO) and (dz^2/dx^2-y^2/dxy)$\rightarrow\pi^*$ (HOMO→bridge) character. This band shows increased positive solvatochromic behaviour in comparison to $(CO)_5M{=}C(OMe)Fc$ (M = Cr, W) and thus incorporates greater HOMO→LUMO character than the directly bound systems. On going from cyclohexane to more polar solvents such as methanol, red shifts of 8 nm (552 – 560 nm) and 10 nm (560 – 570 nm) are observed for the chromium and tungsten derivatives respectively.

Both methoxy-carbenes studied here display an identical first oxidation of the ferrocene based HOMO orbital ($E_{1/2}$ = 0.146 V). However the tungsten complex does show a lower reduction of the $C_{carbene}(p_x)$ based LUMO orbital (E_{pc} = -1.514 *vs.* -1.548 V). This may explain the red shift observed in the low energy MLCT band on

going from chromium to tungsten for (*E*)-$(CO)_5M{=}C(OMe)C_2H_2Fc$ (552 → 560 nm in cyclohexane) and backs up the contribution from the HOMO→LUMO transition. Figure 3 – 51 gives an overlay of the UV-vis absorption spectra of (*E*)-$(CO)_5Cr{=}C(OMe)C_2H_2Fc$ and (*E*)-$(CO)_5Cr{=}C(OMe)C_2H_2Ph$. The latter complex does not exhibit a low energy band corroborating its assignment as a ferrocene based MLCT transition.

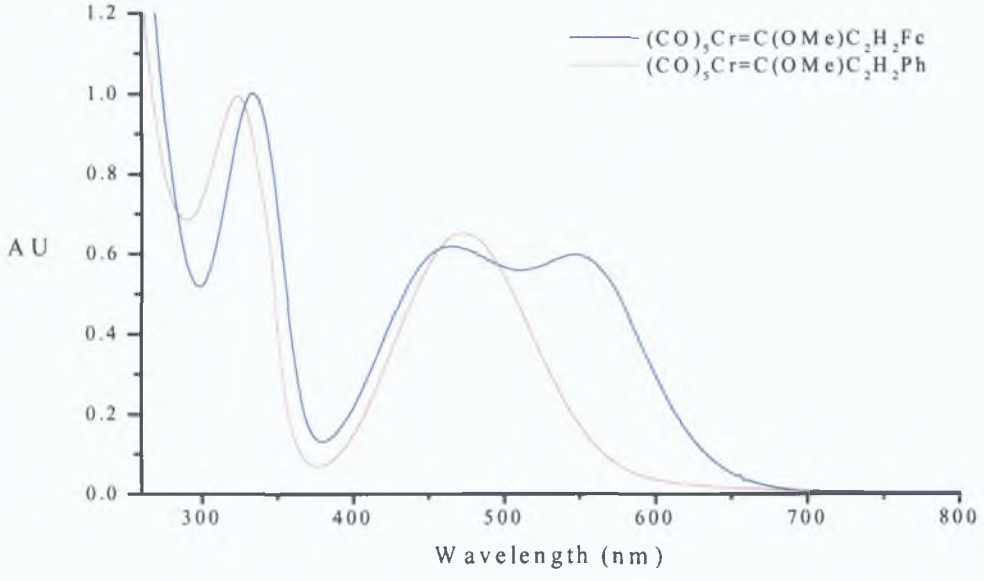

Fig. 3 – 51: An overlay of the UV-vis absorption spectra of (*E*)-$(CO)_5Cr{=}C(OMe)C_2H_2Fc$ and (*E*)-$(CO)_5Cr{=}C(OMe)C_2H_2Ph$ in cyclohexane.

The higher energy bands of (*E*)-$(CO)_5M{=}C(OMe)C_2H_2Fc$ (M = Cr, W) occurring at 466 nm and 444 nm for the chromium and tungsten complexes respectively are dominated by the Fischer–carbene based MLCT transition (chromium/tungsten based $dyz \rightarrow C_{carbene}(p_x)$). Similarly to the Fischer-carbene complexes discussed in chapter 2, negative solvatochromic behaviour is observed on increasing solvent polarity. As for the directly bound systems, the absorption band of (*E*)-$(CO)_5M{=}C(OMe)C_2H_2Fc$ with λ_{max} = 466 and 444 nm for M = Cr, W respectively, may contain bridge→acceptor, i.e. $\pi \rightarrow C_{carbene}(p_x)$, charge transfer character. A red shift is observed on increasing the number of vinyl spacers in the bridge due to an increase in the π-bridge orbital energy.[8(a), 13(d)] The low-energy Fischer-carbene LF transition (chromium/tungsten based $dyz \rightarrow dz^2$) also absorbs in this region of the spectrum.

On comparing the UV-vis spectra of the pyrrolidino complexes (*E*)-$(CO)_5M{=}C(NC_4H_8)C_2H_2Fc$ (M = Cr, W) with their methoxy analogues it can be concluded that each band is shifted to higher energy to the extent where each excited state is impossible to populate independently of any other, apart from the MLCT band which still absorbs at a lower energy The latter band is significantly reduced in intensity relative to the higher energy bands It is suggested here that the HOMO→LUMO character of the low-energy band is reduced, in comparison to the methoxy-carbenes, due to the increased energy of the LUMO orbital and also reduced π-overlap between the Fischer-carbene and vinylferrocene moieties

Although it is not possible to accurately determine the λ_{max} of the higher energy CT band for these systems (*ca* 360 and 380 nm for (*E*)-$(CO)_5M{=}C(NC_4H_8)C_2H_2Fc$ where M = Cr and W respectively), they do show negative solvatochromic behaviour implying the presence of the zwitteriomc resonance structure in the ground state The $\pi \rightarrow C_{carbene}(p_x)$ (bridge→LUMO) character of this band is most likely reduced in comparison to the methoxy complexes, again due to an increased LUMO energy and reduced π-overlap between the Fischer-carbene and vinyl moieties Resonance structures for the complexes (*E*)-$(CO)_5M{=}C(X)C_2H_2Fc$ (M = Cr, W, X = -OMe, -NC_4H_8) are shown in scheme 3 – 6 As for the complexes studied in chapter 2, the zwitterionic resonance form II dominates the ground state

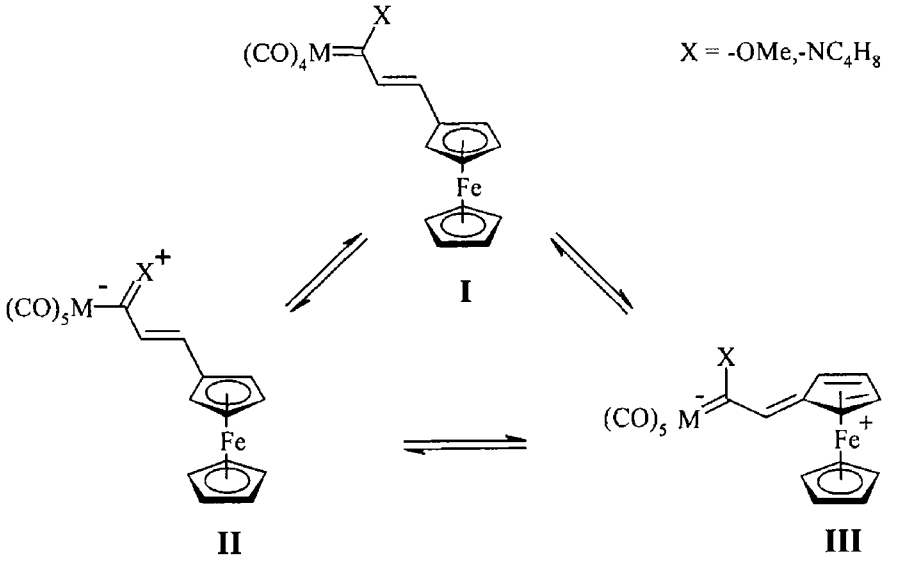

Scheme 3 – 6 Resonance forms of (*E*)-$(CO)_5M{=}C(OMe)C_2H_2Fc$ (M = Cr, W)

Similar to the carbene complexes studied in chapter 2, the vinyl-carbene complexes (*E*)-$(CO)_5M{=}C(OMe)C_2H_2Fc$ (M = Cr, W) undergo photoinduced CO loss following irradiation of their high-energy bands (λ_{max} = 334 and 338 nm for M = Cr, W respectively) This transition is thus assigned to the high-energy Fischer-carbene LF transition (chromium/tungsten based $dyz \rightarrow dx^2\text{-}y^2$) A similar assignment is made for the high-energy bands of (*E*)-$(CO)_5M{=}C(NC_4H_8)C_2H_2Fc$ (M = Cr, W), which occur at 315 and 298 nm for the chromium and tungsten complexes respectively The low-energy LF band of (*E*)-$(CO)_5W{=}C(NC_4H_8)C_2H_2Fc$ appears to be more resolved than its chromium analogue with λ_{max} of 322 nm

3 5 2 Steady state and laser flash photolysis of (*E*)-$(CO)_5M=C(OMe)C_2H_2Fc$ and (*E*)-$(CO)_5M=C(NC_4H_8)C_2H_2Fc$ (M = Cr, W)

Laser flash photolysis of (*E*)-$(CO)_5Cr=C(OMe)C_2H_2Fc$ at 355 nm gives rise to CO loss at the chromium and tungsten centres The parent compound is regenerated after time under an atmosphere of CO The lifetime of this transient species was determined to be 7 ± 0 66 ms under one atmosphere of CO The transient absorption difference spectrum obtained following flash photolysis of (*E*)-$(CO)_5Cr=C(OMe)C_2H_2Fc$ is dominated by the depletion of the parent compound in the region of 390 – 630 nm and 290 – 340 nm, together with absorptions with λ_{max} = 370 and 290 nm

This transient species is tentatively assigned to the η^3-vinyl-carbene complex, T-I as shown in scheme 3 - 7 This assignment is based on the relatively small second-order rate constant for the reaction of the chromium methoxy-carbene transient species with CO (k_2 = 16 33 ± 1 6 M^{-1} s^{-1}), and the negative entropy value calculated for the regeneration of (*E*)-$(CO)_5Cr=C(OMe)C_2H_2Fc$ (-89 ± 9 J K^{-1} mol^{-1}) Similar species have been previously isolated, fully characterised and identified as intermediates in the Dotz benzannulation reaction [24 25 26] Such negative entropy values are unusual for a chromium species and indicate that the parent compound is regenerated through an associative process (scheme 3 – 8) [27] The enthalpy of activation ($\Delta H^{\neq}$ = 23 ± 2 kJmol $^{-1}$) is similar to that of the solvated species $Cr(CO)_5$(cyclohexane) observed by Creaven et al [27(a)]

Three other transient species are possible following photoinduced CO loss from (*E*)-$(CO)_5Cr=C(OMe)C_2H_2Fc$, i e T-II, T-III and T-IV as shown in scheme 3 – 7 It has been postulated that population of the Fischer-carbene MLCT transition gives rise to the metal-ketene transient species (T-II, scheme 3 – 7) *via* CO insertion into the metal-carbene bond The presence of this intermediate has only been imparted by chemical reaction and has remained elusive to spectroscopic characterisation [28 29] The results from this study did not suggest the presence of a ketene intermediate

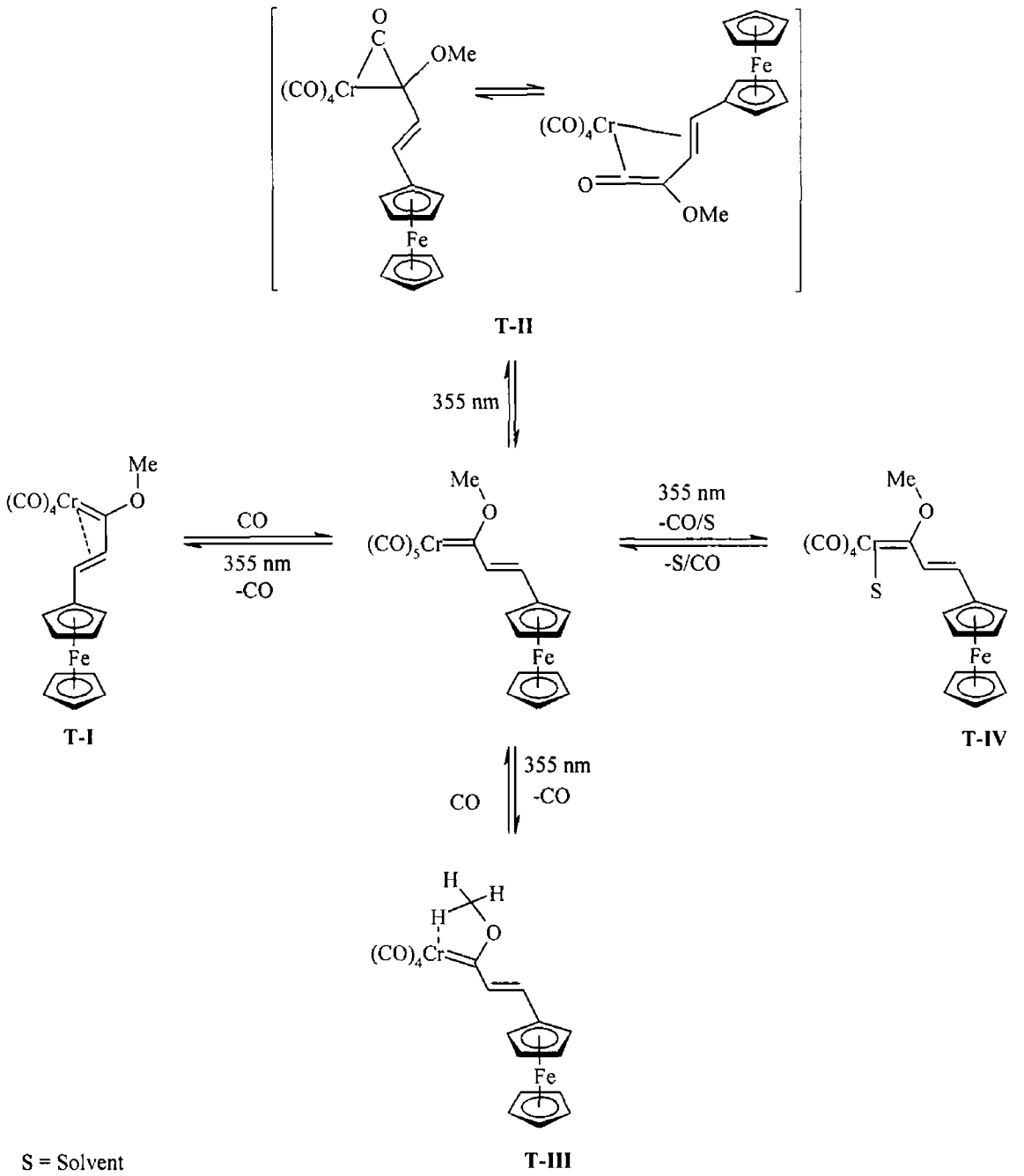

Scheme 3 – 7 Possible transient species which may occur following photoinduced CO loss from (*E*)-$(CO)_5Cr{=}C(OMe)C_2H_2Fc$

Formation of the agostic interaction T-III (scheme 3 – 7) is unlikely as such transient species have only been reported for tungsten Fischer-carbene complexes [30] [31] [32] The agostic interaction reported by McGarvey et al following laser flash photolysis of $(CO)_5W{=}C(OMe)Ph$ is relatively short lived (4 6 μs) in comparison to the transient species observed following laser flash photolysis of (*E*)-$(CO)_5Cr{=}C(OMe)C_2H_2Fc$ (7

± 0.66 ms).[31] Existence of T-IV is also unlikely because of the long lifetime of the transient species observed. Following laser flash photolysis of $Cr(CO)_6$ in cyclohexane the transient species formed, $Cr(CO)_5$(cyclohexane), decays with a second order rate constant of 2.3×10^{-6} M^{-1} s^{-1} on reaction with CO. [33] No evidence for *anti-syn* isomerisation was observed in this study. [34, 35]

Similarly, a transient species tentatively attributed to the tungsten methoxy η^3-vinyl-carbene intermediate was observed at 380 nm with depletion of the parent compound evident at 440 nm. A transient absorption difference spectrum could not be plotted, as the signals recorded were not sufficiently intense. The lifetime of this transient species was too long lived to be measured, and indicates a more stable metal centre for the tungsten based transient species in comparison to the chromium analogue. Additional investigations are currently in progress to further characterise both the chromium and tungsten methoxy-carbene transient species.

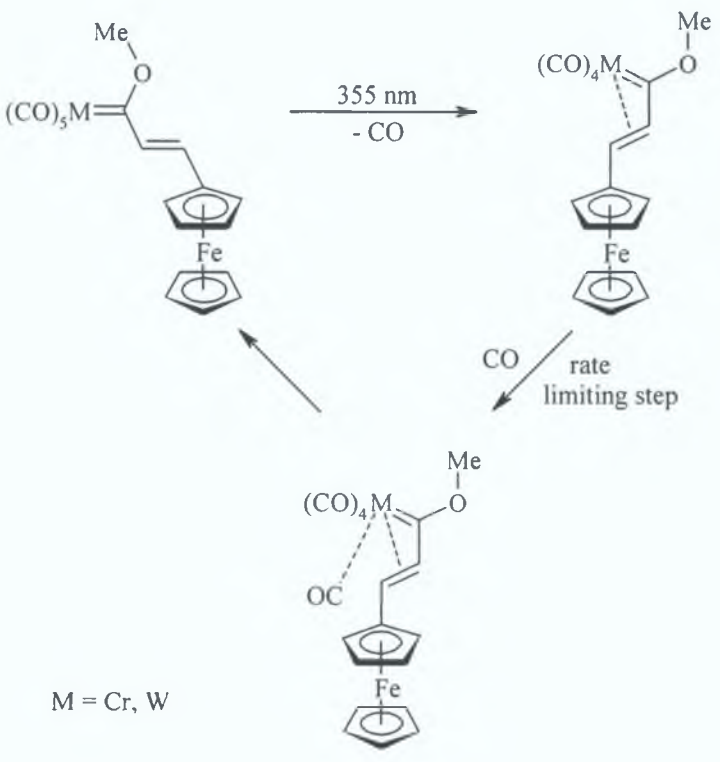

Scheme 3 – 8: Proposed mechanism for regeneration of (*E*)-$(CO)_5Cr{=}C(OMe)C_2H_2Fc$ following photoinduced CO loss under an atmosphere of CO.

These experiments were repeated in the absence of CO, under an atmosphere of argon for each of the methoxy-carbene complexes Following laser flash photolysis experiments, both the chromium and tungsten methoxy-carbenes failed to regenerate the parent compound under these conditions (fig 3 – 16 and fig 3 – 33)

The photochemistry of the pyrrolidino analogues was also investigated Laser flash photolysis of (*E*)-$(CO)_5Cr{=}C(NC_4H_8)C_2H_2Fc$ at 355 nm gives rise to CO loss at the chromium centre The parent compound is regenerated after time under an atmosphere of CO, however the lifetime of this species was too long lived to be measured by the instrumentation available Unlike the methoxy-carbenes, when this experiment was repeated under an atmosphere of argon regeneration of the parent compound was observed This is evident in the UV-vis spectra of (*E*)-$(CO)_5Cr{=}C(NC_4H_8)C_2H_2Fc$, which remained unchanged throughout the experiment Three possible mechanisms are proposed for the regeneration of (*E*)-$(CO)_5Cr{=}C(NC_4H_8)C_2H_2Fc$ following photoinduced CO loss (scheme 3 – 9),

(i) reversible formation of the η^4-metal-ketene transient species T-V (scheme 3 – 9)

(ii) photoinduced dissociation of a CO ligand and formation of the η^3-vinyl-carbene transient species T-VI (scheme 3 – 9) followed by regeneration of the parent compound by recombination with CO liberated into the solution

(iii) photoinduced dissociation of a CO ligand and formation of the solvated transient species T-VII (scheme 3 – 9) followed by regeneration of the parent compound by recombination with CO liberated into the solution

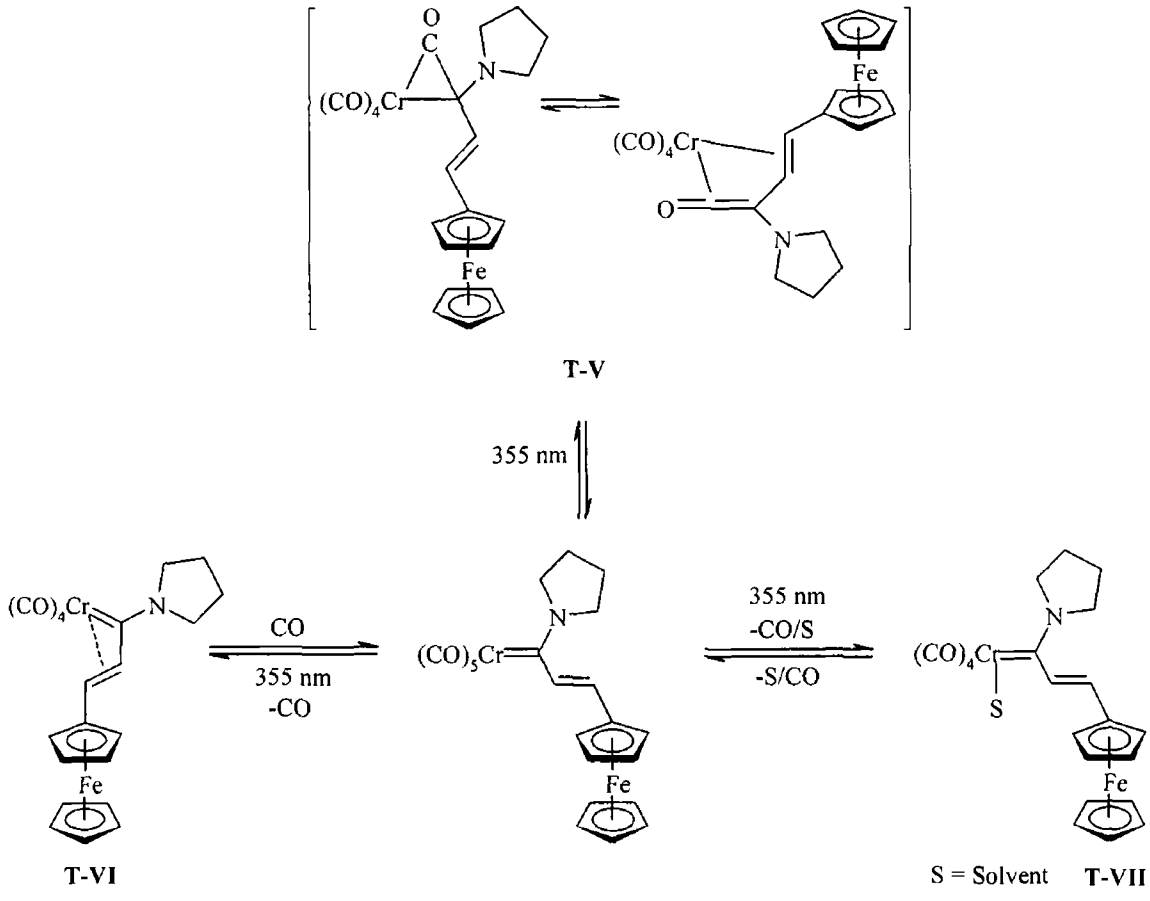

Scheme 3 - 9

Such a long lived transient species is unlikely to be as a result of T-VII considering previously reported lifetimes for solvated tetracarbonyl amino-carbene transient species [29] An amino η^4-metal-ketene has been isolated by Anderson and Wulff, however this complex contained a $Cr(CO)_3$ moiety [36] Such species are known intermediates in the Dotz benzannulation reaction [24 25 26] Attempts to isolate any of the suggested transient species by scaled up low-temperature photolysis were unsuccessful Further investigations are currently underway to identify the intermediate following laser flash photolysis of (*E*)-$(CO)_5Cr{=}C(NC_4H_8)C_2H_2Fc$

No transient signals were detected following flash photolysis of (*E*)-$(CO)_5W{=}C(NC_4H_8)C_2H_2Fc$ at 355 nm in both the presence and absence of CO

Steady state photolysis at λ_{exc} > 320 nm and laser flash photolysis at 355 nm in the presence of triphenylphosphine as a trapping ligand confirmed CO loss for all four complexes (rxn. 3 – 4).

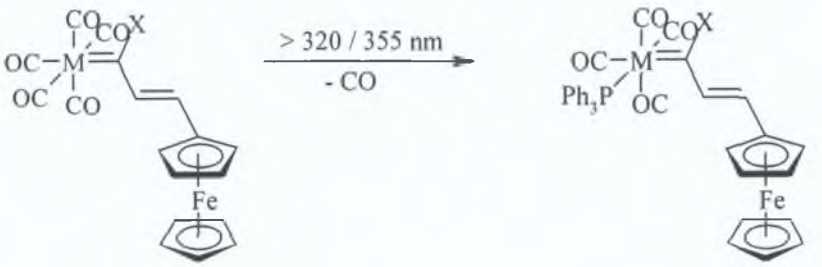

X = -OMe, $-NC_4H_8$
M = Cr, W

Rxn. 3 – 4

Irradiation λ_{exc} > 320 nm and laser flash photolysis at 355 nm is thought to populate the high-energy LF state of the carbene complexes, which populates the chromium and tungsten valence dx^2-y^2 orbital giving rise to loss of an equatorial CO ligand thereby resulting in the *cis*-substituted product. There appears to be complete conversion of (*E*)-$(CO)_5Cr{=}C(OMe)C_2H_2Fc$ to the tetracarbonyl product when photolysed at λ_{exc} > 320 nm in the presence of excess of triphenylphosphine (fig. 3 – 24). Irradiation of (*E*)-$(CO)_5Cr{=}C(NC_4H_8)C_2H_2Fc$ at λ_{exc} > 320 nm and at λ_{exc} ≈ 355 nm also populates the lower energy excited states. Again, CO loss is the only photoprocess observed, however, the reaction does not go to completion. It is possible that efficient intersystem crossing occurs to the π-bridge→carbene state and the MLCT states. Due to increased spin-orbit coupling of the heavier tungsten atom, relative to the chromium atom, with the ligand orbitals the tungsten carbene complexes are expected to show a lower efficiency towards photoinduced CO loss. Indeed the formation of (*E*)-*cis*-$(PPh_3)(CO)_4W{=}C(OMe)C_2H_2Fc$ does not go to completion as is evident by the pentacarbonyl parent compound still present in the infrared spectrum after photolysis ceased. The quantum yield for CO loss from $(CO)_5W{=}C(OMe)Ph$ has previously been determined as 0.017.[35]

Only (*E*)-$(CO)_5Cr{=}C(OMe)C_2H_2Fc$ showed formation of tetracarbonyl following photolysis at λ_{exc} > 400 nm. CO loss is thought to occur here through population of the low-energy LF state of the carbene moiety in the complex.[37] The fact that CO loss

does occur following irradiation of the absorption band at 466 nm suggests that the low-energy carbene LF state does absorb in this region of the spectrum. The inefficiency of CO loss following population of this excited state is most probably due to efficient intersystem crossing to the lower lying CT states. These CT transitions are expected to be inactive with respect to CO loss as they involve population of the carbene LUMO orbital. Irradiation of both low- and high-energy LF bands results in the *cis*-CO loss product even though irradiation of the low energy LF band is expected to result in *trans*-CO loss due to population of the metal dz^2 orbital. It is thought that on loss of a CO ligand from the metal centre *trans* to the carbene ligand, following irradiation of the low-energy LF band, rapid rearrangement of the remaining CO ligands occur resulting in a vacant site on the metal centre in a *cis* position with respect to the carbene ligand.[38] It has been shown that in solution at room temperature the four CO ligands of a $16e^-$ chromium carbene complex are actually in a fluxional state, i.e. the vacant site is not in a fixed position on the metal centre.[22] The *cis*-substituted product must therefore be the thermodynamically favoured product. It has been suggested that the population of Fischer-carbene based MLCT transition also gives rise to *anti-syn* isomerisation of the alkoxy moiety on the carbene ligand.[34, 35] As mentioned earlier, no evidence of *anti-syn* isomerisation was observed for the methoxy complexes (*E*)-$(CO)_5M{=}(OMe)C_2H_2Fc$ (M = Cr, W).

The transient absorption difference spectra recorded following flash photolysis of (*E*)-$(CO)_5Cr{=}C(OMe)C_2H_2Fc$ under CO are quite similar to those recorded in the presence of excess triphenylphosphine, both having λ_{max} between 370 – 380 nm (fig. 3 – 52). In contrast, the transient absorption difference spectra recorded following flash photolysis of (*E*)-$(CO)_5Cr{=}C(NC_4H_8)C_2H_2Fc$ in the presence of CO or argon are different to the spectra recorded in the presence of excess triphenylphosphine (fig. 3 – 53). The latter spectra have a λ_{max} at 380 nm whereas the transient species observed under carbon monoxide or argon conditions has a λ_{max} at 420 nm. TRIR measurements are still required to confirm the nature of this transient species.

The tungsten pyrrolidino-carbene complex was completely converted to the tetracarbonyl complex (*E*)-*cis*-$(PPh_3)(CO)_4W{=}C(NC_4H_8)C_2H_2Fc$ following steady state photolysis at $\lambda_{exc} > 320$ nm. This was a surprising result and was unexpected

based on the current literature data where tungsten-carbenes have been shown to have low quantum efficiencies for CO loss.[37]

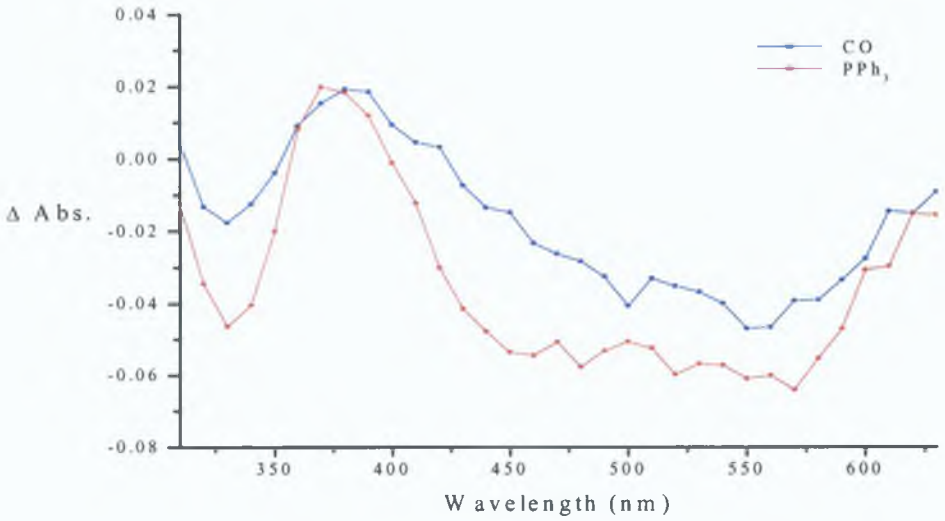

Fig. 3 – 52: An overlay of transient difference absorption spectra recorded 2 ms following laser flash photolysis of (*E*)-$(CO)_5Cr{=}C(OMe)C_2H_2Fc$ under CO and in the presence of excess triphenylphosphine. The transient absorption difference spectra are plotted point-by-point every 10 nm.

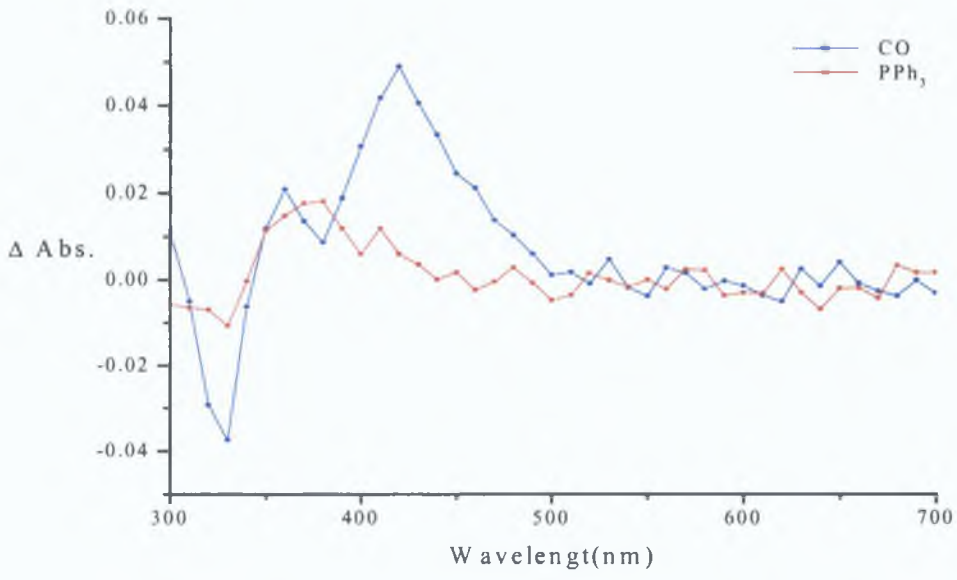

Fig. 3 – 53: An overlay of transient difference absorption spectra recorded 2 ms following laser flash photolysis of (*E*)-$(CO)_5Cr{=}C(NC_4H_8)C_2H_2Fc$ under CO and in the presence of excess triphenylphosphine. The transient absorption difference spectra are plotted point-by-point every 10 nm.

3 5 3 Photoinduced *cis-trans* isomerisation of (*E*)-$(CO)_5M{=}C(OMe)C_2H_2Fc$ and (*E*)-$(CO)_5M{=}C(NC_4H_8)C_2H_2Fc$ (M = Cr, W)

As it is possible to selectively irradiate the lower energy bands of the complexes (*E*)-$(CO)_5M{=}C(X)C_2H_2Fc$ (M = Cr, W, X = -OMe, $-NC_4H_8$) their photochemistry was also investigated at longer wavelength radiation Laser flash photolysis studies were carried out at 532 nm, thereby populating the low-energy CT excited states

Cis-trans isomerisation of vinylferrocene complexes is known to occur *via* the singlet excited state of the vinyl bridge which allows rotation about the vinyl σ-bond [39 40 41] Isomerisation of *cis*-stilbene to *trans*-stilbene occurs *via* a singlet excited state resulting in predominantly *trans*-stilbene, however *cis-trans* isomerisation of *cis*-styrylferrocene is suppressed by ferrocene [40] In replacing one of the phenyl groups of stilbene with a ferrocene group, the Fe centre of ferrocene promotes intersystem crossing from the singlet excited state to the triplet excited state which is then quenched by the ferrocene moiety resulting in inefficient isomerisation This is not the case for (*E*)-$(CO)_5Cr{=}(OMe)C_2H_2Fc$ for which a transient species was observed at a monitoring wavelength of 610 nm with a lifetime of τ = 190 ± 19 ns (k = 5 2664 ± 0 53 x 10^6 s^{-1}) attributed to *cis-trans* isomerisation of the vinyl unit This transient species is present both under an atmosphere of argon and in the presence of oxygen, i e under atmospheric conditions, suggesting that isomerisation here occurs *via* a singlet excited state (this also dismisses the possibility of the transient being due to *anti-syn* isomerisation of methoxy moiety on carbene) A transient species attributed to *cis-trans* isomerisation was also observed for the vinyl-phenyl carbene complex (*E*)-$(CO)_5Cr{=}(OMe)C_2H_2Ph$ at 610 nm with a lifetime of τ = 262 ± 26 ns (k = 3 82 ± 0 40 x 10^6 s^{-1})

In contrast to similar studies, the excited state species returns completely to the *trans*-isomer [40 42] This is evident in the UV-vis spectra, which remain unchanged and also the transient signals, which recover to the pre-irradiated baseline Isomerisation occurs *via* excitation of the low-energy ferrocene based HOMO→LUMO MLCT transition of the complex as the redistribution of electron density involved reduces the bond order of the vinyl spacer thus facilitating rotation about the carbon-carbon σ-

bond (scheme 3 – 9)[42] No such isomerisation was observed for (*E*)-$(CO)_5W{=}(OMe)C_2H_2Fc$ It is proposed here that the heavier tungsten atom promotes intersystem crossing to a triplet MLCT state, which is thus quenched by the ferrocene unit

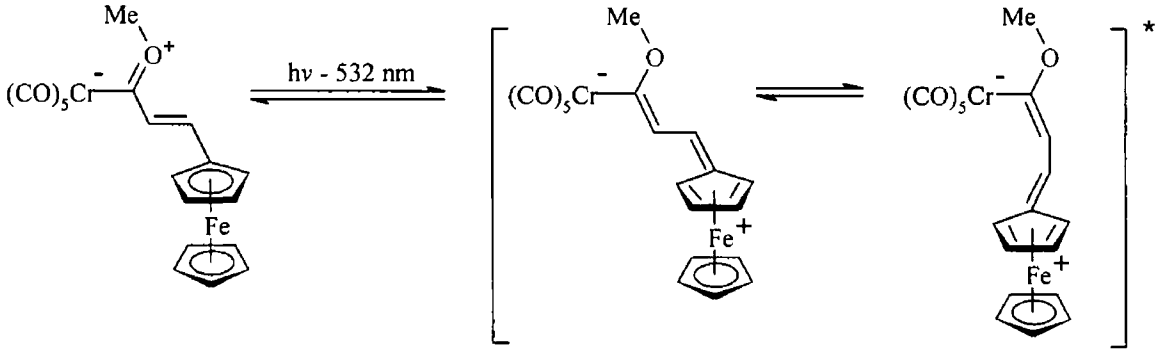

singlet charge-transfer excited state

Scheme 3 – 9

3 6 Conclusions

The photochemistry of two methoxy-stabilised Fischer-carbene complexes and their corresponding pyrrolidino analogues were investigated using a combination of laser flash photolysis and steady state photolysis All complexes showed evidence for tetracarbonyl formation when irradiated in the presence of excess triphenylphosphine Transients assigned to a CO loss species were observed following laser flash photolysis of all but the (*E*)-$(CO)_5W{=}C(NC_4H_8)C_2H_2Fc$ Fischer-carbene complex In the case of the methoxy derivatives the transients observed have tentatively been assigned to a η^3-vinyl-carbene complex However they cannot be accurately assigned without further experimental evidence UV-vis and electrochemical data of all complexes show a decreased interaction between the ferrocene and pyrrolidino-carbene moieties in comparison to the methoxy-carbenes This is supported by the crystal structure of (*E*)-$(CO)_5Cr{=}C(NC_4H_8)C_2H_2Fc$ where the ferrocene and pyrrohdino-carbene moieties are out of plane with one another

[1] For comprehensive reviews on the non-linear optical properties of organometallic complexes the reader is recommended the following publications, (a) N J Long, *Angew Chem Int Ed Engl* **1995**, 34, 21 (b) S Di Bella, *Chem Soc Rev* **2001**, 30, 355 (c) B J Coe in *Comprehensive Coordination Chemistry II*, eds J A McCleverty, T J Meyer, M D Ward, Elsevier, 9, 621

[2] M L H Green, S R Marder, M E Thompson, J A Bandy, D Bloor, P V Kolinksy, R J Jones, *Nature* **1987**, 330, 360

[3] See chapter 1, section 1 8 for an explanation of the static molecular hyperpolarisability

[4] J L Oudar, D S Chemla, *J Chem Phys* **1977**, 66, 2664

[5] J L Oudar, *J Chem Phys* **1977**, 67, 446

[6] S R Marder, D N Beratan, L -T Cheng, *Science* **1991**, 252, 103

[7] T Verbiest, S Houbrechts, M Kauranen, K Clays, A Persoons, *J Mat Chem* **1997**, 7(11), 2175

[8] (a) J C Calabrese, L –T Cheng, J C Green, S R Marder, W Tam, *J Am Chem* **1991**, 113, 7227 (b) G Doisneau, G Balavoine, T Fillebeen-Khan, J –C Clinet, J Delaire, I Ledoux, R Loucif, G Puccetti, *J Organomet Chem* **1991**, 1991, 299 (c) R Louicif-Saibil, J A Delaire, L Bonazzola, G Doisneau, G Balavoine, T Fillebeen-Khan, I Ledoux, G Puccetti, *Chem Phys* **1992**, 167, 369 (d) Z Yuan, N J Taylor, Y Sun, T B Marder, I D Williams, L -T Cheng, *J Organomet Chem* **1993**, 449, 27 (e) M Blanchard-Desce, C Runser, A Fort, M Barzoukas, J -M Lehn, V Bloy, V Alain, *Chem Phys* **1995**, *199*, 253 (f) V Alain, M Blanchard-Desce, C -T Chen, S R Marder, A Fort, M Barzoukas, *Synth Met* **1996**, *81*, 133 (g) V Alain, A Fort, M Barzoukas, C -T Chen, M Blanchard-Desce, S R Marder, J W Perry, *Inorg Chim Acta* **1996**, *242*, 43 (h) S Barlow, H E Bunting, C Ringham, J C Green, G U Bublitz, S G Boxer, J W Perry and S R Marder, *J Am Chem Soc* **1999**, 121, 3715 (i) S Barlow, S R Marder, *Chem Comm* **2000**, 1555 (j) D R Kanis, M A Ratner, T J Marks, *J Am Chem Soc* **1990**, 121, 8203 (k) D R Kanis, M A Ratner, T J Marks, *J Am Chem Soc* **1992**, 114, 10338 (l) D R Kanis, M A Ratner, T J Marks, *Chem Rev* **1994**, 94, 195

[9] G. Doisneau, G. Balavoine, T. Fillebeen-Khan, J. -C. Clinet, J. Delaire, I. Ledoux, R. Loucif and G. Puccetti, *J. Organomet. Chem.* **1991**, 421, 299.

[10] (a) J. Mata, S. Uriel, E. Peris, R. Llusar, S. Houbrechts, A. Persoons, *J. Organomet. Chem.* **1998**, 562, 197. (b) I.-S. Lee, S.-S. Lee, Y.-K. Chung, D. Kim, N.-W. Song, *Inorg. Chim. Acta* **1998**, 279, 243. (c) J. Heck, S. Dabek, T. Meyer-Friedrichsen, H. Wong, *Coord. Chem. Rev.* **1999**, 190-192, 1217. (d) M. Malaun, R. Kowallick, A. M. McDonagh, M. Marcaccio,R. L. Paul, I. Asselberghs, K. Clays, A. Persoons, B. Bildstein, C. Fiorini, J.-M. Nunzi, M. D. Ward, J. A. McCleverty, *J. Chem. Soc., Dalton Trans.* **2001**, 3025. (e) D. Prim, A. Auffrant, Z. F. Plyta, J.-P. Tranchier, F. Rose-Munch, E. Rose, *J. Organomet. Chem.* **2001**, 624, 124. (f) Z. F. Plyta, D. Prim, J.-P. Tranchier, F. Rose-Munch, E. Rose, *Tetrahedron Lett.* **1999**, 40, 6769. (g) T. J. J. Muller, *J. Organomet. Chem.* **1999**, 578, 95. (h) T. J. J. Muller, A. Netz, M. Ansorge, E. Schmalzlin, C. Brauchle, K. Meerholz, *Organometallics* **1999**, 18, 5066. (i) J. A. Mata, E. Peris, R. Llusar,S. Uriel, M. P. Cifuentes, M. G. Humphrey, M. Samoc, B. Luther-Davies, *Eur. J. Inorg. Chem.* **2001**, 2113. (j) E. Peris, *Coord. Chem. Rev.* **2004**, 248, 279.

[11] J. C. Kotz, C. L. Nivert, J. M. Lieber, R. C. Reed, *J. Organomet. Chem.* 1975, 91, 87.

[12] S. Maiorana, A. Papagni, E. Licandro, A. Persoons, K. Clay, S. Houbrechts, W. Porzio, *Gazz. Chim. Ital.*, **1995**, 125, 377.

[13] (a) H. Fischer, O. Podschadly, G. Roth, S. Herminghaus, S. Klewitz, J. Heck, S. Houbrechts, T. Meyer, *J. Organomet. Chem.* **1997**, 541, 321.(b) G. Roth, H. Fischer, T. Meyer-Friedrichsen, J. Heck, S. Houbrechts, André Persoons, *Organometallics* **1998**, 17, 1511. (c) L. Lancellotti, R. Tubino, S. Luzzati, E. Licandro, S. Maiorana, A. Papagni, *Synth. Met.* **1998**, 93, 27. (d) K. N. Jayaprakash, P. C. Ray, I. Matsuoka, M. M. Bhadbhade, V. G. Puranik, P. K. Das, H. Nishihara, A. Sarkar, *Organometallics*, **1998**, 18, 3851. (e) O. Briel, A. Fehn, W. Beck, *J. Organomet. Chem.* **1999**, 578, 247. (f) E. Licandro, S. Maiorana, A. Papagni, P. Hellier, L. Capella, A. Persoons, S. Houbrechts, *J. Organomet. Chem.* **1999**, 583, 111.

[14] J. A. Connor, J. P. Lloyd, *J. Chem. Soc. Dalton Trans.* **1972**, 1470, 1476.

[15] J. Barluenga, A. Fernandez-Acebes, A. A. Trabanco, J. Florez, *J. Am. Chem. Soc.* **1997**, 119, 7591.

[16] (a) J A Connor, J P Lloyd, *J Chem Soc Dalton Trans* **1972**, 1470 (b) J A Connor, J P Lloyd, *J Chem Soc Perkin Trans* I **1973**, 17 (c) J Barluenga, A Fernandez-Acebes, A A Trabanco, J Florez, *J Am Chem Soc* **1997**, 119, 7591

[17] E O Fischer, A Maasbol, *Angew Chem* **1964**, 76, 645

[18] C P Casey, W R Brunswald, *J Organomet Chem* **1974**, 77, 345

[19] For comparitive spectra see H Fischer, E O Fischer, *Chem Ber* **1974**, 107, 673

[20] L J Farrugia, *J Appl Cryst* **1997**, 30, 565

[21] D W Macomber, P Madhukar, R D Rogers, *Organometallics* **1989**, 8, 1275

[22] H Nakatsuji, J Ushio, S Han, T Yonezawa, *J Am Chem Soc* **1983**, 105, 426

[23] see chapter 2

[24] J Barluenga, F Aznar, A Martin, S Garcia-Granda, E Perez-Carreno, *J Am Chem Soc* **1994**, 116, 11191

[25] M L Waters, T A Brandvolt, L Isaacs, W D Wulff, A L Rheingold, *Organometallics* **1998**, 17, 4298

[26] J Barluenga, F Aznar, I Guitierrez, A Martin, S Garcia-Granda, M A Llorca-Baragano, *J Am Chem Soc* **2000**, 122, 1314

[27] (a) B S Creaven, M W George, A G Ginzburg, C Hughes, J M Kelly, C Long, I M McGrath, M T Pryce, *Organometallics* **1993**, 12, 3127 (b) S Zhang, G R Dobson, V Zhang, H C Bajaj, R van Eldik, *Inorg Chem* **1990**, 29, 3477

[28] M L Gallagher, J B Greene, A D Rooney, *Organometallics* **1997**, 16, 5260

[29] K O Doyle, M L Gallagher, M T Pryce, A D Rooney, *J Organomet Chem* **2001**, 617-618, 269

[30] P C Servaas, D J Stufkens, A Oskam, *J Organomet Chem* **1990**, 390, 61

[31] J N Bechara, S E J Bell, J J McGarvey, J J Rooney, *J Chem Soc, Chem Comm* **1986**, 1785

[32] S E J Bell, K C Gordon, J J McGarvey, *J Am Chem Soc* **1988**, 110, 3107

[33] C J Breheny, J M Kelly, C J Long, S O'Keeffe, M T Pryce, G Russell, M W Walsh, *Organometallics* **1998**, 17, 3690

[34] A D Rooney, J J McGarvey, K C Gordon, *Organometallics* **1995**, 14, 107

[35] H P Gut, N Welte, U Link, H Fischer, U E Steiner, *Organometallics* **2000**, 19, 2354

[36] B A Anderson, W D Wulff, *J Am Chem Soc* **1990**, 112, 8615

[37] L K Fong, N J Cooper, *J Am Chem Soc* **1984**, 106, 2595

[38] C P Casey, N W Vollendorf, K J Haller, *J Am Chem Soc* **1984**, 106, 3754

[39] J H Richards, N Pisker-Trifunac, *J Paint Technology* **1969**, 41, 363

[40] T Arai, Y Ogawa, H Sakuragi, K Tokumaru, *Chem Phys Letters* **1992**, 196, 145

[41] H Gorner, *J Chem Soc Faraday Trans* **1993**, 89 (22), 4027

[42] D F Perepichka, I F Perepichka, A F Popov, M R Bryce, A S Batsanov, A Chesney, J A K Howard, N I Sokolov, *J Organomet Chem* **2001**, 637-639, 445

Chapter 4

Synthesis and ^{1}H-NMR Study of *meso*-Thienyl and *meso*-Ferrocenyl Porphyrins

4 1 Aims and objectives

The following outlines the synthesis and characterisation of a series of *meso*-substituted thienyl and ferrocenyl porphyrins

The new *meso*-tetrathien-2-ylporphyrins zinc(II)-5,10,15,20-tetra(5'-bromothien-2'-yl)porphyrin (ZnTBrThP), zinc(II)-5,10,15,20-tetra(5'-ethynylthien-2'-yl)-porphyrin (ZnTEtThP) and zinc(II)-5,10,15,20-tetra(5'-(trimethylsilylethynyl)thien-2'-yl)porphyrin (ZnTTMSEtThP) are reported and their ^{1}H-NMR spectra discussed with respect to zinc(II)-5,10,15,20-tetra(thien-2'-yl)porphyrin (ZnTThP) and zinc(II)-5,10,15,20-tetraphenylporphyrin (ZnTPP) Also reported is the synthesis of the unsymmetrically substituted porphyrins zinc(II)-5-(5'-(trimethylsilylethynyl)thien-2'-yl)-10,15,20-triphenylporphyrin (ZnTMSEtThTPP), zinc(II)-5,10-di(5'-(trimethylsilylethynyl)thien-2'-yl)-15,20-diphenylporphyrin & zinc(II)-5,15-di(5'-(trimethylsilylethynyl)thien-2'-yl)-10,20-diphenylporphyrin (ZnDTMSEtThDPP), zinc(II)-5,10,15-tri(5'-(trimethylsilylethynyl)thien-2'-yl)- 20-phenylporphyrin (ZnTTMSEtThPP) and their desilylated derivatives zinc(II)-5-(5'-ethynylthien-2'-yl)-10,15,20-triphenylporphyrin (ZnEtThTPP), zinc(II)-5,10-di(5'-ethynylthien-2'-yl)-15,20-diphenylporphyrin & zinc(II)- 5,15-di(5'-ethynylthien-2'-yl)-10,20-diphenylporphyrin (ZnDEtThDPP), zinc(II)-5,10,15-di(5'-ethynylthien-2'-yl)-20-phenylporphyrin (ZnTEtThPP) and zinc(II)-5-(5'-(5''-ethynyl-2''-thiophenecarboxaldehyde)thien-2'-yl)-10,15,20-triphenylporphyrin (ZnPald) The ^{1}H-NMR spectra of these compounds are also discussed

Synthesis of the new *meso*-substituted ferrocenyl porphyrins zinc(II)-5-ferrocenyl-10,15,20-triphenylporphyrin (ZnFcTPP), nickel(II)-5-ferrocenyl-10,15,20-triphenylporphyrin (NiFcTPP), zinc(II)-5-ferrocenyl-10,15,20-tri(thien-2'-yl)porphyrin (ZnFcTThP) is reported and their ^{1}H-NMR spectra discussed

4.2 An introduction to porphyrin synthesis

The construction of porphyrins and their metal complexes, which mimic heme-containing proteins as well as the photosynthetic reaction centres, has been the foundation of many studies across a broad spectrum of scientific disciplines. The synthetic goal of many of these studies is to gain control over the arrangement of diverse substituents in specific patterns about the periphery of the porphyrin macrocycle. Porphyrins can be designed and tailored for specific applications by controlling the substituents attached at the periphery of the macrocycle. Most existing model systems are based on two distinct families of porphyrins; the β-substituted porphyrins and the *meso*-substituted porphyrins (fig. 4 - 1). The β-substituted porphyrins closely resemble naturally occurring porphyrins. The *meso*-substituted porphyrins have no direct biological counterparts but have found wide application as biomimetic models and as useful components in materials chemistry.[1]

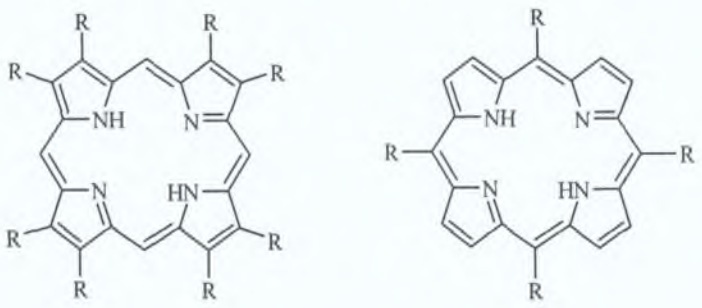

β-substituted porphyrin *meso*-substituted porphyrin

Fig. 4 - 1

Synthetic approaches to octa-alkylporphyrins and natural porphyrins related to heme and chlorophyll have reached a high degree of sophistication in the past sixty years, from monopyrrole tetramerisations (rxn. 4 - 1),[2] through Fischer's dipyrromethane self-condensation in organic acid melts (rxn. 4 - 2),[3] to MacDonald's 2 + 2 methodology (rxn. 4 - 3)[4] and the cyclisation of unsymmetrically substituted b-bilenes and a,c-biladienes (rxn. 4 - 4).[5] The most often studied synthetic porphyrin group are the *meso*-tetraarylporphyrins (A_4-porphyrin), tetraphenylporphyrin (TPP) being the classical example (rxn. 4 – 5). These porphyrins also being the most used for physical and spectroscopic studies.

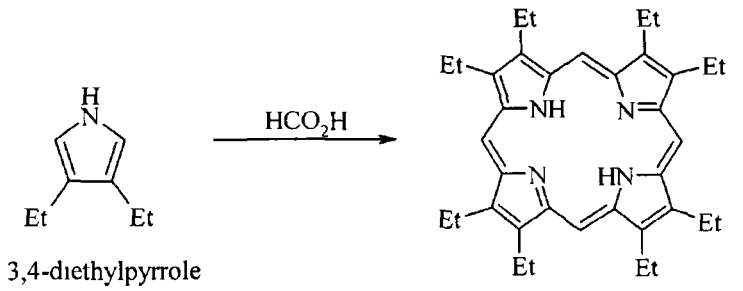

3,4-diethylpyrrole

β-octaethylporphyrin

Rxn 4 – 1

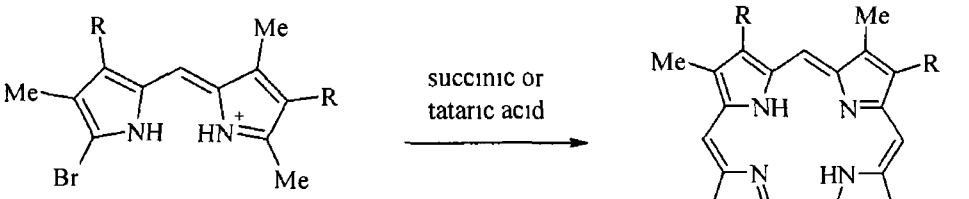

R = Et, $CH_2CH_2CO_2H$

R = Et, $CH_2CH_2CO_2H$

Rxn 4 – 2

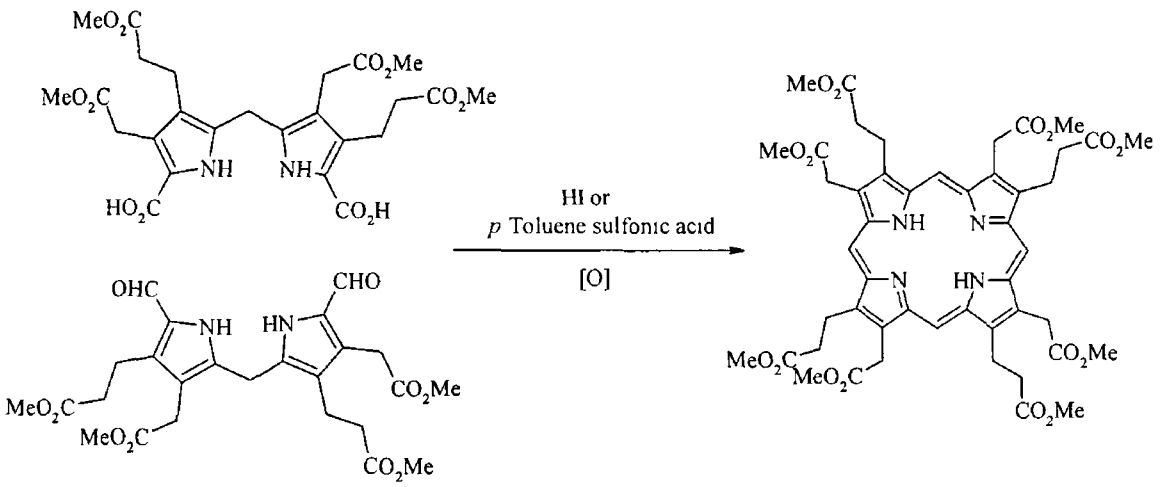

Rxn 4 – 3

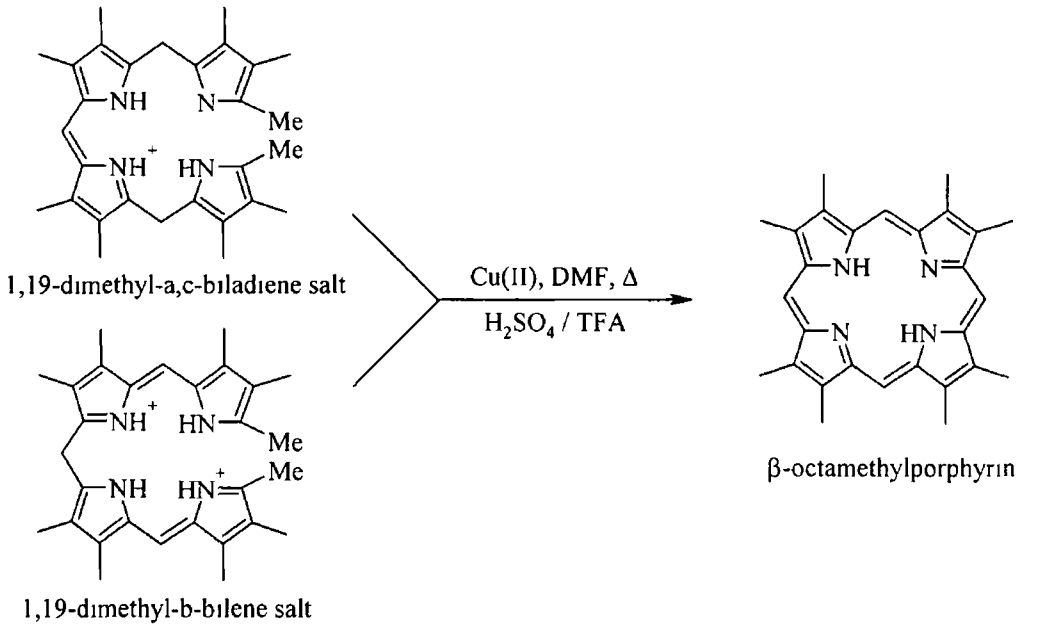

Rxn 4 – 4

Rothemund first attempted the synthesis of *meso*-substituted porphyrins in 1935[6] and succeeded in synthesising TPP a year later by heating benzaldehyde and pyrrole in a sealed bomb at 150 ^{0}C for 24 hours [7] Due to the harsh conditions the aldehyde could not be varied much and yields were also very low Adler and Longo modified the Rothemund reaction by allowing pyrrole and benzaldehyde to react for 30 minutes at reflux temperature in propionic acid (rxn 4 - 5) [8] The yields were above 20% and the milder reaction conditions allowed the use of a wider selection of substituted benzaldehydes

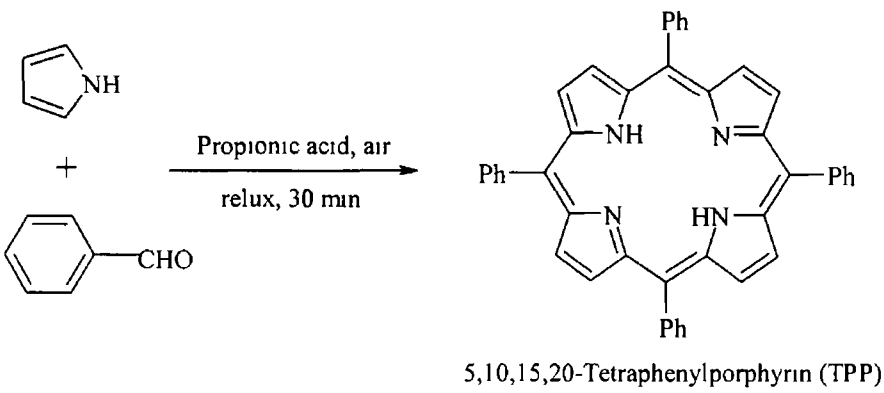

Rxn 4 - 5

Dolphin provided some insight into the course of the reaction by examining the condensation products formed under anaerobic conditions The reaction of pyrrole or 3,4-dimethylpyrrole with benzaldehyde in anaerobic refluxing acetic acid afforded tetraphenylporphyrmogen and octamethyltetraphenylporphyrmogen in 7 % and 30 % yields respectively while oxidation resulted in formation of the respective porphyrins (scheme 4 - 1) [9]

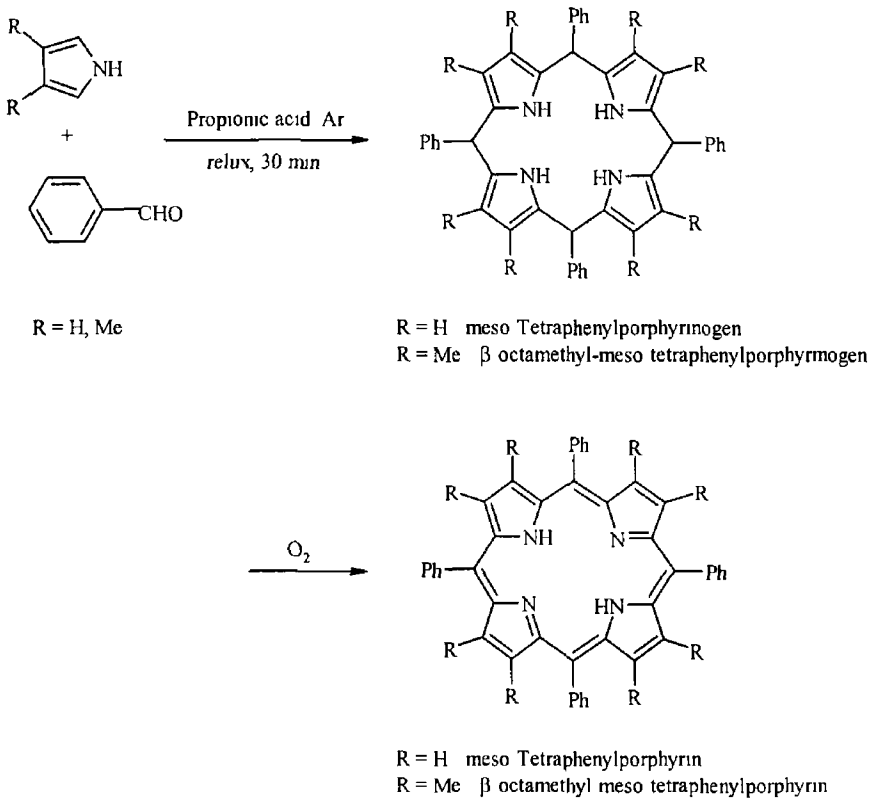

Scheme 4 - 1

These experiments provided strong evidence that the porphyrinogen is the key intermediate formed upon pyrrole-aldehyde condensation leading to the porphyrin Collman and co-workers developed the most celebrated example of *meso*-substituted porphyrins when they reduced *meso*-tetrakis(*o*-nitrophenyl)porphyrin to *meso*-tetrakis(*o*-aminophenyl)porphyrin affording the readily separable four atropisomers (fig 4 - 2) [10] The *o*-aminophenyl porphyrins, often called "picket-fence" porphyrins, are easily derivatised leading to a variety of supramolecular porphyrin systems (fig 4 - 3) [11]

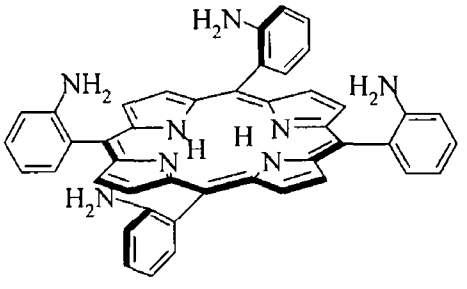

a,a,a,a-atropisomer

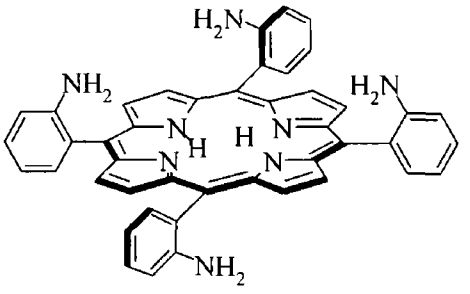

a,a,a,b-atropisomer

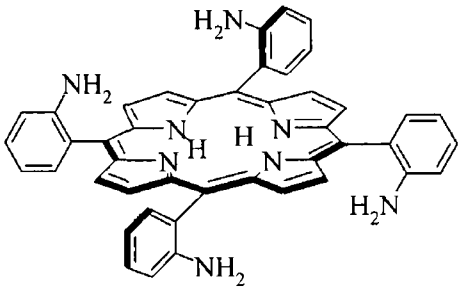

a,a,b,b-atropisomer

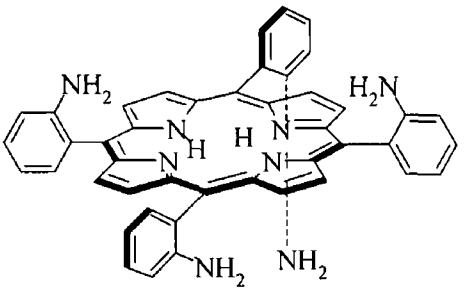

a,b,a,b-atropisomer

Fig 4 - 2

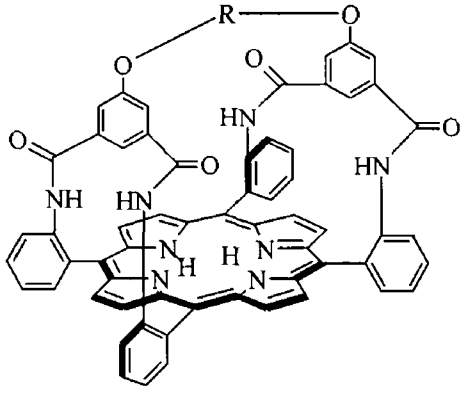

R

$(CH_2)_n$, n = 2, 4, 6, 8, 10

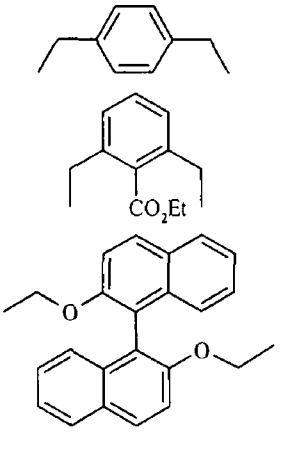

Fig 4 – 3

Lindsey improved tetraarylporphyrin synthesis further by reacting pyrrole and benzaldehyde in dichloromethane under argon in the presence of borontrifluoride etherate at room temperature to give a porphyrinogen, and then oxidising with *p*-chloranil to produce porphyrins in the range 30 – 40 %.[12] Trifluoroacetic acid and 2,3-dichloro-5,6-dicyano-1,4-benzoquinone (DDQ) were also effective reagents for the condensation and oxidation steps respectively (scheme 4 - 2).

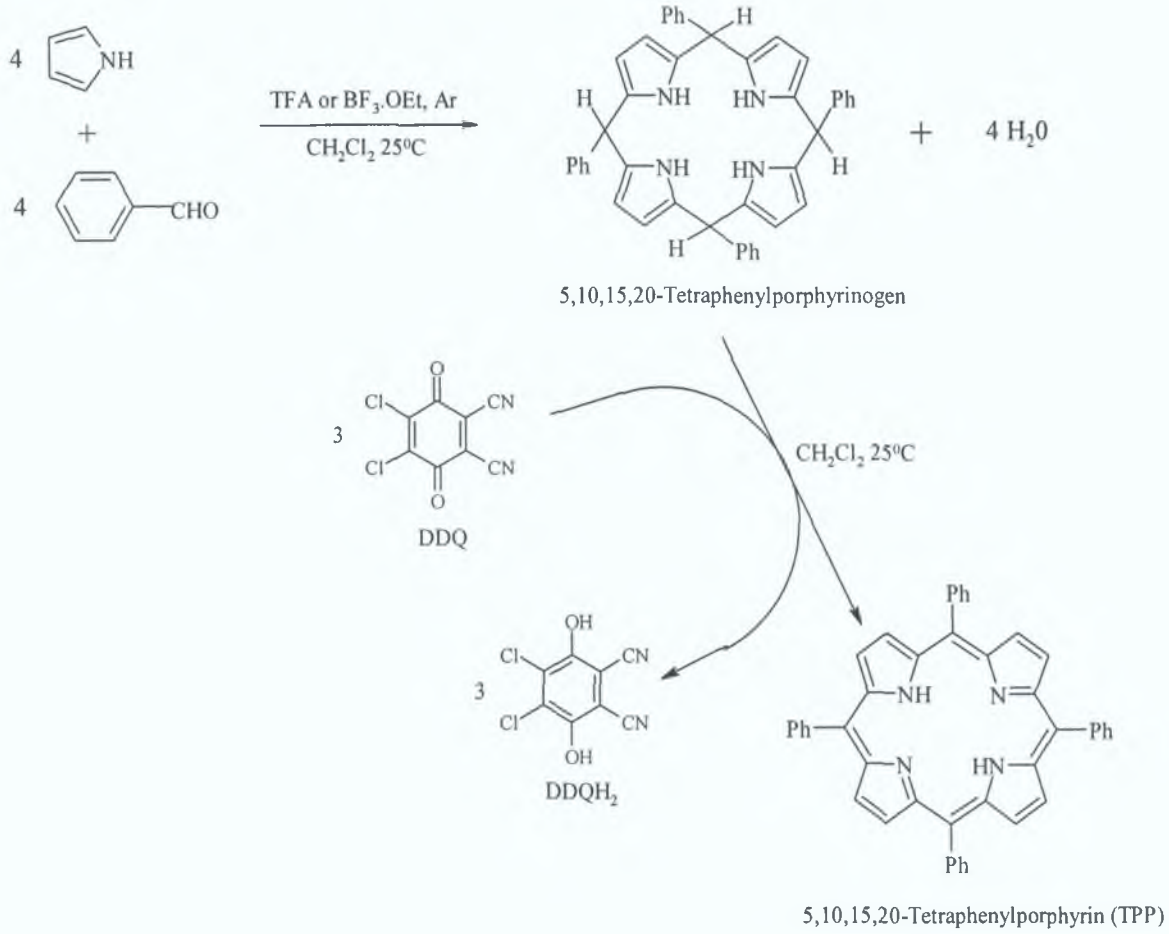

Scheme 4 - 2

The scope of the "Lindsey method" is much wider than both the Rothemund and Adler methods due to the milder reaction conditions employed and has given rise to a diverse catalogue of porphyrin systems. Yields have varied from 5 % to over 60 % using the Lindsey method when the mono-aldehydes used in the synthesis has varied from *p*-, *o*- and *m*-substituted benzaldehydes to heterocyclic aldehydes and even some organometallic aldehydes. Fig. 4 - 4 illustrates some examples of aldehydes used in

both the Adler[13 14 15 16 17, 18 19] and Lindsey[20 21 22 23 24 25] methods for the synthesis of A_4-porphyrins [26]

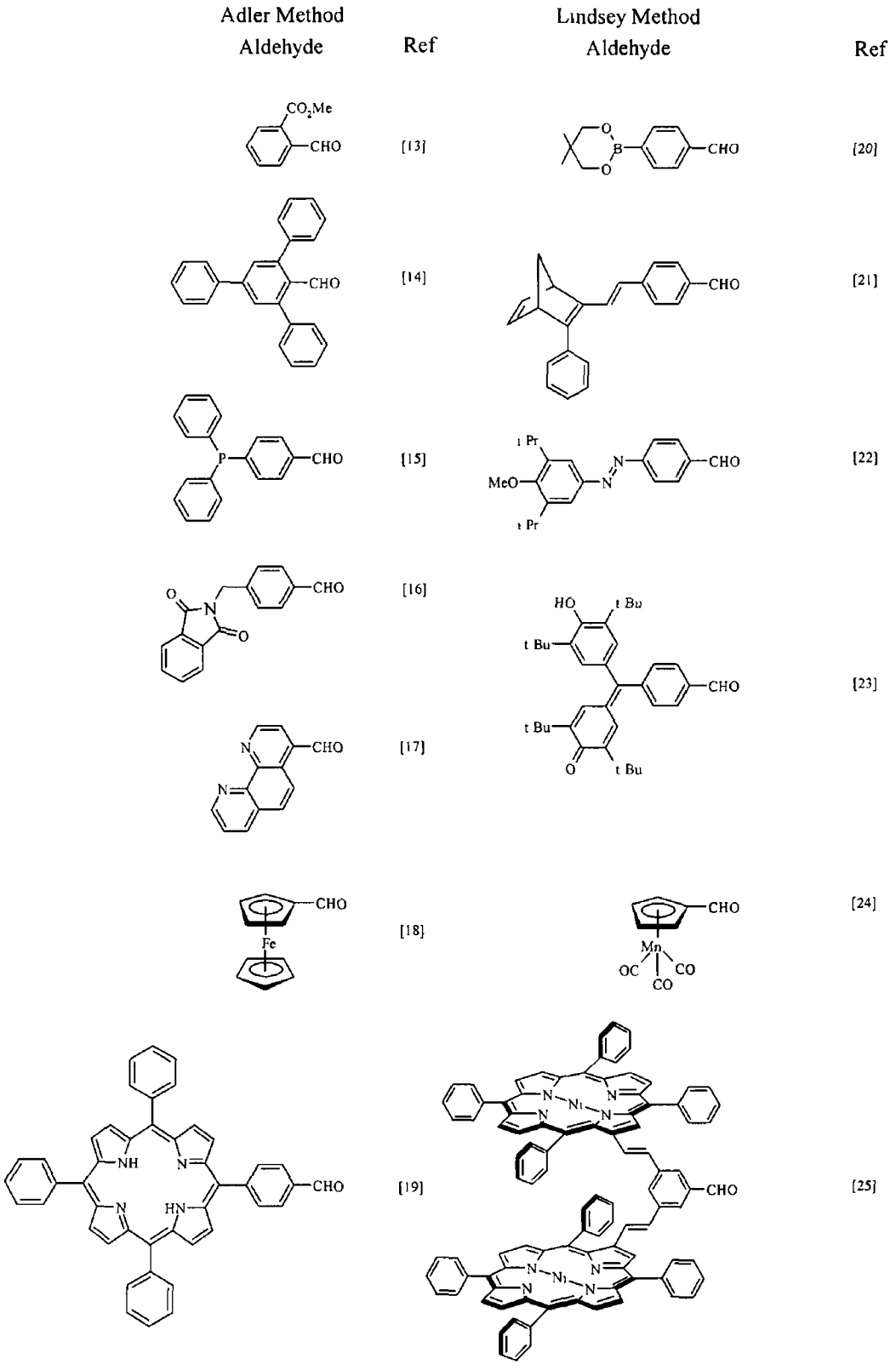

Fig 4 – 4

Condensation of an aldehyde with pyrrole affords the porphyrin having four identical *meso*-substituents, however, *meso*-substituted porphyrins bearing multiple substituents arranged regiospecifically about the porphyrin periphery are of huge interest due to their potential application in the synthesis of porphyrin-based biomimetic systems for the supramolecular and material sciences [1] Although mixed-aldehyde condensations forgo the necessity for elaborate synthesis they do require intensive chromatographic separation and purification of the porphyrin mixtures resulting in poor overall yields The ease of separation is usually determined by the differences in polarity between the two types of *meso*-substituents The reaction of a pyrrole with a mixture of two aldehydes, A and B, results in a mixture of six porphyrins A_4-, A_3B-, A_2B_2- (*cis* and *trans* isomers), AB_3- and B_4- porphyrins (rxn 4 - 6)

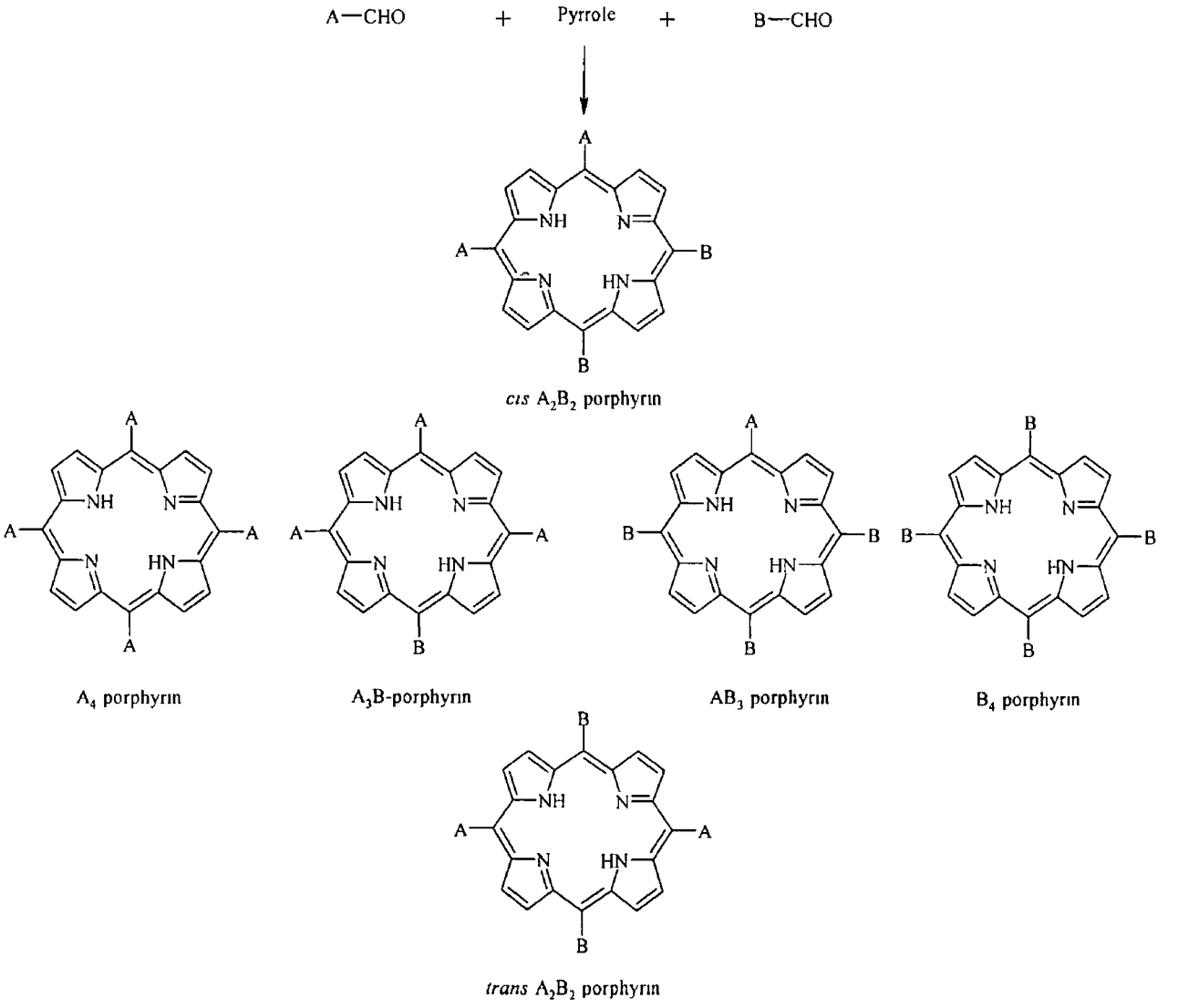

Rxn 4 - 6

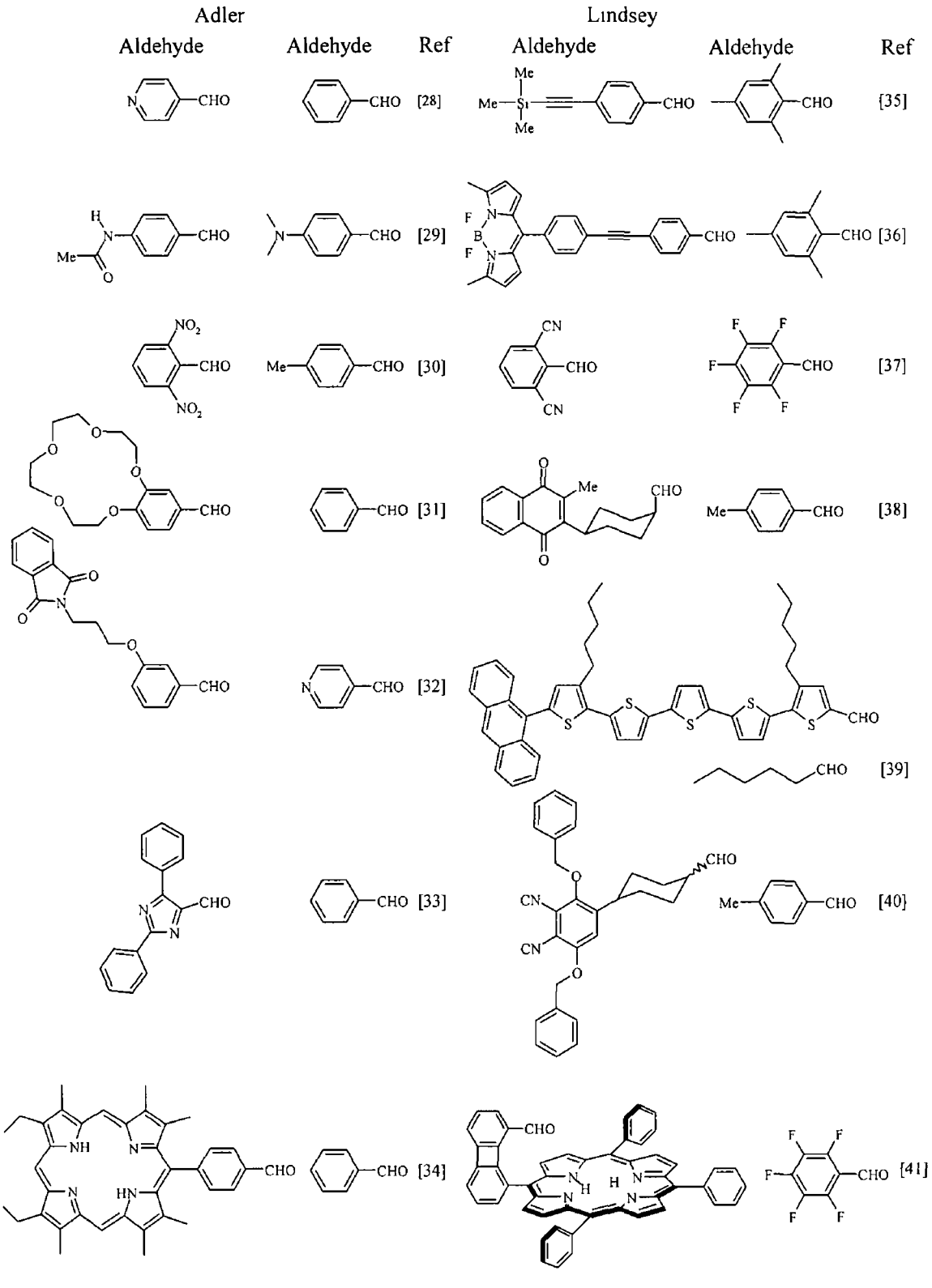

Fig 4 – 5 Examples of various aldehydes used in mixed aldehyde porphyrin synthesis for both the Adler and Lindsey methods

The A_3B-porphyrin is often the most sought after product of the mixed-aldehyde condensation as it has the ideal symmetry for the synthesis of artificial photosynthetic devices The fraction of A_3B-porphyrin is, in theory, maximised by reaction of a 4 3 1 ratio of pyrrole and aldehydes A and B respectively, however, the ratio giving the highest isolated yield of A_3B-porphyrin also depends on the actual reactivities of the two aldehydes This approach of mixed-aldehyde condensations was first used by Little et al [27] *via* the Adler method to prepare mono-hydroxy and mono-pyridyl porphyrins and quickly gained acceptance leading to the preparation of a wide variety of porphyrins bearing two different types of substituents *via* both the Adler[28 29 30 31 32 33 34] and Lindsey[35 36 37 38 39 40 41] methods (fig 4 - 5) [26] Condensations using a higher number of aldehydes leads to very low isolated yields of the various porphyrins (< 1 %), e g the reaction of a pyrrole with a mixture of three aldehydes should result in a mixture of 21 porphyrins

Even though Rothemund's original method for porphyrin synthesis has been improved and refined by subsequent investigations, the Adler and Lindsey methods remain the most efficient Nevertheless, there is still an inherent difficulty in each of these methods due to the fact that the condensation reaction between eight molecules (four pyrroles and four aldehydes) results in concomitant formation of many undesirable polymeric products A key intermediate in the pyrrole-aldehyde condensation reaction is believed to be the pyrrole-carbinol Carbinol synthesis has been investigated, both for comparison with the pyrrole-aldehyde condensation aswell as for preparative purposes Three synthetic methods exist for the preparation of pyrrole-carbinols (fig 4 - 6) [42]

Method I

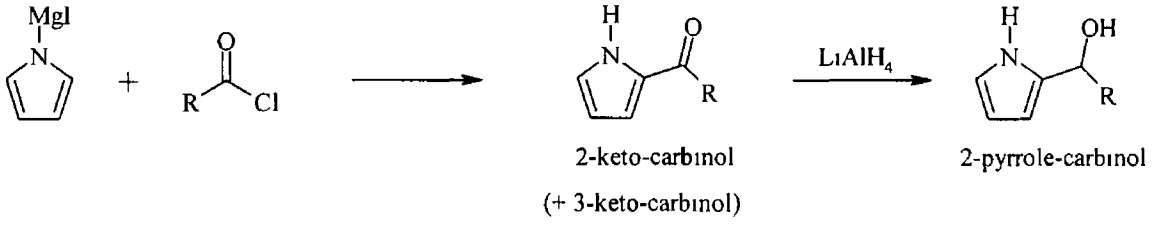

2-keto-carbinol
(+ 3-keto-carbinol)

2-pyrrole-carbinol

Method II

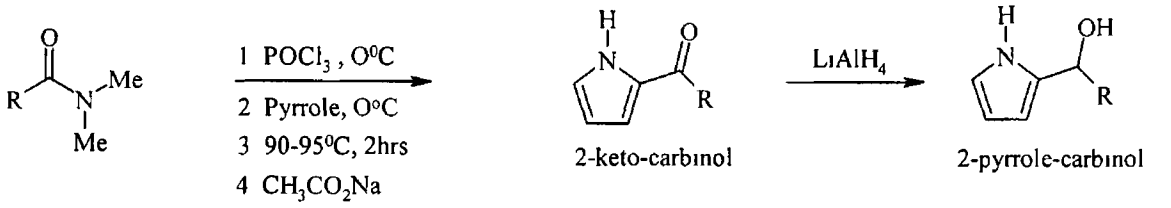

2-keto-carbinol

2-pyrrole-carbinol

Method III

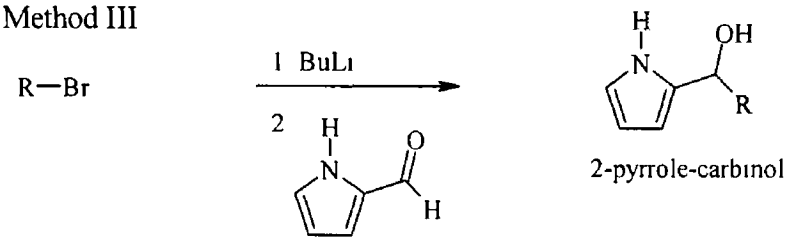

2-pyrrole-carbinol

Fig 4 - 6

Pyrrole-carbinols are known to undergo self-condensation in acidic solution forming the *meso*-substituted porphyrin Several pyrrole-carbinols have been treated in hot-propionic acid under conditions identical to that in the Adler method In each case yields were similar to that of the corresponding pyrrole-aldehyde condensation reaction (rxn 4 - 7) [43]

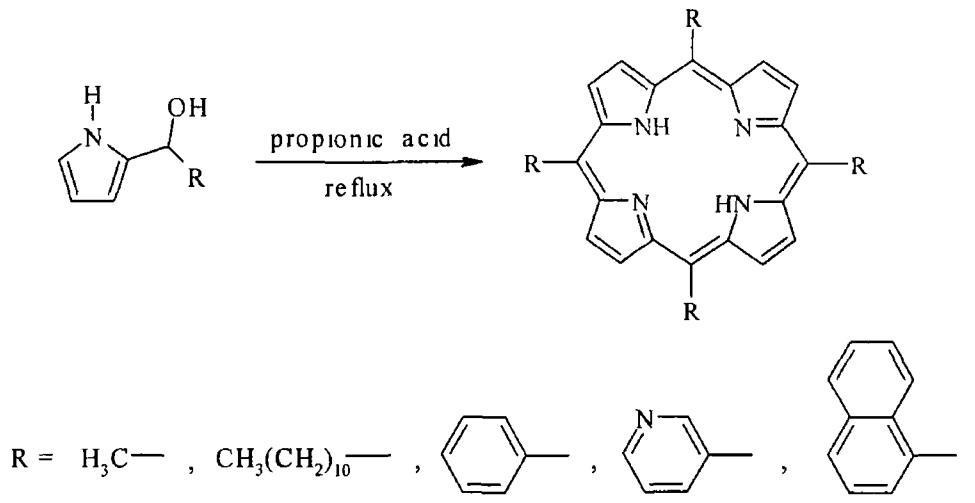

Rxn 4 - 7

A considerable increase in metalloporphyrin yields was observed when $Zn(OAc)_2$ was added to the mixture containing the pyrrole-carbinol [42(c)] This was attributed to a reduction in the number of coordinating reactants at the Zn atom, prior to condensation, from four pyrroles and four aldehydes to just four pyrrole-carbinol molecules Some pyrrole-carbinol condensations have not been so successful and have only yielded porphyrin when the azeotropic removal of water has been applied to the reaction [44]

Synthetic developments in the area of unsymmetrically functionalised tetraarylporphyrins have progressed in recent years, as porphyrins bearing specific patterns of substituents are crucial building blocks in biomimetic and materials chemistry One successful approach to minimize the chromatographic separation generally required for mixed condensations towards A_3B-substituted porphyrins involves the covalent attachment of one aldehyde to a solid phase (scheme 4 - 3),[45] however this method is constrained to those aldehydes that have a functional group that can successfully be attached to a solid phase resin

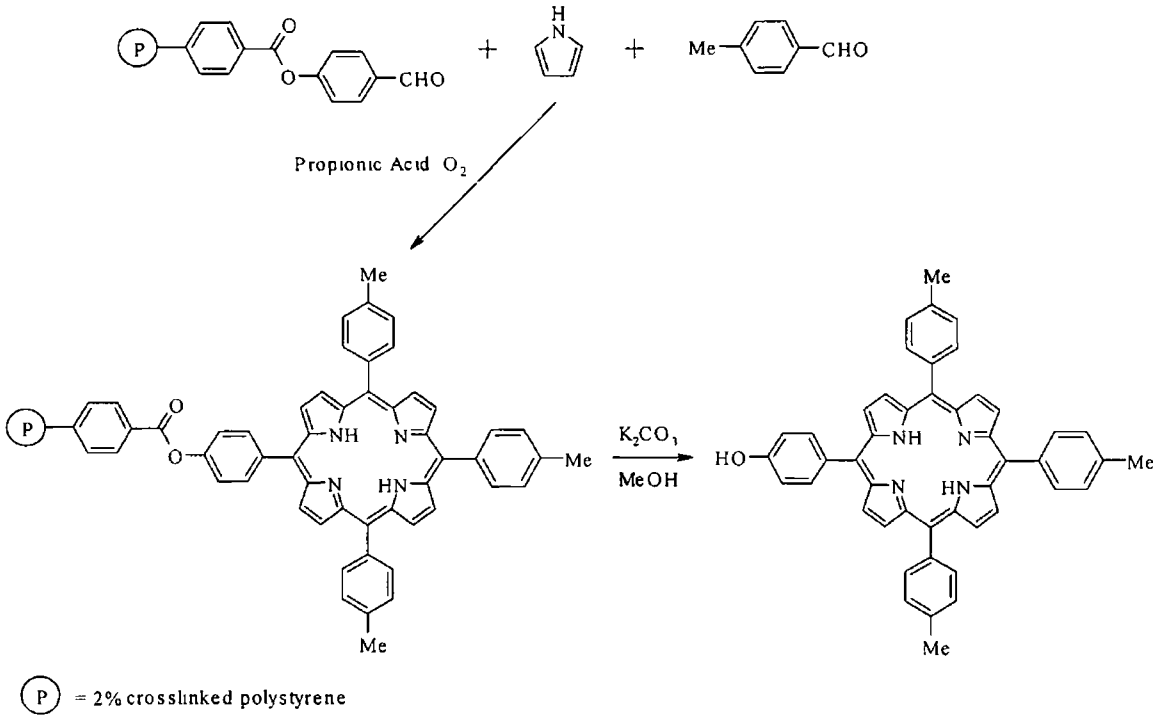

Scheme 4 - 3

Porphyrins bearing substituents in the 5,15-positions are useful for diverse applications however the *cis*- and *trans*-substituted porphyrins are often very difficult to separate by column chromatography Rational synthesis of *trans*-substituted porphyrins with C_2 symmetry has been developed based on the MacDonald 2+2 condensation of a dipyrromethane and an aldehyde [4] In the initial development of the MacDonald 2+2 condensation, the dipyrromethanes were prepared following methods established during the course of the synthesis of naturally occurring porphyrins Such dipyrromethanes were substituted at the β-positions but lacked *meso*-substituents Gunter and Mander established a high yielding route to the formation of 5,15-substituted porphyrins by reaction of meso-unsubstituted, β-substituted dipyrromethanes with an aryl aldehyde in methanol containing *p*-TsOH at 20 ^{0}C for 6 hours (rxn 4 - 8) [46] The resulting porphyrinogen was then isolated by cooling the reaction mixture to 4^{0}C for 16 hours and oxidised with DDQ in THF, resulting in the corresponding porphyrin A small portion of the mono 5-substituted porphyrin was also formed

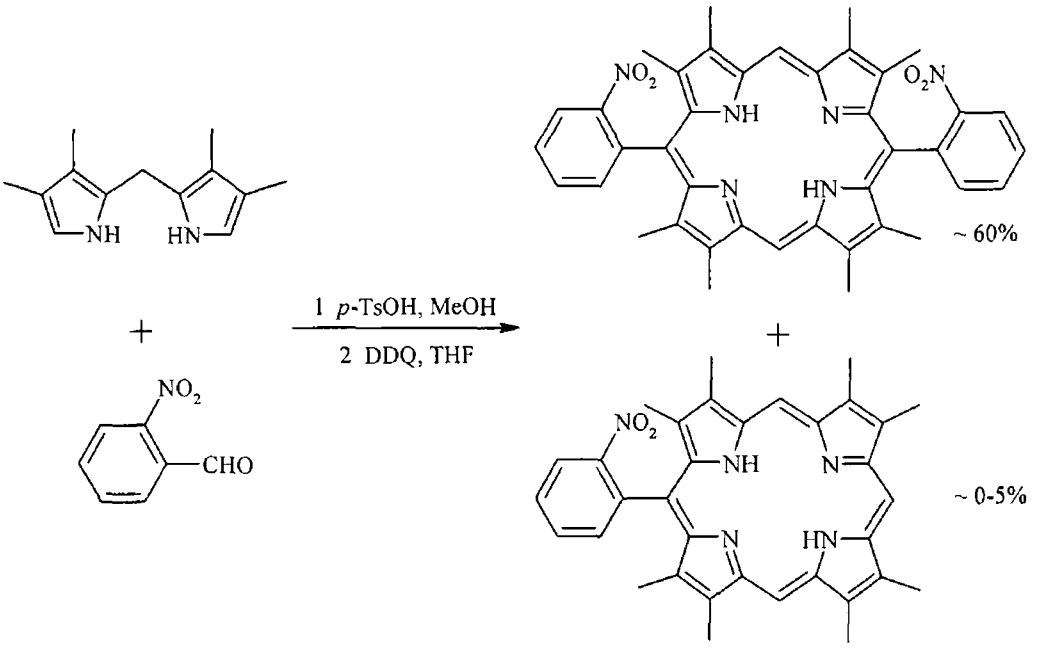

Rxn 4 – 8

Osuka further developed the method of Gunter and Mander to incorporate acid labile substrates such as acetals in the aldehyde unit [47] The condensation was carried out at room temperature in acetonitrile using trichloroacetic acid as a catalyst, oxidation of the porphyrinogen was carried out with *p*-chloranil in THF Lindsey developed this method even further by carrying out the dipyrromethane-aldehyde condensation reaction in a two-step one-flask room-temperature procedure in dichloromethane with borontrifluoride-etherate as the catalyst followed by oxidation with *p*-chloraml [48] These routes have been employed to prepare a variety of *trans*-substituted porphyrins through variation of the aldehyde and also the dipyrromethane,[49] [50] [51] a number of examples are shown in fig 4 – 7

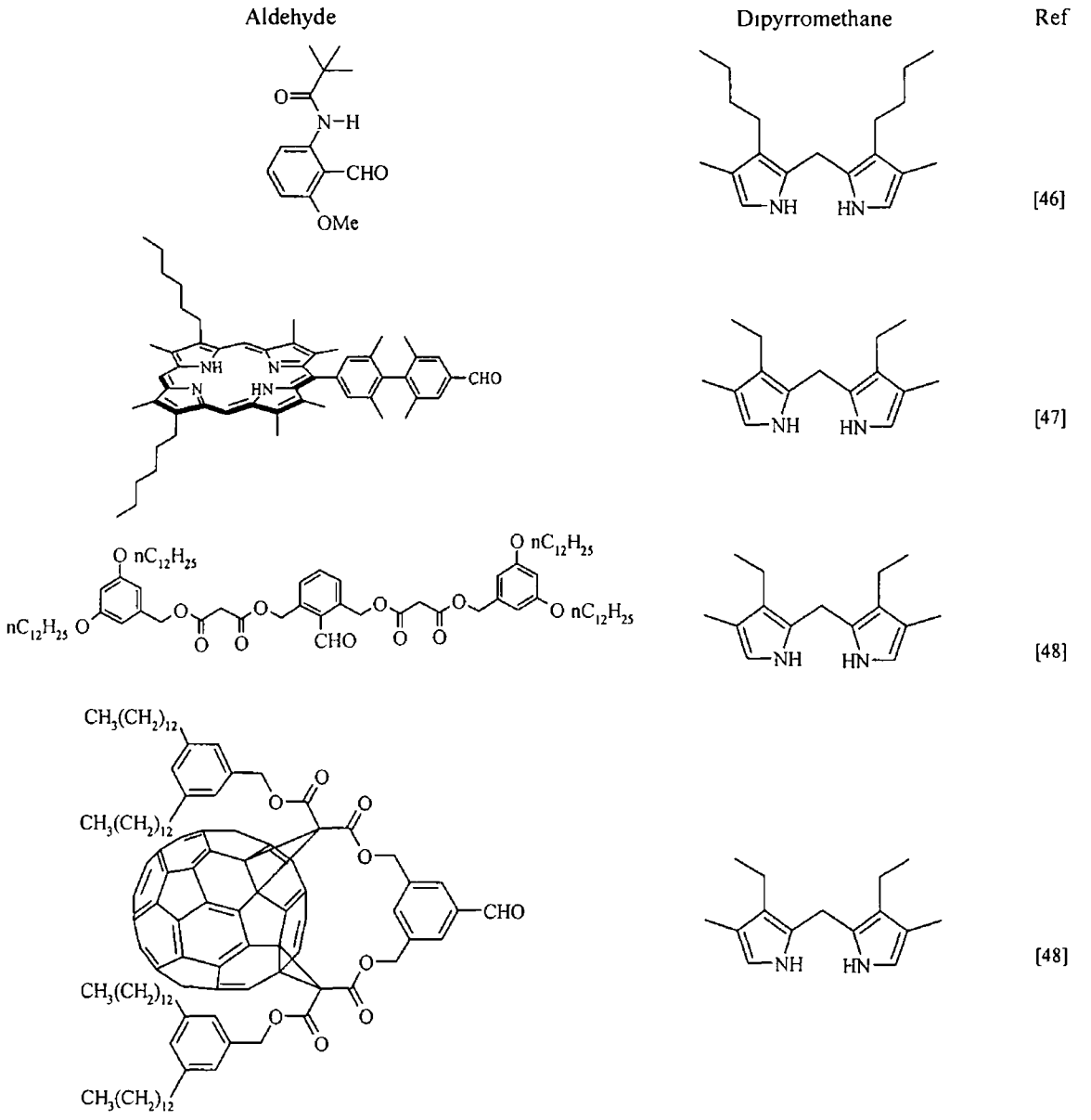

Fig 4 - 7

Another route to *trans*-substituted porphyrins with C_2 symmetry or with different *meso*-substituents is the direct coupling of a 1,9-unsubstituted dipyrromethane and a 1,9-dipyrromethanedicarboxaldehyde [52] This method can also be used to synthesise less symmetrical porphyrins by the condensation of porphyrins with dissimilar β-substituents however this may lead to a mixture of products that can be difficult to separate, e g rxn 4 – 9

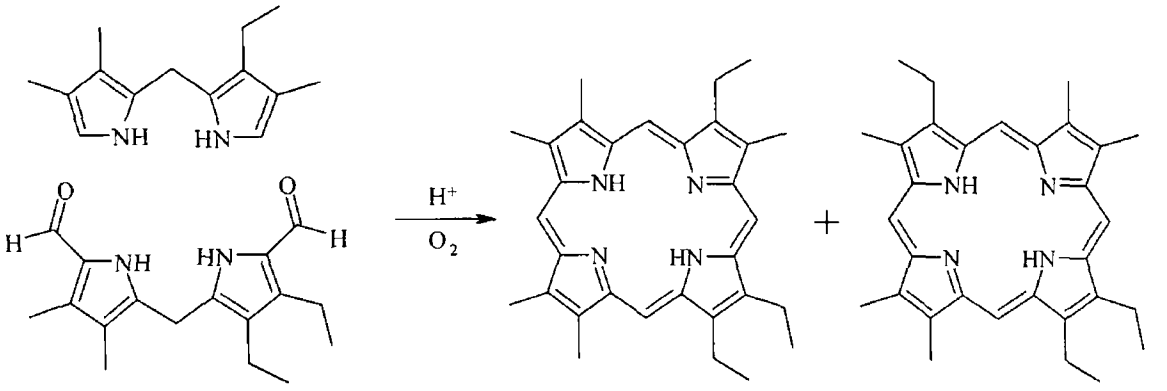

Rxn 4 - 9

Montierth et al have successfully carried out such a 2+2 MacDonald-type porphyrin synthesis using dissimilar dipyrromethanes by linking one of the dipyrromethanes to a solid support proving that the synthesis and, most importantly, the purification of a single completely unsymmetrical porphyrin is possible (rxn 4 – 10) [52]

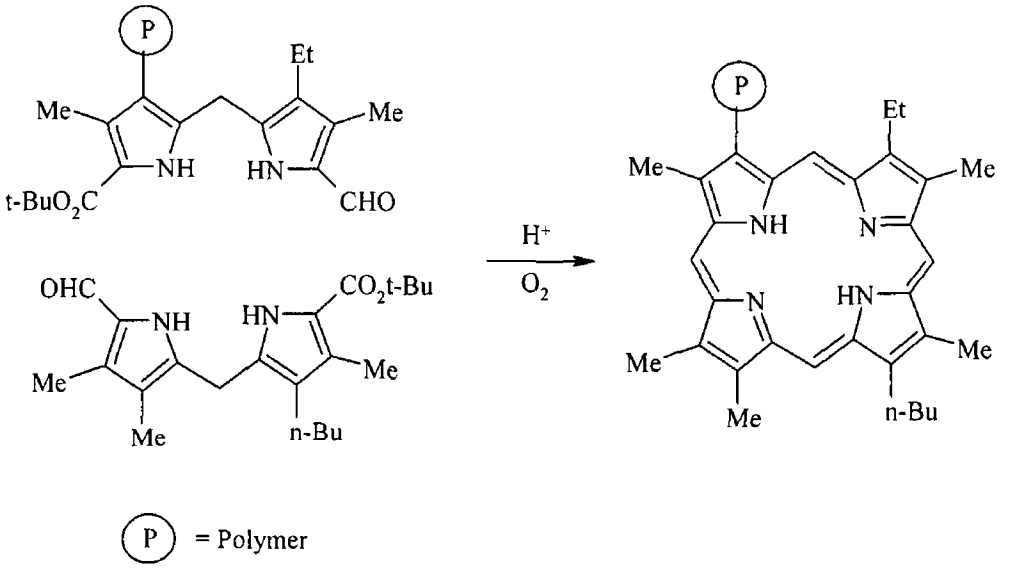

Rxn 4 - 10

The accessible routes to porphyrins *via* the MacDonald 2 + 2 condensation depend directly on the availability of various types of dipyrromethanes Unsubstituted dipyrromethane was first synthesised by Clezy in 1969 using a three-step procedure, which involved the use of the highly toxic thiophosgene [53] Recent methodology has since been established for preparing dipyrromethane in one step,[54] Lindsey has also developed a procedure that affords control over the substituents at their *meso* and β positions (fig 4 - 8) [55]

(a) Clezy route

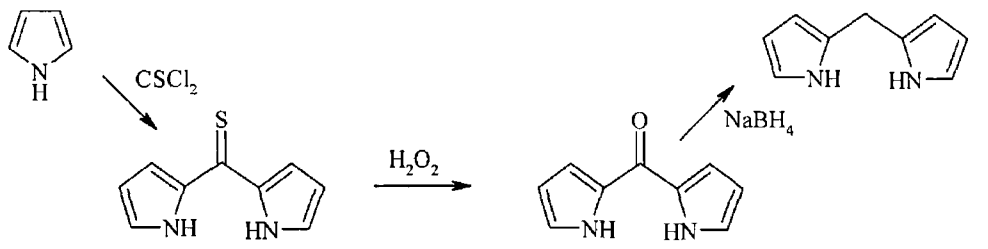

(b) Wang and Bruce route

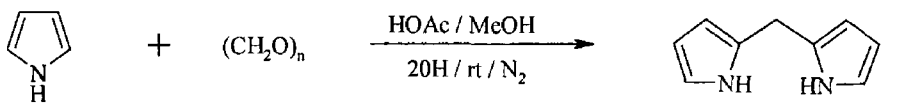

40 1

(c) Lindsey route

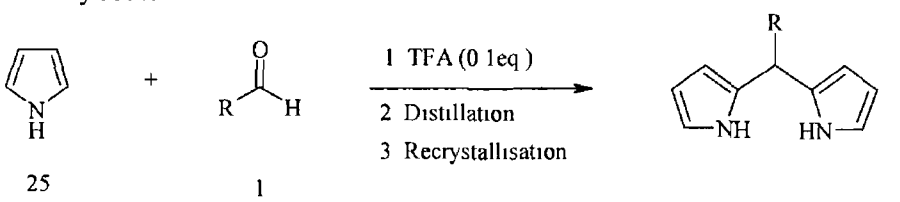

25 1

R = H, CH_3

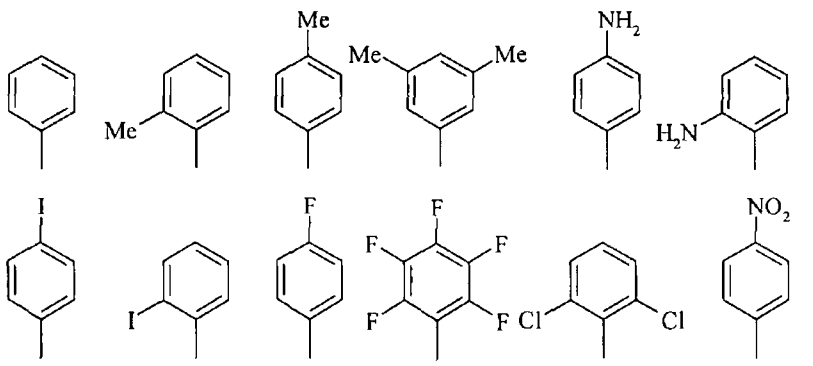

Fig 4 - 8

However, scrambling can occur in an acid catalysed dipyrromethane-aldehyde condensation This can result in a product distribution equal that of a mixed aldehyde condensation The successful implementation of a MacDonald 2 + 2 condensation therefore requires minimisation of the scrambling processes An example of how a *cis*-A_2B_2-porphyrin is formed *via* scrambling during the condensation of a *meso*-A-dipyrromethane and a B-aldehyde is shown in scheme 4 - 4

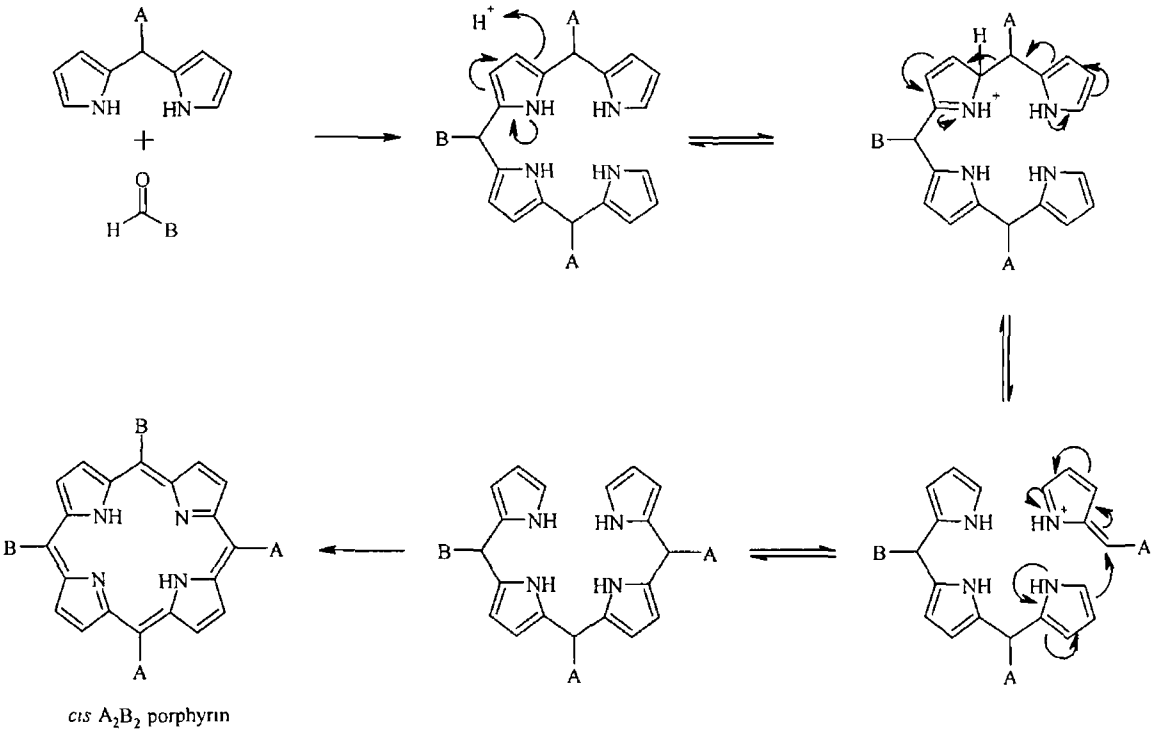

Scheme 4 - 4

Littler and co workers have carried out a detailed study investigating the conditions giving minimal scrambling in the synthesis of *trans*-porphyrins in gram quantities from dipyrromethanes and aldehydes [56] Sterically hindered dipyrromethanes such as 5-mesityldipyrromethane completely suppress scrambling when using (rxn 4 - 11) However this is very difficult to achieve for sterically unhindered dipyrromethanes such as 5-phenyldipyrromethane The effect of scrambling can only therefore be minimised when using sterically unhindered dipyrromethanes and also yields were relatively poor under the conditions used by Littler et al (rxn 4 - 12)

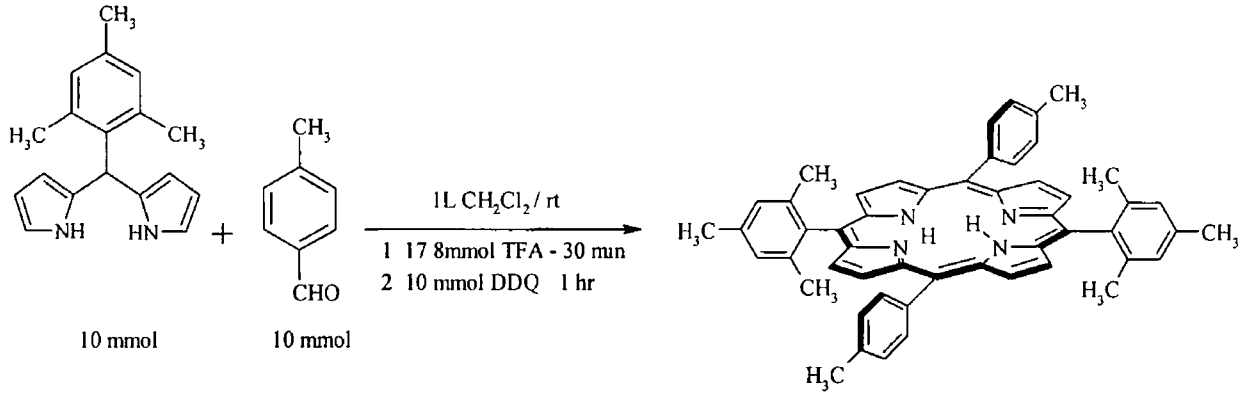

Rxn 4 - 11

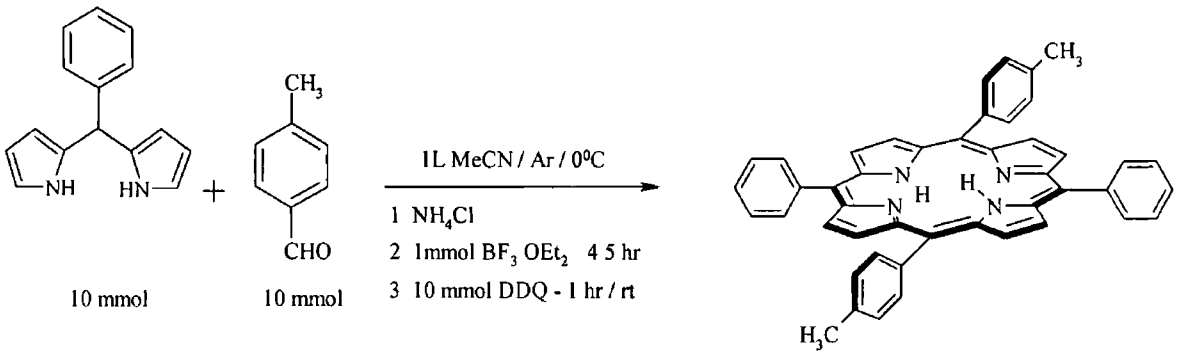

Rxn 4 - 12

Rao et al took an alternative approach to the synthesis of *trans*-porphyrins bearing sterically unhindered substituents *via* the self-condensation of a dipyrromethanecarbinol [57] An efficient and selective procedure was developed for the monoacylation of dipyrromethanes affording the direct precursor to the desired dipyrromethanecarbinols on the gram scale This procedure was successfully applied to a wide range of aryl substituents, an example of which is shown in scheme 4 - 5

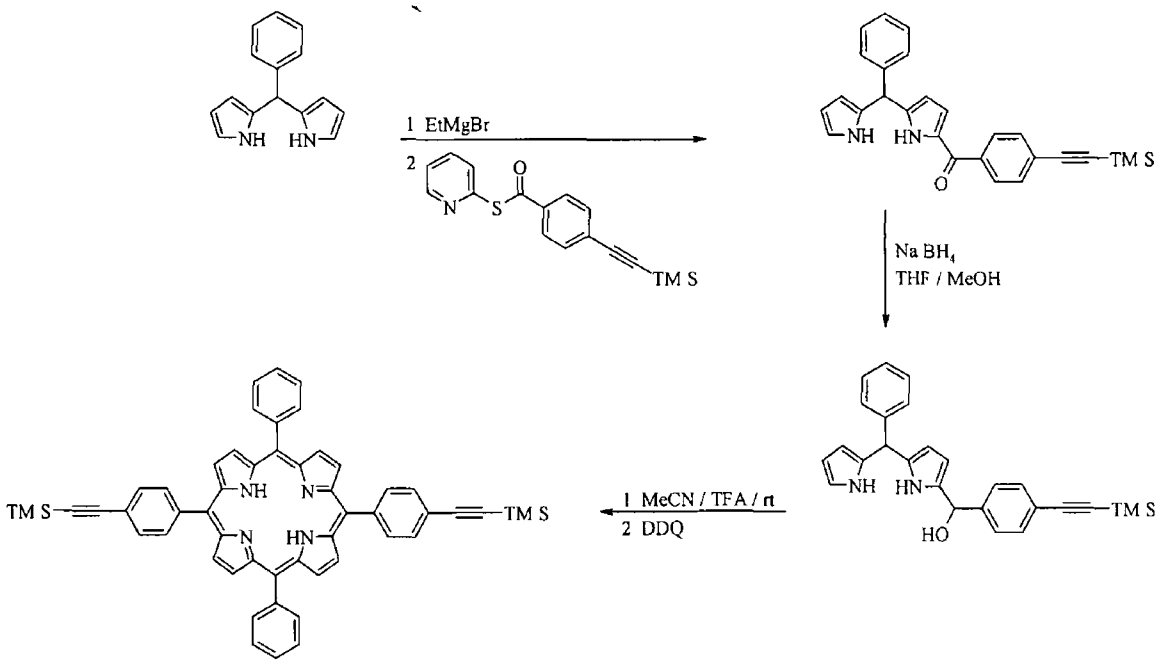

Scheme 4 - 5

Due to the complexity of syntheses required for the preparation of less symmetrical members of the *meso*-substituted porphyrin family such studies have been quite infrequent Recently however, Brinas and Bruckner have published the stepwise synthesis of 5,10-diphenylporphyrin based on the known 2 + 2 methodology and a number of successful 3 + 1 approaches toward the synthesis of porphyrins and porphyrin analogues [58] The 3 + 1 methodology was quickly abandoned due to the large susceptibility of tripyrranes to acid catalysed scrambling as compared to that of dipyrranes (rxn 4 – 13) The key intermediate in the 2 + 2 condensation was identified as the benzoylformyl-dipyrromethane, which was reduced to the dicarbinol and condensed in situ with dipyrromethane under the low scrambling conditions as found by Lindsey (scheme 4 – 6) This procedure afforded analytically pure 5,10-diphenylporphyrin in 10 – 20 % yield

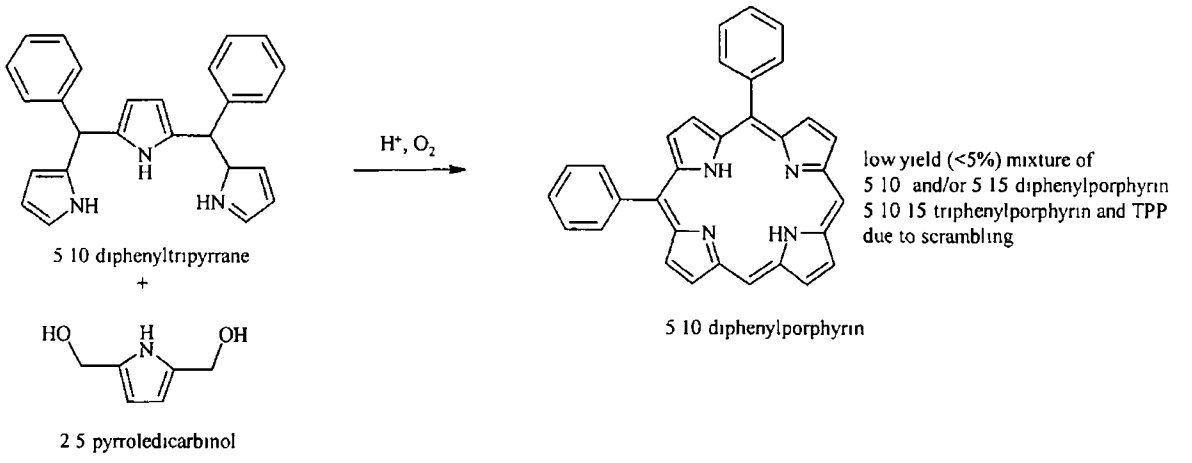

Rxn 4 – 13

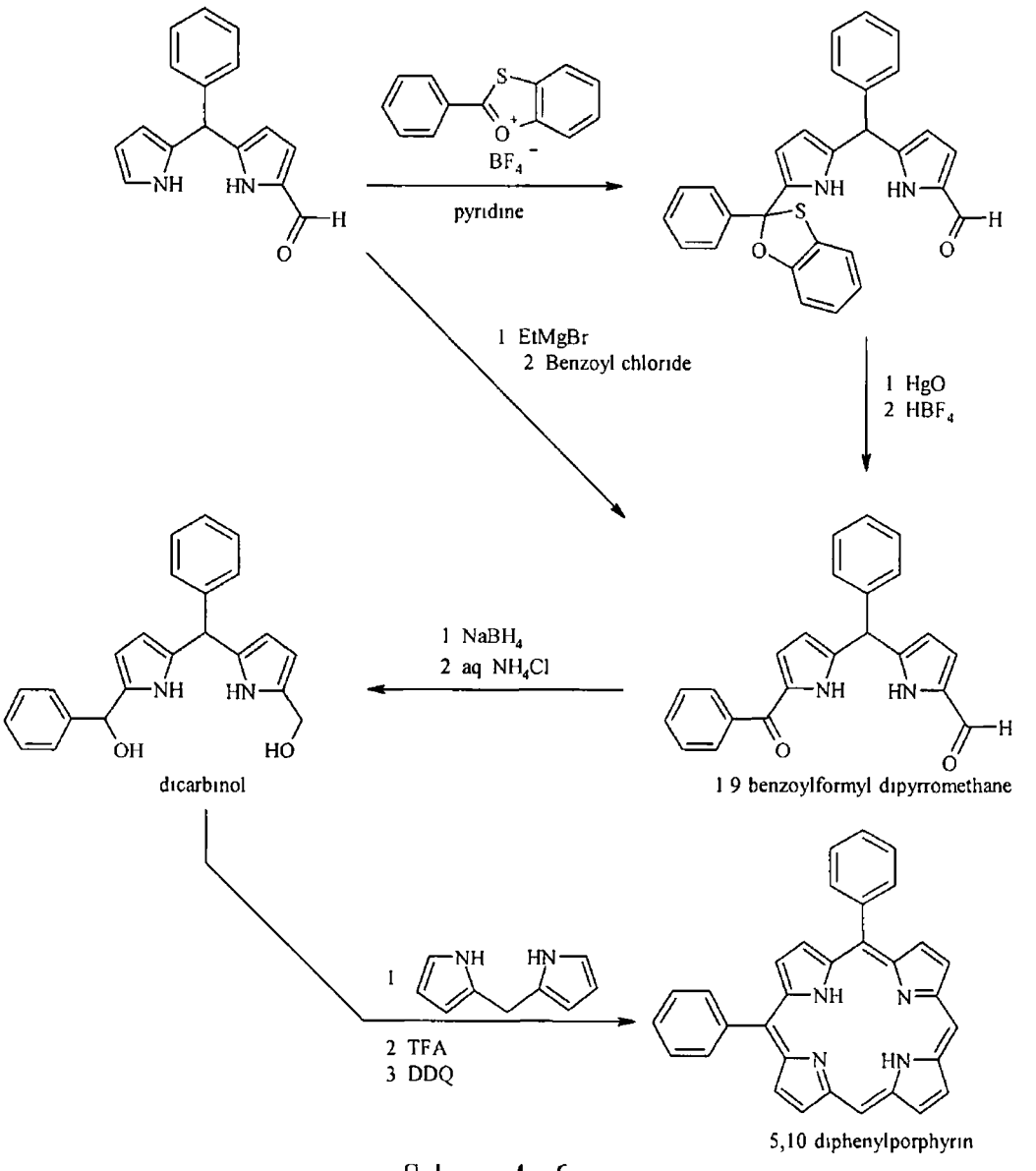

Scheme 4 - 6

Hatscher and Senge extended this method to prepare a range of aryl and aliphatic 5,10-substituted porphyrins with similar yields using a variation of the 3 + 1 methodology Although no scrambling was observed in this method some 5-mono-substituted porphyrin was always formed in the reaction (rxn 4 - 14) [59] In the same study a different approach was taken to the same synthesis by adding three equivalents of the hthiated-desired substituent to one equivalent of unsubstituted porphine This resulted in yields of up to 75 % of the 5,10-disubstituted porphyrinogen, which was easily oxidised to the corresponding 5,10-disubstituted porphyrin using DDQ (scheme 4 - 7)

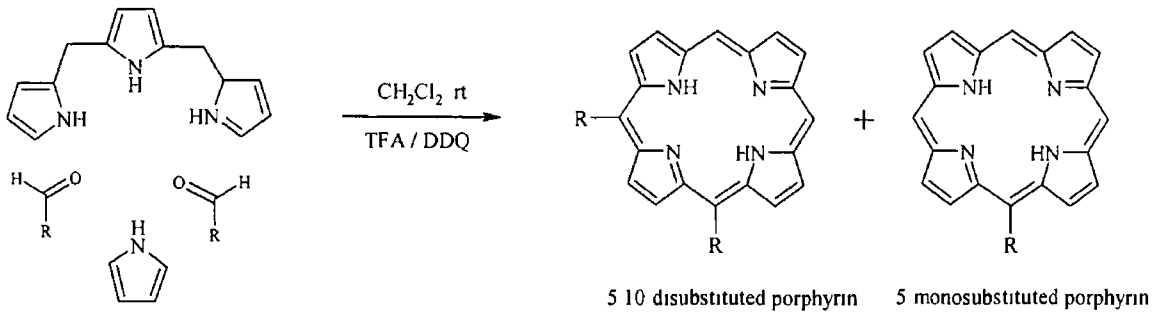

Rxn 4 - 14

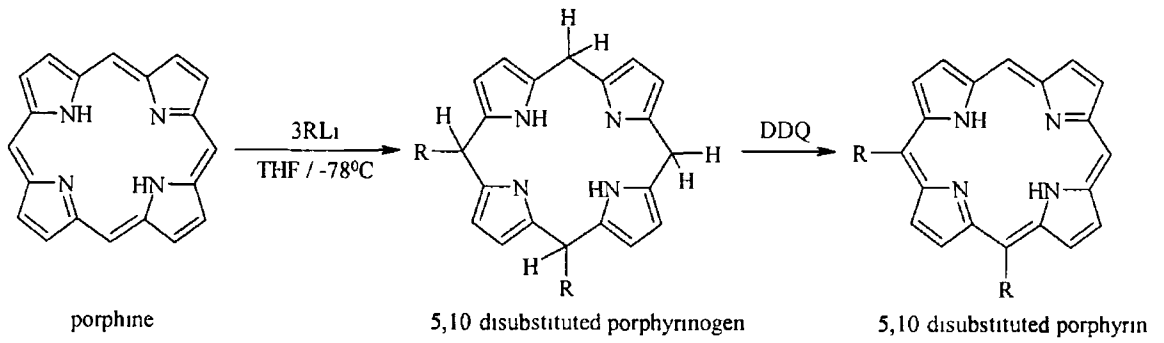

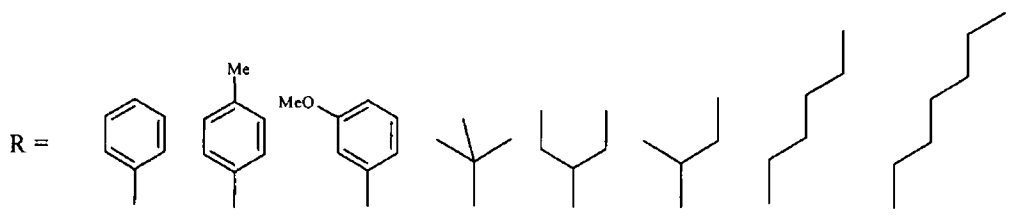

Scheme 4 - 7

The synthesis of tetra-aryl porphyrins of the A_3B-type and those bearing three (*cis*-AB_2C, *trans*- AB_2C) or four (ABCD) different substituents in pure form have remained elusive until recently due to the complexity of syntheses required for the preparation of less symmetrical members of the *meso*-substituted porphyrin family

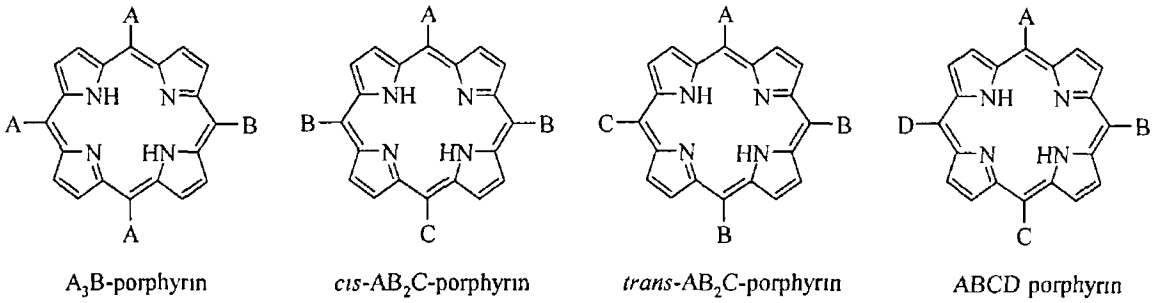

A_3B-porphyrin *cis*-AB_2C-porphyrin *trans*-AB_2C-porphyrin ABCD porphyrin

Fig 4 - 9

Rao et al prepared an A_3B-porphyrin *via* two routes involving the condensation of an A_3-dipyrromethanedicarbinol and a B-dipyrromethane (scheme 4 - 8) or an ABA-dipyrromethanedicarbinol and an A-dipyrromethane [60] The key to the success of these syntheses relies on the use of analytically pure dipyrromethanes thus ruling out the formation of unwanted porphyrin contaminant in the final product

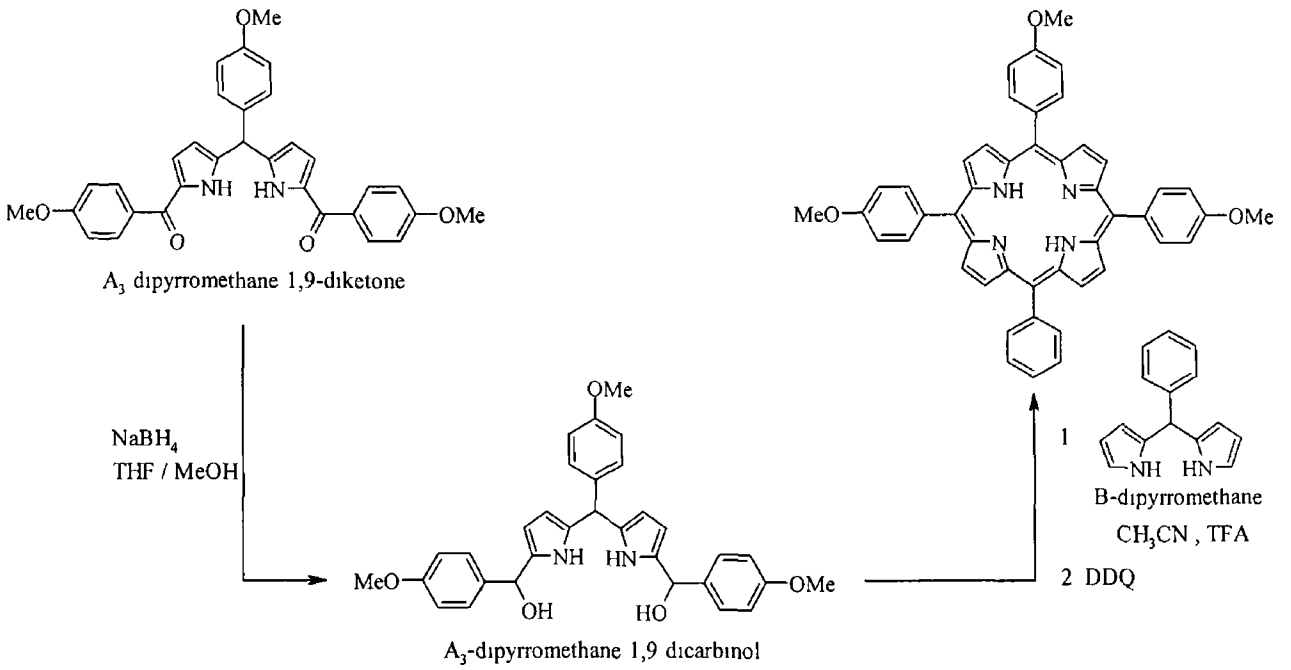

Scheme 4 - 8

trans-AB_2C-porphyrins were also prepared by Rao et al *via* the condensation of an ABA-dipyrromethanedicarbinol and a C-dipyrromethane (scheme 4 - 9) [62] Again, the use of analytically pure dipyrromethanes was instrumental in the success of these syntheses

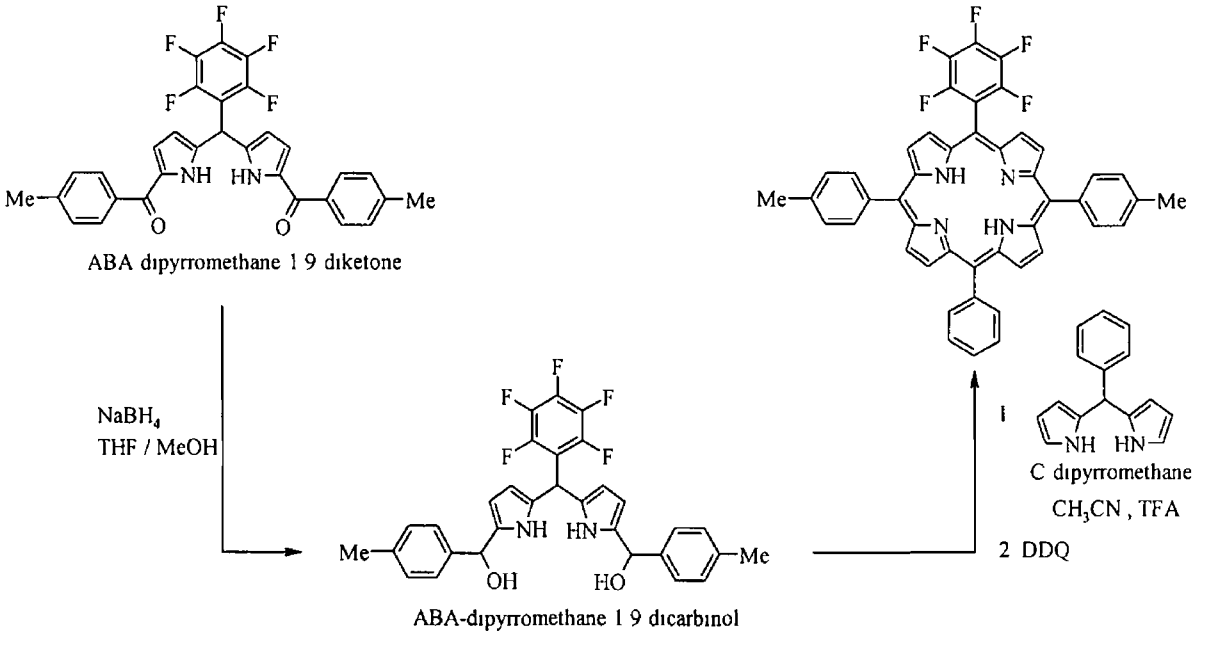

Scheme 4 - 9

The alternative route involving the condensation of an ABC-dipyrromethane-dicarbinol with a B-dipyrromethane is less efficient as it requires the unsymmetrical acylation of a dipyrromethane in the 1,9-positions This is the only viable route to *trans*-AB_2C-porphyrins with mesityl groups occupying the *trans* positions as the required ABA-dipyrromethane-1,9-diketone (A = mesityl) could not be reduced to the corresponding dicarbinol *cis*-AB_2C-porphyrins were prepared in a similar manner by Lindsey *via* the condensation of an ABC-dipyrromethanedicarbinol and an A-dipyrromethane (Scheme 4 - 10) An alternative route involving the condensation of an AAB-dipyrromethane-dicarbinol and a C-dipyrromethane was also carried out successfully

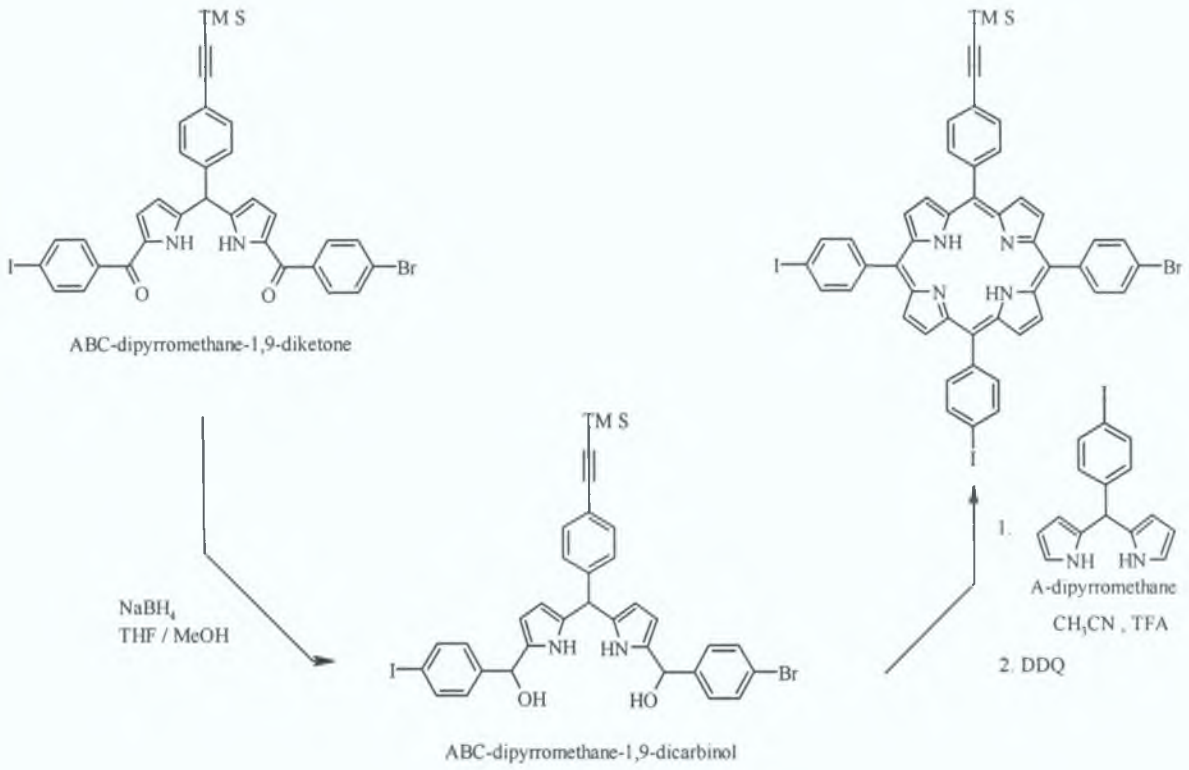

Scheme 4 - 11

The first account of a stepwise synthesis of unsymmetrical tetra-arylporphyrins of the ABCD-type was reported by Smith and Wallace in 1990, however they used a synthetic route involving the condensation of two dissimilar dipyrromethanes that resulted in a mixture of porphyrin products.[61] The rational synthesis of unsymmetrical *meso*-substituted porphrins devised by Rao et. al proved successful one again in the preparation of ABCD-porphyrins, five ABCD-porphyrins were prepared in all.[62] Porphyrins II-V were designed as potential building blocks with the possibility of further coupling at each *meso*-substituent (fig. 4 - 10). Porphyrins II, III and IV each bear three functional groups that can be selectively manipulated and are potential building blocks for "T-shaped" porphyrin architechtures. The former two both contain one iodo group and two protected ethynes, while the latter contains three ethynes that can be reacted sequentially (unprotected, TMS-protected and TIPS-protected). Porphyrin V bears four different functional groups for sequential elaboration *via* Pd coupling reactions.

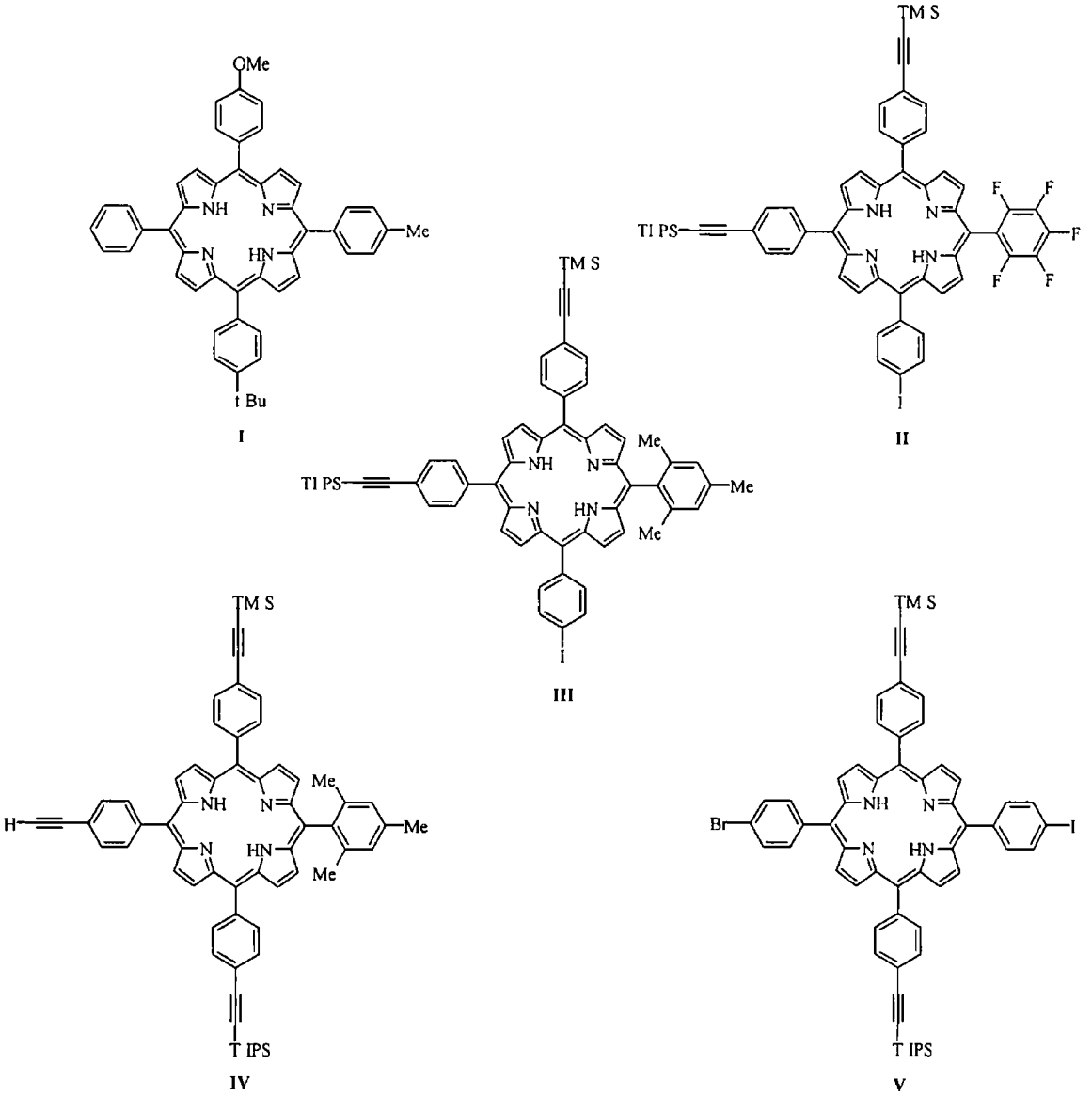

Fig 4 - 10

4 3 Experimental

4 3 1 Reagents

Pyrrole was purchased from the Aldrich Chemical Company and was freshly distilled over potassium hydroxide before use Aldrich Chemical Company supplied all solvents Pentane was of HPLC grade and used without any further purification Dichloromethane was dried over $MgSO_4$ prior to use Benzaldehyde, zinc(II) acetate, nickel(II) acetate, 2-thiophenecarboxaldehyde, 5-bromo-2-thiophenecarboxaldehyde, ferrocenecarboxaldehyde, dimethylamine, diisopropylamine, trimethylamine, *n*-butyl lithium, trimethylsilylacetylene, silver tetrafluoroborate, tetrakis(triphenylphosphine)palladium(0), potassium carbonate and ammonium fluoride (0 1 M in tetrahydrofuran) were all purchased from the Aldrich Chemical Company and used without further purification Silica gel (Merck) was used as received All mobile phases were dried over $MgSO_4$ prior to use

4 3 2 Equipment

All infra red spectra were obtained on a Perkin-Elmer 2000 FTIR spectrometer in a 0 1 mm sodium chloride liquid solution cell using spectroscopic grade dichloromethane as the solvent ^{1}H and ^{13}C NMR spectra were recorded on a Bruker model AC 400 MHz spectrometer in the appropriate deuterated solvent at room temperature with external TMS as a standard All UV spectra were measured in spectroscopic grade solvents on a Hewlett Packard 8452A-photodiode array spectrometer using a 1cm quartz cell

4 3 3 Synthesis [62]

4 3 3 1 5-(trimethylsilylethynyl)-2-thiophenecarboxaldehyde

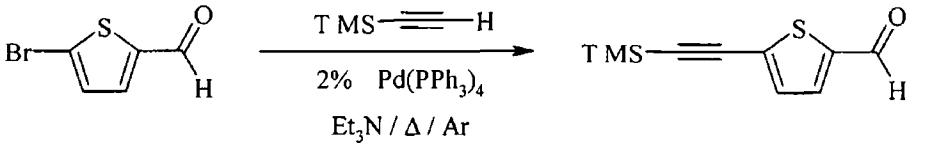

Rxn 4 – 15

5-(Trimethylsilylethynyl)-2-thiophenecarboxaldehyde was prepared *via* the Sonogashira coupling reaction [63] 5-bromo-2-thiophenecarboxaldehyde (25 mmol/2 97 ml) was dissolved in 25 ml Et_3N and purged with argon for 10 minutes A 2 % equivalent of tetrakis(triphenylphosphine)palladium(0) was then added (0 50 mmol/575 mg) followed by an excess of trimethylsilylacetylene (35 mmol/4 95 ml) in quick succession [Note the reaction vessel must be sealed effectively and the Ar pressure sufficiently lowered due to the high volatility of trimethylsilylacetylene (b p 53 ^{0}C)] The reaction mixture was refluxed for 12 hours and then allowed to cool The Et_3N and excess trimethylsilylacetylene were removed under reduced pressure The crude product was extracted from the remaining brown oil by first dissolving in *ca* 5 ml of dichloromethane followed by addition of *ca* 30 ml of petroleum ether (40 - 60) The solvent was then decanted off This process was repeated several times until the washings remained colourless The washings were combined and the solvent was removed under reduced pressure *via* rotary evaporator affording a dark brown oil The product was then purified by careful Kugelrohr distillation (110 ^{0}C/0 04 mmHg) affording a 5 g of a pale yellow solid (24 mmol/96 %) Spectroscopic data were in good agreement with the reported data [64]

^{1}H NMR ($CDCl_3$) δ 9 85 (1H, s), 7 63 (1H, d, ^3J = 3 6 Hz), 7 26 (1H, d, ^3J = 3 6 Hz), 0 27 (9H, s) ppm

^{13}C NMR ($CDCl_3$) δ 182 85, 144 20, 136 36, 133 52, 105 06, 96 77, -0 41 ppm

IR (pentane) ν(CO) 1671 cm $^{-1}$, ν(C≡C) 2149 cm $^{-1}$

4 3 3 2 5-ethynyl-2-thiophenecarboxaldehyde

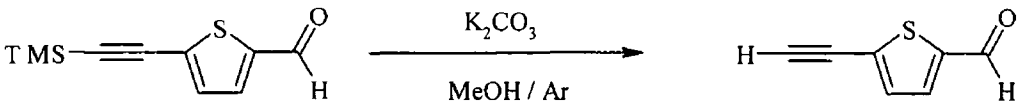

Rxn 4 – 16

5-(trimethylsilylethynyl)-2-thiophenecarboxaldehyde was deprotected yielding 5-ethynyl-2-thiophenecarboxaldehyde by adapting a known procedure [65] Anhydrous K_2CO_3 (1 mmol/0 138 g) was added to a solution of 5-(trimethylsilylethynyl)-2-thiophenecarboxaldehyde (10 mmol/2 08 g) in 15 ml of methanol The mixture was allowed to stir for 3 hours at room temperature under an atmosphere of argon and the solvent was then removed under reduced pressure The crude material was dissolved in 50 ml of CH_2Cl_2 and washed with 2 x 50 ml aliquots of a 5 % $NaHCO_3$ solution The organic phase was dried over $MgSO_4$ Removal of the solvent afforded 1 01 g of a light yellow oil (7 30 mmol/73 %) Spectroscopic data were in good agreement with reported data [64]

^{1}H NMR ($CDCl_3$) δ 9 87 (1H, s), 7 64 (1H, d, ^3J = 3 6 Hz), 7 32 (1H, d, ^3J = 3 6 Hz), 3 58 (1H, s) ppm

^{13}C NMR ($CDCl_3$) δ 182 46, 144 24, 135 66, 133 67, 131 20, 85 87, 76 04 ppm

IR (pentane) ν(CO) 1671 cm $^{-1}$, ν(C≡C) 2108 cm $^{-1}$

4.3 3 3 dipyrromethane

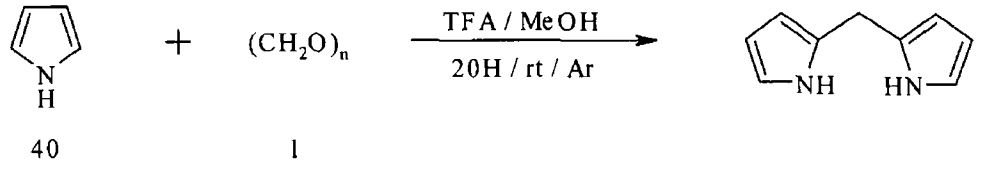

40 1

Rxn 4 – 17

Dipyrromethane was prepared *via* a one-step synthetic route similar to the method used by Bruce and Wang [56] Pyrrole (144 mmol / 10 ml) and paraformaldehyde (108 mg/3 6 mmol) were treated with trifluoroacetic acid (3 6 mmol/96 μl) under an atmosphere of argon and allowed to stir for 20 hours The reaction mixture was then diluted with 50 cm^3 CH_2Cl_2, washed with water (2 x 30 cm^3), aqueous KOH (0 1 mol dm^3, 2 x 30 cm^3) and then water (2 x 30 cm^3) The organic phase was then dried over $MgSO_4$ and the solvent removed under reduced pressure affording a dark brown oil Unreacted pyrrole was removed by vacuum distillation taking care not to heat the crude mixture too much The dark residue was passed through a silica gel column (CH_2Cl_2 Et_3N/99 1) affording 178 mg of a colourless to light-brown product (1 21 mmol/33 61 %) Analytical data were in good agreement with the reported data [56]

^{1}H NMR ($CDCl_3$) δ 7 82 (2H, s), 6 64 (2H, m), 6 05 (4H, m), 3 96 (2H, s) ppm

4 3 3 4 *meso*-phenyldipyrromethane

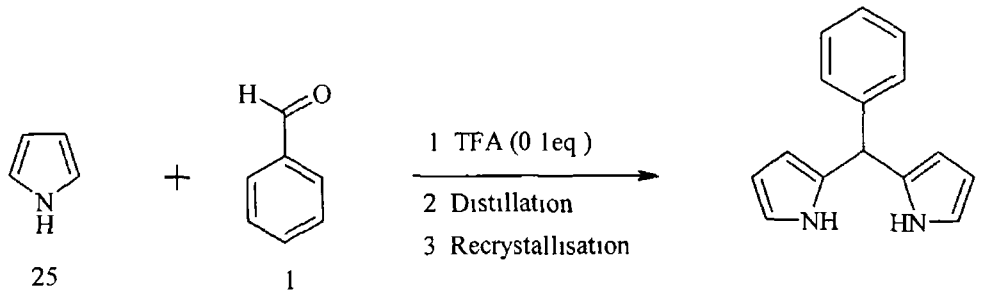

25 1

Rxn 4 – 18

meso-Phenyldipyrromethane was prepared *via* a one-step synthetic route as reported by Lindsey et al [57] Pyrrole (250 mmol/17 40 ml) and benzaldehyde (1 ml/5 mmol) were added to a dry round bottomed flask and purged with argon for 5 minutes Trifluoroacetic acid (0 50 mmol/13 33 μl) was added and the solution was allowed stir for 5 minutes after which time the reaction was quenched with 50 ml 0 1 M NaOH and extracted into 50 ml ethyl acetate The organic phase was washed with water and dried over $MgSO_4$ The solvent and excess pyrrole was removed under reduced pressure resulting in a brown oil The pure product was isolated after chromatography on a silica gel column (CH_2Cl_2 Et_3N/99 1) affording 307 mg of a colourless solid (1 38 mmol/27 63 %) Analytical data were in good agreement with the reported data [57]

^{1}H NMR ($CDCl_3$) δ 7 87 (2H, s), 7 10 – 7 24 (5H, m), 6 63 (2H, m), 6 08 (2H, m), 5 85 (2H, m), 5 42 (1H, s) ppm

4 3 3 5 5,10,15,20-tetraphenylporphyrin (H_2TPP)

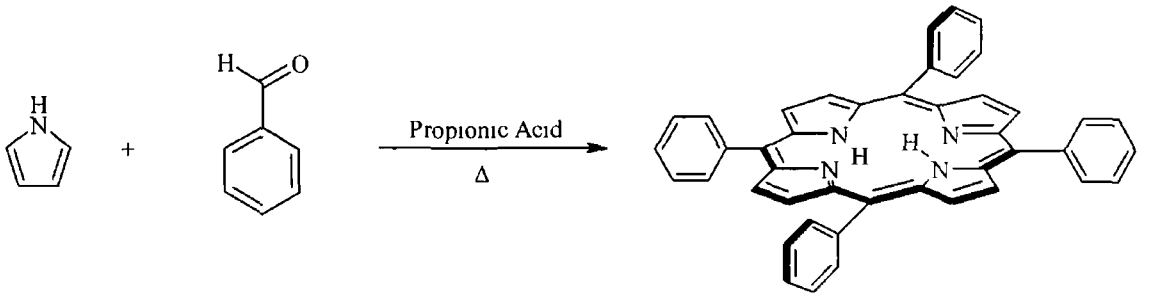

Rxn 4 - 19

H_2TPP was prepared following the synthetic procedure developed by Adler et al [8] Benzaldehyde (0 03 mol/3 05 ml) and pyrrole (0 03 mol/2 08 ml) were added to 100 ml of propionic acid The reaction mixture was brought to reflux temperature for 90 minutes and then allowed to cool, and left overnight The porphyrin was filtered off and repeatedly washed with cold methanol leaving 920 mg of a purple powder (1 73 mmol, 23 % yield) Analytical data were in good agreement with the reported data [8]

^1H NMR ($CDCl_3$) δ 8 77 (8H, s), 8 15 (8H, m), 7 70 – 7 67 (12H, m), -2 86 (2H, s) ppm

^{13}C NMR ($CDCl_3$) δ 142 11, 134 52, 127 67, 126 65, 120 09 ppm

4 3 3 6 5,10,15,20-tetra(thien-2'-yl)porphyrin (H_2TThP)

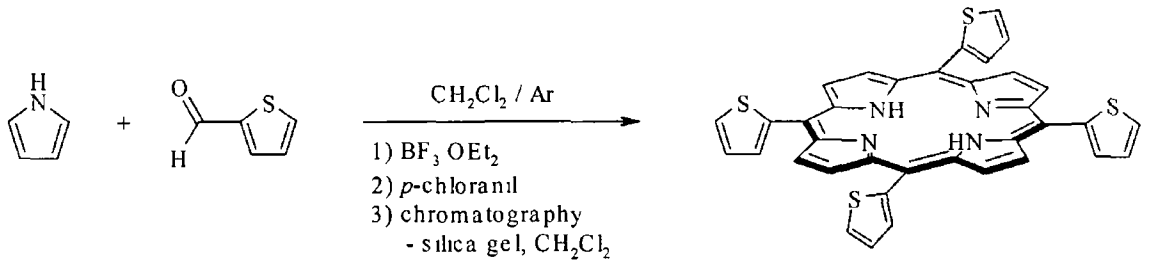

Rxn 4 - 20

H_2TThP[66] was readily prepared *via* a modified version of Lyndsey's two-step one-flask room temperature reaction for the synthesis of *meso*-substituted porphyrins [12] 5 mmol (0 35 ml) pyrrole and 5 mmol (0 47 ml) of 2-thiophenecarboxaldehyde were dissolved in 200 ml CH_2Cl_2 and the solution was purged with argon for 10 minutes The reaction mixture was then cooled to 0 ^{0}C, treated with 0 50 mmol (63 36 μl) BF_3 OEt_2 and allowed to stir overnight (10 - 12 hours) at room temperature 3 75 mmol (922 mg) of *p*-chloranil was added to the solution and stirring was continued for a further 6 hours [note as *p*-chloranil is an oxidising agent the solution no longer needs to be kept under argon at this point] The volume of solvent was then reduced to *ca* 25 ml and the crude mixture was chromatographed over silica using CH_2Cl_2 as the mobile phase yielding 145 mg pure porphyrin (2 3 x 10^4 mol/18 %)

^{1}H NMR ($CDCl_3$) δ 8 97 (8H, s), 7 85 (4H, q, ^3J = 3 2 Hz, ^4J = 1 2 Hz), 7 78 (4H, q, ^3J = 5 2 Hz, ^4J = 1 2 Hz), 7 44 (4H, q, ^3J = 5 2 Hz, ^3J = 3 2 Hz), - 2 72 (2H, s) ppm
^{13}C NMR ($CDCl_3$) δ 146 90, 142 62, 133 89, 127 90, 126 08, 112 38 ppm

4 3 3 7 5,10,15,20-tetra(5'-bromothien-2'-yl) porphyrin (H_2TBrThP)

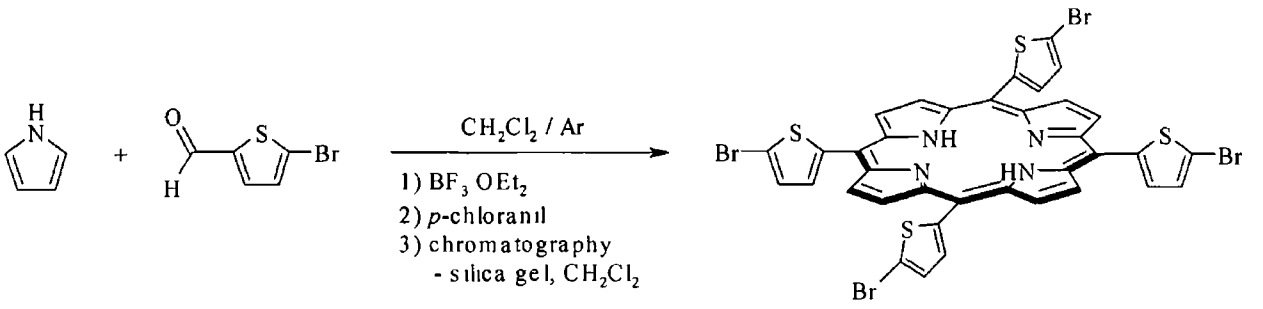

Rxn 4 - 21

H_2TBrThP was prepared following a similar procedure to H_2TThP 5 mmol (0 35 ml) pyrrole and 5 mmol (0 59 ml) of 5-bromo-2-thiophenecarboxaldehyde were dissolved in 200 ml CH_2Cl_2 and the solution was purged with argon for 10 minutes The reaction mixture was then treated with 0 50 mmol (63 36 μl) BF_3OEt_2 at room temperature and allowed to stir overnight (10 - 12 hours) 3 75 mmol (922 mg) of *p*-chloranil was added to the solution and stirring was continued for a further 6 hours The volume of solvent was then reduced to *ca* 25 ml and the crude mixture was chromatographed over silica using CH_2Cl_2 as the mobile phase affording 255 mg pure porphyrin (2 7 x 10^{-4} mol/21 40 %)

^{1}H NMR ($CDCl_3$) δ 9 03 (8H, s), 7 58 (4H, d, ^3J = 3 6 Hz), 7 42 (4H, d, ^3J = 3 6 Hz), -2 85 (2H, s) ppm

^{13}C NMR ($CDCl_3$) δ 143 90, 133 96, 131 40, 129 44, 114 78, 111 61 ppm

FAB MS [M-1] observed 953 Calcd 953 44

4 3 3 8 5,10,15,20-tetra(5'-(trimethylsilylethynyl)thien-2'-yl)porphyrin (H_2TTMSEtThP)

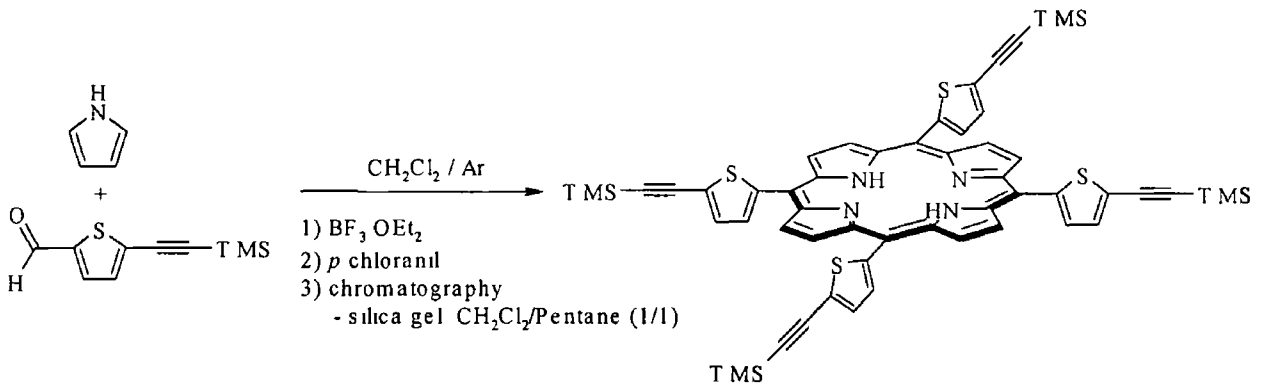

Rxn 4 - 22

H_2TTMSEtThP was prepared in a two-step one-flask reaction following the same procedure as for H_2TThP 5 mmol (0 35 ml) pyrrole and 5 mmol (1 04 g) of 5-trimethylsilylethynyl-2-thiophenecarboxaldehyde were dissolved in 200 ml CH_2Cl_2 and the solution was purged with argon for 10 minutes The reaction mixture was then cooled to *ca* -70 ^{0}C with a liquid nitrogen/acetone slurry, treated with 0 50 mmol (63 36 μl) BF_3 OEt_2 and stirred overnight allowing the reaction mixture to slowly reach room temperature (10 - 12 hours) 3 75 mmol (922 mg) of *p*-chloranil was added to the solution and stirring was continued for a further 6 hours The volume of solvent was subsequently reduced to *ca* 25 ml and the crude mixture was chromatographed over silica using a 1 1 mixture of CH_2Cl_2 pentane as the mobile phase, which afforded 358 mg of pure porphyrin (3 5 x 10 ^{4} mol/28 %)

^{1}H NMR ($CDCl_3$) δ 8 99 (8H, s), 7 67 (4H, d, ^3J = 3 6 Hz), 7 58 (4H, d, ^3J = 3 6 Hz), 0 29 (36H, s), -2 80 (2H, s) ppm

IR (CH_2Cl_2) ν(C≡C) 2145 cm ^{1}

FAB MS [M-1] observed 1023 Calcd 1022 68

4 3 3 9 5,10,15,20-tetra(5'-ethynylthien-2'-yl)porphyrin (H_2TEtThP)

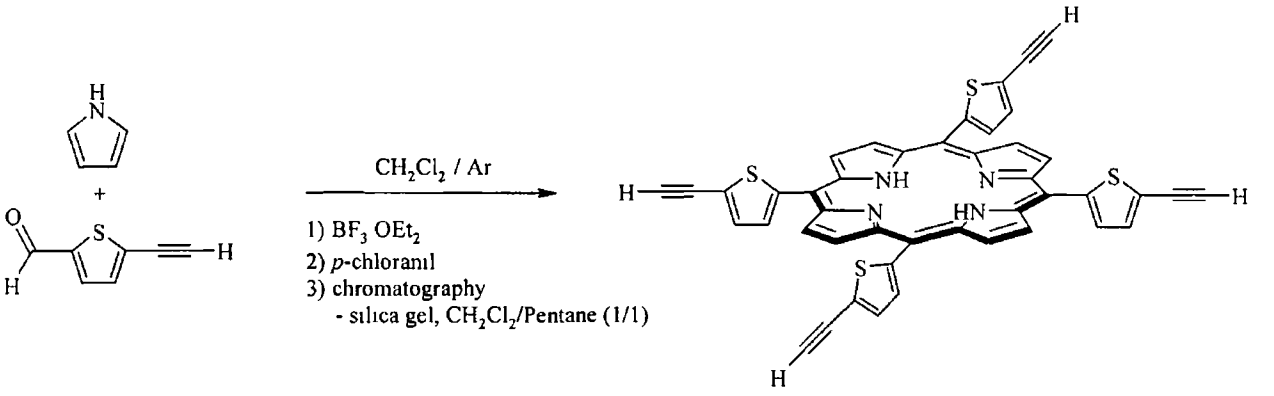

Rxn 4 - 23

H_2TEtThP was prepared in an analogous manner to H_2TTMSEtThP 5 mmol (0 35 ml) pyrrole and 5 mmol (0 69 g) of 5-ethynyl-2-thiophenecarboxaldehyde were dissolved in 200 ml CH_2Cl_2 and the solution was purged with argon for 10 minutes The reaction mixture was then cooled to *ca* -70 ^{0}C with a liquid nitrogen/acetone slurry, treated with 0 50 mmol (63 36 μl) BF_3 OEt_2 and stirred overnight allowing the reaction mixture to slowly reach room temperature (10 - 12 hours) 3 75 mmol (922 mg) of *p*-chloranil was added to the solution and stirring was continued for a further 6 hours The volume of solvent was then reduced to *ca* 25 ml and the crude mixture was chromatographed over silica using a 1 1 mixture of CH_2Cl_2 pentane as the mobile phase affording 165 mg pure porphyrin (2 3 x 10 ^{4} mol/18 %)

^{1}H NMR ($CDCl_3$) δ 9 01 (8H, s), 7 71 (4H, d, ^3J = 3 6 Hz), 7 63 (4H, d, ^3J = 3 6 Hz), 3 52 (4H, s), -2 84 (2H, s) ppm

IR (CH_2Cl_2) ν(C≡C) 2108 cm ^{1}

FAB MS [M-1] observed 734 Calcd 733 95

4 3 3 10 mixed aldehyde synthesis of *meso*-substituted phenyl/5-bromothien-2-yl porphyrins

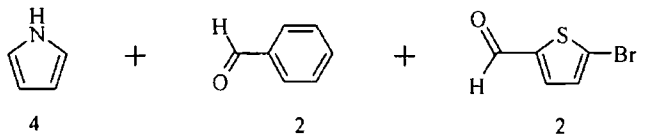

CH_2Cl_2
Ar / r t

1) BF_3 OEt_2
2) *p* chloranil
3) chromatography
silica gel, CH_2Cl_2/Pentane (1/3)

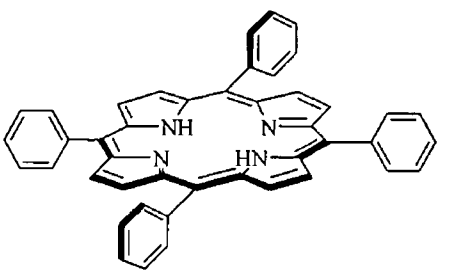

H_2TPP

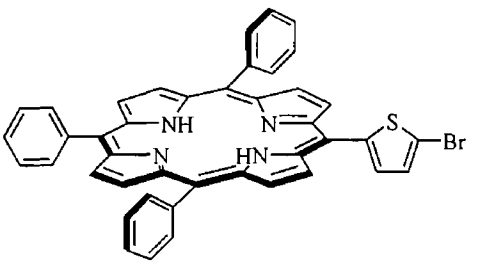

5-(5' bromothien-2' yl)-10 15,20-triphenylporphyrin

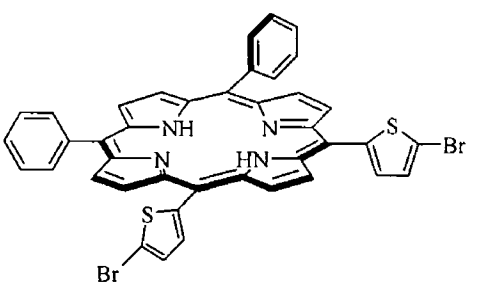

cis 5 10 di(5'-bromothien 2'-yl) 15 20-diphenylporphyrin

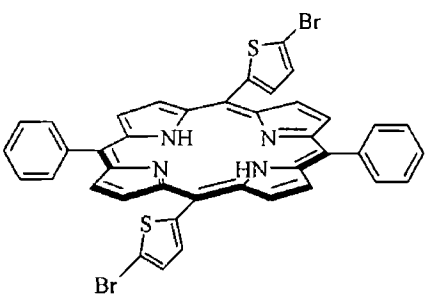

trans 5 15 di(5' bromothien 2'-yl) 10 20-diphenylporphyrin

(*inseparable*)

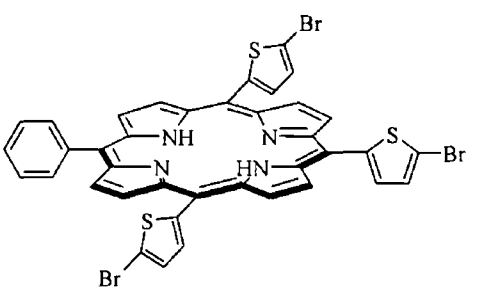

5 10,15-tri(5' bromothien-2'-yl) 20 phenylporphyrin

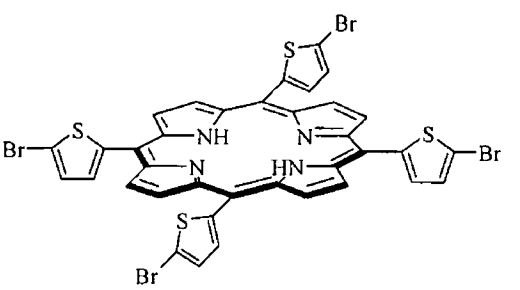

5 10 15,20-tetra(5'-bromothien-2' yl)porphyrin

Rxn 4 - 24

The mixture of six *meso*-substituted phenyl/5-bromothien-2-yl porphyrins were prepared *via* a mixed aldehyde condensation reaction in a two-step one-flask room temperature reaction following the same procedure as for H_2TBrThP 5 mmol (0 35 ml) pyrrole, 2 5 mmol (0 25 ml) benzaldehyde and 2 5 mmol (0 30 ml) of 5-bromo-2-thiophenecarboxaldehyde were added to 200 ml CH_2Cl_2 The solution was purged with argon for 10 minutes, followed by addition of 0 50 mmol (63 36 μl) BF_3 OEt_2 The solution was stirred overnight at room temperature (10 - 12 hours) 3 75 mmol (922 mg) of *p*-chloranil were then added to the solution and stirring was continued for a further 6 hours The volume of solvent was then reduced to *ca* 25 ml and the crude mixture was chromatographed over silica using CH_2Cl_2 as the mobile phase affording a purple powder, which consisted of six porphyrins Careful separation of the fractions by chromatography on a silica gel column (pentane CH_2Cl_2 / 3 1) afforded each porphyrin in high purity apart from both the *cis*- and *trans*- di(5-bromothien-2-yl)diphenylporphyrins which are inseparable The order of elution was tetra-, tri-, *cis*- and *trans*-di- and mono-2-bromothiophene substituted porphyrins respectively followed by H_2TPP Analytical data for H_2TPP and H_2TBrThP were as reported above

4 3 3 10 1 5-(5'-bromothien-2'-yl)-10,15,20-triphenylporphyrin

6 3 x 10^{-5} mol, 44 mg, 5 % yield

^{1}H NMR ($CDCl_3$) δ 8 99 (2H, d, ^3J = 4 8 Hz), 8 77 (2H, d, ^3J = 4 8 Hz), 8 75 (4H, q AB, ^3J = 4 8 Hz), 8 08 - 8 10 (6H, m), 7 63 (9H, m), 7 52 (1H, d, ^3J = 3 6 Hz), 7 32 (1H, d, ^3J = 3 6 Hz), -2 84 (2H, s) ppm

^{13}C NMR ($CDCl_3$) δ 144 78, 141 91, 134 53, 133 58, 129 26, 127 81, 126 73, 121 36, 120 74, 114 14, 109 31 ppm

FAB MS [M-1] observed 700 Calcd 699 67

4 3 3 10 2 5,10-di(5'-bromothien-2'-yl)-15,20-diphenylporphyrin and 5,15-di(5'-bromothien-2'-yl)-10,20-diphenylporphyrin

1 x 10^{-4} mol, 78 mg, 8 % yield

^{1}H NMR ($CDCl_3$) δ 9 00 - 9 05 (4H, m), 8 74 – 8 79 (4H, m), 8 13 (4H, m), 7 67 – 7 73 (6H, m), 7 58 (2H, d, ^3J = 3 6 Hz), 7 40 (2H, dd, ^3J = 3 6 Hz), -2 82 (2H, m) ppm

^{13}C NMR ($CDCl_3$) 144 76, 142 33, 135 02, 134 27, 129 49, 128 14, 127 04, 123 12, 122 49, 113 33, 110 50 δ ppm

FAB MS [M-1] observed 784 Calcd 783 60

4 3 3 10 3 5,10,15-tri(5'-bromothien-2'-yl)-20-phenylporphyrin

7 55 x 10^{-5} mol, 65 mg, 6 % yield

^{1}H NMR ($CDCl_3$) δ 9 04 (4H, q AB, ^3J = 4 8 Hz), 9 01 (2H, d, ^3J = 4 8 Hz), 8 77 (2H, d, ^3J = 4 8 Hz), 8 13 (2H, m), 7 66 - 7 75 (3H, m), 7 57 (3H, d, ^3J = 3 6 Hz), 7 40 (3H, dd, ^3J = 3 6 Hz), -2 83 (2H, s) ppm

^{13}C NMR ($CDCl_3$) 144 20, 134 50, 133 84, 129 39, 128 06, 126 84, 122 35, 114 57, 111 15 δ ppm

FAB MS [M-1] observed 869 Calcd 868 52

(H_2TPP and H_2TBrThP were isolated in 2 and 1 % respectively from the crude mixture)

4 3 3 11 5-ferrocenyl-10,15,20-triphenylporphyrin (H_2FcTPP)

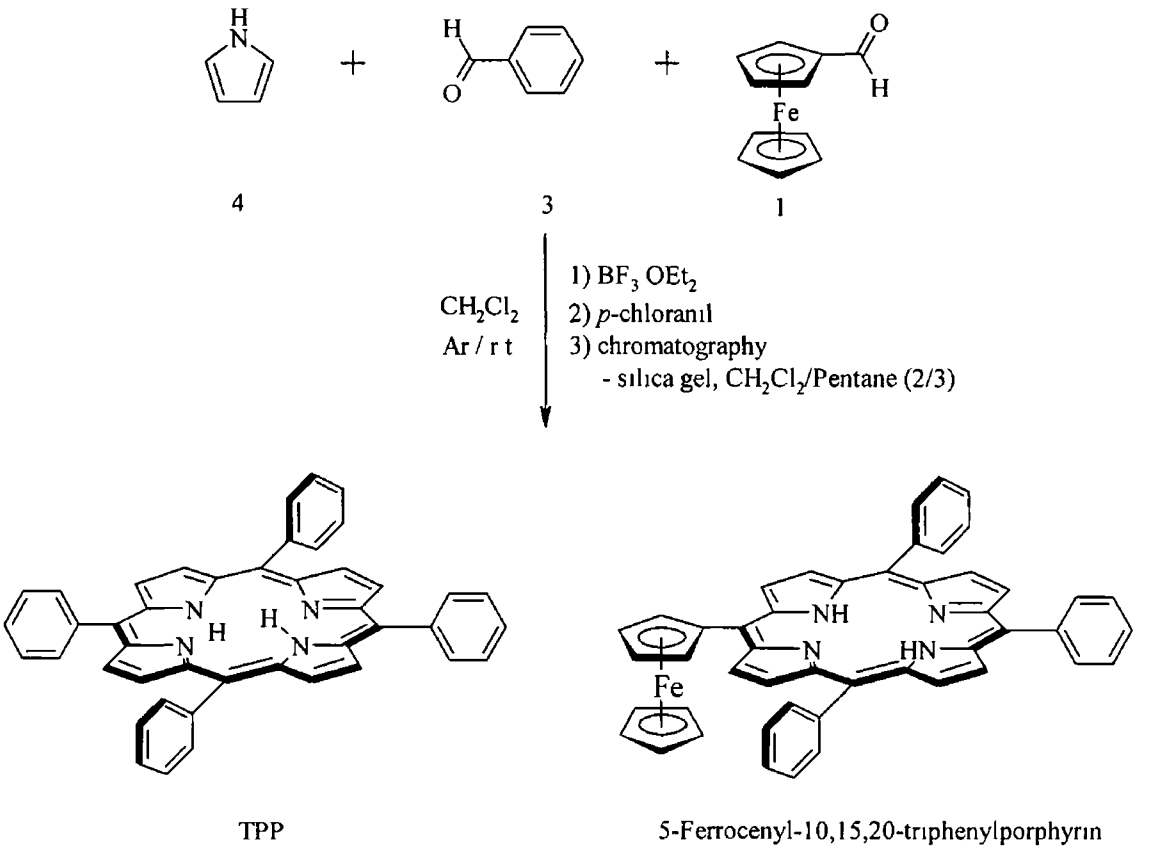

Rxn 4 - 25

H_2FcTPP was prepared *via* a mixed aldehyde condensation reaction in a two-step one-flask room temperature reaction 5 mmol (0 35 ml) pyrrole, 3 75 mmol (0 38 ml) of benzaldehyde and 1 25 mmol (268 mg) were added to 200 ml CH_2Cl_2 The solution was purged with argon for 10 minutes, followed by addition of 0 50 mmol (63 36 μl) BF_3 OEt_2 The solution was allowed to stir overnight at room temperature (10 - 12 hours) 3 75 mmol (922 mg) of *p*-chloranil was added to the solution and stirring was continued for a further 6 hours The volume of solvent was then reduced to ca 25 ml and the crude mixture was chromatographed over silica using CH_2Cl_2 as the mobile phase affording a purple powder consisting of a mixture of porphyrins

Careful separation by chromatography on a silica gel column (pentane CH_2Cl_2 / 3 2) afforded H_2TPP followed by H_2FcTPP in high purity (1 01 x 10^{-4} mol, 73 mg, 8 09 %) Analytical data for H_2TPP was identical with that of reported data

^1H NMR ($CDCl_3$) δ 9 88 (2H, d, J = 4 4 Hz), 8 64 – 8 69 (6H, m), 8 08 – 8 12 (6H, m), 7 60 – 7 69 (9H, m), 5 42 (2H, dd), 4 68 (2H, dd), 4 04 (5H, s), -2 37 (2H, s) ppm
^{13}C NMR ($CDCl_3$) δ 142 45, 134 50, 127 66, 126 77, 126 62, 120 15, 89 53, 77 46, 70 61, 69 02 ppm
FAB MS [M-1] observed 722 Calcd 721 68

4 3 3 12 5-ferrocenyl-10,15,20-tri(thien-2'-yl)porphyrin (H_2FcTThP)

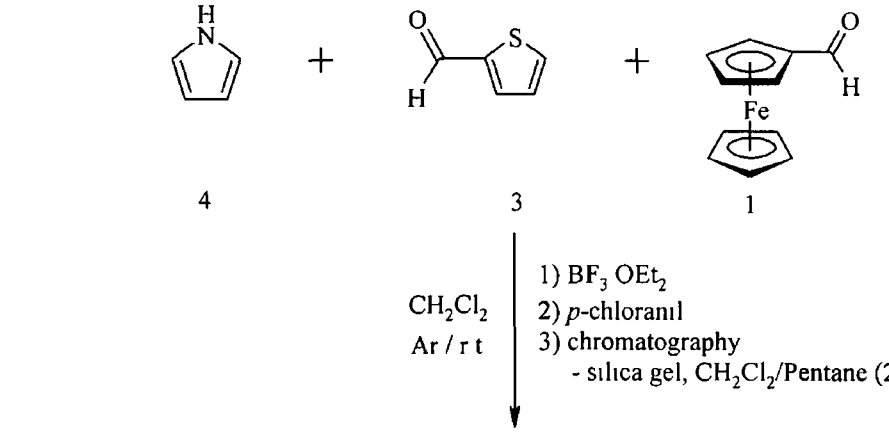

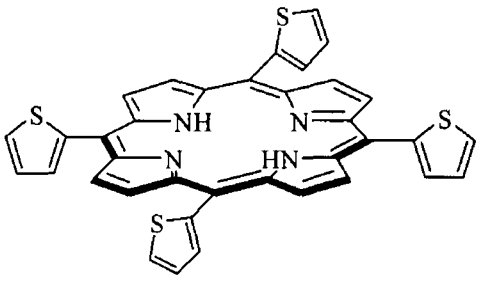

TThP

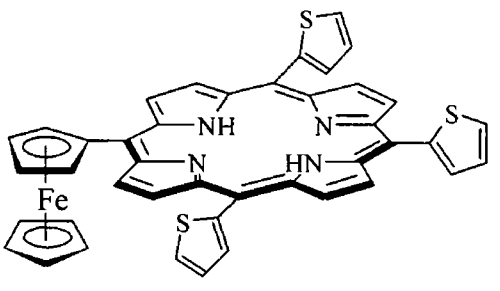

5-Ferrocenyl-10,15,20-tri(thien-2'-yl)porphyrin

+ inseparable mixture

Rxn 4 - 26

H_2FcTThP was prepared *via* a mixed aldehyde condensation reaction in a two-step one-flask room temperature reaction in a similar manner to H_2FcTPP 5 mmol (0 35 ml) pyrrole, 3 75 mmol (0 35 ml) of 2-thiophenecarboxaldhyde and 1 25 mmol (268 mg) were added to 200 ml CH_2Cl_2 The solution was purged with argon for 10 minutes, and then treated with 0 50 mmol (63 36 µl) BF_3 OEt_2 The mixture was stir red overnight at room temperature (10 - 12 hours) 3 75 mmol (922 mg) of *p*-chloranil was added to the solution and stirring was continued for a further 6 hours The volume of solvent was then reduced to *ca* 25 ml and the crude mixture was chromatographed over silica using CH_2Cl_2 as the mobile phase affording a purple powder, which consisted of a mixture of porphyrins

Careful separation by chromatography on a silica gel column (pentane CH_2Cl_2/9 1) afforded H_2TThP followed by H_2FcTThP in high purity (8 9 x 10^{-5} mol, 66 mg, 7 12 %) No other porphyrins could be isolated from the crude mixture

^{1}H NMR ($CDCl_3$) δ 9 84 (2H, d, ^3J = 4 0 Hz), 8 86 (6H, m), 7 81 – 7 70 (6H, m), 7 38 – 7 34 (3H, m), 5 41 (2H, dd), 4 68 (2H, dd), 4 02 (5H, s), -2 26 (2H, s) ppm
^{13}C NMR ($CDCl_3$) δ 143 19, 142 47, 133 80, 133 57, 128 78, 127 89, 127 75, 126 20, 125 99, 120 13, 112 04, 111 16, 89 14, 77 61, 70 67, 69 24 ppm
FAB MS [M-1] observed 741 Calcd 740 75

4 3 3 13 General procedure for metallation of porphyrins

The appropriate porphyrin was dissolved in *ca* 20 ml CH_2Cl_2 and the solution was purged with argon for 10 minutes 1 5 equivalents of $M(OAc)_2$ (M = Zn, Ni) was first dissolved in 5 ml MeOH and then added to the porphyrin solution The reaction mixture was allowed to stir for *ca* 10 hours All solvents were removed under reduced pressure leaving a purple solid This solid was dissolved in CH_2Cl_2 and washed successively with 5 % aqueous $NaHCO_3$, followed by water The organic layer was dried over $MgSO_4$ and the solvent removed under reduced pressure The metalloporphyrins were usually obtained in > 95 % yield (unless otherwise stated) following column chromatography (silica, neat CH_2Cl_2)

4 3 3 13 1 zinc(II)-5,10,15,20-tetraphenylporphyrin (ZnTPP)

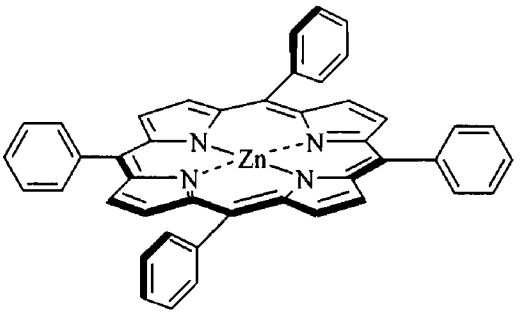

Fig 4 – 11

Analytical data were in good agreement with the reported data [67]

^{1}H NMR ($CDCl_3$) δ 8 87 (8H, s), 8 16 (8H, m), 7 72 –7 64 (12H, m) ppm

^{13}C NMR ($CDCl_3$) δ 150 16, 142 77, 134 39, 131 95, 127 45, 126 51, 121 09 ppm

4 3 3 13 2 nickel(II)-5,10,15,20-tetraphenylporphyrin (NiTPP)

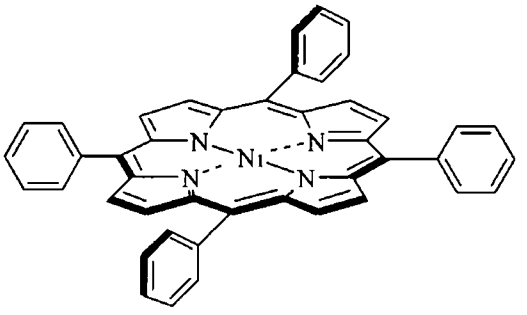

Fig 4 – 12

Analytical data for NiTPP were in good agreement with the reported data [69]

^{1}H NMR ($CDCl_3$) δ 8 67 (8H, s), 7 95 (8H, m), 7 62 (12H, m) ppm

4 3 3 13 3 zinc(II)-5,10,15,20-tetra(thien-2'-yl)porphyrin (ZnTThP)

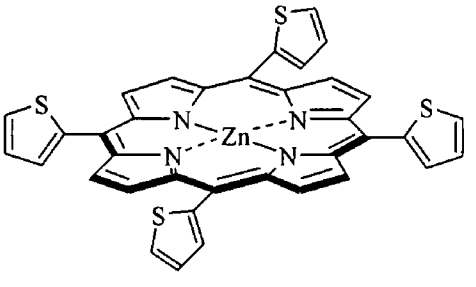

Fig 4 – 13

Analytical data for ZnTThP were in good agreement with the reported data [68]

^{1}H NMR ($CDCl_3$) δ 9 07 (8H, s), 7 84 (4H, dd, ^3J = 3 6 Hz, ^4J = 1 2 Hz), 7 77 (4H, dd, ^3J = 3 6 Hz, ^3J = 5 2 Hz), 7 44 (4H, dd, ^3J = 3 6 Hz, ^4J = 1 2 Hz) ppm

^{13}C NMR ($CDCl_3$) δ 151 34, 143 00, 133 53, 132 15, 127 45, 125 94, 115 93, 113 17 ppm

4 3 3 13 4 zinc(II)-5,10,15,20-tetra(5'-bromothien-2'-yl)porphyrin (ZnTBrThP)

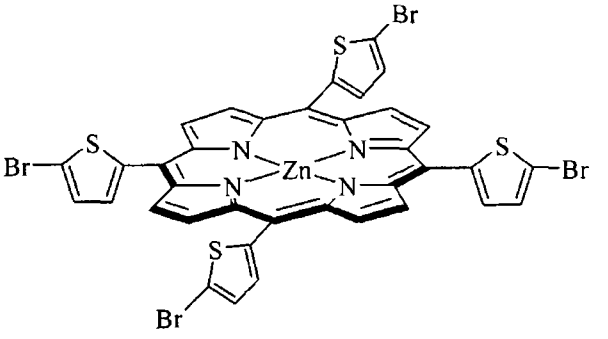

Fig 4 – 14

^{1}H NMR ($CDCl_3$) δ 9 12 (8H, s), 7 56 (4H, d, J = 3 6 Hz), 7 41 (4H, d, J = 3 6 Hz) ppm

^{13}C NMR ($CDCl_3$) δ 151 23, 144 70, 133 59, 132 27, 132 13, 129 28, 114 19, 112 41 ppm

MALDI MS [M+1] observed 1018 8 Calcd 1018 79

4 3 3 13 5 zinc(II)-5-(5'-bromothien-2'-yl)-10,15,20-triphenylporphyrin

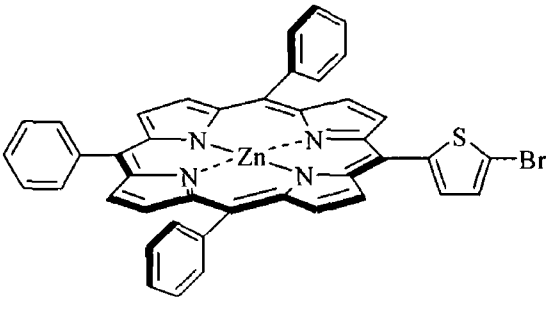

Fig 4 – 15

^{1}H NMR ($CDCl_3$) δ 9 11 (2H, d, J = 4 8 Hz), 8 88 (2H, d, ^{3}J = 4 8 Hz), 8 85 (4H, q AB, ^{3}J = 4 8 Hz), 8 13 (6H, m), 7 68 (9H, m), 7 56 (1H, d, ^{3}J = 3 6 Hz), 7 38 (1H, d, ^{3}J = 3 6 Hz) ppm

^{13}C NMR ($CDCl_3$) δ 150 96, 150 51, 150 27, 150 04, 145 52, 142 57, 134 40, 133 24, 132 53, 132 26, 131 98, 131 41, 130 87, 129 12, 127 58, 126 58, 122 26, 121 65, 113 64, 110 19 ppm

MALDI MS [M+1] observed 763 0 Calcd 763 03

4 3 3 13 6 zinc(II)-5,10-di(5'-bromothien-2'-yl)-15,20-diphenylporphyrin & zinc(II)-5,15-di(5'-bromothien-2'-yl)-10,20-diphenylporphyrin

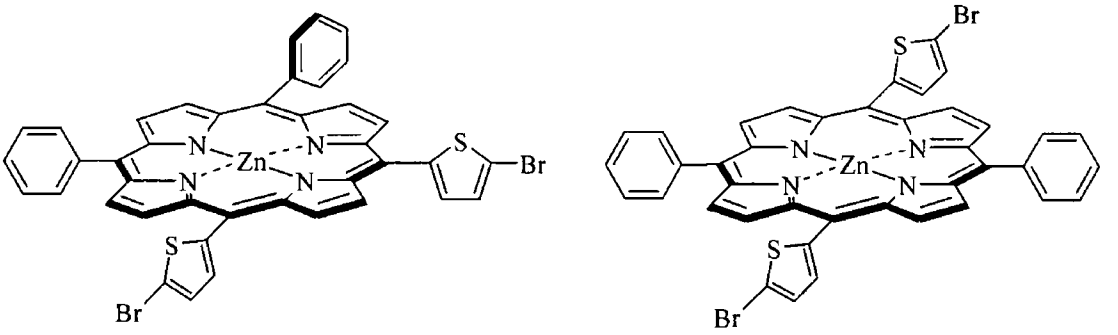

Fig 4 – 16

^{1}H NMR ($CDCl_3$) δ 9 08 – 9 13 (4H, m), 8 83 – 8 87 (4H, m), 8 11 (4H, m), 7 66 – 7 69 (6H, m), 7 55 (2H, d, ^3J = 3 6 Hz), 7 37 (2H, dd, ^3J = 3 6 Hz) ppm

^{13}C NMR ($CDCl_3$) δ 151 21, 151 09, 150 87, 150 68, 150 44, 150 24, 144 89, 142 11, 134 91, 134 13, 132 82, 132 63, 132 36, 132 07, 131 83, 131 59, 129 75, 128 36, 127 19, 123 05, 122 56, 113 58, 110 63 ppm

MALDI MS [M+1] observed 848 0 Calcd 847 95

4 3 3 13 7 zinc(II)-5,10,15-tri(5'-bromothien-2'-yl)-20-phenylporphyrin

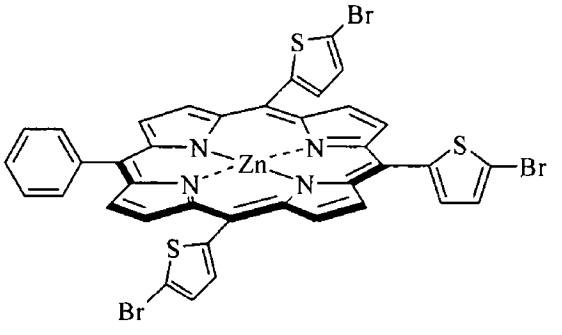

Fig 4 – 17

^{1}H NMR ($CDCl_3$) δ 9 11 (4H, q AB, ^3J = 4 8 Hz), 9 09 (2H, d, ^3J = 4 8 Hz), 8 86 (2H, d, ^3J = 4 8 Hz), 8 10 (2H, m), 7 64 – 7 72 (3H, m), 7 55 (3H, d, ^3J = 3 6 Hz), 7 37 (3H, dd, ^3J = 3 6 Hz) ppm

^{13}C NMR ($CDCl_3$) 151 22, 150 74, 150 49, 150 23, 144 20, 134 50, 133 84, 129 39, 126 84, 122 35, 114 57, 111 15, δ ppm

FAB MS [M-1] observed 932 Calcd 931 88

4 3 3 13 8 zınc(II)-5-ferrocenyl-10,15,20-trıphenylporphyrın (ZnFcTPP)

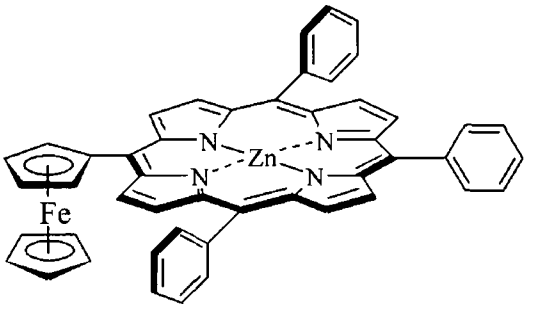

Fıg 4 – 18

^{1}H NMR ($CDCl_3$) δ 9 98 (2H, d, ^{3}J = 4 0 Hz), 8 73 (6H, m), 8 07 (6H, m), 7 57 (9H, m), 5 26 (2H, dd), 4 51 (2H, dd), 3 90 (5H, s) ppm

^{13}C NMR ($CDCl_3$) δ 151 06, 150 18, 149 91, 149 32, 142 93, 142 76, 134 42, 132 47, 131 79, 130 98, 127 42, 126 52, 121 13, 120 82, 118 74, 90 66, 77 61, 70 48, 68 53 ppm

FAB MS [M-1] observed 785 Calcd 785 03

4 3 3 13 9 nıckel(II)-5-ferrocenyl-10,15,20-trıphenylporphyrın (NıFcTPP)

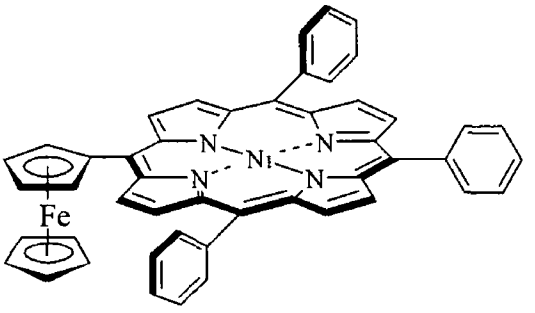

Fıg 4 – 19

^{1}H NMR ($CDCl_3$) δ 9 58 (2H, d, ^{3}J = 4 8 Hz), 8 62 (2H, d, ^{3}J = 4 8 Hz), 8 59 (4H, q AB, ^{3}J = 4 8 Hz), 7 90 (6H, m), 7 61 (9H, m), 5 07 (2H, dd), 4 63 (2H, dd), 3 90 (5H, s) ppm

FAB MS [M-1] observed 778 Calcd 778 37

4 3 3 13 10 zınc(II)-5-ferrocenyl-10,15,20-trı(thıen-2'-yl)porphyrın (ZnFcTThP)

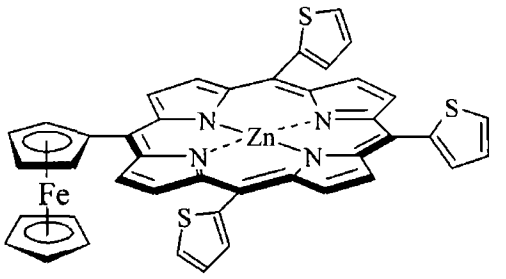

Fıg 4 – 20

^{1}H NMR ($CDCl_3$) δ 10 06 (2H, d, ^{3}J = 4 8 Hz), 8 97 (6H, m), 7 70 – 7 80 (6H, m), 7 39 (3H, m), 5 40 (2H, dd), 4 69 (2H, dd), 4 07 (5H, s) ppm

^{13}C NMR ($CDCl_3$) δ 151 34, 151 15, 149 55, 149 23, 143 48, 143 26, 133 44, 132 72, 131 95, 131 77, 130 81, 129 82, 127 57, 127 33, 125 87, 113 09, 91 62, 77 22, 70 11, 69 77 ppm

FAB MS [M-1] observed 804 Calcd 803 91

4 3 3 14 General procedure for Sonogashira coupling of 5-bromothien-2-yl porphyrins

The appropriate porphyrin was first dissolved in 10 ml of amine and the solution was purged with argon for 10 minutes Me_2NH was used for the synthesis of zinc(II)-5-(5'-(trimethylsilylethynyl)thien-2'-yl)-10,15,20-triphenylporphyrin and for the *cis*- and *trans*-, i e zinc(II)-5,10-di(5'-(trimethylsilylethynyl)thien-2'-yl)-15,20-diphenylporphyrin and zinc(II)-5,15-di(5'-(trimethylsilylethynyl)thien-2'-yl)-10,20-diphenylporphyrin, mixture *i*-Pr_2NH was used for the synthesis of zinc(II)-5,10,15-tri(5'-(trimethylsilylethynyl)thien-2'-yl)-20-phenylporphyrin and zinc(II)-5,10,15,20-tetra(5'-(trimethylsilylethynyl)thien-2'-yl)porphyrin A 2 % equivalent of tetrakis(triphenylphosphine)palladium(0) was then added followed by an excess of trimethylsilylacetylene in quick succession The reaction mixture was allowed to reflux for 1 hour and subsequently allowed to cool The solvent and excess trimethylsilylacetylene were removed under reduced pressure The crude product was then chromatographed over silica affording pure porphyrin in > 95 % yield

4 3 3 14 1 zinc(II)-5-(5'-(trimethylsilylethynyl)thien-2'-yl)-10,15,20-triphenylporphyrin (ZnTMSEtThTPP)

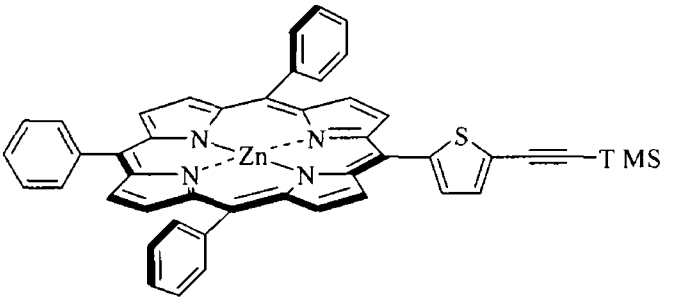

Fig 4 – 21

^{1}H NMR ($CDCl_3$) δ 9 09 (2H, d, ^{3}J = 4 8 Hz), 8 88 (2H, d, ^{3}J = 4 8 Hz), 8 85 (4H, q AB, ^{3}J = 4 8 Hz), 8 14 (6H, m), 7 72 – 7 63 (10H, m), 7 57 (1H, d, ^{3}J = 3 6 Hz), 0 28 (9H, s) ppm

^{13}C NMR ($CDCl_3$) δ 150 95, 150 52, 150 28, 150 09, 145 76, 142 58, 134 41, 133 17, 132 55, 132 28, 132 02, 131 88, 131 52, 127 59, 126 60, 125 05, 122 22, 121 67, 110 38, 99 79, 97 70, 1 08 ppm

IR (CH_2Cl_2) ν(C≡C) 2145 cm ^{1}

MALDI MS [M+1] observed 779 1 Calcd 779 34

4 3 3 14 2

zinc(II)-5,10-di(5'-(trimethylsilylethynyl)thien-2'-yl)-15,20-diphenylporphyrin & zinc(II)-5,15-di(5'-(trimethylsilylethynyl)thien-2'-yl)-10,20-diphenylporphyrin (ZnDTMSEtThDPP)

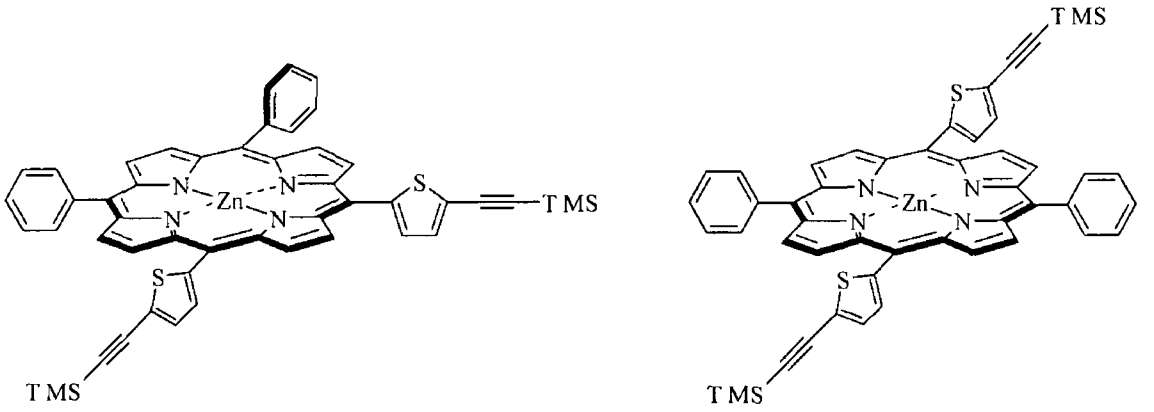

Fig 4 – 22

^{1}H NMR ($CDCl_3$) δ 9 03 – 9 06 (4H, m), 8 77 – 8 82 (4H, m), 8 05 (4H, m), 7 57 – 7 62 (8H, m), 7 51 (2H, dd, ^3J = 3 6 Hz), 0 24 (18H, m) ppm

^{13}C NMR ($CDCl_3$) δ 151 17, 151 02, 150 78, 150 58, 150 39, 150 17, 145 45, 142 35, 134 40, 133 26, 132 78, 132 55, 132 29, 132 04, 131 89, 131 78, 131 53, 127 70, 126 65, 125 23, 122 67, 122 11, 111 48, 110 96, 99 94, 97 63, 1 11 ppm

IR (CH_2Cl_2) ν(C≡C) 2145 cm^{-1}

FAB MS [M-1] observed 882 Calcd 882 57

4 3 3 14 3

zınc(II)-5,10,15-trı(5'-(trımethylsılylethynyl)thıen-2'-yl)- 20-phenylporphyrın (ZnTTMSEtThPP)

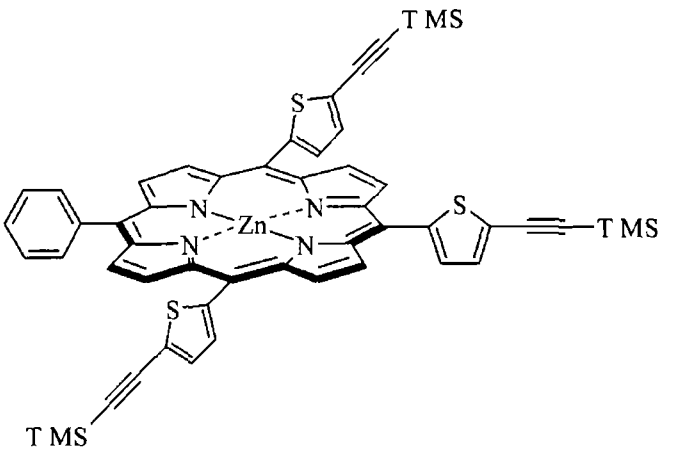

Fıg 4 – 23

^{1}H NMR ($CDCl_3$) δ 9 08 (4H, q AB, ^{3}J = 4 4 Hz), 9 04 (2H, d, ^{3}J = 4 4 Hz), 8 83 (2H, d, ^{3}J = 4 8 Hz), 8 11 (2H, m), 7 71 – 7 65 (6H, m), 7 56 (3H, dd, ^{3}J = 3 6 Hz), 0 28 (27H, m) ppm

^{13}C NMR ($CDCl_3$) δ 151 27, 151 14, 151 01, 150 84, 150 49, 145 75, 142 20, 134 33, 133 32, 132 78, 132 21, 131 85, 131 76, 127 79, 126 65, 125 34, 123 08, 111 99, 100 06, 97 59, 1 10 ppm

IR (CH_2Cl_2) ν(C≡C) 2145 cm ^{1}

FAB MS [M-1] observed 984 Calcd 983 81

4 3 3 14 4

zinc(II)-5,10,15,20-tetra(5'-(trimethylsilylethynyl)thien-2'-yl)porphyrin (ZnTTMSEtThP)

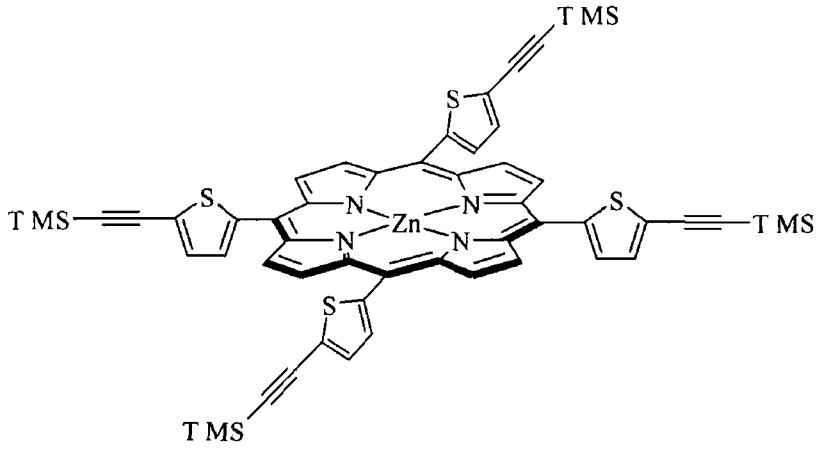

Fig 4 – 24

^{1}H NMR ($CDCl_3$) δ 9 08 (8H, s), 7 64 (4H, d, ^{3}J = 3 6 Hz), 7 56 (4H, d, ^{3}J = 3 6 Hz), 0 34 (36H, s) ppm

^{13}C NMR ($CDCl_3$) δ 151 29, 145 00, 133 52, 132 38, 131 94, 125 64, 112 54, 100 18, 97 53, 1 09 ppm

IR (CH_2Cl_2) ν(C≡C) 2144 cm ^{1}

FAB MS [M-1] observed 1086 Calcd 1086 03

4 3 3 15 General procedure for desilylation of 5-(trimethylsilylethynyl)thien-2-yl porphyrins

An slight excess of tetrabutylammonium fluoride (1 1 M in THF, 0 5 ml, 0 55 mmol) was added dropwise to a solution of the appropriate 5-(trimethylsilylethynyl)thien-2-yl substituted porphyrin (*ca* 5 x 10^{5} mol) in dichloromethane (10 ml) at room temperature, e g 1 2 equivalents were used in the desilylation of ZnTMSEtThTPP whereas 4 8 equivalents were used in the desilylation of ZnTTMSEtThP as there are four trimethylsilyl moieties present The reaction mixture was allowed to stir for 1 hour and then washed with water (10 ml) and brine (10 ml) The organic phase was separated, dried over $MgSO_4$ and evaporated to dryness Column chromatography of the crude product (SiO_2, pentane dichloromethane 1 2) afforded pure porphyrin in all cases in yields of > 95 %

4 3 3 15 1 zinc(II)-5-(5'-ethynylthien-2'-yl)-10,15,20-triphenylporphyrin (ZnEtThTPP)

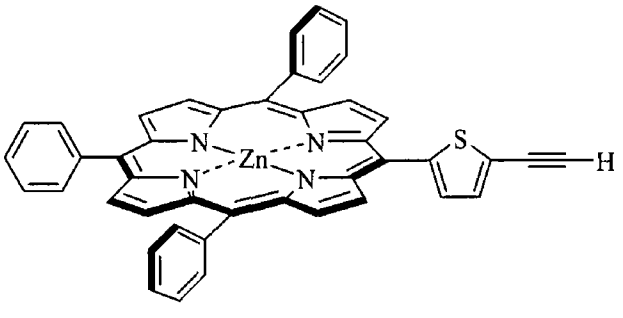

Fig 4 – 25

^{1}H NMR ($CDCl_3$) δ 9 07 (2H, d, ^{3}J = 4 8 Hz), 8 87 (2H, d, ^{3}J = 4 8 Hz), 8 83 (4H, q AB, ^{3}J = 4 8 Hz), 8 10 (6H, m), 7 53 – 7 65 (10H, m), 7 70 (1H, d, ^{3}J = 3 6 Hz), 3 37 (1H, s) ppm

^{13}C NMR ($CDCl_3$) δ 150 90, 150 48, 150 24, 149 96, 145 48, 142 55, 134 40, 133 03, 132 57, 132 31, 132 17, 131 83, 131 49, 127 57, 126 59, 123 79, 122 18, 121 69, 110 12, 82 05, 77 03 ppm

IR (CH_2Cl_2) ν(C≡C) 2108 cm ^{1}

MALDI MS [M+1] observed 709 2 Calcd 709 17

4 3 3 15 2

zinc(II)-5,10-di(5'-ethynylthien-2'-yl)-15,20-diphenylporphyrin &

zinc(II)- 5,15-di(5'-ethynylthien-2'-yl)-10,20-diphenylporphyrin (ZnDEtThDPP)

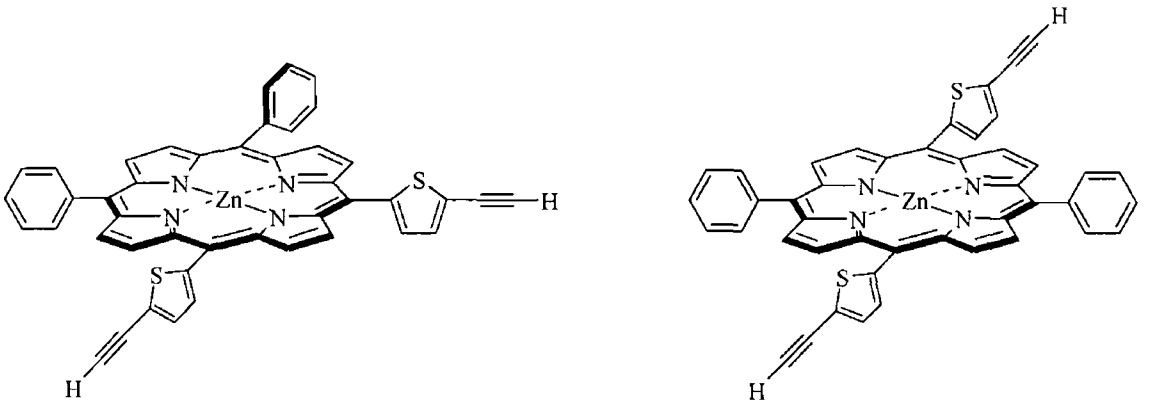

Fig 4 – 26

^{1}H NMR ($CDCl_3$) δ 9 08 (4H, m), 8 86 (4H, m), 8 10 (4H, m), 7 66 (8H, m), 7 56 (2H, d, ^{3}J = 3 6 Hz), 3 41 (2H, m) ppm

^{13}C NMR ($CDCl_3$) δ 151 12, 150 97, 150 73, 150 60, 150 40, 150 16, 145 77, 142 39, 134 40, 133 10, 132 81, 132 57, 132 30, 132 20, 132 00, 131 73, 131 46, 127 68, 126 63, 123 96, 122 70, 122 11, 111 23, 110 68, 82 12, 77 09 ppm

IR (CH_2Cl_2) ν(C≡C) 2108 cm ^{1}

MALDI MS [M+1] observed 739 3 Calcd 739 21

4 3 3 15 3 zinc(II)-5,10,15-di(5'-ethynylthien-2'-yl)-20-phenylporphyrin (ZnTEtThPP)

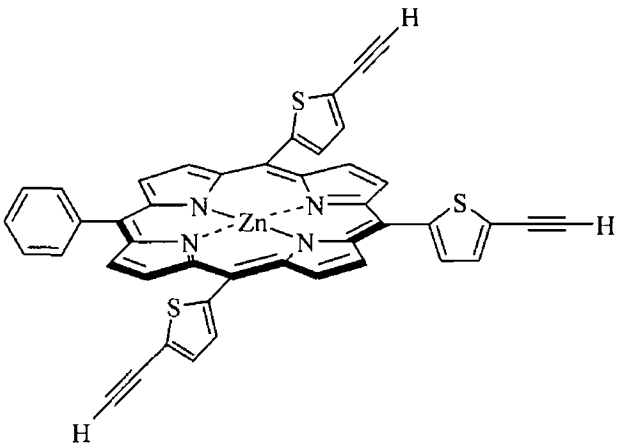

Fig 4 – 27

^{1}H NMR ($CDCl_3$) δ 9 11 (6H, m), 8 88 (2H, d, ^{3}J = 4 0 Hz), 8 12 (2H, m), 7 68 (6H, m), 7 60 (3H, dd, ^{3}J = 3 6 Hz), 3 47 (3H, m) ppm

^{13}C NMR ($CDCl_3$) δ 151 22, 151 10, 150 97, 150 83, 150 47, 145 44, 142 17, 134 32, 133 18, 132 80, 132 24, 132 00, 131 72, 127 77, 126 64, 124 09, 123 10, 111 73, 82 20, 77 14 ppm

IR (CH_2Cl_2) ν(C≡C) 2108 cm ^{1}

MALDI MS [M+1] observed 769 3 Calcd 769 26

4 3 3 15 4 zinc(II)-5,10,15,20-tetra(5'-ethynylthien-2'-yl)-porphyrin (ZnTEtThP)

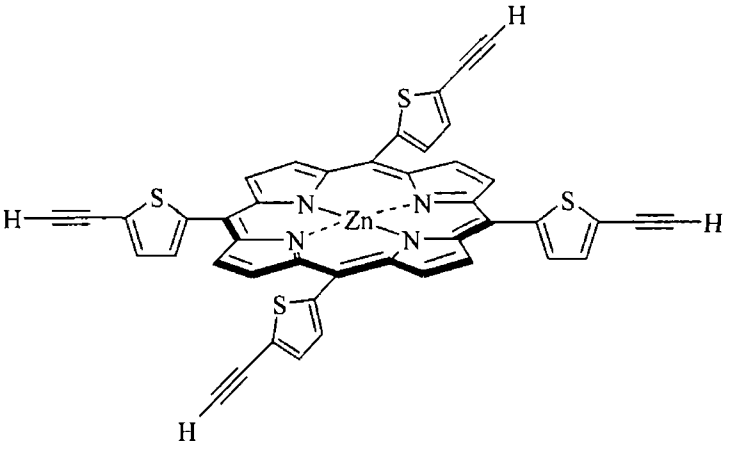

Fig 4 – 28

^{1}H NMR ($CDCl_3$) δ 9 10 (8H, s), 7 68 (4H, d, ^{3}J = 3 6 Hz), 7 61 (4H, d, ^{3}J = 3 6 Hz), 3 49 (4H, s)

^{13}C NMR ($CDCl_3$) δ 151 10, 145 36, 133 26, 132 21, 124 24, 112 09, 82 27, 65 79 ppm

IR (CH_2Cl_2) ν(C≡C) 2108 cm^{-1}

MALDI MS [M+1] observed 800 4 Calcd 799 31

4 3 3 16 zmc(II)-5-(5'-(5''-ethynyl-2''-thiophenecarboxaldehyde)thien-2'-yl)-10,15,20-triphenylporphyrin (ZnPald)

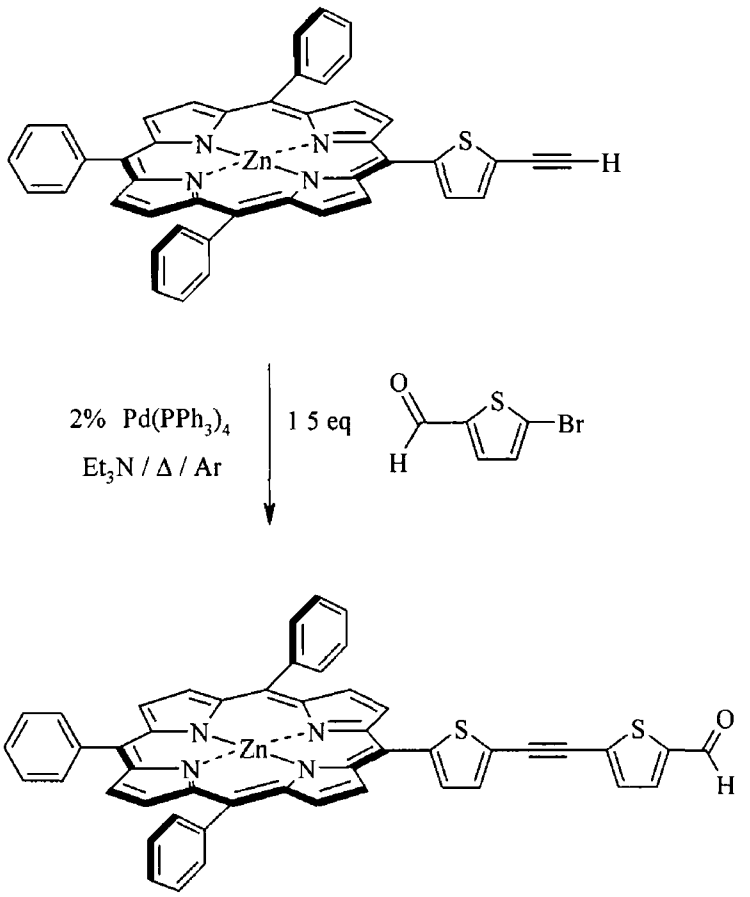

Rxn 4 – 27

ZnPald was prepared *via* the Sonogashira coupling reaction Zinc(II)-5-(5'-ethynylthien-2'-yl)-10,15,20-triphenylporphyrin (35 mg/5 x 10^{-5} mol) and 5-bromo-2-thiophenecarboxaldehyde (1 5 x 10^{-4} mol/18 μl) were added to 10 ml Et_3N and purged with argon for 10 minutes A 2 % equivalent (1 x 10^{6} mol, 1 15 mg) of tetrakis(triphenylphosphine)palladium(0) was added The reaction mixture was allowed to reflux for 8 hours and then allowed to cool Et_3N was removed under reduced pressure The residue was washed with petroleum ether (40 – 60) to remove any unreacted aldehyde from the crude mixture Column chromatography of the crude product (SiO_2, pentane dichloromethane 1 2) afforded 26 mg of pure porphyrin (33 mmol/94 %)

^{1}H NMR ($CDCl_3$) δ 9 50 (1H, s), 9 10 (2H, d, ^3J = 4 8 Hz), 8 90 (2H, d, ^3J = 4 8 Hz), 8 86 (4H, q AB, ^3J = 4 8 Hz), 8 13 (6H, m), 7 74 (1H, d, ^3J = 3 6 Hz), 7 67 (10H, m), 7 40 (1H, d, ^3J = 3 6 Hz), 7 15 (1H, d, ^3J = 3 6 Hz) ppm

IR (pentane) ν(C≡O) 1670 cm ^{1}, ν(C≡C) 2191 cm ^{1}

FAB MS [M-1] observed 818 Calcd 818 30

4 4 Results and discussion

4 4 1 *meso*-Tetrathien-2-ylporphyrins

Apart from H_2TPP, which was synthesised *via* the Adler method, all porphyrins in this study were synthesised *via* a modification of the Lindsey procedure Attempts to reproduce the reported synthesis of H_2TThP *via* the Adler method were unsuccessful This was attributed to possible decomposition of the porphyrin at the elevated temperatures of the reaction (141 ^{0}C) aswell as high solubility of the porphyrin in the propionic acid solvent This synthesis was successfully carried out however by employing the Lindsey method at low temperature Similar conditions have been employed by Anderson et al for the synthesis of *meso*-ethynylporphyrins [69] H_2TThP was obtained in 18 % yield following the Lindsey synthesis where the $BF_3 OEt_2$ catalyst was introduced to the reaction at of 0 ^{0}C before allowing the reaction mixture to slowly reach room temperature A yield of 21 40 % was obtained for $H_2TBrThP$ following a similar procedure where the $BF_3 OEt_2$ catalyst was added at room temperature Porphyrins $H_2TTMSEtThP$ and $H_2TEtThP$ were obtained in low yields (< 5%) *via* the Lindsey method at room temperature On cooling the reaction mixture to *ca* -70 ^{0}C with a liquid nitrogen/acetone slurry before addition of $BF_3 OEt_2$, the yields were improved to 28 % for $H_2TTMSEtThP$ and 18 % for the desilylated analogue $H_2TEtThP$

Metallation of H_2TThP and $H_2TBrThP$ with zinc(II) was carried out quantitatively Zinc(II) insertion of the 5-(trimethylsilylethynyl)thien-2-yl and 5-ethynylthien-2-yl substituted porphyrins, $H_2TTMSEtThP$ and $H_2TEtThP$, resulted in yields of ~ 2 %, the major product being a dark brown crude material The reasons for such low yields have not yet been identified ZnTTMSEtThP was successfully synthesised in high yield (> 95 %) by an alternative route *via* the Sonogashira coupling of ZnTBrThP with trimethylsilylacetylene ZnTEtThP was subsequently synthesised in high yield (> 95 %) *via* the desilylation of ZnTTMSEtThP in the presence of Bu_4NF Fig 4 – 29 gives an overlay of the aromatic region of the ^{1}H-NMR spectra for the *meso*-tetrasubstituted porphyrins ZnTPP, ZnTThP, ZnTBrThP, ZnTEtThP and ZnTTMSEtThP

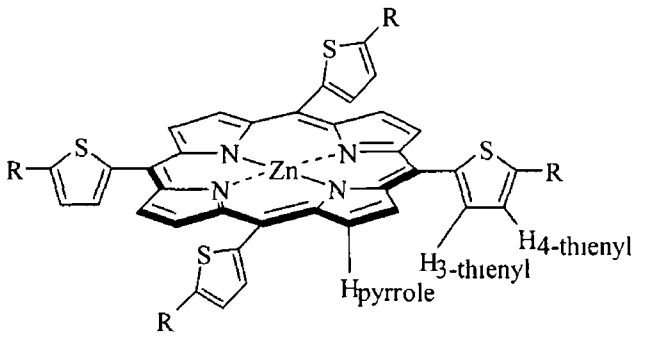

porphyrin	R
ZnTThP	−H (5-thienyl)
ZnTBrThP	−Br
ZnTEtThP	—≡—H
ZnTTMSEtThP	—≡—T MS

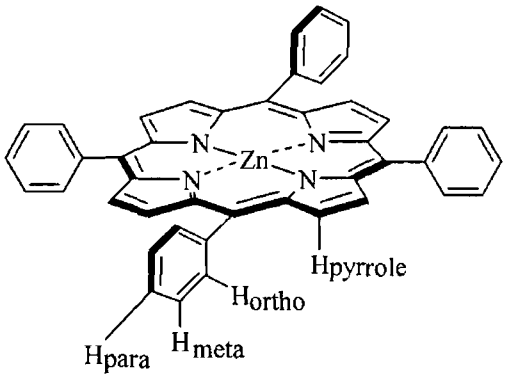

ZnTPP

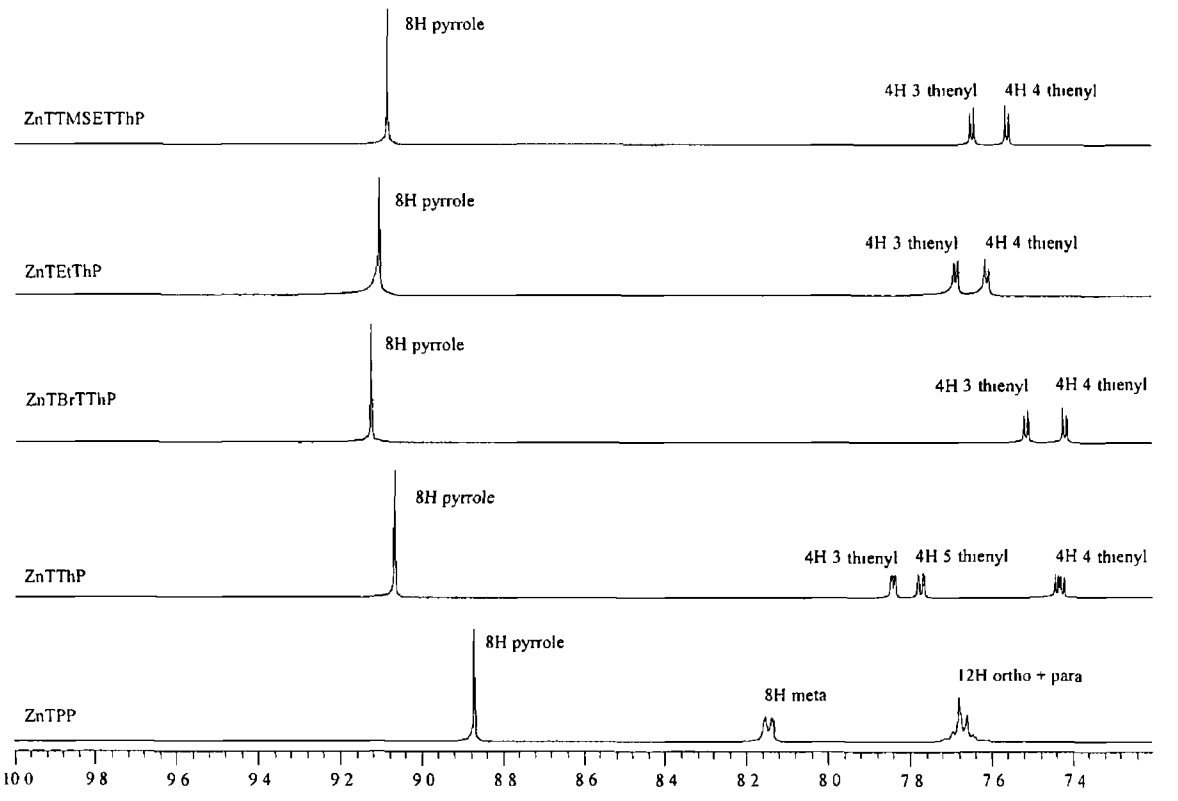

Fig 4 – 29 An overlay of the aromatic region of the 400 MHz ^{1}H-NMR spectra (δ ppm) for the *meso*-tetrasubstituted porphyrins ZnTPP, ZnTThP, ZnTBrThP, ZnTEtThP and ZnTTMSEtThP recorded in $CDCl_3$

All of the A_4-type *meso*-substituted porphyrins ZnTPP, ZnTThP, ZnTBrThP, ZnTEtThP and ZnTTMSEtThP are of S_4 symmetry and posses a C_4 rotational axis through the metal centre perpendicular to the plane of the ring (fig 4 – 30) Each of the β-pyrrolic protons are therefore in an identical magnetic environment as is evident in the ^{1}H-NMR spectra by their appearance as a sharp singlet This singlet occurs at 8 87 ppm for ZnTPP however is shifted slightly downfield for the *meso*-tetrathien-2-yl porphyrins The singlet β-pyrrolic proton signal occurs at 9 07 ppm for ZnTThP, 9 12 ppm for ZnTBrTThP, 9 10 ppm for ZnTEtThP and 9 08 ppm for ZnTTMSEtThP This deshielding effect of the β-pyrrolic protons observed for the *meso*-tetrathien-2-yl porphyrins is possibly a result of an increase in the ring current of the porphyrin ring The thienyl protons are typical of a 2-substituted thiophene system for ZnTThP and of a 2,5-disubstituted thiophene system for ZnTBrThP, ZnTEtThP and ZnTTMSEtThP, however they are shifted slightly downfield due to the close proximity of the porphyrin ring current

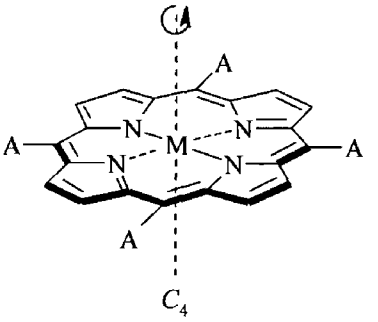

Fig 4 - 30

4 4 2 *meso*-Substituted phenyl/thien-2-yl porphyrins

The mixed aldehyde synthesis of porphyrins H_2TBrThP, H_2TBrThPP, H_2DBrThDPP and H_2BrThTPP was carried out *via* the Lindsey method at room temperature with yields close to the expected statistical ratio [26] Zinc(II) insertion was carried out quantitatively for all porphyrins The 5-(trimethylsilylethynyl)thien-2-yl substituted porphyrins were successfully synthesised *via* Sonogashira coupling of their 5-bromothien-2-yl precursors This reaction was carried out in refluxing dimethylamine for ZnTMSEtThTPP and ZnDTMSEtThDPP, however the higher boiling point amine, diisopropylamine, was required for porphyrins ZnTTMSEtThPP and ZnTTMSEtThP Desilylation in the presence of Bu_4NF formed the 5-ethynylthien-2-yl substituted porphyrins in high yield The *cis*- and *trans*-isomers of ZnDTMSEtThDPP and ZnDEtThDPP, aswell as their synthetic precursors, proved inseparable and were thus used as a mixture throughout

Synthesis of the 5-(trimethylsilylethynyl)thien-2-yl and 5-ethynylthien-2-yl substituted porphyrins was also carried out *via* the direct condensation of pyrrole with the aldehydes 5-(trimethylsilylethynyl)thiophene-2-carboxaldehyde and 5-ethynylthiophene-2-carboxaldehyde respectively (fig 4 – 33) The resulting mixtures proved inseparable in both cases The direct synthesis of 5,15-(trimethylsilylethynyl)thien-2-yl-10,20-diphenylporphyrin was also attempted *via* the condensation of 5-(trimethylsilylethynyl)thiophene-2-carboxaldehyde and 5-phenyldipyrromethane however the occurrence of scrambling resulted in the formation of the six products seen in the mixed aldehyde reaction (fig 4 – 33) The condensation of 5-(trimethylsilylethynyl)thiophene-2-carboxaldehyde with dipyrromethane also proved unsuccessful

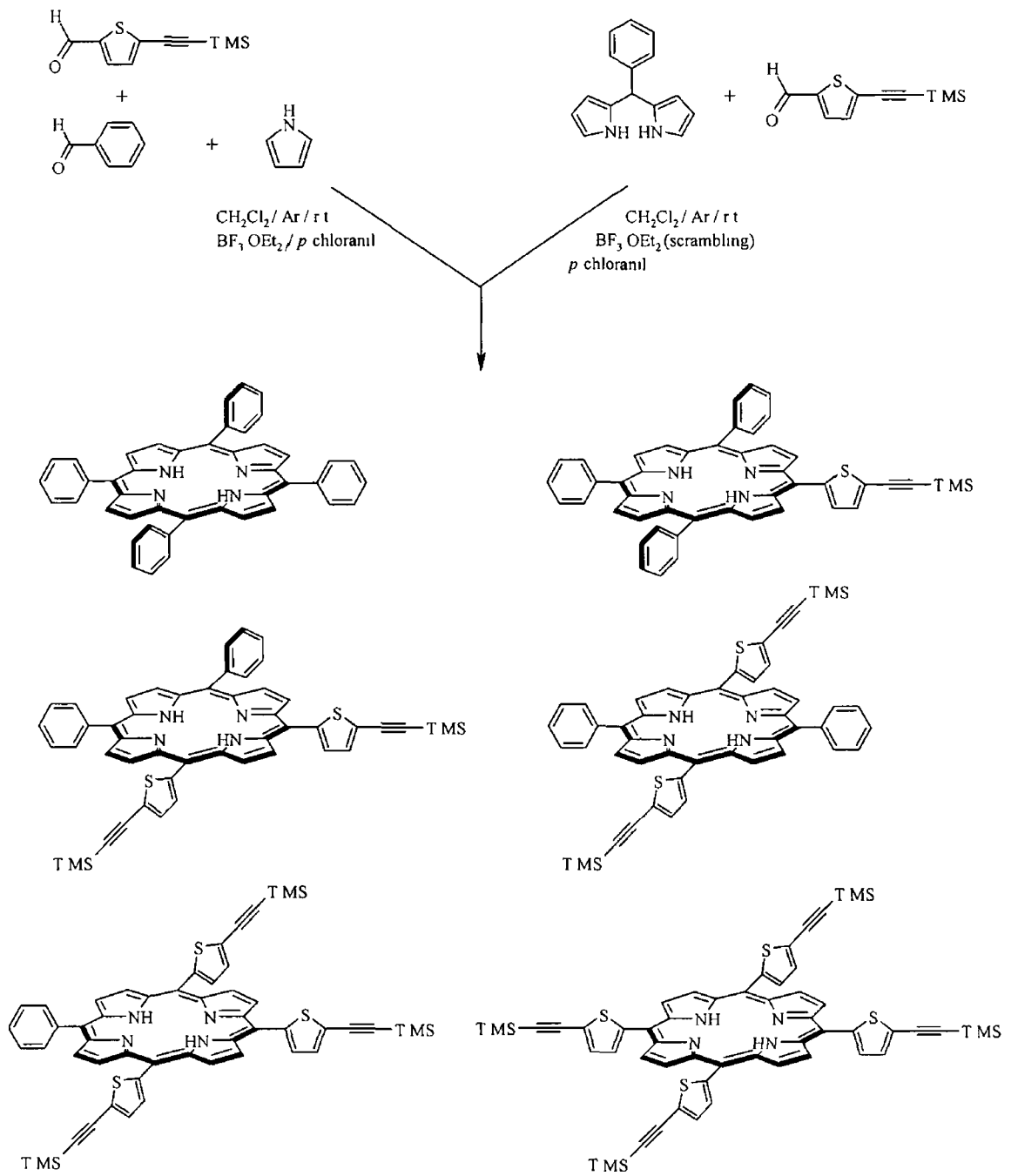

Fig 4 – 33 The mixed aldehyde condensation of pyrrole with benzaldehyde and 5-(trimethylsilylethynyl)thiophene-2-carboxaldehyde and the condensation of 5-(trimethylsilylethynyl)thiophene-2-carboxaldehyde with 5-phenyldipyrromethane both resulted in the same inseparable mixture of 5-(trimethylsilylethynyl)thien-2-yl substituted porphyrins

On lowering the symmetry of the ring by introducing non-equivalent groups at the *meso*-position of the porphyrin ring the ^{1}H-NMR spectra become more complex. AB_3 and A_3B-type porphyrins, i.e. ZnTMSEtThTPP and ZnTTMSEtThPP, are of C_{2v} symmetry. The *cis*- and *trans*-isomers of ZnDTMSEtThDPP, A_2B_2-type porphyrins, are of C_{2v} and D_{2h} symmetry respectively (fig. 4 – 34).

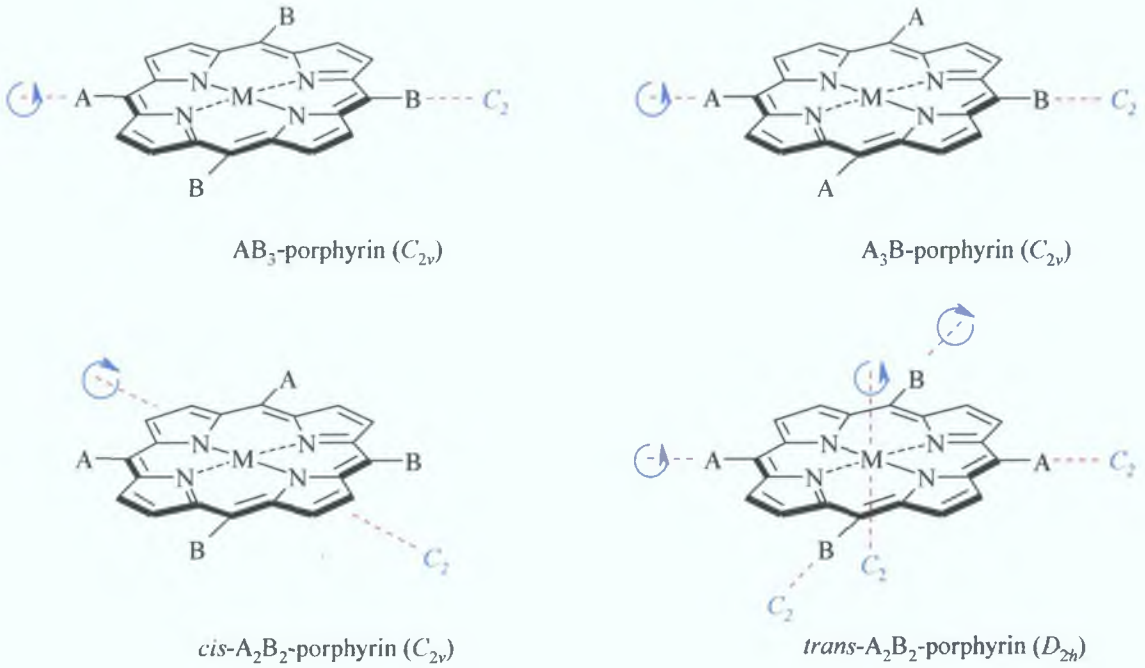

Fig. 4 – 34

Fig. 4 – 35 gives an overlay of the aromatic region of the ^{1}H-NMR spectra for the 5-(trimethylsilylethynyl)thien-2-yl substituted porphyrins. The 3,7-β-pyrrolic protons of ZnTMSEtThTPP, i.e. those closest to the *meso*-5-(trimethylsilylethynyl)thien-2-yl substituent, occur downfield of the other β-pyrrolic protons for ZnTMSEtThTPP as a doublet at 9.09 ppm (^3J = 4.8 Hz). These protons are coupled to the adjacent 2,8-β-pyrrolic protons, which occur at 8.88 ppm also as a doublet (^3J = 4.8 Hz). The 12,13,17,18-β-pyrrolic protons occur at 8.85 ppm as an AB-type quartet (^3J = 4.8 Hz). The meta-, ortho- and para-phenyl protons do not differ significantly from ZnTPP. The ortho- and para-phenyl protons obscure the 3-thienyl proton of ZnTMSEtThTPP, however the 4-thienyl proton is still visible at 7.65 ppm as a doublet (^3J = 3.6 Hz). The trimethylsilyl protons occur at 0.28 ppm as a singlet.

As the *cis*- and *trans*-isomers of ZnDTMSEtThDPP were obtained as a mixture the β-pyrrolic protons occur as a complex multiplet The *cis*-isomer, of C_{2v} symmetry, typically displays two doublets corresponding to the 3,12- and 2,13-β-pyrrolic protons whereas the 7,8- and 17,18-β-pyrrolic protons give rise to two singlets [59] The *trans*-isomer, of D_{2h} symmetry, typically displays two singlets corresponding to the 2,8,12,18- and 3,7,13,17-β-pyrrolic protons [72] Two singlets appear at 0 23 and 0 24 ppm corresponding to the trimethylsilyl protons of the *cis*- and *trans*-isomers of ZnDTMSEtThDPP These signals are only slightly resolved and were therefore integrated as an 18 proton multiplet

ZnTTMSEtThPP which incorporates the 5-(trimethylsilylethynyl)thien-2-yl substituent in three of its *meso*-positions is of identical symmetry to the mono 5-(trimethylsilylethynyl)thien-2-yl porphyrin ZnTMSEtTPP The β-pyrrolic proton signals of ZnTTMSEtThPP appear almost as a mirror image to those of ZnTMSEtTPP The 7,8,12,13,-β-pyrrolic protons of ZnTMSEtThTPP occur as an AB-type quartet at 9 08 ppm (^3J = 4 8 Hz) The 3,17-β-pyrrolic protons occur slightly upfield at 9 04 ppm as a doublet (^3J = 4 8 Hz) and are coupled to the adjacent 2,18-β-pyrrolic protons, which occur at 8 83 ppm also as a doublet (^3J = 4 8 Hz) The meta-, ortho- and para-phenyl protons do not differ significantly from ZnTMSEtTPP apart from a decreased integration from 6 to 2 protons The 3',4'-thienyl protons of the 5-(trimethylsilylethynyl)thien-2-yl substituent in the 10-*meso*-position are in a slightly different magnetic environment than the 3,4-thienyl protons of the 5-(trimethylsilylethynyl)thien-2-yl substituents in the 5- and 15-*meso*-positions This is evident by the appearance of the 4- and 4'-thienyl protons as a double doublet at 7 56 ppm (^3J = 3 6 Hz) Again, the ortho- and para-phenyl protons obscure the 3- and 3'-thienyl protons of ZnTTMSEtThPP resulting in a multiplet at 7 71 – 7 65 ppm The trimethylsilyl protons of ZnTTMSEtThPP appear as two slightly resolved singlets at 0 28 ppm ZnTTMSEtThP is of S_4 symmetry and its ^{1}H-NMR is described in the previous section

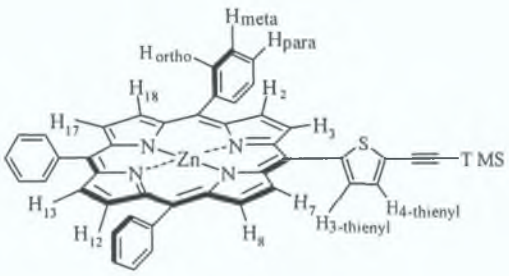

ZnTMSEtThTPP

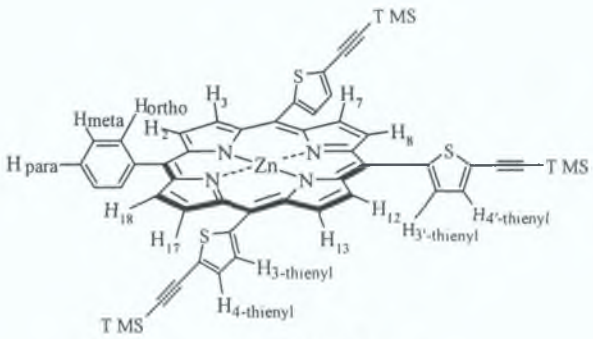

ZnTMSTEtThPP

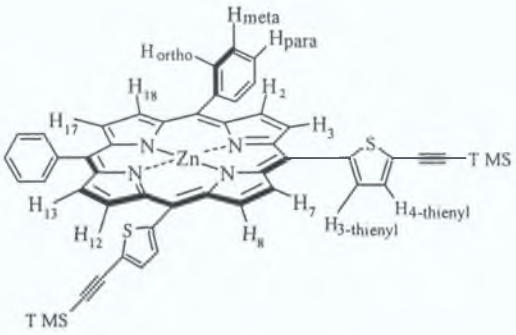

cis-ZnDTMSEtThDPP

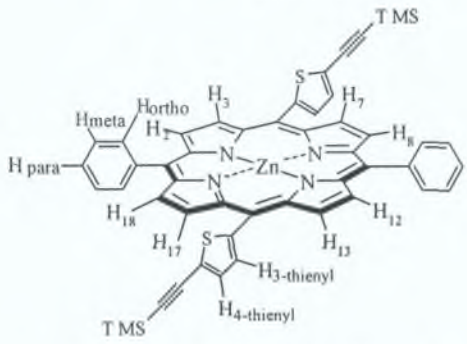

trans-ZnDTMSEtThDPP

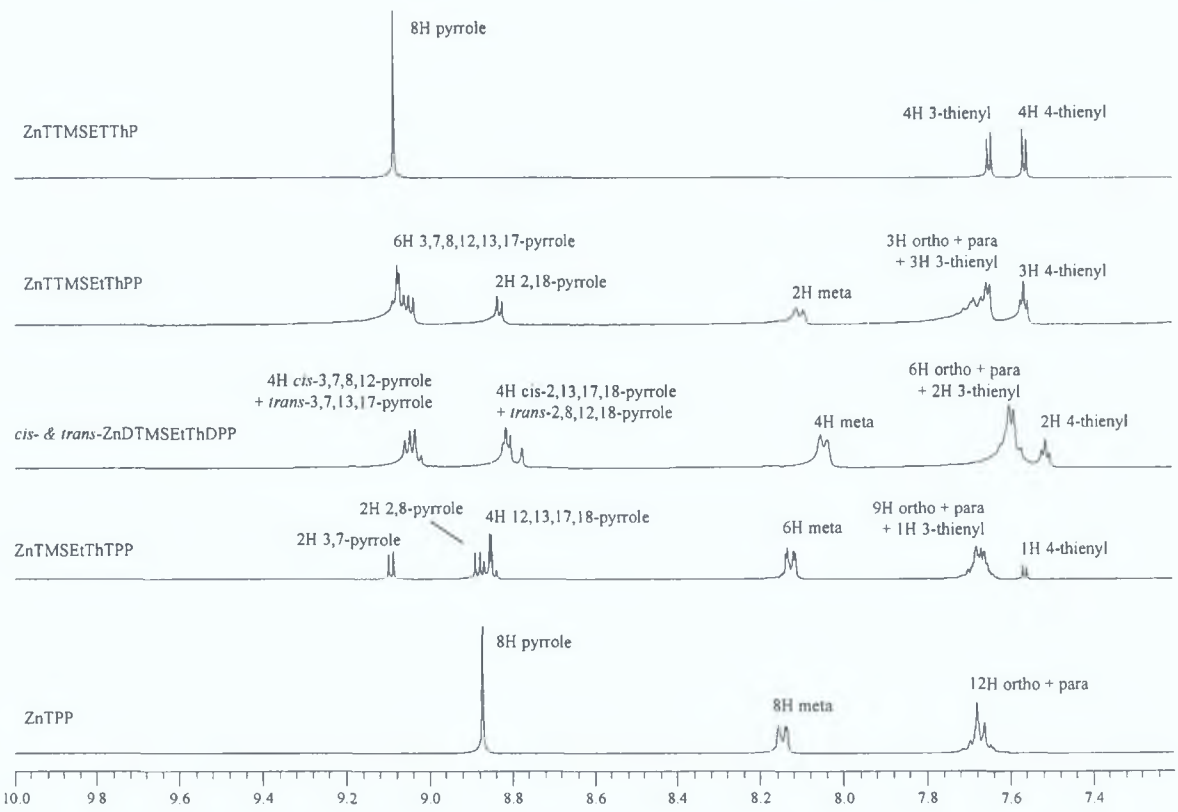

Fig. 4 – 35: An overlay of the aromatic region of the 400 MHz ^{1}H-NMR spectra (δ ppm) for ZnTPP and the 5-(trimethylsilylethynyl)thien-2-yl substituted porphyrins ZnTMSEtThTPP, ZnDTMSEtThDPP, ZnTTMSEtThPP and ZnTTMSEtThP recorded in $CDCl_3$.

The ^{1}H-NMR spectra of the 5-ethynylthien-2-yl substituted porphyrins are not described here as they are quite similar to their 5-(trimethylsilylethynyl)thien-2-yl substituted analogues Fig 4 – 36 gives an overlay of the aromatic region of the ^{1}H-NMR spectra for the various 5-ethynylthien-2-yl substituted porphyrins The ethynyl protons are also shown As with the TMS signals for the *cis*- and *trans*-isomers of ZnDTMSEtThDPP, two slightly resolved singlets are observed for the ethynyl protons of the *cis*- and *trans*-isomers of ZnDEtThDPP at 3 41 ppm Also, as observed for ZnTTMSEtThPP, the 5-(trimethylsilylethynyl)thien-2-yl substituent in the 10-*meso*-position is in a slightly different magnetic environment than the 5-(trimethylsilylethynyl)thien-2-yl substituents in the 5- and 15-*meso*-positions The ethynyl protons therefore appear as two slightly resolved singlets at 3 47 ppm

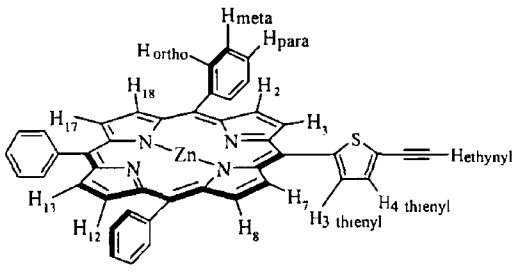

ZnEtThTPP

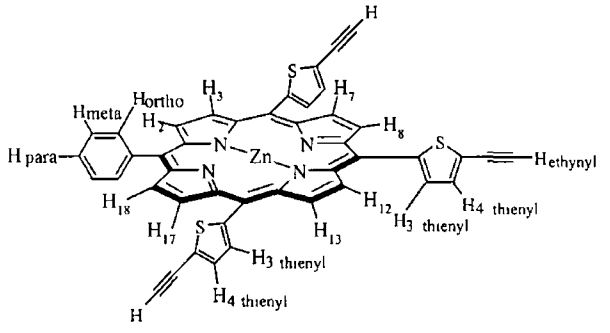

ZnTEtThPP

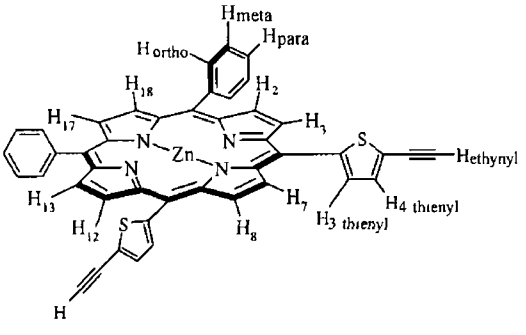

cis ZnDEtThDPP

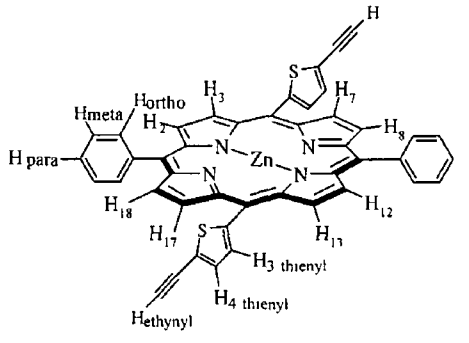

trans ZnDEtThDPP

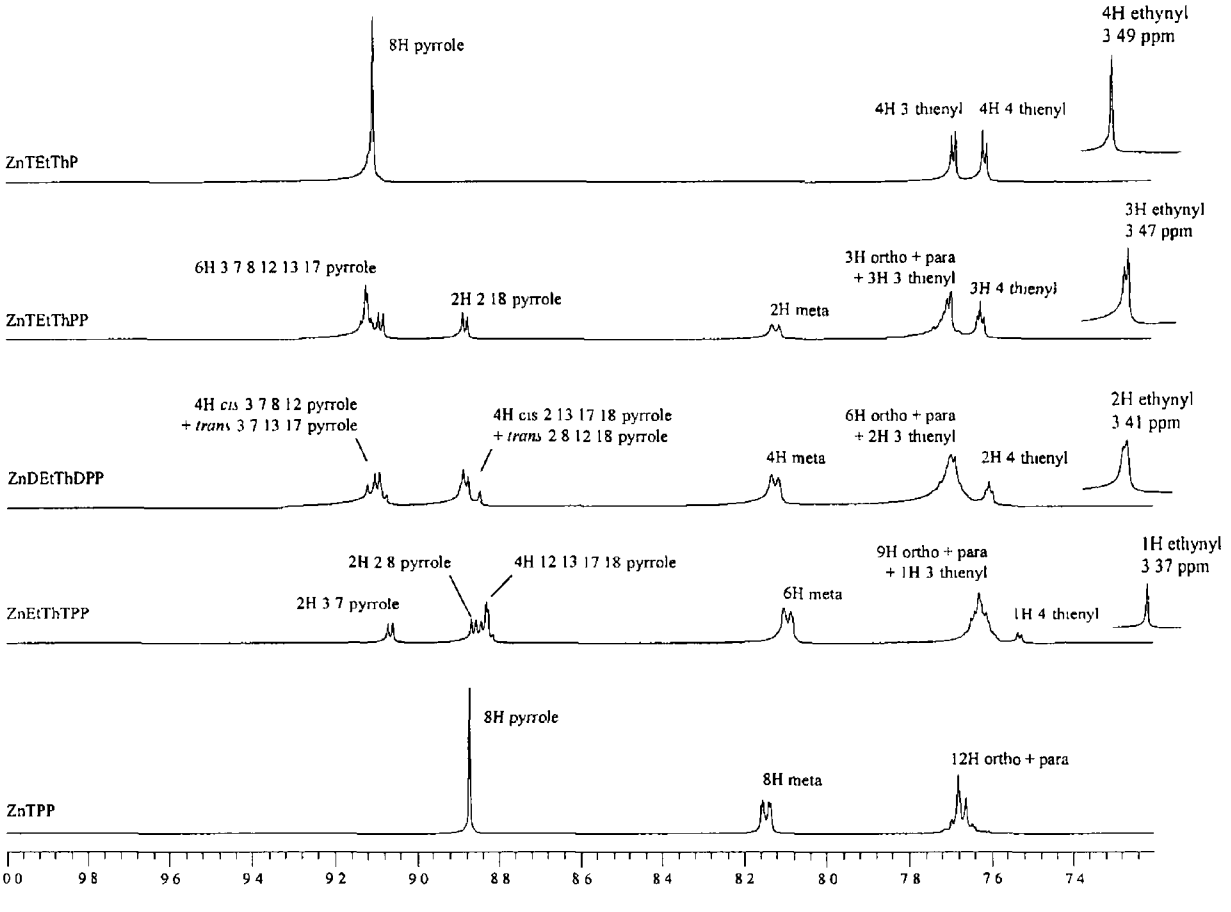

Fig 4 – 36 An overlay of the aromatic region of the 400 MHz ^{1}H-NMR spectra (δ ppm) for ZnTPP and the 5-ethynylthien-2-yl substituted porphyrins ZnEtThTPP, ZnDEtThDPP, ZnTEtThPP and ZnTEtThP recorded in $CDCl_3$

ZnEtThTPP was further coupled, under Sonogashira conditions, at the terminal ethynyl moiety to 5-bromo-2-thiophenecarboxaldehyde giving the porphyrin zinc(II)-5-(5'-(5''-ethynylthiophene-2'-carboxaldehyde)thien-2'-yl)-10,15,20-triphenylporphyrin (ZnPald) in high yield The symmetry of the porphyrin remains the same on going from ZnEtThTPP to ZnPald (C_{2v}) therefore there is little difference in the ^{1}H-NMR spectra (fig 4 – 37) All of the signals are shifted slightly downfield on going from ZnEtThTPP to ZnPald with the 3,4-thienyl protons showing the largest shift The two extra 3',4'-thienyl protons occur as doublets at 7 40 and 7 15 ppm respectively (^3J = 3 6 Hz) The single aldehyde proton occurs as a singlet downfield from the β-pyrrolic protons at 9 50 ppm

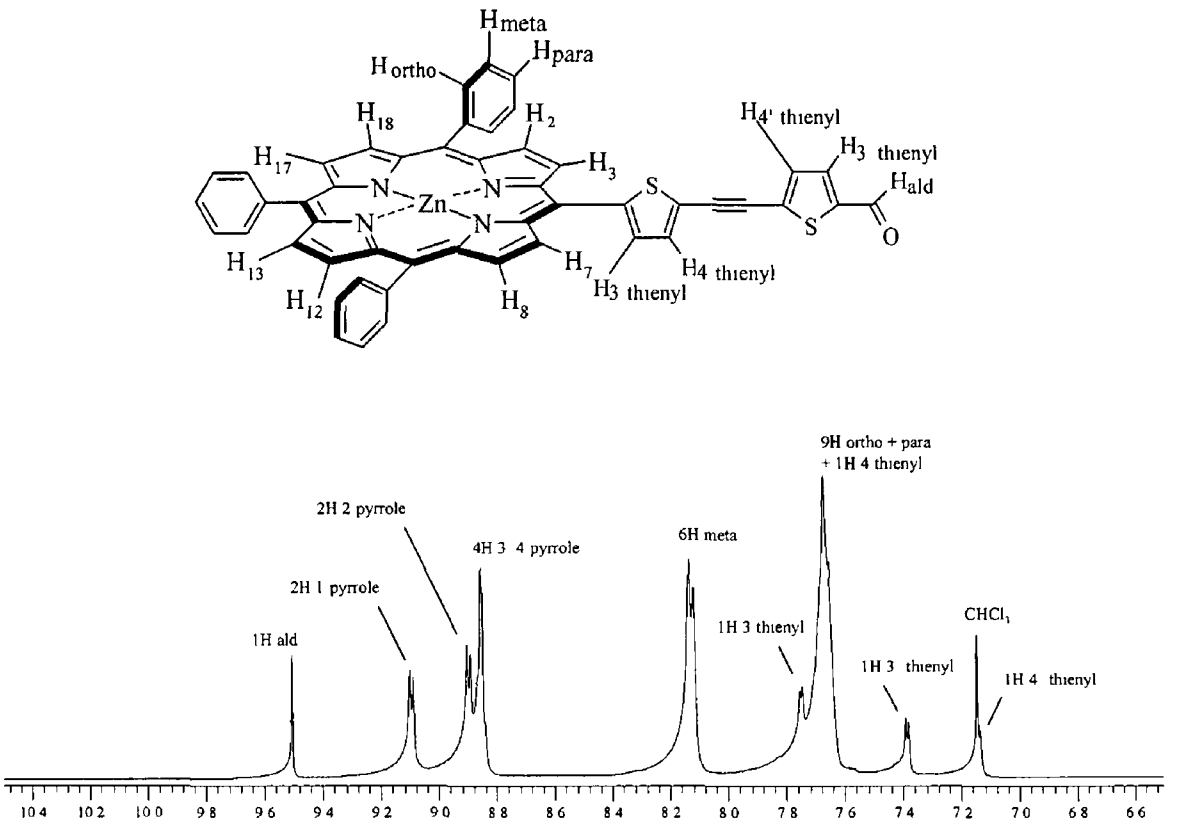

Fig 4 – 37 The aromatic region of the 400 MHz ^{1}H-NMR spectra (δ ppm) for ZnPald recorded in $CDCl_3$

4 4 3 *meso*-Ferrocenyl porphyrins

The mixed aldehyde synthesis of H_2FcTPP and H_2FcTThP were both carried out at by the Lindsey method at room temperature with yields of 8 and 7 % respectively Attempts to isolate any bis-, tri-, or tetra-ferrocenyl porphyrin were unsuccessful in both cases Metallation of H_2FcTPP with zinc(II) and nickel(II) was carried out quantitatively Metallation of H_2FcTThP with zinc(II) was also carried out in high yield ZnFcTPP, NiFcTPP and ZnFcTThP are all examples of AB_3-type porphyrins Free rotation of the ferrocene moiety at the *meso*-position of a porphyrin has been previously reported and is again evident here in the ^{1}H-NMR spectra of ZnFcTPP, NiFcTPP and ZnFcTThP [70] Each compound can thus be considered to be of *pseudo*-C_{2v} symmetry

An overlay of the ^{1}H-NMR spectra for ZnFcTPP and NiFcTPP is shown in fig 4 – 38 The 3,7-β-pyrrolic protons occur as a doublet at 9 98 ppm (^3J = 4 0 Hz) and 9 58 ppm (^3J = 4 8 Hz) for ZnFcTPP and NiFcTPP respectively The 2,8,12,13,17,18-β-pyrrolic protons occur as a multiplet for ZnFcTPP at 8 73 ppm These protons are more resolved for NiFcTPP with a doublet occurring at 8 62 ppm (^3J = 4 8 Hz) corresponding to the 2,8 -β-pyrrolic protons The 12,13,17,18 -β-pyrrolic protons of NiFcTPP give rise to an AB-type quartet at 8 59 ppm (^3J = 4 8 Hz) Nickel(II) porphyrins are known to have a non-planar distorted conformation in contrast to the planar zinc(II) porphyrin systems [71] This distortion from planarity may lead to a decrease in the ring current of the porphyrin macrocycle which could explain why the β-pyrrolic protons of NiFcTPP are slightly upfield of the zinc(II) analogue ZnFcTPP The β-pyrrolic protons of NiTPP occur upfield with respect to those of ZnTPP, i e 8 67 *vs* 8 87 ppm respectively The Cp' and Cp'' protons occur as double doublets at 5 26 and 4 51 ppm for ZnFcTPP and at 5 07 and 4 63 ppm for NiFcTPP The larger separation of these signals for ZnFcTPP indicates that they are less equivalent than in the nickel(II) analogue This is possibly due to increased communication between the porphyrin and ferrocene π-systems in NiFcTPP promoted by the distorted non-planar porphyrin ring The five Cp protons occur as a sharp singlet at 3 90 ppm for both ZnFcTPP and NiFcTPP

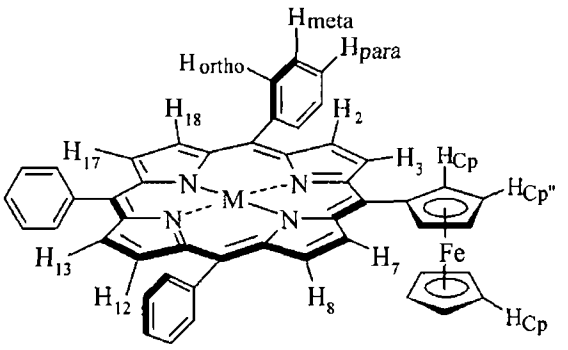

M = Zn(II), Ni(II)

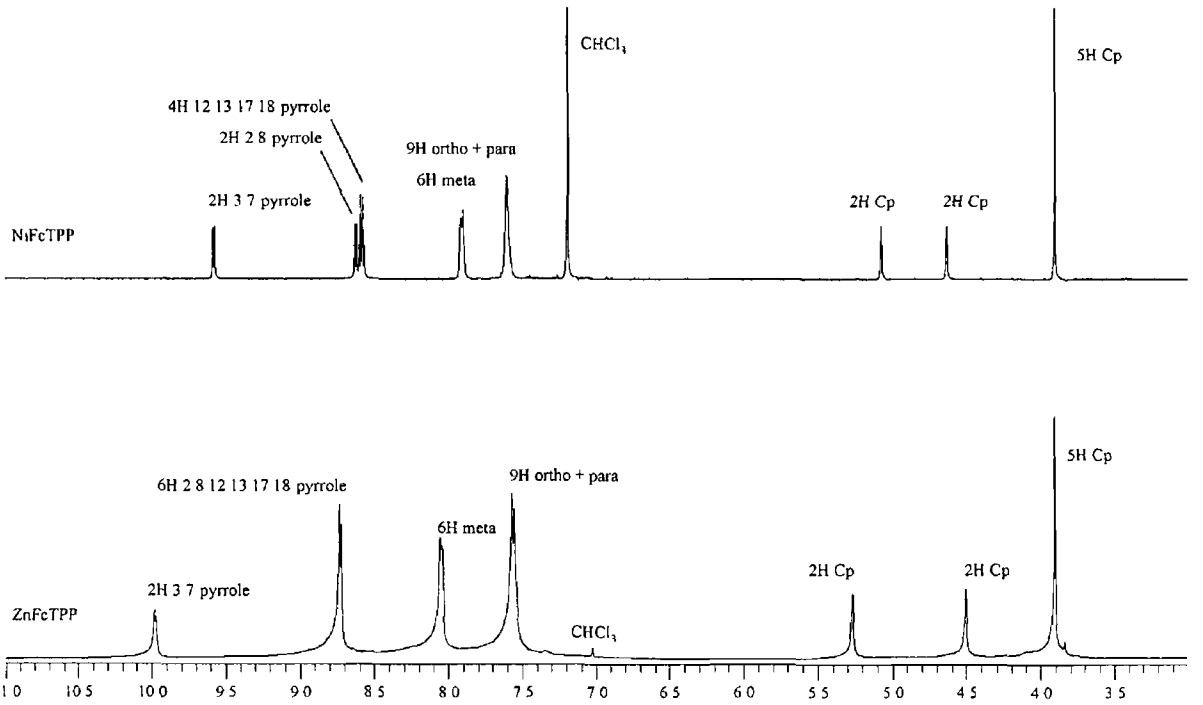

Fig 4 – 38 An overlay of the 400 MHz ^{1}H-NMR spectra (δ ppm) for ZnFcTPP and NiFcTPP recorded in $CDCl_3$

The ^{1}H-NMR spectrum of ZnFcTThP, also of *pseudo*-C_{2v} symmetry, shows a similar splitting pattern as for the ZnFcTPP and NiFcTPP porphyrins (fig 4 – 39) The 3,7-β-pyrrolic protons occur further downfield as a doublet at 10 06 ppm (^3J = 4 8 Hz) The 2,8,12,13,17,18-β-pyrrolic protons are unresolved as for ZnFcTPP and occur as a multiplet at 8 97 ppm The 3- and 5-thienyl protons occur as a multiplet in the range 7 70 – 7 80 ppm The 4-thienyl protons also occur as a multiplet at 7 39 ppm The Cp'

and Cp'' protons occur as double doublets at 5 40 and 4 69 ppm for ZnFcTThP with the five Cp protons occurring as a sharp singlet at 4 07 ppm The β-pyrrolic protons aswell as the ferrocenyl protons all occur slightly downfield for ZnFcTThP in comparison to ZnFcTPP suggesting a greater ring current in the former compound

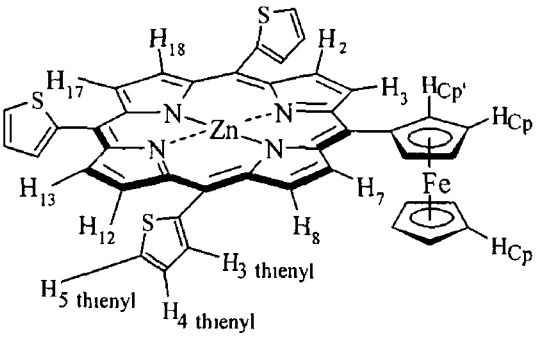

ZnFcTThP

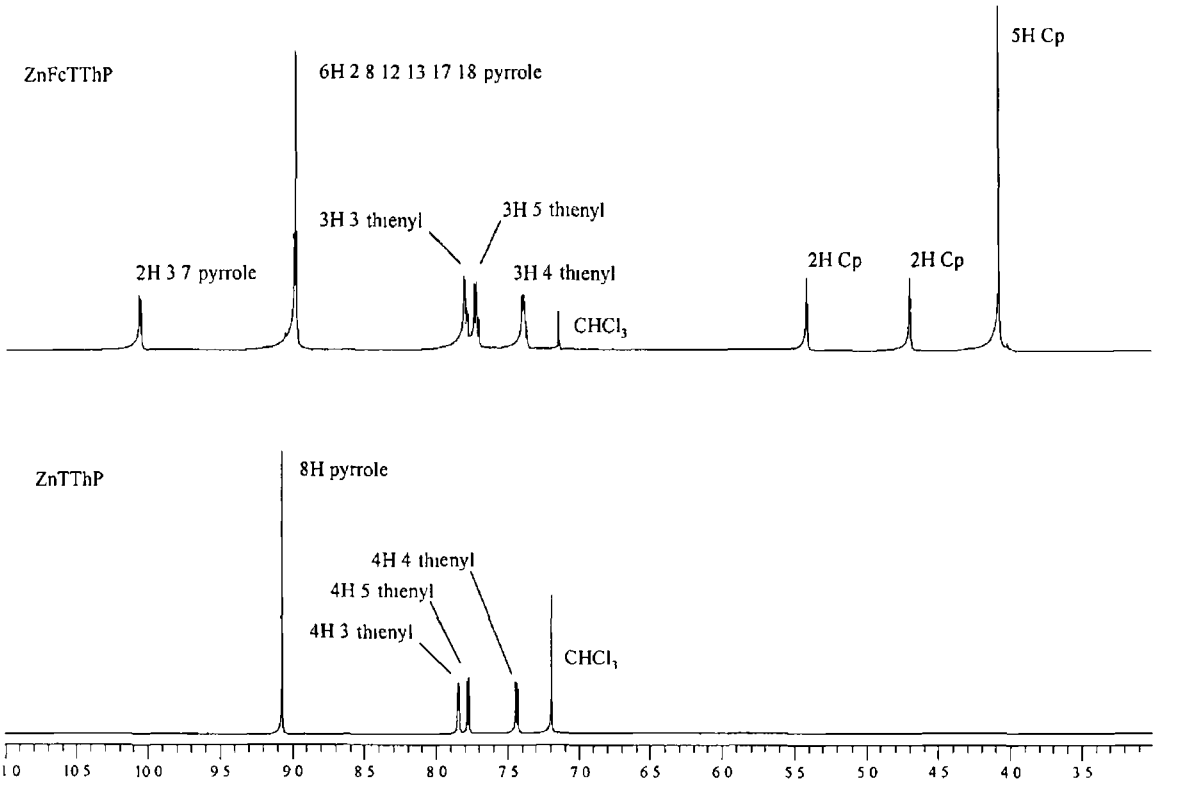

Fig 4 – 39 An overlay of the 400 MHz ^{1}H-NMR spectra (δ ppm) for ZnFcTThP and ZnTThP recorded in $CDCl_3$

4 5 Conclusions

A series of *meso*-tetrathien-2-yl porphyrins and *meso*-phenyl/thien-2-yl porphyrins have been successfully prepared via a modification of the Lindsey synthetic procedure The Sonogishira coupling reaction was carried out successfully for a series of mono-, di-, tri- and tetra-(5-bromothien-2-yl) porphyrin systems ^{1}H-NMR studies suggest an increase in the ring current of ZnTThP, ZnTBrThP, ZnTEtThP and ZnTTMSEtThP relative to ZnTPP This is also demonstrated by successively increasing the number of thien-2-yl substituents from one to four at the *meso*-position of the porphyrin ring A similar increase in ring current was also observed for ZnFcTThP in comparison to ZnFcTPP

[1] (a) C M Drain, J T Hupp, K S Suslick, M R Wasielewski, X Chen, *J Porph Phtal* **2002**, 6, 243 (b) M Calvete, G Ying Yang, M Hanack, *Synth Metals* **2003**, 141, 231 (c) *The Porphyrin Handbook*, eds K M Kadish, K M Smith, R Guilard, Academic Press Boston, 2000, Vol 18

[2] (a) H Fischer, H Orth, *Die Chemie des Pyrrols*, Akademische Verlagsgesellschaft Leipzig, 1937, Vol II, part 1, p 175

[3] (a) H Fischer, J Klarer, *Ann Chem* **1926**, 448, 178 (b) H Fischer, H Friedrich, W Lamatsch, K Morgenroth, *Ann Chem* **1928**, 466

[4] (a) G P Arsenault, E Bullock, S F MacDonald, *J Am Chem Soc* **1960**, 82, 4384 (b) J A S Cavaleiro, A M d'A Rocha Gonsalves, G W Kenner, K M Smith, *J Chem Soc , Perkin Trans 1* **1974**, 1771 (c) J A S Cavaleiro, G W Kenner, K M Smith, *J Chem Soc , Perkin Trans 1* **1974**, 1188

[5] (a) A W Johnson, I T Kay, *J Chem Soc C* **1961**, 2418 (b) I D Dicker, R Grigg, A W Johnson, H Pinnock, K Richardson, P van der Broek, *J Chem Soc C* **1971**, 536

[6] P J Rothemund, *J Am Chem Soc* **1935**, 57, 2010

[7] P J Rothemund, *J Am Chem Soc* **1936**, 58, 625

[8] A D Adler, F R Longo, J D Finarelli, J Goldmacher, J Assour, L Korsakoff, *J Org Chem* **1967**, 32, 476

[9] D Dolphin, *J Heterocyclic Chem* **1970**, 7, 275

[10] J P Collman, R R Gagne, C A Reed, T R Halbert, G Lang, W T Robinson, *J Am Chem Soc* **1975**, 97, 1427

[11] J P Collman , J I Brauman , J P Fitzgerald , P D Hampton , Y Naruta , J W Sparapany , J A Ibers, *J Am Chem Soc* **1988,** 110, 3477

[12] J S Lindsey, I C Schreiman, H C Hsu, P Kearney, A M Marguerettaz, *J Org Chem* **1987**, *52*, 827

[13] T Fujimoto, H Umekawa, N Nishino, *Chem Lett* **1992**, 37

[14] K S Suslick, M M Fox, *J Am Chem Soc* **1983**, 105, 3507

[15] G Markl, M Reiss, P Kreitmeier, H Noth, *Angew Chem Int Ed Eng* **1995**, 34, 2230

[16] D K Lavallee, Z Xu, R Pina, *J Org Chem* **1993**, 58, 6000

[17] P Kus, G Knerr, L Czuchajowski, *J Heterocyclic Chem* **1990**, 27, 1161

[18] R G Wollmann, D N Hendrickson, *Inorg Chem* **1977**, 16, 3079

[19] O Wennerstrom, H Ericsson, I Raston, S Svensson, W Pimlott, *Tetrahedron Lett* **1989**, 30, 1129

[20] H Toi, Y Nagai, Y Aoyama, H Kawabe, K Aizawa, H Ogoshi, *Chem Lett* **1993**, 1043

[21] F Ludley, E Breitmaier, *Synthesis* **1994**, 949

[22] C A Hunter, L D Sarson, *Tetrahedron Lett* **1996**, 37, 699

[23] D A Schultz, D A Knox, L W Morgan, K Sandberg, G N Tew, *Tetrahedron Lett* **1993**, 34, 3975

[24] (a) N M Loim, E V Grishko, N I Pyshnograeva, E V Vorontsov, V I Sokolov, *Russ Chem Bull* **1994**, 43, 871 (b) N M Loim, M A Kondratenko, E V Grishko, V I Sokolov, *Russ Chem Bull* **1994**, 43, 905

[25] D L Officer, A K Burrell, D C W Reid, *Chem Commun* **1996**, 1657

[26] J S Lindsey in *The Porphyrin Handbook*, eds K M Kadish, K M Smith, R Guilard, Academic Press Boston, 2000, Vol 1, ch 2

[27] R G Little, J A Anton, P A Loach, J A Ibers, *J Heterocyclic Chem* **1975**, 12, 343

[28] (a) E B Fleischer, A M Schacter, *Inorg Chem* **1991**, 30, 3763 (b) C M Dram, J -M Lehn, *J Chem Soc , Chem Commun* **1994**, 2313

[29] D Gust, T A Moore, A L Moore, L Leggett, S Lin, J M DeGraziano, R M Hermant, D Nicodem, P Craig, G R Seely, R A Nieman, *J Phys Chem* **1993**, 97, 7926

[30] R G Little, *J Heterocyclic Chem* **1981**, 18, 129

[31] V Thanabal, V Krishnan, *J Am Chem Soc* **1982**, 104, 3643

[32] M Perree-Fauvet, C Verchere-Beaur, E Tarnaud, G Anneheim-Herbelin, N Bone, A Gaudemer, *Tetrahedron* **1996**, 52, 13569

[33] P Suriyanarayanan, V Krishnan, *Photochem Photobiol* **1983**, 38, 533

[34] K Kadish, N Guo, E V Caemalbecke, A Froiio, R Paolesse, D Monti, P Taglıatesta, T Boschi, L Prodi, F Bolletta, N Zaccheroni, *Inorg Chem* **1998**, 37, 2358

[35] R W Wagner, T E Johnson, J S Lindsey, *J Am Chem* **1996**, 118, 11166.

[36] F Li, S I Yang, Y Ciringh, J Seth, C H Martin III, D L Singh, D Kim, R R Birge, D F Bocian, D Holten, J S Lindsey, *J Am Chem* **1998**, 120, 10001

[37] Z Gross, I Toledano, *J Org Chem* **1994**, 59, 8312

[38] H Dieks, M O Senge, B Kirste, H Kurreck, *J Org Chem* **1997**, 62, 8666

[39] M S Vollmer, F Wurthner, F Effenberger, P Emele, D U Meyer, T Stumpfig, H Port, H C Wolf, *Chem Eur J* **1998**, 4, 260

[40] H Szelinski, D Niethammer, P Tian, H Kurreck, *Tetrahedron* **1996**, 52, 8497

[41] J P Collmann, D A Tyvoll, L L Chng, H T Fish, *J Org Chem* **1995**, 60, 1926

[42] (a) H Volz, G Herb, *Z Naturforsch* **1984**, 39b, 1393 (b) R G Little, *J Heterocyclic Chem* **1981**, 18, 833 (c) Y Kuroda, H Murase, Y Suzuki, H Ogoshi, *Tetrahedron Lett* **1989**, 30, 2411 (d) H Volz, H Schaffer, *Chem Zeit* **1985**, 109, 308 (e) H Volz, M Hassler, H Schaffer, *Z Naturforsch* **1986**, 41b, 1265 (f) H Volz, M Hassler, *Z Naturforsch* **1988**, 43b, 1043

[43] R G Little, *J Heterocyclic Chem* **1981**, 18, 833

[44] S G DiMagno, R A Williams, M J Therien, *J Org Chem* **1994**, 59, 6943

[45] C C Leznoff, P I Svirskaya, *Angew Chem Int Ed Eng* **1978**, 17, 947

[46] M J Gunter, L N Mander, *J Org Chem* **1981**, 46, 4792

[47] A Osuka, T Nagata, F Kobayashi, K Maruyama, *J Heterocyclic Chem* **1990**, 27, 1657

[48] J S Lindsey, I C Schreiman, H C Hsu, P C Kearney, A M Marguerettaz, *J Org Chem* **1987**, 52, 827

[49] H -A Wagenknecht, W -D Woggon, *Angew Chem Int Ed Eng* **1997**, 36, 390

[50] T Nagata, A Osuka, K Maruyama, *J Am Chem Soc* **1990**, 112, 3054

[51] J -F Nierengarten, L Oswald, J -F Nicoud, *Chem Commun* **1998**, 1545

[52] J M Montierth, A G Duran, S H Leung, K M Smith, N E Schore, *Tetrahedron Lett* **2000**, 41, 7423

[53] (a) P S Clezy, G A Smith, *Aust J Chem* **1969**, 22, 239

[54] Q M Wang, D W Bruce, *Synlett* **1995**, 1267

[55] (a) C -H Lee, J S Lindsey, *Tetrahedron* **1994**, 50, 11427 (b) B J Littler, M A Miller, C -H Hung, R W Wagner, D F O'Shea, P D Boyle, J S Lindsey, *J Org Chem* **1999**, 64, 1391

[56] B J Littler, Y Ciringh, J S Lindsey, *J Org Chem* **1999**, 64, 2864

[57] P D Rao, B J Littler, G R Geier III, J S Lindsey, *J Org Chem* **2000**, 65, 1084

[58] R P Brinas, C Bruckner, *Tetrahedron* **2002**, 58, 4375

[59] S Hatscher, M O Senge, *Tetrahedron Lett* **2003**, 44, 157

[60] P D Rao, S Dhanalekshmi, B J Littler, J S Lindsey, *J Org Chem* **2000**, 65, 7323

[61] D M Wallace, K M Smith, *Tetrahedron Lett* **1990**, 31, 7265

[62] All thienylporphyrins synthesised in this study, in particular Zn(II)-5,10,15,20-tetrathien-2-ylporphyrin, were found to slowly decompose when left exposed to the atmosphere and were therefore stored in a refrigerator under an atmosphere of argon upon isolation

[63] (a) K Sonogashira, Y Tohda, N Hagihara, *Tetrahedron Lett* **1975**, 4467 (b) E -I Negishi, L Anastacia, *Chem Rev* **2003**, 103, 1979

[64] I -Y Wu, J T Lin, J Luo, C -S Li, C Tsai, Y S Wen, C -C Hsu, F -F Yeh, S Liou, *Organometallics* **1998**, 17, 2188

[65] W B Austin, N Bilow, W J Kelleghan, K S Y Lau, *J Org Chem* **1981**, 46, 2280

[66] N Ono, H Miyagawa, T Ueta, T Ogawa, H Tani, *J Chem Soc , Perkin Trans 1* **1998**, 1595

[67] A D Adler, F R Longo, F Kampas, J Kim, *J Inorg Nucl Chem* **1970**, 32, 2443

[68] P Bhavana, B Verghese, P Bhyrappa, *Acta Crysta* C 57 **2001**, 252

[69] H L Anderson, *Inorg Chem* **1994**, 33, 972

[70] V A Nadtochenko, N N Denisov, V Yu Gak, N V Abramova, and N M Loim, **1999**, 10, 1900

[71] C J Medforth, R E Haddad, C M Muzzi, N R Dooley, L Jaquinod, D C Shyr, D J Nurco, M M Olmstead, K M Smith, J -G Ma, J A Shelnutt, *Inorg Chem* **2003**, 42, 2227

Chapter 5

Photophysical and Electrochemical Properties of *meso*-Thienylporphyrms

5 1 Aims and objectives

The aim of this chapter was to investigate the influence of the thiophene ring on the photophysical and electrochemical properties of the porphyrin macrocyles, when substituted at the *meso*-position A series of *meso*-tetrathien-2-yl and *meso*-phenyl/thien-2-yl porphyrins were synthesised as described in the previous chapter The photophysical properties of the porphyrins synthesised m this study were investigated by the techniques of UV-vis absorption spectroscopy, steady state fluorescence spectroscopy, laser flash photolysis and time correlated single photon counting Electrochemical analysis was also carried out by cyclic voltammetry

5 2 Literature survey

The diverse applications for porphyrins and their metallated analogues are derived from their stable and rigid structure, which possesses unique photophysical and electrochemical properties At present porphyrin-based systems are widely studied because of their catalytic,[1] therapeutic[2] and potential optoelectronic applications [3] Extended π-conjugated porphyrin systems are increasingly investigated due to their applications towards advanced technologies, which includes nonlinear optical materials [3] The properties of the porphyrin macrocycle in such systems can easily be modulated by appending various chemical moieties onto the periphery of the ring, and also by varying the metal centre Desirable molecular and material properties, such as large hyperpolarisabilities, can therefore be imparted on the porphyrin ring by appropriate substitution and metallation The reversibility of the redox chemistry shown by porphyrins, i e the stability of both their mono- and di- cationic π-radicals, makes them particularly attractive for photoionisation and photoconductive processes Such studies are well documented in the mimicking of the photosynthetic reaction centre by photoinduced electron transfer using porphyrin based electron reservoirs [4]

In the following chapter the ground and excited state photophysical properties of some novel zinc-*meso*-thienylporphyrins are discussed Also, as the HOMO and LUMO energies are closely related to the reversible half-wave oxidation and reduction potentials, the redox properties of thienylporphyrins are also reported, as they can provide an indication of the magnitude of the HOMO-LUMO energy gap in the porphyrin macrocycle There exists an appreciable amount of literature on the synthesis and properties of pseudo-porphyrins and core modified porphyrins containing the thiophene ring, however the following discussion will deal only with porphyrins containing the traditional N_4-core, peripherally substituted with the thiophene ring [5]

Ono et al have synthesised a series of *meso*- and *β*-dodecasubstituted thienylporphyrins in an attempt to alter the redox potentials of the macrocyclic structure by causing ruffling of its planar geometry (fig 5 – 1) [6] It is well established that the HOMO orbital of the porphyrin macrocycle is destabilised upon reduction of its planarity, which thus lowers the HOMO-LUMO energy gap [7] Only the redox properties of the copper(II) metallated

derivatives were reported by Ono et al Substitution of the porphyrin ring with thien-2-yl moieties in the *meso*- and *β*-positions increased the energy of the HOMO orbital as expected, however a stabilisation of the LUMO orbital also occurred resulting in a decreased energy gap of 1 63 V for Cu(II)-2,3,5,7,8,10,12,13,15,17,18,20-dodeca(thien-2-yl)porphyrin and only 1 48 V for Cu(II)-2,3,5,7,8,10,12,13,15,17,18,20-dodeca(5-(methylthio)thien-2-yl)porphyrin HOMO-LUMO energy gaps of 2 34 V and 2 20 V were reported for Cu(II)-TPP and Cu(II)-*meso*-tetra(thien-2-yl)porphyrin Remarkable bathochromic shifts of up to 100 nm of the Soret bands were also observed for these highly distorted porphyrin systems H_2-2,3,5,7,8,10,12,13,15,17,18,20-dodeca(5-(methylthio)thien-2-yl)porphyrin showed a λ_{max} at 520 nm in comparison to 417 nm and 425 nm for H_2TPP and H_2-*meso*-tetra(thien-2-yl)porphyrin

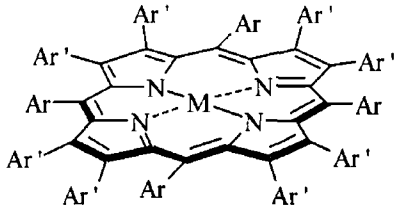

Ar	Ar'	M
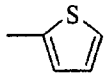	—H	2H
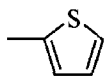	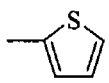	2H, Zn(II), Cu(II), Ni(II)
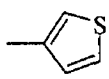	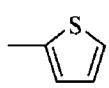	2H, Cu(II)
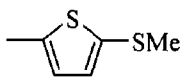	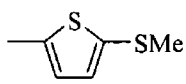	2H, Zn(II), Cu(II)

Fig 5 – 1

A non-planar saddled conformation (fig 5 – 2a) was proposed for these dodecaarylporphyin systems by Ono et al based on low temperature ^{1}H-NMR studies A wave conformation of the porphine ring was later confirmed for Zn-*meso*-tetra(thien-2-yl)porphyrm (fig 5 – 2b) [8]

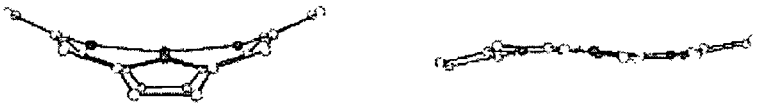

(a) (b)

Fig 5 – 2 (a) Saddled and (b) wave conformations of the porphine ring system

Meso-tetra(thien-3-yl)porphyrin has also since been reported by Bhyrappa and Bhavana [9] In the latter study the electrochemical and UV-vis absorption properties of *meso*-tetra(thien-3-yl)porphyrin and *meso*-tetra(thien-2-yl)porphyrin aswell as their zinc(II) and copper(II) complexes were reported (fig 5 – 3) A decrease in the HOMO-LUMO energy gap was observed for *meso*-tetra(thien-2-yl)porphyrin with respect to *meso*-tetra(thien-3-yl)porphyrin and tetraphenylporphyrin (H_2TPP) *Meso*-tetra(thien-2-yl)porphyrin shows a HOMO-LUMO energy gap of 1 98 V compared to 2 18 V and 3 23 V for *meso*-tetra(3-thienyl)porphyrin and tetraphenylporphyrin (H_2TPP) respectively Similar trends were observed for the metallated analogues with the Zn(II)- and Cu(II)-*meso*-tetra(thien-3-yl)porphyrin redox potentials approaching those of Zn(II)- and Cu(II)-TPP Moderate bathochromic shifts were also observed for the Soret and Q bands in the UV-vis spectra of the thienyl porphyrins of *ca* 5 – 10 nm with *meso*-tetra(thien-2-yl)porphyrin again showing the more pronounced perturbation with respect to the tetraphenylporphyrins These changes brought about in the UV-vis spectra aswell as in the redox properties of the compounds studied were attributed to inductive effects of the thienyl groups as opposed to increased conjugation of the porphyrin π-system

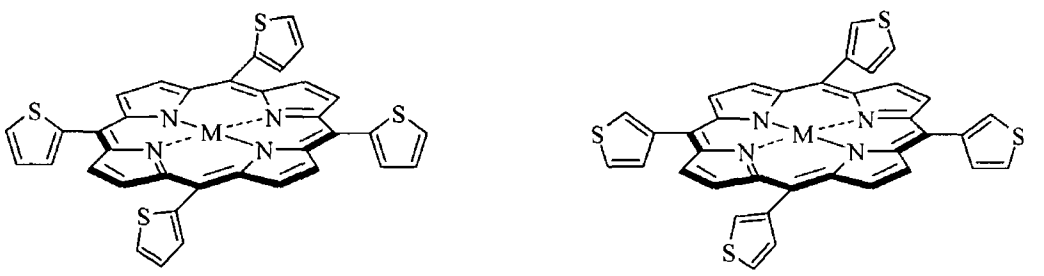

M = 2H, Zn(II), Cu(II)

Fig 5 – 3

Medforth et al have investigated the barriers for rotation of *meso*-aryl groups in uncrowded *meso*-tetraaryl and 2,3,7,8,12,13,17,18-octaaryl porphyrins aswell as in highly substituted very non-planar crowded 2,3,5,7,8,10,12,13,15,17,18,20-dodecaaryl and 5,10,15,20-tetraryl-2,3,7,8,12,13,17,18-octaphenyl porphyrins [10] Some intermediately crowded systems, such as 2,3-diaryl-5,10,15,20-tetraphenylporphyrms, were also investigated The effect of metal size was investigated by using complexes with a small, nickel(II), and large, zinc(II), metal while the effect of protonation was examined using the free base porphyrin (M = 2H) and the porphyrin dication (M = $4H^{2+}$) Medforth and coworkers synthesised a number of thien-3-yl substituted porphyrins for this study (fig 5 – 4) A lower aryl-porphyrin rotational barrier of up to 20 kJmol ^{1} was observed for the thien-3-yl substituted porphyrins in comparison to the phenyl substituted analogues

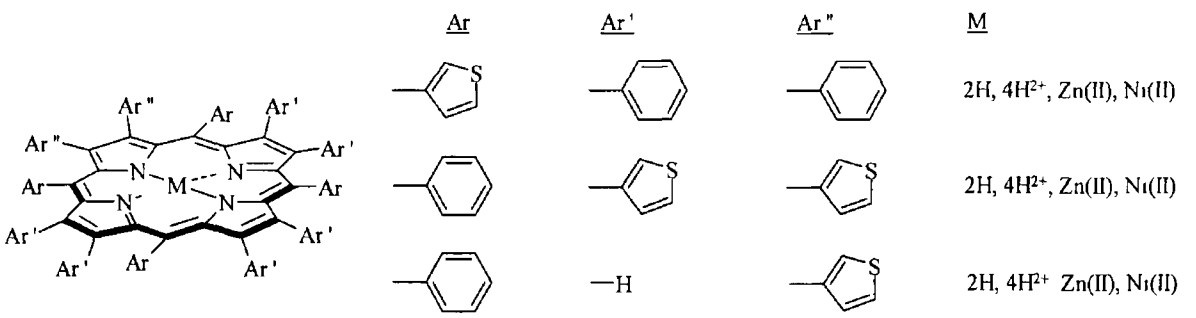

Fig 5 – 4

There have been a number of reports in the literature of photoelectrochemical cells containing oligothiophene backbones with porphyrin photosensitisers Conjugated polythiophene derivatives have been extensively studied in part due to their chemical and thermal stability and their synthetic accessibility, but also due to their electroluminescent properties and potential applications in non-linear optics and molecular wire technologies [11] Ohgothiophene based photovoltaic cells show excellent energy conversion efficiencies upon monochromatic irradiation, however their efficiencies are poor under polychromatic irradiation thus the incorporation of an efficient photosensitiser is required [11]

Recently Chen et al have investigated the photoelectrochemical properties of *trans*-5,15-bis((2',2'' 5'',2'''-terthiophene)-3''-yl)-2,8,12,18-tetra-*n*-butyl-3,7,13,17-tetra-methylporphyrin (fig 5 – 5a) when copolymerised with 2',2'' 5'',2'''-terthiophene (fig 5 – 5b) [12] Significant enhancements in the energy conversion efficiencies were observed in comparison to the poly(2',2'' 5'',2'''-terthiophene) homopolymer due to the introduction of the porphyrin moiety A small increase was also observed in the efficiency of the copolymer after soaking in a zinc(II) solution due to metallation of 25 % of the porphyrin units on the polymer backbone

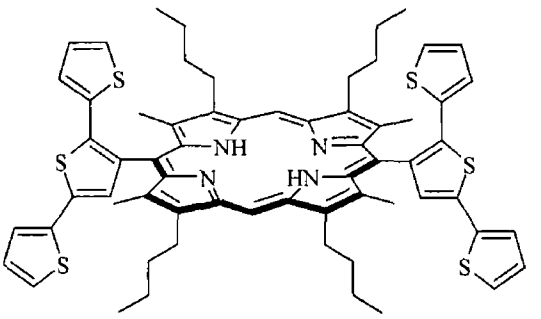

(a) (b)

Fig 5 – 5

Schaferling and Bauerle have investigated the properties of some metallated tetraphenylporphyrins covalently linked to bi- and terthiophenes units via a pentyloxy spacer (fig 5 – 6) [13] Cyclic voltammetry and UV-vis absorption studies confirmed a lack of electronic communication between the two chromophores due to the pentyloxy spacer Polymerisation of the monomer units was achieved by electrochemical oxidation The polymers displayed a combination of the reversible redox waves of the conducting polythiophene backbone and the porphyrin redox centres This is in contrast to a similar study by Ballarin et al who observed irreversible oxidation of the porphyrin moiety in a copolymer of 2,2'-bithiophene and a tetraphenylporphyrin-alkoxy- monothiophene unit [14] Schaferling and Bauerle did not observe reduction of the metal centres or of the porphyrin units at negative potentials due to the insulating/semiconducting character of the polythiophene backbone in this potential region

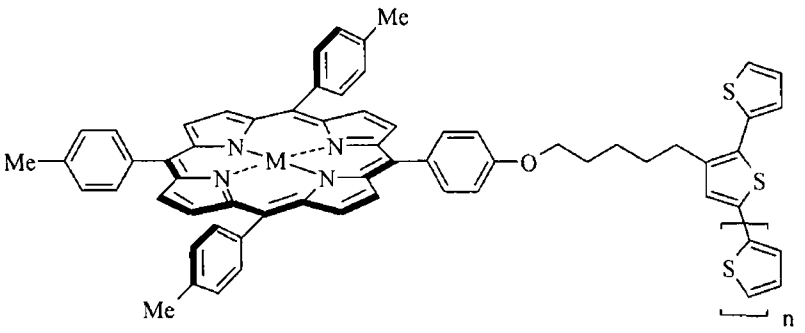

n = 0, M = Zn(II), Ni(II), Co(II), Fe(III)Cl, Mn(III)Cl
n = 1, M = Ni(II), Co(II), Fe(III)Cl

Fig 5 - 6

Segawa et al have synthesised a number of phosphorous(V)-tetraphenylporphyrin derivatives where monothiophene, 2,2'-bisthiophene and 2',2'' 5'',2'''-terthiophene units are linked axially through a phosphorous centre (fig 5 – 7) [15]

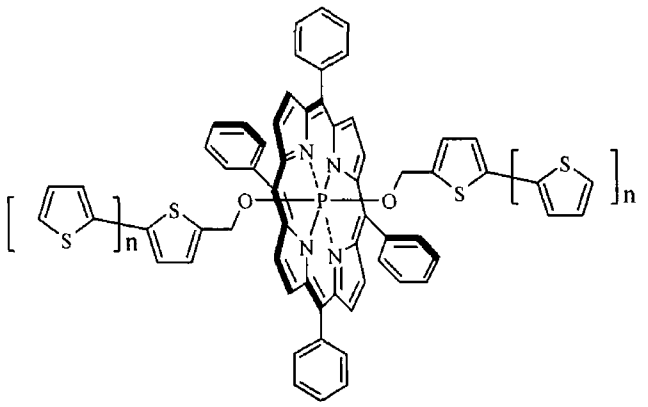

n = 0, 1, 2

Fig 5 – 7

The fluorescence quantum yields and lifetimes in these systems are dependent on the number of thiophene units in the system A slight red shift was observed on increasing the number of thiophene units aswell as a decrease in the fluorescence lifetimes and quantum yields Surprisingly the 2,2'-bisthiophene system showed a larger decrease in fluorescence lifetime and quantum yield than the 2',2'' 5'',2'''-terthiophene analogue

The conductivity of the 2,2'-bis- and 2',2'' 5'',2'''-terthiophene systems was investigated following the formation of one-dimensional polymers via electrochemical oxidation (fig 5 – 8) [16] The mono-thiophene system did not polymerise

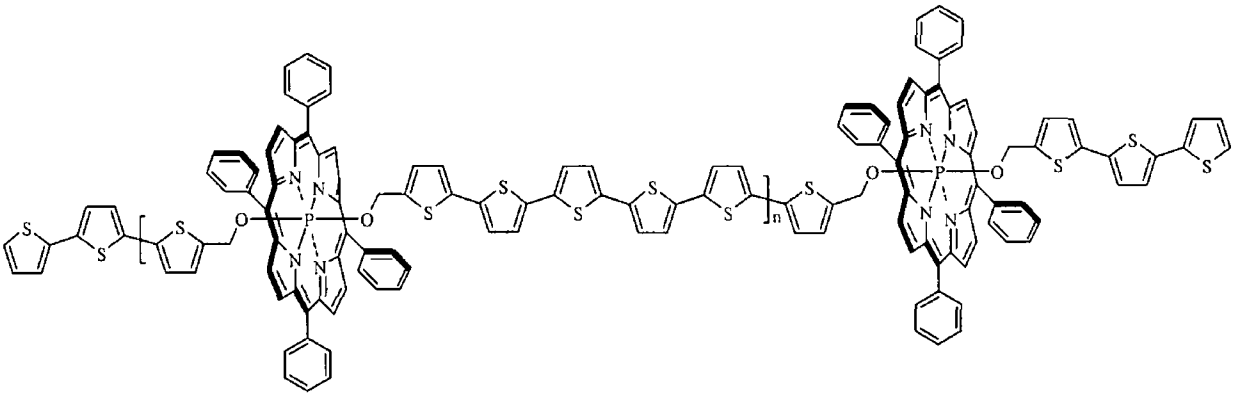

Fig 5 - 8

In the latter study zinc(II) and palladium(II) metalled *meso*-tetra(2,2'-bisthiophene)porphyrin and *meso*-tetra(2',2'' 5'',2'''-terthiophene)porphyrin were also synthesised and polymerised via electrochemical oxidation The proposed quasi two-dimensional structures of the Zn(II)- and Pd(II) *meso*-tetra(2',2'' 5'',2'''-terthiophene)porphyrin polymers are shown m fig 5 – 9

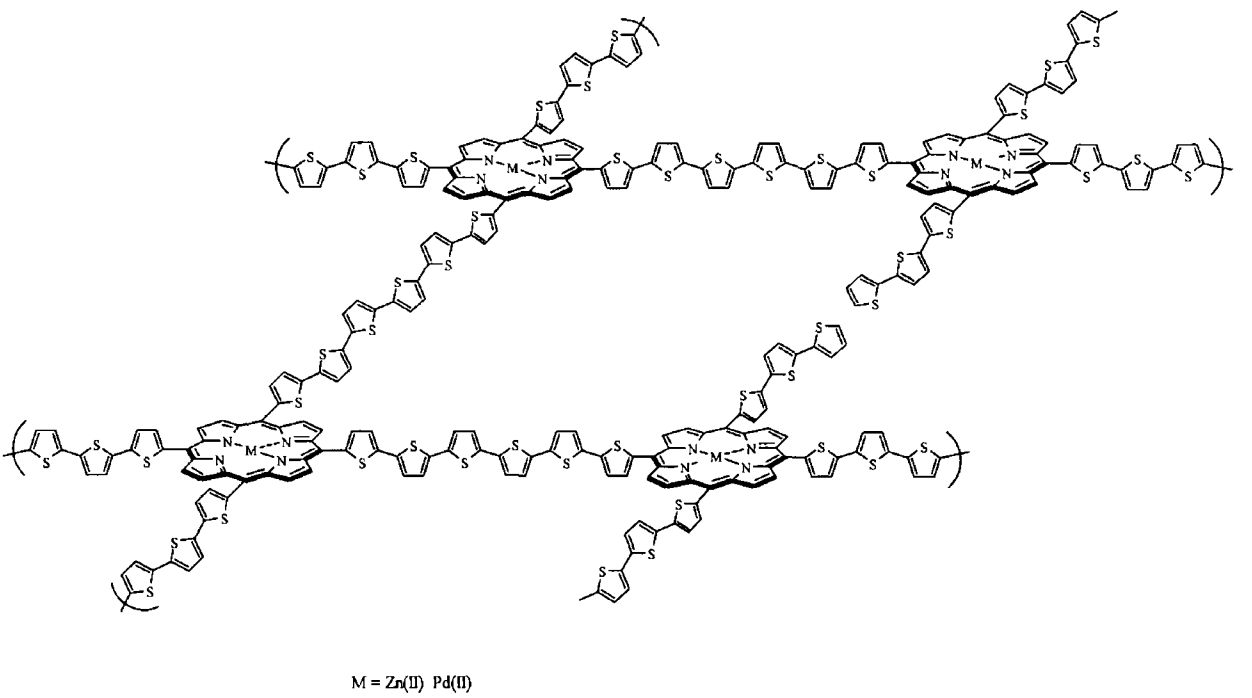

Fig 5 – 9

Ever increasing attention is being paid to π-conjugated metalloporphyrin polymeric systems where the porphyrin unit is incorporated into the backbone of the polymer as opposed to being a peripheral substituent [12 13] Yamamoto et al have successfully carried out the synthesis of one-dimensional π-conjugated zinc(II)-porphyrin polymers with *meso*-linked aryl and ethynyl spacers via a $Ni(cod)_2(bpy)$ coupling reaction and Stille, Sonogashira palladium coupling techniques [17] The porphyrin monomers were directly coupled to form homopolymers and also coupled to aryl units to form copolymers The thiophene-based systems are shown in fig 5 – 10

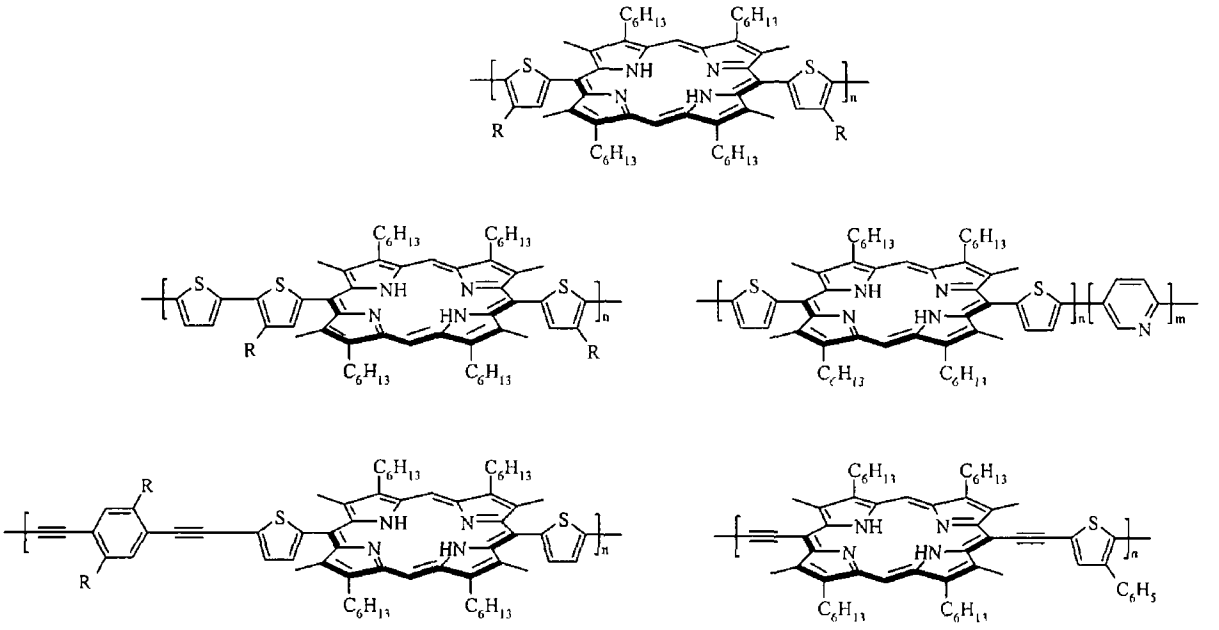

R = C_6H_{13} R = H $OC_{12}H_{25}$

Fig 5 - 10

Electronic coupling between the adjacent porphyrin units in the polymer backbone resulted in a bathochromic shift and splitting of the Soret band in the UV-vis spectra The polymers with an ethynyl spacer directly bound to the *meso*-position of the porphyrin ring showed the largest shift with the lower energy Soret band occurring at *ca* 490 nm

Li et al have recently reported the synthesis of H_2- and Zn(II)-5,15-bis(acetylene-4-(ethylenedioxy)thiophene)-10,20-bis(4-methoxycarbonylphenyl)porphyrins and their hydrophilic disodium dicarboxylate derivatives (fig 5 – 11a) [18] Polymerisation of the free base and the zinc(II) derivatives to their respective homopolymers was carried out by electrochemical oxidation The zinc metallated monomers were also successfully polymerised by chemical oxidation with iron(III) chloride Again, a large red shift and splitting of the Soret band was observed on formation of the conjugated polymers The 4-methoxycarbonyl zinc(II) monomer has a Soret band at 460 nm in dichloromethane whereas its polymeric derivative has two Soret absorptions at 434, 570 nm in dimethylsulfoxide Images of the sodium derivative of the zinc(II) polymer (fig 5 – 11b) were recorded by transmission electron microscopy (TEM) and atomic force microscopy (AFM) The formation of uniform porphyrin wires of up to 2 5 mm in length (*ca* 1200 monomer units) was confirmed, with a thickness of about 2 nm corresponding to the width of the porphyrin unit The zinc/sodium derivatised polymer showed efficient conductivity on oxidation to the porphyrin monocation species

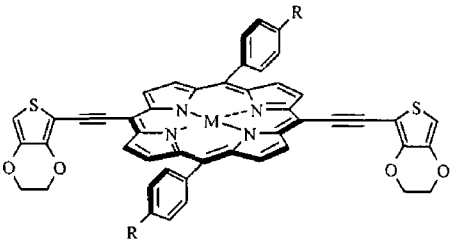

(a)

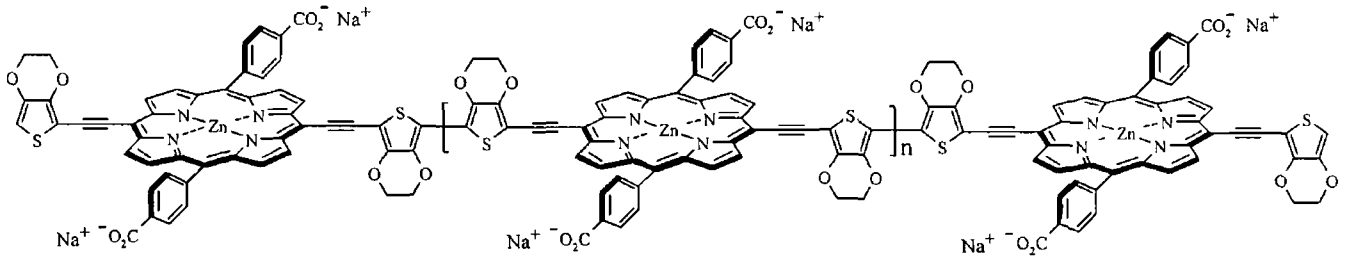

(b)

Fig 5 - 11

Crossley and Prashar reported the design and synthesis of a series of thiophene appended porphyrin systems where the thiophene ring is fused to the periphery of the macrocycle via two aza linkages (fig 5 – 12) [19] The aim of their work was to attach the highly conjugated porphyrins systems to a gold surface through the sulphur atom of the fused thiophene ring however these experiments have not been reported in the literature to date

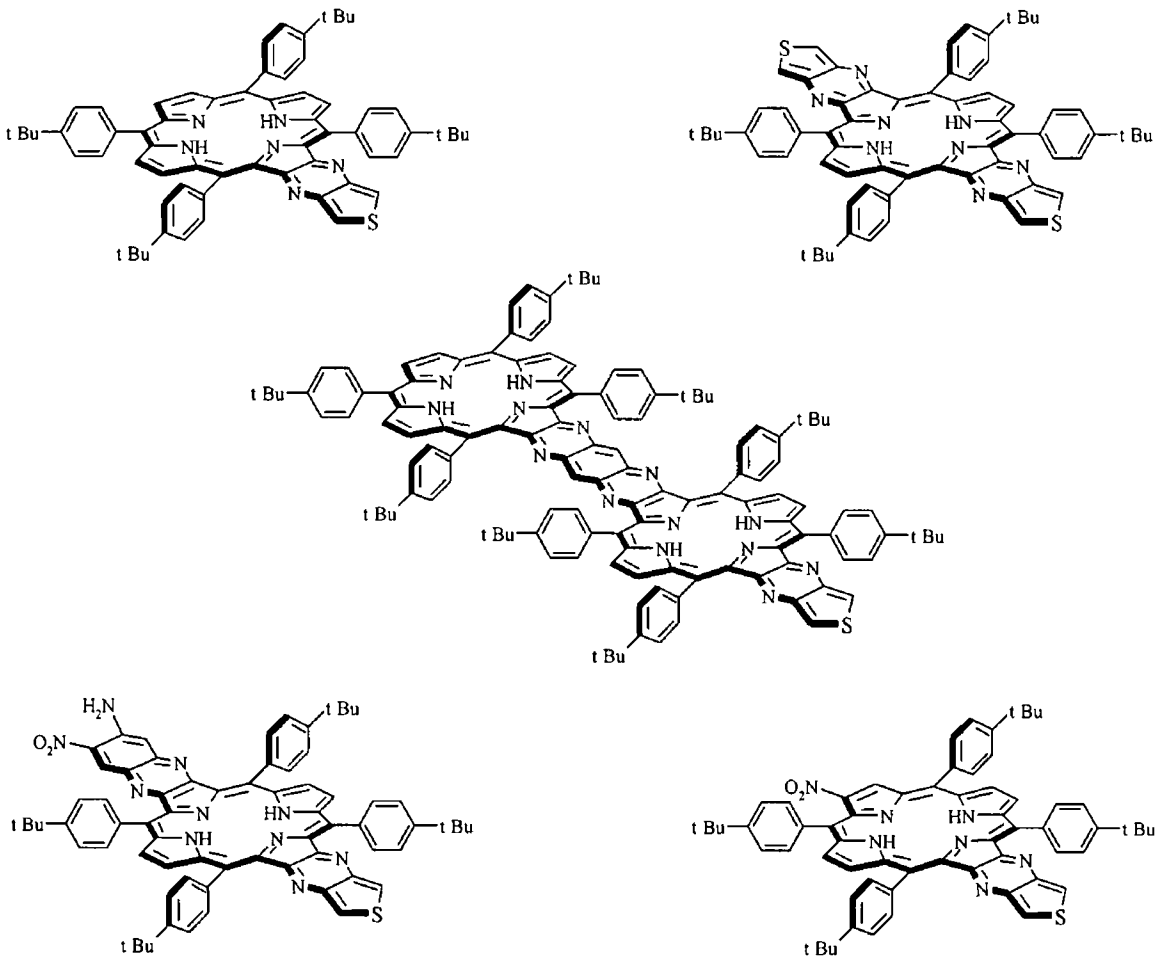

Fig 5 - 12

Ono et al have synthesised a series of naphtoporphyrin systems by the condensation of isomdole derivatives [20] Among the systems studied were the thiophene derivatives shown in figure 5 – 13(a) The extended π-system of these compounds resulted in red shifted Soret and Q bands The diprotonated species shows the most pronounced shift with λ_{max} of 462 and 659 nm The zinc(II) and nickel(II) derivatives showed a reduced HOMO-LUMO energy gap of 26 and 29 mV realative to ZnTPP A similar fused porphyrin-thiophene system has also been reported by Callot et al (fig 5 – 13b) [21]

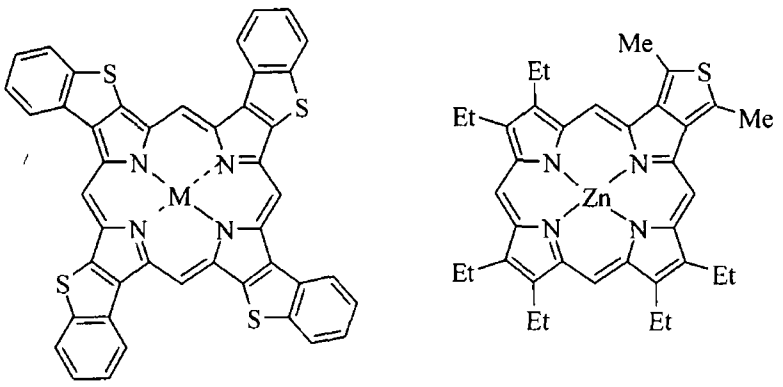

M = 2H, Zn(II), Ni(II), $4H^{2+}$

(a) (b)

Fig 5 – 13

Odebel et al [22] reported that a strong electronic communication exists in a zinc/free-base porphyrin dyad mediated by a 5,5'''-bis(ethynyl)-3,3'''-bis(octyl)-2,2' 5',2'' 5'',2'''-quaterthiophene unit The distance between the two macrocycles is 28 Å Highly efficient energy transfer was observed for all of the zinc/free-base dyad systems studied (fig 5 – 14), however an increased rate was observed with enhanced ground-state electronic communication between the two porphyrin units, when ethynyl units were used at the *meso*-position of both porphyrin rings Vinyl or ethynyl substitution at the *meso*-position both gave rise to enhanced coupling between the two porphyrin units in comparison to the directly linked quaterthiophene bridge which only displayed weak ground state interaction due to decoupling of the porphyrin units

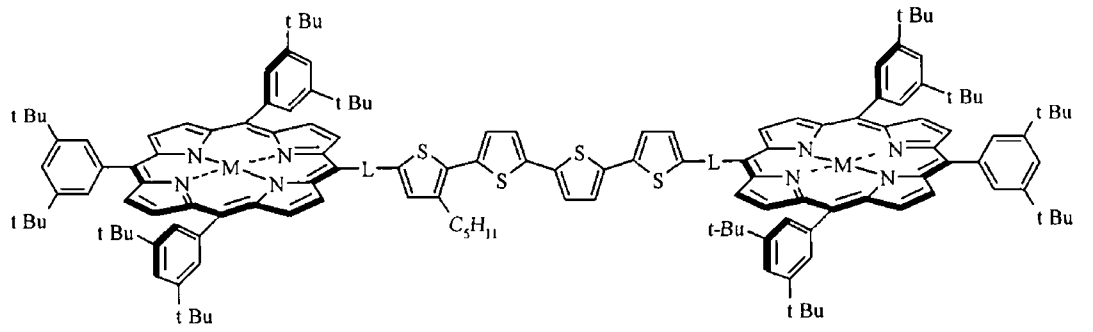

M = 2H, 2H, Zn(II), 2H, Zn(II), Zn(II)

L = direct link, 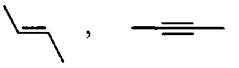

Fig 5 - 14

Wurthner et al have reported efficient intramolecular energy transfer from an anthryl donor moiety to a porphyrin acceptor via terminally substituted oligothiophene bridging units in a large series of compounds (fig 5 – 15) [23]

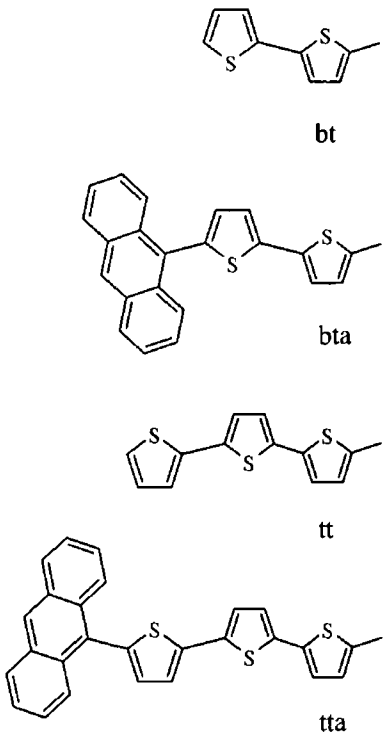

	R^1	R^2	R^3	R^4
(i)	bt	bt	bt	bt
(ii)	tt	tt	tt	tt
(iii)	bta	n-pentyl	n-pentyl	n-pentyl
(iv)	bta	n-pentyl	bta	n-pentyl
(v)	bta	bta	n-pentyl	n-pentyl
(vi)	bta	bta	bta	n-pentyl
(vii)	bta	bta	bta	bta
(viii)	tta	n-pentyl	n-pentyl	n-pentyl
(ix)	tta	n-pentyl	tta	n-pentyl
(x)	tta	tta	n-pentyl	n-pentyl
(xi)	tta	tta	tta	n-pentyl
(xii)	tta	tta	tta	tta

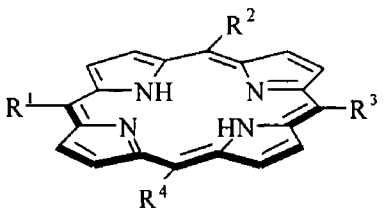

Fig 5 – 15

Only slight vibronic coupling was observed in the UV-vis spectrum between the anthryl donor and the oligothiophene bridge whose conjugated π-networks are almost perpendicular in the ground state It is therefore possible to selectively excite the anthryl unit with almost 90 % efficiency for the mono-anthryl systems and even greater efficiency for the higher substituted systems

Temperature dependent steady-state and time-resolved fluorescence studies suggest that, upon excitation of the anthryl moiety, the π-π interaction between the anthryl ring and the oligothiophene unit is increased. The authors show however that the rate of energy transfer from the anthryl donor to the porphyrin acceptor takes place on a faster timescale than this conformational change (< 10 ns vs. 10 ns) resulting in emission solely from the porphyrin S_1 excited state with quantum efficiencies of almost 100 % for all systems studied (triplet emissions were not reported).

Similar results were found on increasing the length of the oligothiophene chain to a 3,3''''-di-*n*-pentyl-2,2':5',2'':5'',2''':5''',2'''':5'''',2''''-quinquethiophene unit (fig. 5 – 16).[24] *n*-Pentyl groups were incorporated into the oligothiophene chain to increase their solubility.

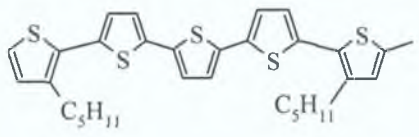

qt

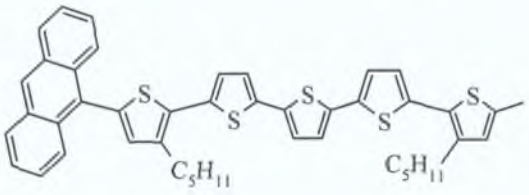

qta

	R^1	R^2	R^3	R^4
(i)	qt	n-pentyl	n-pentyl	n-pentyl
(ii)	qt	n-pentyl	qt	n-pentyl
(iii)	qt	qt	n-pentyl	n-pentyl
(iv)	qt	qt	qt	n-pentyl
(vi)	qta	n-pentyl	n-pentyl	n-pentyl
(vi)	qta	n-pentyl	qta	n-pentyl
(vii)	qta	qta	n-pentyl	n-pentyl
(viii)	qta	qta	qta	n-pentyl
(ix)	qta	qta	qta	qta

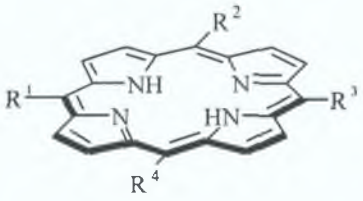

Fig. 5 - 16

A red shift and broadening of the porphyrin absorption and emission spectra was observed for all compounds and attributed to coupling of the porphyrin π-system with the conjugated oligothiophene chains. The mechanism of energy transfer, i.e. Forster or Dexter, could not be clearly defined for these systems. The authors do suggest however

that due to vibromc coupling, energy is also transferred from the anthryl donor to the porphyrin acceptor via an intramolecular relaxation process mediated by the oligothiophene chain On comparing these result with similar polyene based systems Wurthner et al concluded that oligothiopenes are far superior with regard to mediating energy transfer and show a greater potential for application in molecular electronics

Liddell et al have reported the synthesis and photophysical properties of a photonic switch consisting of a dithienylethene (DTE)-tetraphenylporphyrin-fullerene (C_{60}) triad molecule (fig 5 – 17) [25] The dyad molecule consisting of the DTE and porphyrin units was also synthesised to investigate the affect of the DTE moiety on the excited state dynamics of the porphyrin chromophore

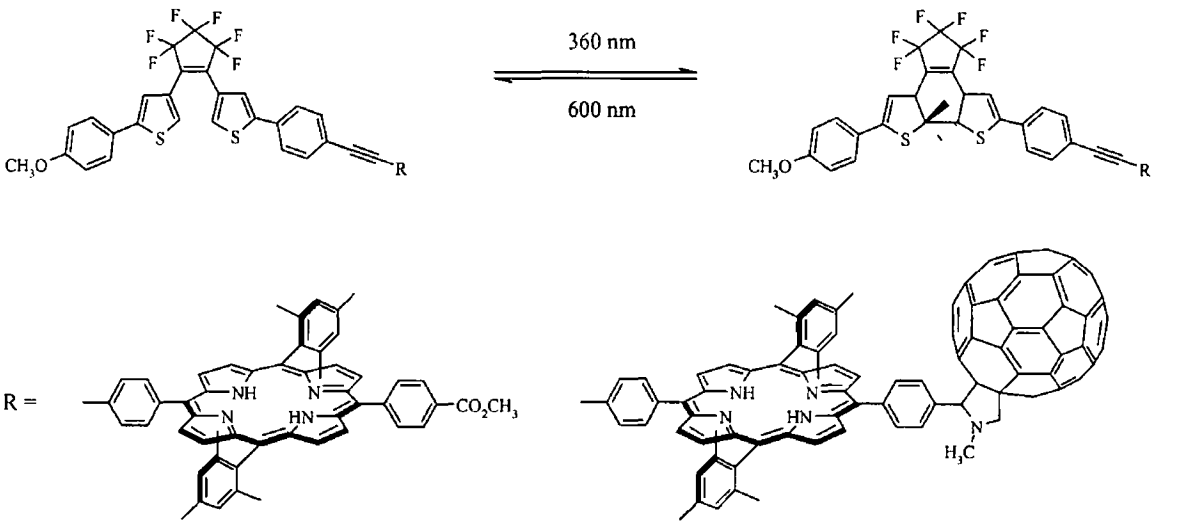

Fig 5 – 17

When the DTE is in its open configuration in the triad system the porphyrin excited state donates an electron to C_{60} with a quantum yield of unity forming the charge separated species DTE-P^{+}-C_{60}^{-} Irradiation of the triad at 360 nm converts the DTE moiety to its closed configuration In this form the porphyrin excited state is quenched by singlet-singlet energy transfer to the closed DTE moiety in 2 3 ps, and electron transfer to the fullerene acceptor is reduced by a factor of 10 Irradiation of the triad at 600 nm regenerates the original state with an open DTE moiety The open and closed forms of the dyad displayed fluorescence from the porphyrin (10 5 ns) and DTE (~ 3 ps) moieties

respectively The very short-lived fluorescence from the closed form of the dyad corresponds well the closed form of the triad system

In the following chapter the photophysical properties of some novel thien-2-yl porphyrins are investigated by laser flash photolysis and by steady state and time resolved fluorescence techniques Electrochemical data are also presented

5 3 Experimental and results

5 3 1 UV-vis absorption spectra

All UV-vis spectra were measured in spectroscopic grade solvents at room temperature on a Hewlett Packard 8452A-photodiode array spectrometer using a 1 cm quartz cell

Porphyrin	Soret (nm)	FWHM (nm)	Q bands (nm)
ZnTPP	422 (2 55)[a]	12	548 (9 72)[b]
			588 (1 90)
ZnTThP	430 (2 84)	15	556 (9 48)
			600 (1 97)
ZnTBrThP	434 (2 82)	17	558 (8 57)
			600 (2 20)
ZnTEtThP	436 (2 42)	20	560 (10 32)
			600 (2 64)
ZnTTMSEtThP	438 (2 21)	22	560 (11 8)
			606 (3 48)
ZnEtThTPP	426 (2 28)	14	552 (9 51)
			592 (1 97)
ZnDEtThDPP	430 (2 76)	15	554 (9 29)
			596 (2 87)
ZnTEtThPP	432 (2 96)	18	556 (8 96)
			598 (2 46)
ZnTMSEtThTPP	426 (2 18)	14	552 (9 62)
			594 (2 01)
ZnDTMSEtThDPP	430 (2 37)	16	554 (9 64)
			598 (2 78)
ZnTTMSEtThPP	434 (2 23)	19	556 (8 92)
			600 (2 94)
ZnPald	428 (2 60)	17	552 (9 81)
			594 (1 87)

Table 5 - 1 UV-vis absorption data of porphyrins recorded in toluene [a] Values in brackets refer to ε (x 10^5 $M^{-1}cm^{-1}$) [b] Values in brackets refer to ε (x 10^3 $M^{-1}cm^{-1}$)

Solvent	Soret (nm)	FWHM (nm)	Q bands (nm)
Pentane	420	15	548, 582
Toluene	428	17	552, 594
DMSO	432	19	562, 606

Table 5 - 2 Solvatochromic behaviour of ZnPald in pentane, toluene and DMSO

5 3 2 Steady state and time resolved fluorescence studies

Steady state fluorescence measurements were carried out on a Perkin Elmer LS50 luminescence spectrometer at room temperature An excitation wavelength of 550 nm was used for all quantum yield measurements Excitation and emission slits were both set at 10 nm Time resolved fluorescence studies were were carried out at the Central Laser Facility, Rutherford Appleton Laboratories [26]

Porphyrin	λ_{max} (nm)	Φ_F	$^1\tau$ (ns)
ZnTPP	596, 647	0 033	1 98
ZnTThP	617, 657	0 010	1 36 / 0 51 *
ZnTBrThP	636	0 006	0 52
ZnTEtThP	639, ~ 650(sh)	0 014	0 74
ZnTTMSEtThP	629, ~ 650(sh)	0 018	0 76
ZnEtThTPP	606, 651	0 040	1 92
ZnDEtThDPP	614, 652	0 038	1 56
ZnTEtThPP	618, 650	0 026	1 10
ZnTMSEtThTPP	607, 651	0 046	1 94
ZnDTMSEtThDPP	615, ~ 647(sh)	0 042	1 48
ZnTTMSEtThPP	622, ~ 643(sh)	0 028	1 07

Table 5 - 3 Fluorescence maxima, quantum yields (Φ_F) and singlet lifetimes ($^1\tau$) of ZnTPP, ZnTThP, ZnTBrThP and the various 5-trimethylsilylethynylthien-2-yl and 5-ethynylthien-2-yl substituted porphyrins in toluene at room temperature

* Dual emission was observed for ZnTThP with an almost 1 1 ratio, 1 36 ns (52%) 0 51 ns (48%)

Solvent	λ_{max} (nm)	Φ_F	$^1\tau$ (ns)
Pentane	604, 653	0 047	1 77
Toluene	614, 644(sh)	0 043	1 92
DMSO	623, 655(sh)	0 037	1 20

Table 5 - 4 Fluorescence maxima, quantum yields (Φ_F) and singlet lifetimes ($^1\tau$) of ZnPald in pentane, toluene and DMSO

5 3 3 Laser flash photolysis studies

Transient absorption measurements following laser flash photolysis at 355 and 532 nm were carried out in toluene under one atmosphere of argon at room temperature with a typical sample absorbance of 0 05 (± 0 01) AU All transient species observed were independent of excitation wavelength and formed within the lifetime of the laser pulse (*ca* 10 ns) All porphyrins studied gave rise to a transient signal, with a maximum absorbance *ca* 470 - 500 nm This transient species is attributed to the lowest energy $^3(\pi$-$\pi^*)$ triplet excited state of the porphyrin chromophores A depletion of the parent compound was also observed in the Soret region of the spectrum *ca* 400 - 435 nm The lifetimes of the triplet excited states ($^3\tau$) are given in table 5 - 5 Table 5 - 6 gives the results of a solvatochromic study of ZnPald carried out in pentane, toluene and DMSO

Porphyrin	$^3\tau$ (μs)
ZnTPP	24
ZnTThP	20
ZnTBrThP	7
ZnTEtThP	13
ZnTTMSEtThP	12
ZnEtThTPP	15
ZnDEtThDPP	12
ZnTEtThPP	8
ZnTMSEtThTPP	16
ZnDTMSEtThDPP	11
ZnTTMSEtThPP	11

Table 5 - 5 Triplet lifetimes ($^3\tau$) of ZnTPP, ZnTThP, ZnTBrThP and the various 5-trimethylsilylethynylthien-2-yl and 5-ethynylthien-2-yl substituted porphyrins recorded in toluene at room temperature

Solvent	$^3\tau$ (μs)
Pentane	6
Toluene	6
DMSO	5

Table 5 - 6 Triplet lifetimes ($^3\tau$) of ZnPald recorded in pentane, toluene and DMSO at room temperature

5 3 4 Electrochemistry

All cyclic voltammetry measurements were carried out under an atmosphere of argon at room temperature with a conventional three-electrode configuration consisting of a glassy carbon working electrode (2 mm diameter), a platinum wire auxiliary electrode and a saturated calomel reference electrode The solvent used in all experiments was dichloromethane, which was obtained in spectrophotometric grade from Sigma-Aldrich and used as received The supporting electrolyte was 0 1 M tetra-*n*-butylammonium tetrafluoroborate, which was purchased from Fluka Chemicals The half-wave potential ($E_{1/2}$) values were determined as (E_{pa} + E_{pc})/2, where E_{pa} and E_{pc} are the anodic and cathodic peak potentials respectively (it is assumed that $E_{1/2} \cong E^0$ for all measurements) All potentials are quoted in reference to the ferrocene/ferrocenium couple Table 5 - 7 contains a list of the redox potentials recorded Where $E_{1/2}$ could not be calculated due to irreversible oxidation or reduction processes E_{pa} and E_{pc} are quoted respectively

Porphyrin	oxidation		
	1st	2nd	
	$E_{1/2}$	$E_{1/2}$	
ZnTPP	0 344	0 664	-
ZnTThP	0 429	0 625	-
ZnTBrThP	0 613	0 522	-
ZnTEtThP	0 485	0 694	-
ZnTTMSEtThP	0 491	0 655	-
ZnEtThTPP	0 412	0 674	-
ZnDEtThDPP	0 457	0 692	-
ZnTEtThPP	0 492	0 700	-
ZnTMSEtThTPP	0 420	0 674	-
ZnDTMSEtThDPP	0 442	0 674	-
ZnTTMSEtThPP	0 443	0 664	-
ZnPald	0 421	0 681	-

reduction						
1st			2nd			3rd
E_{pc}	E_{pa}	$E_{1/2}$	E_{pc}	E_{pa}	$E_{1/2}$	E_{pc}
1 907	-1 786	-1 847	-2 283	-2 139	-2 211	~
1 787	-1 637	-1 712	-2 131	-1 964	-2 048	~
1 664	~	~	-1 939	~	~	~
1 699	~	~	-2 184	~	~	~
1 690[r]	-1 659	-1 675	-2 028	~	~	~
1 865	~	~	-2 056	~	~	~
1 766	~	~	-2 088	~	~	~
1 722	~	~	-2 099	~	~	~
1 862	~	~	-2 041	~	~	-2 204
1 743	~	~	-2 056	~	~	-2 304
1 725	~	~	-2 017	~	~	-2 402
1 809	-1 836	-1 823	-2 198	~	~	~

Table 5 – 7

5.4 Discussion

5.4.1 Zinc(II)-*meso*-tetrathien-2-ylporphyrins

There have been mixed reports in the literature of whether there exists electronic communication between the porphyrin ring and thienyl substituents via the *meso*-position of the macrocycle.[9, 23, 24, 27] The systems investigated in this study suggest that direct attachment of the aromatic thiophene ring at the *meso*-position of the porphyrin ring does lead to electronic interaction between the two π-systems, which can be enhanced through appropriate substitution. Fig. 5 – 17 shows an overlay of the UV-vis spectra of ZnTPP and the various zinc(II)-*meso*-tetrathienylporphyrins investigated in this study.

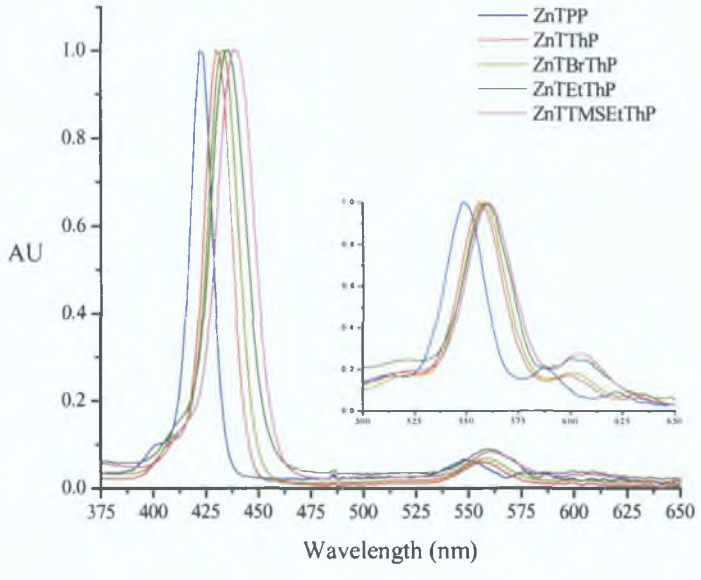

Fig. 5 – 17: UV-vis spectra of ZnTPP, ZnTThP, ZnTBrThP, ZnTEtThP and ZnTTMSEtThP in toluene at room temperature. All spectra have been normalised at their λ_{max}.

By varying the substituent on the 5-position of the thiophene ring a red shift can be induced in the Soret absorption of the porphyrin ring. The Soret band is red shifted by 8 nm for ZnTThP, 12 nm for ZnTBrThP, 14 nm for ZnTEtThP and 16 nm for ZnTTMSEtThP with respect to ZnTPP (see table 5 – 1 for λ_{max}). Such a strong shift would not be anticipated on the basis of an inductive effect of the thienyl substituents

alone [28] Also, as the Soret band is shifted to lower energy the FWHM increases This suggests increased electronic coupling between the π-systems of the porphyrin and thienyl rings Similar changes are observed for the Q bands A slight increase in the relative intensity of the Q(0,0) band occurs as the electronic communication between the porphyrin and thienyl rings is increased The ratio of the intensity of Q(0,0)/Q(1,0) bands increases in the order ZnTThP < ZnTBrThP < ZnTEtThP < ZnTTMSEtThP According to Gouterman's four orbital model, the intensity of the Q(0,0) transition is dependent on the energy difference between the porphyrin $a_{1u} \rightarrow e_g$ and $a_{2u} \rightarrow e_g$ transitions and thus the relative energies of the a_{1u} and a_{2u} orbitals [29]

An overlay of the fluorescence emission spectra of ZnTPP and the *meso*-tetrathienylporphyrins recorded in toluene is shown in fig 5 – 18 The first striking feature of these spectra is that the emission bands which arise from the $Q(1,0)^*$ and $Q(0,0)^*$ excited states are almost completely unresolved for the *meso*-tetrathienylporphyrins due the large red shift of the higher energy $Q(0,0)^*$ band The $Q(1,0)^*$ band, for all thienyl porphyrins, only shows a slight red shift when compared to ZnTPP (see table 5 – 3 for emission data)

The fluorescence quantum yields for each of the *meso*-tetrathienyl porphyrins are reduced relative to ZnTPP This is expected due to the presence of the four sulphur atoms on the periphery of the ring and especially for the ZnTBrThP molecule, which in addition contains four heavy bromine atoms The phosphorescence quantum yield is dependent on the rate of intersystem crossing (k_{isc}) which heavy atoms, such as sulphur and bromine, through enhanced spin-orbit coupling, promote Unfortunately the phosphorescence quantum yields are not available for these systems due to the instrumental limitation of the detection range

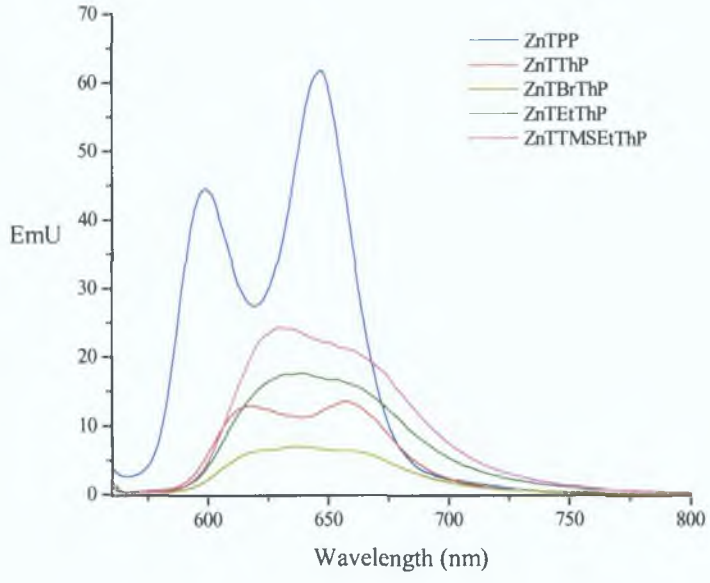

Fig. 5 – 18: Luminescence spectra (λ_{exc} = 550 nm, abs. = 0.2 at 550 nm) of ZnTPP, ZnTThP, ZnTBrThP, ZnTEtThP and ZnTTMSEtThP recorded in toluene at room temperature.

The fluorescence lifetimes recorded in toluene are also included in table 5 – 3. A lifetime of 1.98 (± 0.02) ns was observed for ZnTPP, which is in excellent agreement with the literature reported value of 2.0 ns.[30] The *meso*-tetrathienylporphyrins all show a slightly reduced fluorescence lifetime relative to ZnTPP, which is attributed to an increase in k_{isc} for these systems. Increased orbital overlap of the thienyl substituents, in comparison to *meso*-phenyl groups,[31] with the a_{2u} orbital of the porphyrin and also a stabilisation of the e_g orbitals (see table 5 – 7 for reduction potentials) should lead to an increased shift of electron density onto the thienyl rings upon excitation. This effect serves to increase spin-orbit coupling and k_{isc}, due to the presence of four heavy sulphur atoms on the periphery of the ring, and also four heavy bromine atoms in the case of ZnTBrThP. The trend seen in the decreasing fluorescence lifetimes corresponds to the effects seen in the fluorescence quantum yields for these systems.[32] As expected, ZnTBrThP displays the shortest lifetime of 0.52 (± 0.01) ns. Typical fluorescence decays observed for ZnTBrThP and ZnTTMSEtThP are shown in fig. 5 – 19.

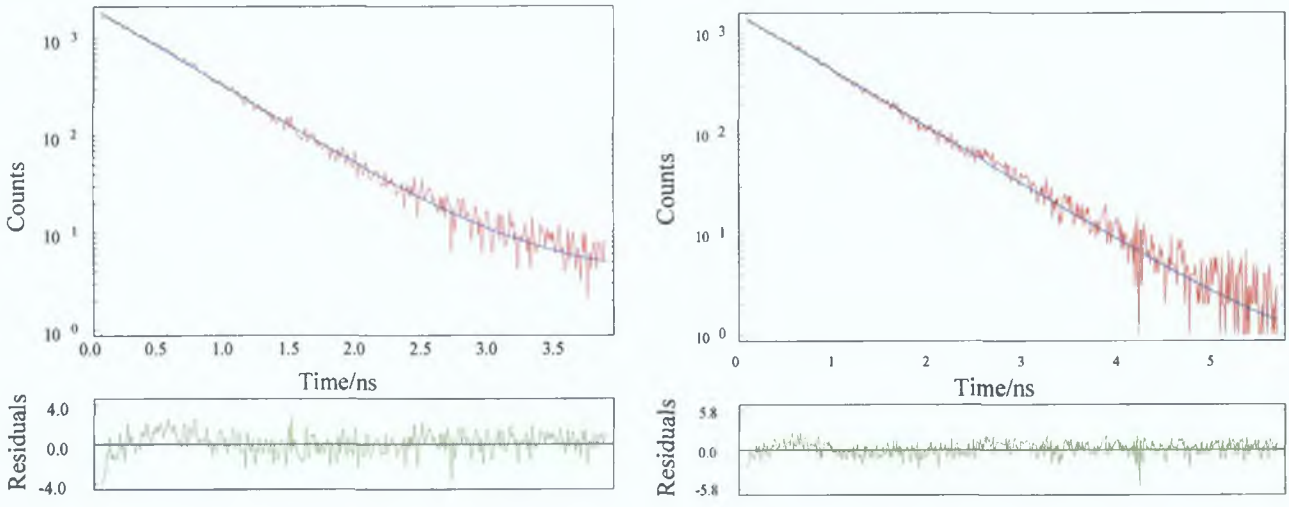

(a) (b)

Fig. 5 – 19: Typical fluorescence decays observed for (a) ZnTBrThP (τ = 0.52 ns) and (b) ZnTTMSEtThP (τ = 0.74 ns) at 636 and 629 nm respectively, following excitation at 435 nm.

The triplet lifetimes of the porphyrins were measured by laser flash photolysis in toluene at room temperature following excitation at both 355 and 532 nm excitation under an atmosphere of argon. The profile of the transient difference absorption spectra and the lifetimes of the transient signals recorded were all independent of the excitation wavelength. The transient absorption difference spectra are attributed to the lowest $^3(\pi$-$\pi^*)$ porphyrin triplet excited state. Second-order kinetics have previously been used to determine the triplet decay of similar porphyrin complexes due to competition between first-order decay and bimolecular triplet-triplet annihilation.[33] All of the transient signals recorded in this study fit well with mono-exponential kinetics indicating unimolecular decay. A lifetime of 24 (± 0.02) μs was observed for ZnTPP. A decrease in the triplet lifetime was observed for the *meso*-tetrathienylporphyrins (table 5 – 7). The shortest lifetime is again displayed by ZnTBrThP of 7 (± 0.07) μs. Transient absorption difference spectra of ZnTPP and ZnTTMSEtThP are shown in fig. 5 – 20 and fig. 5 – 21 respectively. An overlay of transient difference absorption spectra of ZnTPP, ZnTThP, ZnTBrThP, ZnTEtThP and ZnTTMSEtThP are shown in fig. 5 - 22.

The absorption difference spectrum of ZnTPP is characterised by a weak absorption from 300 – 390 nm in the UV region and from 435 – 538 nm in the visible with a λ_{max} at 470 nm Saturation of the detector occurs between 400 - 435 nm, which corresponds to the Soret band of the parent species Isosbestic points are present at 400, 435 and 538 nm Only weak absorptions are observed at longer wavelengths

The *meso*-tetrathienylporphyrins show a red shifted transient absorption difference spectrum relative to ZnTPP with the λ_{max} occurring at *ca* 490 - 500 nm Also, there is a substantial increase in the lower energy absorption which stretches from *ca* 580 nm right out to 750 nm (i e the detection limit of the instrument) and possibly into the near-IR region of the spectrum These characteristic excited state properties suggest a relatively strong increase in the electronic coupling of the porphyrin ring and the thienyl π-network upon excitation The broad low-energy excited state absorbance is possibly due to charge transfer of electron density from the central porphyrin macrocycle to the surrounding thienyl rings Indeed this low energy absorbance is most prominent for the 5-(trimethylsilylethynyl)thien-2-yl and 5-ethynylthien-2-yl substituted porphyrins, which would be expected to show the strongest electron accepting ability due to the ethynyl moieties An overlay of the transient decay signals for all of the *meso*-tetrathienylporphyrins is shown in fig 5 – 23

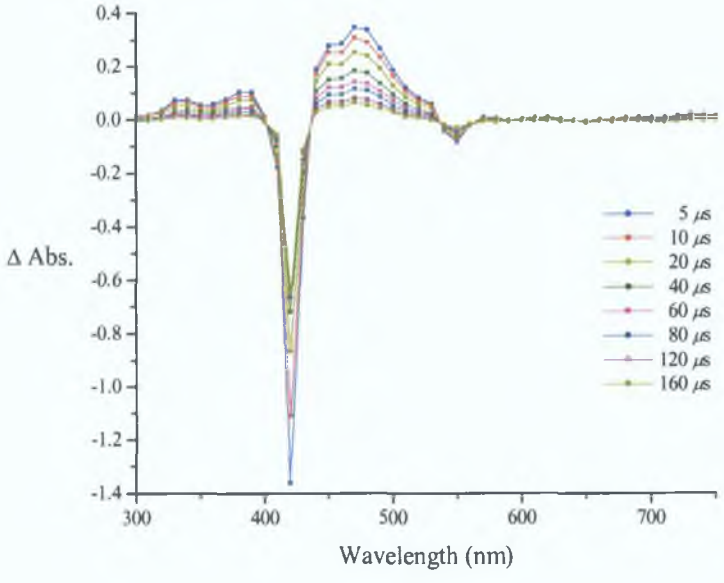

Fig. 5 – 20: Transient absorption difference spectra of ZnTPP in toluene following 532 nm excitation under 1 atm of argon.

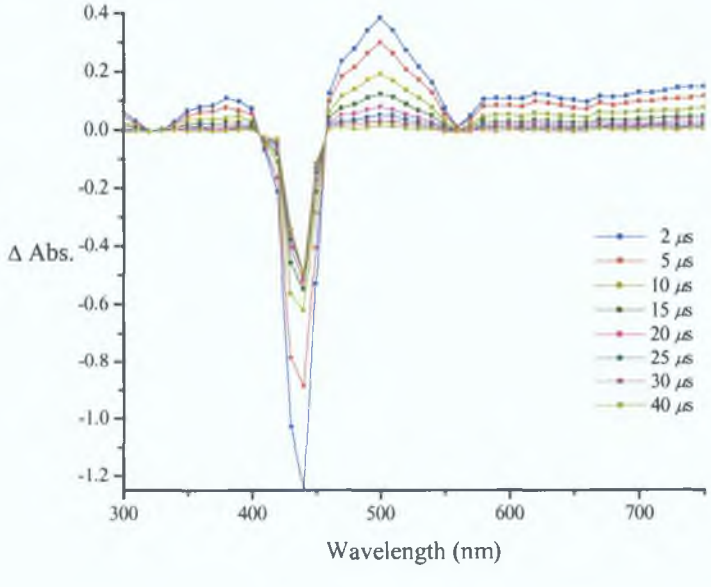

Fig. 5 – 21: Transient difference absorption spectra of ZnTTMSEtThP following 532 nm excitation in toluene under 1 atm of argon.

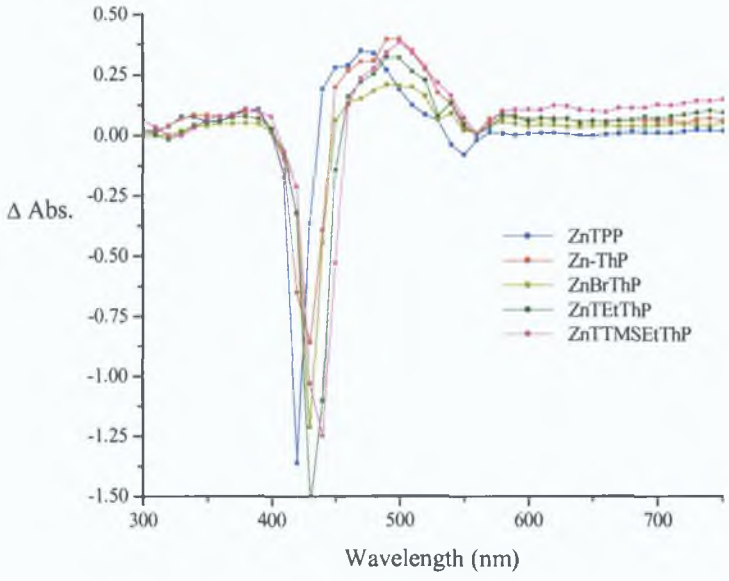

Fig. 5 – 22: An overlay of transient absorption difference spectra of ZnTPP, ZnTThP, ZnTBrThP, ZnTEtThP and ZnTTMSEtThP following 532 nm excitation in toluene under 1 atm of argon. Each plot is taken 2 μs after the laser pulse and all spectra have been recorded with an equal absorbance at 532 nm (~ 0.05 AU).

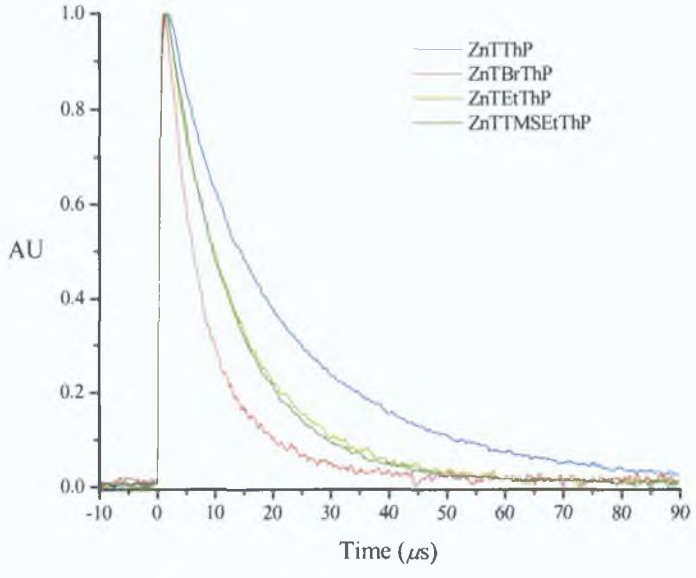

Fig. 5 – 23: An overlay of the transient signals recorded at 500 nm, following excitation of ZnTThP, ZnTBrThP, ZnTEtThP and ZnTTMSEtThP in toluene under 1 atm of argon. All signals have been normalised at their absorption maxima.

Substitution at the *meso* position of the porphyrin ring also has a significant effect on the electrochemistry of the porphyrin ring The two $E_{1/2}$ values observed at positive potential (table 5 – 7) correspond to the first and second reversible oxidations of the porphyrin ring, which result in the formation of the porphyrin cation radical and porphyrin dication respectively There are generally two redox couples also present at negative potential corresponding to the formation of the porphyrin anion radical and dianion species All of the *meso*-tetrathienyl compounds studied show two reversible redox processes at positive potential however, in contrast to ZnTPP, only ZnTThP and ZnTTMSEtThP show a reversible first reduction on formation of the radical anion None of the *meso*-tetrathienyl compounds show reversible formation of the diamon species

All of the *meso*-tetrathienylporphyrins show an increase in their first oxidation relative to ZnTPP indicating a stabilisation of the a_{2u} (HOMO) orbital of the porphyrin ring in these systems ZnTBrThP displays the largest effect with a $E_{1/2}$ value 269 mV greater than the first oxidation of ZnTPP The e_g (LUMO) orbitals are also stabilised upon *meso*-thienyl substitution relative to ZnTPP, however due to the irreversibility of the majority of these processes the HOMO-LUMO energy gap can only be calculated for ZnTThP and ZnTTMSEtThP These compounds show a reduced HOMO-LUMO energy gap of 35 and 70 mV respectively relative to ZnTPP ZnTBrThP again shows the largest effect with a decrease in the potential of the first cathodic reduction peak of over 240 mV ZnTThP, ZnTEtThP and ZnTTMSEtThP each show a decrease in the first cathodic reduction peak by 85, 141 and 147 mV respectively The ethynyl appended systems show a greater perturbation of the ground and $^3(\pi\text{-}\pi^*)$ excited state UV-vis spectra as they have a less stabilised a_{2u} orbital and they also have a greater ability to delocalise the electron density of the porphine ring Fig 5 – 25 shows an overlay of the cyclic voltammograms recorded for ZnTThP, ZnTBrThP and ZnTEtThP

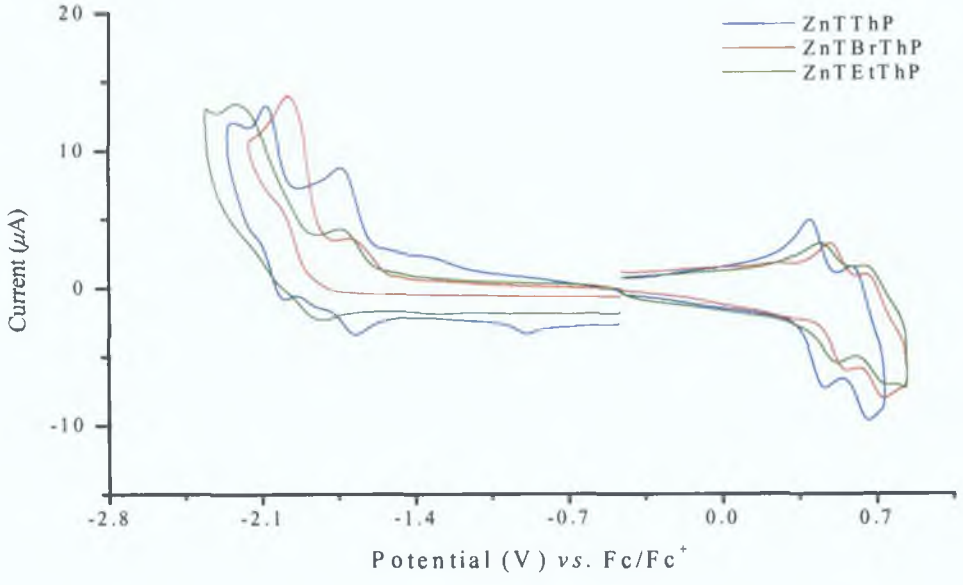
ZnTThP
ZnTBrThP
ZnTEtThP
20
10
0
-10
Current (μA)
-2.8
-2.1
-1.4
-0.7
0.0
0.7
Potential (V) vs. Fc/Fc+

Fig. 5 - 25

5.4.2 *meso*-5-(trimethylsilylethynyl)thien-2-yl and *meso*-5-ethynylthien-2-yl substituted porphyrins

Given the differences observed from having four symmetrical *meso*-thienyl groups on the periphery of the porphine ring a study was then undertaken to investigate the properties of mono-, di- and tri-substituted analogues. As the strongest changes were observed for ZnTTMSEtThP and its deprotected ethynyl analogue ZnTEtThP, these substituents were chosen for the study. [note: the di(5-(trimethylsilylethynyl)thien-2-yl) and di(5-ethynylthien-2-yl) derivatives contain a mixture of *cis*- and *trans*- structural isomers as they are inseparable by chromatography[34]]. Fig. 5 – 26 shows an overlay of UV-vis spectra of ZnTPP and the various *meso*-5-(trimethylsilylethynyl)thien-2-yl substituted porphyrins recorded in toluene.

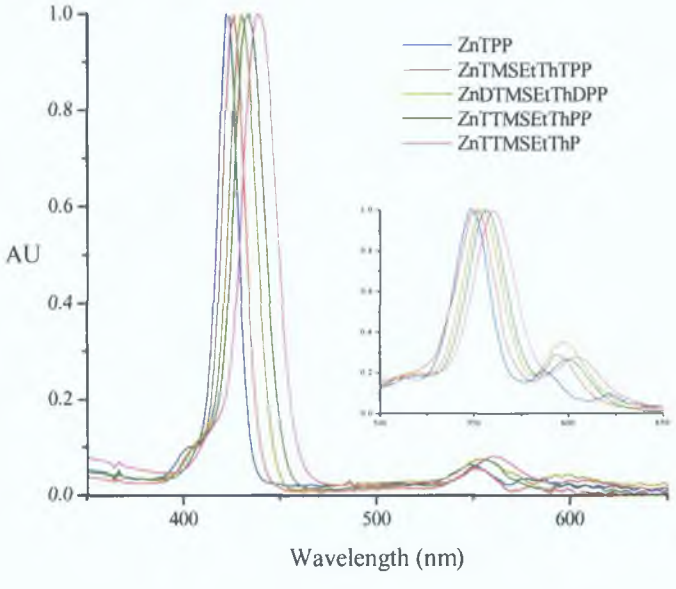

Fig. 5 – 26: UV-vis absorption spectra of ZnTPP, ZnTMSEtThTPP, ZnDTMSEtThDPP, ZnTTMSEtThPP and ZnTTMSEtThP, recorded in toluene at room temperature. All spectra have been normalised at their absorption maxima

By increasing the number of thienyl substituents at the *meso*-position of the porphyrin ring a red shift is induced in the Soret absorption (table 5 – 1). The Soret band is red shifted by 4 nm for every 5-(trimethylsilylethynyl)thien-2-yl group resulting in a total shift of 16 nm for ZnTTMSEtThP with respect to ZnTPP (see table 5 – 1 for λ_{max}). There is also a corresponding increase in the FWHM of the Soret band associated with

increasing thienyl substitution. These trends in results relate well with those observed for the *meso*-tetrathienylporphyrins in the previous section and indicate an increased electronic coupling between the π-systems of the porphyrin and thienyl rings on increased thienyl substitution. Analogous red shifts are observed in the Q band region.

Fig. 5 – 27 shows an overlay of the fluorescence emission spectra for the *meso*-5-(trimethylsilylethynyl)thien-2-yl substituted porphyrins. Similar spectra are observed for the *meso*-5-ethynylthien-2-yl substituted porphyrins with a slight decrease in quantum yield (see table 5 – 3 for emission data). These spectra differ to that of ZnTPP in that there is an increase in intensity of the higher energy $Q(0,0)^*$ emission band relative to the $Q(1,0)^*$ emission band. The mono- and di-thienyl porphyrins each show an increased quantum yield of fluorescence with respect to ZnTPP which can be attributed to this increased $Q(0,0)^*$ emission. As the number of thienyl substituents on the ring increases the intensity of both emission bands decreases with a concurrent red shift of their λ_{max}. This is expected in lieu of the properties of the *meso*-tetrathienylporphyrins. The higher energy $Q(0,0)^*$ band shows a much stronger red shift and decrease in intensity ultimately resulting in an overlap of both bands which appear to have equal intensity for the tetrathienyl compounds.

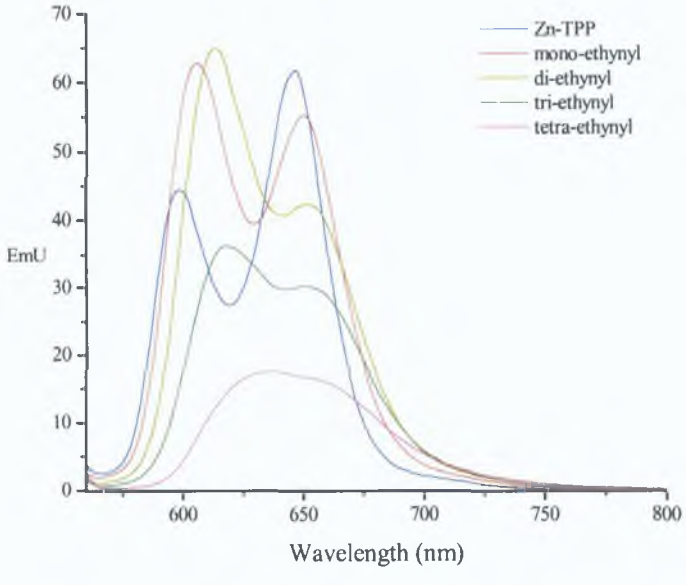

Fig. 5 – 27: Fluorescence spectra (λ_{exc} = 550 nm) of ZnTPP, ZnEtThTPP, ZnDEtThDPP, ZnTEtThPP and ZnTEtThPP, recorded in toluene at room temperature.

It is possible that a shift of electron density onto the thienyl ring upon excitation results in decreased spin-orbit coupling and k_{isc} for ZnTMSEtThTPP relative to ZnTPP, i.e. one heavy sulphur atom on the periphery of the ring will have a decreased spin-orbit coupling in comparison to the central metal. However, spin-orbit coupling and k_{isc} are increased as the number of thienyl units is increased thus becoming more efficient than for the central zinc atom of ZnTPP. This hypothesis is backed up by the trend seen in the decreasing fluorescence lifetimes and quantum yields observed upon increasing the number of thienyl substituents.

The fluorescence quantum yield decreases upon increased *meso*-thienyl substitution, which is expected due to the increase in the number of heavy sulphur atoms in the conjugated system. A plot of 'number of thienyl substituents *vs* quantum yield' (fig. 5 – 28) illustrates how the fluorescence quantum yield decreases with increasing thienyl substitution for both the 5-(trimethylsilylethynyl)thien-2-yl and 5-ethynylthien-2-yl *meso*-substituted porphyrins. A reduction in the fluorescence lifetime is observed on increasing thienyl substitution of the porphine ring (table 5 – 3) with the tetrathienyl compounds displaying the shortest lifetimes.

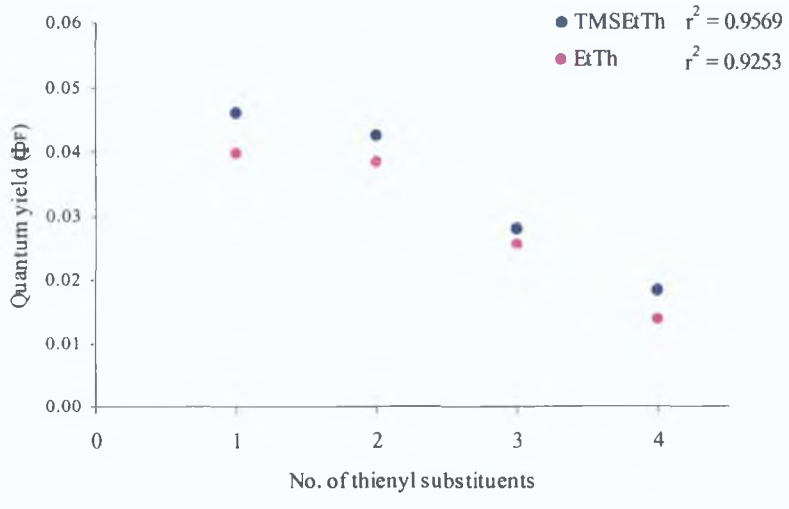

Fig. 5 – 28: The above graph illustrates how the fluorescence quantum yield decreases with increasing thienyl substitution for both the *meso*-5-(trimethylsilylethynyl)thien-2-yl and *meso*-5-ethynylthien-2-yl substituted porphyrins.

The triplet lifetimes of the porphyrins were measured by laser flash photolysis in toluene at room temperature following excitation at both 355 and 532 nm excitation under an atmosphere of argon. As with the *meso*-tetrathienyl porphyrins, all of the transient signals obtained are assigned to the lowest $^3(\pi\text{-}\pi^*)$ porphyrin triplet excited state. These transient signals are independent of the excitation wavelength and fit well with mono-exponential kinetics indicating unimolecular decay. A decrease in the triplet lifetime is observed on increasing thienyl substitution of the porphine ring (table 5 – 7). Shown in fig. 5 – 29 are the transient absorption difference spectra for ZnTPP, ZnEtThTPP, ZnDEtThDPP, ZnTEtThPP and ZnTEtThP.

The difference absorption spectra of the triplet-excited thienylporphyrins are all red shifted relative to ZnTPP with the λ_{max} occurring at *ca.* 480, 480, 490 and 500 nm for the mono-, di-, tri- and tetra- substituted compounds respectively (λ_{max} does not vary between the 5-(trimethylsilylethynyl)thien-2-yl and 5-ethynylthien-2-yl series). The low energy absorption at > 580 nm is present for these thienyl porphyrins as was observed previously for the *meso*-tetrathienylporphyrins. This low energy absorption becomes more pronounced on increasing thienyl substitution on the porphine ring thus further suggesting the possibility of it being a charge transfer band. These results suggest an increase in the electronic coupling of the excited porphyrin ring with the peripheral thienyl substituents on increasing *meso*-thienyl substitution.

Analogous to the *meso*-tetrathienyl compounds studied, the mono-, di- and tri-thienyl porphyrins show two reversible redox processes at positive potential however, none of them display reversible formation of the radical anion or dianion species. Enhanced stabilisation of both the HOMO and LUMO orbitals is observed on increasing thienyl substitution. This stabilisation is more pronounced for the LUMO orbitals. This decrease in reduction potential on increasing thienyl substitution is thus the dominant affect which determines the red shift of the Soret band in the ground state UV-vis spectrum and may also be involved in the charge transfer transition observed in the $^3(\pi\text{-}\pi^*)$ excited state difference absorption spectrum. A third irreversible reduction process is observed for the mono-, di- and tri- 5-(trimethylsilylethynyl)thien-2-yl substituted porphyrins. This reduction was not observed for the tetra-substituted analogue, however it may be occurring at too low a potential to be observed under the conditions used. This peak has

not been assigned. A typical cyclic voltammogram of ZnDTMSEtThDPP is shown in fig. 5 – 30.

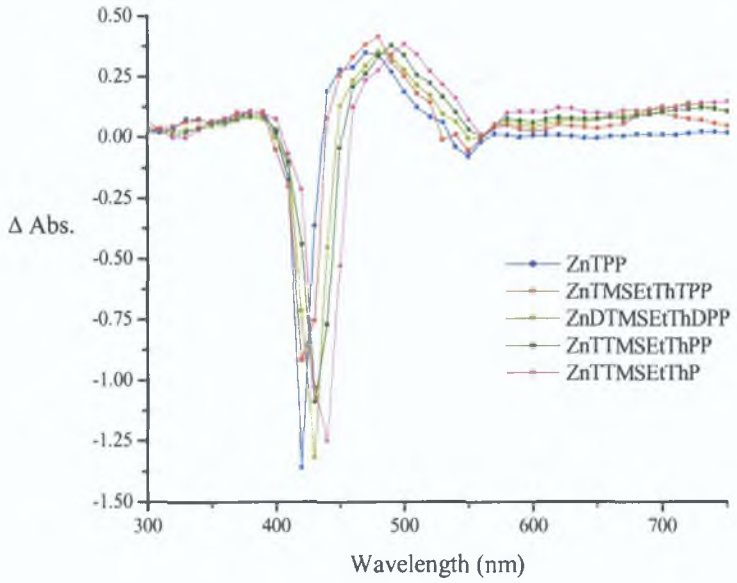

Fig. 5 – 29: An overlay of the transient absorption difference spectra of ZnTPP, ZnTMSEtThTPP, ZnDTMSEtThDPP, ZnTTMSEtThPP and ZnTTMSEtThP following laser excitation at 532 nm under 1 atm of argon. Each plot is taken 2 μs after the laser pulse and all spectra have been recorded in toluene with equal absorbance at 532 nm (~ 0.05 AU).

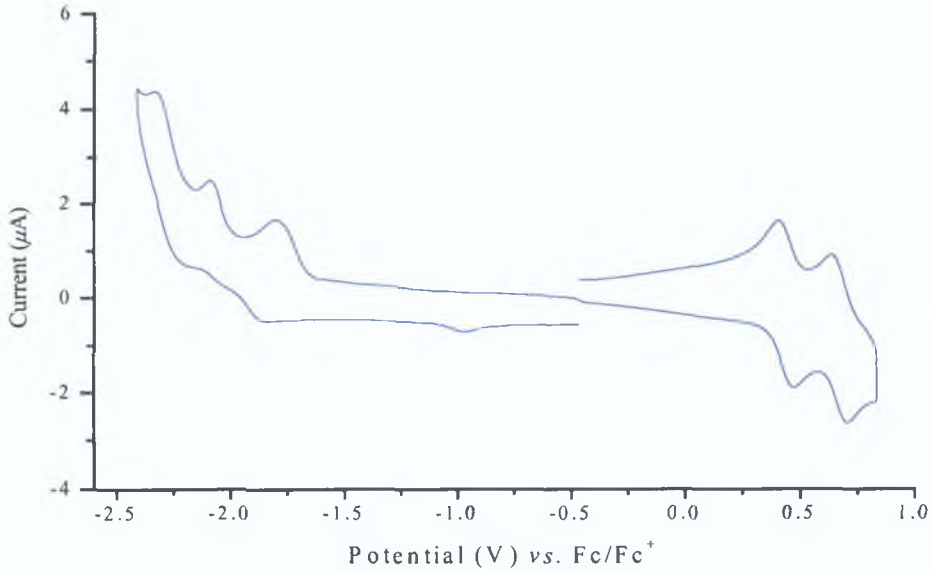

Fig. 5 – 30: Cyclic voltammogram of ZnDTMSEtThDPP

5.4.3 zinc(II)-5-(5'-(5''-ethynylthiophene-2'-carboxaldehyde)thien-2'-yl)-10,15,20-triphenylporphyrin (ZnPald)

Zinc(II)-5-(5'-ethynylthien-2'-yl)-10,15,20-triphenylporphyrin was successfully coupled at the terminal ethynyl moiety to 5-bromo-2-thiophenecarboxaldehyde via Sonogashira coupling giving the porphyrin zinc(II)-5-(5'-(5''-ethynylthiophene-2'-carboxaldehyde)thien-2'-yl)-10,15,20-triphenylporphyrin (ZnPald) in high yield.[34] Figure 5 – 31 shows an overlay of the UV-vis absorption spectra of ZnPald recorded in pentane, toluene and DMSO. Sizeable red shifts are observed in the UV-vis spectra for the Soret band aswell as a concurrent increase in the FWHM on going from pentane (λ_{max} = 420 nm, FWHM = 15 nm) to toluene (λ_{max} = 428 nm, FWHM, =17 nm) and DMSO (λ_{max} = 432 nm, FWHM = 19 nm). Similarly red shifts are observed in the Q band region of the spectrum on going from pentane ($\lambda_{Q(1,0)}$ = 548 nm $\lambda_{Q(0,0)}$ = 582 nm) to toluene ($\lambda_{Q(1,0)}$ = 552 nm $\lambda_{Q(0,0)}$ = 594 nm) to DMSO ($\lambda_{Q(1,0)}$ = 562 nm $\lambda_{Q(0,0)}$ = 606 nm). An increase in the ratio of absorbance of Q(0,0)/Q(1,0) is also observed indicating a solvent dependency on the energy difference between the $a_{1u} \rightarrow e_g$ and $a_{2u} \rightarrow e_g$ transitions.

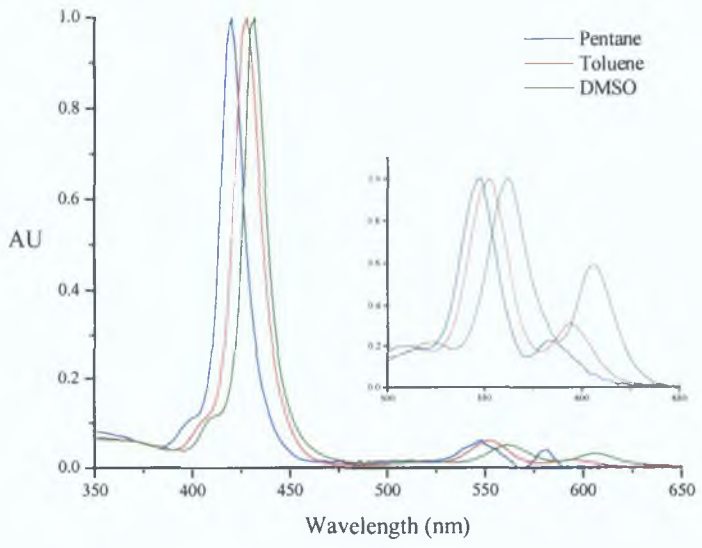

Fig. 5 – 31: UV-vis absorption spectra of zinc(II)-5-(5'-(5''-ethynylthiophene-2'-carboxaldehyde)thien-2'-yl)-10,15,20-triphenylporphyrin in pentane, toluene and DMSO.

The fluorescence spectra show similar solvatochromic behaviour with a decreased quantum yield as the solvent polarity increases (fig. 5 – 32). The $Q(0,0)^*$ emission band is red shifted from 604 nm in pentane to 614 nm in toluene and to 623 nm in DMSO. The $Q(1,0)^*$ emission band is also red shifted on increasing solvent polarity, however this shift is not as strong as that for the $Q(0,0)^*$ emission band thus resulting in a slight convergence of the two peaks in toluene and DMSO. Surprisingly the fluorescence lifetime is identical to ZnEtThTPP in toluene (1.92 ns), however the triplet lifetime is reduced by more than 50 % from 15 μs for ZnEtThTPP to 6 μs for ZnPald in toluene. A typical transient decay observed following flash photolysis of ZnPald at 532 nm excitation in toluene is shown in figure 5 – 33. Both the singlet and triplet lifetimes are slightly shorter in DMSO (1.20 ns and 5 μs respectively).

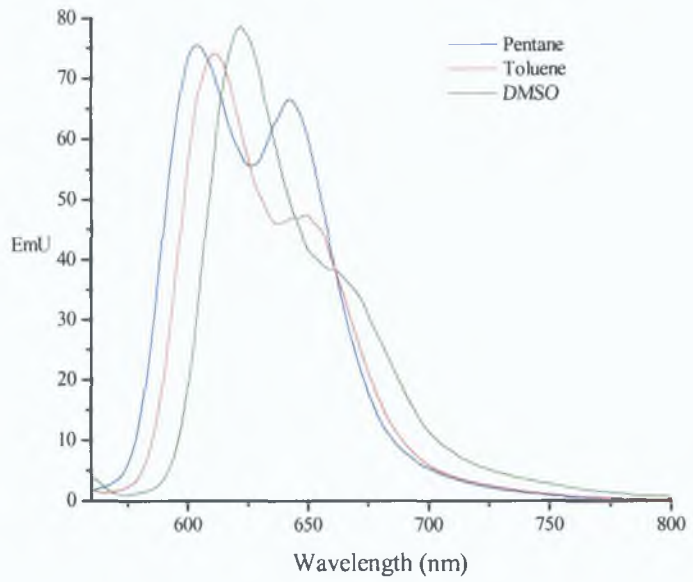

Fig. 5 – 32: Fluorescence spectra of ZnPald recorded in pentane, toluene and DMSO at room temperature at λ_{exc} = 544, 550 and 560 nm excitation respectively.

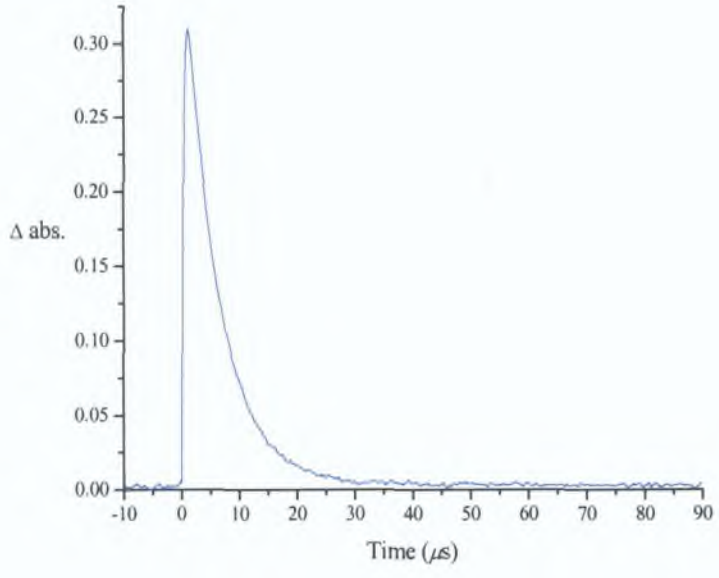

Fig. 5 – 33: A typical transient observed for ZnPald at 480 nm in toluene following 532 nm excitation under 1 atm of argon.

The transient absorption difference spectra of ZnPald in toluene (fig. 5 – 34) displays similar characteristics to that of ZnEtThTPP, however there is a substantial increase in the intensity of low energy absorption, which validates the hypothesis that this is a charge transfer type $^{3}(\pi\text{-}\pi^{*})$ excited state transition. This transition gains in oscillator strength on increasing the solvent polarity as seen in fig. – 35. The appearance of this low energy band suggests that there is enhanced electronic communication between the porphyrin π-system and the *meso*-thienyl moiety on going from the ground state to the excited state of the porphyrin.

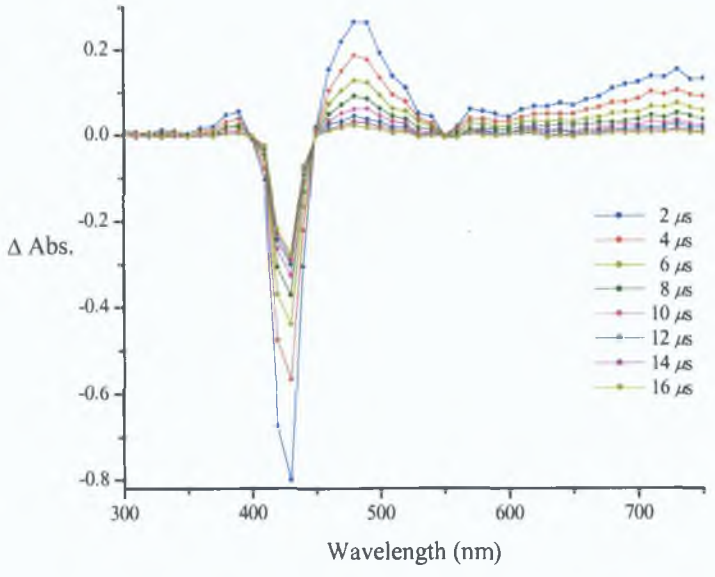

Fig. 5 – 34: Transient absorption difference spectra of ZnPald in toluene following 532 nm excitation under 1 atm of argon.

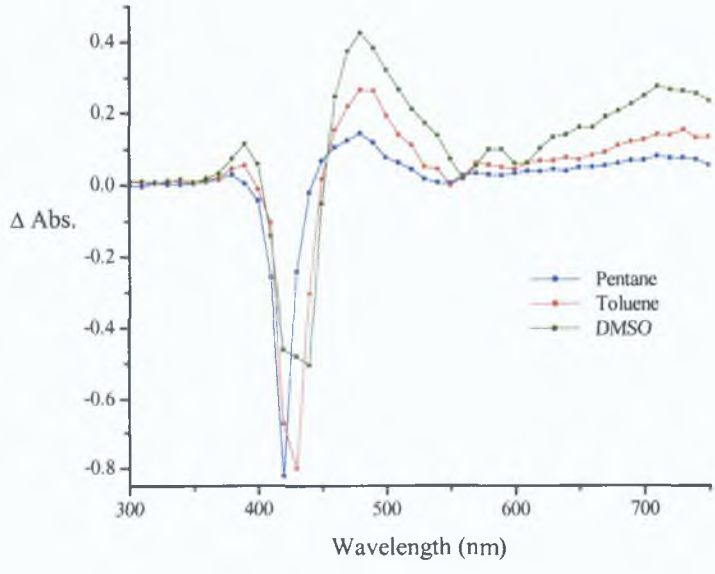

Fig. 5 – 35: An overlay of the transient absorption difference spectra of ZnPald in pentane, toluene and DMSO following 532 nm excitation under 1 atm of argon. Each plot is taken 2 μs after the laser pulse and all spectra have been recorded with an equal absorbance at 532 nm.

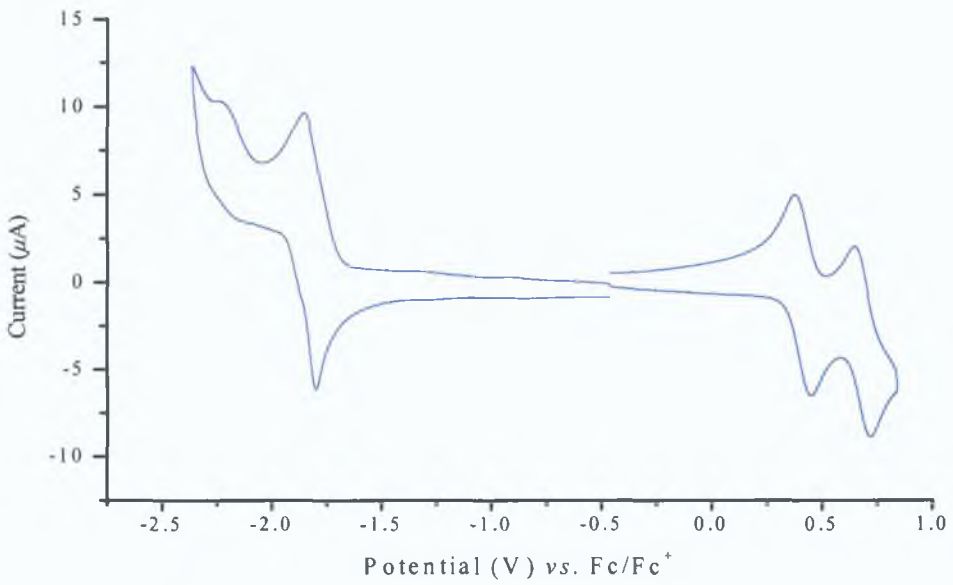

Fig. 5 - 36

The cyclic voltammogram of ZnPald (fig. 5 – 36) is similar to that obtained for ZnEtThTPP in that it displays two reversible porphyrin based oxidations and two reduction processes, however the first reduction process corresponding to the formation of the radical anion species is now reversible. The second reduction corresponding to the dianion is still irreversible. Both the HOMO and LUMO orbitals are stabilised by 77 and 98 mV respectively with respect to ZnTPP resulting in a decrease in the HOMO-LUMO energy gap of 21 mV.

5 5 Conclusions

The photophysical properties of some novel *meso*-substituted thien-2-yl zinc(II)-porphyrins were investigated by laser flash photolysis and by steady state and time resolved fluorescence techniques A red shift of the porphyrin Soret band was observed upon introduction of a thienyl substituent into the *meso*-position of the ring A red shift of the fluorescence maxima was also observed Reduction in the quantum yield and lifetime of fluorescence was observed upon increased thienyl substitution at the *meso*-position of the porphyrin ring Reduction of the $^{3}(\pi\text{-}\pi^{*})$ porphyrin triplet excited state was also observed upon increased thienyl substitution Electochemical studies showed the stabilisation of both the HOMO and LUMO orbitals on increasing thienyl substitution of the porphyrin macrocycle

5 6 Bibliography

[1] G Simonneaux, P Le Maux, *Coord Chem Rev* **2002**, 228, 43

[2] K Lang, J Mosinger, D M Wagnerova, *Coord Chem Rev* **2004**, 248, 321

[3] M Calvete, G Ying Yang, M Hanack, *Synth Metals* **2003**, 141, 231

[4] (a) *The Porphyrin Handbook*, eds K M Kadish, K M Smith, R Guilard, Academic Press Boston, 2000, Vol 8 (b) *The Porphyrin Handbook*, eds K M Kadish, K M Smith, R Guilard, Academic Press Boston, 2003, Vol 18

[5] (a) *The Porphyrin Handbook*, eds K M Kadish, K M Smith, R Guilard, Academic Press Boston, 2000, Vol 2 (b) *The Porphyrin Handbook*, eds K M Kadish, K M Smith, R Guilard, Academic Press Boston, 2000, Vol 9 (c) *The Porphyrin Handbook*, eds K M Kadish, K M Smith, R Guilard, Academic Press Boston, 2003, Vol 14

[6] N Ono, H Miyagawa, T Ueta, T Ogawa, H Tam, *J Chem Soc , Perkin Trans 1* **1998**, 1595

[7] (a) K M Kadish, E Van Caemelbecke, G Royal in *The Porphyrin Handbook*, eds K M Kadish, K M Smith, R Guilard, Academic Press Boston, **2000**, Vol 8, ch 55 (b) M O Senge in *The Porphyrin Handbook* eds K M Kadish, K M Smith, R Guilard, Academic Press Boston, **2000**, Vol 1, p 239

[8] P Bhavana, B Verghese, P Bhyrappa, Acta Crysta C 57 **2001**, 252

[9] P Bhyrappa, P Bhavana, *Chem Phys Lett* **2001**, 349, 399

[10] C J Medforth, R E Haddad, C M Muzzi, N R Dooley, L Jaqumod, D C Shyr, D J Nurco, M M Olmstead, K M Smith, J -G Ma, J A Shelnutt, *Inorg Chem* **2003**, 42, 2227

[11] J Roncali, *Chem Rev* **1992**, 92, 711

[12] J Chen, A K Burrell, W M Cambell, D L Officer, C O Too, G G Wallace, *Electrochim Acta* **2004**, 49, 329

[13] M Schaferling, P Bauerle, *J Mater Chem* **2004**, 14, 1132

[14] B Ballarin, S Masiero, R Seeber, D Tonelli, *J Electroanal Chem* **1998**, 449, 173

[15] (a) H Segawa, N Nakayama, T Shimidzu, *J Chem Soc , Chem Commun* **1992**, 784 (b) H Segawa, N Nakayama, F Wu, T Shimidzu, *Synth Met* **1993**, 966, 55

[16] T Shimidzu, H Segawa, F Wu, N Nakayama, *J of Photochem Photobiol A Chem* **1995**, 926, 121

[17] T. Yamamoto, N. Fukushima, H. Nakjima, T. Maruyama, I. Yamaguchi, *Macromol.* **2000**, 33, 5988.

[18] G. Li, T. Wang, A. Schulz, S. Bhosale, M. Lauer, P. Espindola, J. Heinze. J.-H. Fuhrhop, *Chem. Commun.* **2004**, 552.

[19] M. J. Crossley, J. K. Prashar, *Tetrahedron. Lett.* **1997**, 38, 6751.

[20] N. Ono, H. Hironaga, K. Ono, S. Kaneko, T. Murashina, T. Ueda, C. Tsukamura, T. Ogawa, *J. Chem. Soc., Perkin Trans. 1* **1996**, 417.

[21] A. Rohrer, R. Ocampo, H. J. Callot, *Bull. Soc. Chim. Fr.* **1997**, 134, 689.

[22] (a) P. Janvier, J.-Y. Lequestel, B. Illien, S. Suresh, E. Blart, J.-P. Quintard, F. Odobel, *Int. J. of Quantum. Chem.* **2001**, 84, 259. (b) F. Odobel, S. Suresh, E. Blart, Y. Nicolas, J.-P. Quintard, P. Janvier, J.-Y. Le Questel, B. Illien, D. Rondeau, P. Richomme, T. Häupl, S. Wallin, L. Hammarström, *Chem. Euro. J.* **2002**, 8, 3027.

[23] F. Wurthner, M. S. Vollmer, F. Effenberger, P. Emele, D. U. Meyer, H. Port, H. C. Wolf, *J. Amer. Chem. Soc.* **1995**, 117, 8090.

[24] M. S. Vollmer, F. Wurthner, F. Effenberger, P. Emele, D. U. Meyer, T. Stumpfig, H. Port, H. C. Wolf, *Chem. Eur. J.* **1998**, 4, 260.

[25] P. A. Liddell, G. Kodis, A. L. Moore, T. A. Moore, D. Gust, *J. Amer. Chem. Soc.* **2002**, 124, 7668.

[26] A schematic diagram of the experimental set-up is available at http://www.clf.rl.ac.uk/Facilities/LSF/LML/confocal/resources/spc.htm

[27] R. Friedlein, X. Crispin, W. Osikowicz, S. Braun, M. P. de Jong, C. D. Simpson, M. D. Watson, F. von Kieseritzky, P. Samorí, S. K. M. Jönsson, M. Fahlman, F. Jäckel, J.P. Rabe, J. Hellberg, K. Müllen, W. R. Salaneck, *Synthetic Metals* **2004**, 147, 79.

[28] Uv-vis spectra of analogous tetraaryl free base porphyrins show little difference from H_2TPP; (a) J. S. Lindsey, S. Prathapan, T. E. Johnson, R. W. Wagner, *Tetrahedron* **1994**, 50, 8941. (b) F. Li, S. Gentemann, W. A. Kalsbeck, J. Seth, J. S. Lindsey, D. Holten, D. F. Bocian, *J. Mater. Chem.* **1997**, 7, 1245.

[29] P. J. Spellane, M. Gouterman, A. Antipas, S. Kim, Y. C. Liu, *Inorg. Chem.* **1980**, 19, 386.

[30] E. G. Azenha, A. C. Serra, M. Pineiro, M. M. Pereira, J. Seixas de Melo, L. G. Arnaut, S. J. Formosinho, A. M. d'A. Rocha Gonsalves, *Chem. Phys.* **2002**, 280, 177.

[31] The 3-thienyl group is known to have a lower barrier to rotation by 20 kJ mol^{-1} than *meso*-phenyl goups (see ref. 13).

[32] When the short lifetime of ZnTThP is considered only, ZnTThP displays dual emission in an almost 1 1 ratio with lifetimes of 1 36 (± 0 01) and 0 51 (± 0 01) ns

[33] (a) C J Aspley, J R Lindsay Smith, R N Perutz, D Pursche, *J Chem Soc , Dalton Trans* **2002**, 170 (b) A Prodi, M T Indelli, C J Kleverlaan, F Scandola, E Alessio, T Gianferrara, L G Marzilli, *Chem Eur J* **1999**, 5, 2668

[34] See chapter 4

Chapter 6

A Photophysical Study of *meso*-Ferrocenylporphyrins and their Tetrafluoroborate Ferrocenium Salts

6 1 Aims and objectives

The aim of this chapter was to study the influence of the ferrocenyl moiety on the photophysical properties of the porphyrin ring when directly bound at one of the *meso*-positions of the ring The ferrocene moiety was subsequently oxidised to the ferrocemum salt, using silver tetrafluoroborate, and the photochemistry of these salts was also investigated The synthesis of the *meso*-ferrocenyl porphyrins zinc(II)-5-ferrocenyl-10,15,20-triphenylporphyrin (ZnFcTPP), mckel(II)-5-ferrocenyl-10,15,20-triphenylporphyrin (NiFcTPP) and zmc(II)-5-ferrocenyl-10,15,20-tri(thien-2'-yl)porphyrin (ZnFcTThP) was previously in chapter 4 Techniques used included, UV-vis absorption spectroscopy, steady state fluorescence spectroscopy, laser flash photolysis and time correlated single photon counting Spectro-electrochemical analysis is also carried out on the ferrocenyl systems monitored by UV/Vis/NIR absorption spectroscopy and steady state fluorescence spectroscopy

6 2 Literature survey

Considerable research effort has been devoted to mimicking photoinduced electron transfer and charge separation within the natural photosynthetic reaction centre Great interest is currently paid to the synthesis of polynuclear transition metal complexes and the study of their photochemical, photophysical and electrochemical properties [1] This interest is stimulated, in particular, by attempts to design and construct supramolecular systems capable of performing light- and/or redox-induced functions Central to supramolecular chemistry is the concept that assemblies of molecular components can be designed to perform relatively elaborate and useful tasks thus mimicking, at the molecular level, functions normally performed by artificial macroscopic devices [2] Modelling of the photosynthetic reaction centre often involves the synthesis of covalently or non-covalently (*via* hydrogen bonding or Van der Waal forces) linked donor-acceptor multicomponent transition metal systems Often in such systems the metal-ligand interaction is sufficiently weak enough to allow the manifestation of intrinsic properties of the metal and ligand (e g ligand centred absorption bands and redox waves) and at the same time sufficiently strong enough to cause the appearance of new properties characteristic of the whole compound (e g metal-to-ligand or ligand-to-metal charge-transfer bands) Porphyrins and metalloporphyrins are particularly attractive towards such applications as they can introduce a variety of desired features such as a rigid, planar geometry (depending on central metal in metalloporphyrins), high stability, an intense electronic absorption, a strong fluorescence emission and a small HOMO-LUMO energy gap, as well as flexible tunability of their optical and redox properties by appropriate metallation

Porphyrins can be found in a variety of multicomponent supramolecular systems for artificial photosynthesis and light harvesting arrays[3] and in the construction of extended π-systems as organic semiconductors,[4] liquid crystals,[5] optical limiters,[6] photovoltaic devices,[7] light-emitting diodes[8] and non-linear optical materials [6] The combination of porphyrin and ferrocene units within the same system can be interesting in terms of intramolecular charge-transfer due to the reversibility of the Fe(II)/Fe(III) couple

Wollman and Hendrickson claimed the first report of a porphyrin synthesis bearing an organometallic moiety at the periphery of the ring in 1977 (Figure 6 - 1) [9] The synthesis and physical properties of *meso*-tetraferrocenylporphyrin (H_2TFcP), its copper complex *meso*-tetraferrocenylporphyrincopper (Cu(II)TFcP) and their various oxidation products were discussed in an attempt to investigate the thermal transfer of an electron from Fe(II) to Fe(III) *via* the ferrocene/ferrocenium couple across the conjugated porphyrin bridge

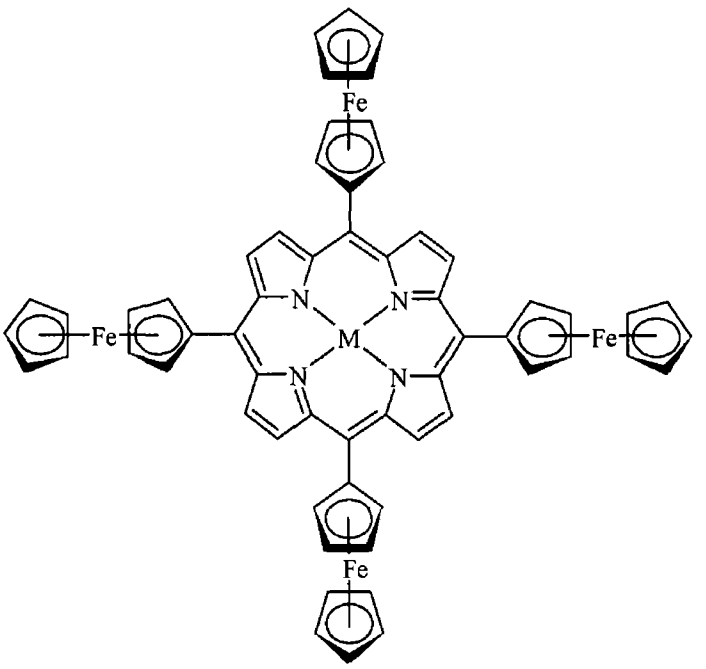

M = 2H, Cu(II)

Fig 6 – 1

The ^{1}H-NMR spectrum of H_2TFcP reported by Wollman and Hendrickson was not well defined and the authors suggested that this was due to the presence of four inseparable atropisomers (α,α,α,α-H_2TFcP, α,α,α,β-H_2TFcP, *cis*-α,α,β,β-H_2TFcP, *trans*-α,α,β,β-H_2TFcP) Also the electronic absorption spectra of H_2TFcP in chloroform reported by Wollman and Hendrickson showed a blue shifted Soret band at 350 nm and a broad, partially resolved band at *ca* 450 nm which tails off gradually with optical density extending out as far as 1200 nm Again, the authors attribute the overall broadness and poor resolution of the electronic absorption to the presence of the four atropisomers

Mixing of the porphyrin π-system with the Fe d-orbitals *via* the Cp ring of the ferrocene moiety was said to be responsible for the shift of the Soret band. Also, the broad band at 450 nm was assigned to a charge-transfer (CT) transition largely localised on the ferrocene subunits. A similar UV/Vis spectrum was observed for Cu(II)TFcP with additional bands at 424 nm and *ca.* 665 nm, the latter was assigned to a copper based ligand-field (LF) transition. The band at 424 nm was not assigned. The ^{1}H-NMR and UV/Vis data reported by Wollman and Hendrickson are not typical of *meso*-substituted porphyrins. Wollman and Hendrickson went further to discuss the mixed-valence oxidation products of H_2TFcP and Cu(II)TFcP in the presence of I_2 or 2,3-dichloro-5,6-dicyanoquinone (DDQ). The electronic absorption spectra of these oxidation products showed no evidence of intervalence-transfer (IT) bands leading the authors to assume that there was no communication between the ferrocenium centres and the Cu(II) ion or the ferrocene centres at nearby methine positions. They concluded that this was as a result of the localised charge deficiency on the porphyrin ring, in the form of a porphyrin π-cation radical.

The synthesis of H_2TFcP and *meso*-tetraruthenocenylporphyrin (H_2TRcP) were later reported by Loim et al. *via* the Lindsey method with yields of 56 % and 40 % respectively.[10] This synthetic approach contrasted with the Adler method, which was used by Wollman and Hendrickson in obtaining H_2TFcP (40 % reported yield). H_2TFcP and H_2TRcP both showed electronic absorption spectra typical of *meso*-tetraarylporphyrins with an extra charge-transfer band at *ca.* 480 nm due to the metallocene moiety. The ^{1}H-NMR spectra were also typical of *meso*-tetraarylporphyrins and showed evidence of free rotation around the C-C bond between the *meso*-carbon atoms and the metallocenyl substituents.

Boyd et al. synthesised a single atropisomer of α,α-5,15-bis(ferrocenyl)-2,8,12,18-tetrabutyl-3,7,13,17-tetramethlporphyrin and the corresponding Ni(II) complex in order to investigate possible electrochemical communication between the ferrocenyl moieties (fig. 6 - 2).[11] They found that free rotation of the ferrocenyl units at the *meso*-positions was prevented by steric interaction with the β-methyl substituents, thus resulting in the formation of the single *a,a*-atropisomer. The steric effect of both ferrocenyl moieties also leads to a strongly ruffled porphyrin core and hence a bathochromically shifted

Soret band Boyd et al had anticipated that oxidation of one of the ferrocenyl groups, to the ferrocenium ion, in this system would result in a mixed valence state with delocalisation of the cationic charge across the highly conjugated porphyrin macrocycle

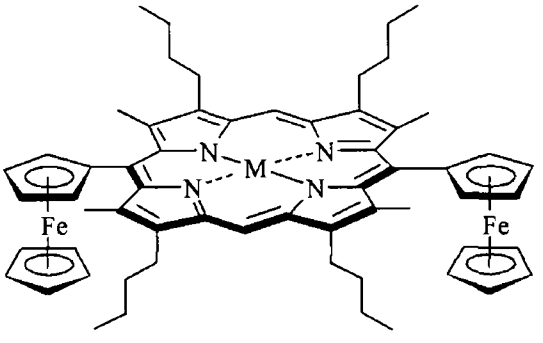

M = 2H, Ni(II)

Fig 6 - 2

When Boyd et al conducted electrochemical studies on the free-base and Ni(II) porphyrins two consecutive, ferrocene based, one-electron oxidation waves separated by $\Delta E_{1/2}$ = 0 19 and 0 41 V respectively The appearance of independent redox couples for each ferrocene unit verifies the presence of strong communication between the two ferrocene moieties over the porphyrin ring (a distance of > 10 Å) Spectroelectrochemical UV/Vis studies of both the free-base and Ni(II) porphyrin complexes revealed the growth of intravalence charge-transfer (IVCT) bands at 1080 nm and 946 nm respectively upon single electron oxidation This is again indicative of strong coupling between the ferrocene units *via* extensive mixing of both ferrocenyl orbital systems with that of the porphyrin π-system Upon oxidation of ferrocene, a hole is introduced into the e_{2g} *d*-orbitals of one of the ferrocene moieties The lowest energy band in the ultraviolet-visible-near infrared spectra is thus an IVCT transition from the highest filled *d*-orbital of Fe(II) to the partially occupied orbital of Fe(III)

The separation in $E_{1/2}$ between the two oxidations of the bis-ferrocenyl complex parallels the intensity of an IVCT transition that arises from electron-transfer between the two sites on the mixed valence singly oxidised complex [12] $E_{1/2}$ is dependent on stabilising factors in the Fe(II)/Fe(II), Fe(II)/Fe(III) and Fe(III)/Fe(III) species and

through space electrostatic effects However, its value can provide an indication of the strength of through bond metal-metal interaction Previous studies on bisferrocene found a peak splitting of $E_{1/2}$ = 0 33 V over a much shorter distance of < 5 4 Å [13] Barlow et al have recently reported the synthesis and characterisation of a range of 1,3-di-(metallocenyl)allylium cations,[14] e g scheme 6 - 1 In this class of compounds there is an overall positive charge stabilised by contributions from (η^6-fulvene)(η^5-cyclopentadienyl)metal cation resonance structures The difference in the half-wave redox potential of the two iron centres for the bis-ferrocenyl structure shown below is $\Delta E_{1/2}$ = 0 61 V

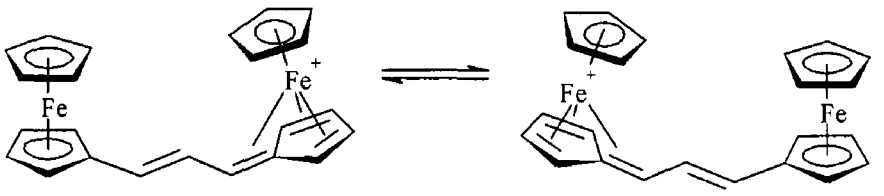

Scheme 6 - 1

Burrell et al have reported a series of ferrocenyl- and ruthenocenyl-porphyrin dyads connected *via* a vinyl spacer at the β-position of the porphyrin ring (fig 6 - 4) [15] Spectroscopic and electrochemical studies showed little evidence for communication between the porphyrin and metallocene

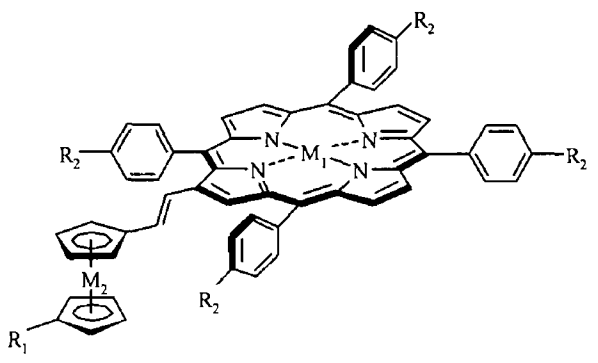

1a M_1 = 2H M_2 = Fe R_1 = H R_2 = H
1b M_1 = Cu, M_2 = Fe, R_1 = H R_2 = H
1c M_1 = Ni M_2 = Fe, R_1 = H R_2 = H
1d M_1 = Zn, M_2 = Fe R_1 = H R_2 = H

2a M_1 = 2H M_2 = Fe R_1 = CHO, R_2 = H
2b M_1 = Cu M_2 = Fe R_1 = CHO R_2 = H
2c M_1 = Ni, M_2 = Fe R_1 = CHO R_2 = H
2d M_1 = Zn M_2 = Fe R_1 = CHO R_2 = H

3 M_1 = 2H M_2 = Ru R_1 = CHO R_2 = H

4 M_1 = 2H M_1 = Fe R_1 = H R_2 = Cl

Fig 6 - 4

Burrell et al also reported the synthesis of a series of novel dimeric porphyrins linked by a similar vinylferrocene spacer (fig 6 - 5) [16] However there were no electrochemical or spectroscopic studies reported for these complexes

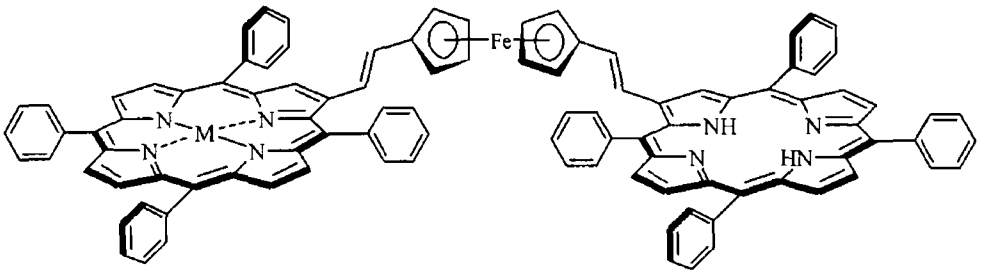

trans,trans

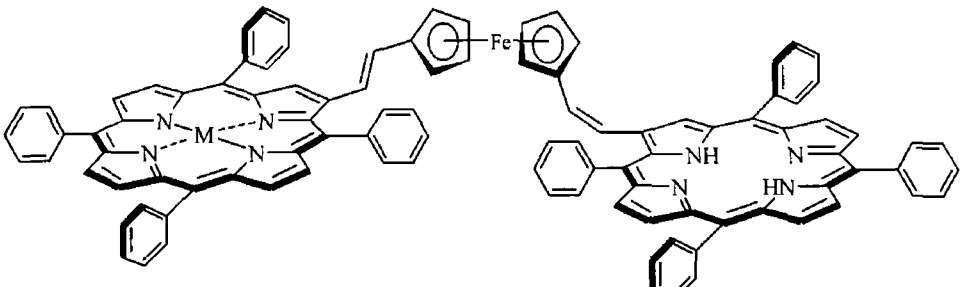

trans cis

M = 2H Cu Ni

Fig 6 - 5

Consistent with the work of Burrell et al , Kim and co-workers reported the synthesis of α,α-5,15-diferrocenyl-2,8,12,18-tetraethyl-3,7,13,17-tetramethylporphyrin (H_2DFcTTP) in 41 % yield as a single atropisomer [17] 5-ferrocenyl-15-phenyl-2,8,12,18-tetraethyl-3,7,13,17-tetramethylporphyrin (H_2FcPTTP) was also synthesised in 27 % yield as well as the Zn(II) (Zn(II)FcPTTP, Zn(II)DFcTTP), Ni(II) (Ni(II)FcPTTP, Ni(II)DFcTTP) and Mn(III)Cl (Mn(III)ClFcPTTP, Mn(III)ClDFcTTP) metallated analogues (fig 6 - 6a) [18] [19] Electrochemical analyses showed that the oxidation of the ferrocene subunit is strongly affected by the central metal as well as the porphyrin ring through extended π-conjugation

The ferrocenyl group of H_2FcPTTP undergoes a reversible one-electron oxidation at $E_{1/2}$ = 0 30 V with respect to the ferrocene/ferrocenium (Fc/Fc^+) couple The oxidation potential of Ni(II)FcPTTP ($E_{1/2}$ = 0 28 V) shifts towards the positive direction

compared with that of Zn(II)FcPTTP ($E_{1/2}$ = 0 23 V) This was attributed to reduced electron density at the porphyrin ring on going from Zn(II) to Ni(II) due to the greater electronegativity of the nickel atom In the case of Mn(III)ClFcPTTP ($E_{1/2}$ = 0 36 V), the higher oxidation state of Mn(III) reduces the electron releasing ability of the porphyrin ring, making ferrocene oxidation more difficult Two reversible ferrocene based one-electron processes are observed upon oxidation of H_2DFcTTP ($\Delta E_{1/2}$ = 0 21 V) The positive charges developed in the monocation and dication species are stabilised by delocalisation over the porphyrin ring π-system and strong coupling appears because of extensive mixing of the ferrocenyl molecular orbital systems with the porphyrin ring π-system Similar changes were observed for the nickel derivative Ni(II)DFcTTP, which displayed the strongest communication between the two metal centres ($\Delta E_{1/2}$ = 0 39 V) in agreement with Burrell et al [8]

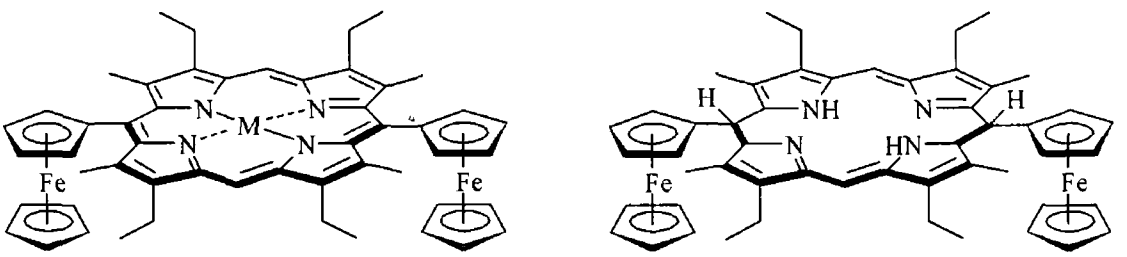

M = 2H, Zn(II), Ni(II), Mn(III)Cl

(a) (b)

Fig 6 - 6

Rhee et al have reported the synthesis of α,α-5-ferrocenyl-15-phenyl-2,8,12,18-tetraethyl-3,7,13,17-tetramethyl-5,15-dihydroporphyrin in 31 % yield (fig 6 - 6b) As a result of the reduced π-conjugation of 5,15-dihydroporphyrms (or porphodimethines) in comparison to porphyrins, these systems show some characteristic properties Most notably is the lack of ring current, which is evident in the ^{1}H-NMR spectrum The usual downfield shift of the porphyrin N-H protons (typically found between -2 to -4 ppm) is not present, with the N-H protons of the porphodimethine occurring at *ca* 8 to 12 ppm The electronic absorption spectrum of the bisferrocenylporphodimethine studied by Rhee is typical of porphodimethmes showing an intense band at 431 nm with a weak broad shoulder at 522 nm, and no Q-bands are observed for these systems The

bisferrocenylporphodimethine shows one two-electron oxidation at $E_{1/2}$ = 0 33 V (*vs* Ag/AgCl) in contrast to the two one-electron oxidations observed for the bisferrocenylporphyrin at $E_{1/2}$ = 0 08 / 0 29 V (*vs* Ag/AgCl, $\Delta E_{1/2}$ = 0 21 V) emphasising the lack of communication across the porphodimethine spacer in comparison to the porphyrin macrocycle

In an effort to model photoinduced electron transfer in photosynthesis Schmidt et al investigated the electrochemistry of *meso*-tetrakis(4-ferrocenylphenyl)porphyrin, H_2TFcPP, and its Zn(II) derivative, Zn-TFcPP (fig 6 - 7) [20] There exists little or no coupling between the ferrocene moieties of H_2TFcPP or Zn-TFcPP and the π-system of the porphyrin ring The phenyl substituents are out of plane with the porphyrin ring so that they serve only as spacer groups allowing rotational freedom to the ferrocene while providing for a rather rigid system with a fixed distance between the donor and acceptor groups This is evident in the electronic absorption spectra of these complexes, which are almost identical with those of *meso*-tetraphenylporphyrin and (*meso*-tetraphenylporphyrinato)zinc

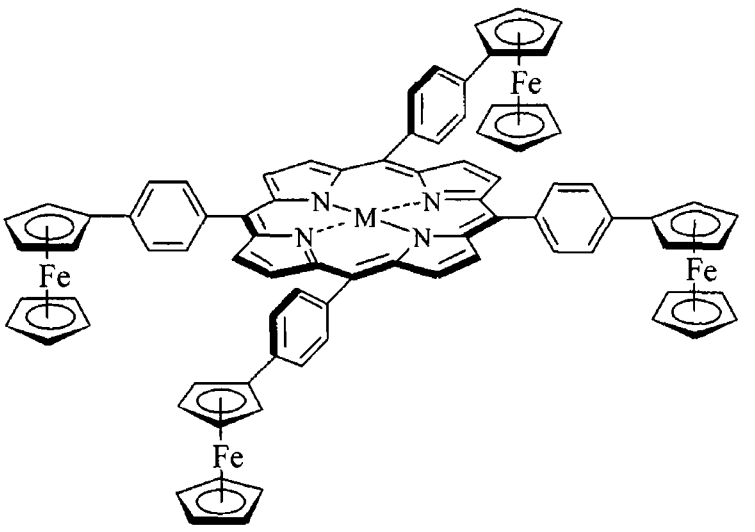

M = 2H, Zn(II)

Fig 6 - 7

Cyclic voltammetry of both H_2TFcPP and Zn-TFcPP showed a four-electron oxidation wave at 0 64 V (*vs* Ag/AgCl), which indicates the lack of communication between the four ferrocene subunits Little change was observed in the electronic absorption spectra on oxidation of the ferrocene subunits to the ferrocemum ion, an increase in fluorescence was reported however The lowest excited singlet state of ferrocene is higher in energy than the lowest excited singlet state of the porphyrin thus ruling out efficient singlet energy-transfer from the excited porphyrin to ferrocene The authors attributed the increased fluorescence in this system to a decrease in reductive quenching ability *via* electron-transfer of the ferrocenium ion with respect to the ferrocene moiety

Similarly, a series of ferrocene-naphthalimide dyads synthesised by Wang et al showed no evidence in the electronic absorption spectra of ground state communication between the two subunits, however, a large decrease in fluorescence intensity was observed for the naphthalimide moiety *via* efficient electron-transfer and energy-transfer involving the ferrocene unit [21] Emission was recovered upon oxidation of the ferrocenyl 4-pyrrolidine-1,8-naphtalimide to its ferrocenium ion (fig 6 - 8)

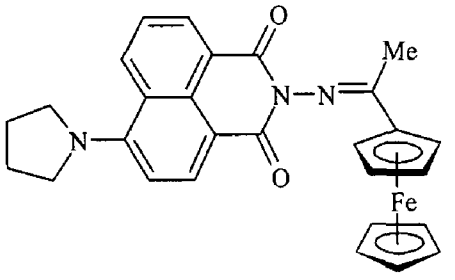

Fig 6 - 8

Similar to porphyrins, ruthenium(II) oligopyridine complexes exhibit unique photophysical, photochemical and redox properties and are often employed as photosensitisers in supramolecular assemblies [22] Siemeling et al recently carried out a thorough investigation of the photophysical properties of a series of ferrocenyl functionalised ruthenium(II) terpyridines [23] The ferrocene moiety acts as an efficient quencher for the ^{3}MLCT state in these compounds however a marked increase in emission intensity was observed for a number of these compounds on oxidation to the ferrocenium ion (fig 6 - 9)

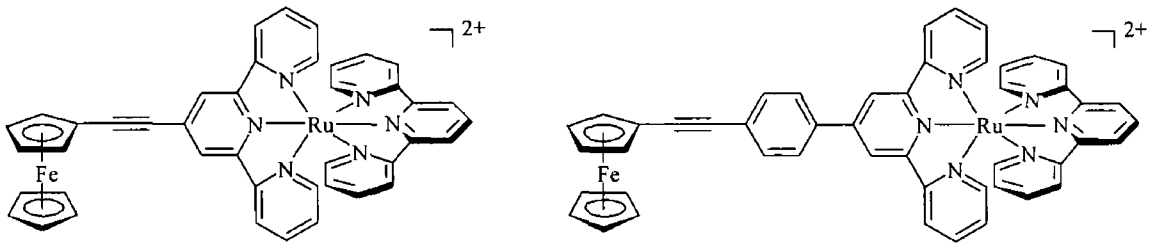

Fig 6 - 9

Beer and Kureck observed intramolecular electron-transfer in a porphyrin-ferrocene-quinone triad resulting in quenching of the porphyrin fluorescence (fig 6 - 10) [24] In this case, quenching was attributed to fast electron-transfer between the excited porphyrin and the electron-acceptor quinone

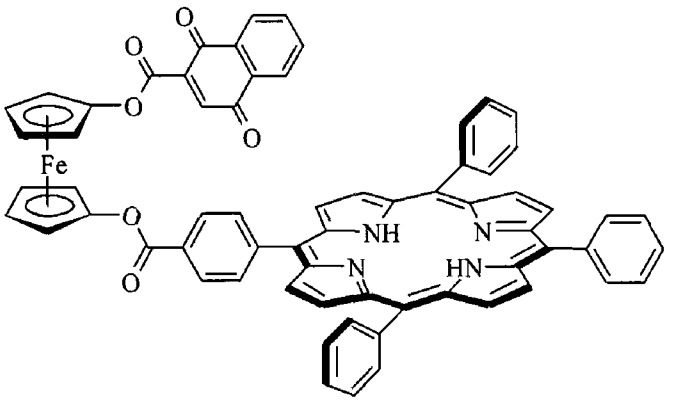

Fig 6 - 10

A strong decrease in the fluorescence efficiency of two ferrocene-porphyrin dyads was observed by Giasson et al (fig 6 - 11 b and c) *via* electron transfer from the ferrocene centre to the porphyrin excited singlet state [25] This represents another example where there exists relatively no ground state electronic interaction between the ferrocene and the π-system of the porphyrin ring due to the presence of the phenyl spacer group The electronic absorption spectra of compounds (a), (b) and (c) shown m figure 6 – 11 are almost identical All three species show two emission bands centred at 630 and 698 nm Relative quantum yields of fluorescence for compounds (b) and (c) are 0 38 and 0 84 respectively when compared to (a) Quenching was attributed to electron-transfer from

the ferrocenyl moiety to the excited porphyrin Photoinduced electron-transfer from the ferrocene centre to the singlet excited state of compounds (b) and (c) was calculated to be exothermic by 0 07 eV and 0 11 eV respectively, whereas energy transfer from the same excited state to the ferrocene is endothermic by 0 49 eV

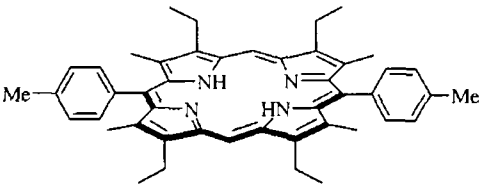

(a)

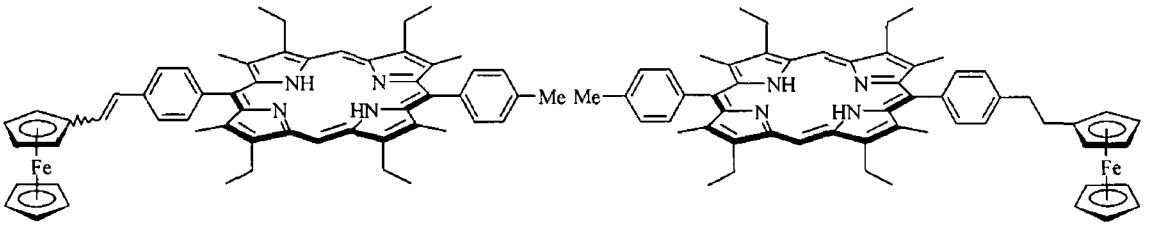

(b) (c)

Fig 6 – 11

Ferrocene has a low-lying triplet excited state and is known to be an effective triplet quencher It has also been observed that ferrocene quenched the triplet excited-state of two germanium porphyrins *via* energy transfer leading to the photochemical stabilisation of these compounds (fig 6 - 12) [26] The triplet-triplet transient absorption spectra for both (TPP)Ge(C_6H_5)(Fc) and (TPP)Ge($Fc)_2$ at 480 nm excitation follows a first order decay with rate constants of 4 1 x 10^4 s^{-1} and 9 8 x 10^4 s^{-1} respectively for the two systems Intramolecular quenching of the triplet excited state is twice as efficient for the bis-ferrocenyl complex, when compared to the mono-ferrocenyl analogue Independent redox couples were observed for the two ferrocene centres in (TPP)Ge($Fc)_2$ with $\Delta E_{1/2}$ = 0 21 V [27]

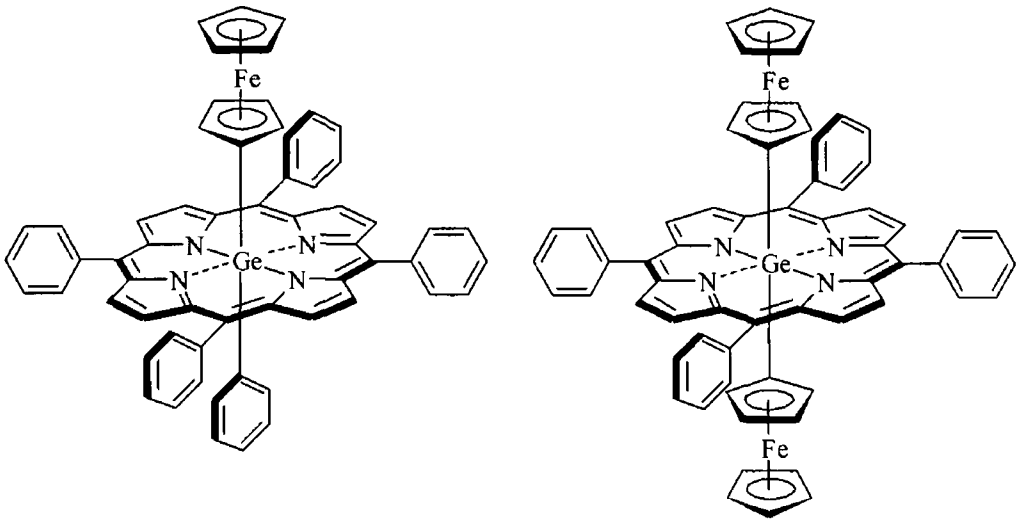

Fig 6 - 12

Generating photocurrents is of major interest for molecular electronics where inducing one directional photoinduced electron-transfer, subsequently leading to vectorial separation of the charges would generate a molecular photodiode Kondo et al achieved an efficient photoinduced current generation at a gold electrode modified with a self-assembled-monolayer (SAM) The SAM consisted of a porphyrin ring, a ferrocene unit and a terminal thiol unit each separated by alkyl chains Each of these units represent the photoactive, electron-transport and surface binding groups of the supramolecular assembly respectively (fig 6 - 13) [28] These triads formed Langmuir-Blodgett (LB) films at the surface of a gold electrode Upon soaking the LB films in a solution of methyl-viologen (MV^+), which acts as an additional electron acceptor, the rate of reverse electron-transfer was reduced Furthermore, the longer the alkyl chain used the larger the photocurrent produced These results suggest that inhibition of energy transfer and reverse electron-transfer are key factors for efficient generation of photocurrents

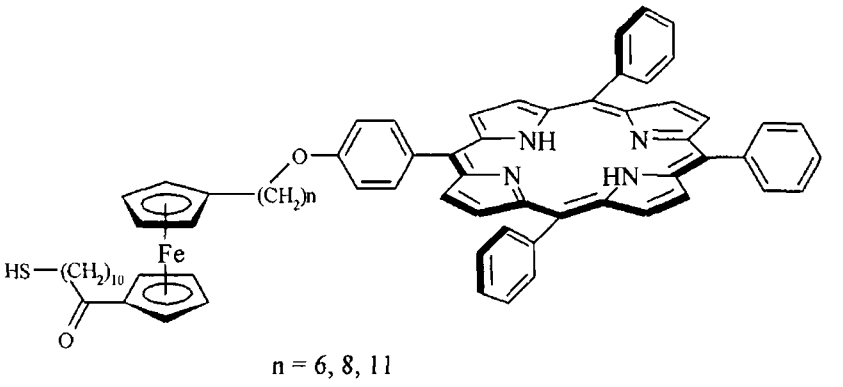

n = 6, 8, 11

Fig 6 - 13

The authors attribute the efficiency of these systems (Φ_{max} = 11 %) to two factors (i) the high electron-transfer rate between the gold electrode and the ferrocene moiety and (ii) the effective inhibition of reverse electron-transfer and/or energy-transfer from the excited state of the porphyrin moiety to the ferrocene or gold electrode Outlined in scheme 6 – 2 is the proposed mechanism for photoinduced current generation for these compounds

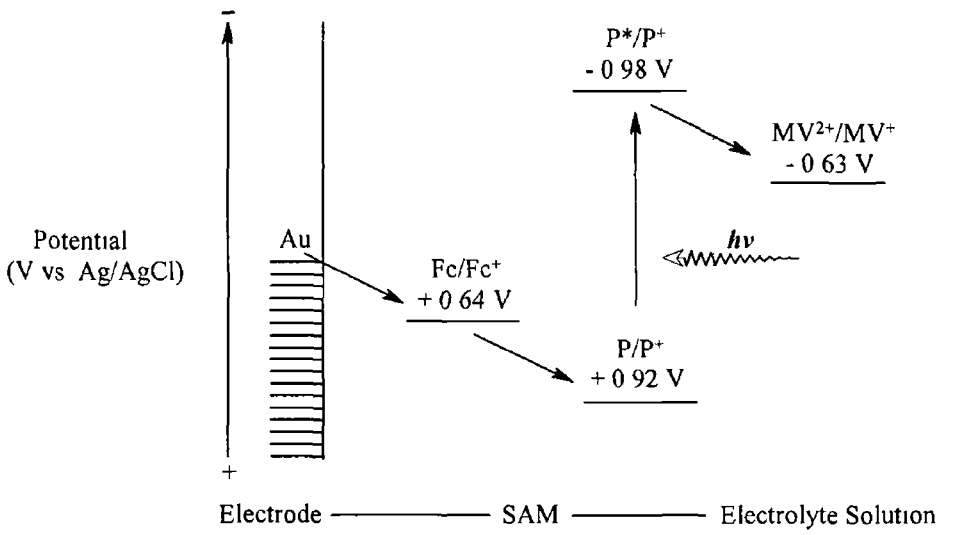

Scheme 6 - 2

Imahori et al also observed efficient photocurrent generation *via* the charge-separated state of a SAM of a ferrocene-porphrin-C_{60} triad (fig 6 - 14) when linked to a gold electrode with a quantum yield of Φ = 25 % [29] Photoinduced electron-transfer occurs from the porphyrin singlet excited state to C_{60} (solution studies showed the C_{60} moiety to be a more efficient fluorescence quencher than the ferrocenyl moiety) The resulting reduced species (C_{60}^{-}) transfers an electron to diffusing electron carriers such as oxygen and/or MV^{+2}, which eventually transfers an electron to the counter electrode During this forward electron-transfer process, electron-transfer also occurs from ferrocene (Fc) to the porphyrin monocation P^{+} (i e a charge shift from Fc- P^{+}- C_{60} to Fc^{+}- P- C_{60}^{-}), and subsequently from the gold electrode to Fc^{+}, thus resulting in the recovery of the initial state and a net vectorial electron flow Imahori and co-workers attributed the efficiency of this system to the efficient electron-transfer from Fc to P^{+}, which competes with charge recombination to the porphyrin ground state, and also to the ability of the C_{60} acceptor unit to compete with deactivation of the porphyrin excited state due energy/electron transfer to the gold electrode

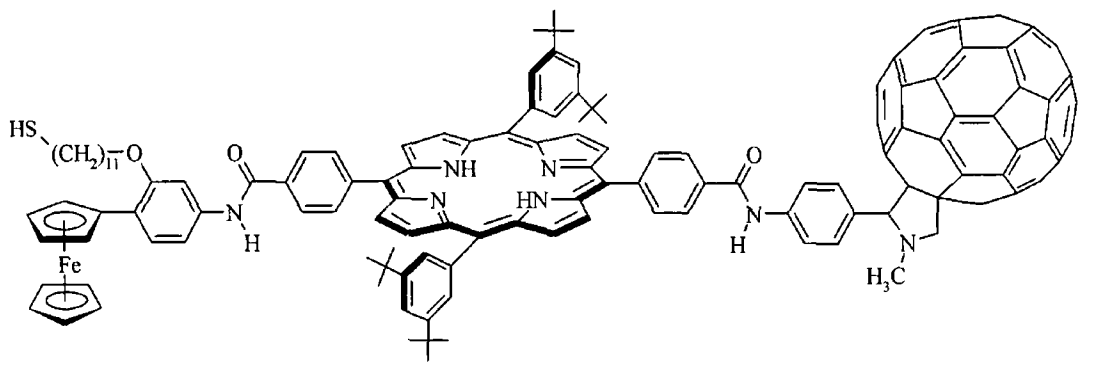

Fig 6 - 14

Imahori and co-workers have also investigated the photophysics of a number of similar triad and tetrad systems (fig 6 – 15) [30] Again, for the triad systems, efficient electron-transfer was observed from the porphyrin singlet excited state to the C_{60} acceptor unit followed by charge shift *via* efficient electron-transfer from Fc to P^{+} Excitation of the zinc-porphyrin (ZnP) in the tetrad system results in energy transfer to the free-base (P) porphyrin and subsequent charge separation The free-base porphyrin can also be excited directly followed by a similar electron-transfer process, i e Fc-ZnP-P^{*}-C_{60} to Fc-ZnP-P^{+}-C_{60} to Fc-ZnP $^{+}$-P-C_{60} to Fc $^{+}$-ZnP-P-C_{60})

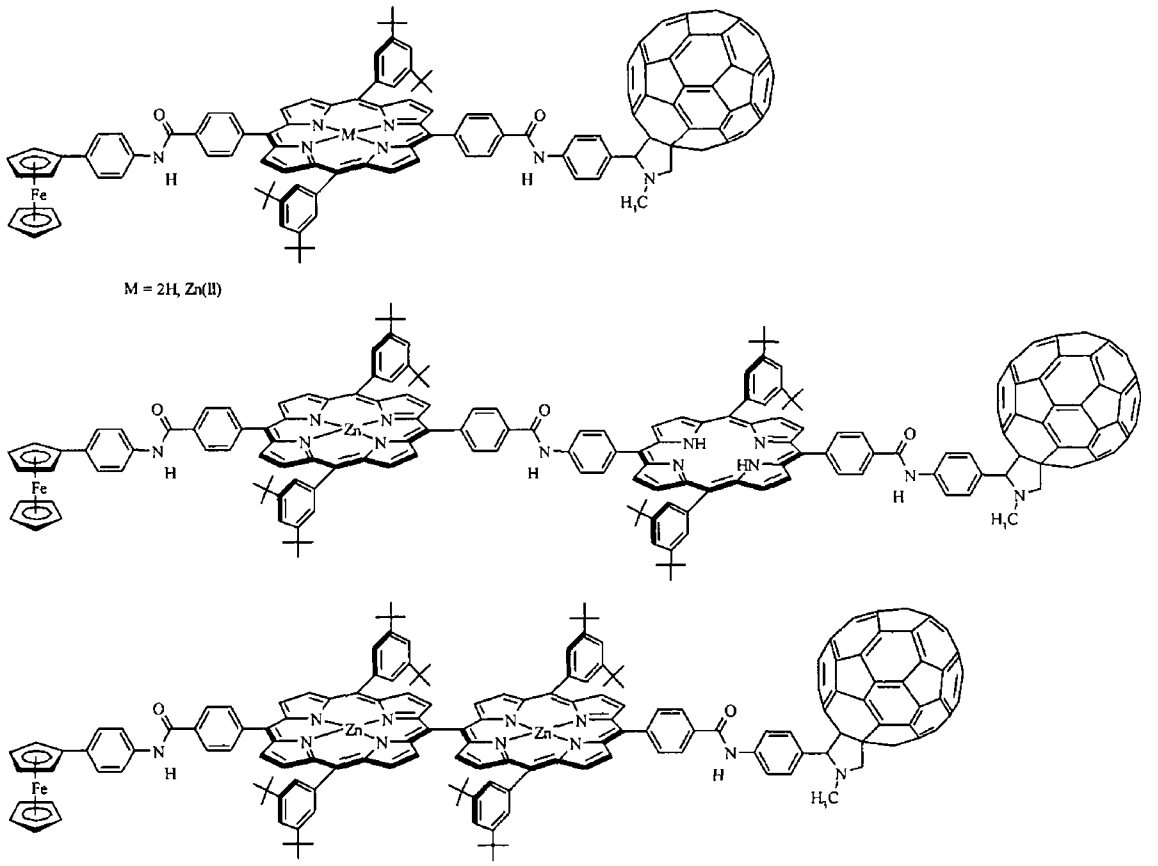

Fig 6 – 15

In an attempt to generate electron-transfer in biological systems and to design new molecular electron-transfer devices Thornton et al linked an electron-donating ferrocenyl derivative to an electron acceptor cationic porphyrin, TMPyFcP (fig 6 - 16) [31] DNA was chosen as a matrix for controlling intramolecular long-distance electron-transfer in this system as it allows the porphyrin moiety to intercalate between two base pairs The driving force for electron-transfer in the system (not including the DNA matrix) was calculated to be ΔG = -0 66 eV (far more efficient than the system studied by Giasson et al) [26] A 99 % reduction in fluorescence was observed, which Thornton et al attributed to fast through bond electron-transfer across the short spacer group employed in the system However, a decrease of only 0 03 ns in emission lifetime was observed on intercalation of the porphyrin subunit into the DNA matrix (0 11 ns *vs* 0 14 ns) Thornton and co-workers suggested that changes in redox potentials, or reorganisation energies upon intercalation either compensate one another or have negligible kinetic consequences

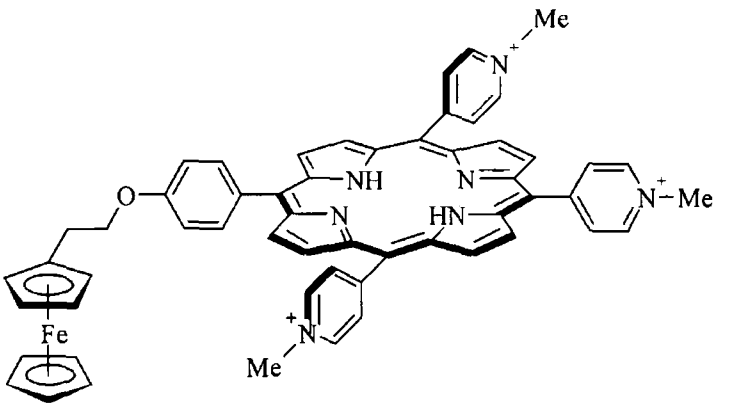

Fig 6 - 16

Tecilla et al used a novel non-covalent approach based on hydrogen-bonded self-assembed chromophores, rather than covalent linkages, in synthesising ferrocenyl porphyrin architectures (fig 6 - 17) [32] The ferrocene-containing molecule was designed with the aim of recognising two porphyrins substituted by a barbiturate derivative

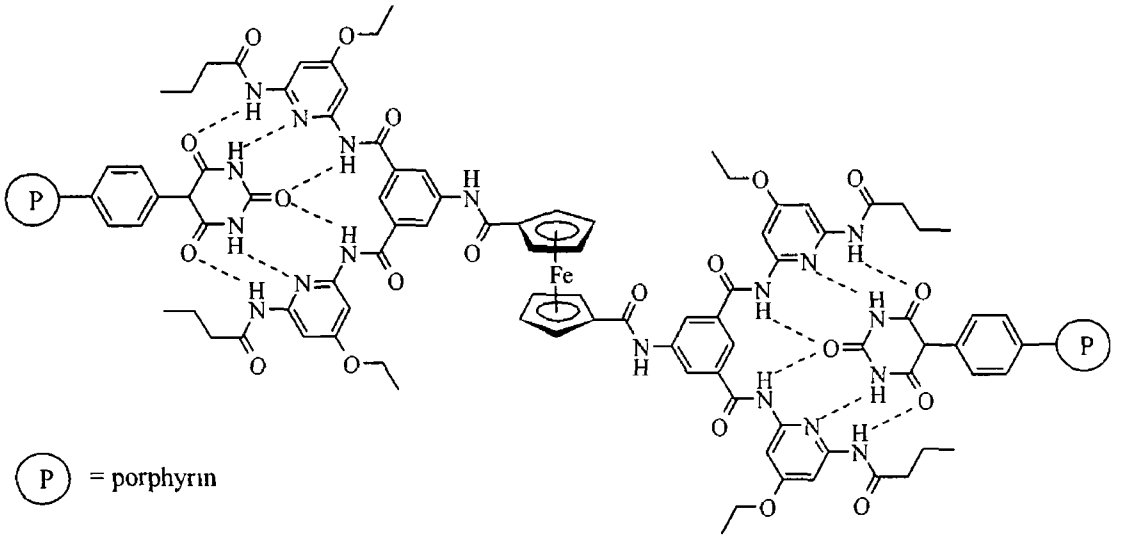

Fig 6 – 17

The molecular recognition of ions is an active area of research as many ions play fundamental roles in biology, in chemical processes and in environmental pollution Upon adding a complexing moiety to a luminescent porphyrin molecule a sensor is constructed with the capability of sensing anions *via* optical and/or electrochemical means

One such system developed by Beer et al was designed for anion recognition (fig 6 - 18)[33] ^{1}H-NMR studies of these tetra-ferrocenyl porphyrins systems revealed the free base compounds as poor complexing agents for the halide, nitrate, hydrogen sulphate and dihydrogen phosphate anions employed in the study In contrast, the zinc metalloporphyrins receptors strongly complex anionic guests and also give trends that are dependent upon the topological arrangement of the ferrocene amide groups of a particular atropisomer The zinc metalloporphyrin receptors were also found to electrochemically recognise anions *via* significant cathodic perturbations of the respective porphyrin and ferrocene redox couples

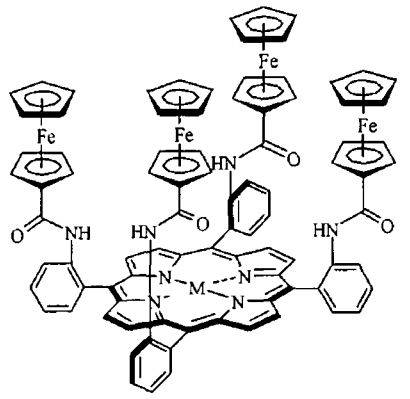

α, α, α, α - atropisomer

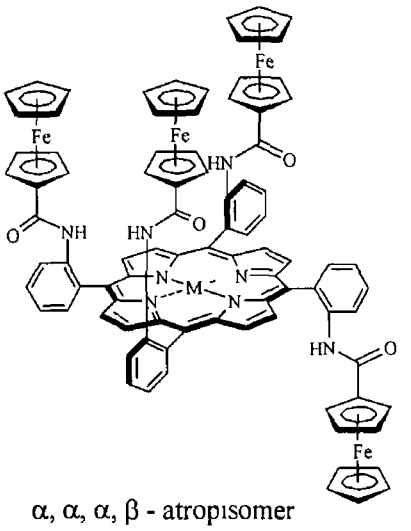

α, α, α, β - atropisomer

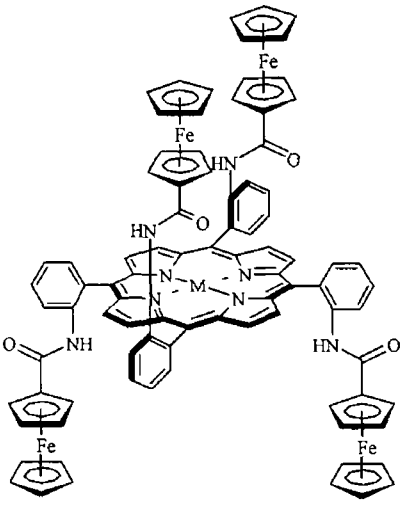

α, β, α, β - atropisomer

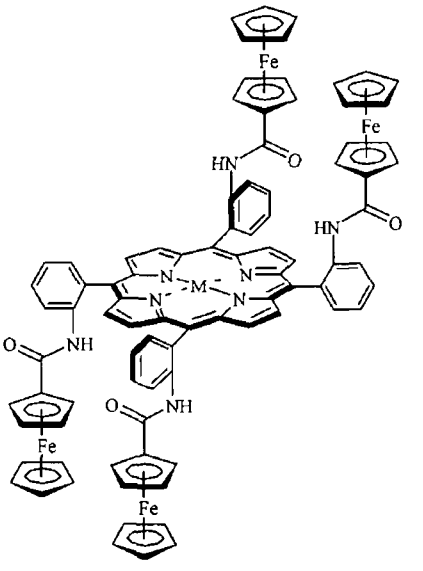

α, α, β, β - atropisomer

Fig 6 - 18 M = 2H, Zn

Similar systems had previously been synthesised by Hisatome[34] *via* Collmans "picket-fence porphyrin" [35] 1,1 - and 1,3- ferrocenoporphyrinophanes were prepared as their free base and Fe(III) and Fe(II) complexes, however the photochemistry of these systems was never studied (fig 6 – 19)

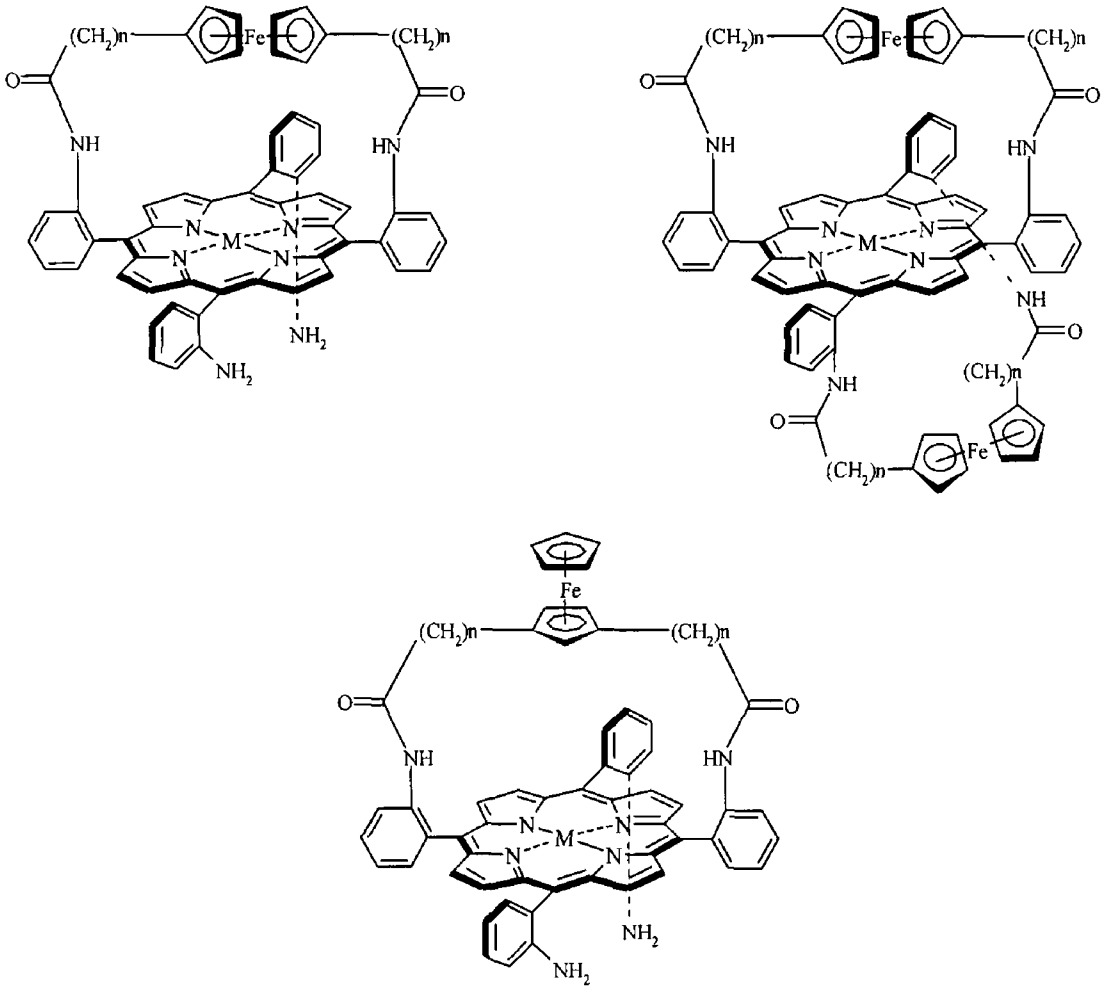

Fig 6 - 19

A number of 1,1 -ferrocenoporphyrinophanes were later prepared by Lindsey et al using the appropriate bis-aldehyde in an effort to understand the effects of strap structural features in porphyrin synthesis (fig 6 – 20) [36] The ferrocene-porphyrin-quinone triad was synthesised *via* a mixed aldehyde synthesis in 4 2 % Although this is quite a low yield it gives ready access to a very complex molecule Quenching of the porphyrin fluorescence was also reported for this triad system however it was neither attributed to the ferrocene or the quinone moiety

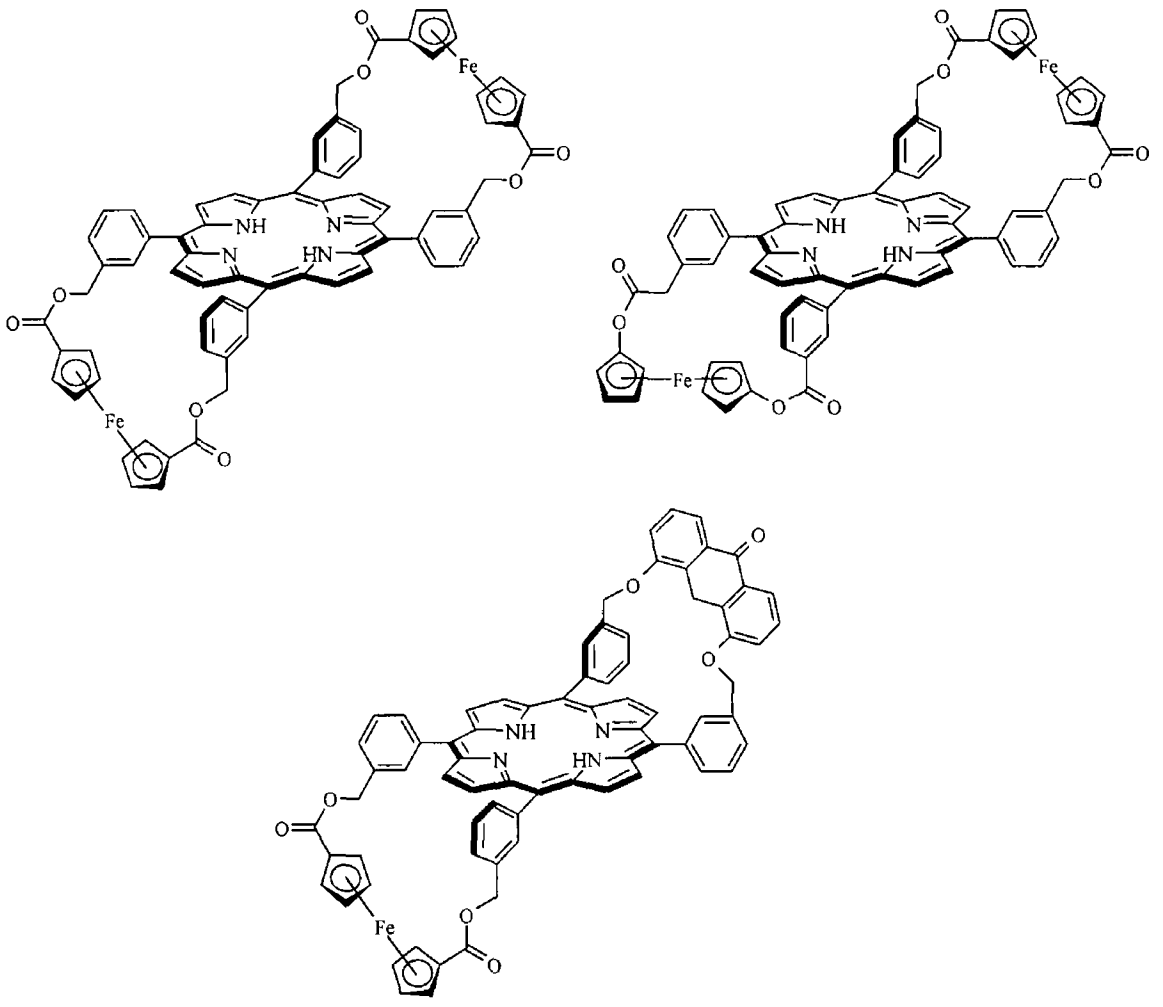

Fig 6 - 20

A synthetic approach for molecular-based multi-bit information storage devices that employ a SAM of redox-active molecules attached to a gold microelectrode[37] or silicon oxide surface has been reported [38] Information is stored in the distinct oxidation states of the redox-active molecules Molecules with an increased number of cationic oxidation states can afford increased memory density A ferrocenyl porphyrin can be cycled between four states (neutral, ferrocene monocation, monocation and dication states of the porphyrin) Thiol and benzylphosphonic acid tethers were utilised for attachment to the gold and silicon oxide surfaces respectively (some examples are shown in figure 6 – 21)

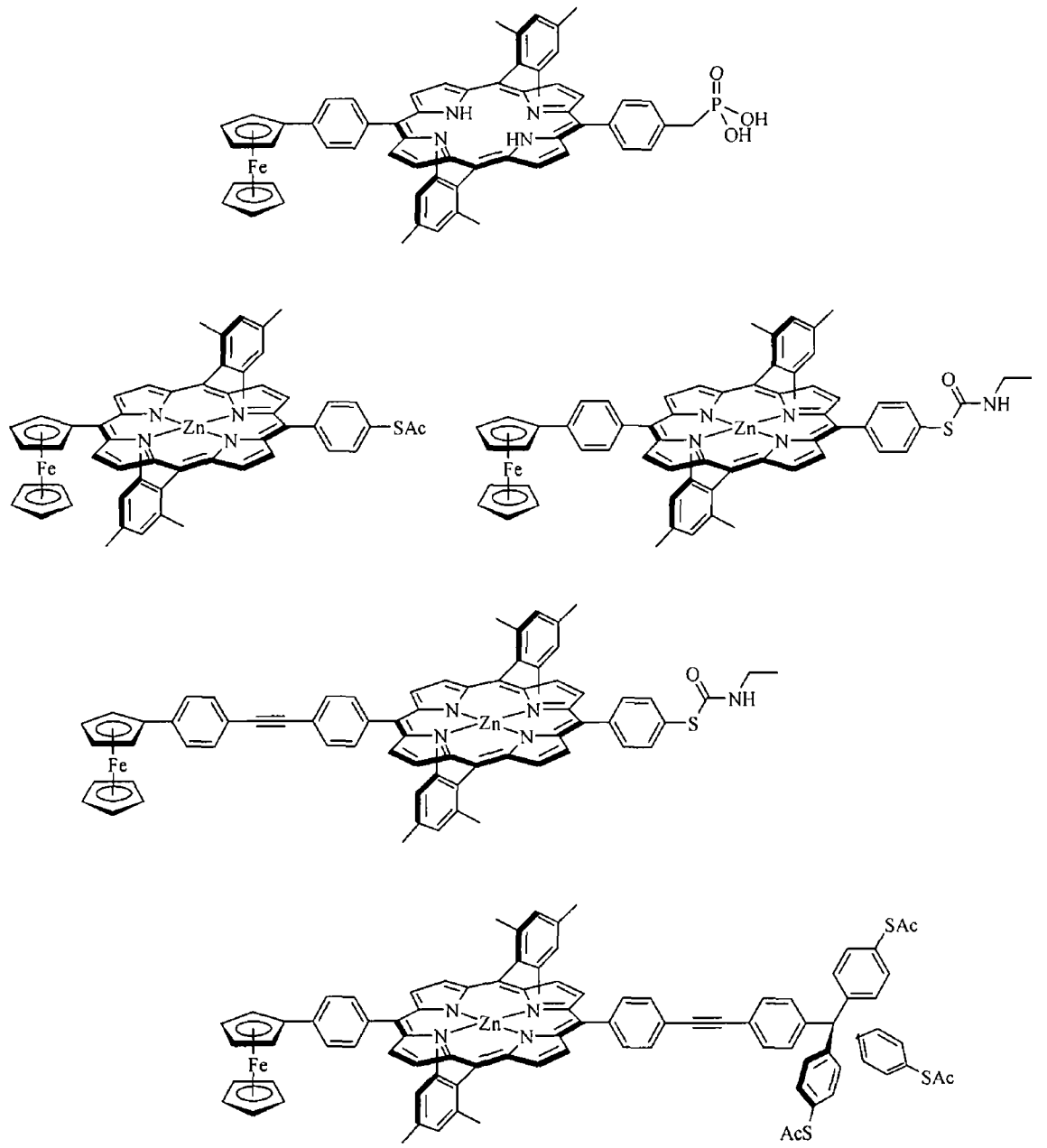

Fig 6 – 21 Some examples of the ferrocenyl porphyrins with applications in multi-bit information storage

All of the compounds studied were each shown to form a robust SAM with reversible electrochemistry The three expected oxidation waves are all well resolved indicating that the ferrocene and porphyrin moieties are electronically isolated from each other A bis-ferrocenyl porphyrin was also studied which showed only one ferrocene based oxidation due to the two identical and electronically isolated metal centres (fig 6 – 22)

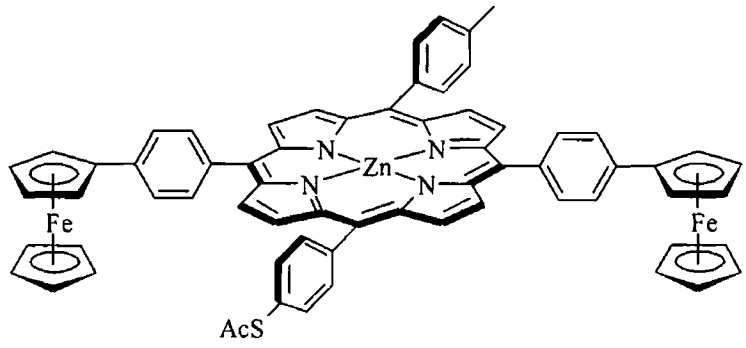

Fig 6 – 22

Recently the synthesis of a series of *meso*-ferrocenylethynyl-5,15-diphenylporphyrins have been reported (fig 6 – 23) [39] The photophysical and electrochemical properties of these systems have not yet been reported however such structures are expected to show interesting non-linear optical properties due to their highly conjugated donor-(π-bridge)-acceptor architecture

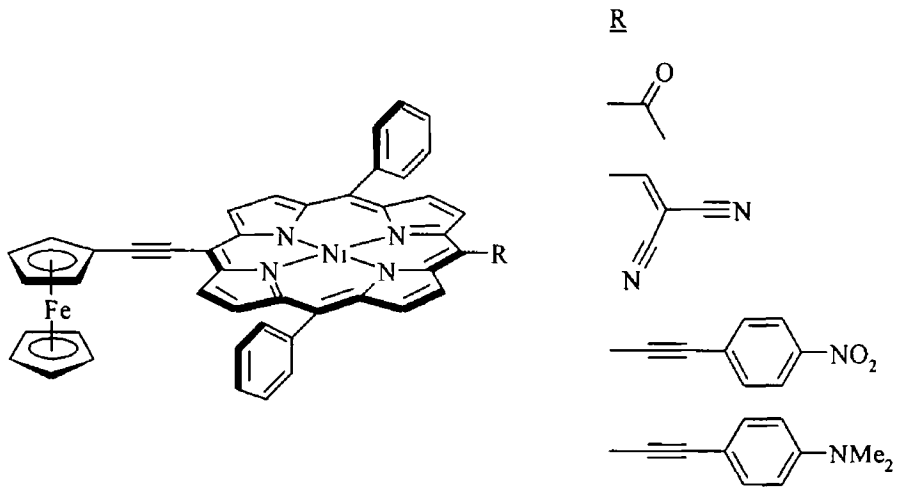

Fig 6 - 23

A novel approach to incorporating the ferrocene moiety into a porphyrin framework was taken by Wang et al who synthesised a bis-porphyrin-ferrocene system where the two cyclopentadienyl rings of the ferrocene unit are fused at the β-positions of two porphyrin rings (fig 6 – 24 a) [40] This unusual complex displayed a broad Soret band with λ_{max} at 416 nm, in addition to a broad absorption at 530 nm in the Q-band region

An analogous mono-porphyrin ruthenium complex was also synthesised, and displayed a λ_{max} at 412 nm with lower energy bands at 450, 534, 576 and 640 nm. The origin of these transitions was not reported. These complexes may display interesting photophysical and electrochemical properties as the metallocene moiety is directly incorporated into the π-system of the porphyrin macrocycle.

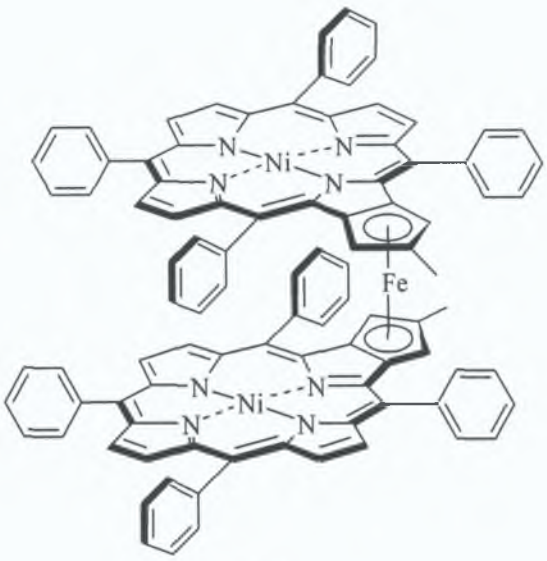

(a)

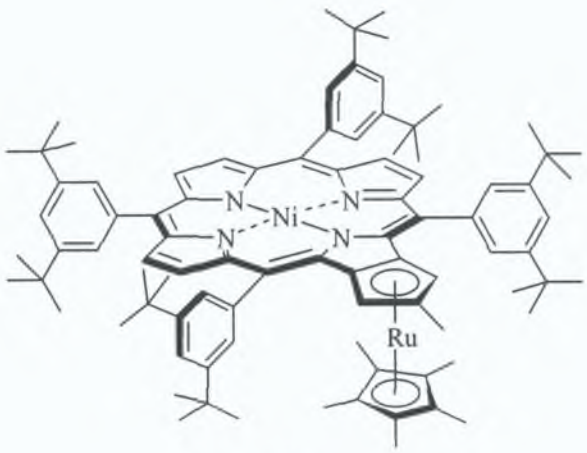

(b)

Fig. 6 - 24

In the following chapter the photophysical properties of *meso*-ferrocenyl porphyrins and their ferrocenium analogues are investigated by laser flash photolysis and by steady state and time resolved fluorescence techniques.

6 3 Experimental and results

6 3 1 Synthesis

ZnFcTPP, NiFcTPP and ZnFcTThP were synthesised as described in chapter 4 The ferrocenium salts [ZnFcTPP][BF_4], [NiFcTPP][BF_4] and [ZnFcTThP][BF_4] were synthesised from their ferrocene precursors, i e ZnFcTPP, NiFcTPP and ZnFcTThP, following a reported procedure [41] 0 05 mmol of ferrocenyl porphyrin was dissolved in 10 ml of THF under an atmosphere of argon The solution was cooled to 0 ^{0}C and 0 75 mmol of $AgBF_4$ (14 60 mg) was added The reaction mixture was allowed to reach room temperature and stirred for an additional hour Any elemental silver was removed by filtration The solvent was subsequently reduced to 1 - 2 ml ex vacuo and the porphyrinatoferrocenium salt was precipitated out by the slow addition of diethyl ether The product was filtered and washed with diethyl ether yielding a dark purple solid (yield *ca* 80 %) ^{1}H-NMR characterisation of the complexes proved unfeasible due to the paramagnetic Fe(III) metal centre The high instability of the ferrocenium salts restricted their characterisation to UV/Vis/NIR and fluorescence spectroscopy by comparison to the spectroelectrochemical spectra of the ferrocenyl precursors

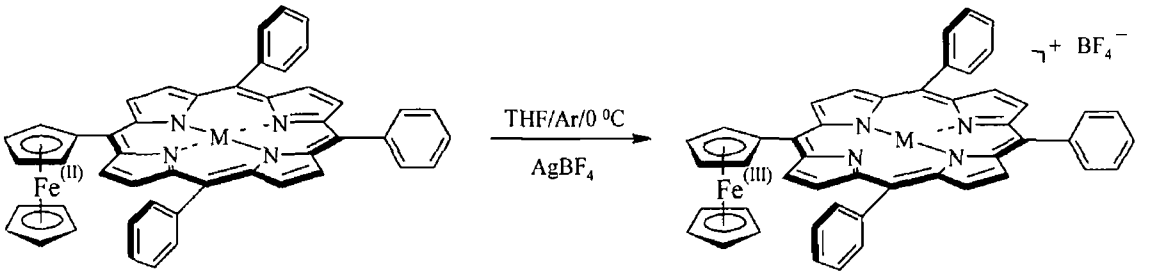

(a)

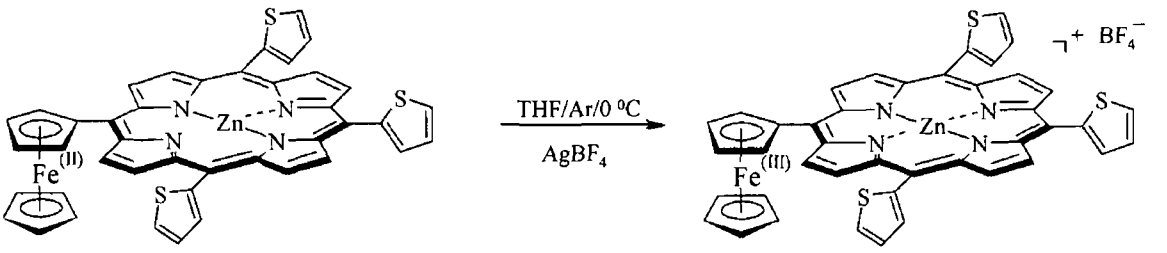

(b)

Rxn 6 – 1 Synthesis of the ferrocenium salts (a) [ZnFcTPP][BF_4], [NiFcTPP][BF_4] and (b) [ZnFcTThP][BF_4]

6 3 2 UV/Vis/NIR absorption spectra

All UV/Vis/NIR spectra were measured in spectroscopic grade solvents at room temperature on a Schimadzu 3100 spectrometer using a 1 cm quartz cell

Porphyrin	Soret (nm)	FWHM (nm)	Q bands (nm)	C T (nm)
ZnTPP	421 (25 26)	9	556 (1 00)	~
			595 (0 38)	
			620 (0 19)	
ZnFcTPP	424 (28 06)	15	572 (1 00)	532 (0 46)
			620 (1 12)	
[ZnFcTPP][BF_4]	423 (13 96)	19	539 (1 00)	789 (0 22)
ZnTThP	428 (21 52)	12	562 (1 00)	~
			604 (0 27)	
ZnFcTThP	429 (24 64)	17	577 (1 00)	535 (0 54)
			626 (0 96)	
[ZnFcTThP][BF_4]	426 (10 73)	28	573 (1 00)	767 (0 25)
			631 (0 86)	
NiTPP	414 (15 82)	18	524 (1 00)	~
			612 (0 15)	
NiFcTPP	412 (11 67)	32	542 (1 00)	691 (0 10)
			587 (0 69)	1175 (0 04)
[NiFcTPP][BF_4]	412 (9 91)	32	542 (1 00)	~ 680 (0 11)
			587 (0 69)	1181 (0 07)

Table 6 - 1 UV/Vis/NIR absorption data of ZnTPP, ZnTThP, NiTPP and their mono-ferrocenyl and ferrocenium analogues recorded in ethanol at room temperature Relative peak intensities are given in brackets

6 3 3 Fluorescence spectra and time correlated single photon counting (TCSPC) measurements

Steady state fluorescence measurements were carried out on a Perkin Elmer LS50 luminescence spectrometer at room temperature All fluorescence spectra were independent of excitation wavelength Excitation and emission slits were both set at 10 nm TCSPC measurements were carried out at the Central Laser Facility, Rutherford Appleton Laboratories [42]

Porphyrin	λ_{max} (nm)	Φ_{Fl} [I, II]	$^{1}\tau$ (ns)
ZnTPP	606, 656	1	1 96
ZnFcTPP	~	~	~
$[ZnFcTPP]^{+}$ [III]	610, 660	0 145	0 51 / 0 94[IV]
ZnTThP	630, 664	1	0 56 / 1 32[IV]
ZnFcTThP	632, 656	0 018	~
$[ZnFcTThP]^{+}$ [III]	622, 666	0 627	0 31 / 1 92[IV]

Table 6 - 2 Fluorescence maxima, relative quantum yields (Φ_{Frel}) and singlet lifetimes ($^{1}\tau$) of ZnTPP, ZnTThP and their mono-ferrocenyl and ferrocemum analogues recorded in ethanol at room temperature

[I] Fluorescence quantum yields were calculated relative to the appropriate tetra-arylporphyrin

[II] All spectra were recorded with excitation wavelength equivalent to the Q band λ_{max} of respective tetra-aryl reference compound, i e 556 and 562 nm for the phenyl- and thienyl compounds respectively

[III] Due to the instability of the tetrafluoroborate salts the time resolved fluorescence studies were carried out on $[ZnFcTPP]^{+}$ and $[ZnFcTThP]^{+}$ following in-situ oxidation with ceric(IV) ammonium nitrate

[IV] Dual emission was observed for porphyrins $[ZnFcTPP]^{+}$, ZnTThP and $[ZnFcTThP]^{+}$ The signals observed consisted of 22 78 %, 70 30 % and 4 96 % of the shorter longer lifetimes respectively

6 3 4 Laser flash photolysis studies

Transient absorption measurements following pulsed laser excitation at 532 nm and 355nm were carried out in spectroscopic grade ethanol under one atmosphere of argon at room temperature A typical sample absorbance of 0 05 (± 0 01) AU was required for ZnTPP and ZnTThP to give intense signals, however more concentrated sample with a typical absorbance of 0 75 (± 0 10) AU was required for the ferrocemum complexes All transient species observed were independent of excitation wavelength and formed within the lifetime of the laser pulse (*ca* 10 ns) A transient species was typically observed for ZnTPP and ZnTThP over the entire range monitored, i e from 750 – 300 nm, with λ_{max} at 460 and 490 nm respectively A depletion of the parent compound was also observed in the Soret region of the spectrum from *ca* 400 - 430 nm The ferrocenium complexes, [ZnFcTPP][BF_4] and [ZnFcTThP][BF_4], showed transient signals of weaker intensity with analogous λ_{max} at 460 and 490 nm respectively All transient species observed are attributed to the lowest lying triplet excited state $^3(\pi\text{-}\pi^*)$ of the porphyrin chromophores The lifetimes of the triplet excited states ($^3\tau$) are given in table 6 - 3 No transient signals were observed for ZnFcTPP, ZnFcTThP, NiTPP and NiFcTPP

Porphyrin	$^3\tau$ (μs)
ZnTPP	22
[ZnFcTPP][BF_4]	12
ZnTThP	40
[ZnFcTThP][BF_4]	20

Table 6 - 3 Triplet lifetimes ($^3\tau$) of ZnTPP, [ZnFcTPP][BF_4], ZnTThP and [ZnFcTThP][BF_4] recorded in ethanol at room temperature

6 3 5 Electrochemistry

All measurements were carried out at room temperature with a conventional three-electrode configuration consisting of a glassy carbon working electrode (2 mm diameter), a platinum wire auxiliary electrode and a SCE reference electrode The solvent used in all experiments was dichloromethane, which was obtained in spectrophotometric grade from Sigma-Aldrich and used as received The supporting electrolyte was 0 1 M tetra-*n*-butylammonium tetrafluoroborate $E_{1/2}$ values were determined as $(E_{pa} + E_{pc})/2$, where E_{pa} and E_{pc} are the anodic and cathodic peak potentials All potentials are quoted in reference to the ferrocene/ferrocemum couple Table 6 - 4 contains a list of the redox potentials recorded Overlays of oxidative and reductive cyclic voltammograms for (a) ZnTPP and ZnFcTPP and (b) ZnTThP and ZnFcTThP are shown in figure 6 – 25

	oxidation			reduction				
	1st	2nd	3rd	1st	2nd			3rd
	$E_{1/2}$	$E_{1/2}$	$E_{1/2}$	$E_{1/2}$	E_{pc}	E_{pa}	$E_{1/2}$	E_{pc}
ZnTPP	0 344	0 664	~	-1 847	-2 283	-2 139	-2 211	~
ZnFcTPP	0 023	0 448	0 695	-1 852	-2 298	-2 113	-2 206	~
ZnTThP	0 429	0 625	~	-1 712	-2 131	-1 964	-2 048	~
ZnFcTThP	0 043	0 469	0 182	-1 753	-2 196	-2 024	-2 110	~
NiTPP	0 546	0 799	~	-2 021	-2 725	~	~	-2 358
NiFcTPP	0 068	0 667	0 841	-2 078	-2 558	~	~	~

Table 6 - 4 Electrochemical data for all compounds studied

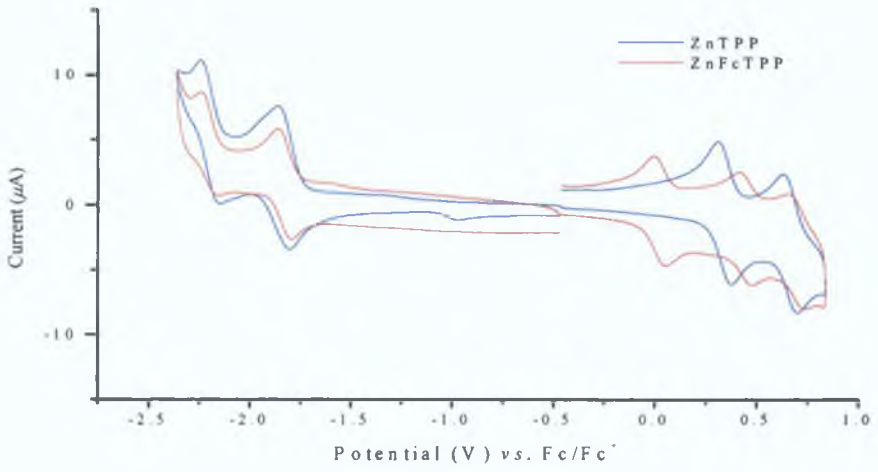

(a)

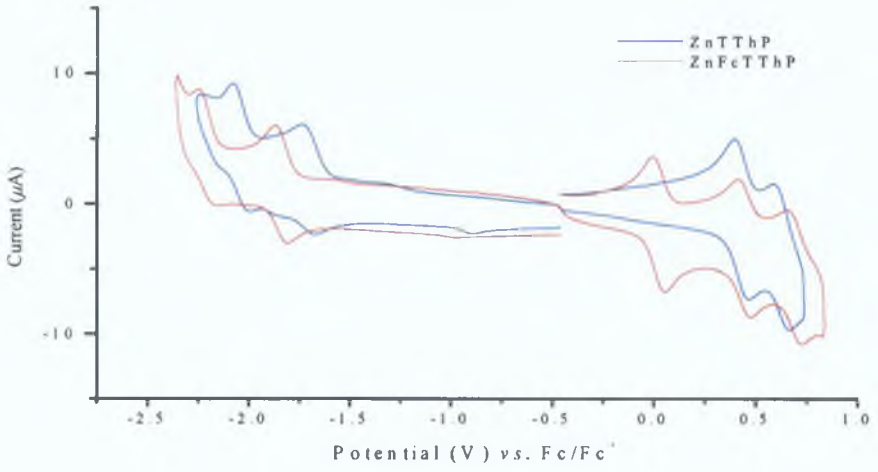

(b)

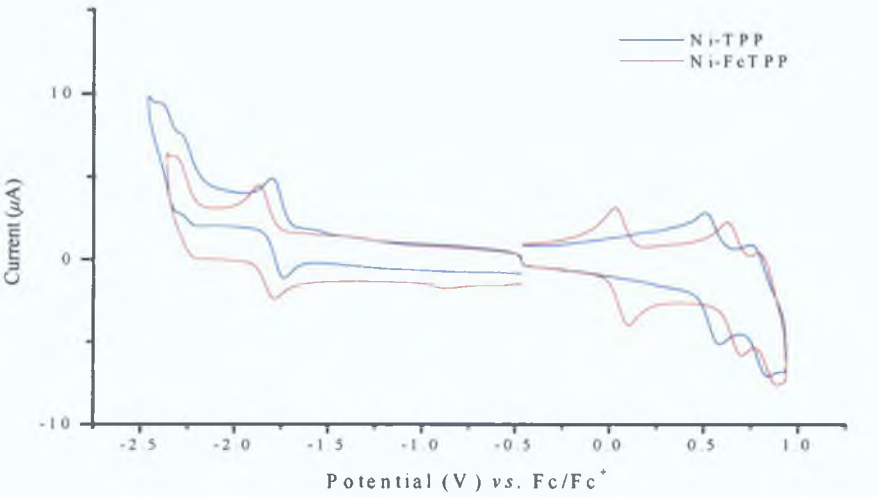

(c)

Fig. 6 – 25: An overlay of oxidative and reductive cyclic voltammograms for (a) ZnTPP and ZnFcTPP (b) ZnTThP and ZnFcTThP and (c) NiTPP and NiFcTPP.

6 3 6 Spectroelectrochemistry

Spectroelectrochemistry was carried out using a platinum-rhodium gauze working electrode, a Ag/AgCl reference electrode and a platinum wire counter electrode 0 1 M tetrabutlyammonium tetrafluoroborate in dichloromethane was used as the electrolyte Spectroelectrochemistry experiments were monitored in the UV/Vis/NIR using a 1 mm path length thin layer Pyrex glass cell on Schimadzu 3100 spectrometer Fluorescence monitored spectroelectrochemistry experiments were recorded on a Perkin-Elmer LS50 luminescence spectrometer using a conventional 1 cm path length quartz cell For all experiments the working electrode was kept at the required potential (+ 0 7 V) during the spectral scan using a CH instrument model 660 potentiostat electrochemical workstation

6.4 Discussion

6.4.1 Photophysical and electrochemical properties of zinc(II)-5-ferrocenyl-10,15,20-triphenylporphyrin and zinc(II)-5-ferrocenium-10,15,20-trithienylporphyrin and their ferrocenium salts

The incorporation of redox-active ferrocene into the porphyrin system allows the photophysical properties of the macrocycle to be modulated by changing the oxidation state of the iron centre. By converting the electron-donating substituent, i.e. ferrocene, to an electron-withdrawing substituent, i.e. the ferrocenium ion, significant changes are induced in the conjugated system. Shown in figure 6 – 26 are the UV/Vis/NIR absorption spectra for ZnTPP, ZnFcTPP, [ZnFcTPP][BF_4], ZnTThP, ZnFcTThP and [ZnFcTThP][BF_4].

Similar changes are observed in the Soret and Q band absorptions for both the phenyl- and thienylporphyrins on going from the tetra-aryl substituted system to the mono-ferrocenyl system. The Soret absorption of ZnTPP is red shifted by 3 nm on replacing one of the *meso*-phenyl groups with a ferrocene moiety. A similar shift of only 1 nm is observed on going from ZnTThP to ZnFcTThP. This shift is not as pronounced for the *meso*-thienyl system as the electron density of the central porphyrin core is already delocalised onto the peripheral *meso*-thienyl rings, whereas there is little electronic communication between the porphyrin ring and the *meso*-phenyl rings of ZnTPP in the ground state (a red shift of 7 nm is observed for the Soret absorption on going from ZnTPP to ZnTThP).[43] The FWHM of the Soret absorption shows an increase (15 nm and 17 nm for ZnFcTPP and ZnFcTThP respectively) in conjunction with this red shift of the λ_{max}. This also suggests increased electronic coupling between the π-systems of the porphyrin and *meso*-aryl substituents. Both of the ferrocenylporphyrins also display a ferrocene based MLCT transition, which absorbs at 532 and 535 nm for ZnFcTPP and ZnFcTThP respectively. The observation of this MLCT transition is further evidence for considerable electronic communication between the ferrocene and porphyrin systems. In previous studies, where a spacer group between the ferrocene and porphyrin π-systems prevents electronic communication, there is no change in the porphyrin

absorbance and no evidence of ferrocene transitions due to their relatively weak absorbance.[20, 25]

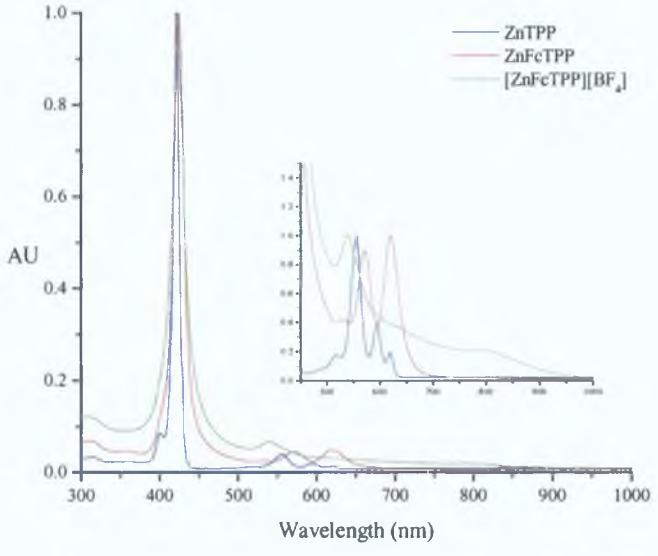

(a)

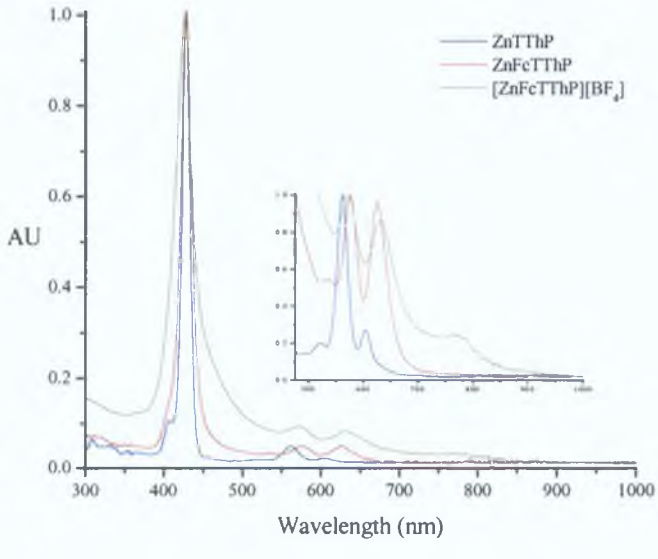

(b)

Fig. 6 - 26: UV/Vis/NIR absorption spectra of (a) ZnTPP, ZnFcTPP, [ZnFcTPP][BF_4] and (b) ZnTThP, ZnFcTThP, [ZnFcTThP][BF_4] in ethanol at room temperature. All spectra have been normalised at their λ_{max}.

More substantial red shifts are seen for the Q bands on replacing one of the *meso*-aryl groups with a ferrocene moiety Also, the relative intensity of the Q(0,0) band increases considerably Gouterman's four-orbital model predicts that the Q(0,0) band intensity is correlated to the energy separation between the nearly degenerate $a_{2u}^{1}e_g^{1}$ and $a_{1u}^{1}e_g^{1}$ transitions of the porphyrin macrocycle [44] The first porphyrin based oxidation increases from 0 344 to 0 448 V on going from ZnTPP to ZnFcTPP and from 0 429 to 0 469 V on going from ZnTThP to ZnFcTThP As there is a stabilisation of the a_{2u} HOMO orbital of ZnFcTPP and ZnFcTThP relative to ZnTPP and ZnTThP respectively the a_{1u} orbital must be stabilised by a greater amount thus increasing the energy difference between the a_{2u}^{1}-LUMO and a_{1u}^{1}-LUMO transitions (as the overall symmetry of the ring is reduced, the degeneracy of the e_g orbitals is broken)

On conversion of the electron-donating ferrocene moiety to the electron-withdrawing ferrocenium ion a small blue shift is induced in the Soret absorption of 1 and 3 nm for [ZnFcTPP][BF_4] and [ZnFcTThP][BF_4] respectively There is also an associated increase in the FWHM of the Soret absorption (18 and 28 nm for the phenyl and thienyl ferrocenium complexes respectively) The most outstanding feature of the mono-ferrocenium porphyrin absorption spectra is the appearance of a broad low-energy CT transition This absorption occurs with λ_{max} at 789 and 767 nm for [ZnFcTPP][BF_4] and [ZnFcTThP][BF_4] respectively This absorption resembles the Fe(II)/Fe(III) IVCT band reported by Boyd et al following oxidation of a bis-ferrocenyl porphyrin The CT bands observed here cannot be assigned to a IVCT band due to the presence of only one ferrocene moiety This absorption is tentatively assigned to a LMCT transition involving the redistribution of electron density from the porphyrin macrocycle to the electron deficient Fe(III) centre [45] [46] This may also be viewed as a delocalisation of the electron hole from the ferrocenium cation onto the π-network of the porphyrin ring

Spectroelectrochemical measurements monitored by UV/Vis/NIR absorption were carried out on ZnFcTPP and ZnFcTThP One-electron oxidation of the ferrocene moiety results in the gradual formation of the $[ZnFcTPP]^+$ and $[ZnFcTThP]^+$ species as evident in the UV/Vis/NIR spectra (fig 6 – 27)

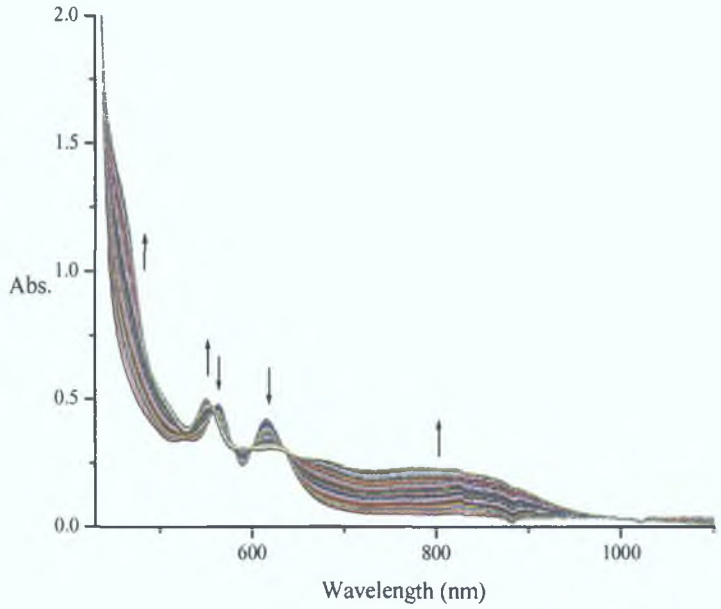

(a)

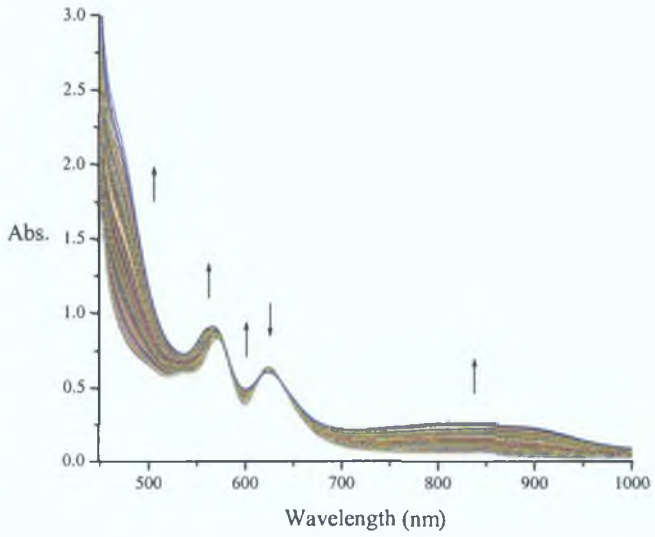

(b)

Fig. 6 – 27: UV/Vis/NIR monitored spectro-electrochemistry of (a) ZnFcTPP and (b) ZnFcTThP in dichloromethane.

ZnTPP and ZnTThP both exhibit strong luminescence, characteristic of porphyrin compounds. By replacing one of the phenyl or thienyl groups of ZnTPP and ZnTThP with a ferrocene moiety their luminescence is quenched. In these complexes ferrocene acts as an efficient electron-donor and quenches the singlet and triplet π–π^* excited

states of the porphyrin by a rapid electron-transfer process followed by vibrational relaxation of the charge transfer excited state ($Fc^{\delta+}$-P^{δ}) to the ground state species (scheme 6 – 3)[47] The fluorescence of the porphyrin ring is completely quenched in ZnFcTPP, whereas ZnFcTThP displays a fluorescence spectrum similar to that of ZnTThP with a relative quantum yield of 0 018 (table 6 – 2) No transient signals attributable to a π–π^* triplet excited state of the porphyrin was observed for either ZnFcTPP or ZnFcTThP

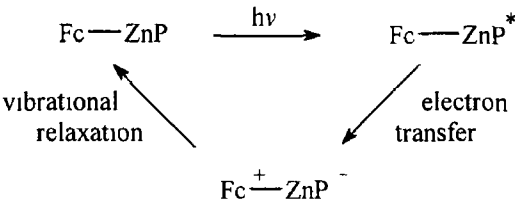

Scheme 6 - 3

In contrast to ferrocene, ferrocenium is a strong electron-acceptor therefore its ability to quench an excited state through an electron-transfer mechanism is reduced On decreasing the electron-transfer efficiency of the iron centre on going from Fe(II) to Fe(III) the luminescent properties of the porphyrin ring are switched on again (fig 6 - 28) The relative fluorescence quantum yield (Φ_F) from both salts is not as efficient as from their tetra-aryl analogues This can be attributed to intersystem crossing of the porphyrin π–π^* excited state to the lower energy LMCT band (scheme 6 – 4) The fluorescence quantum yields of [ZnFcTPP][BF_4] and [ZnFcTThP][BF_4] were calculated to be 0 145 and 0 627 relative to ZnTPP and ZnFcTThP respectively

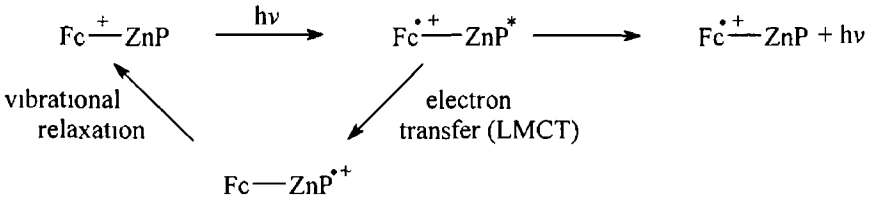

Scheme 6 - 4

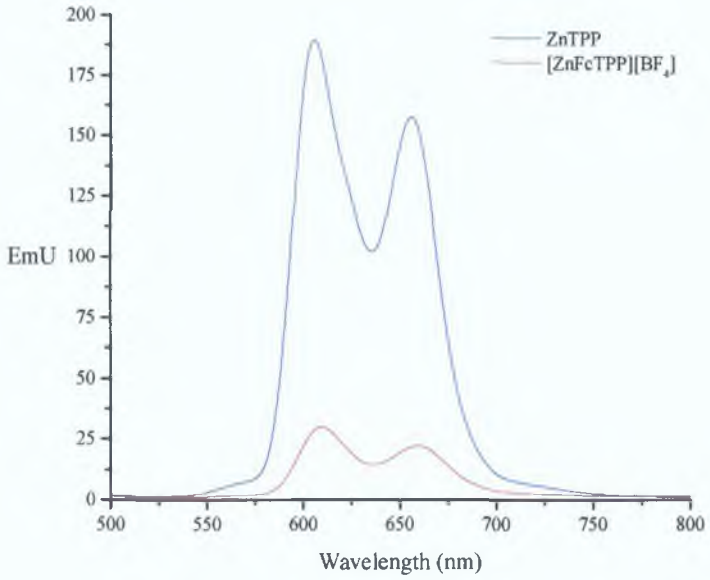

(a)

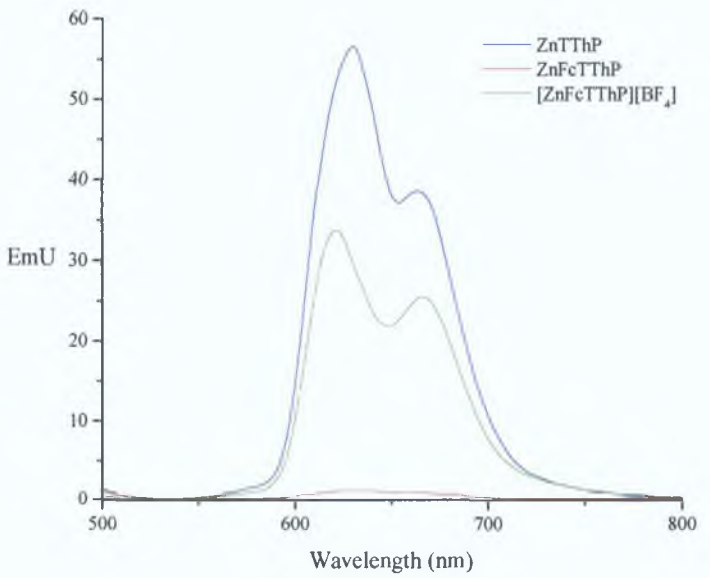

(b)

Fig. 6 – 28: Luminescence spectra of (a) ZnTPP, ZnFcTPP, [ZnFcTPP][BF_4] and (b) ZnTThP, ZnFcTThP, [ZnFcTThP][BF_4] in ethanol at room temperature at 556 and 562 nm excitation respectively.

Spectroelectrochemical measurements were also carried out on ZnFcTPP and ZnFcTThP and monitored by UV/Vis fluorescence. Again, one-electron oxidation of the ferrocene moiety results in the gradual formation of the $[ZnFcTPP]^+$ and $[ZnFcTThP]^+$ species as shown in figure 6 – 29.

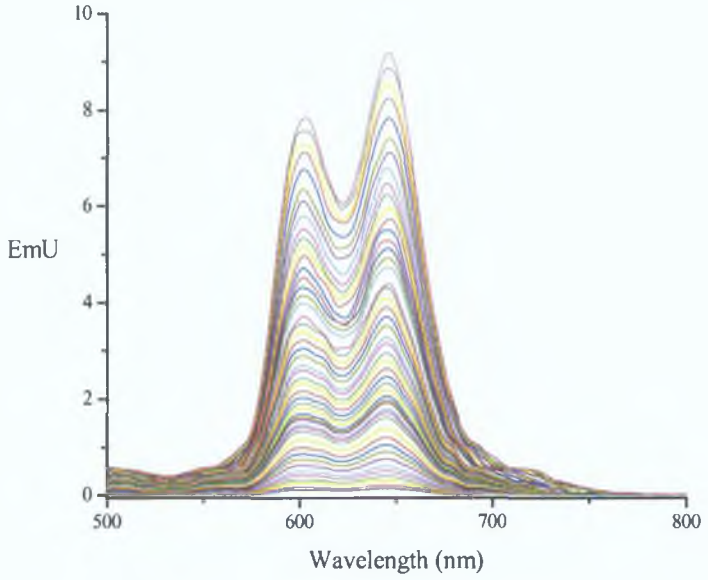

(a)

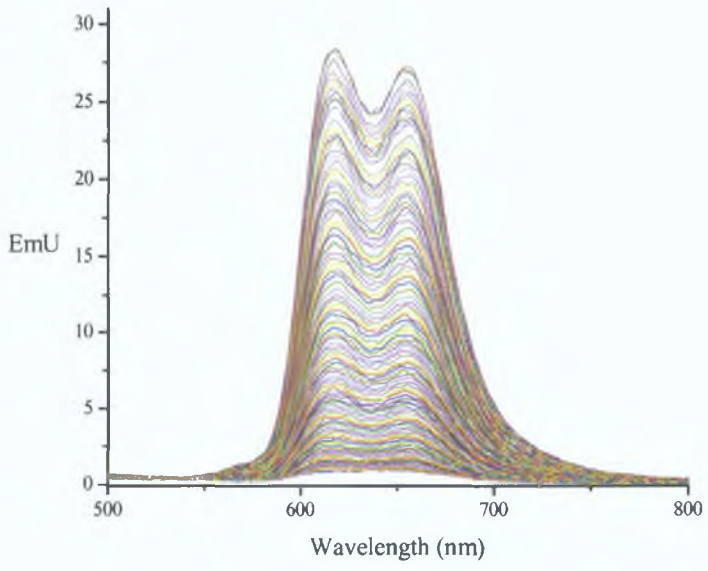

(b)

Fig. 6 – 29: Fluorescence monitored spectroelectrochemistry of (a) ZnFcTPP and (b) ZnFcTThP in dichloromethane.

Following oxidation and formation of the porphyrin salts, the fluorescence of the porphyrin ring is switched on again. The triplet π-π^* excited states of [ZnFcTPP][BF_4] and [ZnFcTThP][BF_4] are again evident in the laser flash photolysis studies. Figure 6 – 30 shows a transient absorption difference spectrum recorded following laser flash photolysis of [ZnFcTPP][BF_4] at 532 nm. The intensity of the transient signal is significantly reduced in comparison to that observed for ZnTPP (fig. 6 – 30), however both λ_{max} are still very evident at 460 nm. ZnTThP and [ZnFcTThP][BF_4] show similar spectra with λ_{max} at 490 nm. [ZnFcTPP][BF_4] also shows a broad depletion from *ca.* 550 – 700 nm most likely due to a decrease in absorption of the CT transition in the excited state compared to the ground state species (fig. 6 – 26 a).

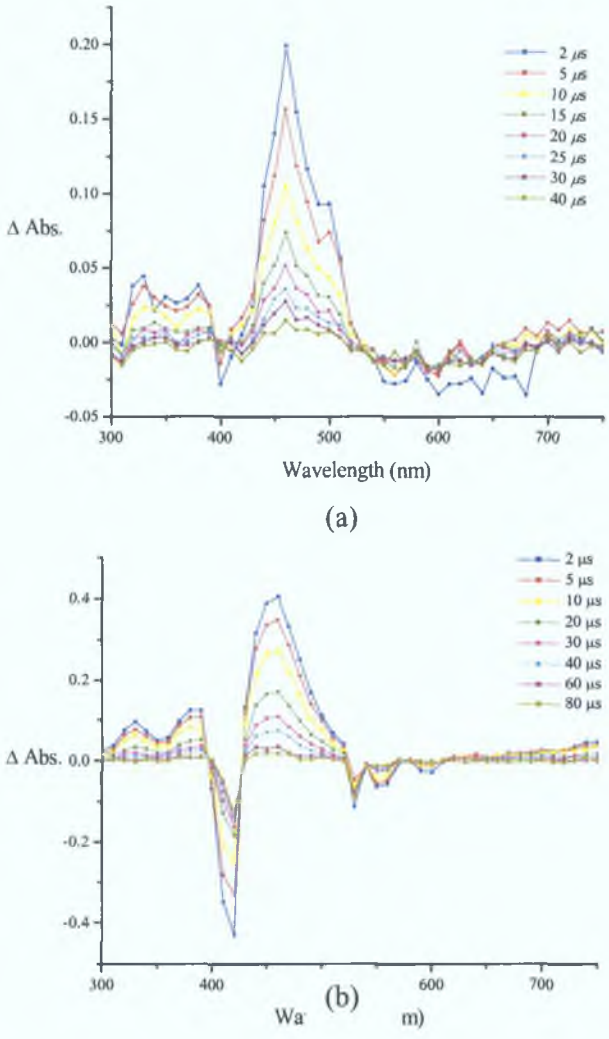

Fig. 6 – 30: Transient difference absorption spectra of (a) [ZnFcTPP][BF_4] and (b) ZnTPP in ethanol following laser excitation at 532 nm under 1 atm argon.

Aswell as a substantial decrease in the intensity of the $^3(\pi\text{-}\pi^*)$ excited state transient signal for the ferrocenium porphyrins there is also a reduction in the lifetime of this species by about 50 %. A lifetime of 12 μs was recorded for [ZnFcTPP][BF_4] in comparison to 22 μs for ZnTPP. Similarly, a lifetime of 20 μs was observed for [ZnFcTThP][BF_4], whereas the triplet $\pi\text{-}\pi^*$ excited state of ZnTThP decays with a lifetime of 40 μs. This reduction in lifetime is attributed to intersystem crossing to the LMCT transition as shown in scheme 6 – 4. An overlay of triplet decays for ZnTThP and [ZnFcTThP][BF_4] is shown in figure 6 – 31.

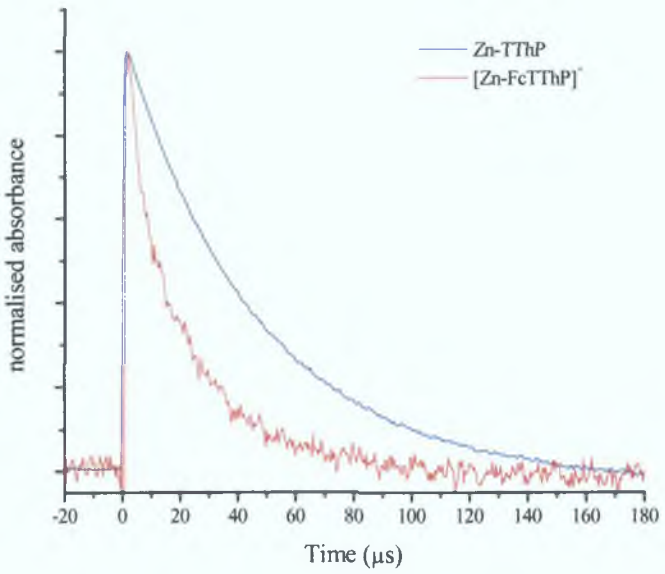

Fig. 6 – 31: An overlay of transient decays of ZnTThP ($^3\tau$ = 40μs) and [ZnFcTThP][BF_4] ($^3\tau$ = 20μs) in ethanol at 490 nm after laser excitation at 532 nm under 1 atm argon. Both signals have been normalised at their absorption maxima.

It should be noted that ZnFcTThP displays an increased first oxidation of + 43 mV in comparison to + 23 mV for ZnFcTPP. This suggests increased communication between the ferrocene unit and the *meso*-thienyl porphyrin ring in comparison to the *meso*-phenyl porphyrin ring. There is also a decrease in the first reduction of the *meso*-thienyl porphyrins with respect to the *meso*-phenyl analogues, which may be a contributing factor to this increased communication. ZnTPP and ZnTThP display first reductions of –1.847 and –1.712 V respectively, whereas ZnFcTPP and ZnFcTThP display first reductions at –1.852 and –1.753 V.

6 4 2 Photophysical and electrochemical properties of nickel(II)-5-ferrocenyl-10,15,20-triphenylporphyrin and its ferrocenium salt

In contrast to ZnTPP, NiTPP does not display any luminescence due to rapid deactivation (< 1 ps) of the porphyrin singlet and triplet $\pi-\pi^*$ excited states *via* the nickel (II) LF excited states [48] Significant changes are again observed in the Soret and Q band absorptions on substitution of a *meso*-phenyl group with a ferrocene unit The UV/Vis/NIR absorption spectrum of NiFcTPP displays a number of differences to its zinc analogue and is more comparable to the ferrocenium complex [ZnFcTPP][BF_4] (fig 6 – 32)

The Soret absorption of NiFcTPP shows a slight blue shift of 2 nm with respect to NiTPP, whereas ZnFcTPP displays a red shift of 3 nm with respect to ZnTPP Similar to the two ferrocenium zinc-porphyrin systems discussed in the previous section, NiFcTPP displays a broad FWHM of the Soret absorption of 32 nm suggesting increased electronic coupling between the π-systems of the porphyrin and *meso*-aryl substituents Due to the broad nature of the Soret absorption, any CT absorptions lying between the Soret and Q bands cannot be observed NiFcTPP does display a low-energy CT transition at 691 nm, which is analogous to the ferrocenium zinc-porphyrin systems There is also a CT transition in the near-infrared evident at 1175 nm The Q(0,0) band of NiTPP is extremely weak in comparison to NiFcTPP suggesting an increased energy difference between the $a_{2u}{}^1$-LUMO and $a_{1u}{}^1$-LUMO transitions similar to the zinc analogues On comparison of the UV/Vis/NIR absorption spectrum of NiFcTPP with the ferrocenium complex [NiFcTPP][BF_4] the Soret and Q bands are identical The two CT bands show small shifts following oxidation of the ferrocene moiety to the ferrocenium tetraflouroborate salt This similarity is also seen in the UV/Vis/NIR monitored spectroelectrochemistry of NiFcTPP where there is only a slight increase in the intensity of the Q(0,0) and CT bands with a weak decrease in the Q(1,0) band (fig 6 – 33)

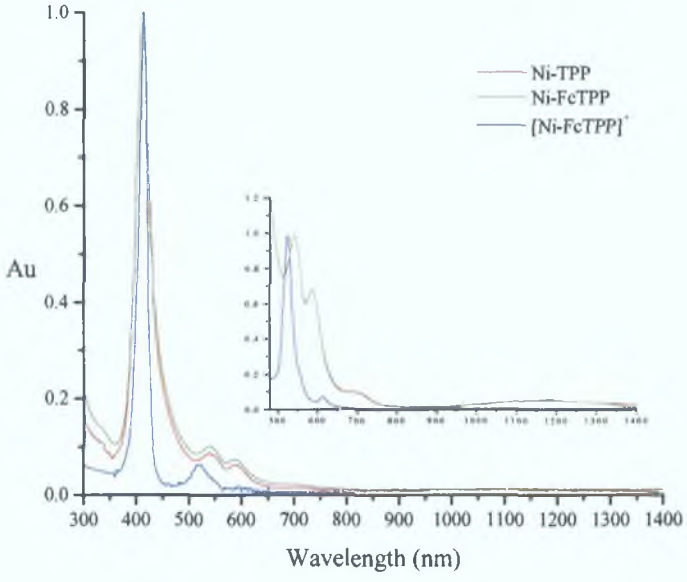

Fig. 6 – 32: Electronic absorption spectra of NiTPP, NiFcTPP, [NiFcTPP][BF_4] in ethanol at room temperature.

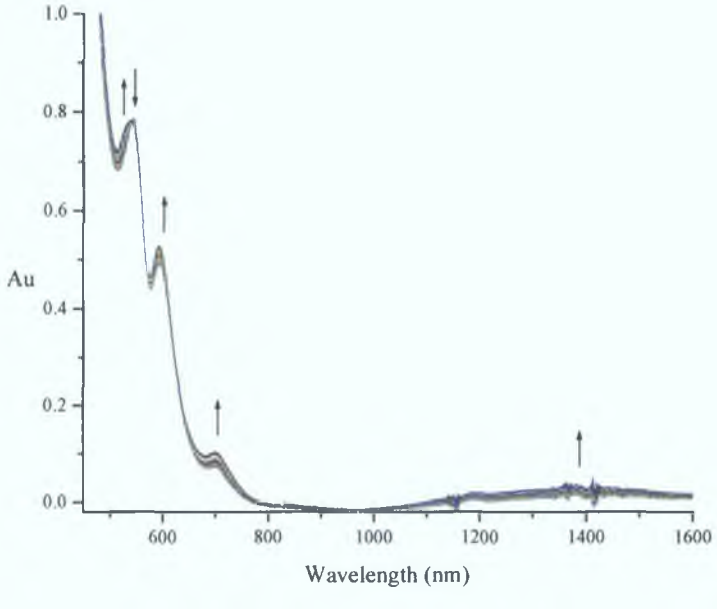

Fig. 6 – 33: UV/Vis/NIR monitored spectroelectrochemistry of NiFcTPP in dichloromethane.

The similarity in the absorption spectra of NiFcTPP and [NiFcTPP][BF_4] is accounted for by the strong ground state communication between the ferrocene/ferrocenium and porphyrin moieties in both systems Such strong communication has been previously reported for similar ferrocenyl nickel-porphyrin systems [11 17 18 19] Possible resonance structures of NiFcTPP and [NiFcTPP][BF_4] are shown in scheme 6 – 5 displaying the similarity between the ferrocene and ferrocenium systems

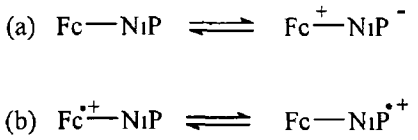

Scheme 6 – 5

The delocalisation of electron density from the ferrocene moiety onto the nickel porphyrin is evident in the electrochemistry of NiFcTPP The first oxidations of ZnFcTTP, ZnFcTThP and NiFcTPP are ferrocene based NiFcTPP shows the most positive potential for this oxidation of + 68 mV with respect to the ferrocene/ ferrocenium redox couple This value is almost three times that observed for ZnFcTPP (+ 23 mV)

6 5 Conclusions

The above studies have proved efficient communication between the porphyrin ring and a *meso*-ferrocenyl moiety exists Fluorescence of the zinc(II)porphyrin macrocycle was quenched by the presence of the ferrocene moiety at the *meso*-position of the macrocycle Oxidation of the ferrocene unit to the ferrocemum salt switched the porphyrin fluorescence back on, with relative quantum yields of 0 145 and 0 627 for [ZnFcTPP][BF_4] and [ZnFcTThP][BF_4] respectively Electrochemical studies indicated a greater communication between the porphyrin and ferrocene units for the nickel(II)porphyrin system NiFcTPP

6 6 Bibliography

[1] (a) R P Kingsborough, T M Swager, "Transition Metals in Polymeric π-Conjugated Organic Frameworks", in *Progress in Inorganic Chemistry*, (Ed K D Karlin, J E), Wiley, **1999**, Vol 48, p 123 (b) N J Long, C K Williams, *Angew Chem Int Ed* **2003**, 42, 2586

[2] V Balzani, F Scandola, "Photochemical and Photophysical Devices", in *Comprehensive Supramolecular Chemistry* (Eds J L Atwood, J E D Davies, D D Macmcol, F Vogtle), Pergamon Press, Oxford, **1996**, Vol 10, p 687

[3] *The Porphyrin Handbook*, eds K M Kadish, K M Smith, R Guilard, Academic Press Boston, 2003, Vol 18

[4] N Aratani, A Osuka, H S Cho, D Kim, *J Photochem Photobiol C Photochem Rev 3* **2002**, 25

[5] T Nakai, K Ban, K Ohta, M Kimura, *J Mater Chem* **2002**, 12, 844

[6] M Calvete, G Ying Yang, M Hanack, *Synth Metals* **2003**, 141, 231

[7] F C Krebs, O Hagemann, M Jorgensen, *Sol Energy Mater Sol Cells* **2004**, 83, 211

[8] C -M Che, Y -J Hou, M C W Chan, J Guo, Y Liu, Y Wang, *J Mater Chem* **2003**, 13, 1362

[9] R G Wollman, D N Hendrickson, *Inorganic Chem* **1977**, 16, 3079

[10] N M Loim, N V Abramova, V I Sokolov, *Mendeleev Commun* **1996**, 46

[11] P D W Boyd, A K Burrell, W M Campbell, P A Cocks, K C Gordon, G B Jameson, D L Officer, Z Zhao, *Chem Commun* **1999**, 637

[12] G M Brown, T J Meyer, D O Cowan, C LeVanda, F Kaufman, P V Roling, M D Rausch, *Inorg Chem* **1975**, 506

[13] W H Morrison, S Krogsrud, D N Hendrickson, *Inorg Chem* **1973**, 12, 1998

[14] (a) S Barlow, S R Marder, *Chem Commun* **2000**, 1555 (b) S Barlow, L M Henling, M W Day, W P Schaefer, J C Green, T Hascall, S R Marder, *J Am Chem Soc* **2002**, 124, 6285

[15] A K Burrell, W Cambell, D L Officer, S M Scott, K C Gordon, M R McDonald, *J Chem Soc , Dalton Trans* **1999**, 3349

[16] A K Burrell, W Cambell, D L Officer, *Tetrahedron Letters*, **1997**, 38, 1249

[17] J Kim, S Woo Rhee, Y H Na, K P Lee, Y Do, S C Jeoung, *Bull Korean Chem Soc* **2000**, 309, 49

[18] S Woo Rhee, B B Park, Y Do, J Kim, *Polyhedron* **2000**, 19, 1961

[19] S Woo Rhee, Y H Na, Y Do, J Kim, *Inorg Chim Acta* **2000**, 309, 49

[20] E S Schmidt, T S Calderwood, T C Bruice, *Inorg Chem* **1986**, 25, 3718

[21] Z H Wang, K C Chen, H Tian, *Chem Lett* 5 **1999**, 423

[22] D P Rillema, J K Nagle, L F Barringer Jr , T J Meyer, *J Am Chem Soc* **1981**, 103, 56

[23] U Siemeling, J Vor der Bruggen, U Vorfeld, B Neumann, A Stammler, H-G Stammler, A Brockhinke, R Plessow, P Zanello, F Laschi, F F de Biani, M Fontani, S Steenken, M Stapper, G Gurzadyan *Chem Eur J* **2003**, 2819

[24] P D Beer, S S Kurek, *J Organomet Chem* **1989**, C6-C8, 366

[25] R Giasson, E J Lee, X Zhao, M S Wrighton, *J Phys Chem* **1993**, 97, 2596

[26] K M Kadish, Q Y Xu and J -M Barbe, *Inorg Chem* **1987**, 26, 2565

[27] G B, Maiya, J -M Barbe and K M Kadish, *Inorg Chem* **1989**, 28, 2524

[28] T Kondo, T Kanai, K Isoo, K Uosaki, *Z Phys Chem* **1999**, 212, 22

[29] H Imahori, H Yamada, S Ozawa, K Ushida, Y Sakata, *Chem Commun* **1999**, 1165

[30] H Imahori, Y Mori, Y Matano, *J Photochem Photobio C Photochem Rev* **2003**, 4, 51

[31] N B Thornton, H Wojtowicz, T Netzel, D W Dixon, *J Phys Chem* B **1998**, 102, 2101

[32] P Tecilla, R P Dixon, G Slobodkin, D S Alavi, D H Waldeck, A D Hamilton, *J Am Chem Soc* **1990**, 112, 9408

[33] (a) P D Beer, M G B Drew, D Hesek, R Jagessar, *J Chem Soc Chem Commun* **1995**, 1187 (b) P D Beer, M G B Drew, R Jagessar, *J Chem Soc Dalton Trans* **1997**, 881

[34] M Hisatome, S Takano, K Yamakawa, *Tetrahedron Letters* **1985**, 26, 2347

[35] J P Collman , J I Brauman , J P Fitzgerald , P D Hampton , Y Naruta , J W Sparapany , J A Ibers, *J Am Chem Soc* **1988**, 110, 3477

[36] R W Wagner, T E Johnson, J S Lindsey, *Tetrahedron* **1997**, 53, 6755

[37] (a) D T Gryko, F Zhao, A A Yasseri, K M Roth, D F Bocian, W G Kuhr, J S Lindsey, *J Org Chem* **2000**, *65*, 7356 (b) L Wei, K Padmaja, W J Youngblood, A B Lysenko, J S Lindsey, D F Bocian, *J Org Chem* **2004**, *69*, 1461

[38] R S Loewe, A Ambroise, K Muthukumaran, K Padmaja, A B Lysenko, G Mathur, Q Li, D F Bocian, V Misra, J S Lindsey, *J Org Chem* **2004**, *69*, 1453

[39] K -L Cheng, H -W Li, D K P Ng, *J Organomet Chem* **2004**, 689, 1593

[40] H J H Wang, L Jaquinod, D J Nurco, M G H Vicente, K M Smith *Chem Commun* **2001**, 2646

[41] J Blumel, N Hebendanz, P Hudeczek, F H Kohler, W Strauss, *J Am Chem Soc* **1992**, 114, 4223

[42] A schematic diagram of the experimental set-up is available at http //www clf rl ac uk/Facilities/LSF/LML/confocal/resources/spc htm

[43] This is elaborated upon in Chapter 5

[44] P J Spellane, M Gouterman, A Antipas, S Kim, Y C Liu, *Inorg Chem* **1980**, 19, 386

[45] Y S Sohn, D N Hendrickson, H B Gray, *J Amer Chem Soc* **1971**, 93, 3603

[46] M Malaun, R Kowallick, A M McDonagh, M Marcaccio,R L Paul, I Asselberghs, K Clays, A Persoons, B Bildstein, C Fiorini, J -M Nunzi, M D Ward, J A McCleverty, *J Chem Soc , Dalton Trans* **2001**, 3025

[47] V A Nadtochenko, D V Khudyakov, N V Abramova, E V Vorontsov, N M Loim, F E Gostev, D G Tovbin, A A Titov, O M Sarkisov, *Russ Chem Bull* **2002**, 51, 986

[48] (a) A Antipas, M Gouterman, *J Am Chem Soc* **1983**, 105, 4896 (b) J Rodriguez, C Kirmaier, D J Holten, *Chem Phys* **1991**, 94, 6020

Chapter 7

Future Work

7 1 Chapters 2 and 3

Steady state and laser flash photolysis studies of the ferrocenyl Fischer-carbenes studied in chapters 2 and 3 indicated CO loss occurs for all compounds studied However, further studies are required, in particular time-resolved infrared (TRIR) and time-resolved resonance Raman (TRrR) to fully characterise the transient species formed following photolysis EFISH measurements of these complexes have to be completed

7.2 Chapter 5

The excited state properties of the *meso*-thienyl substituted porphyrins are attractive towards a number of optoelectronic applications An increased donor-acceptor interaction in the excited state of a molecule can lead to large differences in ground and excited state dipoles ultimately giving rise to large hyperpolarisabilities for nonlinear optical applications Also, such compounds could have potential as optical limiters due to an increased ratio of excited state absorbance cross-section to ground state absorbance cross-section and also their enhanced intersystem crossing

The desilylated tetraethynylporphyrin ZnTEtThP can potentially undergo coupling at each of the terminal ethynyl moieties leading to extended systems and possibly even dendrimetic structures Preliminary studies on the free base analogue H_2TEtThP have shown some positive results When reacted under Sonogashira coupling conditions with an excess of 2-bromothiophene-5-carboxaldehyde, ^{1}H-NMR analysis revealed the presence of the tetra-functionalised porphyrin (rxn 7 – 1) The mono, di and tri-functionalised systems were also present albeit in a lower quantity, however reaction conditions still have to be optimised The porphyrin also appeared to undergo some metallation during the reaction Use of the metallated porphyrin ZnTEtThP should preclude any insertion of the palladium catalyst into the porphyrin centre

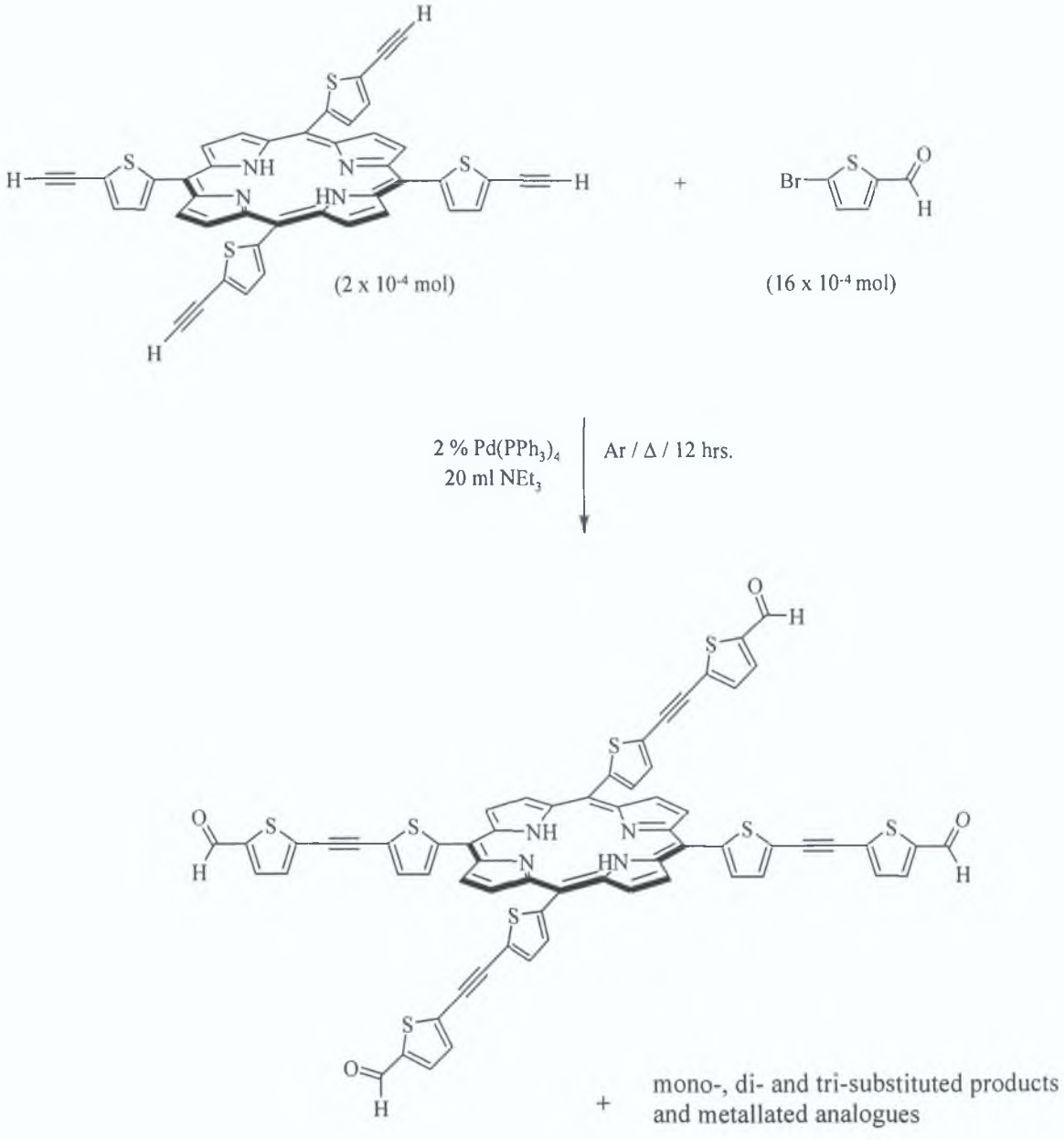

Rxn. 7 - 1

On coupling H_2TEtThP with the (η^5-Cp)Ru(PPh_3)$_2$ moiety at each of the ethynyl positions, the reaction almost went to completion without any metallation occurring (rxn. 7 – 2). Such a complex could have interesting optoelectronic and electrochemical properties. Close inspection of the two free base protons at *ca.* – 2.8 ppm showed slight asymmetry of the peak suggesting the presence of more than one porphyrin. Again, the reaction conditions for this synthesis have yet to be optimised.

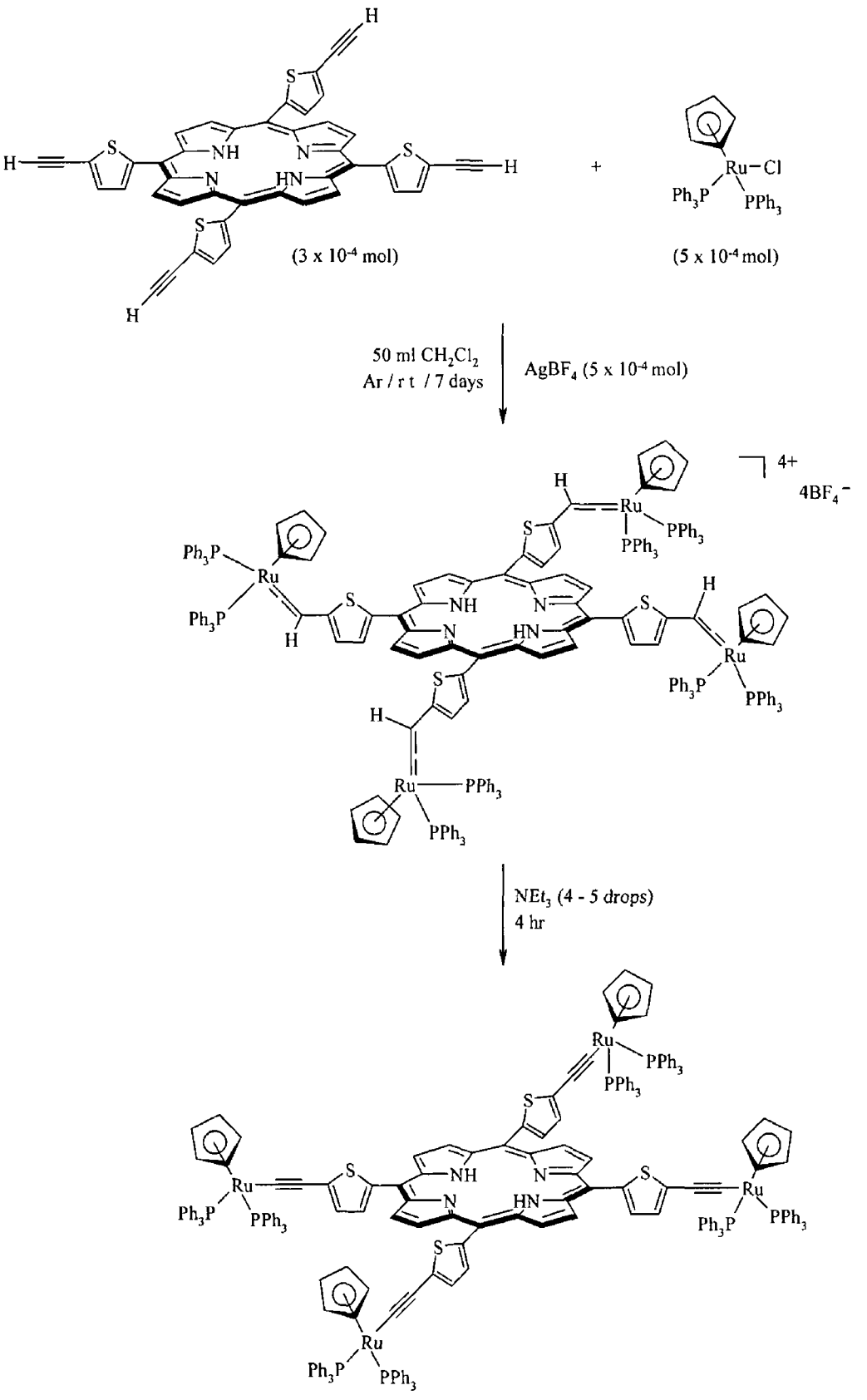
(3 x 10⁻⁴ mol)
(5 x 10⁻⁴ mol)
50 ml CH2Cl2
Ar / r t / 7 days
AgBF4 (5 x 10⁻⁴ mol)
4+
4BF4⁻
NEt3 (4 - 5 drops)
4 hr

Rxn 7 - 2

The photophysical properties of the *meso*-thien-2-yl substituted porphyrins studied in chapter 5 make them attractive towards artificial photosynthetic devices Two compounds are shown in figure 7 – 1 that may show interesting photophysical properties in comparison to previous studies by Benites and co-workers on similar multiporphyrin systems [1]

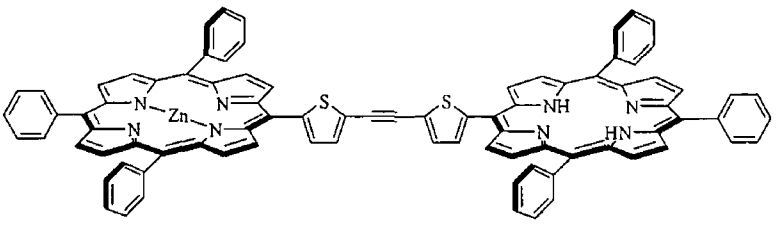

(a)

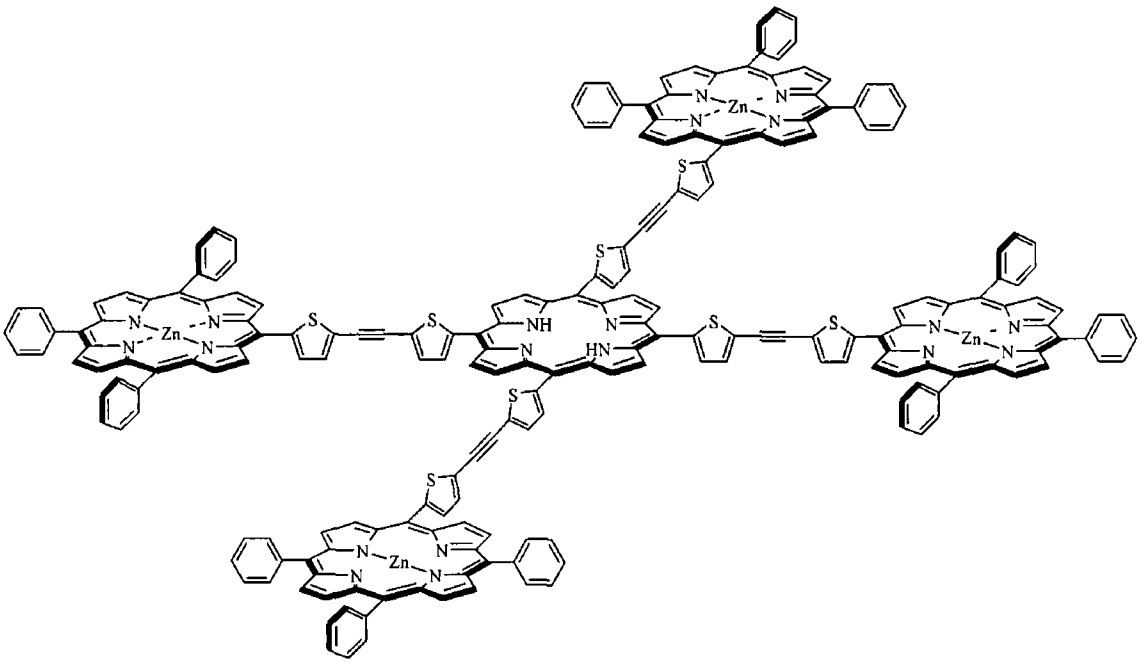

(b)

Fig 7 - 1

7 3 Chapter 6

In view of the results obtained for the *meso*-ferrocenyl porphyrins obtained in chapter 6 synthesis, the synthesis of a *meso*-substituted cobaltocene porphyrin is an attractive prospect (fig 7 – 2) It is anticipated that the latter complex may possess similar properties as the *meso*-ferrocenium complexes studied Unlike ferrocemum however, cobaltocene is relatively stable in the Co(III) oxidation state as a salt Cobaltocene is also diamagnetic thus making characterisation relatively straight forward in comparison to ferrocemum

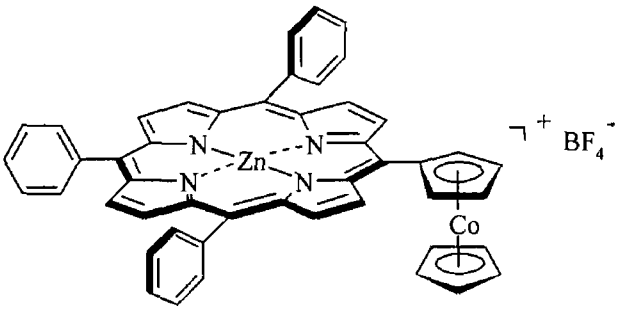

Fig 7 – 2

7 4 $(\eta^5$-Cp)Ru(PPh$_3)_2$ complexes

Preliminary synthetic studies of $(\eta^5$-Cp)Ru(PPh$_3)_2$ appended systems containing dicyanovinyl ligands have shown some interesting results An example of some of the mono- and bis-$(\eta^5$-Cp)Ru(PPh$_3)_2$ systems investigated are shown in figure 7 – 3 Shown in figure 7 – 4 are two examples of the tetra-$(\eta^5$-Cp)Ru(PPh$_3)_2$ systems investigated All complexes were syntesised by a general procedure similar to that reported by Garcia and co-workers [2]

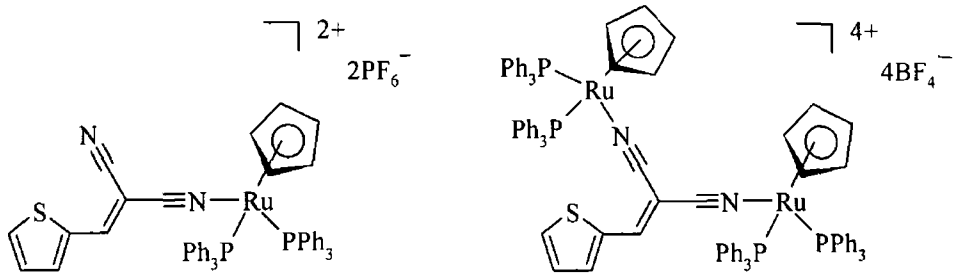

Fig 7 – 3

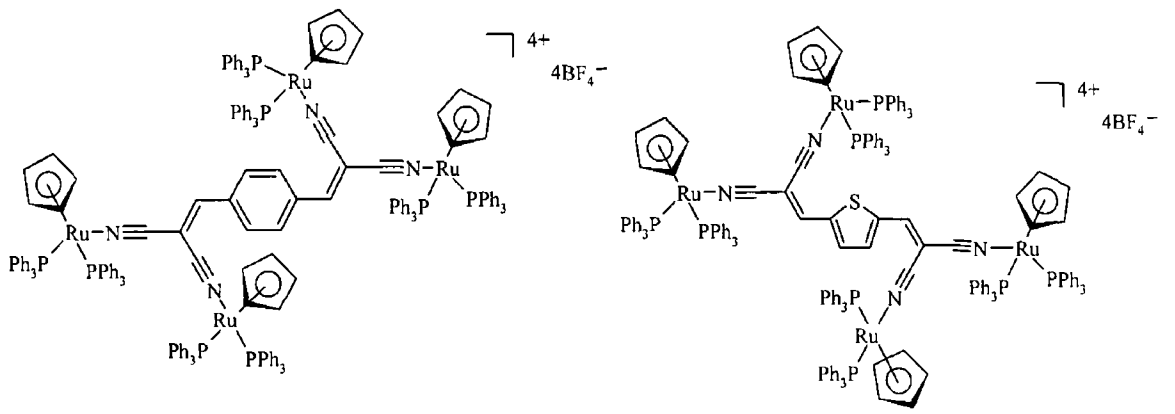

Fig 7 – 4

These poly-ruthenium complexes show CT transitions in the visible region extending out to *ca* 800nm Such complexes may posses interesting third-order nonlinear optical properties [3] A number of derivatives have also been synthesised with a view to couple suitable electron acceptors to the polyruthemum complexes towards second-order nonlinear optical devices (fig 7 – 5)

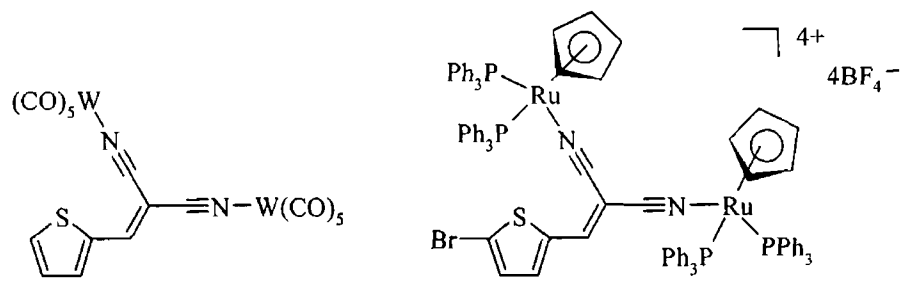

Fig 7 – 5

7 5 Bibliography

[1] M R Benites, T E Johnson, S Weghorn, L Yu, P D Rao, J R Diers, S I Yang, C Kirmaier, D F Bocian, D Holten, J S Lindsey, *J Mater Chem* **2002**, 12, 65

[2] M H Garcia, J C Rodrigues, A R Dias, M F M Piedade, M T Duarte, M P Robalo, N Lopes, *J Organomet Chem* **2001**, 632, 133

[3] C E Powell, M G Humphrey, *Coord Chem Rev* **2004**, 248, 725

Appendix

Appendix

A1 Sample preparation for laser flash photolysis experiments

All samples were prepared for laser flash photolysis in a quartz fluorescence cell attached to a glass degassing bulb by dissolution in the appropriate solvent Each solution was filtered before addition to the fluorescence cell to avoid the presence of light scattering particles The concentration of compound in each sample was adjusted so that the absorbance at the excitation wavelength (λ_{nm} = 532, 355, 266 nm) was between 0 8 and 1 2 absorbance units If needed, the exact concentration could be calculated from previously calculated molar extinction coefficients The sample was then degassed by three cycles of a freeze-pump-thaw procedure to 10^{-3} Torr, followed by a substantial liquid pump phase in order to remove traces of water and carbon dioxide not removed in the degassing procedure Either one atmosphere of argon or a required atmosphere of carbon monoxide is then placed over the sample under the guidance of a pressure gauge The concentration of carbon monoxide in cyclohexane at room temperature at one atmosphere of carbon monoxide has been calculated to be $9\,0 \times 10^{-3} M$ [1] For variable temperature experiments it was assumed that the concentration of carbon monoxide in solution remained constant over the temperature range used

On flashing the sample over a monitoring wavelength range of 800 –2 70nm filters for $\lambda > 500$, 400, 320 nm were employed to reduce excessive photodegradation of the sample The UV-vis absorption spectra were recorded before and after each flash photolysis experiment and also after every 5-15 strikes of the laser (depending on sample sensitivity) to observe any possible spectral changes and to ensure the sample stability

[1] J Makranczy, K Megyery-Balog, L Rosz, D Patyt, *Hung J Ind Chem* , **1976**, 4, 269

A2 Crystal data and experimental parameters for $(CO)_5Cr=C(OMe)Fc$

A2 1 Crystal data and structure refinement for $(CO)_5Cr=C(OMe)Fc$

Identification code	mpome2	
Empirical formula	C17 H12 Cr Fe O6	
Formula weight	420 12	
Temperature	153(2) K	
Wavelength	0 71073 Å	
Crystal system	Orthorhombic	
Space group	Pca2(1)	
Unit cell dimensions	a = 19 941(9) Å	a= 90°
	b = 6 934(3) Å	b= 90°
	c = 11 642(5) Å	g = 90°
Volume	1609 8(12) $Å^3$	
Z	4	
Density (calculated)	1 733 Mg/m^3	
Absorption coefficient	1 607 mm^{-1}	
F(000)	848	
Crystal size	0 69 x 0 60 x 0 26 mm^3	
Theta range for data collection	2 04 to 25 00°	
Index ranges	-23<=h<=21, -8<=k<=7, -13<=l<=13	
Reflections collected	6988	
Independent reflections	2777 [R(int) = 0 0217]	
Completeness to theta = 25 00°	99 7 %	
Absorption correction	Semi-empirical from equivalents	
Max and min transmission	1 0000 and 0 6251	
Refinement method	Full-matrix least-squares on F^2	
Data / restraints / parameters	2777 / 1 / 227	
Goodness-of-fit on F^2	1 031	
Final R indices [I>2sigma(I)]	R1 = 0 0635, wR2 = 0 1490	
R indices (all data)	R1 = 0 0638, wR2 = 0 1496	
Absolute structure parameter	0 25(3)	
Largest diff peak and hole	3 528 and -0 679 e $Å^{-3}$	

A2 2 Atomic coordinates (x 10^4) and equivalent isotropic displacement parameters (Å^{2}x 10^3) for $(CO)_5Cr=C(OMe)Fc$ U(eq) is defined as one third of the trace of the orthogonalized U^{ij} tensor

	x	y	z	U(eq)
Cr(1)	5390(1)	7951(1)	-168(1)	19(1)
Fe(1)	7474(1)	10459(1)	580(1)	19(1)
C(1)	6249(2)	7659(6)	842(4)	19(1)
C(2)	6938(2)	7961(6)	452(4)	17(1)
C(3)	7163(2)	8603(7)	-659(4)	20(1)
C(4)	7885(2)	8661(7)	-631(5)	26(1)
C(5)	8099(2)	8087(6)	462(5)	24(1)
C(6)	7522(2)	7649(7)	1156(5)	20(1)
C(7)	6865(2)	12674(7)	1125(5)	25(1)
C(8)	7201(3)	13208(6)	95(5)	30(1)
C(9)	7906(3)	13103(6)	320(5)	29(1)
C(10)	8007(3)	12533(8)	1485(6)	36(1)
C(11)	7355(3)	12274(7)	1980(5)	29(1)
O(12)	6290(2)	7138(5)	1932(3)	26(1)
C(13)	5732(3)	6641(9)	2630(5)	32(1)
C(14)	5694(2)	10400(6)	-720(4)	23(1)
O(15)	5823(2)	11860(5)	-1081(4)	34(1)
C(16)	4894(2)	9282(7)	982(5)	24(1)
O(17)	4572(2)	10122(6)	1619(3)	35(1)
C(18)	5025(2)	5543(7)	303(5)	28(1)
O(19)	4780(2)	4105(6)	511(4)	42(1)
C(20)	5839(2)	6640(6)	-1404(4)	23(1)
O(21)	6087(2)	5876(6)	-2154(3)	39(1)
C(22)	4659(2)	8225(7)	-1153(5)	26(1)
O(23)	4202(2)	8428(6)	-1739(4)	39(1)

A2 3 Bond lengths [Å] and angles [°] for $(CO)_5Cr=C(OMe)Fc$

Cr(1)-C(22)	1 865(5)
Cr(1)-C(18)	1 901(5)
Cr(1)-C(16)	1 903(5)
Cr(1)-C(14)	1 914(5)
Cr(1)-C(20)	1 923(5)
Cr(1)-C(1)	2 087(5)
Fe(1)-C(3)	2 030(5)
Fe(1)-C(2)	2 041(4)
Fe(1)-C(9)	2 048(5)
Fe(1)-C(4)	2 052(5)
Fe(1)-C(7)	2 059(5)
Fe(1)-C(8)	2 062(5)
Fe(1)-C(6)	2 063(5)
Fe(1)-C(5)	2 067(4)
Fe(1)-C(11)	2 073(5)
Fe(1)-C(10)	2 075(5)
C(1)-O(12)	1 322(6)
C(1)-C(2)	1 462(6)
C(2)-C(3)	1 440(7)
C(2)-C(6)	1 441(6)
C(3)-C(4)	1 439(7)
C(4)-C(5)	1 400(8)
C(5)-C(6)	1 438(7)
C(7)-C(8)	1 422(8)
C(7)-C(11)	1 423(8)
C(8)-C(9)	1 432(8)
C(9)-C(10)	1 427(9)
C(10)-C(11)	1 433(8)
O(12)-C(13)	1 420(6)
C(14)-O(15)	1 126(6)
C(16)-O(17)	1 141(7)
C(18)-O(19)	1 137(7)
C(20)-O(21)	1 135(6)
C(22)-O(23)	1 146(7)
C(22)-Cr(1)-C(18)	88 2(2)
C(22)-Cr(1)-C(16)	88 7(2)

C(18)-Cr(1)-C(16)	91 4(2)
C(22)-Cr(1)-C(14)	87 1(2)
C(18)-Cr(1)-C(14)	175 3(2)
C(16)-Cr(1)-C(14)	88 3(2)
C(22)-Cr(1)-C(20)	87 2(2)
C(18)-Cr(1)-C(20)	88 8(2)
C(16)-Cr(1)-C(20)	175 9(2)
C(14)-Cr(1)-C(20)	91 2(2)
C(22)-Cr(1)-C(1)	176 3(2)
C(18)-Cr(1)-C(1)	93 84(19)
C(16)-Cr(1)-C(1)	94 42(19)
C(14)-Cr(1)-C(1)	90 87(18)
C(20)-Cr(1)-C(1)	89 67(19)
C(3)-Fe(1)-C(2)	41 43(19)
C(3)-Fe(1)-C(9)	126 2(2)
C(2)-Fe(1)-C(9)	165 7(2)
C(3)-Fe(1)-C(4)	41 3(2)
C(2)-Fe(1)-C(4)	69 12(19)
C(9)-Fe(1)-C(4)	106 0(2)
C(3)-Fe(1)-C(7)	120 8(2)
C(2)-Fe(1)-C(7)	110 23(18)
C(9)-Fe(1)-C(7)	68 0(2)
C(4)-Fe(1)-C(7)	154 2(2)
C(3)-Fe(1)-C(8)	108 1(2)
C(2)-Fe(1)-C(8)	128 72(19)
C(9)-Fe(1)-C(8)	40 8(2)
C(4)-Fe(1)-C(8)	118 6(2)
C(7)-Fe(1)-C(8)	40 4(2)
C(3)-Fe(1)-C(6)	69 3(2)
C(2)-Fe(1)-C(6)	41 12(18)
C(9)-Fe(1)-C(6)	151 0(2)
C(4)-Fe(1)-C(6)	68 4(2)
C(7)-Fe(1)-C(6)	129 2(2)
C(8)-Fe(1)-C(6)	167 1(2)
C(3)-Fe(1)-C(5)	68 4(2)
C(2)-Fe(1)-C(5)	68 66(19)
C(9)-Fe(1)-C(5)	116 7(2)
C(4)-Fe(1)-C(5)	39 7(2)

C(7)-Fe(1)-C(5)	165 8(2)
C(8)-Fe(1)-C(5)	151 3(2)
C(6)-Fe(1)-C(5)	40 75(19)
C(3)-Fe(1)-C(11)	155 3(2)
C(2)-Fe(1)-C(11)	120 8(2)
C(9)-Fe(1)-C(11)	67 7(2)
C(4)-Fe(1)-C(11)	162 7(2)
C(7)-Fe(1)-C(11)	40 3(2)
C(8)-Fe(1)-C(11)	67 9(2)
C(6)-Fe(1)-C(11)	108 9(2)
C(5)-Fe(1)-C(11)	127 2(2)
C(3)-Fe(1)-C(10)	163 0(2)
C(2)-Fe(1)-C(10)	153 3(2)
C(9)-Fe(1)-C(10)	40 5(3)
C(4)-Fe(1)-C(10)	124 5(2)
C(7)-Fe(1)-C(10)	68 2(2)
C(8)-Fe(1)-C(10)	68 5(2)
C(6)-Fe(1)-C(10)	117 8(2)
C(5)-Fe(1)-C(10)	106 1(2)
C(11)-Fe(1)-C(10)	40 4(2)
O(12)-C(1)-C(2)	106 2(4)
O(12)-C(1)-Cr(1)	128 2(3)
C(2)-C(1)-Cr(1)	125 6(3)
C(3)-C(2)-C(6)	107 7(4)
C(3)-C(2)-C(1)	128 1(4)
C(6)-C(2)-C(1)	124 2(4)
C(3)-C(2)-Fe(1)	68 9(2)
C(6)-C(2)-Fe(1)	70 2(3)
C(1)-C(2)-Fe(1)	126 3(3)
C(4)-C(3)-C(2)	107 5(4)
C(4)-C(3)-Fe(1)	70 2(2)
C(2)-C(3)-Fe(1)	69 7(2)
C(5)-C(4)-C(3)	108 5(4)
C(5)-C(4)-Fe(1)	70 7(3)
C(3)-C(4)-Fe(1)	68 5(2)
C(4)-C(5)-C(6)	109 1(4)
C(4)-C(5)-Fe(1)	69 6(2)
C(6)-C(5)-Fe(1)	69 5(3)

C(5)-C(6)-C(2)	107 2(5)
C(5)-C(6)-Fe(1)	69 8(3)
C(2)-C(6)-Fe(1)	68 6(3)
C(8)-C(7)-C(11)	108 5(5)
C(8)-C(7)-Fe(1)	69 9(3)
C(11)-C(7)-Fe(1)	70 4(3)
C(7)-C(8)-C(9)	107 2(5)
C(7)-C(8)-Fe(1)	69 7(3)
C(9)-C(8)-Fe(1)	69 1(2)
C(10)-C(9)-C(8)	109 0(5)
C(10)-C(9)-Fe(1)	70 8(3)
C(8)-C(9)-Fe(1)	70 1(2)
C(9)-C(10)-C(11)	106 8(5)
C(9)-C(10)-Fe(1)	68 7(3)
C(11)-C(10)-Fe(1)	69 7(3)
C(7)-C(11)-C(10)	108 5(5)
C(7)-C(11)-Fe(1)	69 3(3)
C(10)-C(11)-Fe(1)	69 9(3)
C(1)-O(12)-C(13)	124 5(4)
O(15)-C(14)-Cr(1)	174 5(4)
O(17)-C(16)-Cr(1)	175 8(4)
O(19)-C(18)-Cr(1)	174 9(5)
O(21)-C(20)-Cr(1)	178 0(4)
O(23)-C(22)-Cr(1)	178 2(5)

Symmetry transformations used to generate equivalent atoms

A2 4 Anisotropic displacement parameters ($Å^2 x\ 10^3$) for $(CO)_5Cr=C(OMe)Fc$ The anisotropic displacement factor exponent takes the form $-2p^2[\ h^2\ a^{*2}U^{11} + + 2\ h\ k\ a^*\ b^*\ U^{12}\ ]$

	U^{11}	U^{22}	U^{33}	U^{23}	U^{13}	U^{12}
Cr(1)	17(1)	20(1)	21(1)	-1(1)	0(1)	-1(1)
Fe(1)	16(1)	14(1)	27(1)	-3(1)	0(1)	0(1)
C(1)	20(2)	20(2)	17(2)	-1(2)	1(2)	-3(2)
C(2)	15(2)	17(2)	20(3)	-3(2)	-7(2)	-2(1)
C(3)	14(2)	23(2)	25(2)	-1(2)	2(2)	0(2)
C(4)	18(2)	23(2)	37(3)	-5(2)	1(2)	0(2)
C(5)	16(2)	18(2)	39(3)	0(2)	6(2)	2(2)
C(6)	20(2)	19(2)	22(3)	-3(2)	-6(2)	-1(2)
C(7)	21(2)	18(2)	37(3)	-7(2)	4(2)	2(2)
C(8)	35(3)	13(2)	42(3)	0(2)	-2(2)	5(2)
C(9)	31(2)	15(2)	40(3)	-8(2)	12(2)	-6(2)
C(10)	27(3)	19(2)	61(4)	-11(3)	-12(2)	-5(2)
C(11)	45(3)	19(2)	21(3)	-7(2)	-1(2)	3(2)
O(12)	22(2)	31(2)	26(2)	6(1)	-2(2)	-2(1)
C(13)	31(3)	39(3)	28(3)	10(2)	-2(2)	-1(2)
C(14)	19(2)	24(2)	27(2)	-1(2)	-3(2)	2(2)
O(15)	32(2)	30(2)	39(2)	6(2)	-1(2)	-6(1)
C(16)	15(2)	27(2)	31(2)	3(2)	-3(2)	-2(2)
O(17)	30(2)	42(2)	33(2)	1(2)	6(2)	8(2)
C(18)	28(3)	29(2)	28(3)	-4(2)	2(2)	-1(2)
O(19)	49(2)	30(2)	46(2)	2(2)	0(2)	-21(2)
C(20)	23(2)	19(2)	26(2)	1(2)	-1(2)	-2(2)
O(21)	45(2)	37(2)	33(2)	-6(2)	4(2)	-1(2)
C(22)	23(2)	26(2)	29(3)	-3(2)	-1(2)	0(2)
O(23)	31(2)	48(2)	36(2)	0(2)	-5(2)	0(2)

A2 5 Hydrogen coordinates (x 10^4) and isotropic displacement parameters ($Å^2$x 10 ^{3}) for $(CO)_5Cr=C(OMe)Fc$

	x	y	z	U(eq)
H(3A)	6872	8928	-1332	25
H(4A)	8182	9066	-1279	31
H(5A)	8575	8036	726	29
H(6A)	7526	7216	1975	24
H(7A)	6368	12599	1231	30
H(8A)	6985	13588	-646	36
H(9A)	8269	13391	-247	35
H(10A)	8447	12352	1881	43
H(11A)	7261	11857	2787	34
H(13A)	5888	6309	3403	49
H(13B)	5499	5533	2293	49
H(13C)	5424	7740	2674	49

A2 6 Torsion angles [°] for $(CO)_5Cr=C(OMe)Fc$

C(22)-Cr(1)-C(1)-O(12)	-169(3)
C(18)-Cr(1)-C(1)-O(12)	-47 1(4)
C(16)-Cr(1)-C(1)-O(12)	44 7(4)
C(14)-Cr(1)-C(1)-O(12)	133 0(4)
C(20)-Cr(1)-C(1)-O(12)	-135 8(4)
C(22)-Cr(1)-C(1)-C(2)	9(3)
C(18)-Cr(1)-C(1)-C(2)	131 3(4)
C(16)-Cr(1)-C(1)-C(2)	-136 9(4)
C(14)-Cr(1)-C(1)-C(2)	-48 6(4)
C(20)-Cr(1)-C(1)-C(2)	42 6(4)
O(12)-C(1)-C(2)-C(3)	-177 8(4)
Cr(1)-C(1)-C(2)-C(3)	3 5(6)
O(12)-C(1)-C(2)-C(6)	2 1(6)
Cr(1)-C(1)-C(2)-C(6)	-176 6(3)
O(12)-C(1)-C(2)-Fe(1)	-87 3(4)
Cr(1)-C(1)-C(2)-Fe(1)	94 0(4)
C(9)-Fe(1)-C(2)-C(3)	33 8(9)
C(4)-Fe(1)-C(2)-C(3)	-38 4(3)
C(7)-Fe(1)-C(2)-C(3)	114 0(3)
C(8)-Fe(1)-C(2)-C(3)	72 1(3)
C(6)-Fe(1)-C(2)-C(3)	-119 0(4)
C(5)-Fe(1)-C(2)-C(3)	-81 2(3)
C(11)-Fe(1)-C(2)-C(3)	157 3(3)
C(10)-Fe(1)-C(2)-C(3)	-164 6(4)
C(3)-Fe(1)-C(2)-C(6)	119 0(4)
C(9)-Fe(1)-C(2)-C(6)	152 8(7)
C(4)-Fe(1)-C(2)-C(6)	80 6(3)
C(7)-Fe(1)-C(2)-C(6)	-127 0(3)
C(8)-Fe(1)-C(2)-C(6)	-168 8(3)
C(5)-Fe(1)-C(2)-C(6)	37 9(3)
C(11)-Fe(1)-C(2)-C(6)	-83 6(3)
C(10)-Fe(1)-C(2)-C(6)	-45 6(5)
C(3)-Fe(1)-C(2)-C(1)	-122 5(5)
C(9)-Fe(1)-C(2)-C(1)	-88 7(9)
C(4)-Fe(1)-C(2)-C(1)	-160 9(5)

C(7)-Fe(1)-C(2)-C(1)	-8 5(5)
C(8)-Fe(1)-C(2)-C(1)	-50 4(5)
C(6)-Fe(1)-C(2)-C(1)	118 5(5)
C(5)-Fe(1)-C(2)-C(1)	156 3(4)
C(11)-Fe(1)-C(2)-C(1)	34 8(5)
C(10)-Fe(1)-C(2)-C(1)	72 9(6)
C(6)-C(2)-C(3)-C(4)	0 6(5)
C(1)-C(2)-C(3)-C(4)	-179 5(4)
Fe(1)-C(2)-C(3)-C(4)	60 3(3)
C(6)-C(2)-C(3)-Fe(1)	-59 7(3)
C(1)-C(2)-C(3)-Fe(1)	120 2(4)
C(2)-Fe(1)-C(3)-C(4)	-118 3(3)
C(9)-Fe(1)-C(3)-C(4)	71 5(3)
C(7)-Fe(1)-C(3)-C(4)	155 5(3)
C(8)-Fe(1)-C(3)-C(4)	113 0(3)
C(6)-Fe(1)-C(3)-C(4)	-80 4(3)
C(5)-Fe(1)-C(3)-C(4)	-36 6(3)
C(11)-Fe(1)-C(3)-C(4)	-170 7(5)
C(10)-Fe(1)-C(3)-C(4)	37 6(8)
C(9)-Fe(1)-C(3)-C(2)	-170 2(3)
C(4)-Fe(1)-C(3)-C(2)	118 3(3)
C(7)-Fe(1)-C(3)-C(2)	-86 2(3)
C(8)-Fe(1)-C(3)-C(2)	-128 6(3)
C(6)-Fe(1)-C(3)-C(2)	37 9(2)
C(5)-Fe(1)-C(3)-C(2)	81 7(3)
C(11)-Fe(1)-C(3)-C(2)	-52 4(6)
C(10)-Fe(1)-C(3)-C(2)	155 9(7)
C(2)-C(3)-C(4)-C(5)	-0 4(4)
Fe(1)-C(3)-C(4)-C(5)	59 6(3)
C(2)-C(3)-C(4)-Fe(1)	-60 0(3)
C(3)-Fe(1)-C(4)-C(5)	-119 9(4)
C(2)-Fe(1)-C(4)-C(5)	-81 3(3)
C(9)-Fe(1)-C(4)-C(5)	112 8(3)
C(7)-Fe(1)-C(4)-C(5)	-174 9(4)
C(8)-Fe(1)-C(4)-C(5)	155 0(3)
C(6)-Fe(1)-C(4)-C(5)	-37 1(3)
C(11)-Fe(1)-C(4)-C(5)	46 9(8)
C(10)-Fe(1)-C(4)-C(5)	72 6(4)

C(2)-Fe(1)-C(4)-C(3)	38 6(2)
C(9)-Fe(1)-C(4)-C(3)	-127 3(3)
C(7)-Fe(1)-C(4)-C(3)	-55 0(5)
C(8)-Fe(1)-C(4)-C(3)	-85 1(3)
C(6)-Fe(1)-C(4)-C(3)	82 8(2)
C(5)-Fe(1)-C(4)-C(3)	119 9(4)
C(11)-Fe(1)-C(4)-C(3)	166 8(7)
C(10)-Fe(1)-C(4)-C(3)	-167 5(3)
C(3)-C(4)-C(5)-C(6)	0 0(5)
Fe(1)-C(4)-C(5)-C(6)	58 3(3)
C(3)-C(4)-C(5)-Fe(1)	-58 3(3)
C(3)-Fe(1)-C(5)-C(4)	37 9(3)
C(2)-Fe(1)-C(5)-C(4)	82 6(3)
C(9)-Fe(1)-C(5)-C(4)	-82 9(3)
C(7)-Fe(1)-C(5)-C(4)	170 9(7)
C(8)-Fe(1)-C(5)-C(4)	-50 6(5)
C(6)-Fe(1)-C(5)-C(4)	120 8(4)
C(11)-Fe(1)-C(5)-C(4)	-164 2(3)
C(10)-Fe(1)-C(5)-C(4)	-125 1(3)
C(3)-Fe(1)-C(5)-C(6)	-82 9(3)
C(2)-Fe(1)-C(5)-C(6)	-38 2(3)
C(9)-Fe(1)-C(5)-C(6)	156 3(3)
C(4)-Fe(1)-C(5)-C(6)	-120 8(4)
C(7)-Fe(1)-C(5)-C(6)	50 0(9)
C(8)-Fe(1)-C(5)-C(6)	-171 4(4)
C(11)-Fe(1)-C(5)-C(6)	75 0(4)
C(10)-Fe(1)-C(5)-C(6)	114 1(3)
C(4)-C(5)-C(6)-C(2)	0 3(5)
Fe(1)-C(5)-C(6)-C(2)	58 7(3)
C(4)-C(5)-C(6)-Fe(1)	-58 4(3)
C(3)-C(2)-C(6)-C(5)	-0 5(5)
C(1)-C(2)-C(6)-C(5)	179 5(4)
Fe(1)-C(2)-C(6)-C(5)	-59 4(3)
C(3)-C(2)-C(6)-Fe(1)	58 9(3)
C(1)-C(2)-C(6)-Fe(1)	-121 0(4)
C(3)-Fe(1)-C(6)-C(5)	80 6(3)
C(2)-Fe(1)-C(6)-C(5)	118 8(5)
C(9)-Fe(1)-C(6)-C(5)	-47 8(6)

C(4)-Fe(1)-C(6)-C(5)	36 2(3)
C(7)-Fe(1)-C(6)-C(5)	-166 0(3)
C(8)-Fe(1)-C(6)-C(5)	161 3(10)
C(11)-Fe(1)-C(6)-C(5)	-125 6(3)
C(10)-Fe(1)-C(6)-C(5)	-82 5(4)
C(3)-Fe(1)-C(6)-C(2)	-38 2(3)
C(9)-Fe(1)-C(6)-C(2)	-166 6(4)
C(4)-Fe(1)-C(6)-C(2)	-82 6(3)
C(7)-Fe(1)-C(6)-C(2)	75 2(4)
C(8)-Fe(1)-C(6)-C(2)	42 5(12)
C(5)-Fe(1)-C(6)-C(2)	-118 8(5)
C(11)-Fe(1)-C(6)-C(2)	115 6(3)
C(10)-Fe(1)-C(6)-C(2)	158 7(3)
C(3)-Fe(1)-C(7)-C(8)	-81 8(3)
C(2)-Fe(1)-C(7)-C(8)	-126 6(3)
C(9)-Fe(1)-C(7)-C(8)	38 2(3)
C(4)-Fe(1)-C(7)-C(8)	-42 9(6)
C(6)-Fe(1)-C(7)-C(8)	-169 2(3)
C(5)-Fe(1)-C(7)-C(8)	150 6(7)
C(11)-Fe(1)-C(7)-C(8)	119 3(4)
C(10)-Fe(1)-C(7)-C(8)	82 0(3)
C(3)-Fe(1)-C(7)-C(11)	158 9(3)
C(2)-Fe(1)-C(7)-C(11)	114 2(3)
C(9)-Fe(1)-C(7)-C(11)	-81 0(4)
C(4)-Fe(1)-C(7)-C(11)	-162 1(4)
C(8)-Fe(1)-C(7)-C(11)	-119 3(4)
C(6)-Fe(1)-C(7)-C(11)	71 5(4)
C(5)-Fe(1)-C(7)-C(11)	31 3(9)
C(10)-Fe(1)-C(7)-C(11)	-37 2(4)
C(11)-C(7)-C(8)-C(9)	0 9(5)
Fe(1)-C(7)-C(8)-C(9)	-59 2(3)
C(11)-C(7)-C(8)-Fe(1)	60 1(3)
C(3)-Fe(1)-C(8)-C(7)	116 5(3)
C(2)-Fe(1)-C(8)-C(7)	75 0(4)
C(9)-Fe(1)-C(8)-C(7)	-118 6(4)
C(4)-Fe(1)-C(8)-C(7)	160 3(3)
C(6)-Fe(1)-C(8)-C(7)	40 3(12)
C(5)-Fe(1)-C(8)-C(7)	-165 5(4)

C(11)-Fe(1)-C(8)-C(7)	-37 5(3)
C(10)-Fe(1)-C(8)-C(7)	-81 2(3)
C(3)-Fe(1)-C(8)-C(9)	-124 9(3)
C(2)-Fe(1)-C(8)-C(9)	-166 4(3)
C(4)-Fe(1)-C(8)-C(9)	-81 2(3)
C(7)-Fe(1)-C(8)-C(9)	118 6(4)
C(6)-Fe(1)-C(8)-C(9)	158 9(10)
C(5)-Fe(1)-C(8)-C(9)	-47 0(6)
C(11)-Fe(1)-C(8)-C(9)	81 1(3)
C(10)-Fe(1)-C(8)-C(9)	37 4(3)
C(7)-C(8)-C(9)-C(10)	-0 8(5)
Fe(1)-C(8)-C(9)-C(10)	-60 3(3)
C(7)-C(8)-C(9)-Fe(1)	59 6(3)
C(3)-Fe(1)-C(9)-C(10)	-165 5(3)
C(2)-Fe(1)-C(9)-C(10)	167 4(7)
C(4)-Fe(1)-C(9)-C(10)	-124 9(3)
C(7)-Fe(1)-C(9)-C(10)	81 7(4)
C(8)-Fe(1)-C(9)-C(10)	119 6(5)
C(6)-Fe(1)-C(9)-C(10)	-50 9(6)
C(5)-Fe(1)-C(9)-C(10)	-83 6(4)
C(11)-Fe(1)-C(9)-C(10)	38 1(3)
C(3)-Fe(1)-C(9)-C(8)	75 0(4)
C(2)-Fe(1)-C(9)-C(8)	47 8(9)
C(4)-Fe(1)-C(9)-C(8)	115 5(3)
C(7)-Fe(1)-C(9)-C(8)	-37 9(3)
C(6)-Fe(1)-C(9)-C(8)	-170 4(4)
C(5)-Fe(1)-C(9)-C(8)	156 8(3)
C(11)-Fe(1)-C(9)-C(8)	-81 5(3)
C(10)-Fe(1)-C(9)-C(8)	-119 6(5)
C(8)-C(9)-C(10)-C(11)	0 3(5)
Fe(1)-C(9)-C(10)-C(11)	-59 6(4)
C(8)-C(9)-C(10)-Fe(1)	59 9(3)
C(3)-Fe(1)-C(10)-C(9)	43 9(9)
C(2)-Fe(1)-C(10)-C(9)	-173 1(4)
C(4)-Fe(1)-C(10)-C(9)	73 1(4)
C(7)-Fe(1)-C(10)-C(9)	-81 2(3)
C(8)-Fe(1)-C(10)-C(9)	-37 6(3)
C(6)-Fe(1)-C(10)-C(9)	154 8(3)

C(5)-Fe(1)-C(10)-C(9)	112 5(3)
C(11)-Fe(1)-C(10)-C(9)	-118 3(5)
C(3)-Fe(1)-C(10)-C(11)	162 2(6)
C(2)-Fe(1)-C(10)-C(11)	-54 8(6)
C(9)-Fe(1)-C(10)-C(11)	118 3(5)
C(4)-Fe(1)-C(10)-C(11)	-168 6(3)
C(7)-Fe(1)-C(10)-C(11)	37 1(3)
C(8)-Fe(1)-C(10)-C(11)	80 7(4)
C(6)-Fe(1)-C(10)-C(11)	-86 8(4)
C(5)-Fe(1)-C(10)-C(11)	-129 2(3)
C(8)-C(7)-C(11)-C(10)	-0 7(6)
Fe(1)-C(7)-C(11)-C(10)	59 1(4)
C(8)-C(7)-C(11)-Fe(1)	-59 8(3)
C(9)-C(10)-C(11)-C(7)	0 2(6)
Fe(1)-C(10)-C(11)-C(7)	-58 7(4)
C(9)-C(10)-C(11)-Fe(1)	59 0(3)
C(3)-Fe(1)-C(11)-C(7)	-47 7(6)
C(2)-Fe(1)-C(11)-C(7)	-85 3(3)
C(9)-Fe(1)-C(11)-C(7)	81 8(4)
C(4)-Fe(1)-C(11)-C(7)	153 3(6)
C(8)-Fe(1)-C(11)-C(7)	37 6(3)
C(6)-Fe(1)-C(11)-C(7)	-129 0(3)
C(5)-Fe(1)-C(11)-C(7)	-170 8(3)
C(10)-Fe(1)-C(11)-C(7)	120 0(5)
C(3)-Fe(1)-C(11)-C(10)	-167 7(5)
C(2)-Fe(1)-C(11)-C(10)	154 7(3)
C(9)-Fe(1)-C(11)-C(10)	-38 2(4)
C(4)-Fe(1)-C(11)-C(10)	33 4(9)
C(7)-Fe(1)-C(11)-C(10)	-120 0(5)
C(8)-Fe(1)-C(11)-C(10)	-82 3(4)
C(6)-Fe(1)-C(11)-C(10)	111 0(3)
C(5)-Fe(1)-C(11)-C(10)	69 3(4)
C(2)-C(1)-O(12)-C(13)	-177 8(4)
Cr(1)-C(1)-O(12)-C(13)	0 8(7)
C(22)-Cr(1)-C(14)-O(15)	14(5)
C(18)-Cr(1)-C(14)-O(15)	12(6)
C(16)-Cr(1)-C(14)-O(15)	-75(5)
C(20)-Cr(1)-C(14)-O(15)	101(5)

C(1)-Cr(1)-C(14)-O(15)	-169(5)
C(22)-Cr(1)-C(16)-O(17)	-19(6)
C(18)-Cr(1)-C(16)-O(17)	-107(6)
C(14)-Cr(1)-C(16)-O(17)	69(6)
C(20)-Cr(1)-C(16)-O(17)	-14(8)
C(1)-Cr(1)-C(16)-O(17)	159(6)
C(22)-Cr(1)-C(18)-O(19)	20(5)
C(16)-Cr(1)-C(18)-O(19)	108(5)
C(14)-Cr(1)-C(18)-O(19)	22(7)
C(20)-Cr(1)-C(18)-O(19)	-68(5)
C(1)-Cr(1)-C(18)-O(19)	-157(5)
C(22)-Cr(1)-C(20)-O(21)	1(12)
C(18)-Cr(1)-C(20)-O(21)	89(12)
C(16)-Cr(1)-C(20)-O(21)	-4(14)
C(14)-Cr(1)-C(20)-O(21)	-86(12)
C(1)-Cr(1)-C(20)-O(21)	-177(100)
C(18)-Cr(1)-C(22)-O(23)	104(17)
C(16)-Cr(1)-C(22)-O(23)	13(17)
C(14)-Cr(1)-C(22)-O(23)	-76(17)
C(20)-Cr(1)-C(22)-O(23)	-167(17)
C(1)-Cr(1)-C(22)-O(23)	-133(15)

Symmetry transformations used to generate equivalent atoms

A3 Crystal data and experimental parameters for 1,1'-$[(CO)_5Cr=C(OMe)]_2Fc$

A3 1 Crystal data and structure refinement for 1,1'-$[(CO)_5Cr=C(OMe)]_2Fc$

Identification code	mpfer	
Empirical formula	C24 H14 Cr2 Fe O12	
Formula weight	654 20	
Temperature	298(2) K	
Wavelength	0 71073 Å	
Crystal system	Orthorhombic	
Space group	Pbcn	
Unit cell dimensions	a = 13 3351(9) Å	a= 90°
	b = 14 3455(9) Å	b= 90°
	c = 13 4177(9) Å	g = 90°
Volume	2566 8(3) $Å^3$	
Z	4	
Density (calculated)	1 693 Mg/m^3	
Absorption coefficient	1 453 mm^{-1}	
F(000)	1312	
Crystal size	0 50 x 0 40 x 0 20 mm^3	
Theta range for data collection	2 09 to 27 49°	
Index ranges	-17<=h<=17, -18<=k<=18, -17<=l<=17	
Reflections collected	26036	
Independent reflections	2915 [R(int) = 0 0359]	
Completeness to theta = 27 49°	98 6 %	
Absorption correction	Semi-empirical from equivalents	
Max and min transmission	1 0000 and 0 7745	
Refinement method	Full-matrix least-squares on F^2	
Data / restraints / parameters	2915 / 0 / 177	
Goodness-of-fit on F^2	0 971	
Final R indices [I>2sigma(I)]	R1 = 0 0355, wR2 = 0 0862	
R indices (all data)	R1 = 0 0491, wR2 = 0 0916	
Largest diff peak and hole	0 430 and -0 242 e $Å^{-3}$	

A3 2 Atomic coordinates (x 10^4) and equivalent isotropic displacement parameters ($Å^2$x 10^3) for 1,1'-[$(CO)_5Cr=C(OMe)]_2Fc$ U(eq) is defined as one third of the trace of the orthogonalized U^{ij} tensor

	x	y	z	U(eq)
Cr(1)	7108(1)	5774(1)	3697(1)	36(1)
Fe(1)	10000	4372(1)	2500	28(1)
C(1)	8660(2)	5819(1)	3649(2)	36(1)
C(2)	9326(2)	5007(1)	3693(1)	32(1)
C(3)	9047(2)	4040(2)	3635(1)	35(1)
C(4)	9930(2)	3494(2)	3711(2)	41(1)
C(5)	10757(2)	4105(2)	3808(1)	41(1)
C(6)	10398(2)	5029(2)	3794(1)	36(1)
C(7)	8912(2)	7491(2)	3628(3)	101(1)
O(8)	9270(1)	6551(1)	3644(1)	54(1)
C(9)	7034(2)	4832(2)	2706(2)	42(1)
O(10)	6911(1)	4266(1)	2124(2)	60(1)
C(11)	7230(2)	4862(2)	4721(2)	40(1)
O(12)	7280(1)	4314(1)	5327(1)	59(1)
C(13)	6959(2)	6714(2)	4694(2)	52(1)
O(14)	6768(2)	7243(1)	5292(2)	84(1)
C(15)	6959(2)	6668(2)	2659(2)	47(1)
O(16)	6818(2)	7186(1)	2033(2)	73(1)
C(17)	5720(2)	5667(2)	3774(2)	58(1)
O(18)	4863(2)	5592(2)	3819(2)	102(1)

A3 3 Bond lengths [Å] and angles [°] for 1,1'-[$(CO)_5Cr$=C(OMe)]$_2$Fc

Cr(1)-C(17)	1 860(3)
Cr(1)-C(9)	1 899(2)
Cr(1)-C(11)	1 903(2)
Cr(1)-C(15)	1 905(2)
Cr(1)-C(13)	1 909(3)
Cr(1)-C(1)	2 072(2)
Fe(1)-C(3)#1	2 0406(19)
Fe(1)-C(3)	2 0406(19)
Fe(1)-C(6)	2 0456(19)
Fe(1)-C(6)#1	2 0456(19)
Fe(1)-C(2)	2 0498(18)
Fe(1)-C(2)#1	2 0498(18)
Fe(1)-C(4)#1	2 058(2)
Fe(1)-C(4)	2 058(2)
Fe(1)-C(5)	2 0601(19)
Fe(1)-C(5)#1	2 0602(19)
C(1)-O(8)	1 327(2)
C(1)-C(2)	1 466(3)
C(2)-C(6)	1 436(3)
C(2)-C(3)	1 440(3)
C(3)-C(4)	1 418(3)
C(4)-C(5)	1 415(3)
C(5)-C(6)	1 409(3)
C(7)-O(8)	1 431(3)
C(9)-O(10)	1 138(3)
C(11)-O(12)	1 134(3)
C(13)-O(14)	1 134(3)
C(15)-O(16)	1 138(3)
C(17)-O(18)	1 150(3)
C(17)-Cr(1)-C(9)	85 91(11)
C(17)-Cr(1)-C(11)	89 34(10)
C(9)-Cr(1)-C(11)	91 21(10)
C(17)-Cr(1)-C(15)	89 51(11)
C(9)-Cr(1)-C(15)	87 79(11)
C(11)-Cr(1)-C(15)	178 52(10)

C(17)-Cr(1)-C(13)	85 13(11)
C(9)-Cr(1)-C(13)	171 01(10)
C(11)-Cr(1)-C(13)	89 36(10)
C(15)-Cr(1)-C(13)	91 47(11)
C(17)-Cr(1)-C(1)	176 79(10)
C(9)-Cr(1)-C(1)	93 00(9)
C(11)-Cr(1)-C(1)	87 67(8)
C(15)-Cr(1)-C(1)	93 46(9)
C(13)-Cr(1)-C(1)	95 99(9)
C(3)#1-Fe(1)-C(3)	152 98(12)
C(3)#1-Fe(1)-C(6)	125 40(8)
C(3)-Fe(1)-C(6)	68 66(9)
C(3)#1-Fe(1)-C(6)#1	68 66(9)
C(3)-Fe(1)-C(6)#1	125 40(8)
C(6)-Fe(1)-C(6)#1	125 11(12)
C(3)#1-Fe(1)-C(2)	163 74(8)
C(3)-Fe(1)-C(2)	41 22(8)
C(6)-Fe(1)-C(2)	41 06(8)
C(6)#1-Fe(1)-C(2)	110 11(8)
C(3)#1-Fe(1)-C(2)#1	41 22(8)
C(3)-Fe(1)-C(2)#1	163 74(8)
C(6)-Fe(1)-C(2)#1	110 11(8)
C(6)#1-Fe(1)-C(2)#1	41 06(8)
C(2)-Fe(1)-C(2)#1	127 17(11)
C(3)#1-Fe(1)-C(4)#1	40 47(8)
C(3)-Fe(1)-C(4)#1	118 35(9)
C(6)-Fe(1)-C(4)#1	160 09(9)
C(6)#1-Fe(1)-C(4)#1	67 90(9)
C(2)-Fe(1)-C(4)#1	155 35(8)
C(2)#1-Fe(1)-C(4)#1	68 63(8)
C(3)#1-Fe(1)-C(4)	118 35(9)
C(3)-Fe(1)-C(4)	40 47(8)
C(6)-Fe(1)-C(4)	67 90(9)
C(6)#1-Fe(1)-C(4)	160 09(9)
C(2)-Fe(1)-C(4)	68 63(8)
C(2)#1-Fe(1)-C(4)	155 36(8)
C(4)#1-Fe(1)-C(4)	104 54(13)
C(3)#1-Fe(1)-C(5)	106 70(9)

C(3)-Fe(1)-C(5)	68 03(9)
C(6)-Fe(1)-C(5)	40 13(8)
C(6)#1-Fe(1)-C(5)	159 34(9)
C(2)-Fe(1)-C(5)	68 40(8)
C(2)#1-Fe(1)-C(5)	122 23(9)
C(4)#1-Fe(1)-C(5)	122 46(9)
C(4)-Fe(1)-C(5)	40 19(9)
C(3)#1-Fe(1)-C(5)#1	68 03(9)
C(3)-Fe(1)-C(5)#1	106 70(9)
C(6)-Fe(1)-C(5)#1	159 34(9)
C(6)#1-Fe(1)-C(5)#1	40 14(8)
C(2)-Fe(1)-C(5)#1	122 23(9)
C(2)#1-Fe(1)-C(5)#1	68 40(8)
C(4)#1-Fe(1)-C(5)#1	40 19(9)
C(4)-Fe(1)-C(5)#1	122 46(9)
C(5)-Fe(1)-C(5)#1	158 60(13)
O(8)-C(1)-C(2)	104 91(18)
O(8)-C(1)-Cr(1)	129 56(15)
C(2)-C(1)-Cr(1)	125 37(15)
C(6)-C(2)-C(3)	106 49(17)
C(6)-C(2)-C(1)	126 14(19)
C(3)-C(2)-C(1)	127 37(19)
C(6)-C(2)-Fe(1)	69 31(10)
C(3)-C(2)-Fe(1)	69 05(10)
C(1)-C(2)-Fe(1)	125 96(13)
C(4)-C(3)-C(2)	108 25(19)
C(4)-C(3)-Fe(1)	70 42(11)
C(2)-C(3)-Fe(1)	69 73(11)
C(5)-C(4)-C(3)	108 2(2)
C(5)-C(4)-Fe(1)	69 99(12)
C(3)-C(4)-Fe(1)	69 11(11)
C(6)-C(5)-C(4)	108 52(19)
C(6)-C(5)-Fe(1)	69 38(11)
C(4)-C(5)-Fe(1)	69 82(12)
C(5)-C(6)-C(2)	108 56(19)
C(5)-C(6)-Fe(1)	70 49(11)
C(2)-C(6)-Fe(1)	69 62(10)
C(1)-O(8)-C(7)	122 75(19)

O(10)-C(9)-Cr(1)	174 6(2)
O(12)-C(11)-Cr(1)	178 4(2)
O(14)-C(13)-Cr(1)	172 8(2)
O(16)-C(15)-Cr(1)	176 4(2)
O(18)-C(17)-Cr(1)	179 3(3)

Symmetry transformations used to generate equivalent atoms

#1 -x+2,y,-z+1/2

A3 4 Anisotropic displacement parameters ($Å^2 x\ 10^3$) for 1,1'-$[(CO)_5Cr=C(OMe)]_2Fc$ The anisotropic displacement factor exponent takes the form $-2p^2[\ h^2\ a^{*2}U^{11} + \quad + 2\ h\ k\ a^*\ b^*\ U^{12}\ ]$

	U^{11}	U^{22}	U^{33}	U^{23}	U^{13}	U^{12}
Cr(1)	29(1)	39(1)	39(1)	1(1)	-1(1)	6(1)
Fe(1)	26(1)	34(1)	26(1)	0	0(1)	0
C(1)	37(1)	34(1)	35(1)	1(1)	-1(1)	1(1)
C(2)	33(1)	40(1)	25(1)	-1(1)	2(1)	4(1)
C(3)	34(1)	37(1)	35(1)	5(1)	6(1)	4(1)
C(4)	43(1)	44(1)	36(1)	10(1)	6(1)	11(1)
C(5)	36(1)	57(1)	29(1)	3(1)	-4(1)	11(1)
C(6)	34(1)	48(1)	27(1)	-5(1)	-4(1)	3(1)
C(7)	62(2)	33(2)	207(4)	4(2)	0(2)	-3(1)
O(8)	40(1)	35(1)	86(1)	0(1)	0(1)	-1(1)
C(9)	36(1)	44(1)	46(1)	5(1)	-3(1)	2(1)
O(10)	64(1)	57(1)	60(1)	-12(1)	-9(1)	-2(1)
C(11)	31(1)	46(1)	43(1)	-4(1)	5(1)	4(1)
O(12)	61(1)	60(1)	55(1)	17(1)	12(1)	7(1)
C(13)	55(2)	50(1)	51(2)	1(1)	-8(1)	14(1)
O(14)	120(2)	67(1)	65(1)	-19(1)	-9(1)	24(1)
C(15)	47(1)	43(1)	51(1)	-3(1)	1(1)	10(1)
O(16)	99(2)	58(1)	64(1)	15(1)	-6(1)	22(1)
C(17)	38(1)	79(2)	58(2)	1(1)	-2(1)	10(1)
O(18)	33(1)	164(3)	108(2)	6(2)	3(1)	4(1)

A3 5 Hydrogen coordinates (x 10^4) and isotropic displacement parameters ($Å^2$x 10 ^{3}) for 1,1'-$[(CO)_5Cr=C(OMe)]_2Fc$

	x	y	z	U(eq)
H(3A)	8363	3799	3561	42
H(4A)	9963	2812	3690	49
H(5A)	11461	3918	3863	49
H(6A)	10812	5592	3844	44
H(7A)	9220	7820	3086	151
H(7B)	9078	7792	4245	151
H(7C)	8197	7491	3542	151

A3 6 Torsion angles [°] for 1,1'-[$(CO)_5Cr{=}C(OMe)]_2Fc$

C(17)-Cr(1)-C(1)-O(8)	-153 6(18)
C(9)-Cr(1)-C(1)-O(8)	136 46(19)
C(11)-Cr(1)-C(1)-O(8)	-132 5(2)
C(15)-Cr(1)-C(1)-O(8)	48 5(2)
C(13)-Cr(1)-C(1)-O(8)	-43 3(2)
C(17)-Cr(1)-C(1)-C(2)	21 1(19)
C(9)-Cr(1)-C(1)-C(2)	-48 86(17)
C(11)-Cr(1)-C(1)-C(2)	42 23(17)
C(15)-Cr(1)-C(1)-C(2)	-136 82(17)
C(13)-Cr(1)-C(1)-C(2)	131 33(17)
O(8)-C(1)-C(2)-C(6)	4 6(3)
Cr(1)-C(1)-C(2)-C(6)	-171 15(14)
O(8)-C(1)-C(2)-C(3)	-174 67(18)
Cr(1)-C(1)-C(2)-C(3)	9 6(3)
O(8)-C(1)-C(2)-Fe(1)	-84 8(2)
Cr(1)-C(1)-C(2)-Fe(1)	99 46(18)
C(3)#1-Fe(1)-C(2)-C(6)	-38 2(3)
C(3)-Fe(1)-C(2)-C(6)	118 00(16)
C(6)#1-Fe(1)-C(2)-C(6)	-120 80(15)
C(2)#1-Fe(1)-C(2)-C(6)	-77 69(11)
C(4)#1-Fe(1)-C(2)-C(6)	158 55(19)
C(4)-Fe(1)-C(2)-C(6)	80 46(13)
C(5)-Fe(1)-C(2)-C(6)	37 13(12)
C(5)#1-Fe(1)-C(2)-C(6)	-163 78(13)
C(3)#1-Fe(1)-C(2)-C(3)	-156 2(2)
C(6)-Fe(1)-C(2)-C(3)	-118 00(16)
C(6)#1-Fe(1)-C(2)-C(3)	121 20(12)
C(2)#1-Fe(1)-C(2)-C(3)	164 32(12)
C(4)#1-Fe(1)-C(2)-C(3)	40 6(2)
C(4)-Fe(1)-C(2)-C(3)	-37 54(12)
C(5)-Fe(1)-C(2)-C(3)	-80 87(13)
C(5)#1-Fe(1)-C(2)-C(3)	78 22(14)
C(3)#1-Fe(1)-C(2)-C(1)	82 1(3)
C(3)-Fe(1)-C(2)-C(1)	-121 7(2)
C(6)-Fe(1)-C(2)-C(1)	120 3(2)

C(6)#1-Fe(1)-C(2)-C(1)	-0 5(2)
C(2)#1-Fe(1)-C(2)-C(1)	42 63(16)
C(4)#1-Fe(1)-C(2)-C(1)	-81 1(3)
C(4)-Fe(1)-C(2)-C(1)	-159 2(2)
C(5)-Fe(1)-C(2)-C(1)	157 5(2)
C(5)#1-Fe(1)-C(2)-C(1)	-43 5(2)
C(6)-C(2)-C(3)-C(4)	0 7(2)
C(1)-C(2)-C(3)-C(4)	-179 95(18)
Fe(1)-C(2)-C(3)-C(4)	60 14(14)
C(6)-C(2)-C(3)-Fe(1)	-59 48(12)
C(1)-C(2)-C(3)-Fe(1)	119 91(19)
C(3)#1-Fe(1)-C(3)-C(4)	46 53(12)
C(6)-Fe(1)-C(3)-C(4)	-80 54(14)
C(6)#1-Fe(1)-C(3)-C(4)	160 78(13)
C(2)-Fe(1)-C(3)-C(4)	-119 06(18)
C(2)#1-Fe(1)-C(3)-C(4)	-169 4(3)
C(4)#1-Fe(1)-C(3)-C(4)	78 9(2)
C(5)-Fe(1)-C(3)-C(4)	-37 22(13)
C(5)#1-Fe(1)-C(3)-C(4)	120 78(14)
C(3)#1-Fe(1)-C(3)-C(2)	165 59(11)
C(6)-Fe(1)-C(3)-C(2)	38 51(11)
C(6)#1-Fe(1)-C(3)-C(2)	-80 16(14)
C(2)#1-Fe(1)-C(3)-C(2)	-50 3(4)
C(4)#1-Fe(1)-C(3)-C(2)	-162 06(12)
C(4)-Fe(1)-C(3)-C(2)	119 06(18)
C(5)-Fe(1)-C(3)-C(2)	81 84(12)
C(5)#1-Fe(1)-C(3)-C(2)	-120 17(12)
C(2)-C(3)-C(4)-C(5)	-0 4(2)
Fe(1)-C(3)-C(4)-C(5)	59 29(14)
C(2)-C(3)-C(4)-Fe(1)	-59 70(13)
C(3)#1-Fe(1)-C(4)-C(5)	82 38(15)
C(3)-Fe(1)-C(4)-C(5)	-119 62(19)
C(6)-Fe(1)-C(4)-C(5)	-37 05(12)
C(6)#1-Fe(1)-C(4)-C(5)	-171 6(2)
C(2)-Fe(1)-C(4)-C(5)	-81 41(13)
C(2)#1-Fe(1)-C(4)-C(5)	53 2(3)
C(4)#1-Fe(1)-C(4)-C(5)	123 52(14)
C(5)#1-Fe(1)-C(4)-C(5)	163 13(11)

C(3)#1-Fe(1)-C(4)-C(3)	-158 00(11)
C(6)-Fe(1)-C(4)-C(3)	82 57(14)
C(6)#1-Fe(1)-C(4)-C(3)	-52 0(3)
C(2)-Fe(1)-C(4)-C(3)	38 21(12)
C(2)#1-Fe(1)-C(4)-C(3)	172 87(18)
C(4)#1-Fe(1)-C(4)-C(3)	-116 85(15)
C(5)-Fe(1)-C(4)-C(3)	119 62(19)
C(5)#1-Fe(1)-C(4)-C(3)	-77 24(15)
C(3)-C(4)-C(5)-C(6)	0 0(2)
Fe(1)-C(4)-C(5)-C(6)	58 74(14)
C(3)-C(4)-C(5)-Fe(1)	-58 74(14)
C(3)#1-Fe(1)-C(5)-C(6)	125 61(13)
C(3)-Fe(1)-C(5)-C(6)	-82 52(13)
C(6)#1-Fe(1)-C(5)-C(6)	51 9(3)
C(2)-Fe(1)-C(5)-C(6)	-37 96(12)
C(2)#1-Fe(1)-C(5)-C(6)	83 27(14)
C(4)#1-Fe(1)-C(5)-C(6)	166 98(12)
C(4)-Fe(1)-C(5)-C(6)	-119 99(18)
C(5)#1-Fe(1)-C(5)-C(6)	-162 13(12)
C(3)#1-Fe(1)-C(5)-C(4)	-114 40(13)
C(3)-Fe(1)-C(5)-C(4)	37 47(12)
C(6)-Fe(1)-C(5)-C(4)	119 99(18)
C(6)#1-Fe(1)-C(5)-C(4)	171 9(2)
C(2)-Fe(1)-C(5)-C(4)	82 03(13)
C(2)#1-Fe(1)-C(5)-C(4)	-156 74(12)
C(4)#1-Fe(1)-C(5)-C(4)	-73 02(18)
C(5)#1-Fe(1)-C(5)-C(4)	-42 14(11)
C(4)-C(5)-C(6)-C(2)	0 4(2)
Fe(1)-C(5)-C(6)-C(2)	59 43(12)
C(4)-C(5)-C(6)-Fe(1)	-59 02(14)
C(3)-C(2)-C(6)-C(5)	-0 7(2)
C(1)-C(2)-C(6)-C(5)	179 94(17)
Fe(1)-C(2)-C(6)-C(5)	-59 96(13)
C(3)-C(2)-C(6)-Fe(1)	59 31(12)
C(1)-C(2)-C(6)-Fe(1)	-120 09(18)
C(3)#1-Fe(1)-C(6)-C(5)	-72 79(15)
C(3)-Fe(1)-C(6)-C(5)	80 80(14)
C(6)#1-Fe(1)-C(6)-C(5)	-160 15(14)

C(2)-Fe(1)-C(6)-C(5)	119 46(17)
C(2)#1-Fe(1)-C(6)-C(5)	-116 54(13)
C(4)#1-Fe(1)-C(6)-C(5)	-33 9(3)
C(4)-Fe(1)-C(6)-C(5)	37 10(13)
C(5)#1-Fe(1)-C(6)-C(5)	161 51(18)
C(3)#1-Fe(1)-C(6)-C(2)	167 74(12)
C(3)-Fe(1)-C(6)-C(2)	-38 66(11)
C(6)#1-Fe(1)-C(6)-C(2)	80 39(11)
C(2)#1-Fe(1)-C(6)-C(2)	123 99(14)
C(4)#1-Fe(1)-C(6)-C(2)	-153 4(2)
C(4)-Fe(1)-C(6)-C(2)	-82 37(13)
C(5)-Fe(1)-C(6)-C(2)	-119 46(17)
C(5)#1-Fe(1)-C(6)-C(2)	42 0(3)
C(2)-C(1)-O(8)-C(7)	-178 5(2)
Cr(1)-C(1)-O(8)-C(7)	-3 0(3)
C(17)-Cr(1)-C(9)-O(10)	-2(2)
C(11)-Cr(1)-C(9)-O(10)	88(2)
C(15)-Cr(1)-C(9)-O(10)	-91(2)
C(13)-Cr(1)-C(9)-O(10)	-6(3)
C(1)-Cr(1)-C(9)-O(10)	175(2)
C(17)-Cr(1)-C(11)-O(12)	14(8)
C(9)-Cr(1)-C(11)-O(12)	-72(8)
C(15)-Cr(1)-C(11)-O(12)	-25(10)
C(13)-Cr(1)-C(11)-O(12)	99(8)
C(1)-Cr(1)-C(11)-O(12)	-165(8)
C(17)-Cr(1)-C(13)-O(14)	8 9(18)
C(9)-Cr(1)-C(13)-O(14)	13(2)
C(11)-Cr(1)-C(13)-O(14)	-80 4(18)
C(15)-Cr(1)-C(13)-O(14)	98 3(18)
C(1)-Cr(1)-C(13)-O(14)	-168 0(18)
C(17)-Cr(1)-C(15)-O(16)	-16(3)
C(9)-Cr(1)-C(15)-O(16)	70(3)
C(11)-Cr(1)-C(15)-O(16)	23(6)
C(13)-Cr(1)-C(15)-O(16)	-101(3)
C(1)-Cr(1)-C(15)-O(16)	162(3)
C(9)-Cr(1)-C(17)-O(18)	32(21)
C(11)-Cr(1)-C(17)-O(18)	-59(21)
C(15)-Cr(1)-C(17)-O(18)	120(21)

C(13)-Cr(1)-C(17)-O(18)	-148(21)
C(1)-Cr(1)-C(17)-O(18)	-38(22)

Symmetry transformations used to generate equivalent atoms

#1 -x+2,y,-z+1/2

A4 Crystal data and experimental parameters for 1,1'-[(CO)$_5$W=C(OMe)]$_2$Fc

A4 1 Crystal data and structure refinement for 1,1'-[(CO)$_5$W=C(OMe)]$_2$Fc

Identification code	mpe1	
Empirical formula	C24 H14 Fe O12 W2	
Formula weight	917 90	
Temperature	153(2) K	
Wavelength	0 71073 Å	
Crystal system	Orthorhombic	
Space group	Pbcn	
Unit cell dimensions	a = 13 6026(6) Å	a= 90°
	b = 14 3049(6) Å	b= 90°
	c = 13 2640(6) Å	g = 90°
Volume	2581 0(2) Å^3	
Z	4	
Density (calculated)	2 362 Mg/m^3	
Absorption coefficient	9 510 mm^{-1}	
F(000)	1712	
Crystal size	0 50 x 0 23 x 0 14 mm^3	
Theta range for data collection	2 07 to 29 00°	
Index ranges	-18<=h<=8, -15<=k<=19, -17<=l<=18	
Reflections collected	13092	
Independent reflections	3426 [R(int) = 0 0297]	
Completeness to theta = 29 00°	99 8 %	
Absorption correction	Semi-empirical from equivalents	
Max and min transmission	0 3494 and 0 1113	
Refinement method	Full-matrix least-squares on F^2	
Data / restraints / parameters	3426 / 0 / 177	
Goodness-of-fit on F^2	1 057	
Final R indices [I>2sigma(I)]	R1 = 0 0293, wR2 = 0 0759	
R indices (all data)	R1 = 0 0336, wR2 = 0 0787	
Largest diff peak and hole	2 934 and -2 810 e Å^{-3}	

A4 2 Atomic coordinates (x 10^4) and equivalent isotropic displacement parameters ($Å^2$x 10^3)for 1,1'-$[(CO)_5W{=}C(OMe)]_2Fc$ U(eq) is defined as one third of the trace of the orthogonalized U^{ij} tensor

	x	y	z	U(eq)
W(1)	2073(1)	820(1)	1285(1)	15(1)
Fe(1)	5000	-560(1)	2500	12(1)
O(1)	1631(3)	2363(2)	-393(2)	39(1)
C(1)	1856(3)	1828(3)	199(3)	25(1)
C(2)	1893(3)	1782(3)	2418(3)	23(1)
O(2)	1748(2)	2303(2)	3046(2)	35(1)
O(3)	-236(2)	571(3)	1162(3)	51(1)
C(3)	606(4)	665(3)	1211(3)	28(1)
C(4)	2019(2)	-194(3)	2361(3)	21(1)
O(4)	1911(2)	-777(2)	2942(3)	30(1)
O(5)	2320(2)	-736(2)	-417(2)	28(1)
C(5)	2236(2)	-170(3)	185(3)	19(1)
C(6)	3697(3)	888(2)	1330(2)	15(1)
O(6)	4277(2)	1633(2)	1332(2)	26(1)
C(7)	3889(4)	2565(3)	1351(4)	55(2)
C(8)	4347(3)	81(2)	1287(2)	15(1)
C(9)	5406(3)	105(2)	1195(2)	16(1)
C(10)	5751(3)	-826(2)	1183(2)	18(1)
C(11)	4940(3)	-1438(3)	1270(2)	19(1)
C(12)	4070(3)	-892(2)	1344(2)	17(1)

A4 3 Bond lengths [Å] and angles [°] for 1,1'-$[(CO)_5W{=}C(OMe)]_2Fc$

W(1)-C(3)	2 011(5)
W(1)-C(4)	2 036(4)
W(1)-C(5)	2 047(4)
W(1)-C(2)	2 051(4)
W(1)-C(1)	2 060(4)
W(1)-C(6)	2 212(4)
Fe(1)-C(12)	2 044(3)
Fe(1)-C(12)#1	2 044(3)
Fe(1)-C(9)#1	2 051(3)
Fe(1)-C(9)	2 051(3)
Fe(1)-C(8)	2 053(3)
Fe(1)-C(8)#1	2 053(3)
Fe(1)-C(10)	2 060(3)
Fe(1)-C(10)#1	2 060(3)
Fe(1)-C(11)	2 060(3)
Fe(1)-C(11)#1	2 060(3)
O(1)-C(1)	1 138(5)
C(2)-O(2)	1 135(5)
O(3)-C(3)	1 155(6)
C(4)-O(4)	1 144(5)
O(5)-C(5)	1 142(4)
C(6)-O(6)	1 327(4)
C(6)-C(8)	1 455(5)
O(6)-C(7)	1 433(5)
C(8)-C(12)	1 444(5)
C(8)-C(9)	1 445(5)
C(9)-C(10)	1 413(5)
C(10)-C(11)	1 413(5)
C(11)-C(12)	1 421(5)
C(3)-W(1)-C(4)	85 39(14)
C(3)-W(1)-C(5)	89 74(15)
C(4)-W(1)-C(5)	90 58(16)
C(3)-W(1)-C(2)	89 53(16)
C(4)-W(1)-C(2)	87 74(16)
C(5)-W(1)-C(2)	178 22(13)

C(3)-W(1)-C(1)	84 31(16)
C(4)-W(1)-C(1)	169 68(14)
C(5)-W(1)-C(1)	90 05(15)
C(2)-W(1)-C(1)	91 49(16)
C(3)-W(1)-C(6)	175 92(15)
C(4)-W(1)-C(6)	92 76(12)
C(5)-W(1)-C(6)	86 64(12)
C(2)-W(1)-C(6)	94 03(13)
C(1)-W(1)-C(6)	97 57(13)
C(12)-Fe(1)-C(12)#1	153 14(19)
C(12)-Fe(1)-C(9)#1	125 07(15)
C(12)#1-Fe(1)-C(9)#1	68 95(14)
C(12)-Fe(1)-C(9)	68 96(14)
C(12)#1-Fe(1)-C(9)	125 06(15)
C(9)#1-Fe(1)-C(9)	124 74(19)
C(12)-Fe(1)-C(8)	41 26(13)
C(12)#1-Fe(1)-C(8)	163 55(15)
C(9)#1-Fe(1)-C(8)	109 75(13)
C(9)-Fe(1)-C(8)	41 23(13)
C(12)-Fe(1)-C(8)#1	163 55(15)
C(12)#1-Fe(1)-C(8)#1	41 26(13)
C(9)#1-Fe(1)-C(8)#1	41 23(13)
C(9)-Fe(1)-C(8)#1	109 75(13)
C(8)-Fe(1)-C(8)#1	126 96(19)
C(12)-Fe(1)-C(10)	68 15(16)
C(12)#1-Fe(1)-C(10)	106 63(15)
C(9)#1-Fe(1)-C(10)	159 29(15)
C(9)-Fe(1)-C(10)	40 21(13)
C(8)-Fe(1)-C(10)	68 45(13)
C(8)#1-Fe(1)-C(10)	122 18(14)
C(12)-Fe(1)-C(10)#1	106 63(15)
C(12)#1-Fe(1)-C(10)#1	68 14(16)
C(9)#1-Fe(1)-C(10)#1	40 21(13)
C(9)-Fe(1)-C(10)#1	159 29(15)
C(8)-Fe(1)-C(10)#1	122 18(14)
C(8)#1-Fe(1)-C(10)#1	68 45(13)
C(10)-Fe(1)-C(10)#1	158 66(18)
C(12)-Fe(1)-C(11)	40 52(14)

C(12)#1-Fe(1)-C(11)	118 49(14)
C(9)#1-Fe(1)-C(11)	160 11(15)
C(9)-Fe(1)-C(11)	67 98(14)
C(8)-Fe(1)-C(11)	68 58(13)
C(8)#1-Fe(1)-C(11)	155 45(14)
C(10)-Fe(1)-C(11)	40 12(14)
C(10)#1-Fe(1)-C(11)	122 62(14)
C(12)-Fe(1)-C(11)#1	118 49(14)
C(12)#1-Fe(1)-C(11)#1	40 52(14)
C(9)#1-Fe(1)-C(11)#1	67 97(14)
C(9)-Fe(1)-C(11)#1	160 11(15)
C(8)-Fe(1)-C(11)#1	155 45(14)
C(8)#1-Fe(1)-C(11)#1	68 57(13)
C(10)-Fe(1)-C(11)#1	122 62(14)
C(10)#1-Fe(1)-C(11)#1	40 11(14)
C(11)-Fe(1)-C(11)#1	104 89(19)
O(1)-C(1)-W(1)	172 6(4)
O(2)-C(2)-W(1)	176 8(3)
O(3)-C(3)-W(1)	179 5(4)
O(4)-C(4)-W(1)	174 4(3)
O(5)-C(5)-W(1)	178 6(3)
O(6)-C(6)-C(8)	106 0(4)
O(6)-C(6)-W(1)	129 0(3)
C(8)-C(6)-W(1)	124 9(3)
C(6)-O(6)-C(7)	121 9(3)
C(12)-C(8)-C(9)	106 7(3)
C(12)-C(8)-C(6)	127 1(3)
C(9)-C(8)-C(6)	126 2(3)
C(12)-C(8)-Fe(1)	69 04(18)
C(9)-C(8)-Fe(1)	69 29(16)
C(6)-C(8)-Fe(1)	125 88(19)
C(10)-C(9)-C(8)	108 1(3)
C(10)-C(9)-Fe(1)	70 24(18)
C(8)-C(9)-Fe(1)	69 48(16)
C(11)-C(10)-C(9)	108 8(3)
C(11)-C(10)-Fe(1)	69 96(18)
C(9)-C(10)-Fe(1)	69 55(17)
C(10)-C(11)-C(12)	108 4(3)

C(10)-C(11)-Fe(1)	69 93(18)
C(12)-C(11)-Fe(1)	69 14(18)
C(11)-C(12)-C(8)	107 9(3)
C(11)-C(12)-Fe(1)	70 34(19)
C(8)-C(12)-Fe(1)	69 70(18)

Symmetry transformations used to generate equivalent atoms

#1 -x+1,y,-z+1/2

A4 4 Anisotropic displacement parameters ($Å^2 x\ 10^3$) for 1,1'-$[(CO)_5W{=}C(OMe)]_2Fc$ The anisotropic displacement factor exponent takes the form $-2p^2[\ h^2\ a^{*2}U^{11} + \quad + 2\ h\ k\ a^*\ b^*\ U^{12}\ ]$

	U^{11}	U^{22}	U^{33}	U^{23}	U^{13}	U^{12}
W(1)	13(1)	16(1)	18(1)	-1(1)	1(1)	2(1)
Fe(1)	11(1)	14(1)	12(1)	0	0(1)	0
O(1)	52(2)	31(2)	33(1)	9(1)	2(1)	10(1)
C(1)	25(2)	23(2)	28(2)	-2(2)	6(1)	3(2)
C(2)	20(2)	19(2)	28(2)	6(1)	-1(1)	4(1)
O(2)	43(2)	27(2)	34(1)	-10(1)	1(1)	10(1)
O(3)	14(2)	85(3)	55(2)	-4(2)	0(1)	-3(2)
C(3)	23(2)	34(2)	27(2)	2(1)	4(1)	1(2)
C(4)	19(2)	20(2)	24(2)	-6(1)	0(1)	2(1)
O(4)	35(2)	24(2)	30(2)	5(1)	2(1)	-1(1)
O(5)	30(2)	26(2)	28(1)	-7(1)	-4(1)	4(1)
C(5)	13(1)	20(2)	23(2)	3(1)	-2(1)	1(1)
C(6)	15(2)	16(2)	15(2)	-1(1)	-1(1)	1(1)
O(6)	19(1)	15(1)	43(2)	-3(1)	1(1)	0(1)
C(7)	26(2)	14(2)	126(6)	-6(2)	5(2)	1(2)
C(8)	12(2)	18(2)	14(2)	-2(1)	-2(1)	4(1)
C(9)	15(2)	22(2)	12(1)	3(1)	1(1)	0(1)
C(10)	15(2)	25(2)	14(1)	0(1)	2(1)	6(1)
C(11)	22(2)	20(2)	15(1)	-4(1)	-4(1)	7(1)
C(12)	22(2)	16(2)	15(2)	-1(1)	-3(1)	-1(1)

A4 5 Hydrogen coordinates (x 10^4) and isotropic displacement parameters ($Å^2$x 10 ^{3}) for 1,1'-$[(CO)_5W{=}C(OMe)]_2Fc$

	x	y	z	U(eq)
H(7A)	4433	3014	1354	83
H(7B)	3490	2649	1959	83
H(7C)	3481	2667	753	83
H(9A)	5821	680	1147	20
H(10A)	6456	-1021	1134	21
H(11A)	4973	-2136	1291	23
H(12A)	3385	-1138	1414	21

A4 6 Torsion angles [°] for 1,1'-[$(CO)_5W$=C(OMe)]$_2$Fc

C(3)-W(1)-C(1)-O(1)	1(3)
C(4)-W(1)-C(1)-O(1)	-3(3)
C(5)-W(1)-C(1)-O(1)	91(3)
C(2)-W(1)-C(1)-O(1)	-88(3)
C(6)-W(1)-C(1)-O(1)	177(3)
C(3)-W(1)-C(2)-O(2)	9(6)
C(4)-W(1)-C(2)-O(2)	-77(6)
C(5)-W(1)-C(2)-O(2)	-57(8)
C(1)-W(1)-C(2)-O(2)	93(6)
C(6)-W(1)-C(2)-O(2)	-169(6)
C(4)-W(1)-C(3)-O(3)	-103(61)
C(5)-W(1)-C(3)-O(3)	-12(61)
C(2)-W(1)-C(3)-O(3)	169(100)
C(1)-W(1)-C(3)-O(3)	78(61)
C(6)-W(1)-C(3)-O(3)	-40(62)
C(3)-W(1)-C(4)-O(4)	11(3)
C(5)-W(1)-C(4)-O(4)	-79(3)
C(2)-W(1)-C(4)-O(4)	101(3)
C(1)-W(1)-C(4)-O(4)	15(4)
C(6)-W(1)-C(4)-O(4)	-165(3)
C(3)-W(1)-C(5)-O(5)	-66(13)
C(4)-W(1)-C(5)-O(5)	19(13)
C(2)-W(1)-C(5)-O(5)	0(15)
C(1)-W(1)-C(5)-O(5)	-151(13)
C(6)-W(1)-C(5)-O(5)	112(13)
C(3)-W(1)-C(6)-O(6)	160 7(17)
C(4)-W(1)-C(6)-O(6)	-136 5(3)
C(5)-W(1)-C(6)-O(6)	133 1(3)
C(2)-W(1)-C(6)-O(6)	-48 5(3)
C(1)-W(1)-C(6)-O(6)	43 5(3)
C(3)-W(1)-C(6)-C(8)	-14(2)
C(4)-W(1)-C(6)-C(8)	48 5(2)
C(5)-W(1)-C(6)-C(8)	-41 9(2)
C(2)-W(1)-C(6)-C(8)	136 4(2)
C(1)-W(1)-C(6)-C(8)	-131 6(2)

C(8)-C(6)-O(6)-C(7)	178 8(3)
W(1)-C(6)-O(6)-C(7)	3 0(5)
O(6)-C(6)-C(8)-C(12)	175 1(3)
W(1)-C(6)-C(8)-C(12)	-8 9(4)
O(6)-C(6)-C(8)-C(9)	-3 8(4)
W(1)-C(6)-C(8)-C(9)	172 2(2)
O(6)-C(6)-C(8)-Fe(1)	85 5(3)
W(1)-C(6)-C(8)-Fe(1)	-98 5(3)
C(12)#1-Fe(1)-C(8)-C(12)	156 5(3)
C(9)#1-Fe(1)-C(8)-C(12)	-121 1(2)
C(9)-Fe(1)-C(8)-C(12)	118 3(3)
C(8)#1-Fe(1)-C(8)-C(12)	-164 2(2)
C(10)-Fe(1)-C(8)-C(12)	81 0(2)
C(10)#1-Fe(1)-C(8)-C(12)	-78 2(2)
C(11)-Fe(1)-C(8)-C(12)	37 7(2)
C(11)#1-Fe(1)-C(8)-C(12)	-41 1(4)
C(12)-Fe(1)-C(8)-C(9)	-118 3(3)
C(12)#1-Fe(1)-C(8)-C(9)	38 1(5)
C(9)#1-Fe(1)-C(8)-C(9)	120 6(2)
C(8)#1-Fe(1)-C(8)-C(9)	77 47(18)
C(10)-Fe(1)-C(8)-C(9)	-37 34(19)
C(10)#1-Fe(1)-C(8)-C(9)	163 47(19)
C(11)-Fe(1)-C(8)-C(9)	-80 6(2)
C(11)#1-Fe(1)-C(8)-C(9)	-159 4(3)
C(12)-Fe(1)-C(8)-C(6)	121 3(4)
C(12)#1-Fe(1)-C(8)-C(6)	-82 2(6)
C(9)#1-Fe(1)-C(8)-C(6)	0 2(4)
C(9)-Fe(1)-C(8)-C(6)	-120 3(4)
C(8)#1-Fe(1)-C(8)-C(6)	-42 9(3)
C(10)-Fe(1)-C(8)-C(6)	-157 7(4)
C(10)#1-Fe(1)-C(8)-C(6)	43 1(4)
C(11)-Fe(1)-C(8)-C(6)	159 1(4)
C(11)#1-Fe(1)-C(8)-C(6)	80 3(5)
C(12)-C(8)-C(9)-C(10)	0 7(3)
C(6)-C(8)-C(9)-C(10)	179 9(3)
Fe(1)-C(8)-C(9)-C(10)	59 88(19)
C(12)-C(8)-C(9)-Fe(1)	-59 13(18)
C(6)-C(8)-C(9)-Fe(1)	120 0(3)

C(12)-Fe(1)-C(9)-C(10)	-80 6(2)
C(12)#1-Fe(1)-C(9)-C(10)	73 2(3)
C(9)#1-Fe(1)-C(9)-C(10)	160 5(2)
C(8)-Fe(1)-C(9)-C(10)	-119 1(3)
C(8)#1-Fe(1)-C(9)-C(10)	116 9(2)
C(10)#1-Fe(1)-C(9)-C(10)	-162 0(3)
C(11)-Fe(1)-C(9)-C(10)	-36 9(2)
C(11)#1-Fe(1)-C(9)-C(10)	35 4(5)
C(12)-Fe(1)-C(9)-C(8)	38 47(19)
C(12)#1-Fe(1)-C(9)-C(8)	-167 66(19)
C(9)#1-Fe(1)-C(9)-C(8)	-80 37(18)
C(8)#1-Fe(1)-C(9)-C(8)	-124 0(2)
C(10)-Fe(1)-C(9)-C(8)	119 1(3)
C(10)#1-Fe(1)-C(9)-C(8)	-42 9(5)
C(11)-Fe(1)-C(9)-C(8)	82 2(2)
C(11)#1-Fe(1)-C(9)-C(8)	154 5(4)
C(8)-C(9)-C(10)-C(11)	-0 3(3)
Fe(1)-C(9)-C(10)-C(11)	59 1(2)
C(8)-C(9)-C(10)-Fe(1)	-59 40(18)
C(12)-Fe(1)-C(10)-C(11)	-37 3(2)
C(12)#1-Fe(1)-C(10)-C(11)	114 7(2)
C(9)#1-Fe(1)-C(10)-C(11)	-170 9(3)
C(9)-Fe(1)-C(10)-C(11)	-120 2(3)
C(8)-Fe(1)-C(10)-C(11)	-81 9(2)
C(8)#1-Fe(1)-C(10)-C(11)	157 1(2)
C(10)#1-Fe(1)-C(10)-C(11)	42 35(18)
C(11)#1-Fe(1)-C(10)-C(11)	73 4(3)
C(12)-Fe(1)-C(10)-C(9)	82 8(2)
C(12)#1-Fe(1)-C(10)-C(9)	-125 1(2)
C(9)#1-Fe(1)-C(10)-C(9)	-50 8(5)
C(8)-Fe(1)-C(10)-C(9)	38 3(2)
C(8)#1-Fe(1)-C(10)-C(9)	-82 8(2)
C(10)#1-Fe(1)-C(10)-C(9)	162 5(2)
C(11)-Fe(1)-C(10)-C(9)	120 2(3)
C(11)#1-Fe(1)-C(10)-C(9)	-166 5(2)
C(9)-C(10)-C(11)-C(12)	-0 3(3)
Fe(1)-C(10)-C(11)-C(12)	58 6(2)
C(9)-C(10)-C(11)-Fe(1)	-58 8(2)

C(12)-Fe(1)-C(11)-C(10)	120 0(3)
C(12)#1-Fe(1)-C(11)-C(10)	-82 0(2)
C(9)#1-Fe(1)-C(11)-C(10)	170 6(4)
C(9)-Fe(1)-C(11)-C(10)	37 0(2)
C(8)-Fe(1)-C(11)-C(10)	81 6(2)
C(8)#1-Fe(1)-C(11)-C(10)	-52 5(4)
C(10)#1-Fe(1)-C(11)-C(10)	-163 08(16)
C(11)#1-Fe(1)-C(11)-C(10)	-123 4(2)
C(12)#1-Fe(1)-C(11)-C(12)	158 01(18)
C(9)#1-Fe(1)-C(11)-C(12)	50 6(5)
C(9)-Fe(1)-C(11)-C(12)	-82 9(2)
C(8)-Fe(1)-C(11)-C(12)	-38 4(2)
C(8)#1-Fe(1)-C(11)-C(12)	-172 5(3)
C(10)-Fe(1)-C(11)-C(12)	-120 0(3)
C(10)#1-Fe(1)-C(11)-C(12)	77 0(2)
C(11)#1-Fe(1)-C(11)-C(12)	116 7(2)
C(10)-C(11)-C(12)-C(8)	0 7(3)
Fe(1)-C(11)-C(12)-C(8)	59 80(19)
C(10)-C(11)-C(12)-Fe(1)	-59 1(2)
C(9)-C(8)-C(12)-C(11)	-0 9(3)
C(6)-C(8)-C(12)-C(11)	180 0(3)
Fe(1)-C(8)-C(12)-C(11)	-60 2(2)
C(9)-C(8)-C(12)-Fe(1)	59 29(18)
C(6)-C(8)-C(12)-Fe(1)	-119 8(3)
C(12)#1-Fe(1)-C(12)-C(11)	-46 75(18)
C(9)#1-Fe(1)-C(12)-C(11)	-161 3(2)
C(9)-Fe(1)-C(12)-C(11)	80 3(2)
C(8)-Fe(1)-C(12)-C(11)	118 8(3)
C(8)#1-Fe(1)-C(12)-C(11)	168 9(4)
C(10)-Fe(1)-C(12)-C(11)	37 0(2)
C(10)#1-Fe(1)-C(12)-C(11)	-121 1(2)
C(11)#1-Fe(1)-C(12)-C(11)	-79 3(3)
C(12)#1-Fe(1)-C(12)-C(8)	-165 5(2)
C(9)#1-Fe(1)-C(12)-C(8)	80 0(2)
C(9)-Fe(1)-C(12)-C(8)	-38 44(19)
C(8)#1-Fe(1)-C(12)-C(8)	50 2(6)
C(10)-Fe(1)-C(12)-C(8)	-81 8(2)
C(10)#1-Fe(1)-C(12)-C(8)	120 2(2)

C(11)-Fe(1)-C(12)-C(8)	-118 8(3)
C(11)#1-Fe(1)-C(12)-C(8)	161 9(2)

Symmetry transformations used to generate equivalent atoms
#1 -x+1,y,-z+1/2

A5 Crystal data and experimental parameters for (*E*)-$(CO)_5Cr=C(C_4H_8N)C_2H_2Fc$

A5 1 Crystal data and structure refinement for (*E*)-$(CO)_5Cr=C(C_4H_8N)C_2H_2Fc$

Identification code	mpcr	
Empirical formula	C22 H19 Cr Fe N O5	
Formula weight	485 23	
Temperature	298(2) K	
Wavelength	0 71073 Å	
Crystal system	Orthorhombic	
Space group	Pbca	
Unit cell dimensions	a = 11 2790(8) Å	a= 90°
	b = 16 6763(11) Å	b= 90°
	c = 22 7532(15) Å	g = 90°
Volume	4279 7(5) $Å^3$	
Z	8	
Density (calculated)	1 506 Mg/m^3	
Absorption coefficient	1 218 mm^{-1}	
F(000)	1984	
Crystal size	0 50 x 0 40 x 0 25 mm^3	
Theta range for data collection	1 79 to 24 99°	
Index ranges	-13<=h<=13, -19<=k<=19, -26<=l<=27	
Reflections collected	38141	
Independent reflections	3760 [R(int) = 0 1240]	
Completeness to theta = 24 99°	100 0 %	
Absorption correction	Semi-empirical from equivalents	
Max and mm transmission	1 0000 and 0 9052	
Refinement method	Full-matrix least-squares on F^2	
Data / restraints / parameters	3760 / 0 / 271	
Goodness-of-fit on F^2	0 942	
Final R indices [I>2sigma(I)]	R1 = 0 0584, wR2 = 0 1159	
R indices (all data)	R1 = 0 1093, wR2 = 0 1330	
Largest diff peak and hole	0 445 and -0 295 e $Å^{-3}$	

A5 2 Atomic coordinates (x 10^4) and equivalent isotropic displacement parameters ($Å^2$x 10^3) for (*E*)-$(CO)_5Cr{=}C(C_4H_8N)C_2H_2Fc$ U(eq) is defined as one third of the trace of the orthogonalized U^{ij} tensor

	x	y	z	U(eq)
Cr(1)	3812(1)	1839(1)	4414(1)	40(1)
Fe(1)	3898(1)	4116(1)	2340(1)	44(1)
C(1)	3677(4)	3085(3)	4586(2)	38(1)
C(2)	3496(4)	3638(3)	4079(2)	48(1)
C(3)	4252(5)	3852(3)	3700(2)	56(1)
C(4)	4080(5)	4421(3)	3210(2)	51(1)
C(5)	5030(5)	4743(3)	2867(2)	56(2)
C(6)	4562(6)	5250(3)	2442(2)	62(2)
C(7)	3310(5)	5251(3)	2506(2)	61(2)
C(8)	3012(5)	4733(3)	2973(2)	55(1)
C(9)	3074(10)	3075(6)	2137(4)	104(3)
C(10)	2964(8)	3601(5)	1680(4)	89(2)
C(11)	4048(11)	3780(5)	1486(3)	98(3)
C(12)	4831(7)	3388(7)	1817(6)	119(4)
C(13)	4274(14)	2943(5)	2226(4)	129(5)
N(14)	3612(3)	3450(2)	5091(2)	38(1)
C(15)	3460(5)	4325(3)	5178(2)	61(2)
C(16)	3439(9)	4449(4)	5813(3)	146(4)
C(17)	3718(6)	3730(3)	6106(2)	83(2)
C(18)	3680(5)	3067(3)	5675(2)	61(2)
C(19)	4992(5)	1995(3)	3835(2)	52(1)
O(20)	5706(4)	2035(2)	3479(2)	81(1)
C(21)	2637(5)	1945(3)	3821(2)	53(1)
O(22)	1944(4)	1971(3)	3465(2)	94(2)
C(23)	2578(5)	1605(3)	4953(2)	50(1)
O(24)	1797(4)	1424(2)	5246(2)	78(1)
C(25)	5060(5)	1733(3)	4969(2)	47(1)
O(26)	5859(3)	1655(2)	5271(2)	76(1)
C(27)	3919(5)	753(3)	4261(2)	57(1)
O(28)	3987(4)	74(2)	4184(2)	89(1)

A5 3 Bond lengths [Å] and angles [°] for (*E*)-$(CO)_5Cr{=}C(C_4H_8N)C_2H_2Fc$

Cr(1)-C(27)	1 848(6)
Cr(1)-C(19)	1 890(6)
Cr(1)-C(23)	1 895(6)
Cr(1)-C(25)	1 899(6)
Cr(1)-C(21)	1 900(6)
Cr(1)-C(1)	2 119(4)
Fe(1)-C(12)	1 999(7)
Fe(1)-C(13)	2 017(7)
Fe(1)-C(9)	2 021(6)
Fe(1)-C(10)	2 025(6)
Fe(1)-C(11)	2 029(6)
Fe(1)-C(8)	2 034(5)
Fe(1)-C(5)	2 041(5)
Fe(1)-C(7)	2 042(5)
Fe(1)-C(6)	2 048(5)
Fe(1)-C(4)	2 055(5)
C(1)-N(14)	1 303(5)
C(1)-C(2)	1 492(6)
C(2)-C(3)	1 264(6)
C(3)-C(4)	1 476(7)
C(4)-C(8)	1 419(7)
C(4)-C(5)	1 431(7)
C(5)-C(6)	1 389(7)
C(6)-C(7)	1 419(8)
C(7)-C(8)	1 411(7)
C(9)-C(10)	1 365(10)
C(9)-C(13)	1 387(12)
C(10)-C(11)	1 335(10)
C(11)-C(12)	1 332(10)
C(12)-C(13)	1 346(11)
N(14)-C(18)	1 476(5)
N(14)-C(15)	1 483(6)
C(15)-C(16)	1 462(7)
C(16)-C(17)	1 407(8)
C(17)-C(18)	1 478(7)

C(19)-O(20)	1 145(5)
C(21)-O(22)	1 126(6)
C(23)-O(24)	1 146(6)
C(25)-O(26)	1 141(6)
C(27)-O(28)	1 149(6)
C(27)-Cr(1)-C(19)	87 6(2)
C(27)-Cr(1)-C(23)	88 2(2)
C(19)-Cr(1)-C(23)	174 8(2)
C(27)-Cr(1)-C(25)	89 2(2)
C(19)-Cr(1)-C(25)	87 4(2)
C(23)-Cr(1)-C(25)	95 5(2)
C(27)-Cr(1)-C(21)	90 1(2)
C(19)-Cr(1)-C(21)	89 0(2)
C(23)-Cr(1)-C(21)	88 1(2)
C(25)-Cr(1)-C(21)	176 4(2)
C(27)-Cr(1)-C(1)	179 6(2)
C(19)-Cr(1)-C(1)	92 53(19)
C(23)-Cr(1)-C(1)	91 75(18)
C(25)-Cr(1)-C(1)	91 27(19)
C(21)-Cr(1)-C(1)	89 44(19)
C(12)-Fe(1)-C(13)	39 2(3)
C(12)-Fe(1)-C(9)	65 5(3)
C(13)-Fe(1)-C(9)	40 2(4)
C(12)-Fe(1)-C(10)	64 9(3)
C(13)-Fe(1)-C(10)	66 6(3)
C(9)-Fe(1)-C(10)	39 4(3)
C(12)-Fe(1)-C(11)	38 6(3)
C(13)-Fe(1)-C(11)	65 9(3)
C(9)-Fe(1)-C(11)	65 4(3)
C(10)-Fe(1)-C(11)	38 4(3)
C(12)-Fe(1)-C(8)	171 1(5)
C(13)-Fe(1)-C(8)	133 2(4)
C(9)-Fe(1)-C(8)	111 7(3)
C(10)-Fe(1)-C(8)	119 0(3)
C(11)-Fe(1)-C(8)	149 3(4)
C(12)-Fe(1)-C(5)	109 3(3)
C(13)-Fe(1)-C(5)	116 1(4)
C(9)-Fe(1)-C(5)	149 5(4)

C(10)-Fe(1)-C(5)	168 2(4)
C(11)-Fe(1)-C(5)	130 7(3)
C(8)-Fe(1)-C(5)	68 4(2)
C(12)-Fe(1)-C(7)	147 6(5)
C(13)-Fe(1)-C(7)	172 3(5)
C(9)-Fe(1)-C(7)	133 6(4)
C(10)-Fe(1)-C(7)	111 2(3)
C(11)-Fe(1)-C(7)	117 4(3)
C(8)-Fe(1)-C(7)	40 51(19)
C(5)-Fe(1)-C(7)	67 6(2)
C(12)-Fe(1)-C(6)	115 8(4)
C(13)-Fe(1)-C(6)	146 4(5)
C(9)-Fe(1)-C(6)	170 7(4)
C(10)-Fe(1)-C(6)	131 8(3)
C(11)-Fe(1)-C(6)	109 5(3)
C(8)-Fe(1)-C(6)	68 4(2)
C(5)-Fe(1)-C(6)	39 71(19)
C(7)-Fe(1)-C(6)	40 6(2)
C(12)-Fe(1)-C(4)	132 1(4)
C(13)-Fe(1)-C(4)	110 0(3)
C(9)-Fe(1)-C(4)	118 6(3)
C(10)-Fe(1)-C(4)	150 6(4)
C(11)-Fe(1)-C(4)	169 3(4)
C(8)-Fe(1)-C(4)	40 62(19)
C(5)-Fe(1)-C(4)	40 89(19)
C(7)-Fe(1)-C(4)	67 9(2)
C(6)-Fe(1)-C(4)	68 0(2)
N(14)-C(1)-C(2)	112 8(4)
N(14)-C(1)-Cr(1)	128 6(3)
C(2)-C(1)-Cr(1)	118 2(3)
C(3)-C(2)-C(1)	127 6(5)
C(2)-C(3)-C(4)	127 4(5)
C(8)-C(4)-C(5)	106 9(4)
C(8)-C(4)-C(3)	129 4(5)
C(5)-C(4)-C(3)	123 7(5)
C(8)-C(4)-Fe(1)	68 9(3)
C(5)-C(4)-Fe(1)	69 0(3)
C(3)-C(4)-Fe(1)	125 6(3)

C(6)-C(5)-C(4)	108 9(5)
C(6)-C(5)-Fe(1)	70 4(3)
C(4)-C(5)-Fe(1)	70 1(3)
C(5)-C(6)-C(7)	108 0(5)
C(5)-C(6)-Fe(1)	69 9(3)
C(7)-C(6)-Fe(1)	69 4(3)
C(8)-C(7)-C(6)	108 3(5)
C(8)-C(7)-Fe(1)	69 4(3)
C(6)-C(7)-Fe(1)	69 9(3)
C(7)-C(8)-C(4)	108 0(5)
C(7)-C(8)-Fe(1)	70 0(3)
C(4)-C(8)-Fe(1)	70 5(3)
C(10)-C(9)-C(13)	107 6(7)
C(10)-C(9)-Fe(1)	70 4(4)
C(13)-C(9)-Fe(1)	69 8(4)
C(11)-C(10)-C(9)	108 2(7)
C(11)-C(10)-Fe(1)	71 0(4)
C(9)-C(10)-Fe(1)	70 2(4)
C(12)-C(11)-C(10)	108 1(8)
C(12)-C(11)-Fe(1)	69 5(4)
C(10)-C(11)-Fe(1)	70 6(4)
C(11)-C(12)-C(13)	110 6(8)
C(11)-C(12)-Fe(1)	71 9(4)
C(13)-C(12)-Fe(1)	71 2(5)
C(12)-C(13)-C(9)	105 5(8)
C(12)-C(13)-Fe(1)	69 7(4)
C(9)-C(13)-Fe(1)	70 1(5)
C(1)-N(14)-C(18)	126 2(4)
C(1)-N(14)-C(15)	125 6(4)
C(18)-N(14)-C(15)	108 2(4)
C(16)-C(15)-N(14)	105 8(4)
C(17)-C(16)-C(15)	110 2(5)
C(16)-C(17)-C(18)	108 4(5)
N(14)-C(18)-C(17)	106 0(4)
O(20)-C(19)-Cr(1)	175 4(5)
O(22)-C(21)-Cr(1)	176 9(5)
O(24)-C(23)-Cr(1)	174 7(5)
O(26)-C(25)-Cr(1)	175 4(5)

O(28)-C(27)-Cr(1)	177 9(5)

Symmetry transformations used to generate equivalent atoms

A5 4 Anisotropic displacement parameters ($Å^2$x 10^3) for (*E*)-$(CO)_5Cr{=}C(C_4H_8N)C_2H_2Fc$ The anisotropic displacement factor exponent takes the form $-2p^2[\ h^2\ a^{*2}U^{11} + \quad + 2\ h\ k\ a^*\ b^*\ U^{12}\ ]$

	U^{11}	U^{22}	U^{33}	U^{23}	U^{13}	U^{12}
Cr(1)	44(1)	33(1)	43(1)	3(1)	2(1)	1(1)
Fe(1)	53(1)	45(1)	35(1)	-2(1)	-1(1)	-3(1)
C(1)	40(3)	31(3)	43(3)	5(2)	1(2)	-1(2)
C(2)	60(3)	38(3)	47(3)	-4(2)	11(3)	1(3)
C(3)	64(4)	49(3)	56(4)	-4(3)	-2(3)	-1(3)
C(4)	85(4)	37(3)	30(3)	-2(2)	-10(3)	6(3)
C(5)	63(4)	58(4)	48(3)	-4(3)	-8(3)	-14(3)
C(6)	97(5)	46(4)	43(3)	8(3)	2(3)	-21(3)
C(7)	92(5)	47(4)	44(4)	3(3)	-4(3)	18(3)
C(8)	67(4)	55(4)	45(3)	-9(3)	14(3)	-2(3)
C(9)	140(8)	95(6)	77(6)	-44(5)	49(6)	-77(6)
C(10)	92(6)	107(6)	69(5)	-51(5)	-40(5)	30(5)
C(11)	168(9)	79(5)	48(4)	-29(4)	47(5)	-24(6)
C(12)	61(5)	117(8)	181(11)	-96(7)	-2(6)	27(5)
C(13)	264(14)	41(5)	81(7)	-13(4)	-84(8)	30(7)
N(14)	46(3)	31(2)	38(2)	3(2)	-1(2)	-3(2)
C(15)	98(4)	32(3)	53(3)	-1(3)	-7(3)	-4(3)
C(16)	329(13)	55(5)	53(4)	-7(4)	-25(6)	21(6)
C(17)	145(6)	58(4)	45(3)	-6(3)	-5(4)	-1(4)
C(18)	102(4)	45(3)	35(3)	3(2)	0(3)	10(3)
C(19)	58(3)	43(3)	55(4)	1(3)	0(3)	2(3)
O(20)	87(3)	83(3)	74(3)	5(2)	34(3)	5(2)
C(21)	55(3)	45(3)	60(4)	3(3)	-5(3)	3(3)
O(22)	89(3)	91(3)	102(4)	0(3)	-46(3)	5(3)
C(23)	54(3)	38(3)	57(3)	5(3)	-9(3)	-3(3)
O(24)	65(3)	91(3)	79(3)	12(2)	19(2)	-18(2)
C(25)	49(3)	41(3)	53(3)	7(3)	9(3)	5(3)
O(26)	54(2)	98(3)	76(3)	23(2)	-13(2)	15(2)
C(27)	63(3)	47(4)	62(4)	-4(3)	6(3)	-1(3)
O(28)	114(3)	37(2)	114(4)	-14(2)	16(3)	-3(2)

A5 5 Hydrogen coordinates (x 10^4) and isotropic displacement parameters ($Å^2$x 10 ^{3}) for (*E*)-$(CO)_5Cr{=}C(C_4H_8N)C_2H_2Fc$

	x	y	z	U(eq)
H(11A)	2738	3850	4036	58
H(42A)	5003	3626	3734	67
H(20A)	5874	4625	2923	67
H(16A)	5016	5552	2149	75
H(17A)	2749	5555	2264	73
H(19A)	2209	4618	3114	66
H(40A)	2422	2827	2356	125
H(27A)	2216	3800	1516	107
H(30A)	4236	4134	1155	118
H(29A)	5693	3412	1765	143
H(32A)	4638	2578	2511	155
H(43A)	4114	4617	5001	73
H(43B)	2725	4507	5001	73
H(45A)	4008	4860	5920	175
H(45B)	2657	4630	5933	175
H(41A)	3150	3633	6419	99
H(41B)	4502	3767	6279	99
H(44A)	4387	2739	5706	73
H(44B)	2991	2731	5742	73

A5 6 Torsion angles [°] for (*E*)-$(CO)_5Cr{=}C(C_4H_8N)C_2H_2Fc$

C(27)-Cr(1)-C(1)-N(14)	124(33)
C(19)-Cr(1)-C(1)-N(14)	-136 1(4)
C(23)-Cr(1)-C(1)-N(14)	46 8(4)
C(25)-Cr(1)-C(1)-N(14)	-48 7(4)
C(21)-Cr(1)-C(1)-N(14)	134 9(4)
C(27)-Cr(1)-C(1)-C(2)	-49(33)
C(19)-Cr(1)-C(1)-C(2)	51 4(4)
C(23)-Cr(1)-C(1)-C(2)	-125 7(4)
C(25)-Cr(1)-C(1)-C(2)	138 8(4)
C(21)-Cr(1)-C(1)-C(2)	-37 6(4)
N(14)-C(1)-C(2)-C(3)	111 8(6)
Cr(1)-C(1)-C(2)-C(3)	-74 6(6)
C(1)-C(2)-C(3)-C(4)	-177 8(5)
C(2)-C(3)-C(4)-C(8)	-14 1(9)
C(2)-C(3)-C(4)-C(5)	168 1(5)
C(2)-C(3)-C(4)-Fe(1)	-104 9(6)
C(12)-Fe(1)-C(4)-C(8)	-172 4(5)
C(13)-Fe(1)-C(4)-C(8)	-134 0(6)
C(9)-Fe(1)-C(4)-C(8)	-90 7(5)
C(10)-Fe(1)-C(4)-C(8)	-56 3(6)
C(11)-Fe(1)-C(4)-C(8)	160 2(13)
C(5)-Fe(1)-C(4)-C(8)	118 8(4)
C(7)-Fe(1)-C(4)-C(8)	38 0(3)
C(6)-Fe(1)-C(4)-C(8)	82 0(3)
C(12)-Fe(1)-C(4)-C(5)	68 7(6)
C(13)-Fe(1)-C(4)-C(5)	107 2(6)
C(9)-Fe(1)-C(4)-C(5)	150 5(5)
C(10)-Fe(1)-C(4)-C(5)	-175 1(5)
C(11)-Fe(1)-C(4)-C(5)	41 4(15)
C(8)-Fe(1)-C(4)-C(5)	-118 8(4)
C(7)-Fe(1)-C(4)-C(5)	-80 8(3)
C(6)-Fe(1)-C(4)-C(5)	-36 8(3)
C(12)-Fe(1)-C(4)-C(3)	-48 4(7)
C(13)-Fe(1)-C(4)-C(3)	-10 0(7)
C(9)-Fe(1)-C(4)-C(3)	33 3(7)

C(10)-Fe(1)-C(4)-C(3)	67 7(7)
C(11)-Fe(1)-C(4)-C(3)	-75 7(15)
C(8)-Fe(1)-C(4)-C(3)	124 0(6)
C(5)-Fe(1)-C(4)-C(3)	-117 1(6)
C(7)-Fe(1)-C(4)-C(3)	162 1(6)
C(6)-Fe(1)-C(4)-C(3)	-154 0(6)
C(8)-C(4)-C(5)-C(6)	1 3(6)
C(3)-C(4)-C(5)-C(6)	179 5(5)
Fe(1)-C(4)-C(5)-C(6)	60 0(4)
C(8)-C(4)-C(5)-Fe(1)	-58 7(3)
C(3)-C(4)-C(5)-Fe(1)	119 6(5)
C(12)-Fe(1)-C(5)-C(6)	107 5(6)
C(13)-Fe(1)-C(5)-C(6)	149 5(6)
C(9)-Fe(1)-C(5)-C(6)	-178 2(5)
C(10)-Fe(1)-C(5)-C(6)	48 7(13)
C(11)-Fe(1)-C(5)-C(6)	69 7(6)
C(8)-Fe(1)-C(5)-C(6)	-81 8(4)
C(7)-Fe(1)-C(5)-C(6)	-37 9(3)
C(4)-Fe(1)-C(5)-C(6)	-119 6(5)
C(12)-Fe(1)-C(5)-C(4)	-132 9(5)
C(13)-Fe(1)-C(5)-C(4)	-90 9(6)
C(9)-Fe(1)-C(5)-C(4)	-58 6(6)
C(10)-Fe(1)-C(5)-C(4)	168 3(11)
C(11)-Fe(1)-C(5)-C(4)	-170 7(4)
C(8)-Fe(1)-C(5)-C(4)	37 8(3)
C(7)-Fe(1)-C(5)-C(4)	81 7(3)
C(6)-Fe(1)-C(5)-C(4)	119 6(5)
C(4)-C(5)-C(6)-C(7)	-0 6(6)
Fe(1)-C(5)-C(6)-C(7)	59 2(4)
C(4)-C(5)-C(6)-Fe(1)	-59 8(4)
C(12)-Fe(1)-C(6)-C(5)	-89 6(6)
C(13)-Fe(1)-C(6)-C(5)	-55 5(7)
C(9)-Fe(1)-C(6)-C(5)	174 2(15)
C(10)-Fe(1)-C(6)-C(5)	-168 1(4)
C(11)-Fe(1)-C(6)-C(5)	-131 0(5)
C(8)-Fe(1)-C(6)-C(5)	81 8(4)
C(7)-Fe(1)-C(6)-C(5)	119 2(5)
C(4)-Fe(1)-C(6)-C(5)	37 9(3)

C(12)-Fe(1)-C(6)-C(7)	151 2(5)
C(13)-Fe(1)-C(6)-C(7)	-174 7(5)
C(9)-Fe(1)-C(6)-C(7)	55 0(17)
C(10)-Fe(1)-C(6)-C(7)	72 7(5)
C(11)-Fe(1)-C(6)-C(7)	109 8(5)
C(8)-Fe(1)-C(6)-C(7)	-37 4(3)
C(5)-Fe(1)-C(6)-C(7)	-119 2(5)
C(4)-Fe(1)-C(6)-C(7)	-81 3(3)
C(5)-C(6)-C(7)-C(8)	-0 4(6)
Fe(1)-C(6)-C(7)-C(8)	59 1(4)
C(5)-C(6)-C(7)-Fe(1)	-59 5(4)
C(12)-Fe(1)-C(7)-C(8)	-173 6(6)
C(13)-Fe(1)-C(7)-C(8)	38(2)
C(9)-Fe(1)-C(7)-C(8)	70 9(5)
C(10)-Fe(1)-C(7)-C(8)	110 2(5)
C(11)-Fe(1)-C(7)-C(8)	152 0(4)
C(5)-Fe(1)-C(7)-C(8)	-82 5(3)
C(6)-Fe(1)-C(7)-C(8)	-119 6(5)
C(4)-Fe(1)-C(7)-C(8)	-38 1(3)
C(12)-Fe(1)-C(7)-C(6)	-54 0(7)
C(13)-Fe(1)-C(7)-C(6)	157 5(19)
C(9)-Fe(1)-C(7)-C(6)	-169 5(5)
C(10)-Fe(1)-C(7)-C(6)	-130 2(5)
C(11)-Fe(1)-C(7)-C(6)	-88 4(5)
C(8)-Fe(1)-C(7)-C(6)	119 6(5)
C(5)-Fe(1)-C(7)-C(6)	37 1(3)
C(4)-Fe(1)-C(7)-C(6)	81 4(3)
C(6)-C(7)-C(8)-C(4)	1 2(6)
Fe(1)-C(7)-C(8)-C(4)	60 6(3)
C(6)-C(7)-C(8)-Fe(1)	-59 4(4)
C(5)-C(4)-C(8)-C(7)	-1 5(6)
C(3)-C(4)-C(8)-C(7)	-179 6(5)
Fe(1)-C(4)-C(8)-C(7)	-60 3(4)
C(5)-C(4)-C(8)-Fe(1)	58 8(3)
C(3)-C(4)-C(8)-Fe(1)	-119 3(5)
C(12)-Fe(1)-C(8)-C(7)	157 3(17)
C(13)-Fe(1)-C(8)-C(7)	-173 5(5)
C(9)-Fe(1)-C(8)-C(7)	-132 5(5)

C(10)-Fe(1)-C(8)-C(7)	-89 4(5)
C(11)-Fe(1)-C(8)-C(7)	-54 5(6)
C(5)-Fe(1)-C(8)-C(7)	80 4(3)
C(6)-Fe(1)-C(8)-C(7)	37 5(3)
C(4)-Fe(1)-C(8)-C(7)	118 5(5)
C(12)-Fe(1)-C(8)-C(4)	38 8(19)
C(13)-Fe(1)-C(8)-C(4)	68 0(6)
C(9)-Fe(1)-C(8)-C(4)	109 0(5)
C(10)-Fe(1)-C(8)-C(4)	152 2(4)
C(11)-Fe(1)-C(8)-C(4)	-173 0(5)
C(5)-Fe(1)-C(8)-C(4)	-38 1(3)
C(7)-Fe(1)-C(8)-C(4)	-118 5(5)
C(6)-Fe(1)-C(8)-C(4)	-80 9(3)
C(12)-Fe(1)-C(9)-C(10)	-79 6(5)
C(13)-Fe(1)-C(9)-C(10)	-118 2(7)
C(11)-Fe(1)-C(9)-C(10)	-37 0(5)
C(8)-Fe(1)-C(9)-C(10)	109 6(5)
C(5)-Fe(1)-C(9)-C(10)	-166 4(5)
C(7)-Fe(1)-C(9)-C(10)	68 3(6)
C(6)-Fe(1)-C(9)-C(10)	21(2)
C(4)-Fe(1)-C(9)-C(10)	154 1(5)
C(12)-Fe(1)-C(9)-C(13)	38 6(5)
C(10)-Fe(1)-C(9)-C(13)	118 2(7)
C(11)-Fe(1)-C(9)-C(13)	81 2(6)
C(8)-Fe(1)-C(9)-C(13)	-132 2(6)
C(5)-Fe(1)-C(9)-C(13)	-48 2(8)
C(7)-Fe(1)-C(9)-C(13)	-173 5(6)
C(6)-Fe(1)-C(9)-C(13)	139 1(18)
C(4)-Fe(1)-C(9)-C(13)	-87 7(6)
C(13)-C(9)-C(10)-C(11)	0 9(8)
Fe(1)-C(9)-C(10)-C(11)	61 1(5)
C(13)-C(9)-C(10)-Fe(1)	-60 2(5)
C(12)-Fe(1)-C(10)-C(11)	-37 1(5)
C(13)-Fe(1)-C(10)-C(11)	-80 2(6)
C(9)-Fe(1)-C(10)-C(11)	-118 4(7)
C(8)-Fe(1)-C(10)-C(11)	152 0(5)
C(5)-Fe(1)-C(10)-C(11)	25 9(15)
C(7)-Fe(1)-C(10)-C(11)	107 8(6)

C(6)-Fe(1)-C(10)-C(11)	66 0(6)
C(4)-Fe(1)-C(10)-C(11)	-169 8(5)
C(12)-Fe(1)-C(10)-C(9)	81 3(6)
C(13)-Fe(1)-C(10)-C(9)	38 3(5)
C(11)-Fe(1)-C(10)-C(9)	118 4(7)
C(8)-Fe(1)-C(10)-C(9)	-89 6(6)
C(5)-Fe(1)-C(10)-C(9)	144 3(12)
C(7)-Fe(1)-C(10)-C(9)	-133 8(6)
C(6)-Fe(1)-C(10)-C(9)	-175 6(5)
C(4)-Fe(1)-C(10)-C(9)	-51 3(7)
C(9)-C(10)-C(11)-C(12)	-1 0(8)
Fe(1)-C(10)-C(11)-C(12)	59 6(5)
C(9)-C(10)-C(11)-Fe(1)	-60 5(5)
C(13)-Fe(1)-C(11)-C(12)	-36 7(6)
C(9)-Fe(1)-C(11)-C(12)	-81 0(6)
C(10)-Fe(1)-C(11)-C(12)	-118 9(8)
C(8)-Fe(1)-C(11)-C(12)	-172 5(6)
C(5)-Fe(1)-C(11)-C(12)	67 9(7)
C(7)-Fe(1)-C(11)-C(12)	151 0(6)
C(6)-Fe(1)-C(11)-C(12)	107 3(6)
C(4)-Fe(1)-C(11)-C(12)	33 1(16)
C(12)-Fe(1)-C(11)-C(10)	118 9(8)
C(13)-Fe(1)-C(11)-C(10)	82 2(6)
C(9)-Fe(1)-C(11)-C(10)	37 9(5)
C(8)-Fe(1)-C(11)-C(10)	-53 5(7)
C(5)-Fe(1)-C(11)-C(10)	-173 2(5)
C(7)-Fe(1)-C(11)-C(10)	-90 1(6)
C(6)-Fe(1)-C(11)-C(10)	-133 8(5)
C(4)-Fe(1)-C(11)-C(10)	152 0(12)
C(10)-C(11)-C(12)-C(13)	0 7(9)
Fe(1)-C(11)-C(12)-C(13)	60 9(6)
C(10)-C(11)-C(12)-Fe(1)	-60 3(5)
C(13)-Fe(1)-C(12)-C(11)	120 2(8)
C(9)-Fe(1)-C(12)-C(11)	80 6(5)
C(10)-Fe(1)-C(12)-C(11)	37 0(5)
C(8)-Fe(1)-C(12)-C(11)	154 4(16)
C(5)-Fe(1)-C(12)-C(11)	-131 9(5)
C(7)-Fe(1)-C(12)-C(11)	-53 4(8)

C(6)-Fe(1)-C(12)-C(11)	-89 3(6)
C(4)-Fe(1)-C(12)-C(11)	-172 2(5)
C(9)-Fe(1)-C(12)-C(13)	-39 6(6)
C(10)-Fe(1)-C(12)-C(13)	-83 2(6)
C(11)-Fe(1)-C(12)-C(13)	-120 2(8)
C(8)-Fe(1)-C(12)-C(13)	34(2)
C(5)-Fe(1)-C(12)-C(13)	107 9(7)
C(7)-Fe(1)-C(12)-C(13)	-173 6(6)
C(6)-Fe(1)-C(12)-C(13)	150 5(6)
C(4)-Fe(1)-C(12)-C(13)	67 7(7)
C(11)-C(12)-C(13)-C(9)	-0 1(9)
Fe(1)-C(12)-C(13)-C(9)	61 3(5)
C(11)-C(12)-C(13)-Fe(1)	-61 4(6)
C(10)-C(9)-C(13)-C(12)	-0 5(9)
Fe(1)-C(9)-C(13)-C(12)	-61 1(6)
C(10)-C(9)-C(13)-Fe(1)	60 6(5)
C(9)-Fe(1)-C(13)-C(12)	115 9(8)
C(10)-Fe(1)-C(13)-C(12)	78 4(6)
C(11)-Fe(1)-C(13)-C(12)	36 2(5)
C(8)-Fe(1)-C(13)-C(12)	-173 1(5)
C(5)-Fe(1)-C(13)-C(12)	-89 0(6)
C(7)-Fe(1)-C(13)-C(12)	153 6(18)
C(6)-Fe(1)-C(13)-C(12)	-53 1(8)
C(4)-Fe(1)-C(13)-C(12)	-133 1(6)
C(12)-Fe(1)-C(13)-C(9)	-115 9(8)
C(10)-Fe(1)-C(13)-C(9)	-37 6(5)
C(11)-Fe(1)-C(13)-C(9)	-79 7(5)
C(8)-Fe(1)-C(13)-C(9)	71 0(6)
C(5)-Fe(1)-C(13)-C(9)	155 1(5)
C(7)-Fe(1)-C(13)-C(9)	38(2)
C(6)-Fe(1)-C(13)-C(9)	-169 0(5)
C(4)-Fe(1)-C(13)-C(9)	110 9(6)
C(2)-C(1)-N(14)-C(18)	176 1(4)
Cr(1)-C(1)-N(14)-C(18)	3 3(7)
C(2)-C(1)-N(14)-C(15)	-4 0(6)
Cr(1)-C(1)-N(14)-C(15)	-176 8(4)
C(1)-N(14)-C(15)-C(16)	-179 9(6)
C(18)-N(14)-C(15)-C(16)	-0 1(7)

N(14)-C(15)-C(16)-C(17)	7 5(9)
C(15)-C(16)-C(17)-C(18)	-12 1(10)
C(1)-N(14)-C(18)-C(17)	173 0(5)
C(15)-N(14)-C(18)-C(17)	-6 9(6)
C(16)-C(17)-C(18)-N(14)	11 6(8)
C(27)-Cr(1)-C(19)-O(20)	1(6)
C(23)-Cr(1)-C(19)-O(20)	-34(7)
C(25)-Cr(1)-C(19)-O(20)	90(6)
C(21)-Cr(1)-C(19)-O(20)	-89(6)
C(1)-Cr(1)-C(19)-O(20)	-179(100)
C(27)-Cr(1)-C(21)-O(22)	1(9)
C(19)-Cr(1)-C(21)-O(22)	88(9)
C(23)-Cr(1)-C(21)-O(22)	-87(9)
C(25)-Cr(1)-C(21)-O(22)	80(10)
C(1)-Cr(1)-C(21)-O(22)	-179(100)
C(27)-Cr(1)-C(23)-O(24)	-44(5)
C(19)-Cr(1)-C(23)-O(24)	-10(7)
C(25)-Cr(1)-C(23)-O(24)	-133(5)
C(21)-Cr(1)-C(23)-O(24)	46(5)
C(1)-Cr(1)-C(23)-O(24)	135(5)
C(27)-Cr(1)-C(25)-O(26)	64(6)
C(19)-Cr(1)-C(25)-O(26)	-24(6)
C(23)-Cr(1)-C(25)-O(26)	152(6)
C(21)-Cr(1)-C(25)-O(26)	-15(8)
C(1)-Cr(1)-C(25)-O(26)	-116(6)
C(19)-Cr(1)-C(27)-O(28)	134(13)
C(23)-Cr(1)-C(27)-O(28)	-49(13)
C(25)-Cr(1)-C(27)-O(28)	47(13)
C(21)-Cr(1)-C(27)-O(28)	-137(13)
C(1)-Cr(1)-C(27)-O(28)	-126(30)

Symmetry transformations used to generate equivalent atoms